

hhu

Heinrich Heine
Universität Düsseldorf 

Elucidate the important role of peroxisomal transport proteins for plant growth and development

Inaugural-Dissertation

zur Erlangung des Doktorgrades
der Mathematisch-Naturwissenschaftlichen Fakultät
der Heinrich-Heine-Universität Düsseldorf

vorgelegt von

Lennart Charton
aus Essen

Düsseldorf, Januar 2020

aus dem Institut für Biochemie der Pflanzen
der Heinrich-Heine-Universität Düsseldorf

Gedruckt mit der Genehmigung der
Mathematisch-Naturwissenschaftlichen Fakultät der
Heinrich-Heine-Universität Düsseldorf

Berichtersteller:

1. Prof. Nicole Linka

2. Prof. Georg Groth

Tag der mündlichen Prüfung:

Erklärung

Ich versichere an Eides statt, dass ich die vorliegende Dissertation eigenständig und ohne unerlaubte Hilfe unter Beachtung der „Grundsätze zur Sicherung guter wissenschaftlicher Praxis“ an der Heinrich-Heine-Universität Düsseldorf angefertigt habe. Die Dissertation habe ich in dieser oder in ähnlicher Form noch bei keiner anderen Institution eingereicht.

Ich habe bisher keine erfolglosen Promotionsversuche unternommen.

Düsseldorf, den

Lennart Charton

Table of contents

I.I Summary	1
I.II Zusammenfassung	3
II. General introduction	5
III. Manuscripts	23
III.I Manuscript 1	
Identification of a novel peroxisomal transport protein involved in the heat shock response of <i>Arabidopsis thaliana</i>	23
III.II Manuscript 2	
Investigation of three candidates for peroxisomal coenzyme A carrier proteins.....	64
III.III Manuscript 3	
Peroxisomal ATP import by PNC1 and PNC2 is required for functional mevalonate-pathway.....	94
IV. Published manuscripts	116
IV.I Published manuscript 1	
Plant peroxisomal solute transporter proteins.....	116
IV.II Published manuscript 2	
The mitochondrial NAD ⁺ transporter (NDT1) plays important roles in cellular NAD ⁺ homeostasis in <i>Arabidopsis thaliana</i>	154
IV.III Published manuscript 3	
Slc25a17 acts as a peroxisomal coenzyme A transporter and regulates multiorgan development in zebrafish.....	173
IV.IV Published manuscript 4	
Analysis of peroxisomal β -oxidation during storage oil mobilization in <i>Arabidopsis thaliana</i> seedlings.....	189
IV.V Published manuscript 5	
The Peroxisomal NAD Carrier from <i>Arabidopsis</i> Imports NAD in Exchange with AMP	
V. Submitted manuscripts	226
V.I Submitted manuscript 1	
Evidence for dual targeting of <i>Arabidopsis</i> plastidial glucose-6-phosphate transporter GPT1 to peroxisomes via the ER.....	226
V.II Submitted manuscript 2	
Biochemical and Functional Characterization of a Mitochondrial Citrate Carrier in <i>Arabidopsis thaliana</i>	264
VI. Acknowledgement	317

I.I Summary

Plant cells are compartmentalized into different organelles separated by membranes, which enables the simultaneous implementation of specialized metabolic reactions. But substrates have to be transported across these barriers in an efficient and controllable way, since many metabolic pathways are shared between different organelles.

Peroxisomes play a central role in a plethora of metabolic reactions covering all stages of plant development from seedling establishment over photosynthesis to reproduction and senescence. But the majority of the transport proteins required for these processes are still unknown. The mitochondrial carrier family represents one of the largest and most diverse group of transport proteins with several peroxisomal representatives in *Arabidopsis*, animals and yeast. This thesis deals with the characterization of four novel peroxisomal MCF carrier that have not been analyzed in detail before. In addition, we aimed to further analyze the importance of the already identified peroxisomal ATP carrier PNC1 and PNC2 beyond their known role in β -oxidation.

The first manuscript deals with the identification of a peroxisomal heat shock responsive carrier (PHS1). PHS1 is the only still unknown MCF carrier that shows a strong transcriptional response upon heat stress, both in microarray and RNA-Seq experiments. Growth of mutant plants is decreased after heat stress concomitant with increased oxidative stress. The evidence for an involvement of PHS1 in peroxisomal ROS homeostasis gets even stronger since *phs1* mutant lines are additionally compromised in post-germinative growth, a process requiring high β -oxidation activity and thus representing a huge source of ROS production. Finally, a *phs1 cat2* double mutant revealed an additive phenotype compared to the respective single mutants. All in all, we could show the involvement of a peroxisomal carrier in the oxidative stress and especially heat stress response, for the first time. But there are still open questions regarding substrate specificity and post-transcriptional regulation, since the heat shock specific role of PHS1 seems to be restricted to the expression of a second isoform.

The second manuscript is about the identification and initial characterization of three closely related peroxisomal MCF carrier. Based on the high similarity to already characterized carrier, we hypothesize that that they mediate the transport of coenzyme A (CoA) to fuel β -oxidation processes like storage oil mobilization and hormone biosynthesis. Hence, we call them peroxisomal CoA carrier (PCC) 1, 2 and 3. Analysis of publicly available RNA-Seq experiments revealed that PCC1 and PCC3 are most highly upregulated upon wounding and germination, respectively, which are both linked to peroxisomal CoA metabolism. In addition, PCC1 was able to complement yeast mutants defective in peroxisomal NAD redox shuttles. Since, CoA and NAD are structurally similar it is unclear, whether this effect is caused by the

natural *in vivo* function of PCC1 or by the heterologous over-expression in yeast. Biochemical approaches could not identify the transported substrates of the PCC proteins, yet.

In the third manuscript we could show, that the already identified peroxisomal ATP carrier PNC1 and PNC2 are required for a functional mevalonate pathway in addition to their known involvement in β -oxidation. Double mutant plants are affected in the biosynthesis of Mev pathway derived isoprenoids like sterols and plant volatiles. In addition, growth experiments in the presence of a specific inhibitor for the parallel working plastidic MEP pathway suggest a crosstalk between both pathways. This should be further analyzed in future studies by additionally knocking out a cytosolic kinase involved in the regeneration of isoprenoid precursors. Moreover, analysis of the *in vivo* ATP pool in the *pnc1/2* double mutant revealed a decrease in the cytosolic ATP level compared to the WT. Hence, future studies should aim to establish a peroxisomal version of this sensor to quantify the effect of the double mutant on peroxisomal ATP levels.

I.II Zusammenfassung

Pflanzliche Zellen sind in Organellen aufgeteilt, die durch Membranen voneinander getrennt sind und dadurch die gleichzeitige Durchführung von spezialisierten Stoffwechselwegen ermöglichen. Jedoch müssen Substrate in einer effizienten und kontrollierbaren Art über diese Grenzen transportiert werden, da viele Stoffwechselwege zwischen verschiedenen Organellen aufgeteilt sind.

Peroxisomen spielen eine zentrale Rolle in einer Vielzahl von Reaktionen, die alle Bereiche der pflanzlichen Entwicklung, von der Keimung, über Photosynthese bis hin zu Reproduktion und Seneszenz, abdecken. Jedoch sind die meisten der daran beteiligten Transportproteine noch unbekannt. Die mitochondriale Carrier Familie (MCF) repräsentiert eine der größten und vielseitigsten Gruppen von Transportproteinen mit mehreren peroxisomalen Vertretern in Arabidopsis, Tieren und Hefe. Diese Arbeit handelt von der Charakterisierung von vier neuen, bisher noch nicht untersuchten peroxisomalen MCF Carrier. Zusätzlich wollten wir die Wichtigkeit der bereits identifizierten peroxisomalen ATP Carrier PNC1 und PNC2, über deren Rolle in der β -Oxidation hinaus, untersuchen.

Das erste Manuskript handelt von der Identifikation eines peroxisomalen Transportproteins (PHS1), das auf Hitzestress reagiert. PHS1 ist der einzige bislang noch unbekannt MCF Carrier mit einer starken transkriptionellen Reaktion auf Hitzestress, sowohl in Microarray, als auch RNA-Seq Experimenten. Das Wachstum von Mutanten nach Hitzestress ist reduziert, begleitet von erhöhtem oxidativem Stress. Die Belege für eine Beteiligung von PHS1 in der peroxisomalen ROS Homöostase werden zudem dadurch deutlich, dass die mutanten Linien zusätzlich einen Wachstumsdefekt nach der Keimung aufweisen, ein Prozess, mit erhöhter β -Oxidationsaktivität und dadurch gesteigerter ROS-Produktion. Schließlich, zeigt eine *phs1 cat2* Doppelmutante einen additiven Phänotypen im Vergleich zu den jeweiligen Einzelmutanten. Alles in Allem konnte wir zum ersten Mal die Beteiligung eines peroxisomalen Transportproteins in der Reaktion auf oxidativen Stress und im Speziellen Hitzestress zeigen. Jedoch gibt es immer noch offene Fragen bezüglich Substratspezifität und post-transkriptioneller Regulierung, da die Hitzeschock-spezifische Rolle von PHS1 wohl nur auf die Expression einer zweiten Isoform beschränkt ist.

Das zweite Manuskript befasst sich mit der Identifizierung und ersten Charakterisierung von drei nah verwandten peroxisomalen MCF Carrier. Basierend auf der großen Ähnlichkeit zu bereits charakterisierten Carrier, hypothesieren wir, dass sie den Transport von Coenzym A (CoA) ermöglichen, welches für β -Oxidationsprozesse wie Speicherölmobilisierung und Hormonbiosynthese benötigt wird. Daher nennen wir sie peroxisomale CoA Carrier (PCC) 1, 2 und 3. Analysen öffentlich zugänglicher RNA-Seq Experimente ergab, dass PCC1 und PCC3 am stärksten durch Verwundung, bzw. während der Keimung hochreguliert sind, beides

Prozesse, die mit dem peroxisomalen Stoffwechsel verbunden sind. Darüber hinaus war PCC1 dazu in der Lage Hefemutanten zu komplementieren, die Defekte in den peroxisomalen NAD Redox-Shuttles aufweisen. Da CoA und NAD strukturell sehr ähnlich sind, ist es unklar, ob der Effekt von der *in vivo* Funktion von PCC1 stammt oder durch die Überexpression in Hefe bedingt ist. Biochemische Ansätze konnten die von den PCC-Proteinen transportierten Substrate bisher nicht identifizieren.

Im dritten Manuskript konnte wir zeigen, dass die bereits charakterisierten peroxisomalen ATP Transporter PNC1 und PNC2 zusätzlich zu ihrer Rolle in der β -oxidation, für einen funktionierenden Mevalonat-Weg benötigt werden. Doppelmutanten sind in der Produktion von Mevalonat-abhängigen Isoprenoiden, wie Sterole und pflanzliche Volatile, beeinträchtigt. Zudem suggerieren Wachstumsexperimente in Anwesenheit eines spezifischen Hemmstoffs des parallel arbeitenden plastidären MEP-Weges, einen Austausch zwischen den beiden Biosynthesewegen. Dieser sollte in zukünftigen Studien durch zusätzliches Ausschalten einer cytosolischen Kinase, die an der Regeneration von Isoprenoidvorläufern beteiligt ist, weiter untersucht werden. Darüber hinaus zeigte die *in vivo* Analyse des ATP-Gehalts in der *pnc* Doppelmutante, dass dieser im Vergleich zum WT verringert ist. Daher sollten zukünftige Studien das Ziel haben, eine peroxisomale Version des Sensors zu etablieren, um den Effekt der Doppelmutante auf den peroxisomalen ATP-Gehalt zu quantifizieren.

II General Introduction

Plant compartmentalization

Eukaryotic cells are highly compartmentalized into different organelles. The physical separation by at least one biological membrane enables the simultaneous implementation of biochemical reactions that demand on different physiological prerequisites. This includes specific sets of enzymes as well as tight regulation of metabolite flux, pH-value and redox-state. The origin of this compartmentalization is still not fully understood and one of the fundamental questions for evolutionary biologists. In general, two different hypotheses exist. One describes the endogenous formation from pre-existing structures which is widely accepted for peroxisomes and the endoplasmatic reticulum (ER) (Schluter et al. 2006; Gabaldon and Pittis 2015). The second mode is based on the endosymbiotic interaction of different cells as it was described for the origin of mitochondria and chloroplasts. The separation into these models appears obvious since in contrast to peroxisomes and the ER, mitochondria and chloroplasts are surrounded by two membranes and possess their own genome.

Peroxisomes

Peroxisome biogenesis and protein import

Peroxisomes are organelles ubiquitous to all eukaryotes and highly dynamic in terms of function and structure. Peroxisome biogenesis is associated to the ER, since phospholipids and some peroxisomal membrane proteins (PMPs) can either be delivered from the ER to preexisting peroxisomes or fuse together for *de novo* biogenesis (Mullen and Trelease 2006). In contrast to yeast and mammals, *de novo* biogenesis is not yet established in plants. Thus, multiplication of plant peroxisomes is most likely restricted to the fission of already existing peroxisomes and can be either constitutively during the cell cycle or inducible i.e. under certain stress conditions (Hu et al. 2012). Peroxisomal matrix proteins are directly imported in a fully-folded state from the cytosol (Lanyon-Hogg et al. 2010; Meinecke et al. 2010). There are two types of peroxisomal target sequences (PTS). PTS1 is a C-terminal tripeptide consisting of a non-polar residue in position 1, a basic amino acid in position 2 and a small and uncharged amino acid in position 3 (Lingner et al. 2011). SKL represents the canonical PTS1 but improvement of mass proteomic studies and targeting of fluorescent fusion protein led to the identification of a broad range of possible PTS1 sequences (Reumann et al. 2012). PTS2 is a N-terminal nonapeptide that consists of two pairs of conserved amino acids separated by 5 non-conserved amino acids and as is the case for PTS1, several alternative sequences have been identified to be functional (Kato et al. 1998; Lingner et al. 2011). PMPs can be sorted into two classes depending on the way of their integration into the peroxisomal membrane. Class-I PMPs are synthesized in the cytosol and are directly integrated into the peroxisomal

membrane. This includes the recognition of a membrane PTS (mPTS) signal by PEX19 in the cytosol. But in contrast to the well-established PTS of soluble proteins, mPTS are highly variable and hence difficult to predict (Rottensteiner et al. 2004; Van Ael and Franssen 2006). Class-II PMPs are first integrated into the ER membrane before they are directed to peroxisomes (Mullen and Trelease 2006).

Photorespiration

The plastidic Ribulose-1,5-bisphosphate carboxylase/oxygenase (Rubisco) is the most abundant enzyme on earth and is responsible for the initial CO₂ fixation in photosynthetic organisms and hence the basis of all carbon on earth (Reumann and Weber 2006). But as the name implies, Rubisco has an additional oxygenase activity that results in the production of the toxic intermediate 2-phosphoglycolate. Even though the affinity to oxygen is very low, the high concentration compared to CO₂ in ambient air leads to a ratio of 1:0.25 up to 1:0.5 between carboxylase and oxygenase activity in C₃ plants (Sharkey 1988). In addition, specific conditions like heat stress can cause a disproportional increase of Rubisco oxygenase activity (Kim and Portis 2004). Since 2-phosphoglycolate cannot enter the Calvin-Benson-Bassham cycle it has to be recycled to 3-phosphoglycerate in a cost-intensive way in a process called photorespiration (Reumann and Weber 2006). The peroxisomal part of photorespiration starts with the oxidation of glycolate to glyoxylate catalyzed by glycolate oxidase concomitant with the production of H₂O₂. Two molecules of glyoxylate are transaminated by serine:glyoxylate and glutamate:glyoxylate aminotransferase, respectively yielding two molecules of glycine that are transferred to mitochondria to produce one molecule of serine. In this step, CO₂ and ammonia are released. Back in peroxisomes the amino group of serine is transferred to glyoxylate resulting in the formation of hydroxypyruvate. Malate dehydrogenase reduces hydroxypyruvate to glycerate by the oxidation of NADH to NAD representing the last peroxisomal step of photorespiration although there is evidence for a cytosolic and plastidic bypass of this reaction (Timm et al. 2008; Timm et al. 2011).

β-oxidation is involved in catabolic reactions

Oil-crops, like rape and the model organism *Arabidopsis thaliana*, store fatty acids in seed cytosolic oil-bodies to provide energy for seedling establishment. Peroxisomes play an essential role in this process since they are the sole site of fatty acid β-oxidation in plants. But β-oxidation of fatty acids is not restricted to the process of storage oil mobilization. During senescence, membrane lipids are degraded to be reused as carbon-source for growth or for storage in sink-tissues like seeds (Troncoso-Ponce et al. 2013). In addition, β-oxidation of guard-cell oil-bodies contributes to the ATP production required for stomatal opening (McLachlan et al. 2016).

In general, released fatty acids are imported as CoA-esters into peroxisomes by the ABC-transporter PXA1 (Footitt et al. 2002; Nyathi et al. 2010). The CoA-moiety is cleaved off during the import which necessitates the re-esterification of fatty acids to CoA prior entering β -oxidation (De Marcos Lousa et al. 2013). This step is catalyzed by two long chain acyl-CoA synthetases (LACS6/7) in an ATP-dependent reaction. The resulting acyl-CoA enters the β -oxidation cycle and is oxidized to 2-trans-enoyl-CoA catalyzed by FAD-dependent acyl-CoA oxidase concurrent with the production of H_2O_2 . The hydratase and dehydrogenase reaction to convert 2-trans-enoyl-CoA to hydroxyl-acyl-CoA and subsequently to 3-ketoacyl-CoA is catalyzed by the multifunctional protein. The dehydrogenase reaction is coupled to the reduction of NAD to NADH. NAD is regenerated by the malate/oxaloacetate shuttle where oxaloacetate is reduced to malate by peroxisomal malate dehydrogenase (Pracharoenwattana et al. 2007). The subsequent regeneration of oxaloacetate occurs in the cytosol catalyzed by the cytosolic malate dehydrogenase. Thus, an efficient exchange of malate and oxaloacetate across the peroxisomal membrane is required to maintain β -oxidation activity. The last step of β -oxidation is mediated by 3-ketoacyl thiolase that cleaves-off the thiol-group using CoA and thus generates acetyl-CoA and acyl-CoA. The latter can re-enter the β -oxidation cycle for further oxidation.

Acetyl-CoA is fueled into the peroxisomal glyoxylate cycle by the reaction with oxaloacetate to form citrate. The conversion of citrate to isocitrate by aconitase is located to the cytosol and hence requires the export of citrate. Citrate or isocitrate can either be respired in the mitochondrion, or reenter peroxisomes in the form of isocitrate to be converted to glyoxylate by isocitrate lyase (Pracharoenwattana et al. 2005). The simultaneously produced succinate is exported from the peroxisomes to be used for gluconeogenesis. Glyoxylate resides in the peroxisome and is converted to malate by malate synthase. Malate is most likely exported to the cytosol for the conversion to oxaloacetate since the peroxisomal malate dehydrogenase was shown to solely catalyze the reverse reaction required for β -oxidation (Pracharoenwattana et al. 2007).

β -oxidation is involved in anabolic reactions

Beside the role in the catabolism of fatty acids, peroxisomal β -oxidation is additionally involved in anabolic reactions including hormone biosynthesis.

The plant hormone jasmonic acid (JA) plays an important role in plant growth and development as well as in the response to biotic and abiotic stress. It is involved in primary root growth, hypocotyl elongation, leaf expansion and reproduction (Huang et al. 2017). JA biosynthesis is initiated by the release of α -linolenic acid from glycerolipids and phospholipids of the plastidic membrane (Hyun et al. 2008). It is converted in a series of enzymatic reactions to 12-oxo-phytodeinic acid (OPDA) which is subsequently transferred to peroxisomes. As it is

the case for fatty acids, OPDA is imported into peroxisomes by PXA1. But in contrast to fatty acids, it is unknown whether OPDA is imported in a free or esterified CoA-bound form (Linka and Theodoulou 2013). In addition, the residual JA biosynthesis rate in a *pxa1* mutant suggests the presence of an alternative import of OPDA either by another carrier or free diffusion across the membrane (Theodoulou et al. 2005; Kienow et al. 2008). Within peroxisomes OPDA is first reduced to OPC8:0 by a NADPH-dependent OPDA reductase before it is esterified to CoA. The OPC8:0 CoA ester is subsequently passed through three rounds of β -oxidation to finally yield JA.

β -oxidation is additionally required for the biosynthesis of indole acetic acid (IAA), the active form of auxin. Auxin is a key player in both cell growth and elongation thus it has to be tightly regulated by modulating biosynthesis, degradation and inactive storage forms (Strader et al. 2011). Indole butyric acid is a two carbon elongated IAA precursor and potential auxin storage form that has to be processed by peroxisomal β -oxidation to its active form (Zolman et al. 2000; Strader et al. 2010). Whereas some enzymes for IBA and fatty acid β -oxidation are identical, three enzymes were shown to be exclusively involved in the conversion of IBA to IAA (Zolman et al. 2000; Zolman et al. 2007; Zolman et al. 2008). 2,4-dichlorophenoxybutyric acid (2,4-DB) is the precursor of the synthetic auxin and herbicide 2,4-dichlorophenoxyacetic acid (2,4-D) and like IBA, it requires peroxisomal β -oxidation for shortening of its carboxyl side-chain (Hayashi et al. 1998). Resistance to 2,4-DB has been extensively used as an assay for the identification of mutants that affected in β -oxidation (Hayashi et al. 1998; Eastmond et al. 2000; Zolman et al. 2001).

β -oxidation-independent peroxisomal anabolism

In addition to its role in β -oxidation, peroxisomes harbor metabolic pathways that, like photorespiration, are independent of the core β -oxidation process.

One of these pathways is the mevalonate (Mev) pathway for the production of isopentenyl-diphosphate (IPP). IPP and its isomer dimethylallyl diphosphate (DMAPP) are the building blocks of isoprenoids that represent one of the most diverse classes of primary and secondary metabolites (Vranova et al. 2013). Despite of being defined as the cytosolic IPP biosynthesis pathway, the last enzymes were shown to be localized to peroxisomes (Sapir-Mir et al. 2008; Simkin et al. 2011). However, the pathway starts in the cytosol with the formation of hydroxymethylglutaryl-coenzyme A, the direct precursor of Mev. After phosphorylation, Mev-phosphate is imported into peroxisomes where it is phosphorylated and subsequently decarboxylated by the phosphomevalonate kinase and ATP-dependent mevalonate-diphosphate decarboxylase, respectively to yield IPP. A peroxisomal isomerase is involved in the interconversion of IPP and DMAPP which are used for the cytosolic production of farnesyl diphosphate, representing the precursor for sterols, brassinosteroids and sesquiterpenes.

Plants have a special role in the production of IPP since they possess the plastidic methylerythritol phosphate (MEP) pathway in addition to the common cytosolic Mev pathway with distinct role in the production of specialized isoprenoids (Hemmerlin et al. 2012). The MEP pathway derived IPP and DMAPP is used for the biosynthesis of photosynthetic related compounds like carotenoids, phytyl-chain and tocopherols. It starts with the condensation of glyceraldehyde-3-phosphate and pyruvate to form deoxy-D-xylulose 5-phosphate (DXP) which is subsequently converted to the name-giving MEP. These two steps, catalyzed by DXP synthase and DXP reductase, respectively, are considered to be the major flux regulators (Simpson et al. 2016). The specific DXP reductase inhibitor fosmidomycin together with mutants affected in either of the pathways has been widely used to analyze the contribution of each pathway to the production of different isoprenoids. It could be shown that a cross-talk between the Mev and MEP pathways exists, even though the loss of one pathway cannot be fully compensated by the action of the other (Kasahara et al. 2002; Laule et al. 2003; Dudareva et al. 2005; Mendoza-Poudereux et al. 2015).

In addition to the *de novo* synthesis, IPP can be generated by the phosphorylation of isopentenyl phosphate (IP) by the cytosolic isopentenyl phosphate kinase (IPK) (Henry et al. 2015). Overexpression of IPK lead to an increase in Mev pathway derived isoprenoids by both, increasing IPP and reducing IP that is a known inhibitor for farnesyl diphosphate synthase. Interestingly, it could be shown that IPK also contributes to the formation of MEP pathway derived isoprenoids which further supports the idea of an exchange between both pathways (Henry et al. 2015).

β -oxidation-independent peroxisomal catabolism

Polyamines (PAs) are low-molecular nitrogenous cations with putrescine, spermidine, spermine and thermospermine being the most dominant representatives (Andronis et al. 2014). Due to their positive charge, free PAs can interact with negatively charged molecules like acidic proteins, membrane phospholipids and nucleic acids to fulfill their divers function in plant growth and development (Igarashi and Kashiwagi 2015). Putrescine is produced in the chloroplasts from arginine and is converted to spermidine and subsequently to spermine by spermidine and spermine synthase, respectively. Elevated levels of spermine by overexpressing spermine synthase are associated with increased tolerance to drought and high salinity (Marco et al. 2011). In contrast, polyamine catabolism has been correlated with several processes including cell growth, development and stress response, but the detailed mechanisms remain largely elusive (Andronis et al. 2014). The back-conversion of spermine to putrescine is located to peroxisomes and mirrors the biosynthesis pathway. In Arabidopsis, three polyamine oxidases (PAOs) were shown to have peroxisomal localization and are responsible for the oxidation of spermine and spermidine to yield putrescine *in vivo* (Fincato et

al. 2011). The terminal oxidation of putrescine is mediated by two copper-containing amine oxidases (CuAO) yielding 4-aminobutanal that is a precursor for 4-aminobutyrate (GABA) (Planas-Portell et al. 2013; Zarei et al. 2016). Thus, the physiological effect of PA catabolism is considered to be not restricted to the regulation of PA levels, but is also associated with the synthesis of GABA and H_2O_2 that is produced by both, PAO and CuAO activity (Planas-Portell et al. 2013).

Peroxisomal antioxidant machinery

β -oxidation and photorespiration are major sources of cellular H_2O_2 production (Foyer and Noctor 2003). Due to its high stability and membrane permeability, H_2O_2 can reach toxic concentrations and hence causing damage to proteins, lipids and DNA (Apel and Hirt 2004). However, at lower concentrations H_2O_2 serves as an important signaling molecule that regulate development, stress response or programmed cell death (Dat et al. 2000; Gechev and Hille 2005). Thus, plants require an efficient system to tightly regulate the production and degradation of H_2O_2 . Catalase is the predominant peroxisomal enzyme for the decomposition of H_2O_2 to water and oxygen with high catalytic rates but low substrate affinity (Noctor and Foyer 1998). Elevated ROS production by for instance abiotic stress may exceeds the capacity of catalase, hence redundant pathways are necessary to protect the cell against oxidative damage.

The coordinated reaction of the two antioxidants ascorbate (ASC) and glutathione (GSH) within the ASC-GSH cycle is an efficient process for the degradation of H_2O_2 and was shown to be active in chloroplasts, mitochondria and peroxisomes (Jimenez et al. 1997; Asada 2006). By this, ascorbate peroxidase reduces H_2O_2 to water concomitant with the oxidation of ASC to dehydro-ASC. A dehydro-ASC reductase is responsible for the regeneration of ascorbate by oxidizing GSH to GSH disulfide (GSSG). The reduction of GSSG is catalyzed by the NADPH dependent glutathione reductase 1 (GR1) that is dually localizes in the cytosol and peroxisomes (Mhamdi et al. 2010).

In peroxisomes, there are two ways for the regeneration of NADPH. One way is mediated by the NADP-dependent isocitrate dehydrogenase (ICDH) that reduces NADP by simultaneously oxidizing isocitrate to 2-oxoglutarate (Corpas et al. 1999). The second way uses the oxidation of glucose-6-phosphate and 6-phosphogluconate catalyzed by respective dehydrogenases as part of the oxidative pentose phosphate pathway (OPPP). The OPPP is found in the cytosol, chloroplasts and at least transiently in peroxisomes (Kruger and von Schaewen 2003; Meyer et al. 2011; Holscher et al. 2014).

ASC and GSH are additionally involved in ROS scavenging independently of the ASC-GSH cycle. The membrane-bound isoforms of peroxisomal ascorbate peroxidase and monodehydroascorbate reductase efficiently prevent H_2O_2 from leaking into the cytosol

(Eastmond 2007). Thereby, H_2O_2 is dissipated concomitantly with the oxidation of ASC to monodehydroascorbate, which is in turn reduced to ASC by the oxidation of NADH to NAD.

In peroxisomes, there are three GSH-S-transferases of the theta family that use GSH for the reduction of toxic fatty acid hydroperoxides to monohydroxy alcohols (Reumann et al. 2007; Dixon et al. 2009). In addition to their peroxidase activity, they also show limited transferase activity conjugating GSH to compounds like xenobiotics to tag them for vacuolar degradation (Kaur et al. 2009).

Diversity of the mitochondrial carrier family

Based on structural similarities, transport proteins can be subdivided into different families. Among them, the mitochondrial carrier family (MCF) represents the largest group of transport proteins with 35 members in *Saccharomyces cerevisiae*, 50 candidates in humans and 58 members in Arabidopsis (Palmieri et al. 2000; Picault et al. 2004; Palmieri et al. 2011). The common structure of all MCF carriers are three tandemly repeated homologous domains consisting of two α -helical transmembrane domains, each (Haferkamp and Schmitz-Esser 2012).

Despite of their structural similarity, MCF carriers are highly diverse in terms of substrate specificity including adenine nucleotides, di- and tricarboxylates and amino acids (Haferkamp and Schmitz-Esser 2012; Palmieri 2014; Taylor 2017). While the majority of the MCF proteins are indeed localized to mitochondria, members of this family have been also found in the plasma membrane, ER, plastids and peroxisomes.

So far, only five peroxisomal transport proteins have been identified and characterized in any species. The peroxisomal import of fatty-acids is mediated by members of the ATP binding cassette family in human, yeast and Arabidopsis (Theodoulou and Kerr 2015). Recently, we could identify the glucose-6-phosphate/phosphate transporter 1 (GPT1) being transiently localized to peroxisomes to fuel the OPPP (Baune et al. submitted). The residual three peroxisomal membrane proteins all belong to the MCF. The first characterized peroxisomal MCF carrier was the yeast adenine nucleotide transporter 1 (Ant1p) shown to mediate the transport of ATP against ADP and AMP (Palmieri et al. 2001; van Roermund et al. 2001). On the basis of amino acid sequence similarity to Ant1p, the two Arabidopsis peroxisomal adenine nucleotide carriers PNC1 and PNC2 were identified and characterized to have equal substrate specificity and strict counter exchange activity (Arai et al. 2008; Linka et al. 2008). The second one is the Arabidopsis peroxisomal NAD carrier PXN, that was initially characterized to transport NAD, NADH, ADP, AMP and CoA *in vitro* (Agrimi et al. 2012; Bernhardt et al. 2012). But experiments using yeast complementation assays suggest that the *in vivo* function of PXN is restricted to the exchange of NAD against AMP (van Roermund et al. 2016). Interestingly, PXN represents the only peroxisomal NAD carrier and the respective

carrier in other species is still unknown. SLC25A17 is the last known peroxisomal MCF carrier that was identified in human and zebrafish to mediate the import of CoA (Agrimi et al. 2012; Kim et al. 2019). But such a transport protein has not been identified in yeast or Arabidopsis, yet.

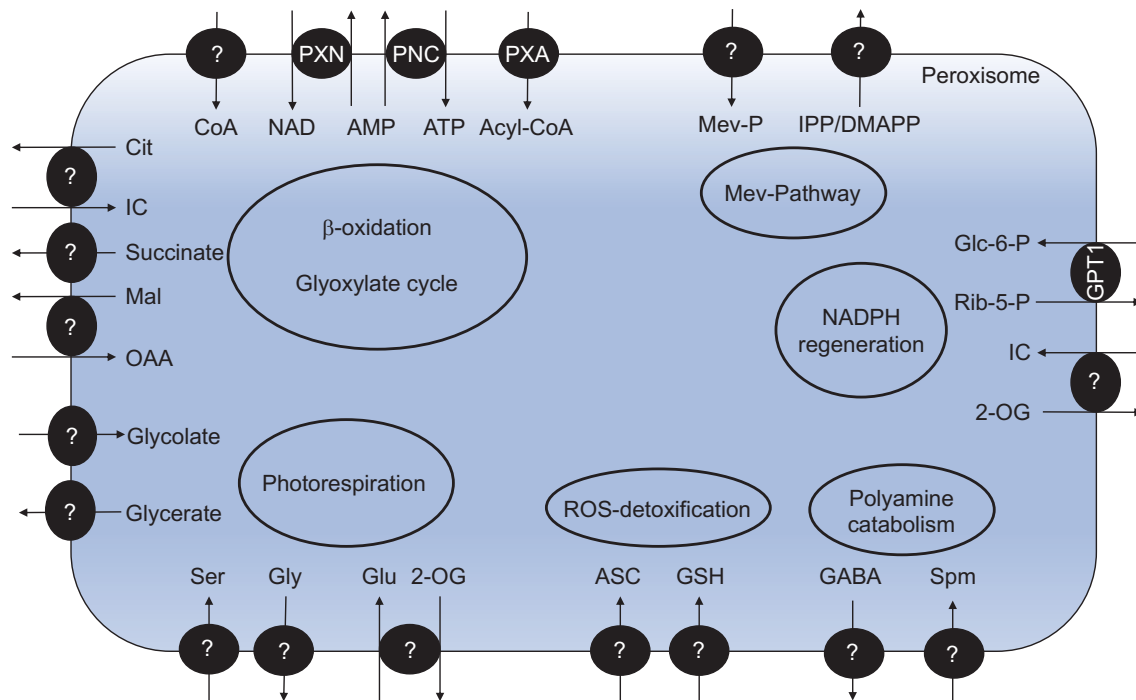


Figure 1: Transport proteins required for plant peroxisomal metabolism

Only four transport proteins are known to supply peroxisomes with substrates and co-factors. Question marks show unknown transport processes either mediated by specific transport proteins or broad-specific carrier. 2-OG: 2-oxoglutarate; AMP: adenosine monophosphate; ASC: Ascorbate; ATP: adenosine triphosphate; Cit: citrate; CoA: coenzyme A; DMAPP: dimethylallyl diphosphate; GABA: 4-aminobutyrate; Glc-6-P: glucose-6-phosphate; Glu: glutamine; Gly: glycine; GPT1: glucose-6-phosphate/phosphate transporter 1; GSH: reduced glutathione; IC: isocitrate; IPP: isopentenyl diphosphate; Mal: malate; Mev-P: mevalonate phosphate; NAD: nicotinamide adenine dinucleotide; OAA: oxaloacetate; PNC: peroxisomal adenine nucleotide carrier; PXA: peroxisomal fatty acid importer; PXN: peroxisomal NAD carrier; Rib-6-P: ribulose-6-phosphate; Ser: serine; Spm: spermine.

In addition, it is still unknown how peroxisomes are provided with smaller molecules like amino, di- and tricarboxylic acids required for photorespiration, glyoxylate cycle and redox shuttles. The presence of pore-forming channels with broad substrate specificity that facilitate the free diffusion of small molecules (< 300 Da) represents one hypothesis (Antonenkov and Hiltunen 2012). The peroxisomal membrane protein 2 from mouse (Pxm2) and the peroxisomal membrane protein of 22 kDa (PMP22) are the only members of the so called PMP22/MPV17 channel family described so far (Tugal et al. 1999; Murphy et al. 2003; Rokka et al. 2009; Vapola et al. 2014). Recombinant Pxm2 was shown to allow free diffusion of organic acids < 300 Da by lipid bilayer experiments. But whether Arabidopsis PMP22 has similar properties *in vitro* or if Pxm2 has indeed channel-activity *in vivo* remain open questions.

But, since mitochondrial localized MCF carrier were shown to transport the majority of the up to now unknown metabolites, the existence of additional peroxisomal representatives of this protein family must not be disregarded (Haferkamp and Schmitz-Esser 2012).

Agrimi, G., A. Russo, C. L. Pierri and F. Palmieri (2012). "The peroxisomal NAD⁺ carrier of *Arabidopsis thaliana* transports coenzyme A and its derivatives." J Bioenerg Biomembr **44**(3): 333-340.

Agrimi, G., A. Russo, P. Scarcia and F. Palmieri (2012). "The human gene SLC25A17 encodes a peroxisomal transporter of coenzyme A, FAD and NAD⁺." Biochem J **443**(1): 241-247.

Andronis, E. A., P. N. Moschou, I. Toumi and K. A. Roubelakis-Angelakis (2014). "Peroxisomal polyamine oxidase and NADPH-oxidase cross-talk for ROS homeostasis which affects respiration rate in *Arabidopsis thaliana*." Front Plant Sci **5**: 132.

Antonenkov, V. D. and J. K. Hiltunen (2012). "Transfer of metabolites across the peroxisomal membrane." Biochim Biophys Acta **1822**(9): 1374-1386.

Apel, K. and H. Hirt (2004). "Reactive oxygen species: metabolism, oxidative stress, and signal transduction." Annu Rev Plant Biol **55**: 373-399.

Arai, Y., M. Hayashi and M. Nishimura (2008). "Proteomic identification and characterization of a novel peroxisomal adenine nucleotide transporter supplying ATP for fatty acid beta-oxidation in soybean and *Arabidopsis*." Plant Cell **20**(12): 3227-3240.

Asada, K. (2006). "Production and scavenging of reactive oxygen species in chloroplasts and their functions." Plant Physiol **141**(2): 391-396.

Bernhardt, K., S. Wilkinson, A. P. Weber and N. Linka (2012). "A peroxisomal carrier delivers NAD(+) and contributes to optimal fatty acid degradation during storage oil mobilization." Plant J **69**(1): 1-13.

Corpas, F. J., J. B. Barroso, L. M. Sandalio, J. M. Palma, J. A. Lupianez and L. A. del Rio (1999). "Peroxisomal NADP-Dependent Isocitrate Dehydrogenase. Characterization and Activity Regulation during Natural Senescence." Plant Physiol **121**(3): 921-928.

Dat, J., S. Vandenabeele, E. Vranova, M. Van Montagu, D. Inze and F. Van Breusegem (2000). "Dual action of the active oxygen species during plant stress responses." Cellular and Molecular Life Sciences **57**(5): 779-795.

De Marcos Lousa, C., C. W. van Roermund, V. L. Postis, D. Dietrich, I. D. Kerr, R. J. Wanders, S. A. Baldwin, A. Baker and F. L. Theodoulou (2013). "Intrinsic acyl-CoA thioesterase activity of a peroxisomal ATP binding cassette transporter is required for transport and metabolism of fatty acids." Proc Natl Acad Sci U S A **110**(4): 1279-1284.

Dixon, D. P., T. Hawkins, P. J. Hussey and R. Edwards (2009). "Enzyme activities and subcellular localization of members of the Arabidopsis glutathione transferase superfamily." J Exp Bot **60**(4): 1207-1218.

Dudareva, N., S. Andersson, I. Orlova, N. Gatto, M. Reichelt, D. Rhodes, W. Boland and J. Gershenzon (2005). "The nonmevalonate pathway supports both monoterpene and sesquiterpene formation in snapdragon flowers." Proc Natl Acad Sci U S A **102**(3): 933-938.

Eastmond, P. J. (2007). "MONODEHYDROASCORBATE REDUCTASE4 is required for seed storage oil hydrolysis and postgerminative growth in Arabidopsis." Plant Cell **19**(4): 1376-1387.

Eastmond, P. J., M. A. Hooks, D. Williams, P. Lange, N. Bechtold, C. Sarrobert, L. Nussaume and I. A. Graham (2000). "Promoter trapping of a novel medium-chain acyl-CoA oxidase, which is induced transcriptionally during Arabidopsis seed germination." J Biol Chem **275**(44): 34375-34381.

Fincato, P., P. N. Moschou, V. Spedaletti, R. Tavazza, R. Angelini, R. Federico, K. A. Roubelakis-Angelakis and P. Tavladoraki (2011). "Functional diversity inside the Arabidopsis polyamine oxidase gene family." J Exp Bot **62**(3): 1155-1168.

Footitt, S., S. P. Slocombe, V. Lerner, S. Kurup, Y. Wu, T. Larson, I. Graham, A. Baker and M. Holdsworth (2002). "Control of germination and lipid mobilization by COMATOSE, the Arabidopsis homologue of human ALDP." EMBO J **21**(12): 2912-2922.

Foyer, C. H. and G. Noctor (2003). "Redox sensing and signalling associated with reactive oxygen in chloroplasts, peroxisomes and mitochondria." Physiologia Plantarum **119**(3): 355-364.

Gabalton, T. and A. A. Pittis (2015). "Origin and evolution of metabolic sub-cellular compartmentalization in eukaryotes." Biochimie **119**: 262-268.

Gechev, T. S. and J. Hille (2005). "Hydrogen peroxide as a signal controlling plant programmed cell death." Journal of Cell Biology **168**(1): 17-20.

Haferkamp, I. and S. Schmitz-Esser (2012). "The plant mitochondrial carrier family: functional and evolutionary aspects." Front Plant Sci **3**: 2.

Hayashi, M., K. Toriyama, M. Kondo and M. Nishimura (1998). "2,4-Dichlorophenoxybutyric acid-resistant mutants of Arabidopsis have defects in glyoxysomal fatty acid beta-oxidation." Plant Cell **10**(2): 183-195.

Hemmerlin, A., J. L. Harwood and T. J. Bach (2012). "A raison d'etre for two distinct pathways in the early steps of plant isoprenoid biosynthesis?" Prog Lipid Res **51**(2): 95-148.

Henry, L. K., M. Gutensohn, S. T. Thomas, J. P. Noel and N. Dudareva (2015). "Orthologs of the archaeal isopentenyl phosphate kinase regulate terpenoid production in plants." Proc Natl Acad Sci U S A **112**(32): 10050-10055.

Holscher, C., T. Meyer and A. von Schaewen (2014). "Dual-targeting of Arabidopsis 6-phosphogluconolactonase 3 (PGL3) to chloroplasts and peroxisomes involves interaction with Trx m2 in the cytosol." Mol Plant **7**(1): 252-255.

Hu, J., A. Baker, B. Bartel, N. Linka, R. T. Mullen, S. Reumann and B. K. Zolman (2012). "Plant peroxisomes: biogenesis and function." Plant Cell **24**(6): 2279-2303.

Huang, H., B. Liu, L. Liu and S. Song (2017). "Jasmonate action in plant growth and development." J Exp Bot **68**(6): 1349-1359.

Hyun, Y., S. Choi, H. J. Hwang, J. Yu, S. J. Nam, J. Ko, J. Y. Park, Y. S. Seo, E. Y. Kim, S. B. Ryu, W. T. Kim, Y. H. Lee, H. Kang and I. Lee (2008). "Cooperation and functional diversification of two closely related galactolipase genes for jasmonate biosynthesis." Dev Cell **14**(2): 183-192.

Igarashi, K. and K. Kashiwagi (2015). "Modulation of protein synthesis by polyamines." IUBMB Life **67**(3): 160-169.

Jimenez, A., J. A. Hernandez, L. A. Del Rio and F. Sevilla (1997). "Evidence for the Presence of the Ascorbate-Glutathione Cycle in Mitochondria and Peroxisomes of Pea Leaves." Plant Physiol **114**(1): 275-284.

Kasahara, H., A. Hanada, T. Kuzuyama, M. Takagi, Y. Kamiya and S. Yamaguchi (2002). "Contribution of the mevalonate and methylerythritol phosphate pathways to the biosynthesis of gibberellins in Arabidopsis." J Biol Chem **277**(47): 45188-45194.

Kato, A., Y. Takeda-Yoshikawa, M. Hayashi, M. Kondo, I. Hara-Nishimura and M. Nishimura (1998). "Glyoxysomal malate dehydrogenase in pumpkin: cloning of a cDNA and functional analysis of its presequence." Plant Cell Physiol **39**(2): 186-195.

Kaur, N., S. Reumann and J. Hu (2009). "Peroxisome biogenesis and function." Arabidopsis Book **7**: e0123.

Kienow, L., K. Schneider, M. Bartsch, H. P. Stuible, H. Weng, O. Miersch, C. Wasternack and E. Kombrink (2008). "Jasmonates meet fatty acids: functional analysis of a new acyl-coenzyme A synthetase family from Arabidopsis thaliana." J Exp Bot **59**(2): 403-419.

Kim, K. and A. R. Portis, Jr. (2004). "Oxygen-dependent H₂O₂ production by Rubisco." FEBS Lett **571**(1-3): 124-128.

Kim, Y. I., I. K. Nam, D. K. Lee, S. Bhandari, L. Charton, S. Kwak, J. Y. Lim, K. Hong, S. J. Kim, J. N. Lee, S. W. Kwon, H. S. So, N. Linka, R. Park and S. K. Choe (2019). "Slc25a17 acts as a peroxisomal coenzyme A transporter and regulates multiorgan development in zebrafish." J Cell Physiol.

Kruger, N. J. and A. von Schaewen (2003). "The oxidative pentose phosphate pathway: structure and organisation." Curr Opin Plant Biol **6**(3): 236-246.

Lanyon-Hogg, T., S. L. Warriner and A. Baker (2010). "Getting a camel through the eye of a needle: the import of folded proteins by peroxisomes." Biol Cell **102**(4): 245-263.

Laule, O., A. Furholz, H. S. Chang, T. Zhu, X. Wang, P. B. Heifetz, W. Gruissem and M. Lange (2003). "Crosstalk between cytosolic and plastidial pathways of isoprenoid biosynthesis in *Arabidopsis thaliana*." Proc Natl Acad Sci U S A **100**(11): 6866-6871.

Lingner, T., A. R. Kataya, G. E. Antonicelli, A. Benichou, K. Nilssen, X. Y. Chen, T. Siemsen, B. Morgenstern, P. Meinicke and S. Reumann (2011). "Identification of novel plant peroxisomal targeting signals by a combination of machine learning methods and in vivo subcellular targeting analyses." Plant Cell **23**(4): 1556-1572.

Linka, N. and F. L. Theodoulou (2013). "Metabolite transporters of the plant peroxisomal membrane: known and unknown." Subcell Biochem **69**: 169-194.

Linka, N., F. L. Theodoulou, R. P. Haslam, M. Linka, J. A. Napier, H. E. Neuhaus and A. P. Weber (2008). "Peroxisomal ATP import is essential for seedling development in *Arabidopsis thaliana*." Plant Cell **20**(12): 3241-3257.

Marco, F., R. Alcazar, A. F. Tiburcio and P. Carrasco (2011). "Interactions between Polyamines and Abiotic Stress Pathway Responses Unraveled by Transcriptome Analysis of Polyamine Overproducers." Omics-a Journal of Integrative Biology **15**(11): 775-781.

McLachlan, D. H., J. Lan, C. M. Geilfus, A. N. Dodd, T. Larson, A. Baker, H. Horak, H. Kollist, Z. He, I. Graham, M. V. Mickelbart and A. M. Hetherington (2016). "The Breakdown of Stored Triacylglycerols Is Required during Light-Induced Stomatal Opening." Curr Biol **26**(5): 707-712.

Meinecke, M., C. Cizmowski, W. Schliebs, V. Kruger, S. Beck, R. Wagner and R. Erdmann (2010). "The peroxisomal importomer constitutes a large and highly dynamic pore." Nat Cell Biol **12**(3): 273-277.

Mendoza-Poudereux, I., E. Kutzner, C. Huber, J. Segura, W. Eisenreich and I. Arrillaga (2015). "Metabolic cross-talk between pathways of terpenoid backbone biosynthesis in spike lavender." Plant Physiol Biochem **95**: 113-120.

Meyer, T., C. Holscher, C. Schwoppe and A. von Schaewen (2011). "Alternative targeting of *Arabidopsis* plastidic glucose-6-phosphate dehydrogenase G6PD1 involves cysteine-dependent interaction with G6PD4 in the cytosol." Plant J **66**(5): 745-758.

Mhamdi, A., J. Hager, S. Chaouch, G. Queval, Y. Han, L. Taconnat, P. Saindrenan, H. Gouia, E. Issakidis-Bourguet, J. P. Renou and G. Noctor (2010). "Arabidopsis GLUTATHIONE REDUCTASE1 plays a crucial role in leaf responses to intracellular hydrogen peroxide and in ensuring appropriate gene expression through both salicylic acid and jasmonic acid signaling pathways." Plant Physiol **153**(3): 1144-1160.

Mullen, R. T. and R. N. Trelease (2006). "The ER-peroxisome connection in plants: development of the "ER semi-autonomous peroxisome maturation and replication" model for plant peroxisome biogenesis." Biochim Biophys Acta **1763**(12): 1655-1668.

Murphy, M. A., B. A. Phillipson, A. Baker and R. T. Mullen (2003). "Characterization of the targeting signal of the Arabidopsis 22-kD integral peroxisomal membrane protein." Plant Physiol **133**(2): 813-828.

Noctor, G. and C. H. Foyer (1998). "ASCORBATE AND GLUTATHIONE: Keeping Active Oxygen Under Control." Annu Rev Plant Physiol Plant Mol Biol **49**: 249-279.

Nyathi, Y., C. De Marcos Lousa, C. W. van Roermund, R. J. Wanders, B. Johnson, S. A. Baldwin, F. L. Theodoulou and A. Baker (2010). "The Arabidopsis peroxisomal ABC transporter, comatose, complements the *Saccharomyces cerevisiae* pxa1 pxa2Delta mutant for metabolism of long-chain fatty acids and exhibits fatty acyl-CoA-stimulated ATPase activity." J Biol Chem **285**(39): 29892-29902.

Palmieri, F. (2014). "Mitochondrial transporters of the SLC25 family and associated diseases: a review." J Inherit Metab Dis **37**(4): 565-575.

Palmieri, F., C. L. Pierri, A. De Grassi, A. Nunes-Nesi and A. R. Fernie (2011). "Evolution, structure and function of mitochondrial carriers: a review with new insights." Plant J **66**(1): 161-181.

Palmieri, L., H. Rottensteiner, W. Girzalsky, P. Scarcia, F. Palmieri and R. Erdmann (2001). "Identification and functional reconstitution of the yeast peroxisomal adenine nucleotide transporter." EMBO J **20**(18): 5049-5059.

Palmieri, L., M. J. Runswick, G. Fiermonte, J. E. Walker and F. Palmieri (2000). "Yeast mitochondrial carriers: bacterial expression, biochemical identification and metabolic significance." J Bioenerg Biomembr **32**(1): 67-77.

Picault, N., M. Hodges, L. Palmieri and F. Palmieri (2004). "The growing family of mitochondrial carriers in Arabidopsis." Trends Plant Sci **9**(3): 138-146.

Planas-Portell, J., M. Gallart, A. F. Tiburcio and T. Altabella (2013). "Copper-containing amine oxidases contribute to terminal polyamine oxidation in peroxisomes and apoplast of Arabidopsis thaliana." BMC Plant Biol **13**: 109.

Pracharoenwattana, I., J. E. Cornah and S. M. Smith (2005). "Arabidopsis peroxisomal citrate synthase is required for fatty acid respiration and seed germination." Plant Cell **17**(7): 2037-2048.

Pracharoenwattana, I., J. E. Cornah and S. M. Smith (2007). "Arabidopsis peroxisomal malate dehydrogenase functions in beta-oxidation but not in the glyoxylate cycle." Plant J **50**(3): 381-390.

Reumann, S., L. Babujee, C. Ma, S. Wienkoop, T. Siemsen, G. E. Antonicelli, N. Rasche, F. Luder, W. Weckwerth and O. Jahn (2007). "Proteome analysis of Arabidopsis leaf peroxisomes reveals novel targeting peptides, metabolic pathways, and defense mechanisms." Plant Cell **19**(10): 3170-3193.

Reumann, S., D. Buchwald and T. Lingner (2012). "PredPlantPTS1: A Web Server for the Prediction of Plant Peroxisomal Proteins." Front Plant Sci **3**: 194.

Reumann, S. and A. P. M. Weber (2006). "Plant peroxisomes respire in the light: Some gaps of the photorespiratory C-2 cycle have become filled - Others remain." Biochimica Et Biophysica Acta-Molecular Cell Research **1763**(12): 1496-1510.

Rokka, A., V. D. Antonenkov, R. Soininen, H. L. Immonen, P. L. Pirila, U. Bergmann, R. T. Sormunen, M. Weckstrom, R. Benz and J. K. Hiltunen (2009). "Pxmp2 is a channel-forming protein in Mammalian peroxisomal membrane." PLoS One **4**(4): e5090.

Rottensteiner, H., A. Kramer, S. Lorenzen, K. Stein, C. Landgraf, R. Volkmer-Engert and R. Erdmann (2004). "Peroxisomal membrane proteins contain common Pex19p-binding sites that are an integral part of their targeting signals." Mol Biol Cell **15**(7): 3406-3417.

Sapir-Mir, M., A. Mett, E. Belausov, S. Tal-Meshulam, A. Frydman, D. Gidoni and Y. Eyal (2008). "Peroxisomal localization of Arabidopsis isopentenyl diphosphate isomerases suggests that part of the plant isoprenoid mevalonic acid pathway is compartmentalized to peroxisomes." Plant Physiol **148**(3): 1219-1228.

Schluter, A., S. Fourcade, R. Ripp, J. L. Mandel, O. Poch and A. Pujol (2006). "The evolutionary origin of peroxisomes: an ER-peroxisome connection." Mol Biol Evol **23**(4): 838-845.

Sharkey, T. D. (1988). "Estimating the Rate of Photorespiration in Leaves." Physiologia Plantarum **73**(1): 147-152.

Simkin, A. J., G. Guirimand, N. Papon, V. Courdavault, I. Thabet, O. Ginis, S. Bouzid, N. Giglioli-Guivarc'h and M. Clastre (2011). "Peroxisomal localisation of the final steps of the mevalonic acid pathway in planta." Planta **234**(5): 903-914.

Simpson, K., L. F. Quiroz, M. Rodriguez-Concepcion and C. R. Stange (2016). "Differential Contribution of the First Two Enzymes of the MEP Pathway to the Supply of Metabolic Precursors for Carotenoid and Chlorophyll Biosynthesis in Carrot (*Daucus carota*)." Front Plant Sci **7**: 1344.

Strader, L. C., A. H. Culler, J. D. Cohen and B. Bartel (2010). "Conversion of endogenous indole-3-butyric acid to indole-3-acetic acid drives cell expansion in Arabidopsis seedlings." Plant Physiol **153**(4): 1577-1586.

Strader, L. C., D. L. Wheeler, S. E. Christensen, J. C. Berens, J. D. Cohen, R. A. Rampey and B. Bartel (2011). "Multiple facets of Arabidopsis seedling development require indole-3-butyric acid-derived auxin." Plant Cell **23**(3): 984-999.

Taylor, E. B. (2017). "Functional Properties of the Mitochondrial Carrier System." Trends Cell Biol **27**(9): 633-644.

Theodoulou, F. L., K. Job, S. P. Slocombe, S. Footitt, M. Holdsworth, A. Baker, T. R. Larson and I. A. Graham (2005). "Jasmonic acid levels are reduced in COMATOSE ATP-binding cassette transporter mutants. Implications for transport of jasmonate precursors into peroxisomes." Plant Physiol **137**(3): 835-840.

Theodoulou, F. L. and I. D. Kerr (2015). "ABC transporter research: going strong 40 years on." Biochem Soc Trans **43**(5): 1033-1040.

Timm, S., A. Florian, K. Jahnke, A. Nunes-Nesi, A. R. Fernie and H. Bauwe (2011). "The hydroxypyruvate-reducing system in Arabidopsis: multiple enzymes for the same end." Plant Physiol **155**(2): 694-705.

Timm, S., A. Nunes-Nesi, T. Parnik, K. Morgenthal, S. Wienkoop, O. Keerberg, W. Weckwerth, L. A. Kleczkowski, A. R. Fernie and H. Bauwe (2008). "A cytosolic pathway for the conversion of hydroxypyruvate to glycerate during photorespiration in Arabidopsis." Plant Cell **20**(10): 2848-2859.

Troncoso-Ponce, M. A., X. Cao, Z. Yang and J. B. Ohlrogge (2013). "Lipid turnover during senescence." Plant Sci **205-206**: 13-19.

Tugal, H. B., M. Pool and A. Baker (1999). "Arabidopsis 22-kilodalton peroxisomal membrane protein. Nucleotide sequence analysis and biochemical characterization." Plant Physiol **120**(1): 309-320.

Van Ael, E. and M. Fransen (2006). "Targeting signals in peroxisomal membrane proteins." Biochim Biophys Acta **1763**(12): 1629-1638.

van Roermund, C. W., R. Drissen, M. van Den Berg, L. Ijlst, E. H. Hetteema, H. F. Tabak, H. R. Waterham and R. J. Wanders (2001). "Identification of a peroxisomal ATP carrier required for medium-chain fatty acid beta-oxidation and normal peroxisome proliferation in *Saccharomyces cerevisiae*." Mol Cell Biol **21**(13): 4321-4329.

van Roermund, C. W., M. G. Schroers, J. Wiese, F. Facchinelli, S. Kurz, S. Wilkinson, L. Charton, R. J. Wanders, H. R. Waterham, A. P. Weber and N. Link (2016). "The Peroxisomal NAD Carrier from Arabidopsis Imports NAD in Exchange with AMP." Plant Physiol **171**(3): 2127-2139.

Vapola, M. H., A. Rokka, R. T. Sormunen, L. Alhonen, W. Schmitz, E. Conzelmann, A. Warri, S. Grunau, V. D. Antonenkov and J. K. Hiltunen (2014). "Peroxisomal membrane channel Pxmp2 in the mammary fat pad is essential for stromal lipid homeostasis and for development of mammary gland epithelium in mice." Dev Biol **391**(1): 66-80.

Vranova, E., D. Coman and W. Gruissem (2013). "Network analysis of the MVA and MEP pathways for isoprenoid synthesis." Annu Rev Plant Biol **64**: 665-700.

Zarei, A., C. P. Trobacher and B. J. Shelp (2016). "Arabidopsis aldehyde dehydrogenase 10 family members confer salt tolerance through putrescine-derived 4-aminobutyrate (GABA) production." Sci Rep **6**: 35115.

Zolman, B. K., N. Martinez, A. Millius, A. R. Adham and B. Bartel (2008). "Identification and characterization of Arabidopsis indole-3-butyric acid response mutants defective in novel peroxisomal enzymes." Genetics **180**(1): 237-251.

Zolman, B. K., M. Nyberg and B. Bartel (2007). "IBR3, a novel peroxisomal acyl-CoA dehydrogenase-like protein required for indole-3-butyric acid response." Plant Mol Biol **64**(1-2): 59-72.

Zolman, B. K., I. D. Silva and B. Bartel (2001). "The Arabidopsis pxa1 mutant is defective in an ATP-binding cassette transporter-like protein required for peroxisomal fatty acid beta-oxidation." Plant Physiol **127**(3): 1266-1278.

Zolman, B. K., A. Yoder and B. Bartel (2000). "Genetic analysis of indole-3-butyric acid responses in Arabidopsis thaliana reveals four mutant classes." Genetics **156**(3): 1323-1337.

III. Manuscripts

III.I Manuscript 1

Identification of a novel peroxisomal transport protein involved in the heat shock response of *Arabidopsis thaliana*

Lennart Charton¹, Felix Holthausen¹, Wiebke Halpape², Andreas Weber¹, Nicole Linka^{1a}

¹Heinrich-Heine-University Düsseldorf, Institute of Plant Biochemistry, Germany

²University of Bielefeld, Center of Biotechnology, Germany

Abstract

As sessile organisms plants have to cope with several environmental stress conditions. Among these, heat stress is considered to be one of the most detrimental ones. Heat stress produces an excess of reactive oxygen species (ROS) that has to be tightly controlled to prevent damage to cellular structures like proteins, lipids and the DNA. Here we identified PHS1, a novel peroxisomal member of the mitochondrial carrier family. RNA-Seq and microarray data revealed a specific upregulation of *PHS1* upon heat stress and a tDNA-induced knock-down of *PHS1* resulted in sensitivity to heat stress that is linked to increased oxidative stress of the plants. Comparative phenotyping with a second *phs1* mutant line obtained by the CRISPR/Cas9 system showed that both lines are compromised in post-germinative growth which is most likely caused by an oxidation and hence inactivation of storage oil mobilizing enzymes. But the heat shock specific phenotype seems to be restricted to the action of a second isoform of PHS1 (PHS1.2) which is not affected in the CRISPR/Cas9 line. *PHS1.2* is strongly upregulated upon heat stress and almost absent under control conditions. The additive phenotype of a *phs1 cat2* double mutant further emphasized the role of PHS1 within the peroxisomal antioxidant machinery by transporting substrates required for the degradation of ROS or for the stress induced cellular signaling in times of elevated oxidative stress.

Introduction

Rising ambient temperature is one of the most detrimental stress conditions for plants (Hasanuzzaman et al. 2013). Each degree of temperature increase is considered to reduce global yields of the four major crop plants wheat, rice, maize and soybean by up to 7.4 % (maize) (Zhao et al. 2017).

Heat stress causes several alterations in plant growth and development, mostly due to the excess production of reactive oxygen species (ROS) (Apel and Hirt 2004). Heat stress related ROS production in mitochondria is considered to be caused by a hyperpolarization of the mitochondrial membrane by an excess activity of the electron transport chain (Fedyeva et al. 2014).

In chloroplasts, photosystem II (PSII) is the most susceptible target for heat stress in the thylakoid membrane complexes. Exposure to high temperatures results in the dissociation of the oxygen evolving complex and the D1 protein leading to the inhibition of the electron transport chain and thus to an excess production of ROS (Havaux and Tardy 1996; Yamane et al. 1998). In addition, Rubisco activase is very sensitive to heat stress which results in the inhibition of Rubisco (Sharkey 2005). Hence, regeneration of NADP required as final electron acceptor is blocked leading to the transfer of electrons to molecular oxygen which results in the formation of ROS like singlet oxygen and H₂O₂ (Asada 2006). But, increasing temperatures also lead to a disproportional increase of the oxygenase reaction of Rubisco resulting in higher rates of photorespiration and hence elevated peroxisomal H₂O₂ production (Kim and Portis 2004).

Since peroxisomes are the sole site of fatty acid degradation in plants (Graham and Eastmond 2002), they also play an important role in membrane remodeling, a process that is required to maintain integrity and fluidity of biological membranes under elevated temperatures (Higashi et al. 2015). Peroxisomal β -oxidation of fatty acids is accompanied by the production of H₂O₂, thus representing another cellular source of heat shock induced ROS production. Membranes can also be directly damaged by ROS. Heat stress-induced ROS promote peroxidation of unsaturated fatty acids (Boca et al. 2014). The primary products of lipid peroxidation are lipid hydroperoxides (LOOH) that can be decomposed by glutathione peroxidases (GPx) to prevent the peroxidative damage. Three theta class glutathione s-transferases (GSTTs) are localized to peroxisomes with GPx activity reducing toxic LOOH to monohydroxy alcohols by the expansion of GSH (Reumann et al. 2007; Dixon et al. 2009).

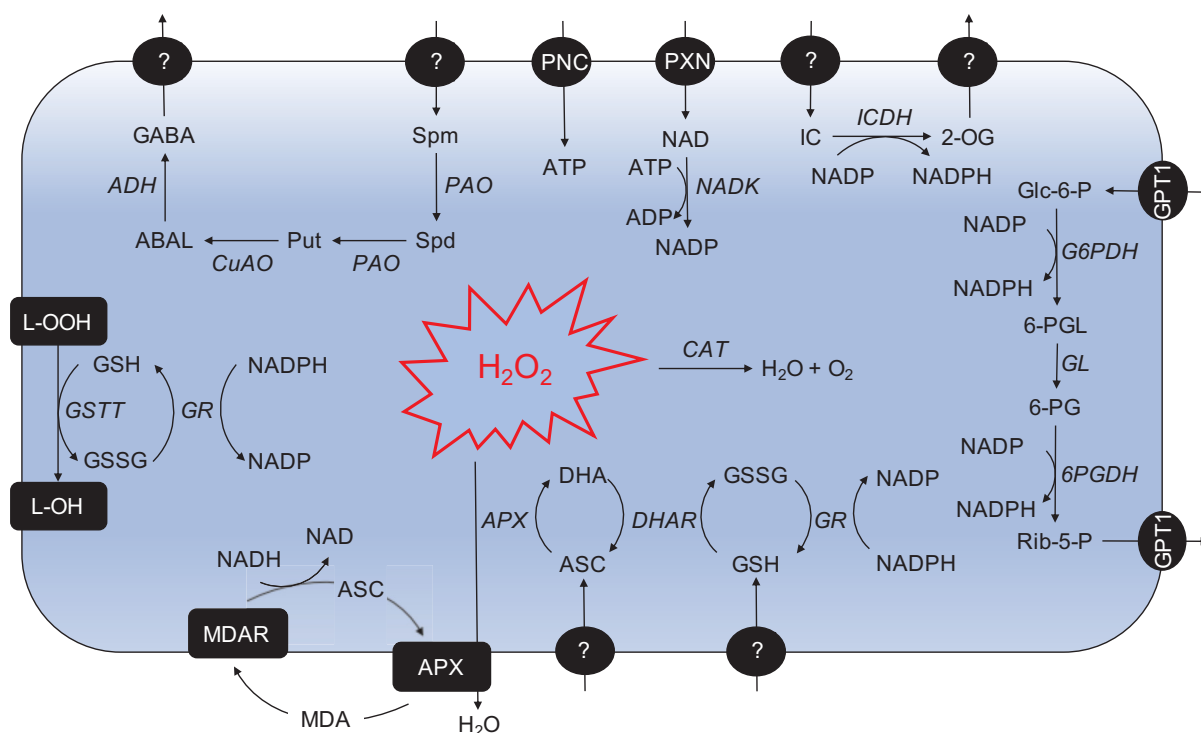


Figure 1: Peroxisomal oxidative stress responsive metabolism

2-OG: 2-oxoglutarate; ABAL: 4-aminobutanal; GABA: 4-aminobutyrate; 6-PG: 6-phosphogluconate; 6PGDH: 6-phosphogluconate dehydrogenase; 6-PGL: 6-phosphogluconolactone; ADP: adenosine diphosphate; ATP: adenosine triphosphate; ADH: aldehyde dehydrogenase; ASC: ascorbate; APX: ascorbate peroxidase; CAT: catalase; CuAO: copper-amine oxidase; DHA: dehydroascorbate; DHAR: dehydroascorbate reductase; GL: gluconolactonase; Glc-6-P: glucose-6-phosphate; G6PDH: glucose-6-phosphate dehydrogenase; GPT1: glucose-6-phosphate transporter 1; GSSG: glutathione (oxidized); GSH: glutathione (reduced); GR: glutathione reductase; GSTT: glutathione s-transferase (theta group); IC: isocitrate; ICDH: isocitrate dehydrogenase; L-OOH: lipid hydroperoxides; L-OH: lipid monohydroxy alcohols; MDAR: monodehydroascorbate reductase; NAD: nicotinamide adenine dinucleotide (oxidized); NADH: nicotinamide adenine dinucleotide (reduced); NADK: nicotinamide adenine dinucleotide kinase; NADP: nicotinamide adenine dinucleotide phosphate (oxidized); nicotinamide adenine dinucleotide phosphate (reduced); PNC: peroxisomal adenine nucleotide carrier; PXN: peroxisomal NAD carrier; PAO: polyamine oxidase; Put: putrescine; Rib-5-P: ribulose-5-phosphate; Spd: spermidine; Spm: spermine.

Since peroxisomes are at the center of several oxidative reactions both under normal and stress conditions, they require an efficient antioxidant system for the decomposition of ROS like H_2O_2 . Catalase is the most dominant peroxisomal enzyme in leaves catalyzing the simultaneous degradation of two molecules of H_2O_2 into water and oxygen (McClung 1997; Noctor and Foyer 1998). Catalase shows highest activity in flowering stems, leaves and flowers but is also extractable from seeds and roots (Mhamdi et al. 2012).

In times of elevated ROS production including biotic and abiotic stress conditions as well as certain developmental processes like germination and senescence, peroxisomes require redundant pathways to cope with increased oxidative stress (del Rio et al. 1998; Graham and Eastmond 2002; Kim and Portis 2004). The ascorbate-glutathione cycle is an

efficient system to degrade H_2O_2 and was found to be localized to chloroplasts, mitochondria and peroxisomes (Jimenez et al. 1997; Asada 2006). It uses the antioxidants ascorbate (ASC) and glutathione (GSH) in a series of coupled enzymatic reactions catalyzed by ascorbate peroxidase, monodehydroascorbate reductase, dehydroascorbate reductase and glutathione reductase (GR) (Jimenez et al. 1997; Noctor and Foyer 1998). The reduction and hence regeneration of oxidized GSH by GR is coupled to the oxidation of NADPH that is in turn regenerated by the action of the oxidative pentose phosphate pathway (OPPP) and NADP-dependent isocitrate dehydrogenase (ICDH) (Corpas et al. 1998; Corpas et al. 1999).

The last barrier to prevent the diffusion of H_2O_2 out of peroxisomes into the cytosol consists of the membrane bound isoforms of ascorbate peroxidase and monodehydroascorbate reductase. They were shown to efficiently prevent the oxidation of cytosolic enzymes even in the absence of catalase (Eastmond 2007).

The role of peroxisomes during heat stress might not be restricted to the degradation of ROS. 4-aminobutyrate (GABA) is a non-proteogenic amino acid that is an important thermo-protectant and signaling molecule in response stress (Jalil et al. 2019; Priya et al. 2019). While the biosynthesis of GABA from glutamate in the cytosol is considered to be the major source of GABA production, there is also evidence for the contribution of polyamine catabolism to GABA synthesis (Shelp and Zarei 2017). The back-conversion of the polyamines spermine and spermidine to putrescine is mediated by a group of polyamine oxidases (PAO2-4) within peroxisomes (Fincato et al. 2011). The peroxisomal copper-containing amine oxidases 2 and 3 are responsible for the subsequent oxidation of putrescine to 4-aminobutanal which is converted to GABA by a peroxisomal aldehyde dehydrogenase (Planas-Portell et al. 2013; Zarei et al. 2016).

For the peroxisomal antioxidant and stress responsive machinery, several substrates and cofactors have to be transported across the peroxisomal membrane. Since the peroxisomal membrane is considered to be impermeable for large molecules, transport proteins are required to mediate an efficient flux of metabolites. But, only a few peroxisomal transport proteins have been identified so far. Cofactors like ATP and NAD are imported by the peroxisomal adenine nucleotide carrier (PNC) and NAD carrier (PXN), respectively (Linka et al. 2008; Bernhardt et al. 2012). The supply of NADPH is mediated by the phosphorylation of NADH by an NADH kinase (Waller et al. 2010).

Together with the group of Antje von Schaewen we could show, that GPT1 is dual-targeted to chloroplasts and peroxisomes and that it is able to exchange glucose-6-phosphate against ribulose-5-phosphate for the peroxisomal oxidative pentose phosphate pathway (OPPP) (Baune et al., submitted). But, no peroxisomal carrier is known to mediate the transport of isocitrate, 2-oxoglutarate, polyamines, GABA, ASC or GSH.

Aim of this thesis

The aim of this thesis was to elucidate the role of peroxisomes in the heat stress response of *Arabidopsis thaliana*. For this we identified a peroxisomal member of the mitochondrial carrier family that is specifically up-regulated upon heat shock. Phenotypical and metabolite analysis will be performed under conditions that lead to elevated oxidative stress and thus require the action of the peroxisomal antioxidant machinery. For these analyzes, a classical tDNA insertion line will be investigated as well as mutants generated by genome editing using the CRISPR/Cas9 system. According to the observed effect, both on phenotype and metabolite level, substrates will be tested in two different heterologous protein expression systems. The findings of this theses will contribute to the understanding of the plants response to heat stress which is highly required to cope with the consequences of climate change.

Material and Methods

Bacteria strains and growth conditions

Chemical competent Mach1 *E.coli* cells (Invitrogen, Karlsruhe, Germany) were used for plasmid transformation and amplification. Cells were grown at 37 °C either in liquid medium shaking at 190 rotations per minute (rpm) or on solid Luria-Bertani (LB) medium. *Agrobacterium tumefaciens* strain GV3103 was used for stable and transient transformation of *Arabidopsis* and *Nicotiana benthamiana*, respectively and was grown at 28 °C either shaking at 150 rpm in liquid YEB medium or on agar plates. For selection purposes, appropriate antibiotics were added to the growth medium.

Transformation of Bacteria

Plasmid DNA was introduced into competent Mach1 *E.coli* cells using heat-shock method (Inoue et al. 1990). Afterwards, the cell suspension was spread on LB-agar plates containing ampicillin and was incubated for at least 8 h (here o/n) at 37 °C.

Chemo-competent *A. tumefaciens* cells were transformed following the freeze-thaw heat-shock method (Hofgen and Willmitzer 1988). Afterwards, single colonies were picked, transferred to new plates and incubated for additional 2 d at 28 °C.

Saccharomyces cerevisiae strain and growth conditions

The uracil auxotrophic *Saccharomyces cerevisiae* strain INVSc1 (Invitrogen) was used in this work. Cells were grown at 30 °C either shaking at 150 rpm in liquid medium or on agar plates. YPD and YNB medium were used as complex and minimal medium, respectively

Transformation of *S. cerevisiae*

For the heterologous expression of proteins in yeast, INVSc1 cells were transformed with yeast expression constructs. The Li/Ac transformation procedure was conducted after standard protocol (Gietz and Schiestl 2007). YNB agar plates lacking the amino acid uracil were used for selection of the auxotrophic yeast strain.

Plant growth conditions

Arabidopsis thaliana ecotype Columbia (Col-0) was used as WT in this thesis. Seeds were surface-sterilized with chloric gas by adding 3 ml concentrated HCl to 100 ml NaClO in a desiccator for 2 hours. Seeds were placed under the clean bench to allow evaporation of residual chloric gas. Stratification was performed for 3 days in the dark at 4°C. If not stated otherwise plants were grown under normal day conditions (12 h light / 12 h dark) at 22/18 °C and a light intensity of 100 $\mu\text{M m}^{-2} \text{s}^{-1}$ on agar plates supplemented with 1 % (w/v) sucrose.

Two to three weeks old seedlings were transferred to soil (3/4 Floraton, 1/4 Arabidopsis substrate) and were further cultivated under long-day conditions.

Transformation of Arabidopsis

For the generation of stable transformed Arabidopsis lines, agrobacterium-mediated transformation was conducted according to the floral-dip method (Zhang et al. 2006). After maturation, seeds of the transformed plants (F_0) were dispersed on MS-agar plates and selected by antibiotic resistance and/or signal of the integrated fluorescence protein.

Isolation of Arabidopsis genomic DNA

Arabidopsis gDNA was isolated by isopropanol precipitation (Weigel and Glazebrook, 2001). For this, one leaf was harvested, frozen in liquid nitrogen and grinded in a bead mill (30 Hz, 30 seconds). Afterwards, 400 μ l extraction buffer (0.2 M Tris-HCl, pH7.5 (HCL), 0.25 M NaCl, 0.025 M EDTA, 0.5 % (w/v) SDS) were added to the powder, inverted several times and centrifuged at maximum speed for 5 min. The resulting supernatant was added to 300 μ l isopropanol, mixed by pipetting up and down and centrifuged again at maximum speed for 5 min. After carefully discarding the supernatant, the pellet was washed 3 times with 70 % ethanol, drained and dried. The dried pellet was subsequently dissolved in 100 μ l TE buffer and stored at -20 °C. For large screening purposes, the Phire Plant gDNA extraction and direct PCR kit (ThermoFischer) was used according to the manufacturer's instructions.

Arabidopsis RNA isolation and cDNA synthesis

Isolation of leaf RNA for cDNA synthesis was performed with the EURx GeneMATRIX Universal RNA purification kit (Roboklon, Berlin, Germany). Prior cDNA synthesis, residual DNA was degraded by RQ1 RNase-free DNase (Promega, Madison, USA). cDNA synthesis itself was performed using the LunaScript RT SuperMix kit (NEB).

Quantitative Real-Time PCR

Quantification of transcript abundance was conducted in a 7500 Fast Real-Time PCR System (Invitrogen) using the Luna Universal qPCR Master Mix (NEB). Primer design, primer efficiency analysis and measurement of transcript abundances were performed according to 'eleven golden rules of quantitative RT-PCR' (Udvardi et al. 2008). The reference gene TIP41-like (At4g34270) was used to normalize the values.

Fatty acid analysis

Per replicate, 5 mg of dry seeds were spread on filter paper on a sucrose containing 0.5 MS-agar plate and grown under normal day conditions. The entire material of one plate was

harvested 0 h, 24 h and 48 h after stratification and the fresh weight was noted. Extraction, derivatization and analysis of fatty acid methyl esters were performed according to Hielscher et al. 2017.

Metabolite analysis

Metabolites were measured from five different 6 weeks old rosettes per genotype. For this, samples were collected and directly frozen in liquid nitrogen and ground to a fine powder. 1.5 ml pre-chilled (-20 °C) extraction solvent mixture (1:2.5:1 H₂O:MeOH:CHCl₃) containing 125 µl internal standard stock (5 mM ribitol + 1 mM dimethyl phenylalanine per 50 ml extraction buffer) were added to 50 mg aliquots of ground sample material. Sample mixture was vortexed for 20 seconds and placed on crushed ice during the processing of other samples. Samples were subsequently gently inverted for 6 min at 4 °C, followed by centrifugation for 2 min at 20,000 g and room temperature. 1 ml of supernatant was transferred to 1.5 ml tube and stored at -80 °C. Metabolites were derivatized by MSTFA and measured by gas chromatography coupled to a time-of-flight mass spectrometer (7200 GC-QTOF, Agilent Technology, Santa Clara, USA). Amino acids were measured by ultra-high-pressure liquid chromatography coupled to a time-of-flight mass spectrometer (1290 UHPLC 6530 QTOF, Agilent Technologies). Response was calculated from the integrated peak areas of the different metabolites using Mass Hunter Software b07 (Agilent Technologies) and expressed relative to the internal standard and fresh weight of the sample.

CLSM of Tobacco protoplasts

Overnight culture of *A. tumefaciens* were harvested via centrifugation (10 min, 3000 g) and resuspended in infiltration buffer (10 mM MgCl₂, 10 mM MES, pH 5.7, 100 µM acetosyringone). Suspension was diluted to an OD₆₀₀ of 0.5. and infiltrated in young *N. benthamiana* leaves. Plants were subsequently grown at long day conditions (16 h/8 h) for two days before protoplast isolation. For this, *N. benthamiana* leaves were cut into small pieces, vacuum infiltrated and incubated in protoplast digestion solution (1.5 % (w/v) cellulase R-10, 0.4 % (w/v) macerozyme R-10, 0.4 M mannitol, 20 mM KCl, 20 mM MES pH 5.6 (KOH), 10 mM CaCl₂, 0.1 % (w/v) BSA) for 2 h at 30 °C. Isolated protoplasts were resuspended in W5 solution (154 mM NaCl, 125 mM CaCl₂, 5 mM KCl, 2 mM MES pH5.6 (KOH)) and peroxisomes were stained by adding 8-(4-Nitrophenyl)-BODIPY (BODIPY) to a final concentration of 5 µM in W5 solution. Protoplasts were directly used for microscopy and analyzed using a Zeiss LSM 780 Confocal Microscope and Zeiss ZEN software. Excitation/emission settings used in this study: BODIPY (488 nm / 490 to 550 nm), mCherry (561 nm / 580 to 625 nm) and Chlorophyll A (488 nm / 640 to 710 nm). Pictures were processed using Fiji software (Schindelin et al. 2012).

CLSM of stable transformed Arabidopsis

Intact leaves of 2 weeks old seedlings were incubated in 0.5 MS medium containing 10 μ M BODIPY solution for 1 h in the dark. Leaves were washed thoroughly before analysis by CLSM. For detailed protocol see CLSM of Tobacco protoplasts.

CLSM of roGFP2

Cytosolic GSH redox state was analyzed in 5 days old hypocotyls of etiolated seedlings using the redox sensitive roGFP2 sensor coupled to glutaredoxin (Schwarzlander et al. 2008). CLSM and image analysis by a custom MatLab analysis suite were performed according to Schwarzlander et al. 2008. 10 mM DTT and 100 mM H₂O₂ were used for the *in vivo* calibration.

Malondialdehyde assay

Malondialdehyde (MDA) was measured as marker of lipid peroxidation in 9 days old seedlings, 4 days after heat-shock for 4 h at 40 °C. About 50 mg pooled seedling were frozen in liquid nitrogen and ground to a fine powder in 2 ml screw cap tubes containing ceramic beads by a precellys (2 x 6500). 0.5 ml 0.1 % TCA were added to the ground sample, vortexed for 10 seconds and centrifuged for 10 minutes at 10,000 g 4 °C. Subsequently, 350 μ l were of the supernatant were transferred to a 15 ml falcon tube having a small hole at the top. 350 μ l 0.1 % TCA were additionally transferred to serve as blanks. 1.65 ml 0.5 % TBA in 20 % TCA were added to the samples and incubated for 25 minutes at 95 °C. Afterwards, samples were cooled down to room temperature and 1.2 ml were transferred to a new tube. After centrifugation for 5 minutes at 10,000 g and 4 °C, 340 μ l of the supernatants were transferred to a 96-well plate (triplicates) and absorbance at 532 nm and 600 nm was measured. MDA content was calculated using the following formula:

$$mmol\ MDA\ g\ FW^{-1} = \frac{\Delta A_{corrected} \times B \times x \times 1000}{\varepsilon \times b \times y}$$

$\Delta A_{corrected} = A_{532} - A_{600}$ subtracted by ΔA_{blank}

b = light path length

ε = millimolar extinction coefficient (155 mM⁻¹ cm⁻¹)

B = dilution factor ((350 μ l supernatant + 1650 μ l 0.5 % TBA in 20 % TCA) / 350 μ l supernatant = 5.7)

x = ml 0.1 % TCA used for extraction

y = g FW used for extraction

1000 = mmol \rightarrow μ mol

Genotyping of tDNA insertion lines

Gene specific and tDNA specific PCRs were performed to verify the tDNA insertion line SALK_030104 of the *PHS1* gene. For the gene specific product, primers were chosen flanking the tDNA insertion site (NL509: TCCTGAGGAGACATACATGGG; NL510: CGCATTTTATAGCAGGAGCAG). For the tDNA specific PCR, each gene specific primer was combined with a tDNA specific primer (P46: TGGTTCACGTAGTGGGCCATCG). For the verification of the *cat2-1* tDNA insertion line SALK_076998 LC11 (CCTCGTGGTTTTGCAGTCAA) and LC12 (TCTCAGCATGACGAACCTGG) were used as gene specific primers and combined with P97 (TGGTTCACGTAGTGGGCCATCG) for the tDNA specific product.

Generation and verification of mutants generated by CRISPR/Cas9

For the phenotypic analysis, additional *phs1* mutant lines were generated using the CRISPR/Cas9 system. Target sites were chosen and integrated into the Cas9 expression vector system as described in Hahn et al. (2017, 2018). For site-specific targeting of Cas9 to *PHS1* the following sgRNA sequences were used: 5'-GGAAATGGCGACGAAGAGCT-3' and 5'-CGAACTGTCTGGGTTGGTGA-3'.

For the screening of positive Cas9 cutting events, a restriction fragment length polymorphism (RFLP) assay was performed. This assay is based on the fact, that the Cas9 cutting site within the first sgRNA target sequence is a *SacI* restriction enzyme recognition site, that, upon Cas9 mediated mutation, gets destroyed. Hence, amplification of the flanking regions with FeH15 (AGTCTGTGCCACCTAGAGTT) and FeH16 (CCAGGAGCAATGCCCCTATA) followed by a restriction digest with *SacI* leads to different cutting patterns visible by agarose gel electrophoresis. In the rare case of a big deletion between both sgRNA sequences, a band-shift of the undigested PCR product is visible.

Expression analysis of RNA-Seq experiments

7143 SRA data files containing non-mutant *Arabidopsis* Illumina samples were downloaded from NCBI and mapped onto the TAIR10 transcriptome, representative isoforms only using kallisto v0.44.0 (for single-end reads: --single -l <as given by SRA-file> -s 30; for paired-end reads default). The resulting data was collated into a single table.

Protein expression and reconstitution into liposomes

Heterologous protein expression for uptake experiments was conducted either in living yeast cell or cell-free using the RTS Wheat Germ CECF kit (biotechrabbit). Yeast galactose-inducible protein expression, harvesting and enrichment of the total membrane fraction was performed according to (Bouvier et al. 2006). Cell-free protein expression was conducted

according to the manufacturers instruction and modified as described in (Bernhardt et al. 2012). Freeze-thaw sonification procedure was used for the reconstitution of heterologous proteins (Palmieri et al. 1995). The non-incorporated counter exchange substrate was removed by passing proteoliposomes over Sephadex PD-10 columns (GE Healthcare) pre-equilibrated with PD-10 buffer (10 mM Tricine-KOH, pH 7.6, 100 mM Na-gluconate, 40 mM Ka-gluconate).

Time dependent uptake experiments

To analyze transport activity, uptake of radioactively labeled substrates was measured at six different time points over 32 min. The reaction was started by adding 950 μ l of the proteoliposome suspension either with or without substrate preloading to 50 μ l transport medium (1 μ Ci radioactively labeled substrate; 4 mM non-labeled substrate; filled up to 50 μ l with PD-10 buffer). The reaction was stopped by loading 140 μ l of the proteoliposomes on Dowex either filled with ion-exchange Resin, 100-200 dry mesh size (Bio-Rad) or Sephadex G-75 size-exclusion column material (s. Table 1). Columns were preequilibrated with Dowex-buffer. The Dowex columns were washed with 350 μ l and 500 μ l Dowex buffer. The flow through was collected in 20 ml scintillation vials either containing 10 ml ddH₂O or Rotiszint® eco plus scintillation cocktail (Carl Roth). The uptake of labeled substrates was measured in a scintillation counter as counts per minute (CPM). For the subsequent analysis of uptake rates three standards were prepared with 10 ml ddH₂O or scintillation cocktail and 5 μ l transport medium to determine the concentration of the labeled molecule as a function of the measured CPM.

Cloning

Sequences for *in silico* cloning were obtained from Aramemnon. Final constructs were verified by sequencing (Macrogen; dna.macrogen.com).

For the complementation of *phs1* mutant plants, PHS1 was fused to the yellow fluorescence protein VENUS by classical restriction-based cloning. For this, *PHS1* was amplified from WT cDNA using the primer MT1 (cacacggatcctgaaccATGGCGACGAAGAGCTCGGA) and MT2 (cacacctcgagACCTTCATGCACTGAAGTAGAAG) to add BamHI and XhoI restriction enzyme sites to the 5' and 3' end of PHS1 coding sequence, respectively. Afterwards, the generated PCR product and the plant binary vector pHyg-VENUS (Grefen et al. 2010) were cut with BamHI and XhoI, purified by gel electrophoresis and ligated to generate a c-terminal YFP fusion of PHS1 under the control of a ubiquitin10 promoter and with hygromycine as plant selection marker (pMT6).

For the localization of PHS1 in stable transformed Arabidopsis, a modified version of the pHyg-VENUS vector (pBH18) was used, where the VENUS fluorescence protein was exchanged by mCherry and an additional multiple cloning site was added (Björn Hielscher PhD thesis, 2018). pBH18 was opened using XhoI and PHS1 coding sequence was inserted by NEB Gibson assembly (Gibson 2011) generating a c-terminal mCherry fusion of PHS1 (pLC2).

Results

Peroxisomes play an important role in the production and scavenging of reactive oxygen species (ROS). Beside naturally occurring processes like fatty acid β -oxidation during germination or photorespiration, biotic and abiotic stress factors influence the oxidative state of peroxisomes. Among the abiotic stress factors, heat stress as a consequence of climate change is one of the biggest threats for future agriculture. Even though metabolites like ascorbate, glutathione or polyamines are major players of the cellular stress response, the mode of transport of these substrates across the peroxisomal membranes has not been identified, yet.

PHS1 is a novel peroxisomal MCF carrier that response to heat stress

The mitochondrial carrier family is known for its broad substrate spectrum and since three of its members are localized to peroxisomes, this family is a promising candidate to search for new peroxisomal transport proteins.

We analyzed publicly available RNA-Seq data to identify so far uncharacterized members of the MCF, that are involved in the heat stress response of Arabidopsis (Figure 2A).

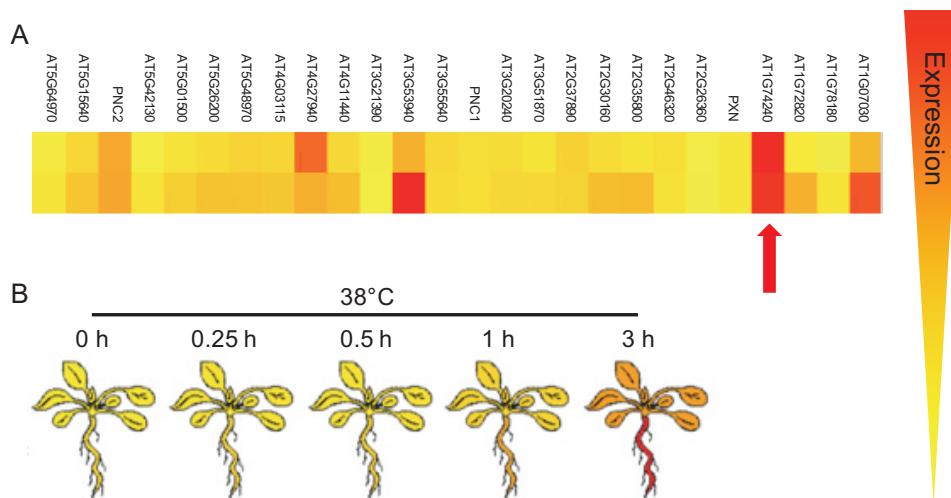


Figure 2: Expression of mitochondrial carrier proteins

(A) Publicly available RNA-Seq data of yet uncharacterized MCFs together with the peroxisomal members PNC1, PNC2 and PXN of two different heat shock experiments with either 37 °C (upper panel; BioProject PRJNA437617) or 42 °C (lower panel; BioProject PRJNA329451). Red arrow highlights MCF carrier upregulated under both conditions. (B) Expression of AT1g74240 (Microarray data) 0, 0.25, 0.5, 1 and 3 h after heat shock at 38 °C (Winter et al. 2007). Color-code from low (yellow) to high expression (red).

Among all uncharacterized MCF carriers and the already known peroxisomal representatives, only At1g74240 was upregulated upon heat stress in two independent experiments. This was further supported by microarray data of the BAR eFP Browser (Figure 2B, Winter et al. 2007) where the expression of the gene increased over time when plants

were exposed to heat stress. Interestingly, this increase was higher in roots than in leaves of 18 days old plants and heat stress represents the only stress factor considerably influencing At1g74240 gene expression.

At1g74240 is a member of the MCF and its amino acid sequence shares high similarity to putative and characterized S-adenosyl-methionine (SAM) and metal transport proteins (Figure 3; blue and grey, respectively), but also to a group of four proteins with completely unknown function.

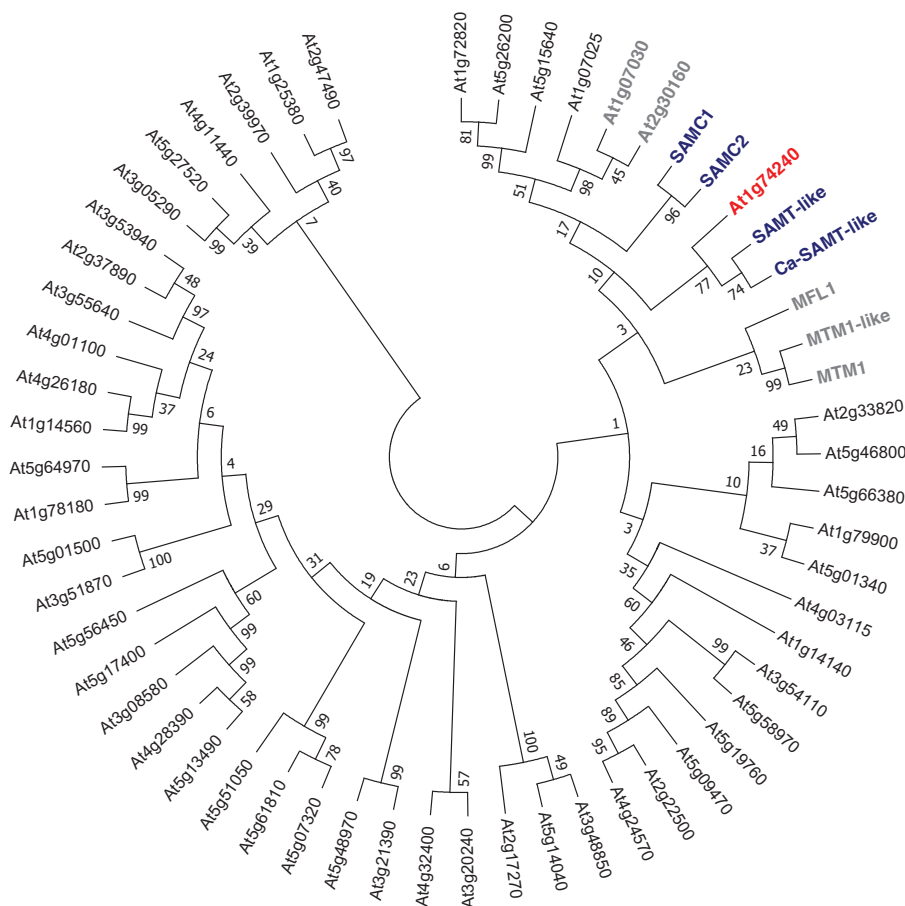


Figure 3: Phylogenetic tree of plant mitochondrial carrier family proteins

Phylogenetic tree of the Arabidopsis mitochondrial carrier family proteins. Tree was generated with mega7 using Neighbor-Joining method and JTT model of amino acid substitution with gaps and missing data being eliminated. Numbers at nodes represent bootstrap values of 1000 replications. Known and putative metal transport related carrier are labeled in grey. Known and putative S-adenosyl-methionine (SAM) carrier are depicted in blue. At1g74240 is highlighted in red. SAMC: S-adenosyl-methionine carrier; SAMT: putative S-adenosyl-methionine transporter; Ca-SAMT: putative calcium dependent SAMT; MFL: Mitoferrin-like protein; MTM: Manganese tracking factor.

Despite their name, members of the MCF have been localized to plastids, peroxisomes, the ER and even the plasma membrane (Haferkamp and Schmitz-Esser 2012). By stable transforming Arabidopsis with an At1g74240-mCherry fusion protein, we could show that the protein is localized to peroxisomes (Figure 4).

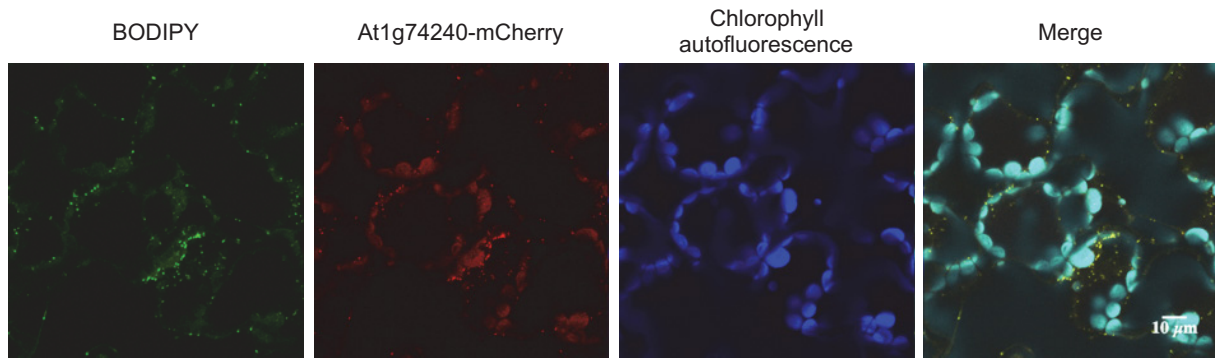


Figure 4: Subcellular localization of At1g74240

Leaf tissue of Arabidopsis stable transformed with an At1g74240-mCherry fusion construct. BODIPY was used as a peroxisome specific dye (1st panel, green). Signal of the mCherry fluorescence protein (red) and the chlorophyll autofluorescence (blue) are shown in the 2nd and 3rd panel, respectively. All channels are combined in a merged picture (4th panel) containing a 10 µm scale bar.

Because of its peroxisomal localization and its response to heat stress, the gene will be referred to as peroxisomal heat stress responsive carrier 1 (*PHS1*).

Establishing and generation of *phs1* tDNA insertion and CRISPR/Cas9 mutant lines

To analyze its physiological role, a tDNA insertion line of *PHS1* was used that harbors a tandem insertion within the fourth intron (Figure 5A). These insertions lead to a downregulation of the carrier to about 40 % of WT transcript level (Figure 5C). A respective stable complementation line (CL) was generated by integrating a PHS1-Venus fusion protein into the *phs1-1* background resulting in a five-fold higher expression compared to the WT (Figure 5C).

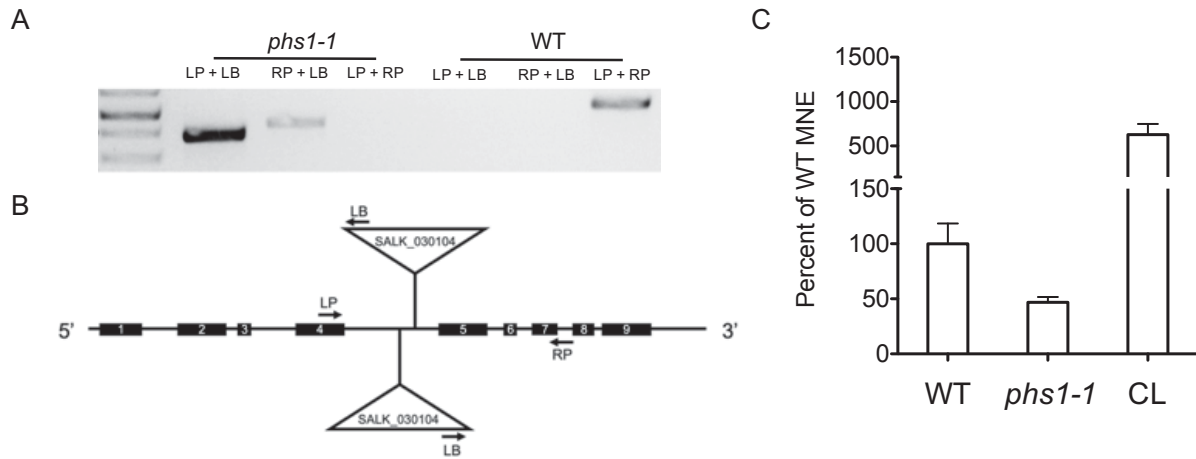


Figure 5: Genotyping of *phs1-1* tDNA insertion line.

(A) Gene- (LP + RP: 1165 bp) and tDNA-specific (RP + LB: 1003 bp; LP + LB: 752 bp) PCR of *phs1-1* and WT gDNA to verify homozygous tDNA insertion. (B) Gene architecture of *PHS1* with exons (boxes) introns (lines), localization of the tDNA (triangle) and primer binding sites (arrows). (C) Quantitative real time PCR of leaf cDNA of four weeks old plants to analyze *PHS1* transcript level in the WT, *phs1-1* and a *phs1-1:PHS1-Venus* complementation line (CL). The reference gene TIP41-like (At4g34270) was used for normalization. Data represent mean normalized expression (MNE) values \pm SD(MNE) of four biological and three technical replicates, each. WT MNE values were set to 100 %.

In addition to the tDNA insertion line, a second independent *phs1* mutant was generated by genome editing using CRISPR/Cas9. The cutting event of Cas9 guided to the first exon of *PHS1* lead to a deletion of 2 bp and thus to a frameshift generating an early stop-codon 24 bp after the start-codon (Figure 6A). The single guide RNA was chosen in a way that Cas9 cuts within a restriction enzyme recognition site which enabled a fast screening of mutants by restriction fragment length polymorphism (RFLP) analysis (Figure 6B). The obtained mutant *phs1-2* is homozygous for the deletion and free of Cas9. The latter is of special importance to exclude the influence of insertional effects on the phenotype and to reduce the probability of off-targeting events in future generations.

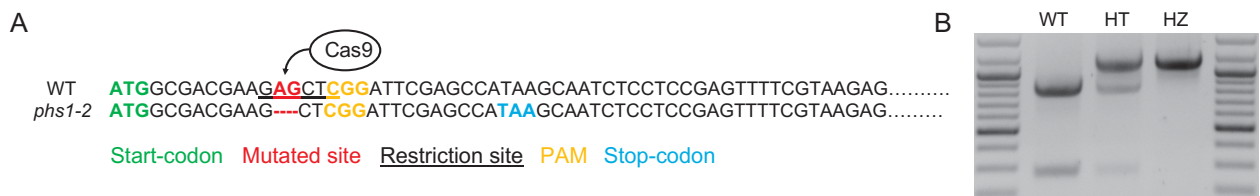


Figure 6: Genotyping of *phs1-2* generated by CRISPR/Cas9

(A) Cutting event of Cas9 9 bp after the start-codon (green) of *PHS1* resulted in a deletion (red) of 2 bp and thus to an early stop-codon (blue). Cas9 cuts within a *SacI* restriction enzyme site (GAGTCT), which enables restriction fragment length polymorphism (RFLP) assay to screen for mutants. (B) Representative image of RFLP result for WT and heterozygous (HT) and homozygous (HZ) mutant alleles.

Analysis of heat shock related *phs1* phenotype

Since the expression data (Figure 2) imply a role of PHS1 in the heat stress response of Arabidopsis, both mutant lines and the tDNA CL were subjected to heat shock for 4 h at 42 °C and root length was measured as a function of plant growth after 10 days of recovery (Figure 7).

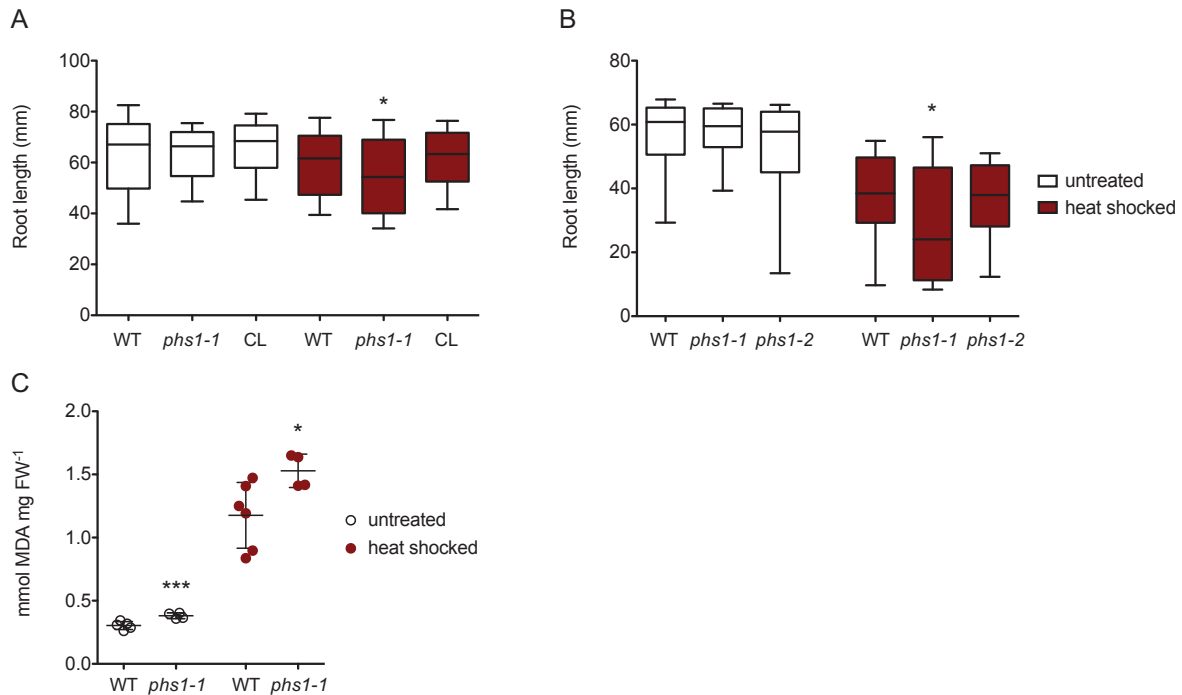


Figure 7: Root length after heat shock.

5 days old seedlings of WT, *phs1-1* and CL (A) as well as *phs1-2* (B) were subjected to heat shock (4 h; 42 °C) and root length was measured after 10 days of recovery. $n > 28$, whiskers span 10-90 percentile (C) Malondialdehyde (MDA) levels as an indicator of membrane peroxidation in 9 days old seedlings, 96 h after heat shock. $n = 5$ biological replicates consisting of 50 mg pooled seedlings, each. Significant difference to the WT determined by one-way ANOVA; *: $p < 0.05$; ***: $p < 0.001$.

Without heat shock treatment, *phs1-1*, *phs1-2* and the CL revealed a WT like growth. But, while the CL also showed WT behavior after HS (Figure 7A, red), the root length of *phs1-1* was significantly reduced in both experiments (Figure 7A and B). The difference in the root length between the experiments might be contributed to the fact that different seed batches were used for the analysis. Contrary to expectations, *phs1-2* did not show a reduced root length after heat shock (Figure 7B). The frame-shift right after the start-codon in *phs1-2* should result in a complete knock-out of the gene and thus to a more severe phenotype compared to *phs1-1*, that still got 40 % of residual WT transcript. Malondialdehyde (MDA) levels as a function of membrane peroxidation were measured 96 h after heat shock of 5 days old WT and *phs1-1* seedlings (figure 7C). In both genotypes, MDA levels were strongly increased after heat shock and the values in *phs1-1* were significantly higher compared to the WT. Interestingly, *phs1-1* also displayed a significant increase under control conditions.

Identification of a second *PHS1* isoform

In order to further analyze the reason for the missing heat shock phenotype of *phs1-2*, we found out that *PHS1* has a second isoform (*PHS1.2*) resulting from an alternative start-codon in the middle of exon 2 (Buels et al. 2016) (Figure 8).

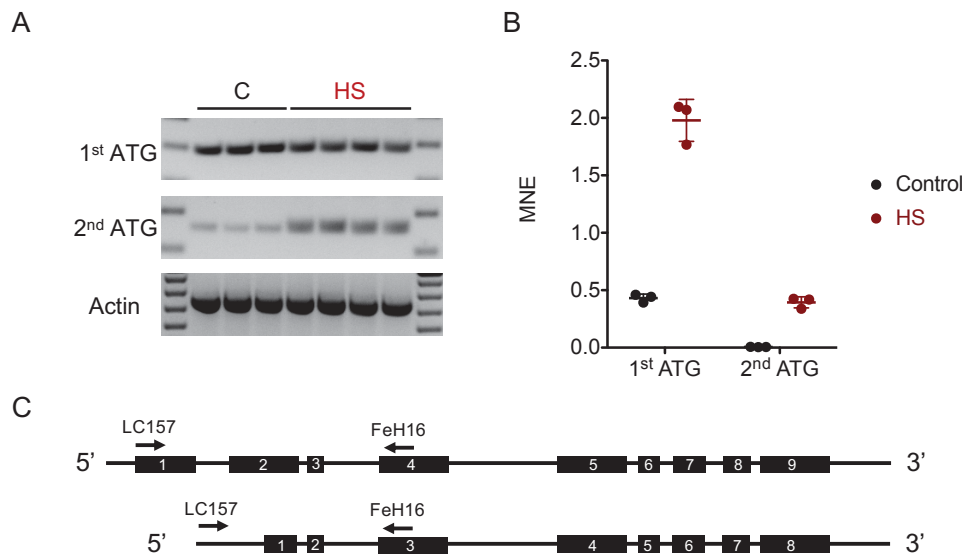


Figure 8: Expression of *PHS1.2* isoform upon heat shock

(A) Amplification of *PHS1* isoforms with specific primer (1st ATG: LC157/FeH16; 2nd ATG: LC239/FeH16) from cDNA (35 PCR cycles) after heat shock (HS; 4 h at 42 °C) or without treatment (control). Four and three biological replicates, respectively. Actin specific primer (P67/P68) were used as loading control. (B) qRT-PCR of both isoforms with (red) or without (black) aforementioned heat shock. Expression of isoforms was normalized by expression of the reference gene TIP41-like (At4g34270). Three biological replicates were measured in triplicates. (C) Gene architecture of *PHS1* (top) and *PHS1.2* (bottom) with exons (boxes), introns (lines) and primer binding sites (arrows).

PCR of cDNA from control and heat stressed plants revealed no obvious difference in the expression of the long isoform *PHS1.1* (Figure 8A). But for the short isoform with the alternative start-codon, there was a strong increase in the band intensity after heat shock. To quantify this effect, qRT-PCR was performed (Figure 8B). It revealed that under control conditions, *PHS1.2* is almost not detectable with 10 times less abundancy compared to *PHS1.1*. Upon heat shock, both isoforms were upregulated but to different extents. While *PHS1.1* expression increased 4.5 times after heat shock, there was a 70-fold upregulation of *PHS1.2*. But the values were still lower than the control values of *PHS1.1*. However, it is conceivable that the truncation of *PHS1.2* leads to different properties of the protein that are especially required during heat stress. One common effect of alternative start-codons or splicing events is a re-localization of the protein to a different organelle. To test this, we transiently expressed a *PHS1.2*-mCherry fusion protein in tobacco leaves and analyzed isolated protoplasts by CLSM (Figure 9).

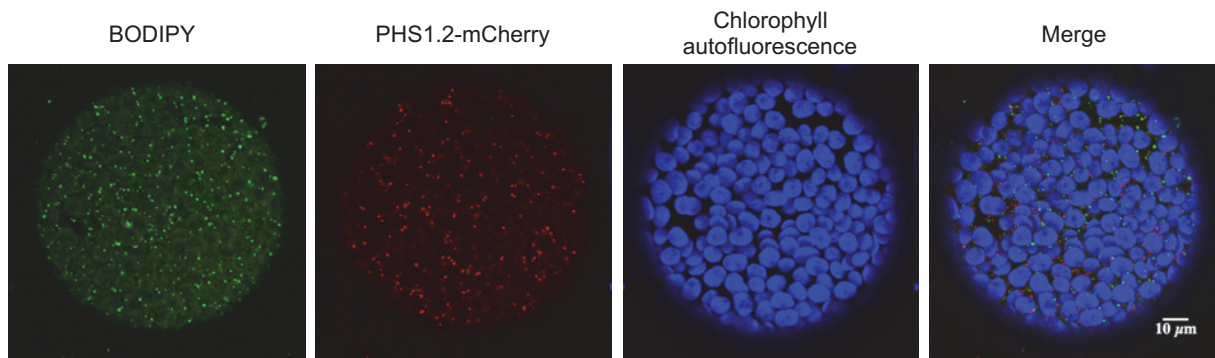


Figure 9: Subcellular localization of PHS1.2

Transient expression of PHS1.2-mCherry fusion protein in tobacco leaves. Protoplasts were isolated 2 days after infiltration. BODIPY was used as a peroxisomal marker (1st panel, green), mCherry fluorescence is shown in red (2nd panel) and chlorophyll autofluorescence in blue (3rd panel). 4th image represents merged picture of all channels including 10 µm scale bar.

Comparing the fluorescence signal of the peroxisomal dye BODIPY and the one of the PHS1.2-mCherry clearly showed that there was no overlay of both signals in the merged picture observable. But the absence of a functional mitochondrial control makes it impossible to draw conclusions about the new subcellular localization.

Assuming that *PHS1.2* is indeed required for a heat stress specific response, we established a second mutant line using genome editing by CRISPR/Cas9 where the gene is further truncated which resulted in the abolishment of the alternative start-codon (Figure 10B).

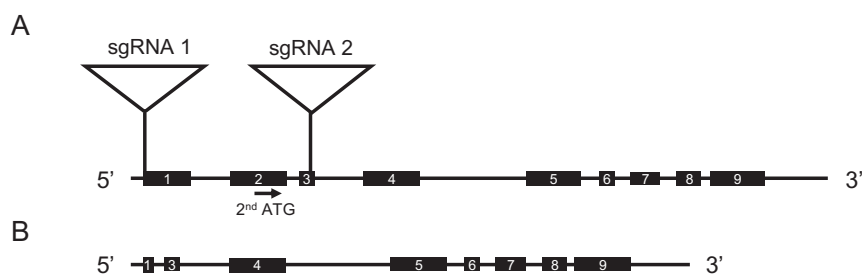


Figure 10: Generation of a *phs1.2* mutant by CRISPR/Cas9

(A) Gene architecture of *PHS1* with sgRNA binding sites (triangles) and the localization of the 2nd start-codon (arrow). (B) Truncated version of *PHS1* where the cutting event of Cas9 resulted in a big deletion of the majority of the first and the complete second exon including the alternative start-codon.

In *phs1-3* the cutting event of Cas9 resulted in a large deletion from the first sgRNA recognition site to the middle of the second intron. Interestingly, there are still minor fractions of the deleted part of *PHS1* present in *phs1-3*, but with low coverage and the alternative start-codon is absent (Figure S1). Unfortunately, *phs1-3* could not be included into the experiments, thus it will be objective of future studies to further confirm the heat shock responsive phenotype of *phs1* mutants.

Post-germinative growth phenotype

To analyze whether *PHS1.2* is only required in the heat stress response or also in other processes producing oxidative stress, we tested the growth behavior of *phs1-1* and *phs1-2* during germination. In this developmental stage there is a high rate of H₂O₂ production resulting from a high β -oxidation activity (Figure 11).

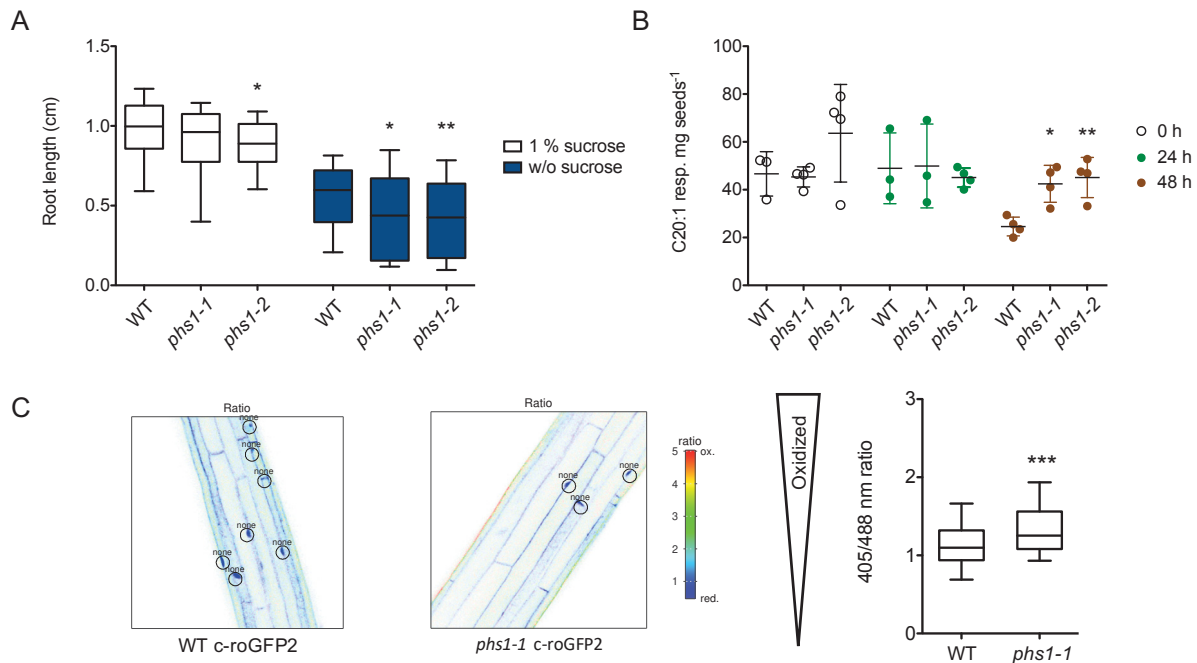


Figure 11: Post-germinative growth phenotype.

(A) WT, *phs1-1* and *phs1-2* were grown for 5 days in the presence (white) or absence (blue) of 1 % (w/v) sucrose. $n > 86$, whiskers span 10-90 percentile. (B) Amount of C20:1 in WT, *phs1-1* and *phs1-2* seeds and seedlings 0h, 24h and 48h after imbibition measured by GC-MS. $n > 3$ biological replicates of pooled seeds and seedlings, respectively. (C) *In vivo* determination of cytosolic redox state in hypocotyls of 5 days old etiolated seedlings with genetically encoded roGFP2 sensor using CLSM. Left panel shows example images of WT and *phs1-1* hypocotyls as false color images. Right panel shows the 405/488 nm ratio of all measured seedlings. The higher the ratio, the higher the oxidative state. $n > 33$ (pooled replicates of at least 2 independent transformed lines). Significant differences to the WT were determined by one-way ANOVA; *: p -value < 0.05 ; **: p -value < 0.01 ; ***: p -value < 0.001 .

In the presence of sucrose, the root lengths of *phs1-1* and *phs1-2* were reduced with *phs1-2* being significant (Figure 11A, white). In the absence of sucrose seedlings fully demand on the degradation of stored fatty acids for energy production which leads to increased β -oxidation activity and hence H₂O₂ production. And indeed, both mutants had significantly shortened roots (Figure 11A, blue). The content of C20:1, a fatty acid found almost exclusively in triacylglycerols of the storage oil reserves, was measured in WT, *phs1-1* and *phs1-2* seeds and seedlings 0h, 24h and 48h after imbibition (Figure 11B). After 48 h there is a decrease in the C20:1 content in the WT which is not observable in *phs1-1* and *phs1-2* indicating a delay in storage oil breakdown. To finally connect this phenotype to oxidative

stress, we measured the oxidative state of the cytosol in WT and *phs1-1* using the genetically encoded redox sensitive GFP sensor roGFP2 (Figure 11C). After 5 days of growing, the cytosol of *phs1-1* was significantly more oxidized compared to the WT as indicated by the higher 405/488 nm ratio of the sensor. The roGFP2 measurements still have to be repeated for *phs1-2* to finally confirm the link between sucrose dependency, storage oil mobilization and oxidative stress.

Generation and analysis of *phs1 cat2-1* double mutants

Under standard growth conditions, there is no obvious phenotype of *phs1-1* observable. Within peroxisomes, there are several redundant pathways for the degradation of H₂O₂ to prevent damage to the cell. Because of this we crossed the *phs1-1* tDNA insertion line with the very same *cat2-1* mutant line to test for an additive phenotype. The results are shown in Figure 12.

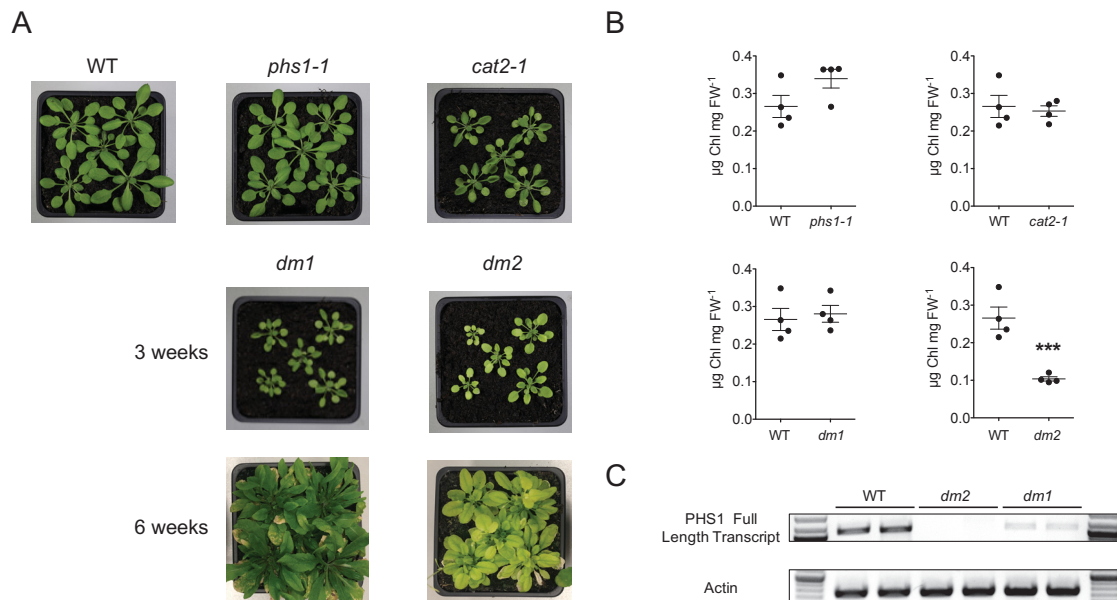


Figure 12: Phenotyping of a *phs1-1 x cat2-1* double mutant

Double mutant of *phs1-1* and *cat2-1* was generated by crossing the individual single tDNA insertion lines. (A) Growth behavior of WT, the respective single tDNA insertion lines and two different T3 double mutants after 3 weeks (top) and of both double mutant lines after 6 weeks (bottom) grown under ambient air conditions. (B) Chlorophyll contents of all four genotypes measured from four individual 6 weeks old plants, each. ***: significant different (p -value < 0.001) to the WT determined by one-way ANOVA. (C) Amplification of PHS1 full length transcript from cDNA of the WT and both double mutant lines. Actin specific primer (P67/P68) were used as loading control.

Crossing of *phs1-1* and *cat2-1* resulted in two different populations. Whereas one group looked like the *cat2-1* single mutant (*dm1*), the second group (*dm2*) showed a reduced growth and brighter leaves after 3 weeks of growing under ambient air conditions (Figure 12A). This phenotype got even stronger after 6 weeks of growing and the chlorophyll content was significantly reduced in these plants (Figure 12B). To analyze the differences between these two genetically identical double mutant lines, we checked for the presence of the PHS1 full length transcript (Figure 12C). This revealed, that in the unaffected *dm1* plants there is still residual transcript detectable whereas it is completely absence in *dm2*. Analysis of metabolites further underlined the severe phenotype of *dm2* (Figure 13).

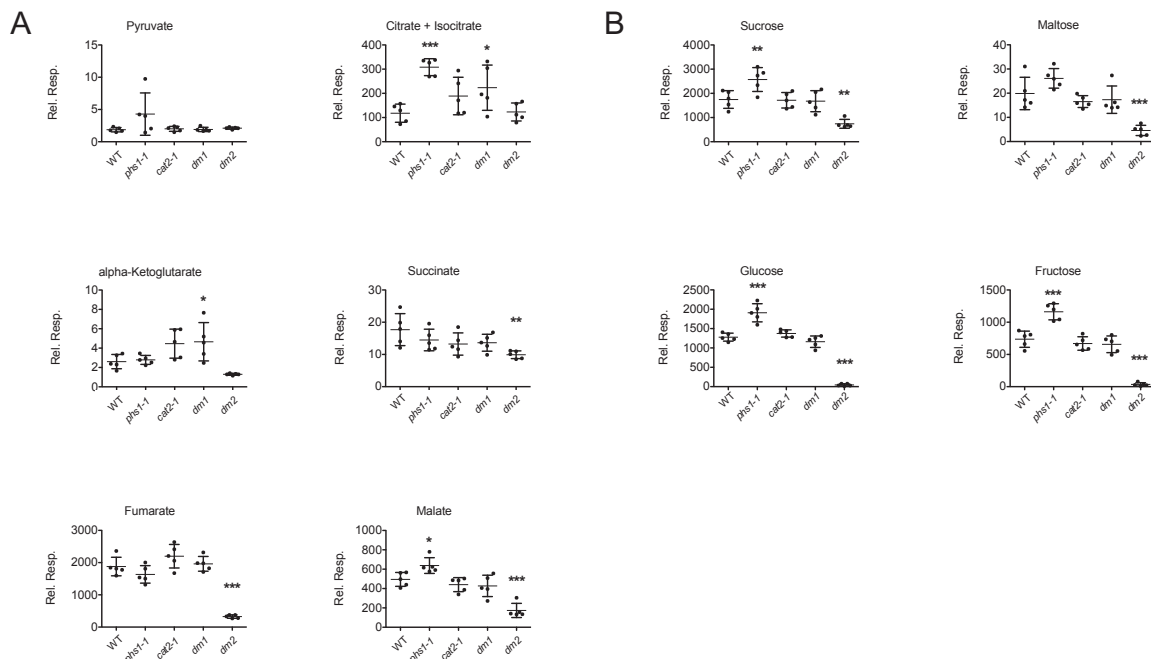


Figure 13: Metabolite analysis

Intermediates of the TCA cycle (A) and photosynthesis related sugars (B) of 5 individual 6 weeks old plants per genotype were measured by GC-MS. Peak intensities were normalized by the internal standard DMAP and the fresh weight of the plants. Significance was determined by one-way ANOVA with *: $p < 0.05$; **: $p < 0.01$ and ***: $p < 0.001$.

The TCA cycle metabolites, succinate, fumarate and malate were specifically and significantly reduced in *dm2* compared to the WT (Figure 13A). In contrast to that, *phs1-1* and *dm1* showed an increase in citrate + isocitrate, *phs1-1* additionally in malate levels and *dm1* had elevated levels of alpha-ketoglutarate. For the photosynthesis related sugars (Figure 13B), only *dm2* had reduced levels of sucrose, maltose, glucose and fructose whereas *dm1* and the *cat2-1* single mutant did not significantly differ from the WT. Interestingly, the *phs1-1* single mutant showed a significant increase in sucrose, glucose and fructose but not in maltose.

After 8 weeks, *dm2* plants set flowers but they rapidly died off and did not produce seeds (Figure 14C).

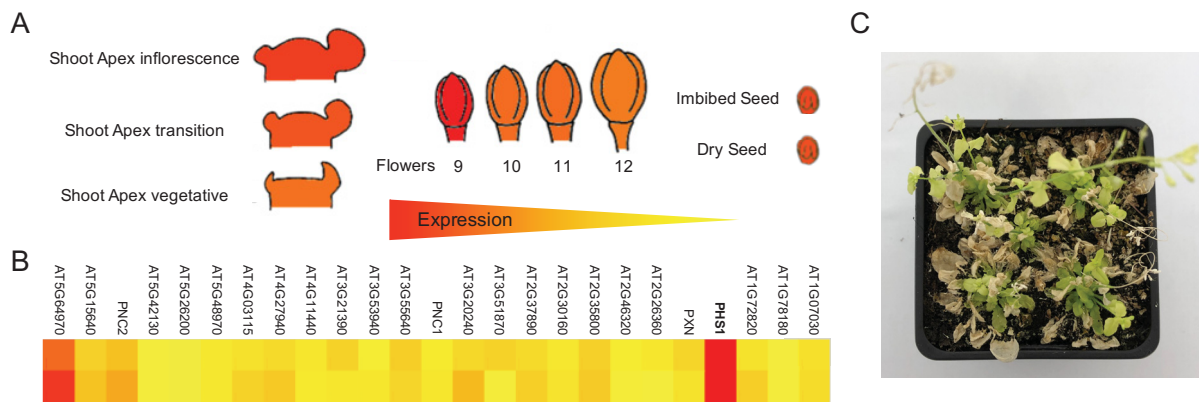


Figure 14: Expression pattern and inflorescence phenotype

(A) Microarray data of the BAR eFP Browser (Winter et al. 2007) showing tissue specific expression of PHS1 in young flowers inflorescence shoot apex as well as dry and imbibed seeds. (B) Foldchange of TPM values calculated from RNA-Seq data revealed that PHS1 shows the highest expression in Stage 5-7 anthers from stage 9 flower buds (Chen et al. 2010) (upper panel) and male meiocytes (Accession PRJNA369070) (lower panel). Color-code from low (yellow) to high expression (red). (C) 8 weeks old *dm2* plants grown at standard conditions.

Microarray data depicted by the BAR eFP browser (Winter et al. 2007) illustrate that PHS1 is highly expressed in young flowers, followed by the shoot apex of vegetative, inflorescence and transition tissues as well as dry and imbibed seeds (Figure 14A). This inflorescence specific expression was further confirmed by RNA-Seq data of two independent experiments (Figure 14B), showing that PHS1 has the highest expression in anthers (Figure 14B, upper panel) and more precisely in male meiocytes (Figure 14B, lower panel).

Biochemical characterization of heterologous expressed PHS1

Because of the stress specific phenotype of *phs1* mutants we analyzed its capability to transport different stress related metabolites and cofactors by heterologous protein expression using either yeast as host cell or wheat germ lysate as a cell-free expression system and subsequent *in vitro* uptake experiments (Table 1).

Table 1: Time dependent uptake experiments using either yeast host cell or the cell-free Wheat-Germ expression kit for PHS1 expression. All uptake experiments were conducted as homo-exchange of substrates except for NAD and CoA. x : no uptake above empty vector control; - : not tested; ✓: uptake activity above empty vector control.

Substrate	Expression system					
	Yeast			Wheat-Germ		
	Uptake	Positive-control	Column material	Uptake	Positive-control	Column material
GSH	x	x	Sephadex G-75	x	-	Sephadex G-75
ASC	x	-	Acetate-Resin	x	-	Acetate-Resin
SAM	x	✓	Hydrogen-Resin	-	-	-
AMP	x	-	Acetate-Resin	x	✓	Acetate-Resin
AMP/NAD	x	-	Acetate-Resin	x	✓	Acetate-Resin
AMP/CoA	x	-	Acetate-Resin	x	✓	Acetate-Resin
Phosphate	x	✓	Chloride-Resin	-	-	-
Sulfate	x	-	Chloride-Resin	-	-	-
GABA	-	-	-	x	-	Sephadex G-75
Spermidine	-	-	-	x	-	Sephadex G-75

ASC and GSH are part of the ASC-GSH cycle within peroxisomes and thus greatly contribute to ROS detoxification. No uptake activity of PHS1 for these substrates could be measured, neither from Yeast nor Wheat-Germ expressed protein. In Yeast, we used the plasma membrane high affinity GSH transport Hgt1p as positive control. But, even Hgt1p did not show transport activity. The polyamine spermidine and the product of peroxisomal polyamine catabolism GABA are important signaling molecules and protectants against oxidative stress and especially involved in the heat stress response. Uptake experiments using PHS1 expressed with Wheat-Germ lysate did not reveal transport activity. The lack of positive controls again questions the suitability of the experimental setup to measure these metabolites. Since PHS1 shows high sequence similarity to already characterized s-adenosyl methionine (SAM) transporters we analyzed its *in vitro* activity using the plastidic SAMT1 as positive control. Whereas SAMT1 was highly active, PHS1 did not show SAM homoexchange activity. Because of the structural similarity of SAM to AMP, we also tested AMP homoexchange and heteroexchange against NAD and Coenzyme A. No uptake activity could be observed for PHS1 neither for the yeast nor the Wheat-Germ expressed protein. But, due to the high activity of PXN as a positive control for the Wheat-Germ system, the general experimental conditions for the *in vitro* experiment seem to be suitable to measure these substrates.

Discussion

PHS1 is involved in plant peroxisomal heat shock response

Except for the fatty acid importer PXA, all peroxisomal transport proteins that have been identified belong to the mitochondrial carrier family (MCF). This and the broad substrate spectrum of MCF proteins make this group a promising basis for searching for new peroxisomal proteins. PHS1 as a member of the MCF is specifically upregulated upon heat shock. Because of the high oxidative character of peroxisomes and the fact, that heat shock results in a massive increase in the production of reactive oxygen species (ROS), we hypothesize that PHS1 is involved in the peroxisomal ROS scavenging machinery.

Therefore, we first tested the influence of heat shock on the root length as a function of plant growth of a *phs1* tDNA insertion line (*phs1-1*) and a mutant line generated by CRISPR/Cas9 (*phs1-2*). It turned out, that the heat shock related phenotype of *phs1-1* is rather mild leading to a slight but significant reduction of the root length in two independent experiments. The less dominant phenotype is probably a consequence of the residual WT transcript that accounts to of 40 % in the tDNA insertion line. The root length of a *phs1-1* complementation line was indispensable to the WT, showing, that this reduction is indeed resulting from the disruption of *PHS1* and not by an insertional effect of the tDNA in another gene.

Malondialdehyde (MDA) is an aldehyde that can be formed as a secondary product during lipid peroxidation and like H₂O₂ can act as both, toxic side product and signaling molecule (Ayala et al. 2014). Hence it is a well-established marker for lipid peroxidation (Lv et al. 2011). After heat shock, MDA levels in *phs1-1* were significantly increased compared to the WT indicating a higher rate of membrane oxidation. Interestingly, even under control conditions the MDA content in *phs1-1* was significantly higher compared to the WT. This might be contributed to a general increased oxidative stress in the mutant line. But the differences under control conditions are small despite of being significantly different. Thus, it might not influence plant growth since the root length of *phs1-1* did not differ from that of the WT.

The colorimetric assay applied for measuring MDA levels has several limitations. First its low specificity, since it measures all thiobarbituric acid reactive substances (TBARS) and not only MDA. In addition, the condensation of MDA with TBA is strongly affected by procedural modifications which exacerbate the reproducibility and generally leads to low recovery test results (Khoubnasabjafari et al. 2015). Therefore, future experiments should measure MDA levels by GC-MS, because it is more sensitive and specific (Liu et al. 1997). However, the TBARS assay is a simple and still sensitive procedure to get a first impression about membrane peroxidation rates between genotypes and conditions.

PHS1 isoform 2 strongly response to heat shock with unclear sub-cellular localization

Contrary to our expectations, *phs1-2* did not show a heat shock phenotype. According to the Araport11 project, there is a second isoform of *PHS1* resulting from an alternative start-codon in the middle of the second exon. Transcript analysis by qRT-PCR clearly showed that *PHS1.2* is almost not expressed under control conditions and that upon heat shock there is a 70-fold upregulation of the gene. Even though it is still lower abundant compared to *phs1.1* (4-fold upregulation upon heat shock) it is conceivable that the truncation of the protein results in different properties of the protein that are especially required during heat stress.

The discovery of alternative open reading frames (ORFs) upstream or downstream of annotated ORFs or even within annotated non-coding-RNAs extended the knowledge about proteome plasticity (Hsu et al. 2016). Alternative ORFs can function as regulators for main ORF translation under stress conditions like oxidative stress and heat stress (Gerashchenko et al. 2012; Zhu et al. 2012). The majority of alternative upstream ORFs have inhibitory effects on the translation of the main ORF either by preventing translation itself or by degrading the produced mRNA by non-sense mediated mRNA decay (Nyiko et al. 2009; von Arnim et al. 2014). Downstream ORFs also have regulatory function, e.g. evading upstream ORF-mediated inhibition of gene expression (Kurihara et al. 2018) or even changing the subcellular localization by alternating the N terminus of proteins that often contains targeting signals. Phytochrome for instance induces alternative promoter selection in Arabidopsis leading to a cytoplasmic localization of the plastidic glycerate kinase under fluctuating light conditions (Ushijima et al. 2017).

Transient expression in tobacco showed an accumulation of the PHS1.2-mCherry signal in distinct dots, but there was no overlay with the peroxisomal BODIPY signal. According to the shape and size of the fluorescence signal, PHS1.2 might be targeted to mitochondria but without colocalization with an organelle specific marker this assumption remains highly speculative. An accumulation in vesicles caused by the artificial overexpression of the protein must also be considered. Additionally, proteins that are overexpressed in a heterologous transient expression system like tobacco might get stuck in the secretory pathway which leads to a mistargeting of the protein (Campanoni et al. 2007). Thus, future studies should aim to do both, co-infiltration of Tobacco leaves with *PHS1-mCherry* together with different organellar specific markers as well as generation of stable transformed Arabidopsis lines. To further analyze the specific role of PHS1.2, *phs1-1* has to be transformed with the alternative isoform to see whether it is able to complement the heat shock phenotype. As a second control, *phs1-1* could be transformed with a *PHS1* construct where the alternative start-codon is mutated to exclude the translation of *PHS1.2*.

A second question that has to be addressed is what is the structural effect of the N-terminal truncation of PHS1.2? MCF carrier contain 3 tandemly repeated motives each consisting of 2 transmembrane domains. According to different prediction programs of the ARAMEMNON database (Schwacke et al. 2003), the truncation of *PHS1.2* results in the abolishment of the first transmembrane domain of the carrier. Thus, the new N-terminus of the protein could be a target of posttranslational modification. For instance, N-terminal acetylation contributes to stress responses by influencing stability, activity, folding and even localization of the protein (Nguyen et al. 2018). This or the structural effect of the deletion on the carriers' pore might contribute to changing properties of PHS1.2 in terms of substrate specificity or affinity. But, different behaviors towards the transported substrate of PHS1.1 and PHS1.2 are not testable at the moment, since the transported substrate has not been identified, yet.

To further confirm the hypothesis that PHS1.2 is especially required during heat stress, we established a third mutant line using genome editing by CRISPR/Cas9. In *phs1-3* there is a big deletion starting 11 bp after the main ORFs start-codon and reaches until the middle of the second intron. Thus, the alternative start-codon and the first TMD are missing in this mutant. Like *phs1-2*, the deletion in *phs1-3* is homozygous and the plants are free of Cas9. As a consequence, *phs1-3* should show at least the same heat stress related phenotype as *phs1-1*. But, due to the fact, that seeds of all lines had to be produced in parallel to guarantee equal preconditions for germination, *phs1-3* could not be included in the root length experiments performed in this study.

Post-germinative growth defect of *phs1* might be linked to increased oxidative stress

Interestingly, even though *phs1-2* did not reveal a heat shock responsive phenotype, *phs1-1* and *phs1-2* both showed a sucrose dependent phenotype when grown in the absence of sucrose. In addition, both mutant lines had reduced root lengths even in the presence of sucrose, with *phs1-2* being significantly different. To test whether the root length phenotype is caused by differences in storage oil content, either caused by a defect in seed filling or fatty acid degradation, we analyzed the content of C20:1, a fatty acid that is almost exclusively present in storage oil reserves (Lemieux et al. 1990).

The C20:1 content of *phs1-1* and *phs1-2* 0h and 24h after imbibition did not significantly differ from that of the WT. But after 48h of growing in the light, the content of C20:1 was reduced in the WT whereas the mutant lines still had significantly higher C20:1 level compared to the WT. This indicates, that a defect in storage oil mobilization rather than in the seed filling process is responsible for the decreased root length of *phs1-1* and *phs1-2*.

Degradation of stored fatty acids during germination requires high β -oxidation activity concomitant with an increased production of H₂O₂. As a consequence, the excess production of H₂O₂ results in oxidative stress of the plants which we could show, at least for *phs1-1* by

using the redox sensitive roGFP2 sensor. The cytosolic lipases SDP1 and SDP1-like are required for the release of free fatty acids from cytosolic oil bodies and thus play an essential role during storage oil mobilization (Eastmond 2006). But both enzymes are susceptible to oxidative stress. Mutants lacking the anti-oxidant peroxisomal membrane bound ascorbate reductase 4 (MDAR4) are compromised in seedling establishment due to the oxidation and hence inactivation of the two lipases (Eastmond 2007). Thus, it is likely that the increased oxidative stress in *phs1* inhibits the cytosolic lipases responsible for lipolysis which results in a delayed breakdown of storage oil reserves.

Genetically encoded sensors are powerful tools to analyze biological parameters like redox status, pH values or ATP in different cellular compartments *in vivo* (Schwarzlander *et al.* 2008; De Col *et al.* 2017). Therefore, future studies should aim to establish WT and *phs1* mutant lines with both, cytosolic and peroxisomal versions of roGFP2 to determine the oxidative state of both compartments during seedling establishment. In addition, this sensor could be applied to further investigate the oxidative state of *phs1* after heat shock. For this, a fluorescence-based plate reader assay has to be established, since working with CLSM is not fast enough to detect rapid changes in the redox state of the plant.

***phs1-1 cat2-1* double mutant has an additive stress related phenotype**

Catalase is a major player in ROS detoxification and all of its three isoforms are localized to peroxisomes with CAT2 being the most dominant isoform (Mhamdi *et al.* 2010). Previous studies analyzing the role of the peroxisomal glutathione reductase 1 (GR1) could show that the phenotype of a *gr1* mutant plant was indispensable from the WT (Mhamdi *et al.* 2010). But a *cat2 gr1* double mutant suffered from increased oxidative stress and growth was severely reduced compared to the *cat2* single mutant. Since *phs1-1* does not show an obvious growth phenotype under standard conditions, we crossed *phs1-1* with the very same *cat2-1* mutant that was used in the study mentioned above.

A small subset of homozygous double mutants (*dm2*) revealed a visible phenotype having light green leaves and a retarded growth even under high CO₂ conditions. However, these plants produced seeds and their descendants were grown in ambient air together with the *cat2-1*-like double mutant (*dm1*), the WT and the *phs1-1* and *cat2-1* single mutants. In *cat2-1* the tDNA is integrated into the second exon and hence represents a full knock-out mutant of CATALASE2 with markedly decreased catalase activity, decreased growth and a daylength dependent formation of lesions (Queval *et al.* 2007). But it is still viable and able to produce seeds even under ambient air conditions when the photoperiod does not exceed 12 h.

The phenotype observed in the progenitor of *dm2* was conserved in the next generation shown by significantly less chlorophyll and a strongly reduced size after 6 weeks

of growing. Amplification of the *PHS1* transcript revealed that the differences between *dm1* and *dm2* result from the amount of residual *PHS1* transcript in the double mutants. Whereas in *dm1* amount of the *PHS1* transcript is lower but still present, it is completely absent in *dm2* mutant plants.

A process called tDNA suppression generally occurs after crossing of two homologous tDNA mutants (in this case SALK tDNA lines) (Osabe et al. 2017). By this, one mutant phenotype is expressed while the other intronic phenotype (in this case *phs1-1*) gets suppressed. This suppression is based on the splicing of tDNA-containing introns caused by extensive methylation and heterochromatinization of tDNA sequences (Sandhu et al. 2013; Osabe et al. 2017). This means, that in the *dm1* plants the 4th tDNA-containing intron of *phs1-1* might be spliced out resulting in plants that are phenotypically indistinguishable from the *cat2-1* single mutant. In contrast to that, *dm2* plants without suppression of the *phs1-1* tDNA show an additive phenotype compared to the respective single mutants. Since tDNA suppression likely occurs directly after sexual crossing, the respective epigenetic state can be maintained for multiple generations (Osabe et al. 2017).

Assuming that PHS1 plays an important role in times of elevated H₂O₂ production, like heat stress and post-germinative growth, plants deficient in both, PHS1 and CAT2 should suffer from severe oxidative stress caused by photorespiration. This is getting obvious by the strong chlorotic phenotype of *dm2*. Reduced chlorophyll content results in a decrease of photosynthesis and thus in the production of sugars. In particular, sucrose as an end product of photosynthesis is the major translocated form in plants and is metabolized into glucose and fructose (Rosa et al. 2009). The low sugar availability is likely connected to reduced starch production which is indicated by the low maltose levels observed in *dm2*. Oxidative stress and or the limited availability of sugars lead to a decrease in TCA cycle metabolites like succinate, fumarate and malate explaining the reduced growth rate of *dm2*.

Whereas *cat2-1* and *dm1* behaved like the WT, *phs1-1* showed a significant increase in metabolites like citrate + isocitrate and malate, but also in sucrose, maltose, glucose and fructose. Interestingly, the chlorophyll content was also increased in *phs1-1* despite not being significant. Biotic and abiotic stress conditions have been associated with the accumulation of soluble sugars as an adaptive response (Roitsch 1999). They can feed anti-oxidant metabolic pathways like the oxidative pentose phosphate pathway that produces NADPH required for the reduction and thus regeneration of oxidized glutathione in the ascorbate-glutathione cycle. In addition, glucose is the main carbon precursor for the synthesis of ascorbate and carbon skeletons of amino acids like cysteine, glutamate and glycine which are the building blocks of glutathione (Noctor and Foyer 1998).

Assuming, that PHS1 is involved in the response to ROS it is conceivable, that in *phs1-1* chlorophyll biosynthesis and thereby the rate of photosynthesis is upregulated to produce

carbon precursor for anti-oxidant processes. This has to be experimentally confirmed by both, PAM measurements to show an increase in photosynthetic efficiency and or electron transport rate as well as measuring the rate of oxidative stress. The latter could be either performed by MDA determination or roGFP2 sensor usage.

In contrast to *dm1*, *dm2* produces flowers that die off without producing seed containing siliques. During fertilization, maintenance of a highly reduced glutathione pool is essential for pollen germination and tube growth (Zechmann et al. 2011; Garcia-Quiros et al. 2019). Besides being toxic at high concentrations, ROS is an important signal for flower meristem initiation with ASC and GSH being involved in the regulation of redox homeostasis (Kocsy et al. 2013). For instance, artificially increasing ASC and GSH lead to delayed bolting and flowering indicating, that a high oxidative state is required for the transition from vegetative to reproductive growth (Kocsy et al. 2013). This goes in line with the expression of *PHS1*. Expression of *PHS1* is increasing from the vegetative to the inflorescence shoot apex. Thus, *PHS1* might be required to prevent a toxic accumulation of ROS above the level required for transition. The high expression of *PHS1* in anthers and especially in male meiocytes, the progenitors of pollen, further underlines the importance of maintaining ROS in reproductive tissues. Since pollen were shown to be susceptible to conditions of high ROS production, like heat stress (Luria et al. 2019), it would be interesting to see whether *phs1* mutants are affected in either pollen viability or pollen tube growth.

All in all, the requirement for a tightly regulation of redox homeostasis in the reproductive tissues might explain the inability of *dm2* to produce seeds. Complementation of *dm2* with both *PHS1* isoforms should be object of future studies to further analyze the role of *PHS1.2*.

Biochemical analysis could not identify the transported substrate

The biochemical analysis using heterologous protein expression in yeast or Wheat-Germ lysate did not reveal the transported substrate of *PHS1*. But, the lack of positive controls for ASC, GABA and spermidine and the non-functional GSH transporter Hgt1p questions the suitability of the used experimental setup. PHT4;4, a member of the phosphate transporter 4 family is the only identified ASC transporter (Miyaji et al. 2015). It is localized to the chloroplast envelope and its activity depends on the presence of chloride and a membrane potential. Thus, using PHT4;4 as a positive control in our *in vitro* system requires the addition of valinomycin to artificially generate a potassium gradient and hence membrane potential.

The same could be applied for the yeast plasma membrane GSH carrier HGT1p that is considered to be a proton-coupled transporter (Bourbouloux et al. 2000). Even in the presence of the uncoupling agent CCCP Hgt1p still had about 60 % of the WT activity. The

application of a membrane potential for Hgt1p uptake experiments could therefore be used to test for the general functionality of the carrier. Interestingly, Yeast Opt2p localizes to peroxisomes and mutants have defects in glutathione redox homeostasis in peroxisomes, mitochondria and chloroplasts (Elbaz-Alon et al. 2014). Hence, yeast complementation of *opt1Δ* with PHS1 might represent an alternative method to test for GSH transport ability. But direct transport of GSH by Opt2p has not been shown, yet.

In plants, the oligopeptide transporter (OPT) family consists of 9 transport proteins. OPT4 was shown to complement the growth phenotype of a yeast mutant deficient in GSH biosynthesis when grown on GSH as sole sulfur source (Zhang et al. 2016) and OPT6 is involved in the long distance transport of GSH (Wongkaew et al. 2018). Both proteins are localized to the plasma membrane. Since Opt2p is considered to be the peroxisomal GSH transporter in Yeast, this family might be a promising target to look for the Arabidopsis one. The closest homologs of Opt2p in Arabidopsis are OPT3 and OPT4. As mentioned above, OPT4 is localized to the plasma membrane and OPT3 was shown to be involved in the phloem loading of iron (Zhai et al. 2014).

In Arabidopsis the L-type amino acid transporter (LAT) family consists of 5 proteins with three representatives showing high affinity polyamine transport activity (Mulangi et al. 2012). LAT1 is localized to the plasma membrane of transgenic Arabidopsis (Fujita et al. 2012) whereas LAT3 and LAT4 localize to the endoplasmatic reticulum and the Golgi, respectively (Li et al. 2013). Because of the different localization of these carriers, LAT2 and LAT5 might be promising candidates for polyamine transporters in other organelles including peroxisomes.

The different localizations of GABA biosynthesis and catabolism require an efficient transport system across biological membranes. Members of the Arabidopsis proline transporter family have been identified to transport GABA in addition to other stress-related compounds across the plasma membrane (Grallath et al. 2005; Meyer et al. 2006). Another transporter is the mitochondrial GABA permease that belong to the same protein family as the above mentioned polyamine transporter (Michaeli et al. 2011). This further underlines the possibility of a peroxisomal member of this group either involved in polyamine or GABA transport.

In addition to the aforementioned metabolites that are required for the peroxisomal antioxidant machinery, NADPH plays an essential role for the reduction of oxidized GSH produced by the reduction of toxic lipid hydroperoxides and dehydroascorbate (Figure 1). Since NADPH is generated by the phosphorylation of NADH within peroxisomes, there is no need for a specific transport protein (Waller et al. 2010). But the regeneration of NADPH necessitates the action of the peroxisomal OPPP and NADP-dependent ICDH. While the substrate and product of the OPPP are exchanged by GPT1 there is no information about a

peroxisomal isocitrate/2-oxoglutarate carrier required for ICDH. Recently the mitochondrial succinate/fumarate carrier 1 (SFC1) was shown to additionally transport citrate and isocitrate but not 2-oxoglutarate (Brito et al., under revisions). Instead, the uncoupling proteins UCP1 and UCP2 are able to catalyze the transport of 2-oxoglutarate but not citrate (Monne et al. 2018). All three carrier belong to the MCF which gives rise to the possibility of a peroxisomal member of this family transporting these substrates. The presence of a peroxisomal dicarboxylate and tricarboxylate carrier is also required for the function of the glyoxylate cycle where citrate/isocitrate and malate/oxaloacetate have to be transported across the peroxisomal membrane. Thus, future studies should include these substrates for PHS1 *in vitro* uptake experiments. Since an impairment in the glyoxylate cycle is also linked to reduced storage oil mobilization and hence sucrose dependency during post-germinative growth, this goes in line with the observed phenotypes of *phs1*.

Conclusion

In this study we could identify a novel peroxisomal MCF member and for could show the involvement of a peroxisomal carrier during plant heat stress for the first time. Interestingly, both isoforms respond to elevated β -oxidation related ROS production during post-germinative growth, but the specific heat shock related role seems to be restricted to a second isoform with so far unknown sub-cellular localization. Hence, future studies should aim to further analyze the transport function and targeting of PHS1 under different environmental conditions. In times of increasing global temperature, the understanding of plant heat stress response is crucial. With our findings, we opened a new opportunity by introducing peroxisomes as potential targets to confer heat shock resistance to plants.

Supplementals

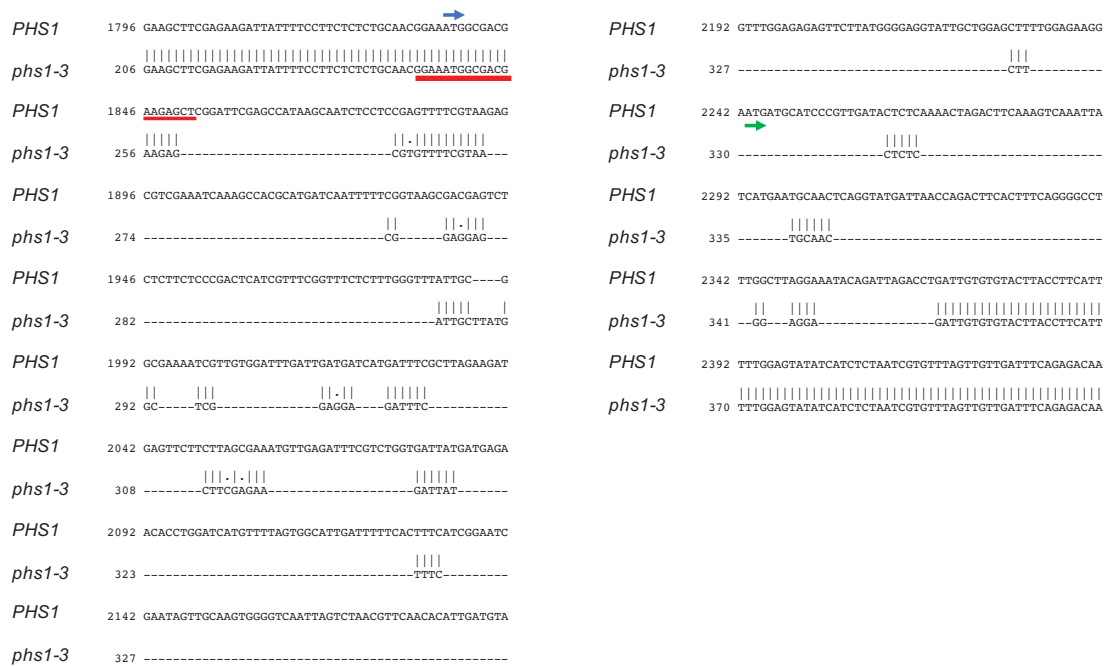


Figure S1: Alignment of WT-*PHS1* and *phs1-3*

Local pairwise alignment of *PHS1* and *phs1-3* generated by ClustalW. Arrows indicate WT (blue) and alternative (green) start-codon. Recognition site of sgRNA1 is underlined in red.

Author contribution

Generating a table with TPM values of SRA RNA-seq experiments was done by Wiebke Halpape. Cloning of pMT6 was done by Maximilian Trippelsdorf. Cloning and transformation of pHHU43 was done by Felix Holthausen. Lennart Charton wrote the manuscript and performed all residual experiments and analyses. Nicole Linka, Georg Groth and Andreas Weber participated in scientific discussions. Nicole Linka and Lennart Charton designed the experiments.

References

- Apel, K. and H. Hirt (2004). "Reactive oxygen species: metabolism, oxidative stress, and signal transduction." Annu Rev Plant Biol **55**: 373-399.
- Asada, K. (2006). "Production and scavenging of reactive oxygen species in chloroplasts and their functions." Plant Physiol **141**(2): 391-396.
- Ayala, A., M. F. Munoz and S. Arguelles (2014). "Lipid peroxidation: production, metabolism, and signaling mechanisms of malondialdehyde and 4-hydroxy-2-nonenal." Oxid Med Cell Longev **2014**: 360438.
- Bernhardt, K., S. Wilkinson, A. P. Weber and N. Linka (2012). "A peroxisomal carrier delivers NAD(+) and contributes to optimal fatty acid degradation during storage oil mobilization." Plant J **69**(1): 1-13.
- Boca, S., F. Koestler, B. Ksas, A. Chevalier, J. Leymarie, A. Fekete, M. J. Mueller and M. Havaux (2014). "Arabidopsis lipocalins AtCHL and AtTIL have distinct but overlapping functions essential for lipid protection and seed longevity." Plant Cell Environ **37**(2): 368-381.
- Bourbouloux, A., P. Shahi, A. Chakladar, S. Delrot and A. K. Bachhawat (2000). "Hgt1p, a high affinity glutathione transporter from the yeast *Saccharomyces cerevisiae*." J Biol Chem **275**(18): 13259-13265.
- Bouvier, F., N. Linka, J. C. Isner, J. Mutterer, A. P. Weber and B. Camara (2006). "Arabidopsis SAMT1 defines a plastid transporter regulating plastid biogenesis and plant development." Plant Cell **18**(11): 3088-3105.
- Buels, R., E. Yao, C. M. Diesh, R. D. Hayes, M. Munoz-Torres, G. Helt, D. M. Goodstein, C. G. Elsik, S. E. Lewis, L. Stein and I. H. Holmes (2016). "JBrowse: a dynamic web platform for genome visualization and analysis." Genome Biol **17**: 66.
- Campanoni, P., J. U. Sutter, C. S. Davis, G. R. Littlejohn and M. R. Blatt (2007). "A generalized method for transfecting root epidermis uncovers endosomal dynamics in Arabidopsis root hairs." Plant J **51**(2): 322-330.
- Chen, C., A. D. Farmer, R. J. Langley, J. Mudge, J. A. Crow, G. D. May, J. Huntley, A. G. Smith and E. F. Retzel (2010). "Meiosis-specific gene discovery in plants: RNA-Seq applied to isolated Arabidopsis male meiocytes." BMC Plant Biol **10**: 280.
- Corpas, F. J., J. B. Barroso, L. M. Sandalio, S. Distefano, J. M. Palma, J. A. Lupianez and L. A. Del Rio (1998). "A dehydrogenase-mediated recycling system of NADPH in plant peroxisomes." Biochem J **330** (Pt 2): 777-784.
- Corpas, F. J., J. B. Barroso, L. M. Sandalio, J. M. Palma, J. A. Lupianez and L. A. del Rio (1999). "Peroxisomal NADP-Dependent Isocitrate Dehydrogenase. Characterization and Activity Regulation during Natural Senescence." Plant Physiol **121**(3): 921-928.
- De Col, V., P. Fuchs, T. Nietzel, M. Elsasser, C. P. Voon, A. Candeo, I. Seeliger, M. D. Fricker, C. Grefen, I. M. Moller, A. Bassi, B. L. Lim, M. Zancani, A. J. Meyer, A. Costa, S. Wagner and M. Schwarzlander (2017). "ATP sensing in living plant cells reveals tissue gradients and stress dynamics of energy physiology." Elife **6**.
- del Rio, L. A., G. M. Pastori, J. M. Palma, L. M. Sandalio, F. Sevilla, F. J. Corpas, A. Jimenez, E. Lopez-Huertas and J. A. Hernandez (1998). "The activated oxygen role of peroxisomes in senescence." Plant Physiol **116**(4): 1195-1200.

- Dixon, D. P., T. Hawkins, P. J. Hussey and R. Edwards (2009). "Enzyme activities and subcellular localization of members of the Arabidopsis glutathione transferase superfamily." J Exp Bot **60**(4): 1207-1218.
- Eastmond, P. J. (2006). "SUGAR-DEPENDENT1 encodes a patatin domain triacylglycerol lipase that initiates storage oil breakdown in germinating Arabidopsis seeds." Plant Cell **18**(3): 665-675.
- Eastmond, P. J. (2007). "MONODEHYDROASCORBATE REDUCTASE4 is required for seed storage oil hydrolysis and postgerminative growth in Arabidopsis." Plant Cell **19**(4): 1376-1387.
- Elbaz-Alon, Y., B. Morgan, A. Clancy, T. N. Amoako, E. Zalckvar, T. P. Dick, B. Schwappach and M. Schuldiner (2014). "The yeast oligopeptide transporter Opt2 is localized to peroxisomes and affects glutathione redox homeostasis." FEMS Yeast Res **14**(7): 1055-1067.
- Fedyaeva, A. V., A. V. Stepanov, I. V. Lyubushkina, T. P. Pobezhimova and E. G. Rikhvanov (2014). "Heat shock induces production of reactive oxygen species and increases inner mitochondrial membrane potential in winter wheat cells." Biochemistry (Mosc) **79**(11): 1202-1210.
- Fincato, P., P. N. Moschou, V. Spedaletti, R. Tavazza, R. Angelini, R. Federico, K. A. Roubelakis-Angelakis and P. Tavladoraki (2011). "Functional diversity inside the Arabidopsis polyamine oxidase gene family." J Exp Bot **62**(3): 1155-1168.
- Fujita, M., Y. Fujita, S. Iuchi, K. Yamada, Y. Kobayashi, K. Urano, M. Kobayashi, K. Yamaguchi-Shinozaki and K. Shinozaki (2012). "Natural variation in a polyamine transporter determines paraquat tolerance in Arabidopsis." Proc Natl Acad Sci U S A **109**(16): 6343-6347.
- Garcia-Quiros, E., J. D. Alche, B. Karpinska and C. H. Foyer (2019). "Glutathione redox state plays a key role in flower development and pollen vigour." J Exp Bot.
- Gerashchenko, M. V., A. V. Lobanov and V. N. Gladyshev (2012). "Genome-wide ribosome profiling reveals complex translational regulation in response to oxidative stress." Proc Natl Acad Sci U S A **109**(43): 17394-17399.
- Gibson, D. G. (2011). "Enzymatic assembly of overlapping DNA fragments." Methods Enzymol **498**: 349-361.
- Gietz, R. D. and R. H. Schiestl (2007). "Large-scale high-efficiency yeast transformation using the LiAc/SS carrier DNA/PEG method." Nat Protoc **2**(1): 38-41.
- Graham, I. A. and P. J. Eastmond (2002). "Pathways of straight and branched chain fatty acid catabolism in higher plants." Prog Lipid Res **41**(2): 156-181.
- Grallath, S., T. Weimar, A. Meyer, C. Gumy, M. Suter-Grotemeyer, J. M. Neuhaus and D. Rentsch (2005). "The AtProT family. Compatible solute transporters with similar substrate specificity but differential expression patterns." Plant Physiol **137**(1): 117-126.
- Grefen, C., N. Donald, K. Hashimoto, J. Kudla, K. Schumacher and M. R. Blatt (2010). "A ubiquitin-10 promoter-based vector set for fluorescent protein tagging facilitates temporal stability and native protein distribution in transient and stable expression studies." Plant J **64**(2): 355-365.

- Haferkamp, I. and S. Schmitz-Esser (2012). "The plant mitochondrial carrier family: functional and evolutionary aspects." Front Plant Sci **3**: 2.
- Hasanuzzaman, M., K. Nahar, M. M. Alam, R. Roychowdhury and M. Fujita (2013). "Physiological, biochemical, and molecular mechanisms of heat stress tolerance in plants." Int J Mol Sci **14**(5): 9643-9684.
- Havaux, M. and F. Tardy (1996). "Temperature-dependent adjustment of the thermal stability of photosystem II in vivo: Possible involvement of xanthophyll-cycle pigments." Planta **198**(3): 324-333.
- Higashi, Y., Y. Okazaki, F. Myouga, K. Shinozaki and K. Saito (2015). "Landscape of the lipidome and transcriptome under heat stress in *Arabidopsis thaliana*." Sci Rep **5**: 10533.
- Hofgen, R. and L. Willmitzer (1988). "Storage of competent cells for *Agrobacterium* transformation." Nucleic Acids Res **16**(20): 9877.
- Hsu, P. Y., L. Calviello, H. L. Wu, F. W. Li, C. J. Rothfels, U. Ohler and P. N. Benfey (2016). "Super-resolution ribosome profiling reveals unannotated translation events in *Arabidopsis*." Proc Natl Acad Sci U S A **113**(45): E7126-E7135.
- Inoue, H., H. Nojima and H. Okayama (1990). "High efficiency transformation of *Escherichia coli* with plasmids." Gene **96**: 23-28.
- Jalil, S. U., M. I. R. Khan and M. I. Ansari (2019). "Role of GABA transaminase in the regulation of development and senescence in *Arabidopsis thaliana*." Current Plant Biology **19**.
- Jimenez, A., J. A. Hernandez, L. A. Del Rio and F. Sevilla (1997). "Evidence for the Presence of the Ascorbate-Glutathione Cycle in Mitochondria and Peroxisomes of Pea Leaves." Plant Physiol **114**(1): 275-284.
- Khoubnasabjafari, M., K. Ansarin and A. Jouyban (2015). "Reliability of malondialdehyde as a biomarker of oxidative stress in psychological disorders." Bioimpacts **5**(3): 123-127.
- Kim, K. and A. R. Portis, Jr. (2004). "Oxygen-dependent H₂O₂ production by Rubisco." FEBS Lett **571**(1-3): 124-128.
- Kocsy, G., I. Tari, R. Vankova, B. Zechmann, Z. Gulyas, P. Poor and G. Galiba (2013). "Redox control of plant growth and development." Plant Sci **211**: 77-91.
- Kurihara, Y., Y. Makita, M. Kawashima, T. Fujita, S. Iwasaki and M. Matsui (2018). "Transcripts from downstream alternative transcription start sites evade uORF-mediated inhibition of gene expression in *Arabidopsis*." Proc Natl Acad Sci U S A **115**(30): 7831-7836.
- Lemieux, B., M. Miquel, C. Somerville and J. Browse (1990). "Mutants of *Arabidopsis* with alterations in seed lipid fatty acid composition." Theor Appl Genet **80**(2): 234-240.
- Li, J., J. Mu, J. Bai, F. Fu, T. Zou, F. An, J. Zhang, H. Jing, Q. Wang, Z. Li, S. Yang and J. Zuo (2013). "Paraquat Resistant1, a Golgi-localized putative transporter protein, is involved in intracellular transport of paraquat." Plant Physiol **162**(1): 470-483.
- Linka, N., F. L. Theodoulou, R. P. Haslam, M. Linka, J. A. Napier, H. E. Neuhaus and A. P. Weber (2008). "Peroxisomal ATP import is essential for seedling development in *Arabidopsis thaliana*." Plant Cell **20**(12): 3241-3257.

- Liu, J., H. C. Yeo, S. J. Doniger and B. N. Ames (1997). "Assay of aldehydes from lipid peroxidation: gas chromatography-mass spectrometry compared to thiobarbituric acid." Anal Biochem **245**(2): 161-166.
- Luria, G., N. Rutley, I. Lazar, J. F. Harper and G. Miller (2019). "Direct analysis of pollen fitness by flow cytometry: implications for pollen response to stress." Plant J **98**(5): 942-952.
- Lv, W. T., B. Lin, M. Zhang and X. J. Hua (2011). "Proline accumulation is inhibitory to Arabidopsis seedlings during heat stress." Plant Physiol **156**(4): 1921-1933.
- McClung, C. R. (1997). "Regulation of catalases in Arabidopsis." Free Radic Biol Med **23**(3): 489-496.
- Meyer, A., S. Eskandari, S. Grallath and D. Rentsch (2006). "AtGAT1, a high affinity transporter for gamma-aminobutyric acid in Arabidopsis thaliana." J Biol Chem **281**(11): 7197-7204.
- Mhamdi, A., J. Hager, S. Chaouch, G. Queval, Y. Han, L. Taconnat, P. Saindrenan, H. Gouia, E. Issakidis-Bourguet, J. P. Renou and G. Noctor (2010). "Arabidopsis GLUTATHIONE REDUCTASE1 plays a crucial role in leaf responses to intracellular hydrogen peroxide and in ensuring appropriate gene expression through both salicylic acid and jasmonic acid signaling pathways." Plant Physiol **153**(3): 1144-1160.
- Mhamdi, A., G. Noctor and A. Baker (2012). "Plant catalases: peroxisomal redox guardians." Arch Biochem Biophys **525**(2): 181-194.
- Mhamdi, A., G. Queval, S. Chaouch, S. Vanderauwera, F. Van Breusegem and G. Noctor (2010). "Catalase function in plants: a focus on Arabidopsis mutants as stress-mimic models." J Exp Bot **61**(15): 4197-4220.
- Michaeli, S., A. Fait, K. Lagor, A. Nunes-Nesi, N. Grillich, A. Yellin, D. Bar, M. Khan, A. R. Fernie, F. J. Turano and H. Fromm (2011). "A mitochondrial GABA permease connects the GABA shunt and the TCA cycle, and is essential for normal carbon metabolism." Plant Journal **67**(3): 485-498.
- Miyaji, T., T. Kuromori, Y. Takeuchi, N. Yamaji, K. Yokosho, A. Shimazawa, E. Sugimoto, H. Omote, J. F. Ma, K. Shinozaki and Y. Moriyama (2015). "AtPHT4;4 is a chloroplast-localized ascorbate transporter in Arabidopsis." Nat Commun **6**: 5928.
- Monne, M., L. Daddabbo, D. Gagneul, T. Obata, B. Hielscher, L. Palmieri, D. V. Miniero, A. R. Fernie, A. P. M. Weber and F. Palmieri (2018). "Uncoupling proteins 1 and 2 (UCP1 and UCP2) from Arabidopsis thaliana are mitochondrial transporters of aspartate, glutamate, and dicarboxylates." J Biol Chem **293**(11): 4213-4227.
- Mulangi, V., M. C. Chibucos, V. Phuntumart and P. F. Morris (2012). "Kinetic and phylogenetic analysis of plant polyamine uptake transporters." Planta **236**(4): 1261-1273.
- Nguyen, K. T., S. H. Mun, C. S. Lee and C. S. Hwang (2018). "Control of protein degradation by N-terminal acetylation and the N-end rule pathway." Exp Mol Med **50**(7): 91.
- Noctor, G. and C. H. Foyer (1998). "ASCORBATE AND GLUTATHIONE: Keeping Active Oxygen Under Control." Annu Rev Plant Physiol Plant Mol Biol **49**: 249-279.

- Nyiko, T., B. Sonkoly, Z. Merai, A. H. Benkovics and D. Silhavy (2009). "Plant upstream ORFs can trigger nonsense-mediated mRNA decay in a size-dependent manner." Plant Mol Biol **71**(4-5): 367-378.
- Osabe, K., Y. Harukawa, S. Miura and H. Saze (2017). "Epigenetic Regulation of Intronic Transgenes in Arabidopsis." Sci Rep **7**: 45166.
- Palmieri, F., C. Indiveri, F. Bisaccia and V. Iacobazzi (1995). "Mitochondrial metabolite carrier proteins: purification, reconstitution, and transport studies." Methods Enzymol **260**: 349-369.
- Planas-Portell, J., M. Gallart, A. F. Tiburcio and T. Altabella (2013). "Copper-containing amine oxidases contribute to terminal polyamine oxidation in peroxisomes and apoplast of Arabidopsis thaliana." BMC Plant Biol **13**: 109.
- Priya, M., L. Sharma, R. Kaur, H. Bindumadhava, R. M. Nair, K. H. M. Siddique and H. Nayyar (2019). "GABA (gamma-aminobutyric acid), as a thermo-protectant, to improve the reproductive function of heat-stressed mungbean plants." Scientific Reports **9**.
- Queval, G., E. Issakidis-Bourguet, F. A. Hoeberichts, M. Vandorpe, B. Gakiere, H. Vanacker, M. Miginiac-Maslow, F. Van Breusegem and G. Noctor (2007). "Conditional oxidative stress responses in the Arabidopsis photorespiratory mutant cat2 demonstrate that redox state is a key modulator of daylength-dependent gene expression, and define photoperiod as a crucial factor in the regulation of H₂O₂-induced cell death." Plant J **52**(4): 640-657.
- Reumann, S., L. Babujee, C. Ma, S. Wienkoop, T. Siemsen, G. E. Antonicelli, N. Rasche, F. Luder, W. Weckwerth and O. Jahn (2007). "Proteome analysis of Arabidopsis leaf peroxisomes reveals novel targeting peptides, metabolic pathways, and defense mechanisms." Plant Cell **19**(10): 3170-3193.
- Roitsch, T. (1999). "Source-sink regulation by sugar and stress." Curr Opin Plant Biol **2**(3): 198-206.
- Rosa, M., C. Prado, G. Podazza, R. Interdonato, J. A. Gonzalez, M. Hilal and F. E. Prado (2009). "Soluble sugars--metabolism, sensing and abiotic stress: a complex network in the life of plants." Plant Signal Behav **4**(5): 388-393.
- Sandhu, K. S., P. S. Koirala and M. M. Neff (2013). "The ben1-1 brassinosteroid-catabolism mutation is unstable due to epigenetic modifications of the intronic T-DNA insertion." G3 (Bethesda) **3**(9): 1587-1595.
- Schindelin, J., I. Arganda-Carreras, E. Frise, V. Kaynig, M. Longair, T. Pietzsch, S. Preibisch, C. Rueden, S. Saalfeld, B. Schmid, J. Y. Tinevez, D. J. White, V. Hartenstein, K. Eliceiri, P. Tomancak and A. Cardona (2012). "Fiji: an open-source platform for biological-image analysis." Nat Methods **9**(7): 676-682.
- Schwacke, R., A. Schneider, E. van der Graaff, K. Fischer, E. Catoni, M. Desimone, W. B. Frommer, U. I. Flugge and R. Kunze (2003). "ARAMEMNON, a novel database for Arabidopsis integral membrane proteins." Plant Physiol **131**(1): 16-26.
- Schwarzlander, M., M. D. Fricker, C. Muller, L. Marty, T. Brach, J. Novak, L. J. Sweetlove, R. Hell and A. J. Meyer (2008). "Confocal imaging of glutathione redox potential in living plant cells." J Microsc **231**(2): 299-316.

- Sharkey, T. D. (2005). "Effects of moderate heat stress on photosynthesis: importance of thylakoid reactions, rubisco deactivation, reactive oxygen species, and thermotolerance provided by isoprene." Plant Cell and Environment **28**(3): 269-277.
- Shelp, B. J. and A. Zarei (2017). "Subcellular compartmentation of 4-aminobutyrate (GABA) metabolism in arabidopsis: An update." Plant Signal Behav **12**(5): e1322244.
- Udvardi, M. K., T. Czechowski and W. R. Scheible (2008). "Eleven golden rules of quantitative RT-PCR." Plant Cell **20**(7): 1736-1737.
- Ushijima, T., K. Hanada, E. Gotoh, W. Yamori, Y. Kodama, H. Tanaka, M. Kusano, A. Fukushima, M. Tokizawa, Y. Y. Yamamoto, Y. Tada, Y. Suzuki and T. Matsushita (2017). "Light Controls Protein Localization through Phytochrome-Mediated Alternative Promoter Selection." Cell **171**(6): 1316-1325 e1312.
- von Arnim, A. G., Q. Jia and J. N. Vaughn (2014). "Regulation of plant translation by upstream open reading frames." Plant Sci **214**: 1-12.
- Waller, J. C., P. K. Dhanoa, U. Schumann, R. T. Mullen and W. A. Snedden (2010). "Subcellular and tissue localization of NAD kinases from Arabidopsis: compartmentalization of de novo NADP biosynthesis." Planta **231**(2): 305-317.
- Winter, D., B. Vinegar, H. Nahal, R. Ammar, G. V. Wilson and N. J. Provart (2007). "An "Electronic Fluorescent Pictograph" browser for exploring and analyzing large-scale biological data sets." PLoS One **2**(8): e718.
- Wongkaew, A., K. Asayama, T. Kitaiwa, S. I. Nakamura, K. Kojima, G. Stacey, H. Sekimoto, T. Yokoyama and N. Ohkama-Ohtsu (2018). "AtOPT6 Protein Functions in Long-Distance Transport of Glutathione in Arabidopsis thaliana." Plant Cell Physiol **59**(7): 1443-1451.
- Yamane, Y., Y. Kashino, H. Koike and K. Satoh (1998). "Effects of high temperatures on the photosynthetic systems in spinach: Oxygen-evolving activities, fluorescence characteristics and the denaturation process." Photosynthesis Research **57**(1): 51-59.
- Zarei, A., C. P. Trobacher and B. J. Shelp (2016). "Arabidopsis aldehyde dehydrogenase 10 family members confer salt tolerance through putrescine-derived 4-aminobutyrate (GABA) production." Sci Rep **6**: 35115.
- Zechmann, B., B. E. Koffler and S. D. Russell (2011). "Glutathione synthesis is essential for pollen germination in vitro." BMC Plant Biol **11**: 54.
- Zhai, Z. Y., S. R. Gayomba, H. I. Jung, N. K. Vimalakumari, M. Pineros, E. Craft, M. A. Rutzke, J. Danku, B. Lahner, T. Punshon, M. L. Guerinot, D. E. Salt, L. V. Kochian and O. K. Vatamaniuk (2014). "OPT3 Is a Phloem-Specific Iron Transporter That Is Essential for Systemic Iron Signaling and Redistribution of Iron and Cadmium in Arabidopsis." Plant Cell **26**(5): 2249-2264.
- Zhang, X., R. Henriques, S. S. Lin, Q. W. Niu and N. H. Chua (2006). "Agrobacterium-mediated transformation of Arabidopsis thaliana using the floral dip method." Nat Protoc **1**(2): 641-646.
- Zhang, Z. C., Q. Q. Xie, T. O. Jobe, A. R. Kau, C. Wang, Y. X. Li, B. S. Qiu, Q. Q. Wang, D. G. Mendoza-Cozatl and J. I. Schroeder (2016). "Identification of AtOPT4 as a Plant Glutathione Transporter." Molecular Plant **9**(3): 481-484.

Zhao, C., B. Liu, S. Piao, X. Wang, D. B. Lobell, Y. Huang, M. Huang, Y. Yao, S. Bassu, P. Ciais, J. L. Durand, J. Elliott, F. Ewert, I. A. Janssens, T. Li, E. Lin, Q. Liu, P. Martre, C. Muller, S. Peng, J. Penuelas, A. C. Ruane, D. Wallach, T. Wang, D. Wu, Z. Liu, Y. Zhu, Z. Zhu and S. Asseng (2017). "Temperature increase reduces global yields of major crops in four independent estimates." Proc Natl Acad Sci U S A **114**(35): 9326-9331.

Zhu, X., S. K. Thaler, Y. Takahashi, T. Berberich and T. Kusano (2012). "An inhibitory effect of the sequence-conserved upstream open-reading frame on the translation of the main open-reading frame of HsfB1 transcripts in Arabidopsis." Plant Cell Environ **35**(11): 2014-2030.

III. Manuscripts

III.II Manuscript 2

Investigation of three candidates for peroxisomal coenzyme A carrier proteins

Lennart Charton¹, Jannika Ewen¹, Wiebke Halpape², Carlo von Roermund³, Andreas Weber¹,
Nicole Linka^{1a}

¹ Heinrich-Heine-University Düsseldorf, Institute of Plant Biochemistry, Germany

² University of Bielefeld, Center of Biotechnology, Germany

³ University of Amsterdam, Laboratory Genetic Metabolic Diseases, Netherlands

^a Corresponding author

Abstract

Coenzyme A (CoA) is an essential cofactor in a plethora of metabolic pathways. Within peroxisomes, it is required for fatty acid degradation, hormone biosynthesis and propionate catabolism. CoA is synthesized in the cytosol; thus, specific transport proteins are required to guarantee an efficient flux across biological membranes. Mitochondrial CoA carrier have been identified and characterized in human, yeast and plants but the knowledge about a peroxisomal CoA carrier is restricted to non-plant organisms. Here we report the identification of three members of the mitochondrial carrier family that are localized to peroxisomes. Their amino acid sequence similarity to already characterized CoA carrier makes them promising candidates to transport CoA across the peroxisomal membrane. Thus, we call them peroxisomal CoA carrier (PCC) 1, 2 and 3. Due to their close homology to each other, functional redundancy cannot be excluded. Therefore, we used the CRISPR/Cas9 approach to generate single and double mutants. But, phenotypic analysis could neither detect a sucrose dependency nor 2,4-DB resistance, two marker assays for β -oxidation. Expression data revealed distinct functions of PCC1, PCC2 and PCC3 in wounding, phosphate starvation and germination, respectively with at least wounding and germination being directly connected to CoA metabolism. PCC1 was able to complement yeast mutants affected in peroxisomal NAD redox shuttles. But whether or not this is linked to its natural *in vivo* function or a result of the heterologous expression remains elusive since biochemical analyses could not reveal the transported substrates of the PCC proteins, yet.

Introduction

Coenzyme A (CoA) is an essential acyl group carrier and carbonyl-activating group and crucial for the proper functioning of fatty acid biosynthesis and β -oxidation, the citric acid cycle, sterol biosynthesis, and amino acid metabolism (Coxon et al. 2005; Tilton et al. 2006). Its biosynthesis starts with the condensation of pantoate and β -alanine to form pantothenate (vitamin B5) catalyzed by pantothenate synthase. While pantoate is synthesized from valine in the mitochondria (Coxon et al. 2005), the source of β -alanine is not known, but putative precursors are spermidine, isoleucine or uracil (Parthasarathy et al. 2019).

The conversion of pantothenate to dephospho-CoA over 4-phosphopantothenate (4-PP), 4-phosphopantothenoyl-CoA and 4-phosphopantothenine is localized to the cytosol (Tilton et al. 2006; Rubio et al. 2006; Rubio et al. 2008). Dephospho-CoA kinase catalyzes the last step by converting dephospho-CoA to CoA. Interestingly, according to proteomic data, dephospho-CoA kinase is localized to peroxisomes, mitochondria and chloroplasts but fluorescence protein fusions only confirmed the peroxisomal localization (Reumann et al. 2009; Ferro et al. 2010; Senkler et al. 2017). In yeast, *C. elegans* and mice CoA is catabolized by a nudix hydrolase to 4-PP and adenosine-3',5'-diphosphate (PAP) (Gasmi and McLennan 2001; AbdelRaheim and McLennan 2002; Reilly et al. 2008). In *Arabidopsis* such an activity has only been shown for the mitochondrial AtNUDT15. AtNUDT15 has a splice variant that unveils a putative peroxisomal targeting signal and masking of the mitochondrial target signal results in peroxisomal localization (Ito et al. 2012). This gives rise to a putative peroxisomal CoA salvage pathway (Figure 1).

CoA plays a central role within peroxisomal metabolism. Fatty acyl-CoA, released during germination in the cytosol is imported into peroxisomes for β -oxidation to provide energy for seedling establishment. The peroxisomal fatty acid transporter CTS cleaves off the CoA moiety during the import (Figure 1). Thus, re-esterification within peroxisomes is required before fatty acids can enter β -oxidation. This re-esterification is catalyzed by LACS6 and LACS7. A double mutant of both LACS genes is unable to degrade stored fatty acids, showing that fatty acids are imported as free fatty acids rather than as CoA esters (Fulda et al. 2004). But whether CoA is released into the peroxisomal lumen or the cytosol remains an open question. Beside storage oil mobilization, β -oxidation related processes like biosynthesis of the plant hormones JA and IAA or catabolism of BCAA also require esterification of the respective precursor with CoA.

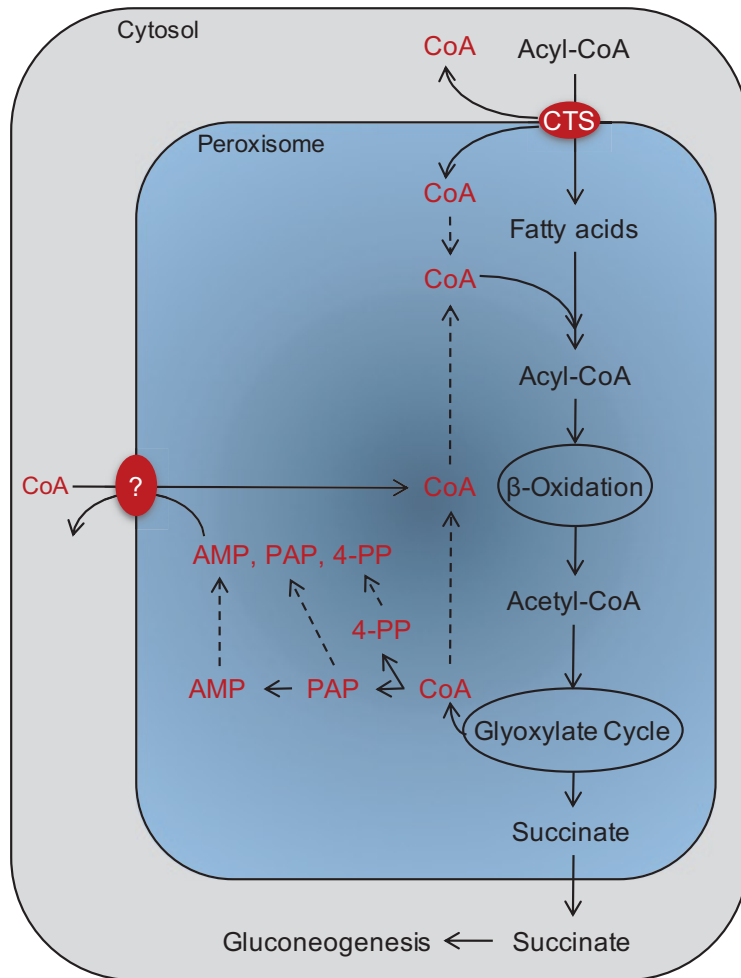


Figure 1: Peroxisomal CoA metabolism

Within peroxisomes CoA is required to activate fatty acids prior entering β -oxidation. The resulting Acetyl-CoA enters the glyoxylate cycle to produce succinate for gluconeogenesis. During this, CoA is cleaved off and can be either reused for esterification or be degraded to PAP and 4-PP. PAP can be further hydrolyzed to AMP. 4-PP, PAP and AMP might serve as an exchange substrate for the CoA import. CoA, Coenzyme A; PAP, adenosine-3',5'-diphosphate; 4-PP, 4-phosphopantothenate; AMP, adenosine monophosphate. Modified after (Charton et al. 2019).

The distribution of CoA biosynthesis and metabolism to different organelles requires an efficient transport system across biological membranes.

Interestingly, all CoA carrier identified so far are members of the mitochondrial carrier family (MCF). Despite their name, these proteins are not restricted to mitochondria. Members of this family have been also found in chloroplasts, peroxisomes, the plasma membrane and the endoplasmatic reticulum (ER).

The first identified CoA carrier was the mitochondrial localized Leu5p in yeast. Cells lacking Leu5p are restricted in growth on non-fermentable carbon sources and mitochondrial CoA levels are reduced (Prohl et al. 2001). Functional complementation of $\Delta leu5$ led to the identification of the mitochondrial CoA carriers in human and its homolog in *Drosophila*

(Slc25a42) as well as to two CoA carriers from Arabidopsis and maize (CoAC1&2) (Fiermonte et al. 2009; Zallot et al. 2013; Vozza et al. 2017).

Biochemical characterization of the human Slc25a42 showed that it is able to additionally catalyze the transport of dephospho-CoA and PAP. However, its homolog in *Drosophila* was shown to be also capable in transporting dephospho-CoA, but no transport activity for CoA could be observed. Because of the proposed subcellular localization of some CoA biosynthetic pathway enzymes and due to the fact that it is still able to complement the $\Delta leu5$ mutant, the authors suggested, that dephospho-CoA is imported into mitochondria for the conversion to CoA or exported for CoA biosynthesis in the cytosol (Vozza et al. 2017).

The first characterized peroxisomal CoA carrier was the human Slc25a17 (Agrimi et al. 2012). The authors showed, that the carrier also accepts dephospho-CoA and PAP in addition to CoA. This gives rise to the question, whether CoA or dephospho-CoA is imported into peroxisomes and if peroxisomes harbor a salvage pathway for CoA. More recently the homolog of Slc2517 was identified in zebrafish to transport CoA (Kim et al. 2019). The carrier is able to transport AMP against CoA *in vitro* and the β -oxidation phenotype of zebrafish embryos with reduced Slc25a17 activity could be rescued by the injection of CoA.

The respective plant peroxisomal CoA carrier is still missing. A putative candidate to mediate this transport was the peroxisomal NAD carrier PXN since it was shown to accept CoA as substrate *in vitro* (Agrimi et al. 2012; Bernhardt et al. 2012). But due to its low affinity to CoA it is unlikely that PXN is able to transport CoA under physiological conditions (van Roermund et al. 2016).

Material and Methods

Bacteria strains and growth conditions

Chemical competent Mach1 *E.coli* cells (Invitrogen, Karlsruhe, Germany) were used for plasmid transformation and amplification. Cells were grown at 37 °C either in liquid medium shaking at 190 rotations per minute (rpm) or on solid Luria-Bertani (LB) medium. *Agrobacterium tumefaciens* strain GV3103 was used for transient transformation of *Nicotiana benthamiana* and was grown at 28 °C either shaking at 150 rpm in liquid YEB medium or on agar plates. For selection purposes, appropriate antibiotics were added to the growth medium.

Transformation of Bacteria

Plasmid DNA was introduced into competent Mach1 *E.coli* cells using heat-shock method (Inoue et al. 1990). Afterwards, the cell suspension was spread on LB-agar plates containing appropriate antibiotics and was incubated overnight at 37 °C.

Chemo-competent *A. tumefaciens* cells were transformed following the freeze-thaw heat-shock method (Hofgen and Willmitzer 1988). Afterwards, single colonies were picked, transferred to new selection plates and incubated for additional 2 d at 28 °C.

Saccharomyces cerevisiae strain and growth conditions

The uracil auxotrophic *Saccharomyces cerevisiae* strain INVSc1 (Invitrogen) was used for heterologous protein expression. For the complementation assay, the following mutants were used: *mdh3* Δ (malate dehydrogenase 3), *gpd1* Δ (glycerol-3-phosphate dehydrogenase 1) and *ant1* Δ (peroxisomal adenine nucleotide transporter 1) and combinations thereof. Mutants were constructed from BJ1991 as described by van Roermund et al. 1995. Cells were grown at 30 °C either shaking at 150 rpm in liquid medium or on agar plates. YPD and YNB medium were used as complex and minimal medium, respectively.

Transformation of *S. cerevisiae*

Transformation of Yeast cells was conducted after standard protocol (Gietz and Schiestl 2007). Yeast cells were selected on synthetic complete medium (SC; 0.67% (w/v) YNB supplemented with appropriate amino acids for auxotrophy and a carbon source).

Determination of β -oxidation activity

β -oxidation activity assays in intact yeast cells were performed as described previously (van Roermund et al. 1995). For this, cells were grown 17 h in oleate-containing media to induce β -oxidation. β -oxidation activity was measured in 200 μ l of 50 mM MES (pH 6.0) and 0.9%

(w/v) NaCl supplemented with 10 μM [1- ^{14}C]-octanoate. Subsequently, [1- ^{14}C]- CO_2 was trapped with 2 M NaOH and used to quantify the rate of fatty acid oxidation. Results are presented as relative activity with WT values set to 100 %.

Plant growth conditions

Arabidopsis thaliana ecotype Columbia (Col-0) was used as WT in this thesis. Seeds were surface-sterilized with chloric gas by adding 3 ml concentrated HCl to 100 ml NaClO in a desiccator for 2 hours. Seeds were placed under the clean bench to allow evaporation of residual chloric gas. Stratification was performed for 3 days in the dark at 4°C. If not stated otherwise plants were grown under normal day conditions (12 h light / 12 h dark) at 22/18 °C and a light intensity of 100 $\mu\text{M m}^{-2} \text{ s}^{-1}$ on agar plates supplemented with 1 % (w/v) sucrose. Two to three weeks old seedlings were transferred to soil (3/4 Floraton, 1/4 Arabidopsis substrate) and were further cultivated under long-day conditions.

Transformation of Arabidopsis

For the generation of stable transformed Arabidopsis lines, agrobacterium-mediated transformation was conducted according to the floral-dip method (Zhang et al. 2006). After maturation, seeds of the transformed plants (F_0) were dispersed on MS-agar plates and selected by antibiotic resistance.

Isolation of Arabidopsis genomic DNA

Arabidopsis gDNA was isolated by isopropanol precipitation (Weigel and Glazebrook, 2001) For this, one leaf was harvested, frozen in liquid nitrogen and grinded in a bead mill (30 Hz, 30 seconds). Afterwards, 400 μl extraction buffer (0.2 M Tris-HCl, pH7.5 (HCL), 0.25 M NaCl, 0.025 M EDTA, 0.5 % (w/v) SDS) were added to the powder, inverted several times and centrifuged at maximum speed for 5 min. The resulting supernatant was added to 300 μl isopropanol, mixed by pipetting up and down and centrifuged again at maximum speed for 5 min. After carefully discarding the supernatant, the pellet was washed 3 times with 70 % ethanol, drained and dried. The dried pellet was subsequently dissolved in 100 μl TE buffer and stored at -20 °C. For large screening purposes, the Phire Plant gDNA extraction and direct PCR kit (ThermoFischer) was used according to the manufacturer's instructions.

Arabidopsis RNA isolation and cDNA synthesis

Isolation of leaf RNA for cDNA synthesis was performed with the EURx GeneMATRIX Universal RNA purification kit (Roboklon, Berlin, Germany). Prior cDNA synthesis, residual DNA was degraded by RQ1 RNase-free DNase (Promega, Madison, USA). cDNA synthesis itself was performed using the LunaScript RT SuperMix kit (NEB).

CLSM of Tobacco protoplasts

Overnight culture of *A. tumefaciens* were harvested via centrifugation (10 min, 3000 g) and resuspended in infiltration buffer (10 mM MgCl₂, 10 mM MES, pH 5.7, 100 μM acetosyringone). For colocalization, young *N. benthamiana* leaves were co-infiltrated with the protein of interest fused to a yellow fluorescent protein (VENUS) together with a cyan fluorescent protein (CFP) c-terminally fused to a peroxisomal target signal (SKL). Suspension was diluted to an OD₆₀₀ of 0.5 before infiltration. Plants were subsequently grown at long day conditions (16 h/8 h) for two days before protoplast isolation. For protoplast isolation, *N. benthamiana* leaves were cut into small pieces, vacuum infiltrated and incubated in protoplast digestion solution (1.5 % (w/v) cellulase R-10, 0.4 % (w/v) macerozyme R-10, 0.4 M mannitol, 20 mM KCl, 20 mM MES pH 5.6 (KOH), 10 mM CaCl₂, 0.1 % (w/v) BSA) for 2 h at 30 °C. Isolated protoplasts were resuspended in W5 solution (154 mM NaCl, 125 mM CaCl₂, 5 mM KCl, 2 mM MES pH5.6 (KOH)). Protoplasts were directly used for microscopy and analyzed using a Zeiss LSM 780 Confocal Microscope and Zeiss ZEN software. Excitation/emission settings used in this study: YFP (514 nm / 493 to 550 nm), CFP (405 nm / 435 to 485 nm) and Chlorophyll A (488 nm / 640 to 710 nm). Pictures were processed using Fiji software (Schindelin et al. 2012).

Genotyping of tDNA insertion lines

Gene specific and tDNA specific PCRs were performed to verify the tDNA insertion line SAIL_736_H08 of the *PCC1* gene. For the gene specific product, primer were chosen flanking the tDNA insertion site (AK7: ACCATGATAGGGGAATCATGG; AK8: GTCATTTTCATCGAGCGAGAAG). For the tDNA specific PCR, each gene specific primer was combined with a tDNA specific primer (P48: TTCATAACCAATCTCGATACAC).

Generation and verification of mutants generated by CRISPR/Cas9

For the phenotypic analysis, *pcc1*, *pcc2* and *pcc3* single as well as *pcc2/pcc3* double mutant lines were generated using the CRISPR/Cas9 system. Target sites were chosen and integrated into the Cas9 expression vector system as described in Hahn et al. (2017, 2018).

For the screening of positive Cas9 cutting events, a restriction fragment length polymorphism (RFLP) assay was performed. This assay is based on the fact, that the Cas9 cutting site within the sgRNA target sequence encodes for a restriction enzyme recognition site, that, upon Cas9 mediated mutation, gets destroyed. Hence, amplification of the flanking regions with followed by a restriction digest leads to different cutting patterns visible by agarose gel electrophoresis. sgRNA sequences, primer combinations and enzymes used for RFLP are listed in table X. Primer sequences and sgRNA positions are shown in Figure S1.

Table 1: CRISPR/Cas9 and RFLP related sequences and products

Gene	sgRNA sequence	Primer	PCR product	Enzyme	RFLP
PCC1	CTAGGGTTGGTGTGAGCTCAGG	LC200/LC201	682 bp	SacI-HF	508 + 174 bp
PCC2	AGAGTCGGTGTTCGGTCGATGG	LC204/LC205	245 bp	TaqI	165 + 80 bp
PCC3	TCTTGAGCAGTCCAAACATTTGG	LC207/LC208	906 bp	BstXI	574 + 332 bp

Expression analysis of RNA-Seq experiments

7143 SRA data files containing non-mutant *Arabidopsis* Illumina samples were downloaded from NCBI and mapped onto the TAIR10 transcriptome, representative isoforms only using kallisto v0.44.0 (for single-end reads: --single -l <as given by SRA-file> -s 30; for paired-end reads default). The resulting data was collated into a single table.

Protein expression and reconstitution into liposomes

Heterologous protein expression for uptake experiments was conducted either in living yeast cell or cell-free using the RTS Wheat Germ CECF kit (biotechrabbit). Yeast galactose-inducible protein expression, harvesting and enrichment of the total membrane fraction was performed according to (Bouvier et al. 2006). Cell-free protein expression was conducted according to the manufacturers instruction and modified as described in (Bernhardt et al. 2012). Freeze-thaw sonification procedure was used for the reconstitution of heterologous proteins (Palmieri et al. 1995). The non-incorporated counter exchange substrate was removed by passing proteoliposomes over Sephadex PD-10 columns (GE Healthcare) pre-equilibrated with PD-10 buffer (10 mM Tricine-KOH, pH 7.6, 100 mM Na-gluconate, 40 mM Ka-gluconate).

Time dependent uptake experiments

To analyze transport activity, uptake of radioactively labeled substrates was measured at six different time points over 32 min. The reaction was started by adding 950 μ l of the proteoliposome suspension either with or without substrate preloading to 50 μ l transport medium (1 μ Ci radioactively labeled substrate; 4 mM non-labeled substrate; filled up to 50 μ l with PD-10 buffer). The reaction was stopped by loading 140 μ l of the proteoliposomes on Dowex columns filled with anion-exchange Resin, 100-200 dry mesh size, acetate-form (Bio-Rad). Columns were preequilibrated with Dowex-buffer (150 mM Na-acetate, pH 7.6). The Dowex columns were washed with 350 μ l and 500 μ l Dowex buffer. The flow through was collected in 20 ml scintillation vials containing 10 ml ddH₂O. The uptake of labeled substrates was measured in a scintillation counter as counts per minute (CPM). For the subsequent analysis of uptake rates three standards were prepared with 10 ml ddH₂O or scintillation cocktail and 5 μ l transport medium to determine the concentration of the labeled molecule as a function of the measured CPM.

Results

In 2009 the group of Carrie et al. identified At3g55640, a member of the mitochondrial carrier family, to be dual-targeted to mitochondria and peroxisomes (Carrie et al. 2009). Because of its amino acid similarity to calcium dependent ATP/Phosphate carrier (APCs) it was previously termed calcium dependent carrier 1 even though it does not contain calcium binding domains (Haferkamp and Schmitz-Esser 2012; Cassin-Ross and Hu 2014; Lorenz et al. 2015). In Arabidopsis, At3g55640 clusters together with different groups of adenine nucleotide carriers but also with CoA carriers from Arabidopsis, human and Yeast (Figure 2).

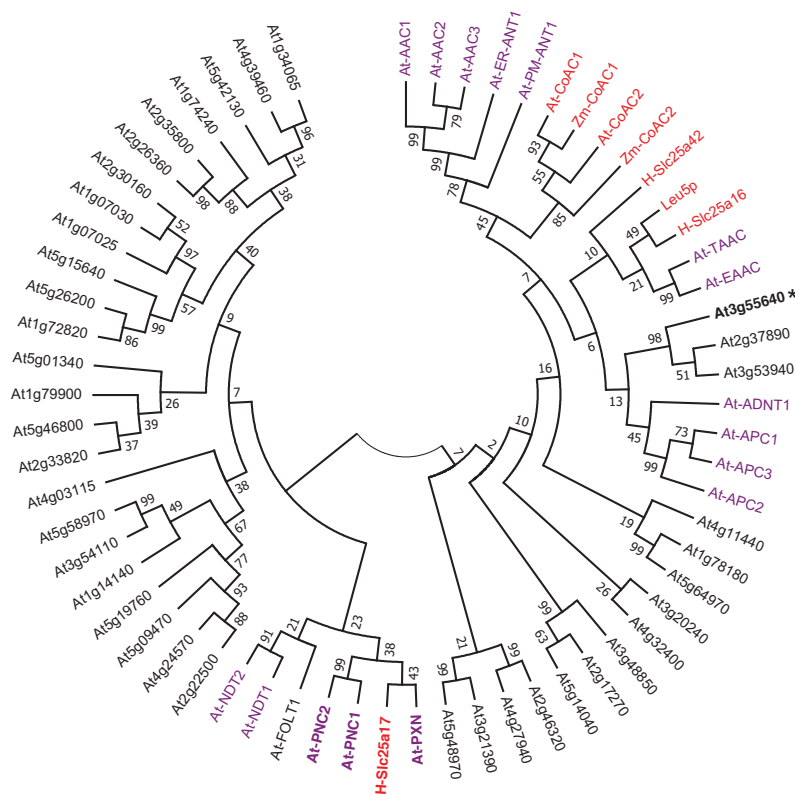


Figure 2: Phylogenetic tree of plant mitochondrial carrier family proteins

Phylogenetic tree of the plant mitochondrial carrier family together with known and putative CoA carriers from maize, human and yeast by amino acid similarities. Tree was generated with Mega7 using Neighbor-Joining method and JTT model of amino acid substitution with gaps and missing data being eliminated. Numbers at nodes represent bootstrap values of 1000 replications. Known adenine nucleotide carriers are labeled in magenta regardless of their subcellular localization. Peroxisomal localized proteins are depicted in bold letters and known and putative CoA carrier are labeled in red. At, *Arabidopsis thaliana*; Zm, *Zea mays*; H, *Homo sapiens*; AAC, ATP/ADP carrier; ER-ANT1, adenine nucleotide carrier 1 of the endoplasmic reticulum; PM-ANT1, ANT1 of the plasma membrane; CoaC, Coenzyme A carrier; Leu5p, yeast mitochondrial CoA carrier; TAAC, thylakoid ATP/ADP carrier; EAAC, putative envelope ATP/ADP carrier; ADNT1, mitochondrial adenine nucleotide transporter 1; APC, calcium-dependent mitochondrial Mg-ATP/Phosphate carrier; PXN, peroxisomal NAD carrier; PNC, peroxisomal adenine nucleotide carrier; FOLT1, mitochondrial folate transporter 1; NDT, mitochondrial NAD carrier.

The closest Arabidopsis homologs of At3g55640 are At2g37890 and At3g53940 with At2g37890 and At3g53940 being more closely related to each other than to At3g55640. All MCF carrier share 3 highly conserved motifs consisting of two alpha helical transmembrane domains, each (Figure 3, underlined).

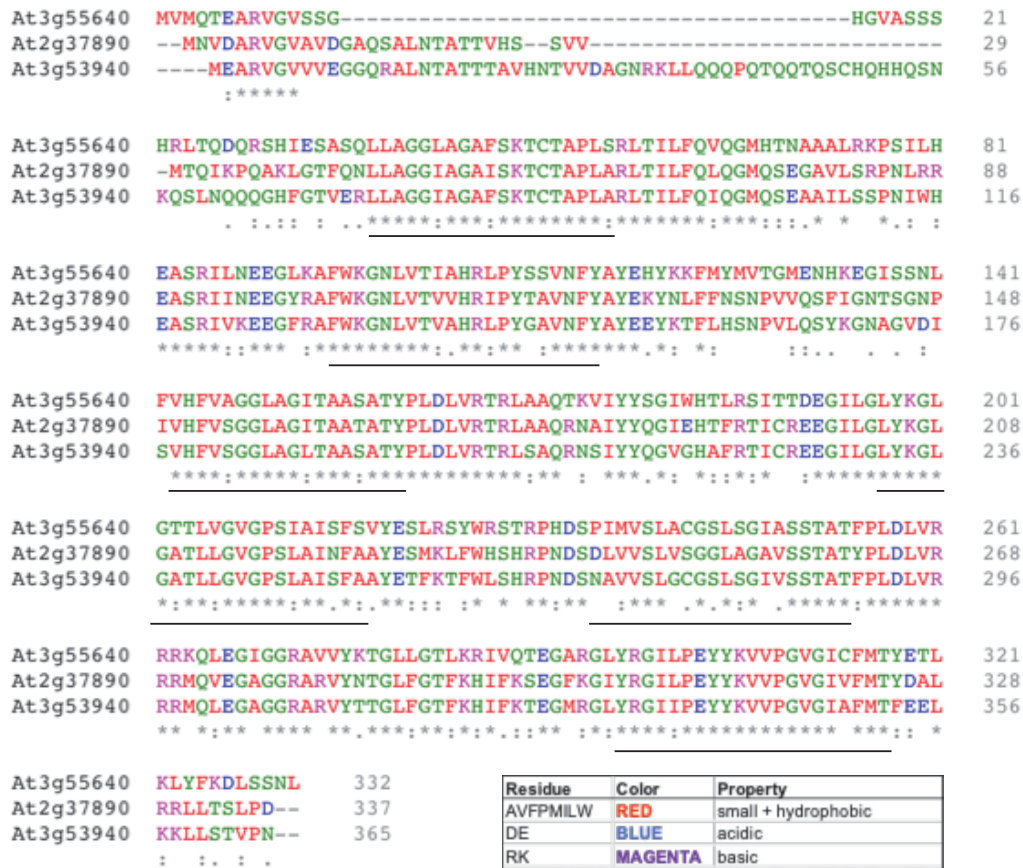


Figure 3: Amino acid sequence alignment

Protein alignment of At3g55640, At2g37890 and At3g53940 generated multiple sequence alignment with Clustal Omega (Sievers et al. 2011). Color code of amino acids as indicated in the table. *: complete alignment; Predicted transmembrane domains of At3g55640 are underlined.

The N-termini differ between these three proteins, whereas the rest of the amino acid sequence is pretty conserved. At3g53940 has the longest N-terminal extension which consists of 38 additional amino acids compared to At3g55640. The N-terminus of At2g37890 contains 7 additional amino acids.

Due to the high similarity of At2g37890 and At3g53940 to At3g55640 we further analyzed their subcellular localization. For this and to confirm the peroxisomal localization of At3g55640, c-terminally tagged yellow fluorescence protein (Venus) versions of all three proteins were transiently expressed in tobacco leaves together with a cyan fluorescence protein (CFP) fused to a peroxisomal targeting signal 1 (PTS1) as peroxisomal marker (Figure 4).

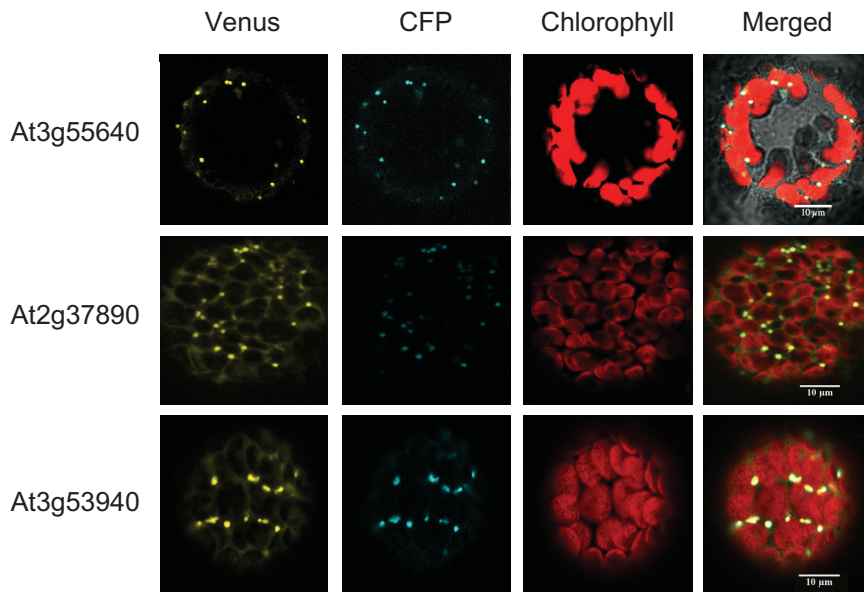


Figure 4: Confocal laser scanning microscopy of tobacco leaf protoplasts

Protein-YFP fusions were transiently expressed in tobacco leaves together with CFP-SKL as peroxisomal marker. Isolated leaf protoplasts were analyzed by confocal laser scanning microscopy (CLSM) after 2 days of expression. First panel on the left shows Venus signal of the protein fusions, followed by the CFP signal of the peroxisomal marker and the autofluorescence of the chlorophyll. The fourth panel shows the merged picture of all three channels.

As indicated by the merged picture (Figure 4) all three proteins localize exclusively to peroxisomes. This, together with the close relationship to already characterized CoA carrier makes them promising candidates for being peroxisomal CoA carrier. Thus, At3g55640, At2g37890 and At3g53940 are further referred to as peroxisomal coenzyme A carrier 1, 2 and 3 (PCC1, PCC2 and PCC3), respectively.

Establishing single and double mutants of *PCCs* by genome editing.

tDNA insertion lines of the PCC genes were ordered to further investigate their role within plant peroxisomal metabolism. For PCC1 there is an insertion line available, where the tDNA is integrated at the very end of the second exon (Figure 5C). The absence of a *pcc1* full length transcript confirmed that *pcc1-1* represents a knock-out of the gene (Figure 5B).

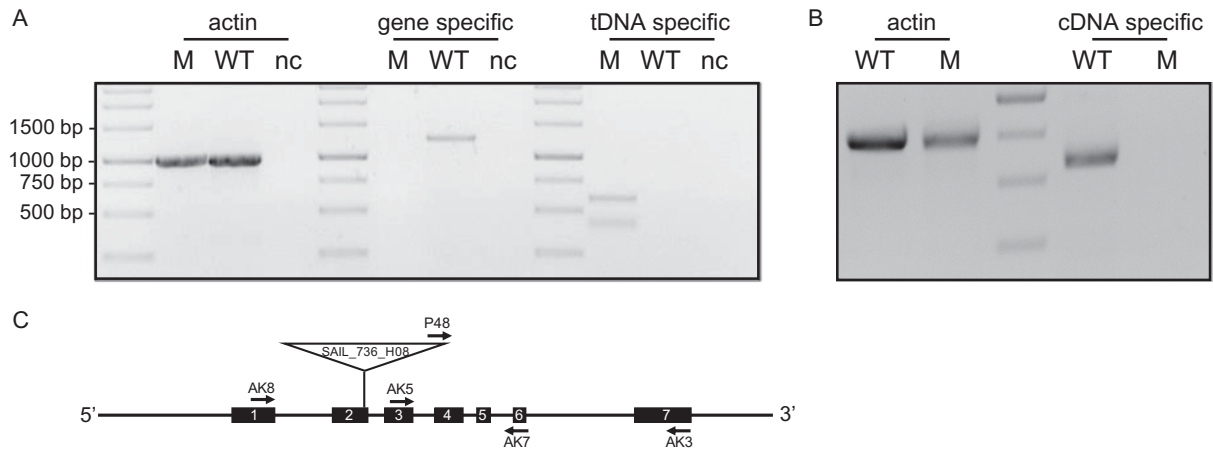


Figure 5: Genotyping of PCC1 tDNA insertion line SAIL_736_H08

(A) Gene (AK8/AK7: 1269 bp) and tDNA (AK8/P48: 400-600 bp) specific PCR on WT and *pcc1-1* gDNA to verify tDNA insertion in *pcc1-1*. Actin specific PCR (P33/P34: 977 bp) was performed as loading and positive control. For negative control (nc) template DNA was substituted by water. (B) Actin (P67/P68: 734 bp) and gene (AK5/AK3: 589 bp) specific PCR on WT and *pcc1-1* cDNA to check for the presence of *pcc1* transcript. (C) Gene architecture of *PCC1* with exons (black squares), introns (lines), primer binding sites and localization of the tDNA insertion (triangle).

In case of PCC2 there are no tDNA lines available carrying the integration in an exon region. The integration within the 5' or 3' UTR leads to rather unpredictable results, since the insertion might additionally regulate the activity of neighboring genes. For a PCC3 tDNA insertion line the integration of the tDNA in the specified exon of the gene could not be confirmed. Thus, genome editing by CRISPR/Cas9 was employed to generate single mutants of each gene (Hahn et al. 2017). Due to the close homology of the PCC proteins and especially of PCC2 and PCC3 (Figure 2), functional redundancy cannot be excluded. Thus, double and triple mutants might be necessary to identify respective phenotypes. So far, single mutants for all three genes and a double mutant for the most closely related genes *pcc2* and *pcc3* could be established (Table 1).

Table 1: Mutant lines of PCC proteins obtained by genome editing using CRISPR/Cas9

Target sequence of the sgRNA and the effect of Cas9 in the mutant line compared to the WT sequence. Changes in the nucleotide sequence are highlighted in red. The protospacer adjacent motif is shown in green. Effect on the protein sequence: WT amino acids are underlined and bold. Amino acids that differ from WT are shown in italic letters. The red asterisk shows the position of the early stop-codon. Protein size shows the number of WT amino acids in the mutant relative to the full-length protein.

Mutant		sgRNA target sequence	Protein sequence	Protein size
<i>pcc1-2</i>	<i>PCC1</i>	WT CTAGGGTTGGTGTGAG--CTCAGG	<u>MVMQTEARVGV</u> <i>RLRTWRSFVSSFNAGPEITYRIGVAALS</i>	12/332 aa
	Mutant	CTAGGGTTGGTGTGAGACTCAGG	<i>RRTRWCF*</i>	
<i>pcc2-1</i>	<i>PCC2</i>	WT AGAGTCGGTGTGCGGT--CGATGG	<u>MNV DARVGVAV</u> <i>RWSSECS*</i>	11/337 aa
	Mutant	AGAGTCGGTGTGCGGTACGATGG		
<i>pcc3-1</i>	<i>PCC3</i>	WT TCTTGAGCAGTCCAAACATTGG	<u>MEARVGVVVEGGQRALNTATTTAVHNTVVDAGNRKLLQQ</u> <u>QPQTQQTSCHQHHQSNKQSLNQQQGHFGTVERLLAGG</u>	111/365 aa
		Mutant TCTTGAGC-----TTTGG	<i>IAGAFSKTCTAPLARLTILFQIQGMQSEAAILSRMKLRVLL</i> <i>RRKVLEHFGKETWLL*</i>	
<i>pcc3-2</i>	<i>PCC3</i>	WT TCTTGAGCAGTCCAAACATTGG	<u>MEARVGVVVEGGQRALNTATTTAVHNTVVDAGNRKLLQQ</u> <u>QPQTQQTSCHQHHQSNKQSLNQQQGHFGTVERLLAGG</u>	113/365 aa
		Mutant TCTTGAGCAGTCCAA---ATTTGG	<i>IAGAFSKTCTAPLARLTILFQIQGMQSEAAILSSPN</i> <i>LA*</i>	
<i>pcc2/3</i>	<i>PCC2</i>	WT AGAGTCGGTGTGCGGT--CGATGG	<u>MNV DARVGVAV</u> <i>RWSSECS*</i>	11/337 aa
		Mutant AGAGTCGGTGTGCGGTCCGATGG		
	<i>PCC3</i>	WT TCTTGAGCAGTCCAAAC--ATTTGG	<u>MEARVGVVVEGGQRALNTATTTAVHNTVVDAGNRKLLQQ</u> <u>QPQTQQTSCHQHHQSNKQSLNQQQGHFGTVERLLAGG</u>	113/365 aa
		Mutant TCTTGAGCAGTCCAAACTATTTGG	<i>IAGAFSKTCTAPLARLTILFQIQGMQSEAAILSSPN</i> <i>YLA*</i>	

In all established mutant lines, the cutting event of Cas9 resulted in a frame shift and as a consequence of this to an altered amino acid sequence and early stop codon. Since the sgRNA target sequence for *PCC1* and *PCC2* directs the Cas9 to the first exon, each, only 12 and 11 amino acids of the resulting proteins correspond to the WT sequence, respectively. For *PCC3*, the target sequence is located in the second exon which is why the deletions in *pcc3-1* (10 bp) and *pcc3-2* (2 bp) result in proteins that still have about one third of the WT length. The same holds true for the single insertion in *PCC3* in the *pcc2/3* double mutant. All lines are homozygous for the respective mutation and free of the Cas9 construct. The latter is of special importance to exclude insertional effects of the Cas9-cassette on the observed phenotype.

Phenotyping of *pcc* mutant plants

Peroxisomal β -oxidation is essential for storage oil mobilization during germination. Thus, mutants that are compromised in this process demand on the supply with an exogenous carbon source to enable seedling establishment. Since CoA plays a pivotal role for the activation of fatty acids prior β -oxidation, plants lacking the ability to import CoA into the peroxisomal lumen should be affected in storage oil mobilization. To test this, *pcc1*, *pcc2* and *pcc3* mutant lines were grown in the presence and absence of sucrose and root length was measured 6 days after germination (Figure 6).

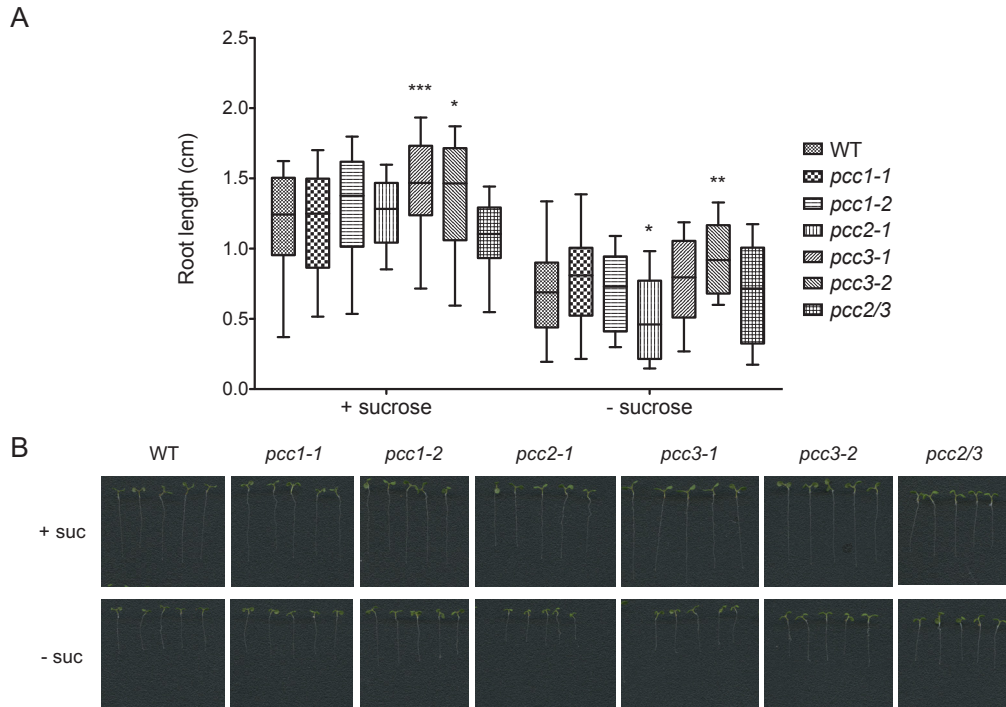


Figure 6: Root growth in the presence and absence of sucrose

Sucrose dependency assay to determine a defect in storage oil mobilization. Plants were grown for 6 days in the presence or absence of 1 % (w/v) sucrose in ambient CO₂ (300 ppm) and a 12 h/12 h (light/dark) day rhythm. (A) Root length was measured as a function of plant growth. Two-way ANOVA was used to test for significant differences; $n > 40$; *: $p < 0.05$; **: $p < 0.01$; ***: $p < 0.001$. (B) Representative images of the different lines grown with (upper panel) or without (lower panel) sucrose.

Interestingly, both mutants of *pcc3* (*pcc3-1* and *pcc3-2*) show an even increased root length in the presence of sucrose, whereas all other lines do not significantly differ from the WT. In the absence of sucrose, only *pcc2-1* revealed a significantly decreased root length compared to the WT. Again, *pcc3-2* showed a significantly increased root length compared to the WT. But in contrast to seedlings grown in the presence of sucrose, the root length of *pcc3-1* is slightly but not significantly increased. The *pcc2/3* double mutant revealed WT-like growth both in the presence and absence of sucrose.

To further narrow down a phenotype of the different *pcc* mutants to the process of β -oxidation, seedlings were grown for 6 days in the presence of the synthetic auxin precursor 2,4-DB. Like IBA, 2,4-DB is processed by one cycle of β -oxidation to yield its active compound 2,4-D which is a strong root growth inhibitor. Mutants that are affected in β -oxidation are more resistant towards 2,4-DB because it cannot be metabolized. Since 2,4-DB has to be activated by esterification with CoA, mutants lacking peroxisomal CoA import should be resistant as well.

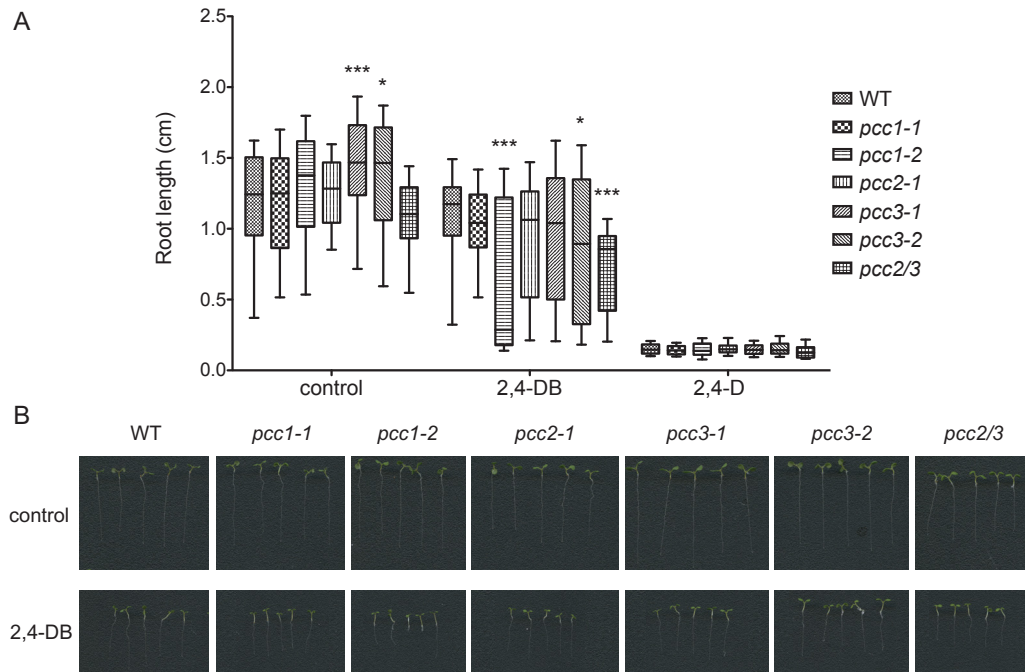


Figure 7: Root growth in the presence of the synthetic auxin precursor 2,4-DB

2,4-DB is a synthetic auxin precursor that is converted by peroxisomal β -oxidation to its active compound 2,4-D, a strong root growth inhibitor. Plants were grown for 6 days in the presence of 0.8 μ M 2,4-DB, 0.2 μ M 2,4-D or without additives (control) in ambient CO₂ (300 ppm) and a 12 h/12 h (light/dark) day rhythm. (A) Root length was measured as a function of plant growth. Two-way ANOVA was used to test for significant differences; $n > 41$; *: $p < 0.05$; ***: $p < 0.001$. (B) Representative images of the different lines grown without additives (upper panel) or in the presence of 2,4-DB (lower panel).

In the presence of 2,4-DB root lengths of *pcc2-1* and the *pcc2/3* double mutant are severely decreased compared to the WT. While *pcc3-2* also showed a decreased root length when grown in the presence of 2,4-DB, *pcc3-1* did not. But, since both mutants had significantly longer roots on the control plate, *pcc3-1* seems to be more sensitive to 2,4-DB, too. There is no significant difference between the lines when grown on plates supplemented with 2,4-D, which indicates, that there is no difference in the perception of the synthetic auxin causing the observed phenotypes.

PCC1 yeast complementation assay

Yeast complementation assays were performed to further analyze the *in vivo* function of PCC1. Therefore, mutants of different peroxisomal proteins were transformed with the Arabidopsis *PCC1* and the rate of C8:0 β -oxidation was measured (Figure 8A). Ant1p is the peroxisomal adenine nucleotide transporter responsible for the exchange of ATP against AMP to enable activation of fatty acids prior entering β -oxidation. Glycerol-3-phosphate dehydrogenase 1 (Gpd1p) and malate dehydrogenase 3 (Mdh3p) are part of the NAD redox shuttles to regenerate NAD that is reduced in the β -oxidation cycle (Figure 8B).

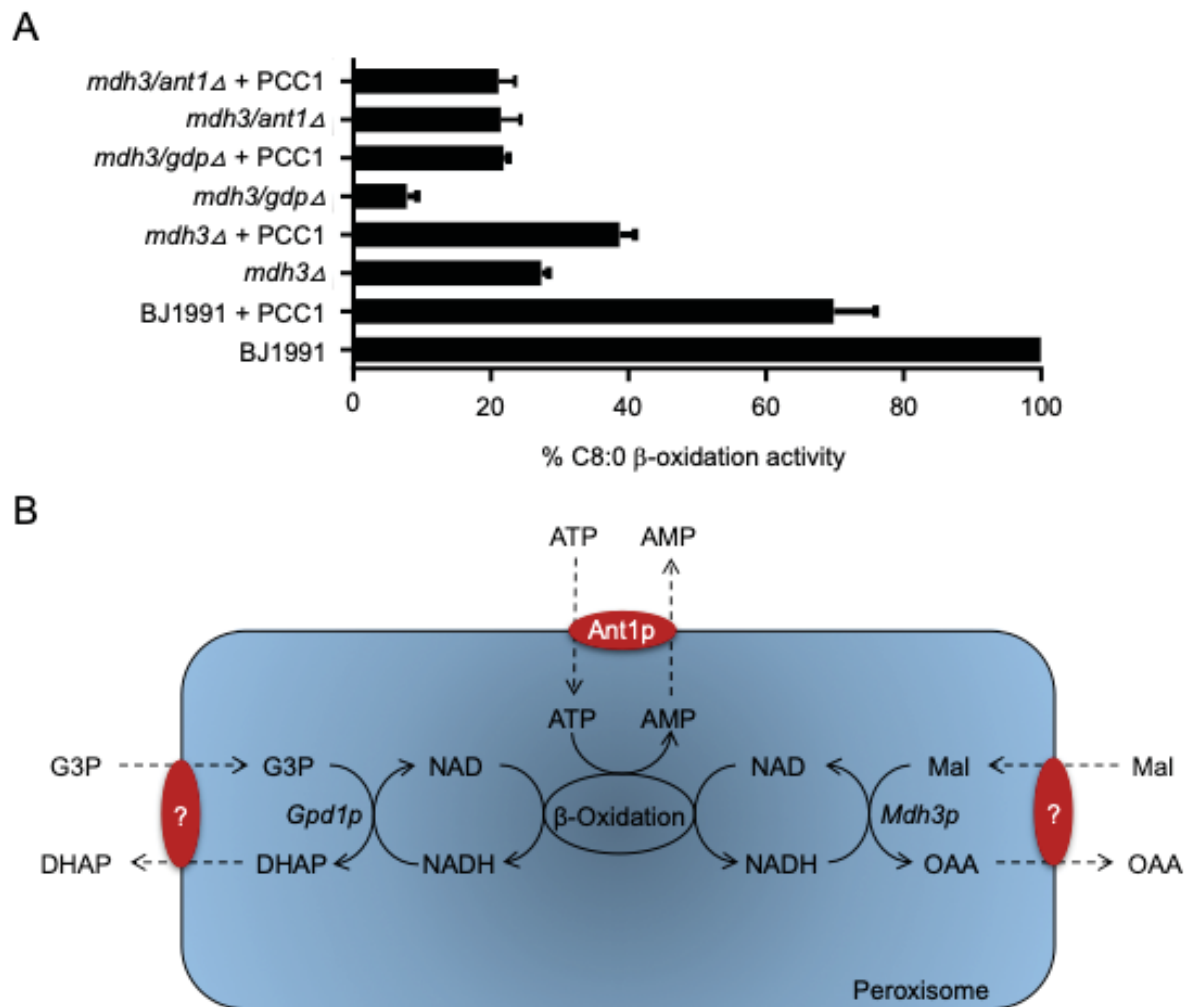


Figure 8: C8:0 β -oxidation activity of different intact yeast mutant and PCC1 complementation lines

(A) β -oxidation activity of C8:0 in oleate-induced yeast WT (BJ1991) and mutant lines either transformed with empty vector or *PCC1*. Activity of the WT was set to 100 %. Data represent mean + SD of technical duplicates. The mutant lines are showed as follows: *mdh3* Δ : malate dehydrogenase 3; *gpd1* Δ : glycerol-3-phosphate dehydrogenase 1; *ant1* Δ : adenine nucleotide transporter 1 and double mutants thereof. (B) Scheme of peroxisomal ATP supply and redox shuttles required for functional β -oxidation in yeast. ATP: adenosine triphosphate; AMP: adenosine monophosphate; G3P: glycerol-3-phosphate; DHAP: dihydroxyacetone phosphate; Mal: malate; NAD nicotinamide dinucleotide (oxidized); NADH: nicotinamide dinucleotide (reduced); OAA: oxaloacetate.

The activity of C8:0 β -oxidation in the WT transformed with PCC1 already resulted in a drop to about 70 % of the control values. Mutants that are affected in the peroxisomal redox shuttle showed a severe decrease in β -oxidation activity to 25 % and 5 % in *mdh3* Δ and *mdh3/gpd1* Δ , respectively. In both mutants, the transformation with *PCC1* lead to an increase of β -oxidation activity to about 40 % (*mdh3* Δ) and 20 % (*mdh3/gpd1* Δ) of the WT values. Interestingly, PCC1 was not able to increase β -oxidation activity in the *mdh3/ant1* Δ double mutant that was reduced to 20 % of control values.

PCC expression data extracted from publicly available RNA-Seq experiments

To further investigate the function of the PCC proteins, RNA-Seq experiments from the sequence read archive (SRA) of the national center for biotechnology information (NCBI) were analyzed and sorted according to the highest expression of the individual PCCs. PCC1 showed the highest expression after methyl-jasmonate (MeJA) treatment and after wounding (Figure 9).

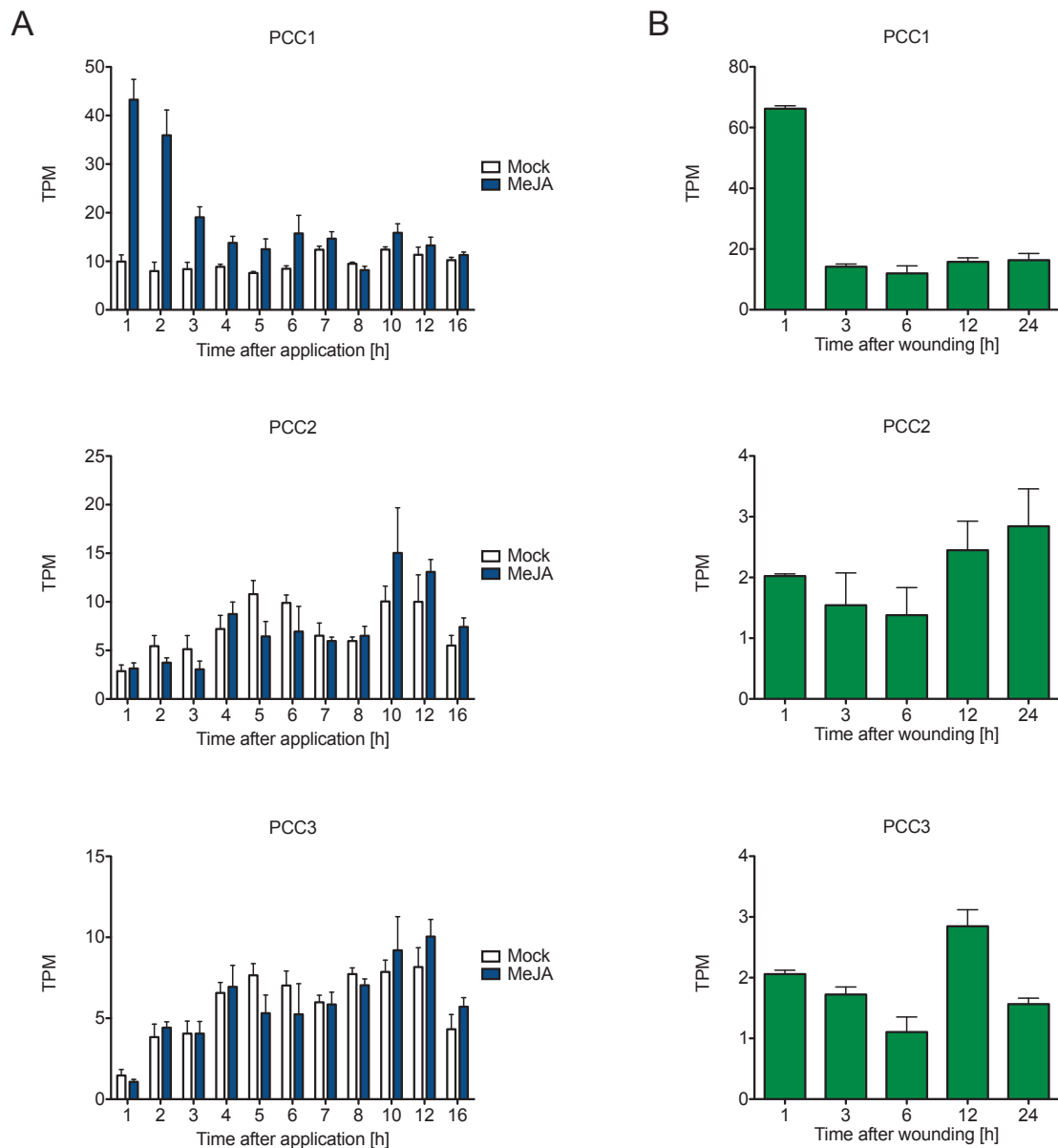


Figure 9: Expression of PCC1, PCC2 and PCC3 upon MeJA treatment and wounding

Transcript per million (TPM) calculated for PCC1, PCC2 and PCC3 from RNA-Seq experiments published in the SRA of NCBI. (A) Samples were taken at the indicated time points after treatment with methyl-jasmonate (MeJA). Bars represent mean + SD of 4 biological replicates. The authors did not provide information about plant age or MeJA concentration (Accession PRJNA224133). Mock treated plants are referred to as control plants. (B) Samples were taken at the indicated time points after piercing the third leaf of 21 days old plants. Bars represent mean + SD of 15 pooled biological replicates measured in duplicates (Accession PRJNA324514).

PCC1 was more than 4-fold upregulated 1 h after MeJA application compared to the Mock treatment (Figure 9A). Afterwards the values declined, but stay higher than the control values even after 6 h. PCC2 and PCC3 did not show a respective response to MeJA. The same could be observed after wounding (Figure 9B). PCC1 was immediately upregulated after 1h followed by a rapid decrease after 3h reaching a plateau until the end of the experiment. TPM values of PCC2 and PCC3 were rather low, almost 10 % of PCC1 levels and did not show a wounding induced change in the expression.

Two RNA-Seq experiment dealt with nutrient starvation and revealed that PCC2 is highly upregulated during phosphate deprivation (Figure 10).

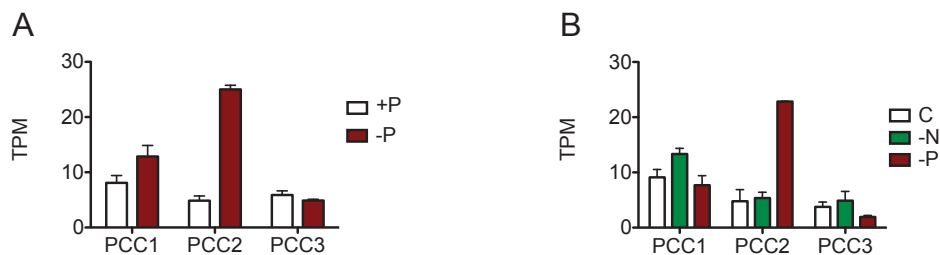


Figure 10: Expression of PCC1, PCC2 and PCC3 under phosphate and nitrogen starvation

TPM values of PCC1, PCC2 and PCC3 calculated from RNA-Seq experiments of the SRA of NCBI. (A) Col-0 plants were grown for 7 days in the presence of phosphate and transferred to phosphate starvation (-P) or control (+P) conditions. Samples were taken 5 days after the transfer. Bars represent mean + SD of 4 biological replicates (Accession PRJNA354802). (B) Col-0 plants were grown either under nitrogen-, phosphate-starvation or control conditions. Bars represent mean + SD of 3 biological replicates. The authors did not provide information about the specified conditions.

When plants were grown for 7 days in the presence of phosphate and then transferred to phosphate starvation conditions, PCC2 revealed a strong increase in the expression of about 5-fold compared to the control plants (Figure 10A). Similar results could be obtained in a second independent experiments, where the expression was analyzed under different nutrient limiting conditions (Figure 10B). The data revealed a high increase in the TPM values of PCC2 under phosphate- but not nitrogen-limiting conditions. In both experiments, PCC1 and PCC2 did not show a nutrient specific change in the expression.

Interestingly, there was no specific stress condition leading to an upregulation of PCC3. But expression was highly increased during germination in the transition from dry seeds to imbibed seeds (Figure 11). Afterwards, there is a rapid decline of PCC3 expression after 1 and 2 DAI. The same could be observed for PCC2 but not for PCC1.

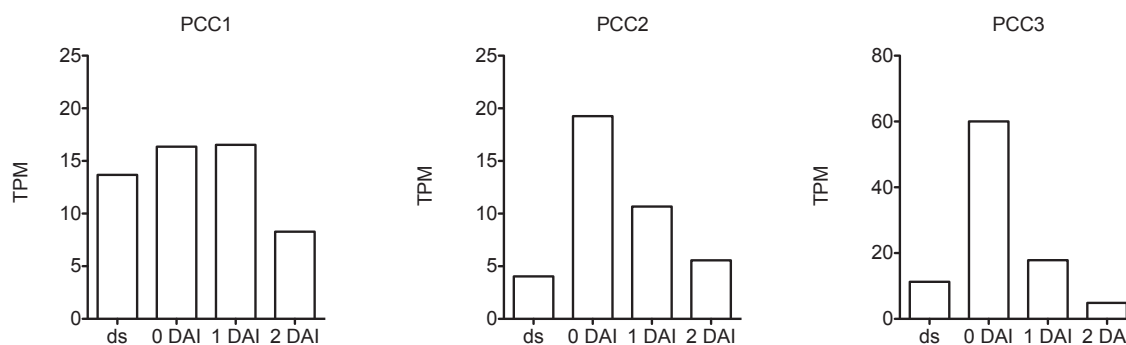


Figure 11: Expression of PNC1, PNC2 and PNC3 during germination

Samples taken from dry seeds (ds) and seedlings 0, 1 and 2 days after 4 days of imbibition (DAI). Data originate from an RNA-Seq experiment of the SRA of NCBI with 1 biological replicate (Accession PRJNA373835).

Biochemical characterization of PCCs using recombinant protein

For the biochemical characterization of PCC1, PCC2 and PCC3 they were expressed either by the plant-based Wheat-Germ cell-free expression kit, or using yeast as host cell. The latter was performed with codon-optimized versions of the PCC proteins adjusted to the yeast codon-usage. According to the hypothesis, proteins were tested for their transport activity of different substrates in *in vitro* uptake experiments (Table 2).

Table 2: Time dependent uptake experiments using either cell-free Wheat-Germ kit or yeast host cells for PCC expression. Radioactively labeled substrate was applied to the outside of preloaded liposomes (X_{out}/Y_{in}). x : no uptake above empty vector control; - : not tested.

	Wheat-Germ			Yeast		
	PCC1	PCC2	PCC3	PCC1	PCC2	PCC3
AMP/CoA	X	X	X	-	-	-
AMP/AMP	X	X	X	X	X	X
ADP/PAP	X	X	X	X	X	X

Unfortunately, for none of the tested substrate combinations uptake activity above the empty vector control values could be observed. The exchange of AMP/CoA was only tested for the Wheat-Germ cell-free expressed proteins with PXN as a positive control. The human peroxisomal CoA carrier Slc25a17 was used as a positive control and revealed high uptake activity for AMP but not for CoA homoexchange. For the exchange of ADP against PAP the human mitochondrial PAP transporter Slc25a42 was used as a positive control but did not show transport activity.

Discussion

PCC1, PCC2 and PCC3 are peroxisomal members of the mitochondrial carrier family

Whereas PCC1 was already identified to be localized to peroxisomes (Carrie et al. 2009), we could show that PCC2 and PCC3 are novel peroxisomal proteins. All three proteins belong to the MCF and analysis of sequence similarity revealed that PCC2 and PCC3 are more closely related to each other than to PCC1 (Figure 2). Amino acid sequence alignments showed, that PCC2 and PCC3 have a prolonged N-terminus compared to PCC1 and that the N-terminus of PCC3 is even longer than the one of PCC2 (Figure 3). Some mitochondrial MCF proteins carry cleavable N-terminal extensions that stimulate but are not essential for insertion into the inner mitochondrial membrane (Murcha et al. 2005). One example are the mitochondrial ATP/ADP carrier (AACs), but the N-terminal extension of PCC3 only consists of 20 amino acids and thus is clearly shorter than the one of the AACs (60 amino acids) and does not share sequence similarity. In addition, there is neither similarity to EF-hand calcium binding domains present in the N-terminus of APCs nor to the N-terminal extension of the adenine nucleotide transporter of the plasma membrane (Rieder and Neuhaus 2011; Lorenz et al. 2015). Thus, the role of the sequence extension of PCC3 is still elusive.

The PCC proteins are closely related to MCF carrier involved in adenine nucleotide transport but also to a group of already characterized CoA carrier (Figure 2). The adenine nucleotide ATP is essential for the activation of fatty acids prior entering β -oxidation and hence plays a pivotal role during storage oil mobilization (Graham 2008; Linka et al. 2008). The activation is conducted by the esterification with CoA. Thus mutants, that are affected in this activation or the subsequent β -oxidation process strongly demand on the supply with exogenous sucrose to enable germination. Because of this, we analyzed the root length as a function of plant growth of *pcc* mutant plants in the presence or absence of sucrose (Figure 6). For PCC1 we analyzed a tDNA insertion knock-out as well as a newly generated CRISPR/Cas9 mutant and both lines did not show a sucrose dependent phenotype. In a systematic phenotypic approach of several peroxisomal proteins with known and unknown function, the very same *pcc1* tDNA insertion line was also shown to be not sucrose dependent (Cassin-Ross and Hu 2014). But in contrast to that study, we could not identify an increased resistance to the synthetic auxin precursor 2,4-DB, indicating, that at least *pcc1-1* is not affected in β -oxidation. Unexpectedly, *pcc1-2* showed a severe decrease in the root length upon treatment with 2,4-DB that was not observed in any other line. To exclude a plate specific effect on the growth behavior, this experiment has to be repeated to confirm or discard the results.

Only *pcc2-1* revealed a significantly decreased root length compared to the WT when grown in the absence of sucrose. Unfortunately, *pcc2-1* is the only *pcc2* mutant that could be obtained by genome editing. Even though off-targeting of Cas9 represents a rather rare event and was controlled *in silico* before cloning, at least one additional independent line is required to confirm the phenotype. This is of special importance, since *pcc2-1* did not reveal a significant different behavior upon 2,4-DB treatment (Figure 7). Interestingly, both *pcc3* mutants had significantly longer roots in the presence of sucrose and increased root lengths in the absence of sucrose with a significant difference for *pcc3-2*. But both lines revealed an increased sensitivity to 2,4-DB. The *pcc2/3* double mutant was generated since PCC2 and PCC3 are closely related to each other and hence might have redundant function. In terms of sucrose dependency, there is no difference to the WT. It seems, that in the *pcc2/3* double mutant line, the decrease that was observed for the *pcc2-1* single mutant compensates for the increased growth of the *pcc3* mutant. For the 2,4-DB assay an additive effect of the two mutations is observable, since *pcc2/3* had severely reduced root lengths compared to the single mutants. All in all, the low connectivity of the phenotypes observed in the assays in terms of both, expected and possible outcomes, doubts the credibility of the experiment. Thus, the experiments have to be repeated including an additional independent line for *pcc2* and double mutant lines for *pcc1/3* and *pcc1/2* as well as triple mutant lines to test for functional redundancy of the carrier.

PCC1 complements yeast mutants affected in peroxisomal NAD redox shuttles

A second approach to determine the *in vivo* function of the PCCs is by yeast complementation assays as it was performed for PCC1 (Figure 8). PCC1 was able to complement the decreased β -oxidation activity of mutants defective in Mdh3p and Gpd1p, two enzymes required for the G3P/DHAP and Mal/OAA shuttle, respectively. Both shuttles are required for the regeneration of NAD that is required for β -oxidation. The same effect could be observed for yeast expressing the peroxisomal NAD carrier PXN (van Roermund et al. 2016). However, PCC1 was not able to complement the phenotype of a *mdh3/ant1 Δ* double mutant. Since Ant1p is able to transport ATP, ADP and AMP (Palmieri et al. 2001) it is conceivable, that PCC1 requires one of these molecules as a counter exchange substrate. Assuming, that PCC1 is indeed a peroxisomal CoA carrier it could transport CoA against AMP. The AMP could then be provided by Ant1p either in the exchange with ATP, or by its uniport transport mode (Lasorsa et al. 2004). Hence, expressing PCC1 in the WT (BJ1991) background could lead to the depletion of the peroxisomal ATP pool explaining the observed drop of the β -oxidation activity. In the *mdh3 Δ* single and *mdh3/gpd1 Δ* mutant, there is an increased demand for NAD. Due to the structural similarity, PXN also accepts CoA as a

substrate (Agrimi et al. 2012). Thus, it might be possible that PCC1 is additionally capable of transporting NAD when present at high concentration.

Ant1p is known to catalyze a proton-coupled import of ATP against AMP resulting in an electro-neutral transport mode that leads to the acidification of the peroxisomal lumen (Lasorsa et al. 2004). Since the peroxisomal pH in tissues of Arabidopsis seedlings with high β -oxidation activity is also more acidic compared to the cytosol, PCC1 might require this proton gradient for its transport function. This kind of proton antiport is known for several members of the MCF (Palmieri and Monne 2016).

Future yeast experiments should aim to analyze whether a mitochondrial targeted version of PCC1 can complement the phenotype of *leu5 Δ* , that is defective in the mitochondrial CoA uptake. By this, the mitochondrial carrier from human, maize and Arabidopsis could be identified (Zallot et al. 2013). In addition, PCC2 and PCC3 have to be included in the complementation assays to see whether they show similar or different effects.

PCC1 is highly upregulated upon wounding which is linked to JA biosynthesis

To further investigate the function of the PCC protein, we mapped and analyzed all WT RNA-Seq experiments in the SRA of the NCBI and searched them for experiments showing the highest expression of each PCC. It turned out, that PCC1 is highly expressed after application of methyl-jasmonate and after wounding (Figure 9).

Jasmonic acid is a plant hormone that is involved in a plethora of biological processes including root growth, reproduction and response to biotic and abiotic stresses (Creelman and Mullet 1997). Its biosynthesis starts in the plastids with the release of linolenic acid that is used for the production of cis-12-oxo-phytodienoic acid (OPDA). OPDA itself can act as a signaling molecule and is considered to be involved in seed dormancy (Dave et al. 2011). Within peroxisomes, OPDA is first reduced by an NADPH-dependent OPDA reductase to OPC-8:0 before it is esterified with CoA to enter β -oxidation for the conversion into jasmonic acid. Wounding results in a signaling cascade that leads to the expression of lipases that release linolenic-acid from the chloroplast membrane and by this, initiate JA biosynthesis (Hyun and Lee 2008). Within 1 min after wounding JA levels increase dramatically, peak after 1 h and remain significantly higher than basal levels for at least 24 h (Glauser et al. 2009). This perfectly fits to the fast increase of PCC1 expression directly after wounding. In addition, JA works in a positive feedback regulatory system for JA biosynthesis which goes in line with the high expression of PCC1 after MeJA application that is still detectable after 6 h. Both experiments indicate a role of PCC1 for JA biosynthesis.

Fatty acids from storage oil or other sources are esterified to CoA in the cytosol which is cleaved of during the peroxisomal import by PXA (Nyathi et al. 2010; De Marcos Lousa et al. 2013). It is unknown whether the CoA moiety is released in the cytosol or in the

peroxisomal lumen. Assuming that CoA is released in the peroxisomal lumen would obviate the necessity of a peroxisomal CoA transporter in fatty acid degradation. However, it is not clear if OPDA and 2,4-DB are transported in a free or esterified form (Linka and Theodoulou 2013; Li et al. 2019). Thus, a peroxisomal CoA carrier would be required for the processing of these substrates even if the CoA from other fatty acids is released into the peroxisomal lumen. This hypothesis fits to the 2,4-DB resistance and sucrose independency observed for *pcc1* by Cassin-Ross et al. but is contradictory to our experiments.

PCC2 gene expression response to phosphate but not nitrogen starvation

Two RNA-Seq experiments where PCC2 showed the highest expression, dealt with nutrient availability (Figure 10). The data revealed that PCC2 is highly upregulated under phosphate but not under nitrogen starvation conditions and that this upregulation is restricted to PCC2 since PCC1 and PCC3 did not show a respective response. Phosphate starvation leads to membrane remodeling by replacing phosphate containing polar head groups of phospholipids with galactose groups (Nakamura 2013). The generated phosphatidylcholine can be dephosphorylated to yield phosphate and choline (Angkawijaya et al. 2019). While the phosphate feeds the cellular phosphate pool, the fate of choline is unknown. Choline could be metabolized by a choline monooxygenase and betaine aldehyde dehydrogenase to glycine betaine. But, *Arabidopsis* does not naturally produce glycine betaine even though a peroxisomal aldehyde dehydrogenase was shown to oxidize betaine aldehyde *in vitro* (Missihoun et al. 2011). Thus, the function of peroxisomes in response to phosphate starvation remains an interesting topic for future studies.

PCC3 gene transcript is highly abundant during first days of germination

The highest expression of PCC3 was not related to a certain stress condition but to the process of germination (Figure 11). PCC3 showed a massive increase in transcript abundance in the transition from dry seeds to imbibed seeds followed by a decrease after 1 and 2 DAI. Interestingly, the same pattern could be observed for PCC2 but with lower total values. This indicates, that both proteins are involved in pathways that are either required within the same developmental stage or share functional redundancy. The fact that *pcc2* showed a sucrose dependent phenotype (Figure 6) fits to its upregulation during germination. PCC1 did not show a respective pattern but was rather constantly expressed throughout the whole experiment with values similar to PCC2. As mentioned above, CoA might not be required for storage oil mobilization if the CoA moiety of the cytosolic fatty acids is released into the peroxisomal lumen.

***In vitro* uptake experiments did not reveal substrate specificity of PCC proteins**

As the predominant hypothesis, the exchange of AMP against CoA was tested for heterologous proteins expressed by the Wheat-Germ cell-free expression kit. Whereas none of the PCC proteins showed uptake activity above the empty vector control, PXN that served as a positive control was highly active. This clearly shows, that the applied experimental setup is suitable to show AMP/CoA transport but gives no information about the functionality of the expressed PCC proteins.

After the initial esterification of fatty acids, CoA can be reused for the next β -oxidation cycle. Beside this, CoA can also be degraded to yield PAP and 4PP that have to be exported out of the peroxisome. The human mitochondrial Slc25a42, first characterized as a CoA carrier, was shown to rather mediate the exchange of ADP against PAP (Fiermonte et al. 2009). Hence, we used this transporter as a positive control to test ADP/PAP heteroexchange capacity of the PCC proteins. None of the PCC proteins regardless of the expression system showed uptake activity for ADP into liposomes with PAP preloading. But, since Slc25a42 was not active, as well, the applied experimental set-up might not be suitable to measure this specific transport. Like the majority of the MCF proteins, the biochemical characterization of Slc25a42 was performed with recombinant protein expressed in *E.coli* and solubilized from inclusion bodies (Fiermonte et al. 2009). This might indicate, that the expression systems themselves are not suitable to express functional Slc25a42 and hence might also be inappropriate for PCC expression.

Many MCF proteins transport adenine nucleotides *in vitro* despite of having other functions *in vivo* (Fiermonte et al. 2009; Palmieri et al. 2009; Agrimi et al. 2012; Bernhardt et al. 2012). Thus, we tested the AMP uptake activity of the PCCs into liposomes preloaded with AMP and used the human peroxisomal CoA carrier Slc25a17 as positive control. While Slc25a17 revealed a high uptake activity, the PCC proteins stayed inactive either due to offering the wrong substrate or to an inappropriate expression system. However, future studies should include ADP and ATP homoexchange, as well and should aim to establish the *E.coli* expression system for the PCCs. Since at least PCC1 was able to complement the yeast NAD redox-shuttle mutants *mdh3 Δ* and the double mutant *mdh3/gpd1 Δ* , NAD should not be excluded as a putative substrate for all PCC proteins.

Conclusion

In this study, we could show the peroxisomal localization of two previously unknown MCF proteins that are closely related to the already identified but not yet characterized peroxisomal carrier At3g55640. All three proteins share high sequence similarity to already characterized CoA carrier and expression data revealed an involvement in germination and wounding response, which are both related to CoA metabolism. The ability of PCC1 to complement Yeast mutants deficient in the peroxisomal NAD redox shuttles further underlined our hypothesis, that PCC1 might be the so far unknown CoA carrier sharing functional redundancy with PCC2 and PCC3. However, further studies are required to show the transport function biochemically and more mutant combinations are required to test the phenotype in regard of functional redundancy of these carriers.

Supplementals

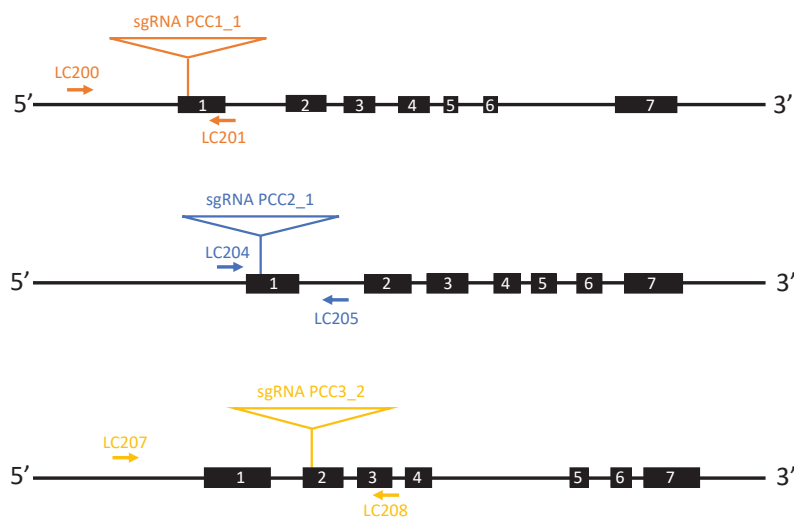


Figure S1: Position of sgRNAs

Position of the sgRNA sequences within the *PCC* genes. Primer for RFLP: LC200: GTAACACCGAAGACACCG; LC201: CTCGCTCGATGAAATGACG; LC204: CTCGCAAACCCAGAAACG; LC205: GTGAGGCGAGCAAGAGGAG; LC207: GATGCGAATTCAGCTTCC; LC208: GATCGAGAGGGTAGGTAG.

Author contribution

Generating a table with TPM values of SRA RNA-seq experiments was done by Wiebke Halpape. Jannika Ewen helped with the establishment of the mutant lines and uptake experiments. Carlo von Roermund performed the yeast complementation assay. Lennart Charton wrote the manuscript and performed all residual experiments and analyses. Nicole Linka, Georg Groth and Andreas Weber participated in scientific discussions. Nicole Linka and Lennart Charton designed the experiments.

References

- AbdelRaheim, S. R. and A. G. McLennan (2002). "The *Caenorhabditis elegans* Y87G2A.14 Nudix hydrolase is a peroxisomal coenzyme A diphosphatase." BMC Biochem **3**: 5.
- Agrimi, G., A. Russo, C. L. Pierri and F. Palmieri (2012). "The peroxisomal NAD⁺ carrier of *Arabidopsis thaliana* transports coenzyme A and its derivatives." J Bioenerg Biomembr **44**(3): 333-340.
- Agrimi, G., A. Russo, P. Scarzia and F. Palmieri (2012). "The human gene SLC25A17 encodes a peroxisomal transporter of coenzyme A, FAD and NAD⁺." Biochem J **443**(1): 241-247.
- Angkawijaya, A. E., A. H. Ngo, V. C. Nguyen, F. Gunawan and Y. Nakamura (2019). "Expression Profiles of 2 Phosphate Starvation-Inducible Phosphocholine/Phosphoethanolamine Phosphatases, PECP1 and PS2, in *Arabidopsis*." Front Plant Sci **10**: 662.
- Bernhardt, K., S. Wilkinson, A. P. Weber and N. Linka (2012). "A peroxisomal carrier delivers NAD(+) and contributes to optimal fatty acid degradation during storage oil mobilization." Plant J **69**(1): 1-13.
- Bouvier, F., N. Linka, J. C. Isner, J. Mutterer, A. P. Weber and B. Camara (2006). "*Arabidopsis* SAMT1 defines a plastid transporter regulating plastid biogenesis and plant development." Plant Cell **18**(11): 3088-3105.
- Carrie, C., K. Kuhn, M. W. Murcha, O. Duncan, I. D. Small, N. O'Toole and J. Whelan (2009). "Approaches to defining dual-targeted proteins in *Arabidopsis*." Plant J **57**(6): 1128-1139.
- Cassin-Ross, G. and J. Hu (2014). "Systematic phenotypic screen of *Arabidopsis* peroxisomal mutants identifies proteins involved in beta-oxidation." Plant Physiol **166**(3): 1546-1559.
- Charton, L., A. Plett and N. Linka (2019). "Plant peroxisomal solute transporter proteins." J Integr Plant Biol.
- Coxon, K. M., E. Chakauya, H. H. Ottenhof, H. M. Whitney, T. L. Blundell, C. Abell and A. G. Smith (2005). "Pantothenate biosynthesis in higher plants." Biochem Soc Trans **33**(Pt 4): 743-746.
- Creelman, R. A. and J. E. Mullet (1997). "Biosynthesis and Action of Jasmonates in Plants." Annu Rev Plant Physiol Plant Mol Biol **48**: 355-381.
- Dave, A., M. L. Hernandez, Z. He, V. M. Andriotis, F. E. Vaistij, T. R. Larson and I. A. Graham (2011). "12-oxo-phytodienoic acid accumulation during seed development represses seed germination in *Arabidopsis*." Plant Cell **23**(2): 583-599.
- De Marcos Lousa, C., C. W. van Roermund, V. L. Postis, D. Dietrich, I. D. Kerr, R. J. Wanders, S. A. Baldwin, A. Baker and F. L. Theodoulou (2013). "Intrinsic acyl-CoA thioesterase activity of a peroxisomal ATP binding cassette transporter is required for transport and metabolism of fatty acids." Proc Natl Acad Sci U S A **110**(4): 1279-1284.
- Ferro, M., S. Brugiére, D. Salvi, D. Seigneurin-Berny, M. Court, L. Moyet, C. Ramus, S. Miras, M. Mellal, S. Le Gall, S. Kieffer-Jaquinod, C. Bruley, J. Garin, J. Joyard, C. Masselon and N. Rolland (2010). "AT_CHLORO, a comprehensive chloroplast proteome database with

subplastidial localization and curated information on envelope proteins." Mol Cell Proteomics **9**(6): 1063-1084.

Fiermonte, G., E. Paradies, S. Todisco, C. M. Marobbio and F. Palmieri (2009). "A novel member of solute carrier family 25 (SLC25A42) is a transporter of coenzyme A and adenosine 3',5'-diphosphate in human mitochondria." J Biol Chem **284**(27): 18152-18159.

Fulda, M., J. Schnurr, A. Abbadi, E. Heinz and J. Browse (2004). "Peroxisomal Acyl-CoA synthetase activity is essential for seedling development in *Arabidopsis thaliana*." Plant Cell **16**(2): 394-405.

Gasmi, L. and A. G. McLennan (2001). "The mouse Nudt7 gene encodes a peroxisomal nudix hydrolase specific for coenzyme A and its derivatives." Biochem J **357**(Pt 1): 33-38.

Gietz, R. D. and R. H. Schiestl (2007). "Large-scale high-efficiency yeast transformation using the LiAc/SS carrier DNA/PEG method." Nat Protoc **2**(1): 38-41.

Glauser, G., L. Dubugnon, S. A. Mousavi, S. Rudaz, J. L. Wolfender and E. E. Farmer (2009). "Velocity estimates for signal propagation leading to systemic jasmonic acid accumulation in wounded *Arabidopsis*." J Biol Chem **284**(50): 34506-34513.

Graham, I. A. (2008). "Seed storage oil mobilization." Annu Rev Plant Biol **59**: 115-142.

Haferkamp, I. and S. Schmitz-Esser (2012). "The plant mitochondrial carrier family: functional and evolutionary aspects." Front Plant Sci **3**: 2.

Hahn, F., O. Mantegazza, A. Greiner, P. Hegemann, M. Eisenhut and A. P. Weber (2017). "An Efficient Visual Screen for CRISPR/Cas9 Activity in *Arabidopsis thaliana*." Front Plant Sci **8**: 39.

Hofgen, R. and L. Willmitzer (1988). "Storage of competent cells for *Agrobacterium* transformation." Nucleic Acids Res **16**(20): 9877.

Hyun, Y. and I. Lee (2008). "Generating and maintaining jasmonic acid in *Arabidopsis*." Plant Signal Behav **3**(10): 798-800.

Inoue, H., H. Nojima and H. Okayama (1990). "High efficiency transformation of *Escherichia coli* with plasmids." Gene **96**: 23-28.

Ito, D., K. Yoshimura, K. Ishikawa, T. Ogawa, T. Maruta and S. Shigeoka (2012). "A comparative analysis of the molecular characteristics of the *Arabidopsis* CoA pyrophosphohydrolases AtNUDX11, 15, and 15a." Biosci Biotechnol Biochem **76**(1): 139-147.

Kim, Y. I., I. K. Nam, D. K. Lee, S. Bhandari, L. Charton, S. Kwak, J. Y. Lim, K. Hong, S. J. Kim, J. N. Lee, S. W. Kwon, H. S. So, N. Linka, R. Park and S. K. Choe (2019). "Slc25a17 acts as a peroxisomal coenzyme A transporter and regulates multiorgan development in zebrafish." J Cell Physiol.

Lasorsa, F. M., P. Scarcia, R. Erdmann, F. Palmieri, H. Rottensteiner and L. Palmieri (2004). "The yeast peroxisomal adenine nucleotide transporter: characterization of two transport modes and involvement in DeltapH formation across peroxisomal membranes." Biochem J **381**(Pt 3): 581-585.

Li, Y., Y. Liu and B. K. Zolman (2019). "Metabolic Alterations in the Enoyl-CoA Hydratase 2 Mutant Disrupt Peroxisomal Pathways in Seedlings." Plant Physiol **180**(4): 1860-1876.

- Linka, N. and F. L. Theodoulou (2013). "Metabolite transporters of the plant peroxisomal membrane: known and unknown." Subcell Biochem **69**: 169-194.
- Linka, N., F. L. Theodoulou, R. P. Haslam, M. Linka, J. A. Napier, H. E. Neuhaus and A. P. Weber (2008). "Peroxisomal ATP import is essential for seedling development in *Arabidopsis thaliana*." Plant Cell **20**(12): 3241-3257.
- Lorenz, A., M. Lorenz, U. C. Vothknecht, S. Niopek-Witz, H. E. Neuhaus and I. Haferkamp (2015). "In vitro analyses of mitochondrial ATP/phosphate carriers from *Arabidopsis thaliana* revealed unexpected Ca²⁺-effects." BMC Plant Biol **15**: 238.
- Missihoun, T. D., J. Schmitz, R. Klug, H. H. Kirch and D. Bartels (2011). "Betaine aldehyde dehydrogenase genes from *Arabidopsis* with different sub-cellular localization affect stress responses." Planta **233**(2): 369-382.
- Murcha, M. W., A. H. Millar and J. Whelan (2005). "The N-terminal cleavable extension of plant carrier proteins is responsible for efficient insertion into the inner mitochondrial membrane." J Mol Biol **351**(1): 16-25.
- Nakamura, Y. (2013). "Phosphate starvation and membrane lipid remodeling in seed plants." Prog Lipid Res **52**(1): 43-50.
- Nyathi, Y., C. De Marcos Lousa, C. W. van Roermund, R. J. Wanders, B. Johnson, S. A. Baldwin, F. L. Theodoulou and A. Baker (2010). "The *Arabidopsis* peroxisomal ABC transporter, comatose, complements the *Saccharomyces cerevisiae* pxa1 pxa2Delta mutant for metabolism of long-chain fatty acids and exhibits fatty acyl-CoA-stimulated ATPase activity." J Biol Chem **285**(39): 29892-29902.
- Palmieri, F., C. Indiveri, F. Bisaccia and V. Iacobazzi (1995). "Mitochondrial metabolite carrier proteins: purification, reconstitution, and transport studies." Methods Enzymol **260**: 349-369.
- Palmieri, F. and M. Monne (2016). "Discoveries, metabolic roles and diseases of mitochondrial carriers: A review." Biochim Biophys Acta **1863**(10): 2362-2378.
- Palmieri, F., B. Rieder, A. Ventrella, E. Blanco, P. T. Do, A. Nunes-Nesi, A. U. Trauth, G. Fiermonte, J. Tjaden, G. Agrimi, S. Kirchberger, E. Paradies, A. R. Fernie and H. E. Neuhaus (2009). "Molecular identification and functional characterization of *Arabidopsis thaliana* mitochondrial and chloroplastic NAD⁺ carrier proteins." J Biol Chem **284**(45): 31249-31259.
- Palmieri, L., H. Rottensteiner, W. Girzalsky, P. Scarcia, F. Palmieri and R. Erdmann (2001). "Identification and functional reconstitution of the yeast peroxisomal adenine nucleotide transporter." EMBO J **20**(18): 5049-5059.
- Parthasarathy, A., M. A. Savka and A. O. Hudson (2019). "The Synthesis and Role of beta-Alanine in Plants." Front Plant Sci **10**: 921.
- Prohl, C., W. Pelzer, K. Diekert, H. Kmita, T. Bedekovics, G. Kispal and R. Lill (2001). "The yeast mitochondrial carrier Leu5p and its human homologue Graves' disease protein are required for accumulation of coenzyme A in the matrix." Mol Cell Biol **21**(4): 1089-1097.
- Reilly, S. J., V. Tillander, R. Ofman, S. E. Alexson and M. C. Hunt (2008). "The nudix hydrolase 7 is an Acyl-CoA diphosphatase involved in regulating peroxisomal coenzyme A homeostasis." J Biochem **144**(5): 655-663.

- Reumann, S., S. Quan, K. Aung, P. Yang, K. Manandhar-Shrestha, D. Holbrook, N. Linka, R. Switzenberg, C. G. Wilkerson, A. P. Weber, L. J. Olsen and J. Hu (2009). "In-depth proteome analysis of Arabidopsis leaf peroxisomes combined with in vivo subcellular targeting verification indicates novel metabolic and regulatory functions of peroxisomes." Plant Physiol **150**(1): 125-143.
- Rieder, B. and H. E. Neuhaus (2011). "Identification of an Arabidopsis plasma membrane-located ATP transporter important for anther development." Plant Cell **23**(5): 1932-1944.
- Schindelin, J., I. Arganda-Carreras, E. Frise, V. Kaynig, M. Longair, T. Pietzsch, S. Preibisch, C. Rueden, S. Saalfeld, B. Schmid, J. Y. Tinevez, D. J. White, V. Hartenstein, K. Eliceiri, P. Tomancak and A. Cardona (2012). "Fiji: an open-source platform for biological-image analysis." Nat Methods **9**(7): 676-682.
- Senkler, J., M. Senkler, H. Eubel, T. Hildebrandt, C. Lengwenus, P. Schertl, M. Schwarzlander, S. Wagner, I. Wittig and H. P. Braun (2017). "The mitochondrial complexome of Arabidopsis thaliana." Plant J **89**(6): 1079-1092.
- Sievers, F., A. Wilm, D. Dineen, T. J. Gibson, K. Karplus, W. Li, R. Lopez, H. McWilliam, M. Remmert, J. Soding, J. D. Thompson and D. G. Higgins (2011). "Fast, scalable generation of high-quality protein multiple sequence alignments using Clustal Omega." Mol Syst Biol **7**: 539.
- Tilton, G. B., W. J. Wedemeyer, J. Browse and J. Ohlrogge (2006). "Plant coenzyme A biosynthesis: characterization of two pantothenate kinases from Arabidopsis." Plant Mol Biol **61**(4-5): 629-642.
- van Roermund, C. W., Y. Elgersma, N. Singh, R. J. Wanders and H. F. Tabak (1995). "The membrane of peroxisomes in *Saccharomyces cerevisiae* is impermeable to NAD(H) and acetyl-CoA under in vivo conditions." EMBO J **14**(14): 3480-3486.
- van Roermund, C. W., M. G. Schroers, J. Wiese, F. Facchinelli, S. Kurz, S. Wilkinson, L. Charton, R. J. Wanders, H. R. Waterham, A. P. Weber and N. Link (2016). "The Peroxisomal NAD Carrier from Arabidopsis Imports NAD in Exchange with AMP." Plant Physiol **171**(3): 2127-2139.
- Vozza, A., F. De Leonardis, E. Paradies, A. De Grassi, C. L. Pierri, G. Parisi, C. M. Marobbio, F. M. Lasorsa, L. Muto, L. Capobianco, V. Dolce, S. Raho and G. Fiermonte (2017). "Biochemical characterization of a new mitochondrial transporter of dephosphocoenzyme A in *Drosophila melanogaster*." Biochim Biophys Acta **1858**(2): 137-146.
- Zallot, R., G. Agrimi, C. Lerma-Ortiz, H. J. Teresinski, O. Frelin, K. W. Ellens, A. Castegna, A. Russo, V. de Crecy-Lagard, R. T. Mullen, F. Palmieri and A. D. Hanson (2013). "Identification of mitochondrial coenzyme a transporters from maize and Arabidopsis." Plant Physiol **162**(2): 581-588.
- Zhang, X., R. Henriques, S. S. Lin, Q. W. Niu and N. H. Chua (2006). "Agrobacterium-mediated transformation of Arabidopsis thaliana using the floral dip method." Nat Protoc **1**(2): 641-646.

III. Manuscripts

III.III Manuscript 3

Peroxisomal ATP import by PNC1 and PNC2 is required for functional mevalonate-pathway

Lennart Charton¹, Laura K. Henry², Natalia Dudareva², Markus Schwarzländer³, Andreas Weber¹, Nicole Linka^{1a}

¹ Heinrich-Heine-University Düsseldorf, Institute of Plant Biochemistry, Germany

² Purdue University, Department of Biochemistry, USA

³ WWU Münster, Institute of Plant Biology and Biotechnology, Germany

Abstract

Metabolic reactions demand on ATP for activation and phosphorylation purposes. Since ATP is produced in the cytosol and mitochondria but is required throughout the whole cell, ATP has to be transported across biological membranes in order to fulfill its diverse tasks. PNC1 and PNC2 are the only known peroxisomal ATP carrier importing ATP against ADP or AMP. Their important role in β -oxidation especially during post-germinative storage oil mobilization is well-established but the knowledge about their involvement in other metabolic processes is little. Here we identified the peroxisomal part of the otherwise cytosolic mevalonate (Mev) pathway for the production of isoprenoid precursors to be dependent on ATP supply by PNC proteins. Double mutants are strongly affected in the production of Mev-pathway derived isoprenoids like campesterol, sitosterol and the plant volatile β -caryophyllene and plants are more sensitive to a block in the parallel acting plastidic MEP pathway. The latter strongly emphasizes a crosstalk between both pathways that has to be further analyzed in the future. In addition, we used the ATP FRET sensor ATeam 1.03-nD/nA to show an overall decreased cytosolic ATP pool in the double mutant. Unfortunately, we could not target the sensor exclusively to peroxisomes to further underline the exclusive role of the PNC proteins for peroxisomal ATP supply. Other putative roles of the PNCs within plant metabolism are discussed.

Introduction

ATP is the major energy currency of the cell and involved in a plethora of metabolic reactions. Its production is compartmentalized to different organelles. Within the cytosol, glycolysis breaks down glucose yielding two net molecules of ATP. Under aerobic conditions, the resulting pyruvate enters mitochondria for its oxidative decarboxylation leading to the production of acetyl-CoA which enters the tricarboxylic acid (TCA) cycle. While some amounts of ATP are produced directly during the TCA cycle, the majority of ATP is generated from reducing equivalents like NADH by the action of the mitochondrial electron transport chain. For this, electrons from NADH and FADH are pumped across the inner mitochondrial membrane to generate a proton gradient. This gradient is used to drive the ATP-ase for the phosphorylation of ADP.

In plants, fatty acid catabolism by β -oxidation occurs exclusively in peroxisomes where the resulting acetyl-CoA is fed into the glyoxylate cycle to produce succinate for gluconeogenesis (Cornah et al. 2004). While this represents the major fate of fatty acid degradation, plants are able, to a lower extent, to respire fatty acids (Graham and Eastmond

2002). For this, citrate or isocitrate produced by the glyoxylate cycle are imported into mitochondria to enter the TCA cycle for further oxidation (Pracharoenwattana et al. 2005).

Plant mitochondria possess three ADP/ATP carrier (AAC1-3) and adenine nucleotide/phosphate carriers (APC1-3). While AACs are involved in the exchange of ATP(out) against ADP(in) for ATP synthesis, the APCs are more likely involved in the net adenine nucleotide supply (Lorenz et al. 2015).

Within chloroplasts ATP and NADPH required for CO₂ fixation in the Calvin-Benson-Bassham (CBB) cycle are produced by the photosynthetic light reaction. Chloroplasts from young seedlings are still able to import ATP from the cytosol by chloroplast nucleotide transporter, but they lose this ability in adult tissues. Thus, the ratio of ATP:NADPH for CBB cycle is maintained by the export of reductants rather than by the import of ATP from the cytosol (Voon et al. 2018).

Two members of the mitochondrial carrier family (MCF) have been identified to be localized to the peroxisomal membrane mediating the transport of ATP (Linka et al. 2008). Peroxisomal nucleotide carrier 1 and 2 (PNC1 and PNC2) were shown to catalyze the import of ATP against ADP or AMP in a strict counter exchange transport mode. The peroxisomal supply with ATP is essential during germination. In this developmental stage, stored fatty acids are degraded by peroxisomal β -oxidation to provide energy for seedling establishment. But before entering the β -oxidation cycle, free fatty acids have to be activated by esterification with coenzyme A in an ATP dependent reaction.

Initial characterization of PNC1 and PNC2 using RNAi lines revealed a sucrose dependent phenotype of the double mutant caused by a block in storage oil degradation. (Linka et al. 2008). Further studies using a double mutant obtained by crossing of PNC1 and PNC2 tDNA insertion lines showed their additional involvement in branched-chain amino acid catabolism and dark induced senescence (Martin Schroers, Sarah Keßel-Vigelius, PhD thesis). All these reactions are linked to peroxisomal β -oxidation, but the knowledge about peroxisomal ATP dependent pathways beside β -oxidation is limited.

The last steps of the cytosolic mevalonate (Mev) pathway for the synthesis of isopentenyl diphosphate (IPP) were shown to be localized to peroxisomes (Sapir-Mir et al. 2008; Simkin et al. 2011). IPP derived from the Mev-pathway is used as a precursor for the synthesis of sterols, brassinosteroids and sesquiterpenes (Figure 1). Sterols are integral components of the membrane with important functions in membrane integrity and fluidity (Clouse 2002). Sitosterol is the most abundant sterol and the direct precursor of stigmasterol. Both sterols play important roles during the embryonic growth phase as well as biotic and abiotic stress response (Schaller 2004; Wang et al. 2012). Campesterol is the precursor of brassinolide, the most active brassinosteroid in most plants (Clouse 2002). Mutants compromised in brassinolide production have a severe dwarfism phenotype. β -caryophyllene

is the main sesquiterpene in *Arabidopsis* and is known to serve as a plant volatile to attract pollinators. Even though *Arabidopsis* is considered to be mostly self-pollinating, insect-mediated pollination might occur in some wild populations (Chen et al. 2003).

The plastidic methyl-erythritol-phosphate (MEP) pathway works in parallel to the Mev pathway and produces IPP for photosynthesis related isoprenoids like carotenoids, phytol-chain and tocopherols. Labeling experiments with Mev and MEP derived precursors as well as genetically or chemically inhibiting either of the pathways revealed a cross-talk between cytosolic and plastidial isoprenoid biosynthesis (Kasahara et al. 2002; Laule et al. 2003; Dudareva et al. 2005; Mendoza-Poudereux et al. 2015).

The peroxisomal part of the Mev pathway starts with the import of mevalonate-phosphate which is phosphorylated by phosphomevalonate kinase (PMK) to mevalonate diphosphate (Figure 1). Mevalonate diphosphate is then converted to IPP by mevalonate diphosphate-decarboxylase (MDD), representing the second ATP dependent reaction. The resulting IPP is either directly exported or converted to dimethylallyl-pyrophosphate (DMAPP).

Beside the *de novo* synthesis plants are able to recycle IPP by phosphorylating IP. This step is catalyzed by the cytosolic isopentenyl phosphate kinase (IPK) (Henry et al. 2015). Double mutants of IPK and MDD have further decreased sterol levels, showing the importance of IPK activity for the cellular IPP pool.

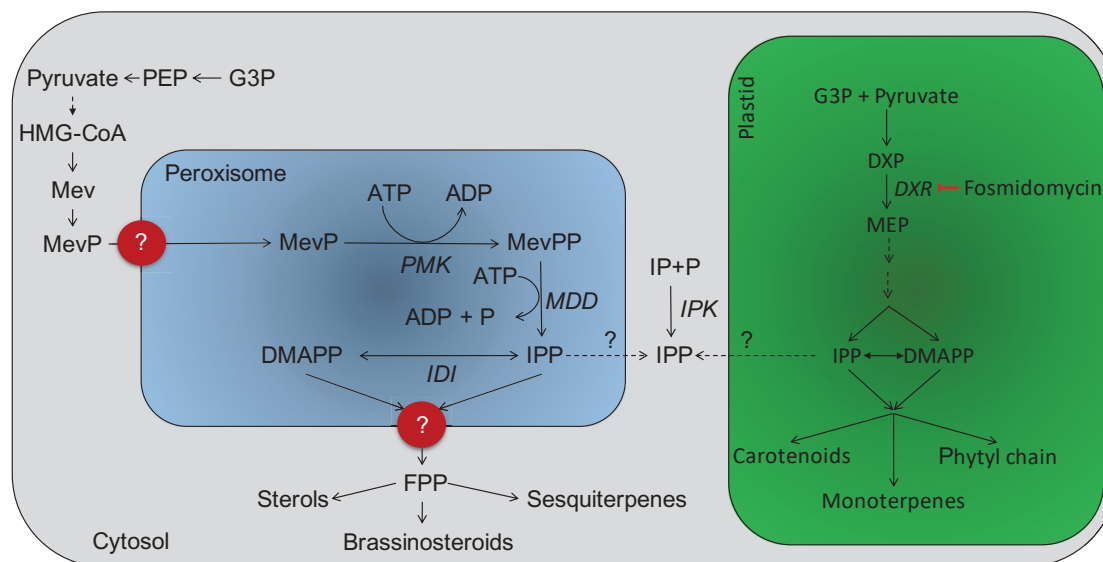


Figure 1: Compartmentalization of IPP production

Synthesis of IPP for the production of isoprenoids is compartmentalized to the cytosol, peroxisome and chloroplasts. Abbreviations: G3P, glyceraldehyde-3-phosphate; PEP, phosphoenolpyruvate; HMG-CoA, hydroxy-methylglutaryl-coenzyme A; Mev, mevalonate; MevP, mevalonate-phosphate; PMK, phosphomevalonate kinase; MevPP, mevalonate-diphosphate; MDD, mevalonate-diphosphate decarboxylase; IP, isopentenyl-phosphate; IPP, isopentenyl-diphosphate; IPK, isopentenyl-phosphate kinase; DMAPP, dimethylallyl-pyrophosphate; IDI, isopentenyl diphosphate isomerase; FPP, farnesyl-diphosphate; DXP, deoxy-D-xylulose 5-phosphate; DXR, deoxy-D-xylulose 5-phosphate reductase; MEP, methylerythritol 4-phosphate.

β -oxidation and the Mev pathway are active throughout the whole life cycle of Arabidopsis. Despite the important role of ATP within peroxisomal metabolism the *pnc1/2* double mutant is still viable after the seedling becomes photoautotrophic. There are three options conceivable that explain the lack of a respective phenotype. (1) ATP for peroxisomal reactions is only required under certain stress conditions. (2) The tDNA insertion in the last exon of *pnc1* only leads to a knock-down of the gene. Hence, residual activity might be sufficient for normal demands, but not during germination. (3) So far PNCs are the only known peroxisomal proteins supplying peroxisomes with ATP, but other import systems cannot be excluded.

The steady state and dynamic responses of ATP have been studied in plants using genetically encoded sensors *in vivo* (Hatsugai et al. 2012; De Col et al. 2017; Voon et al. 2018). The ATP-FRET sensor ATeam 1.03-nD/nA is based on a cyan and yellow fluorescent protein (CFP and YFP, respectively) linked by the ϵ -subunit of the Bacillus sp. PS3 (Imamura et al. 2009; Kotera et al. 2010). Upon binding of ATP there is a conformational change resulting in an energy transfer from CFP to YFP. This ratiometric shift is used to determine ATP levels in different compartments by specific targeting of the sensor. While the sensor was successfully targeted to mitochondria, chloroplasts and the cytosol, it has not been targeted to peroxisomes, yet.

Aim of this thesis

One aim of this study was to establish a peroxisomal version of the ATeam sensor to further investigate the effect of *pnc1/2* on peroxisomal ATP levels. Therefore, WT and mutant plants were stable transformed with a cytosolic and peroxisomal version of the sensor to determine not only the steady state ATP level, but to analyze the dynamic response in both compartments and genotypes by fluorescence plate reader assays. In addition, we identified the peroxisomal part of the mevalonate pathway to be ATP-dependent. Therefore, we further analyzed the role of the PNC proteins for the peroxisomal ATP-supply of the Mev pathway. For this, we used inhibitor assays with the specific MEP pathway inhibitor fosmidomycin and GC-MS analysis of sterols and volatiles derived from the Mev pathway. Other pathways that demand on peroxisomal ATP supply are discussed.

Material and Methods

Bacteria strains and growth conditions

Chemical competent Mach1 *E.coli* cells (Invitrogen, Karlsruhe, Germany) were used for plasmid transformation and amplification. Cells were grown at 37 °C either in liquid medium shaking at 190 rotations per minute (rpm) or on solid Luria-Bertani (LB) medium. *Agrobacterium tumefaciens* strain GV3103 was used for stable and transient transformation of *Arabidopsis* and *Nicotiana benthamiana*, respectively and was grown at 28 °C either shaking at 150 rpm in liquid YEB medium or on agar plates. For selection purposes, appropriate antibiotics were added to the growth medium.

Transformation of Bacteria

Plasmid DNA was introduced into competent Mach1 *E.coli* cells using heat-shock method (Inoue et al. 1990). Afterwards, the cell suspension was spread on LB-agar plates containing ampicillin and was incubated for at least 8 h (here o/n) at 37 °C.

Chemo-competent *A. tumefaciens* cells were transformed following the freeze-thaw heat-shock method (Hofgen and Willmitzer 1988). Afterwards, single colonies were picked, transferred to new plates and incubated for additional 2 d at 28 °C.

Plant growth conditions

Arabidopsis thaliana ecotype Columbia (Col-0) was used as WT in this thesis. Seeds were surface-sterilized with chloric gas by adding 3 ml concentrated HCl to 100 ml NaClO in a desiccator for 2 hours. Seeds were placed under the clean bench to allow evaporation of residual chloric gas. Stratification was performed for 3 days in the dark at 4°C. If not stated otherwise plants were grown under normal day conditions (12 h light / 12 h dark) at 22/18 °C and a light intensity of 100 $\mu\text{M m}^{-2} \text{s}^{-1}$ on agar plates supplemented with 1 % (w/v) sucrose. Two to three weeks old seedlings were transferred to soil (3/4 Floraton, 1/4 Arabidopsis substrate) and were further cultivated under long-day conditions.

Transformation of Arabidopsis

For the generation of stable transformed Arabidopsis lines, agrobacterium-mediated transformation was conducted according to the floral-dip method (Zhang et al. 2006). After maturation, seeds of the transformed plants (F_0) were dispersed on MS-agar plates and selected by fluorescence.

Isolation of Arabidopsis genomic DNA

Arabidopsis gDNA was isolated by isopropanol precipitation (Weigel and Glazebrook, 2001) For this, one leaf was harvested, frozen in liquid nitrogen and grinded in a bead mill (30 Hz, 30 seconds). Afterwards, 400 μ l extraction buffer (0.2 M Tris-HCl, pH7.5 (HCL), 0.25 M NaCl, 0.025 M EDTA, 0.5 % (w/v) SDS) were added to the powder, inverted several times and centrifuged at maximum speed for 5 min. The resulting supernatant was added to 300 μ l isopropanol, mixed by pipetting and centrifuged at maximum speed for 5 min. After carefully discarding the supernatant, the pellet was washed 3 times with 70 % ethanol, drained and dried. The dried pellet was subsequently dissolved in 100 μ l TE buffer and stored at -20 °C.

Cloning

Sequences for *in silico* cloning were obtained from Aramemnon. Final constructs were verified by sequencing (Macrogen; dna.macrogen.com).

For the peroxisomal targeting of ATeam 1.03-nD/nA, the sensor was c-terminally fused to the peroxisomal targeting signal SKL by classical restriction enzyme-based cloning. For this, the sequence was amplified from the cytosolic version using primer LC37 (CCGCACTAGTGATATCACAAAGTTTG) adding a SpeI restriction enzyme site and LC38 (GGTCTAGATTACAGCTTGCTCTCGATGTTGTGG) adding the SKL target-sequence AGCAAGCTG and a XbaI restriction enzyme site. Subsequently, the cytosolic ATeam plasmid and the resulting PCR product were cut with SpeI and XbaI and ligated to yield ATeam-SKL (pLC6).

Quantification of sterols and plant volatiles by GC-MS

Plant cultivation, metabolite extraction and targeted metabolic profiling were performed as described in Henry et al. 2015.

Hypoxia plate reader assay to measure *in vivo* ATP level

Transparent 96-well plates (Sarstedt #82.1581) with a well volume of 400 μ l were filled with 300 μ l assay medium (10 mM MES pH 5.8, 10 mM MgCl₂, 10 mM CaCl₂, 5 mM KCl). Fluorescence was read sequentially for each well using the 'well multichromatics' mode in a . BMG CLARIOstar plate reader equipped with an atmospheric control unit (ACU). The following excitation and emission wavelengths were chosen: Excitation: 435 \pm 10 nm; emission: 485 \pm 10 (CFP) and 540 \pm 7.5 nm (YFP). The 'orbital averaging' mode was used to distribute the 70 excitation light flashes per reading cycle and well on a circle with a 4 mm radius. Hypoxia was induced after 90 minutes of equilibration in the dark. Reoxygenation was conducted after 4.5 h. Fluorescence values were subtracted by non-sensor control plants and the ratio was plotted as a function of relative ATP level.

Results

Establishment of a stable *pnc1/2* double mutant line

Since PNC1 and PNC2 are functional redundant and single mutants do not show a respective phenotype (Linka et al. 2008), a double mutant had to be generated in order to further analyze the physiological role of the PNC proteins. Therefore, individual tDNA insertion lines of *pnc1* (SAIL-H303) and *pnc2* (SALK-014579) were crossed (Sarah Keßel-Vigelius, PhD thesis). The tDNA is inserted in the 5th and 2nd exon of *PNC1* and *PNC2*, respectively (Figure 2A). Analysis of cDNA revealed that only shortened transcripts from 5' UTR to the site of the tDNA insertion are detectable, but the respective full-length transcripts are absent in the double mutant line (Figure 2B).

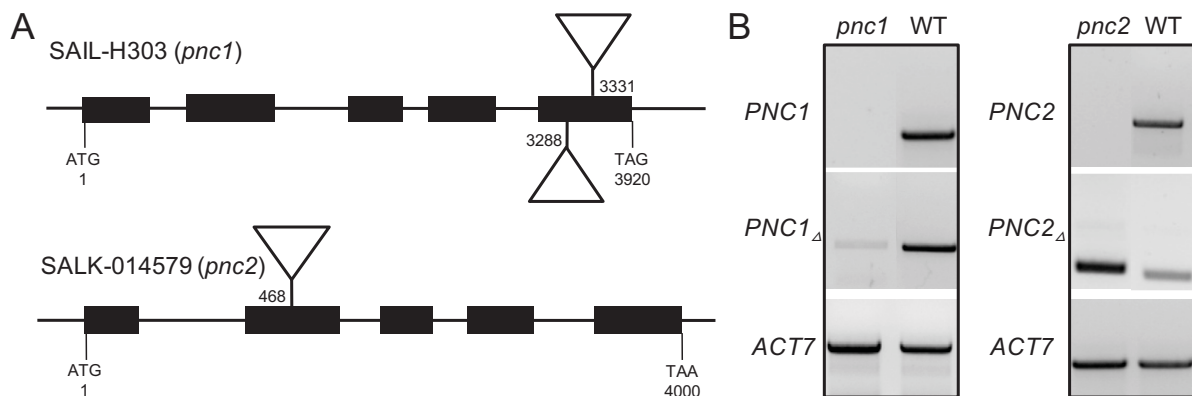


Figure 2: Genotyping of *pnc1/2* double mutant

(A) Gene architecture of *PNC1* (upper panel) and *PNC2* (lower panel) showing the tDNA insertion of *pnc1* and *pnc2*, respectively. Black squares mark exon region, connecting lines represent introns. (B) PCR on cDNA of *pnc1/2* using primer covering the full-length transcript (*PNC1*: 1023 bp; *PNC2*:1050 bp) or the region from 5'-UTR to tDNA insertion site (*PNC1 Δ* : 613 bp, *PNC2 Δ* : 365 bp). Transcript of *ACT7* served as positive control (734 bp).

ATP is required for functional β -oxidation and hence storage oil degradation during germination. Thus, mutants with a block in β -oxidation demand on the supply with an exogenous carbon source like sucrose to enable seedling establishment. The single mutants of *pnc1* and *pnc2* grew like the WT both, in the presence and absence of sucrose (Figure 3). But the *pnc1/2* double mutant was unable to germinate in the absence sucrose (Figure 3B).

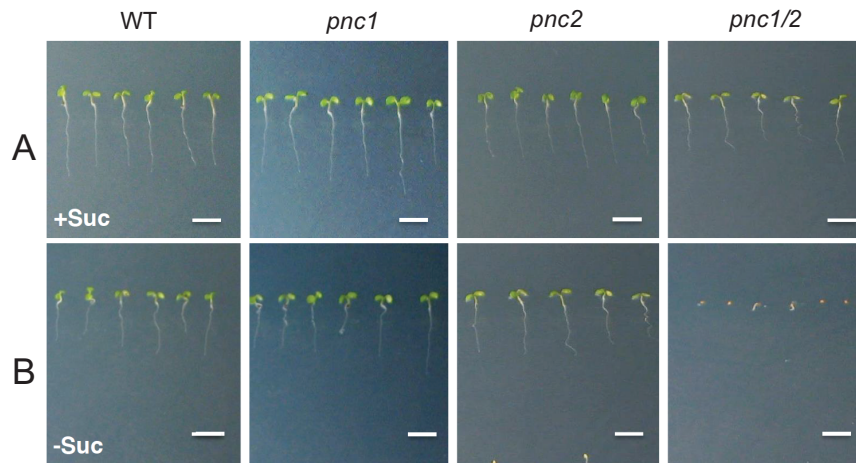


Figure 3: Sucrose dependency assay of *pnc1/2* double mutant

WT, *pnc1*, *pnc2* and *pnc1/2* were grown for 5 days either in the presence (upper panel) or absence (lower panel) of 1 % (w/v) sucrose. Images show representative seedlings of each genotype.

PNCs provide ATP for peroxisomal Mev pathway reactions

The last steps of the cytosolic Mev pathway of the synthesis of IPP used for isoprenoid production, is localized to peroxisomes. Within peroxisomes MevP is first phosphorylated and then decarboxylated to yield IPP. Both reactions require ATP and since PNCs are the so far only known peroxisomal ATP carrier, we hypothesized that they play an important role in this pathway.

To test this, WT and *pnc1/2* were grown in the presence of fosmidomycin, a specific inhibitor of the plastidic MEP pathway for IPP production and root length was measured as a function of plant growth (Figure 1).

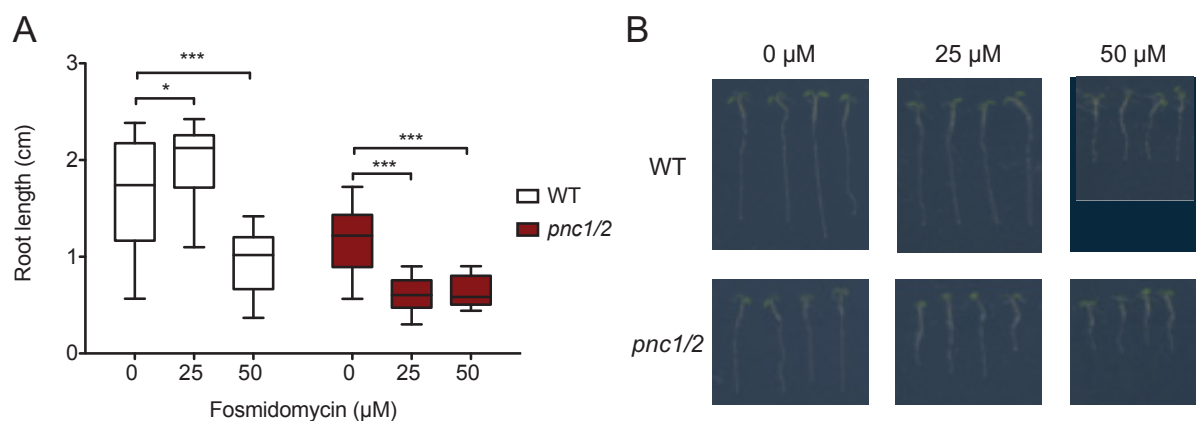


Figure 4: Root growth of WT and *pnc1/2* in the presence of fosmidomycin

(A) Root length of 7 days old WT (white) and *pnc1/2* (red) seedlings grown on 1/2MS + 1b% (w/v) sucrose in the presence or absence of fosmidomycin. $n > 16$, significant differences determined by students t-test; * = $p < 0.05$; *** = $p < 0.001$. (B) Representative images of 7 days old seedlings.

At 25 μM fosmidomycin the WT showed a slight but significant increased root length compared to the control without treatment. Interestingly, root length of *pnc1/2* is already strongly decreased at this concentration. Increasing the fosmidomycin concentration to 50 μM did not lead to a more severe decrease in the root length of *pnc1/2* but the WT revealed a significant decrease at this concentration. By inhibiting the MEP pathway, plants demand on the Mev pathway for the synthesis of IPP. As expected, without peroxisomal ATP supply in the *pnc1/2* mutant line, the Mev pathway cannot compensate for the inhibition of the MEP pathway as seen in the WT. But a complete inhibition at 50 μM fosmidomycin can obviously not be fully compensated by a functional Mev pathway even in the WT.

Campesterol, stigmasterol and sitosterol are sterols derived from IPP of the Mev pathway. They all three share the common precursor 24-methylenelophenol but stigmasterol is a sterol produced downstream of sitosterol. Another group of Mev pathway derived isoprenoids are sesquiterpenes with β -caryophyllene being the most dominant volatile mainly produced in flowers of plants, including *Arabidopsis* (Chen et al. 2003).

Sterols and volatiles of WT and *pnc1/2* were collected from 10 days old seedlings and 4 weeks old flowers, respectively and analyzed by GC-MS to determine the effect of the *pnc1/2* mutant on a metabolic level (Figure 5).

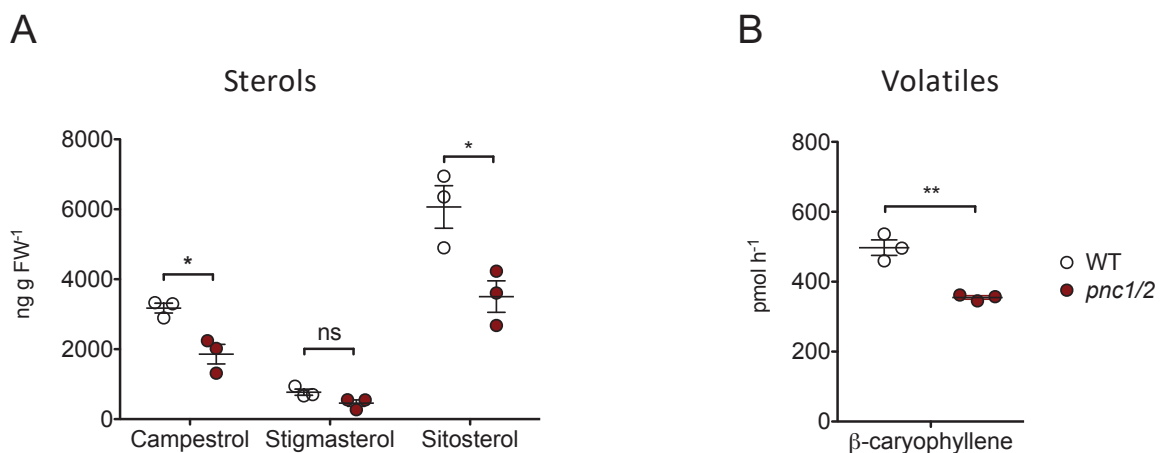


Figure 5: Levels of sterols and volatiles in WT and *pnc1/2*

(A) Amount of sterols in WT and *pnc1/2* seedlings measured by GC-MS. Samples collected from 100 mg pooled 10 days old seedlings. (B) Emission of β -caryophyllene by 50 flowers of 4 weeks old plants measured by GC-MS. $n = 3$; significant differences were determined by students t-test; ns = not significant; * = $p < 0.05$; ** = $p < 0.01$.

The amount of all measured sterols was reduced in the *pnc1/2* double mutant of about 60 % of the WT level (Figure 5A). But only campesterol and sitosterol showed a statistically significant difference to the WT (p -value of stigmasterol 0.07). In case of the volatiles (Figure 5B) the amount of emitted β -caryophyllene per hour is reduced in the *pnc1/2*

mutant to about 70 % of the WT level. This, together with the inhibitor analysis, clearly indicates a role of PNC1 and PNC2 for the ATP supply of the Mev pathway.

Determination of the cytosolic ATP pool *in vivo*

The genetically encoded ATP-FRET sensor ATeam is a powerful tool to analyze ATP levels *in vivo*. For the targeting of the well-established cytosolic version of the sensor, the peroxisomal target sequence 1 (PTS1) consisting of the three amino acids SKL was fused to the C-terminus of the sensor. For initial analysis of the correct localization of ATeam-SKL, the construct was transiently expressed in tobacco leaves and protoplasts were imaged after 2 days of expression using confocal laser scanning microscopy (CLSM) (Figure 6).

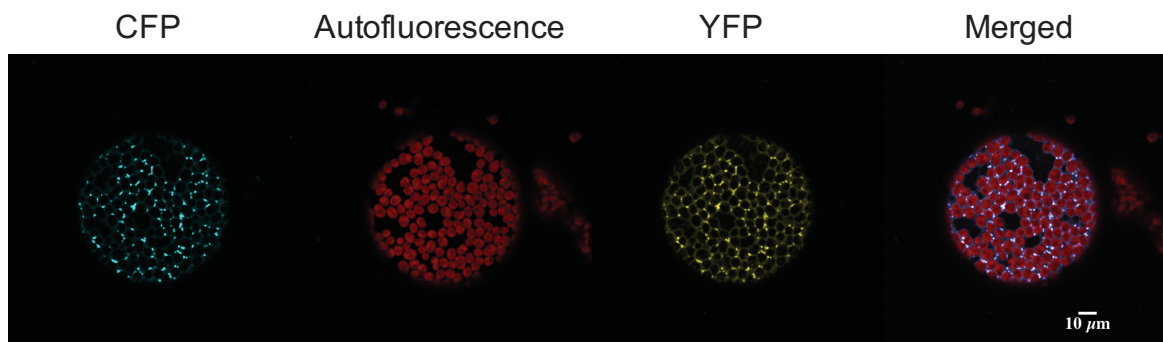


Figure 6: Localization of peroxisomal ATeam sensor transiently expressed in tobacco leaves

Young leaves of tobacco were infiltrated with *Agrobacteria* harboring the peroxisomal ATeam sensor. Protoplasts were isolated 2 days after infiltration and analyzed by CLSM. Both, CFP and YFP of the sensor accumulate in distinct dots, indicating peroxisomal localization of the sensor. Chloroplasts were imaged by autofluorescence of the chlorophyll.

When transiently expressed in tobacco, both fluorescence proteins of ATeam-SKL accumulate in dot-like structures indicating peroxisomal localization.

Since this system is more artificial and may lead to a mis-localization of the sensor, leaf tissue of stable transformed *Arabidopsis* was additionally analyzed (Figure 7).

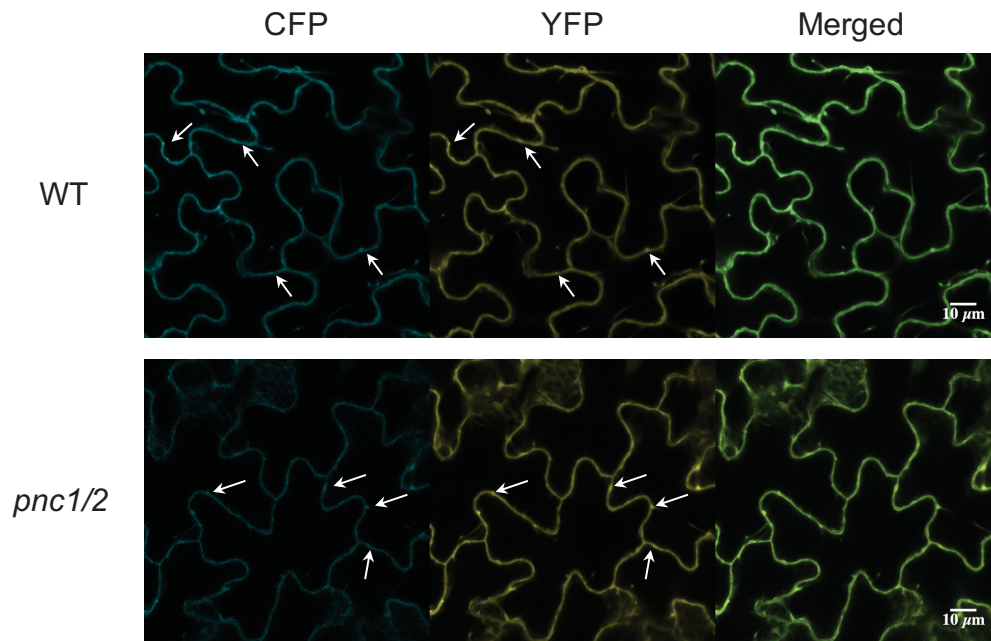


Figure 7: Localization of ATeam-SKL in stable transformed Arabidopsis leaf tissue.

CLSM of stable transformed WT and *pnc1/2* Arabidopsis plants. CFP (left panel) and YFP (middle panel) co-localize as visible in the merged picture (right panel). Beside the dot like structure (white arrows) the sensor has a high background noise.

In contrast to the transient expression in tobacco, stable transformed Arabidopsis plants showed a strong expression of the ATeam-SKL sensor in non-peroxisomal organelles. The peroxisomal localization is still visible (white arrows), but the high background noise prevents the correct measurement of the peroxisomal ATP levels.

To test the dynamic response of the cytosolic ATeam sensor in WT and *pnc1/2* plants, fluorescence was measured in a plate reader equipped with an atmospheric control unit (ACU). The ACU enables the displacement of oxygen by pumping in nitrogen which leads to a rapid decrease in ATP production and hence concentration (Wagner et al. 2019). The subsequent reoxygenation leads to an increase in the ATP production. The combination of rapid de- and reoxygenation allows to draw inferences about the dynamic response of ATP depletion and recovery in the mutant compared to the WT (Figure 8).

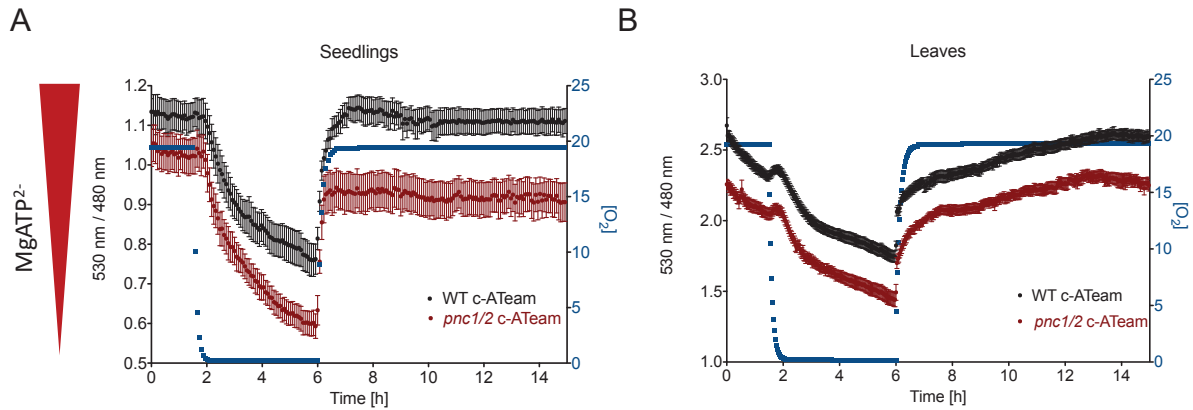


Figure 8: Hypoxia assay of WT and *pnc1/2*

7 days old seedlings (A) and leaf discs from 4 weeks old plants (B) harboring the cytosolic ATeam sensor were analyzed by fluorescence plate reader assays using an ACU. Hypoxia was induced after 90 minutes of equilibration for 4.5 h. Fluorescence emission of CFP (480 nm) and YFP (530 nm) was detected, subtracted by non-sensor control plants and the ratio was plotted as a function of relative ATP level. Values represent means and SEM of 12 replicates pooled from 2 independent sensor lines, each.

For seedlings (Figure 8A) a steady state of the cytosolic ATP level was maintained before the application of hypoxia (90 minutes). After this, the oxygen depletion results in a rapid drop of the MgATP levels in both genotypes. This depletion further increased throughout the whole time of oxygen deprivation to 68% and 60% of the steady state level in the WT and *pnc1/2* mutant, respectively. Upon reoxygenation after 4.5 h of hypoxia, the MgATP level rose rapidly, but only the WT could reach the values of the equilibration phase. *pnc1/2* reached a steady state after reoxygenation at about 91% of the initial values.

In case of the leaf discs (Figure 8B), no steady state was reached during the equilibration state, neither for WT, nor for *pnc1/2*. Upon hypoxia, MgATP levels dropped at the same rate in both genotypes. WT and *pnc1/2* also behaved the same when it comes to reoxygenation and both reached the same values as measured before oxygen deprivation. But, cytosolic MgATP levels in both, seedlings and leaves are generally lower in *pnc1/2* compared to the WT.

Discussion

MgATP levels are reduced in the cytosol of *pnc1/2*

ATP is essential for fatty acid activation prior β -oxidation. The *pnc1/2* double mutant of both peroxisomal ATP transport proteins is unable to germinate in the absence of an exogenous carbon source (Figure 3) which implies, that at least during this developmental stage PNC proteins are the major contributors to peroxisomal ATP supply. Under standard growth conditions the double mutant does not show an obvious growth phenotype after the seedling becomes photoautotrophic. Since the effect of the tDNA insertion within the last exon of *pnc1* is difficult to be determined, the ATP-FRET sensor ATeam was employed to measure MgATP levels in the cytosol and peroxisomes both, in the WT and *pnc1/2* double mutant. Even though when transiently expressed in tobacco, the peroxisomal ATeam version is targeted almost exclusively to peroxisome-like structures, stable transformed Arabidopsis show additional background fluorescence, that prevents the usage of a fluorescence plate reader to detect the peroxisomal signal specifically (Figure 7). For both, transient expression in tobacco as well as stable transformation of Arabidopsis, an Agrobacteria strain was used that carries the viral silencing repressor p19 from *Cymbidium ringspot virus* (Lakatos et al. 2004) to maximize the fluorescence intensity which is required for plate reader measurements. But it is conceivable that the strong overexpression led to a mis-localization of the ATeam-SKL at least in stable transformed Arabidopsis. Hence, using an Agrobacteria strain without the p19 protein might overcome this issue. However, since nobody could show peroxisomal targeting of the ATeam sensor before, there might be some issues with the import of the sensor into peroxisomes. Unlike mitochondria and chloroplast, peroxisomes are able to import fully folded proteins which might represent a bottleneck for big or structural complex proteins (Walton et al. 1995). Measurements of the cytosolic ATeam revealed reduced MgATP levels in young seedlings and leaf tissue (Figure 8). In seedlings, depletion of MgATP by hypoxia led to a more rapid decrease in the *pnc1/2* and in contrast to the WT, the double mutant did not reach the initial MgATP level after reoxygenation. Whereas in leaf tissue, the rates of MgATP depletion and replenishment were the same but both genotypes did not reach a steady state before the application of hypoxia. However, for future experiments a CCCP treatment should be added to the end of the assay to test whether the difference between the genotypes is real. CCCP uncouples the mitochondrial electron transport chain which leads to a depletion of the cellular ATP pool. By this, the minimal values of the dynamic range of the ATeam sensor can be determined and compared. A difference in the MgATP levels between *pnc1/2* and the WT would imply a general effect of the double mutant on cellular energy metabolism. Without oxygen, mitochondrial respiration is impaired and thus, the cells fully demand on glycolysis and fermentation for ATP

production (Mustroph and Albrecht 2003). In plants, carbon fixed during the day is mainly stored as starch or used for sucrose synthesis (Liang et al. 2015). As a consequence, reduced photosynthetic activity would lead to decreased carbon fixation rates and thus, less carbon stored in the cell for respiration and hence energy production. To test this hypothesis, sugar and starch content should be determined and photosynthetic efficiency as well as gas exchange could be tested.

PNC proteins are required for the production of Mev pathway derived isoprenoids

IPP and DMAPP are the building block for the synthesis of isoprenoids, the most diverse ... group in plants. Their production is compartmentalized to the plastidic MEP pathway and the cytosolic/peroxisomal Mev pathway. While IPP from the MEP pathway is mainly involved in the production of photosynthesis related molecules, IPP from the Mev pathway contributes to the production of different sterols. Since two enzymatic steps of the peroxisomal part of the Mev pathway are ATP-dependent, we hypothesized that the activity of the PNC proteins is crucial for a functional Mev pathway and thus for the production of different sterols.

Indeed, the concentrations of campesterol, sitosterol and β -caryophyllene are significantly reduced in seedlings of *pnc1/2* compared to WT (Figure 5A). Sitosterol is the most abundant sterol in plants and the direct precursor of stigmasterol (Nomura et al. 1999). In *pnc1/2* the amount of stigmasterol is also reduced, but not statistically significant. It seems, that the residual high concentration of sitosterol is still sufficient for the synthesis of stigmasterol. Measurements of sterols in a knockout line of MDD1, the second peroxisomal ATP dependent enzyme, revealed similar results, but with higher stigmasterol levels compared to *pnc1/2* (Henry et al. 2015). In *mdd1* the residual basal activity of the low expressed isoform MDD2 or the fact that in *pnc1/2* both ATP dependent reactions (MPK and MDD) are affected, might explain the additional drop in the double mutant. Interestingly, a complete depletion of sterols is only observed in mutants that are affected in enzymes acting directly upstream of sterol biosynthesis (Clouse 2002; Henry et al. 2015). This implies the existence of an IPP crosstalk between the Mev and MEP pathway. But even though the *pnc1/2* is more sensitive to lower concentrations of the MEP pathway specific inhibitor fosmidomycin, a complete inhibition cannot be compensated by a functional Mev pathway shown by a similar reduction in WT growth at higher fosmidomycin concentrations (Figure 4).

Beside the *de novo* synthesis, IPP can also be regenerated by phosphorylating IP catalyzed by cytosolic IPK (Henry et al. 2015). Hence, lower MgATP levels in the cytosol of *pnc1/2* as measured by the ATeam sensor, might also contribute to the more severe decrease in sterols compared to *mdd1*. But all in all, the reduction of sterols does not lead to an obvious growth phenotype. Mutants that are affected in the biosynthesis of brassinolide, the most active brassinosteroid in plants, have a severe dwarfism phenotype (Clouse 2002).

Brassinolide is synthesized from campesterol, but the reduction observed for *pnc1/2* and *mdd1* might still enable normal values of brassinolide production.

Sitosterol and stigmasterol play important roles during biotic and abiotic stress response (Schaller 2004; Wang et al. 2012). Thus, the reduction of both sterols in *pnc1/2* might not have an effect under normal growth conditions, but future studies should address the question of how the double mutant reacts to for example pathogen attack.

In addition, this study aimed to generate a triple mutant of *pnc1/2* and *ipk*. Measuring sterol levels in this mutant with and without additional inhibition of the MEP pathway by fosmidomycin will show, how *de novo* IPP production and regeneration by IPK contribute to the synthesis of sterols. Further, it would be interesting to know, how the production of MEP pathway derived isoprenoids is affected in these mutants.

Putative role of PNC proteins in photorespiration

It could be shown, that photorespiration plays an important role in maintaining photosynthetic activity by preventing the accumulation of inhibiting metabolites (Kelly and Latzko 1976) and depletion of reducing equivalents to prevent the generation of reactive oxygen species (ROS) especially under high light conditions (Takahashi et al. 2007). Since photorespiration is a highly dynamic process that responds quickly to environmental changes (Eisenhut et al. 2017), it has to be tightly regulated. Many enzymes involved in photorespiration have been shown to be regulated by phosphorylation (Hodges et al. 2013; Kataya et al. 2016) and different kinases have been identified to have peroxisomal localization (Fukao et al. 2002; Turner et al. 2005; Coca and San Segundo 2010). One of these kinases is the NADH kinase 3 (NADK3) that phosphorylates NADH to NADPH (Turner et al. 2005). NADPH is required for the peroxisomal ascorbate glutathione cycle to regenerate oxidized glutathione by glutathione reductase 1 (GR1) and thus, plays an important role in cellular stress response (Noctor et al. 2012). NADP itself is reduced either by the action of the peroxisomal oxidative pentose phosphate pathway or by NADP-dependent isocitrate dehydrogenase (Letierrier et al. 2012; Holscher et al. 2016). RNA-Seq data revealed a strong upregulation of PNC2 but not PNC1 in mutants of the photorespiratory pathway when shifted from high CO₂ (3000 ppm) to ambient air (300 ppm) (Figure SX). Since photorespiratory mutants are linked to increased oxidative stress (Moreno et al. 2005; Li et al. 2019), it is possible that ATP provided by PNC2 is required for peroxisomal NADPH production to protect the cell against oxidative damage. This also implies that PNC1 and PNC2 might have different roles within plant metabolism. Recently, several peroxisomal proteins were identified to be involved in photorespiration under dynamic and fluctuating light conditions when light intensity follows a sinusoidal pattern with high and low light peaks to mimic solar radiation on a cloudy day (Li et al. 2019). Most of

them had no significant phenotype under standard and low light conditions like the mutant of the peroxisomal NAD carrier *pxn1*. The authors supposed that PXN imports additional NAD to compensate for the increased demand of NAD reducing reactions in fluctuating high light. Because of this observation it is conceivable that PNC proteins are required to import ATP especially during fluctuating light conditions to drive regulation by phosphorylation on the one hand and on the other hand to protect from oxidative damage at high light peaks. This phenotypic platform enables the measurement of several photosynthetic parameters during growth and development by fluorescence in a non-disruptive way. In the future, this system will be adapted to genetically encoded fluorescence probes like the ATeam sensor, which allows the determination of additional parameters like pH, redox state and ATP levels (Markus Schwarzländer, personal communication).

In addition to the influence of photorespiration on photosynthetic activity, peroxisomal β -oxidation has been linked to stomatal conductance (McLachlan et al. 2016). They postulate that cytosolic oil bodies in the guard cells are consumed by peroxisomal β -oxidation in order to produce ATP required for stomatal opening. Mutants affected in triacyl-glycerol catabolism have a delayed light-induced opening of the stomata most likely caused by a reduced activity of the plasma membrane ATPase that pumps protons into the apoplast resulting in an acidification and hence opening of the stomata. This might represent another way, how PNC proteins are at least indirectly involved in photorespiration, since a decrease in stomatal conductance prevents an efficient gas exchange which leads to elevated photorespiration rates by increasing the CO₂ concentration within the leaf.

Putative role of PNC proteins in hormone biosynthesis

Peroxisomal β -oxidation is not only required for storage oil mobilization during seedling establishment. It is also involved in the biosynthesis of plant hormones like auxin, jasmonic acid and ABA. Because all these β -oxidation related processes demand on the ATP dependent activation of precursors before entering β -oxidation, a lack of peroxisomal ATP import has to affect many aspects of plant growth and development. However, the *pnc1/2* double mutant does not show an obvious phenotype after the seedlings becomes photoautotrophic.

The conversion of the inactive auxin precursor IBA to the active compound IAA which represents the best studied naturally occurring auxin molecule is mediated by one cycle of β -oxidation. In general auxin is crucial for the regulation of all aspects of plant growth and development. To maintain the homeostasis of active auxin, biosynthesis, transport and inactivation/activation must be tightly regulated. The auxin pool consists of a mixture of free auxin, conjugated auxins and IBA (Korasick et al. 2013). In Arabidopsis, like in many other dicots, the majority of IAA is bound as amino acid conjugates (Bajguz and Piotrowska 2009).

Mutant analyses showed that the conversion of IBA to IAA plays an important role during seedling growth and development (Zolman et al. 2008). Thus, a β -oxidation defect resulting in lower rates of IBA derived IAA might not influence the plants life cycle after the seedling becomes photoautotrophic.

Jasmonic acid (JA) represents another plant hormone that is involved in biotic and abiotic stress response as well as developmental processes such as root growth, reproduction and senescence (Wasternack and Hause 2013; Chini et al. 2016). JA is converted by peroxisomal β -oxidation from 12-oxo-phytodienic acid (OPDA). The accumulation of OPDA in seeds is the reason for the seed dormancy phenotype of the peroxisomal fatty acid importer comatose (*cts1*) (Dave et al. 2011). Defects in the JA biosynthetic pathway lead to male sterility. But, since both *cts1* and *pnc1/2* are able to reproduce there have to be alternative routes for the import and conversion of OPDA within peroxisomes.

Conclusion

ATP is an important substrate and crucial for a plethora of metabolic reactions. While many ATP-dependent pathways have been identified in the cytosol, the mitochondria and the chloroplasts, the knowledge about respective peroxisomal pathways is restricted to β -oxidation activity. Import of ATP into peroxisomes is mediated by two MCF carrier called PNC1 and PNC2. Interestingly, the double mutant has no obvious phenotype under standard growth conditions after the seedling becomes photoautotrophic. Here we could show, that ATP imported by PNC proteins is required for a functional Mev pathway for the production of sterols, hormones and volatiles. Future studies should aim to characterize *pnc1/2* under non-standard conditions, like biotic stress upon wounding (JA response) or dynamic light conditions to test for an involvement in supporting and regulating photorespiration.

Author contribution

Generation and genotyping of *pnc1/2* double mutant was performed by Sarah-Keßel-Vigelius. Plant cultivation for sterol and volatile analysis, extraction and measuring by GC-MS was done by Laura Henry. Markus Schwarzländer provided the cytosolic ATeam sensor and support during sensor measurement. Lennart Charton wrote the manuscript and performed all residual experiments and analyses. Nicole Linka, Andreas Weber, Georg Groth and Markus Schwarzländer participated in scientific discussions. Nicole Linka and Lennart Charton designed the experiments.

References

- Bajguz, A. and A. Piotrowska (2009). "Conjugates of auxin and cytokinin." Phytochemistry **70**(8): 957-969.
- Chen, F., D. Tholl, J. C. D'Auria, A. Farooq, E. Pichersky and J. Gershenzon (2003). "Biosynthesis and emission of terpenoid volatiles from Arabidopsis flowers." Plant Cell **15**(2): 481-494.
- Chini, A., S. Gimenez-Ibanez, A. Goossens and R. Solano (2016). "Redundancy and specificity in jasmonate signalling." Curr Opin Plant Biol **33**: 147-156.
- Clouse, S. D. (2002). "Arabidopsis mutants reveal multiple roles for sterols in plant development." Plant Cell **14**(9): 1995-2000.
- Coca, M. and B. San Segundo (2010). "AtCPK1 calcium-dependent protein kinase mediates pathogen resistance in Arabidopsis." Plant J **63**(3): 526-540.
- Cornah, J. E., V. Germain, J. L. Ward, M. H. Beale and S. M. Smith (2004). "Lipid utilization, gluconeogenesis, and seedling growth in Arabidopsis mutants lacking the glyoxylate cycle enzyme malate synthase." J Biol Chem **279**(41): 42916-42923.
- Dave, A., M. L. Hernandez, Z. He, V. M. Andriotis, F. E. Vaistij, T. R. Larson and I. A. Graham (2011). "12-oxo-phytodienoic acid accumulation during seed development represses seed germination in Arabidopsis." Plant Cell **23**(2): 583-599.
- De Col, V., P. Fuchs, T. Nietzel, M. Elsasser, C. P. Voon, A. Candeo, I. Seeliger, M. D. Fricker, C. Grefen, I. M. Moller, A. Bassi, B. L. Lim, M. Zancani, A. J. Meyer, A. Costa, S. Wagner and M. Schwarzlander (2017). "ATP sensing in living plant cells reveals tissue gradients and stress dynamics of energy physiology." Elife **6**.
- Dudareva, N., S. Andersson, I. Orlova, N. Gatto, M. Reichelt, D. Rhodes, W. Boland and J. Gershenzon (2005). "The nonmevalonate pathway supports both monoterpene and sesquiterpene formation in snapdragon flowers." Proc Natl Acad Sci U S A **102**(3): 933-938.
- Eisenhut, M., A. Brautigam, S. Timm, A. Florian, T. Tohge, A. R. Fernie, H. Bauwe and A. P. M. Weber (2017). "Photorespiration Is Crucial for Dynamic Response of Photosynthetic Metabolism and Stomatal Movement to Altered CO₂ Availability." Mol Plant **10**(1): 47-61.
- Fukao, Y., M. Hayashi and M. Nishimura (2002). "Proteomic analysis of leaf peroxisomal proteins in greening cotyledons of Arabidopsis thaliana." Plant Cell Physiol **43**(7): 689-696.
- Graham, I. A. and P. J. Eastmond (2002). "Pathways of straight and branched chain fatty acid catabolism in higher plants." Prog Lipid Res **41**(2): 156-181.
- Hatsugai, N., V. Perez Koldenkova, H. Imamura, H. Noji and T. Nagai (2012). "Changes in cytosolic ATP levels and intracellular morphology during bacteria-induced hypersensitive cell death as revealed by real-time fluorescence microscopy imaging." Plant Cell Physiol **53**(10): 1768-1775.
- Henry, L. K., M. Gutensohn, S. T. Thomas, J. P. Noel and N. Dudareva (2015). "Orthologs of the archaeal isopentenyl phosphate kinase regulate terpenoid production in plants." Proc Natl Acad Sci U S A **112**(32): 10050-10055.
- Hodges, M., M. Jossier, E. Boex-Fontvieille and G. Tcherkez (2013). "Protein phosphorylation and photorespiration." Plant Biol (Stuttg) **15**(4): 694-706.

- Hofgen, R. and L. Willmitzer (1988). "Storage of competent cells for *Agrobacterium* transformation." Nucleic Acids Res **16**(20): 9877.
- Holscher, C., M. C. Lutterbey, H. Lansing, T. Meyer, K. Fischer and A. von Schaewen (2016). "Defects in Peroxisomal 6-Phosphogluconate Dehydrogenase Isoform PGD2 Prevent Gametophytic Interaction in *Arabidopsis thaliana*." Plant Physiol **171**(1): 192-205.
- Imamura, H., K. P. Nhat, H. Togawa, K. Saito, R. Iino, Y. Kato-Yamada, T. Nagai and H. Noji (2009). "Visualization of ATP levels inside single living cells with fluorescence resonance energy transfer-based genetically encoded indicators." Proc Natl Acad Sci U S A **106**(37): 15651-15656.
- Inoue, H., H. Nojima and H. Okayama (1990). "High efficiency transformation of *Escherichia coli* with plasmids." Gene **96**: 23-28.
- Kasahara, H., A. Hanada, T. Kuzuyama, M. Takagi, Y. Kamiya and S. Yamaguchi (2002). "Contribution of the mevalonate and methylerythritol phosphate pathways to the biosynthesis of gibberellins in *Arabidopsis*." J Biol Chem **277**(47): 45188-45194.
- Kataya, A. R., E. Schei and C. Lillo (2016). "Towards understanding peroxisomal phosphoregulation in *Arabidopsis thaliana*." Planta **243**(3): 699-717.
- Kelly, G. J. and E. Lutzko (1976). "Inhibition of spinach-leaf phosphofructokinase by 2-phosphoglycollate." FEBS Lett **68**(1): 55-58.
- Korasick, D. A., T. A. Enders and L. C. Strader (2013). "Auxin biosynthesis and storage forms." J Exp Bot **64**(9): 2541-2555.
- Kotera, I., T. Iwasaki, H. Imamura, H. Noji and T. Nagai (2010). "Reversible dimerization of *Aequorea victoria* fluorescent proteins increases the dynamic range of FRET-based indicators." ACS Chem Biol **5**(2): 215-222.
- Lakatos, L., G. Szittyá, D. Silhavy and J. Burgyan (2004). "Molecular mechanism of RNA silencing suppression mediated by p19 protein of tombusviruses." EMBO J **23**(4): 876-884.
- Laule, O., A. Furholz, H. S. Chang, T. Zhu, X. Wang, P. B. Heifetz, W. Grissem and M. Lange (2003). "Crosstalk between cytosolic and plastidial pathways of isoprenoid biosynthesis in *Arabidopsis thaliana*." Proc Natl Acad Sci U S A **100**(11): 6866-6871.
- Letierrier, M., J. B. Barroso, R. Valderrama, J. M. Palma and F. J. Corpas (2012). "NADP-dependent isocitrate dehydrogenase from *Arabidopsis* roots contributes in the mechanism of defence against the nitro-oxidative stress induced by salinity." ScientificWorldJournal **2012**: 694740.
- Li, J., S. Tietz, J. A. Cruz, D. D. Strand, Y. Xu, J. Chen, D. M. Kramer and J. Hu (2019). "Photometric screens identified *Arabidopsis* peroxisome proteins that impact photosynthesis under dynamic light conditions." Plant J **97**(3): 460-474.
- Liang, C., Y. Zhang, S. Cheng, S. Osorio, Y. Sun, A. R. Fernie, C. Y. Cheung and B. L. Lim (2015). "Impacts of high ATP supply from chloroplasts and mitochondria on the leaf metabolism of *Arabidopsis thaliana*." Front Plant Sci **6**: 922.
- Linka, N., F. L. Theodoulou, R. P. Haslam, M. Linka, J. A. Napier, H. E. Neuhaus and A. P. Weber (2008). "Peroxisomal ATP import is essential for seedling development in *Arabidopsis thaliana*." Plant Cell **20**(12): 3241-3257.

- Lorenz, A., M. Lorenz, U. C. Vothknecht, S. Niopek-Witz, H. E. Neuhaus and I. Haferkamp (2015). "In vitro analyses of mitochondrial ATP/phosphate carriers from *Arabidopsis thaliana* revealed unexpected Ca(2+)-effects." BMC Plant Biol **15**: 238.
- McLachlan, D. H., J. Lan, C. M. Geilfus, A. N. Dodd, T. Larson, A. Baker, H. Horak, H. Kollist, Z. He, I. Graham, M. V. Mickelbart and A. M. Hetherington (2016). "The Breakdown of Stored Triacylglycerols Is Required during Light-Induced Stomatal Opening." Curr Biol **26**(5): 707-712.
- Mendoza-Poudereux, I., E. Kutzner, C. Huber, J. Segura, W. Eisenreich and I. Arrillaga (2015). "Metabolic cross-talk between pathways of terpenoid backbone biosynthesis in spike lavender." Plant Physiol Biochem **95**: 113-120.
- Moreno, J. I., R. Martin and C. Castresana (2005). "Arabidopsis SHMT1, a serine hydroxymethyltransferase that functions in the photorespiratory pathway influences resistance to biotic and abiotic stress." Plant J **41**(3): 451-463.
- Mustroph, A. and G. Albrecht (2003). "Tolerance of crop plants to oxygen deficiency stress: fermentative activity and photosynthetic capacity of entire seedlings under hypoxia and anoxia." Physiol Plant **117**(4): 508-520.
- Noctor, G., A. Mhamdi, S. Chaouch, Y. Han, J. Neukermans, B. Marquez-Garcia, G. Queval and C. H. Foyer (2012). "Glutathione in plants: an integrated overview." Plant Cell Environ **35**(2): 454-484.
- Nomura, T., Y. Kitasaka, S. Takatsuto, J. B. Reid, M. Fukami and T. Yokota (1999). "Brassinosteroid/Sterol synthesis and plant growth as affected by lka and lkb mutations of Pea." Plant Physiol **119**(4): 1517-1526.
- Pracharoenwattana, I., J. E. Cornah and S. M. Smith (2005). "Arabidopsis peroxisomal citrate synthase is required for fatty acid respiration and seed germination." Plant Cell **17**(7): 2037-2048.
- Sapir-Mir, M., A. Mett, E. Belausov, S. Tal-Meshulam, A. Frydman, D. Gidoni and Y. Eyal (2008). "Peroxisomal localization of Arabidopsis isopentenyl diphosphate isomerases suggests that part of the plant isoprenoid mevalonic acid pathway is compartmentalized to peroxisomes." Plant Physiol **148**(3): 1219-1228.
- Schaller, H. (2004). "New aspects of sterol biosynthesis in growth and development of higher plants." Plant Physiol Biochem **42**(6): 465-476.
- Simkin, A. J., G. Guirimand, N. Papon, V. Courdavault, I. Thabet, O. Ginis, S. Bouzid, N. Giglioli-Guivarc'h and M. Clastre (2011). "Peroxisomal localisation of the final steps of the mevalonic acid pathway in planta." Planta **234**(5): 903-914.
- Takahashi, S., H. Bauwe and M. Badger (2007). "Impairment of the photorespiratory pathway accelerates photoinhibition of photosystem II by suppression of repair but not acceleration of damage processes in Arabidopsis." Plant Physiol **144**(1): 487-494.
- Turner, W. L., J. C. Waller and W. A. Snedden (2005). "Identification, molecular cloning and functional characterization of a novel NADH kinase from *Arabidopsis thaliana* (thale cress)." Biochem J **385**(Pt 1): 217-223.
- Voon, C. P., X. Guan, Y. Sun, A. Sahu, M. N. Chan, P. Gardstrom, S. Wagner, P. Fuchs, T. Nietzel, W. K. Versaw, M. Schwarzlander and B. L. Lim (2018). "ATP compartmentation in

plastids and cytosol of *Arabidopsis thaliana* revealed by fluorescent protein sensing." Proc Natl Acad Sci U S A **115**(45): E10778-E10787.

Wagner, S., J. Steinbeck, P. Fuchs, S. Lichtenauer, M. Elsasser, J. H. M. Schippers, T. Nietzel, C. Ruberti, O. Van Aken, A. J. Meyer, J. T. Van Dongen, R. R. Schmidt and M. Schwarzlander (2019). "Multiparametric real-time sensing of cytosolic physiology links hypoxia responses to mitochondrial electron transport." New Phytol.

Walton, P. A., P. E. Hill and S. Subramani (1995). "Import of stably folded proteins into peroxisomes." Mol Biol Cell **6**(6): 675-683.

Wang, K., M. Senthil-Kumar, C. M. Ryu, L. Kang and K. S. Mysore (2012). "Phytosterols play a key role in plant innate immunity against bacterial pathogens by regulating nutrient efflux into the apoplast." Plant Physiol **158**(4): 1789-1802.

Wasternack, C. and B. Hause (2013). "Jasmonates: biosynthesis, perception, signal transduction and action in plant stress response, growth and development. An update to the 2007 review in *Annals of Botany*." Ann Bot **111**(6): 1021-1058.

Zhang, X., R. Henriques, S. S. Lin, Q. W. Niu and N. H. Chua (2006). "Agrobacterium-mediated transformation of *Arabidopsis thaliana* using the floral dip method." Nat Protoc **1**(2): 641-646.

Zolman, B. K., N. Martinez, A. Millius, A. R. Adham and B. Bartel (2008). "Identification and characterization of *Arabidopsis* indole-3-butyric acid response mutants defective in novel peroxisomal enzymes." Genetics **180**(1): 237-251.

IV. Published Manuscripts

IV.I Published Manuscript 1

Plant peroxisomal solute transporter proteins

Lennart Charton^{1,2}, Anastasija Plett^{1,2}, and Nicole Linka^{1,3}

¹ Institute for Plant Biochemistry and Cluster of Excellence on Plant Sciences (CEPLAS),
Heinrich Heine University, Universitätsstrasse 1, 40225 Düsseldorf, Germany.

² Equal author contribution

³ Corresponding author

Abstract

Plant peroxisomes are unique subcellular organelles which play an indispensable role in several key metabolic pathways, including fatty acid β -oxidation, photorespiration, and degradation of reactive oxygen species. The compartmentalization of metabolic pathways into peroxisomes is a strategy for organizing the metabolic network and improving pathway efficiency. An important prerequisite, however, is the exchange of metabolites between peroxisomes and other cell compartments. Since the first studies in 1970s scientists contributed to understanding how solutes enter or leave this organelle. This review gives an overview about our current knowledge of the solute permeability of peroxisomal membranes described in plants, yeast, mammals and other eukaryotes. In general, peroxisomes contain in their bilayer membrane specific transporters for hydrophobic fatty acids (ABC transporter) and large cofactor molecules (carrier for ATP, NAD and CoA). Smaller solutes with molecular masses below 300–400 Da, like the organic acids malate, oxaloacetate, and 2-oxoglutarate, are shuttled via non-selective channels across the peroxisomal membrane. In comparison to yeast, human, mammals and other eukaryotes, the function of these known peroxisomal transporters and channels in plants are discussed in this review.

Introduction

Peroxisomes are surrounded by a single membrane which functions as a permeability barrier to solutes by forming a confined compartment for peroxisomal metabolism. To connect peroxisomes to the metabolic network of the cell, the peroxisomal bilayer membrane embeds different transport proteins allowing the passage of a variety of solutes (Rottensteiner and Theodoulou 2006; Antonenkov and Hiltunen 2011; Linka and Theodoulou 2013). Since peroxisomes are highly metabolically active, a massive transfer of metabolites across the peroxisomal membrane has to take place (Antonenkov and Hiltunen 2011; Linka and Esser 2012; Linka and Theodoulou 2013). Recent progress defines the permeability of the peroxisomal membrane to solutes into two types of transport proteins: (1) *non-selective pore-forming channels* facilitate the passage of small solutes down the electrochemical gradient, like the β -barrel porins found in the outer membrane of gram-negative bacteria, mitochondria and plastids (Antonenkov and Hiltunen 2011); (2) *specific transporters* mediate the passive flux of larger molecules in a uniport or antiport mechanism, typical for the inner mitochondrial and envelope membrane (Linka and Esser 2012; Linka and Theodoulou 2013). Thus, the peroxisomal bilayer membrane is comparable to the plasma membrane and Endoplasmic Reticulum (ER) membrane, since permeability is conducted by both, channel

and carrier proteins. The combination of non-selective pore-forming channels to transfer small molecules as well as specific carrier proteins for 'bulky' solutes is a highly efficient way to cope with a massive flux of a variety of metabolites across the peroxisomal border. While solute transport through a pore-forming channel occurs at a much faster rate, carriers bind their solutes tightly and are thus highly specific to their transport substrate.

Peroxisomal pore-forming channels are present in the membrane of plants, mammals, and yeast peroxisomes as well as in glycosomal membranes of *Trypanosoma brucei* (Reumann et al. 1995; Reumann et al. 1996; Reumann et al. 1998; Rokka et al. 2009; Antonenkov et al. 2009; Gualdrón-López et al. 2012; Mindthoff et al. 2015). These channel proteins are general pores consisting of transmembrane α -helices and thus distinct to the β -barrel porins. The peroxisomal channels allow the rapid and unrestricted diffusion of small hydrophilic molecules with molecular masses up to 300-400 Da, but prevent diffusion of larger molecules across the peroxisomal membrane (Antonenkov and Hiltunen 2011). The transport is driven by the concentration gradient of the transported solute. Recently, two putative channel proteins have been identified for peroxisomes: the peroxisomal membrane protein of 22 kDa (PMP22) and peroxin 11 (PEX11) (Figure 1) (Rokka et al. 2009; Mindthoff et al. 2015).

Up to now, specific solute transporters belonging to the mitochondrial transporter family (MCF) and the ATP-binding cassette (ABC) transporter family have been found in the peroxisomal membranes of mammals, plants and yeast (Figure 1) (Linka and Esser 2012; Linka and Theodoulou 2013). These two families of proteins each consist of transmembrane α -helical domains and catalyze a passive or active transport, respectively. Three peroxisomal members of the MCF are passive carriers mediating the facilitated diffusion of solutes down their electrochemical gradient (Palmieri et al. 2001; van Roermund et al. 2001; Visser et al. 2002; Linka et al. 2008; Arai et al. 2008; Agrimi et al. 2011; Bernhardt et al. 2012; Agrimi et al. 2012). In contrast, the peroxisomal ABC transporter is an active transporter pumping its substrate across the membrane against their electrochemical gradient, which is coupled to the hydrolysis of ATP as energy source (Morita and Imanaka 2012; Baker et al. 2015; Theodoulou and Kerr 2015). In summary, both peroxisomal carrier types perform the traffic of large molecules (up to < 400 Da), including acyl-CoA esters and some cofactors like ATP, NAD⁺, CoA.

Peroxisomal ABC transporters

The peroxisomal ABC transporter belong to the D subfamily of the ATP-binding cassette (ABC) transporter family (Morita and Imanaka 2012; Baker et al. 2015; Theodoulou and Kerr 2015). Like all eukaryotic ABC transporters, they have a core structure consisting of two

conserved domains: a transmembrane domain (TMD) with multiple α -helices and a nucleotide-binding domain (NBD) with Walker A and Walker B motifs. The TMDs bind and translocate substrates, whereas the NBDs form a 'sandwich dimer' capable of binding and hydrolyzing ATP. The hydrolysis of ATP provides the energy for the translocation of the substrate against an electrochemical gradient across the membrane (Higgins 1992; Rees et al. 2009). The peroxisomal ABCD proteins from human, mammals and fungi function as dimers of two TMD-NBD 'half transporters' (Morita and Imanaka 2012; Theodoulou and Kerr 2015; Baker et al. 2015). In contrast, plant peroxisomes possess a full-sized transporter encoded by a single gene. This plant ABCD protein contains two homologous but distinct halves that are attached as heterodimers with the topology TMD1-NBD1–TMD2-NBD2 (Dietrich et al. 2009). The fusion of two half transporters into one 'pseudo-heterodimeric' protein was a single event in the evolution of the green plant lineage which occurred before the divergence of bryophytes (Morita and Imanaka 2012; Theodoulou and Kerr 2015; Baker et al. 2015). The role of the peroxisomal ABCD proteins has been intensively studied in yeast, human and plants. Cross-species complementation studies revealed a conserved function for members of the ABCD family, mediating the uptake of β -oxidation substrates into peroxisomes (Table 1).

Yeast contains two peroxisomal half-ABC transporters ScPxa1p and ScPxa2p (Hettema et al. 1996; Shani and Valle 1996; Verleur et al. 1997). Single knockout mutants are impaired in growth on oleate-containing medium, indicating that they are unable to utilize oleate (C18:1) as a sole carbon source (Hettema et al. 1996; Verleur et al. 1997). The double yeast mutant *pxa1 Δ /pxa2 Δ* did not display an enhanced phenotype compared to the single mutants, suggesting that the two half-size transporters heterodimerize to form a fully functional transporter. This was confirmed by protein–protein interaction studies (Shani and Valle 1996; Chuang et al. 2014). The growth defect was restricted to only very-long chain fatty acids (VLCFA; >C22:0), indicating that ScPxa1p/ScPxa2p is involved in the import of fatty acids with 18 or more carbons as CoA esters into the peroxisome for their further degradation by β -oxidation (Hettema et al. 1996; Verleur et al. 1997). In yeast an alternative uptake route exists for medium-chain free fatty acids, which is independent of the peroxisomal ABC transporter (van Roermund et al. 2003). These β -oxidation substrates can enter the peroxisome in the non-esterified form via the proposed ScPex11 channel protein (Mindthoff et al. 2015). Inside the peroxisomal matrix, they are activated by the peroxisomal acyl-CoA synthetase ScFaa2p (fatty acid activation protein 2) (Hettema et al. 1996), prior to β -oxidation, a process which requires ATP imported by the peroxisomal ATP carrier ScAnt1p (adenine nucleotide transporter1) (van Roermund et al. 2001; Palmieri et al. 2001).

Humans have three ABCD family members residing in the peroxisomal membrane (ABCD1-3) (Kamijo et al. 1990; Mosser et al. 1993; Lombard-Platet et al. 1996). They are

half transporters and function *in vivo* as active homodimers. The human ABCD proteins have distinct but partially overlapping substrate specificities to different acyl-CoA esters. HsABCD1 shares functional redundancy with HsABCD2 (van Roermund et al. 2008; van Roermund et al. 2011). A defect in the human ABCD1 protein (or ALDP) causes X-linked adrenoleukodystrophy (X-ALD) (Mosser et al. 1993). This most common peroxisomal disorder is characterized by an impaired peroxisomal β -oxidation and consequently accumulation of VLCFA in tissues, especially the brain and the adrenal glands (Wiesinger et al. 2013). Although human ABCD proteins have functional redundancy, the basal expression levels of HsABCD2 and HsABCD3 are not sufficient to compensate the lack of HsABCD1 in X-ALD patients. Human ABCD2 (or ALDR) prefers shorter VLCFA and polyunsaturated fatty acids as transport substrates (van Roermund et al. 2011), whereas human ABCD3 (or PMP70) has the broadest substrate specificity (van Roermund et al. 2013). It is involved in the transport of saturated fatty acids, unsaturated fatty acids, branched-chain fatty acids, dicarboxylic fatty acids, and C27 bile acid intermediates (Ferdinandusse et al. 2015).

The Arabidopsis ABCD1 is the most studied and best understood plant peroxisomal ABC transporter. It has been independently identified by four different groups and hence is also known as CTS (Comatose (Footitt et al. 2002)), PXA1 (peroxisomal ABC transporter 1 (Zolman et al. 2001)), PED3 (peroxisome defective 3 (Hayashi et al. 2002)) and ACN2 (acetate non-utilizing 2) (Hooks et al. 2004). In this review we use the name CTS. Arabidopsis plants defective in CTS exhibit different phenotypes with respect to β -oxidation. Besides fatty acid degradation β -oxidation is involved in a wide range of metabolic and signaling processes in plants, including the synthesis of signaling molecules and secondary products. Hence, Arabidopsis CTS has been implicated not only to import fatty acyl-CoAs into the peroxisome, but also various other β -oxidation substrates, such as the jasmonic acid (JA) precursor 12-oxo-phytodienoic acid (OPDA) (Theodoulou et al. 2005; Dave et al. 2011), the synthetic auxin precursor 2,4-dichlorophenoxybutyric acid (2,4-DB) (Hayashi et al. 2002) and indole butyric acid (IBA) (Zolman et al. 2001), precursors of ubiquinone synthesis (Block et al. 2014) and cinnamic acid (Bussell et al. 2014), which is required for the synthesis of benzoic acid.

An unusual transport mechanism has been proposed for the human and Arabidopsis ABCDs shuttling their substrates across the peroxisomal membrane (Figure 1). Acyl-CoA esters and not 'free' (non-esterified) fatty acids are bound to the human ABCD1-3 and CTS transporter, demonstrated by the stimulated ATPase activity in the presence of fatty acyl-CoA derivatives (Nyathi et al. 2010). Once the acyl-CoA substrate is bound by ABCD or CTS, the CoA moiety is cleaved off during transfer across the lipid bilayer. The CoA cleavage during the transport cycle of CTS was confirmed using isotopic labelling of yeast cells with ^{18}O (van Roermund et al. 2012). Furthermore, it was experimentally shown that the human

ABCD1-3 and CTS itself possess an intrinsic acyl-CoA thioesterase activity (De Marcos Lousa et al. 2013; Geillon et al. 2017; Okamoto et al. 2018), although no motif homologous to either α/β -hydrolases or hot-dog fold thioesterases were detected (De Marcos-Lousa 2013). Such a transport mechanism subsequently requires a re-activation within the peroxisome by a peroxisomal acyl-CoA synthetase (ACS), which interacts with the transporter (De Marcos-Lousa 2013). It was shown that functional complementation of the *pxa1 Δ /pxa2 Δ* yeast mutant by CTS depends on the presence of ScFaa2p or the equivalent Arabidopsis long-chain acyl CoA synthetases 6 and/or 7 (LACS6/7) inside yeast peroxisomes (De Marcos Lousa et al. 2013). Coupling the translocation process to the peroxisomal ATP-dependent re-activation with CoA might be a potential regulation point for the entry of fatty acids and other substrates into the β -oxidation pathway. The cleavage and re-esterification of the acyl-CoA consumes two molecules of ATP and thus seems to be energetically wasteful. Still, it solves the biophysical challenge of shuttling an amphipathic molecule across the peroxisomal membrane and enables separate permeation pathways for the hydrophilic (CoA) and hydrophobic (fatty acid) moieties of β -oxidation substrates. In addition, the human ABCD and plant CTS transporter are able to accept disparate CoA derivatives as transport molecules via the intrinsic thioesterase domain, which recognizes the CoA moiety as an important determinant. We do not know yet, on which side of the peroxisomal membrane the CoA cleavage by the HsABCD1-3 or CTS transporter occurs. If CoA is released in the cytosol, the question how it enters peroxisomes remains to be answered.

Peroxisomal members of the mitochondrial carrier family

The mitochondrial carrier family (MCF) represents the largest group of eukaryotic transport proteins with 35 members in *Saccharomyces cerevisiae* (Palmieri et al. 2000; Palmieri et al. 2006) and more than 50 putative candidates in human (Palmieri 2014). The Arabidopsis genome encodes for 58 MCF members evenly distributed across the five chromosomes (Haferkamp 2007; Palmieri et al. 2011; Haferkamp and Schmitz-Esser 2012). All MCF carriers contain three tandemly repeated homologous domains, each consisting of two hydrophobic membrane spanning α -helices linked by a conserved sequence motif (Palmieri et al. 2011; Haferkamp and Schmitz-Esser 2012; Taylor 2017). They are highly variable in terms of size and charge of the transported molecule and the underlying transport mode. The predominant mechanism follows a 1:1 exchange of solutes (antiport), but unidirectional substrate transport (uniport) and proton compensated anion symport have been shown to be mediated by certain MCF carriers (Palmieri et al. 2011; Haferkamp and Schmitz-Esser 2012; Palmieri 2014; Taylor et al. 2017). According to their substrate specificity they can be divided into four subfamilies. The first group includes the nucleotide and nucleotide derivate

transporters. Carriers for the transport of di- and tri-carboxylates and keto-acids belong to the second subfamily. The third group comprises carriers catalyzing the transport of amino acids and their derivatives. Other carriers are grouped together with uncoupling proteins in the fourth and last subfamily (Palmieri et al. 2011; Haferkamp and Schmitz-Esser 2012; Palmieri 2014; Taylor 2017). Despite their name several MCF carriers have been localized to other cellular compartments, such as plasma membrane, ER membrane, plastids and peroxisomes. Up to now, three peroxisomal MCF carriers have been characterized in human, mammals, fungi and plants mediating the transport of ATP, NAD and CoA (Fig. 1 and Tab. 1) (van Roermund et al. 2001; Palmieri et al. 2001; Arai et al. 2008; Linka et al. 2008; Agrimi et al. 2011; Bernhardt et al. 2012; Agrimi et al. 2012). These essential cofactors are synthesized outside the peroxisomes and therefore have to be imported into the peroxisomal lumen (Figure 1). In all cases a specific carrier is required, because ATP, NAD and CoA cannot be transported through a peroxisomal pore-forming channel due to their size.

The peroxisomal ATP carrier

The first peroxisomal MCF carrier found was the ATP carrier from *S. cerevisiae*, called ScAnt1p (Adenine nucleotide transporter 1) (van Roermund et al. 2001; Palmieri et al. 2001). Based on sequence similarity to ScAnt1p, two Arabidopsis MCF members have been identified called AtPNC1 and AtPNC2 (Peroxisomal adenine Nucleotide Carrier) (Arai et al. 2008; Linka et al. 2008). Their transport function has been investigated by *in vitro* uptake experiments using liposomes reconstituted with recombinantly expressed proteins (Table 1). The yeast and plant carrier accept the adenine nucleotides ATP, ADP and AMP as transport substrates and catalyze a strict counter exchange of ATP against AMP or ADP (Palmieri et al. 2001; Linka et al. 2008). The import of cytosolic ATP into peroxisomes is essential for the ATP-dependent activation of fatty acids for their degradation by peroxisomal β -oxidation (Figure 1) (van Roermund et al. 2001; Palmieri et al. 2001; Arai et al. 2008; Linka et al. 2008). In yeast and plants, the fatty acid β -oxidation exclusively takes place inside peroxisomes (Goepfert and Poirier 2007; Graham 2008; van Roermund et al. 2012). Consequently, yeast cells deficient in ScAnt1p were unable to metabolize medium-chain fatty acids, such as lauric acid (C16:0) as carbon and energy source due to the lack of intraperoxisomal ATP (van Roermund et al. 2001; Palmieri et al. 2001). Arabidopsis PNC1 and PNC2 were shown to be able to complement the β -oxidation phenotype of the *ant1 Δ* yeast mutant, indicating that the plant carrier, like the yeast ortholog, are able to supply β -oxidation with ATP (Linka et al. 2008). A similar phenotype was observed for PNC1 and PNC2 Arabidopsis mutant plants. While the phenotype of single *pnc* Arabidopsis lines was not distinguishable from the wildtype, plants in which both AtPNC proteins are suppressed were impaired in peroxisomal β -oxidation, leading to a block in storage oil mobilization (Linka

et al. 2008). Since storage of carbohydrates (starch) and proteins is minor in *Arabidopsis* seeds (Goepfert and Poirier 2007; Graham 2008), *pnc1/pnc2* *Arabidopsis* seedlings depend on exogenous sucrose to allow seedling establishment (Linka et al. 2008). This strongly emphasizes that AtPNC1 and AtPNC2 are the sole site of peroxisomal ATP supply. The fatty acid activation step by peroxisomal acyl-CoA synthetases produces AMP and PP_i in yeast and *Arabidopsis* (Hettema et al. 1996; Fulda et al. 2004). While AMP is the direct counter-exchange substrate for the peroxisomal ATP carrier-mediated ATP import, the destiny of PP_i remains unknown. So far, a peroxisomal pyrophosphatase, catalyzing the hydrolysis of PP_i to 2 molecules of P_i has not been found in peroxisomes. This raises the question how PP_i and/or P_i are shuttled out of the peroxisomes (Linka and Theodoulou 2013). Due to their polar nature, both solutes are unlikely to freely diffuse across the peroxisomal membrane. Experiments using isolated bovine kidney peroxisomes observed transport activity for P_i and to a lesser extent PP_i (Visser et al. 2005). Whether specific transporters or unspecific channels mediate this solute transport was not addressed in this study.

Beyond fatty acid β -oxidation peroxisomal ATP is required for other enzymatic reactions inside peroxisomal lumen. In plants, for example, β -oxidation is involved in phytohormone biosynthesis (Wasternack and Strnad 2017; Wasternack and Feussner 2018). Jasmonates constitute a family of bioactive oxylipids that regulate a variety of defense responses and developmental processes. Its biosynthesis starts with the production of OPDA and dinor-OPDA in the chloroplasts and continues in peroxisomes by an alternative β -oxidation cycle (Wasternack and Strnad 2017; Wasternack and Feussner 2018). The peroxisomal import of OPDA is at least partially mediated by the peroxisomal ABC transporter CTS in *Arabidopsis* (Theodoulou et al. 2005). Inside the peroxisomal matrix it is then reduced to OPC-8 and activated by peroxisomal AtOPC-8:CoA ligase (Kienow et al., 2008). *Arabidopsis* null mutants lacking this enzyme are compromised in JA biosynthesis, leading to reduced JA levels (50-60%) and hyperaccumulation of OPC8:0 in wound-induced leaves (Koo et al. 2006). Finally, the last steps comprise several cycles of β -oxidation, by which an even number of carbons is removed from the carboxyl side chains of OPC-8, giving rise to JA in *Arabidopsis*. We also observed in the *pnc1/2* *Arabidopsis* silencing mutant significantly reduced JA levels, indicating a role for PNC proteins in JA biosynthesis in plants (personal communication).

In addition to JA, plant peroxisomes are involved in the synthesis of indole-3-acetic acid (IAA), short auxin (Korasick et al. 2013). This phytohormone plays a fundamental role in plant growth and development. It can be stored in inactive forms, conjugated to amino acids or sugars (Korasick et al. 2013). One of several auxin precursors in plants is IBA. Auxin derived from IBA is important during seedling development, when it influences lateral rooting (De Rybel et al. 2012), cotyledon and root hair expansion, and apical hook formation (Strader

et al. 2010; Strader et al. 2011). The synthesis of auxin from IBA occurs in plant peroxisomes by the action of an alternative peroxisomal β -oxidation pathway. Like OPDA and fatty acids, IBA has to be esterified with CoA, an ATP-consuming reaction in plants. However, in contrast to fatty acid β -oxidation, an alternative peroxisomal acyl-CoA synthetase is required, since *Arabidopsis* double knockout mutants of the two *Arabidopsis* fatty acid acyl-CoA synthetases LACS6/7 are sensitive to IBA (Cassin-Ross and Hu 2014a). However, even if catalyzed by another enzyme, ATP is still mandatory for the CoA esterification since *pnc1/pnc2 Arabidopsis* mutant plants are less sensitive to IBA as well as to the synthetic auxin precursor 2,4-DB (Linka et al. 2008; Arai et al. 2008).

Interestingly, there is no obvious phenotype of *Arabidopsis* plants lacking PNC1 and PNC2 after the seedling becomes photoautotrophic (personal communications). Since ATP as the energy currency plays such an important role in the cellular metabolism, it is likely that other peroxisomal pathways in addition to β -oxidation need ATP. This includes the mevalonate pathway (MVA) in plants that is involved in the formation of isopentenyl diphosphate (IPP) and dimethylallyl pyrophosphate (DMAPP), the building blocks of isoprenoids (Simkin et al. 2011; Rodríguez-Concepción and Boronat 2015). In *Arabidopsis* two ATP-dependent enzymes of the mevalonate pathway (MVA) are located to peroxisomes: phosphomevalonate kinase (PMK) and mevalonate diphosphate decarboxylase (MVD) (Sapir-Mir et al. 2008; Simkin et al. 2011). AtPMK catalyzes the phosphorylation of mevalonate phosphate to mevalonate diphosphate, consuming ATP and releasing ADP. Mevalonate diphosphate is subsequently decarboxylated by AtMVD to IPP, coupled to the hydrolysis of ATP to ADP and P_i (Simkin et al. 2011). IPP derived from the MVA pathway is required in plants for the formation of triterpenes, sesquiterpenes, phytosterols, ubiquinone, vitamin D and primary metabolites important for cell integrity (Rodríguez-Concepción and Boronat 2015). In parallel to the MVA, IPP can be produced by the plastidic 2-C-methyl-D-erythritol-4-phosphate (MEP) pathway in plants, which is used as precursor for the synthesis of monoterpenes, carotenoids, apocarotenoids and the side chain of chlorophylls, tocopherols and prenylquinones (Rodríguez-Concepción and Boronat 2015). Interaction between MVA and MEP pathways has been documented, explaining the less prominent phenotype of single mutants in either of the two pathways (Hemmerlin et al. 2012). However, the plant-specific carrier and channel involved in peroxisomal and plastidic transport steps have not been identified, yet (Linka and Theodoulou 2013). Since *Arabidopsis* PNCs are the sole source of peroxisomal ATP, *pnc1/2* mutant plants should be affected in MVA-synthesized isoprenoid molecules, like sterols and volatiles as it was shown for *mvd* mutant plants (Henry et al. 2015). However, a severe phenotype for *Arabidopsis pnc1/2* mutants might not be visible under normal conditions due to the presence of the functional MEP pathway.

Reversible post-translational modification by phosphorylation is an essential fast responding regulatory mechanism that controls many cellular processes (Cohen 2000; Friso and van Wijk 2015). For this, protein kinases transfer the γ -phosphate group from ATP to the hydroxyl group of serine, threonine or tyrosine residues, whereas protein phosphatases hydrolyze the phosphoester bond to dephosphorylate proteins. In plants, several soluble peroxisomal proteins involved in β -oxidation, glyoxylate cycle and photorespiration have been shown to be phosphorylated under certain conditions (Hodges et al. 2013; Kataya et al. 2015). But the physiological effects are still unknown. While many kinases have been identified and characterized, the knowledge about peroxisomal kinases is still limited. The first identified peroxisomal kinase was glyoxysomal protein kinase 1 (GPK1) in *Arabidopsis* (Fukao et al. 2003). AtGPK1 is a serine/threonine protein kinase, most likely anchored to the peroxisomal membrane with its kinase domain facing the peroxisomal lumen. The targets of AtGPK1 have not been identified, but regulation of proteins involved in fatty acid degradation may be required to prevent an overproduction of sucrose and hence protect against waste of energy in early post-germinative seedlings. In addition, *Arabidopsis* calcium-dependent protein kinase 1 (CDPK1) has been localized to peroxisomes and oil bodies and has been reported to be involved in salt and drought stress response as well as pathogen resistance (Coca and San Segundo 2010). It is suggested to play a role in lipid metabolism in plants since *Arabidopsis* mutants are partially resistant to the synthetic auxin precursor 2,4-DB and OPDA (Cassin-Ross and Hu 2014b). Further research is required to determine the signal transduction pathway of AtCDPK1. Although the *Arabidopsis pnc1/2* silencing plants develop normally through the plant life cycle, it might be interesting to investigate, to what extent the peroxisomal phospho-proteome was altered in these plant mutant lines.

NAD and its phosphorylated analog (NADP) have become well established as key energy transducers (Pollak et al. 2007; Houtkooper et al. 2010). The *Arabidopsis* genome harbors about 800 predicted oxidoreductases, which are likely to use NAD or NADP as cofactors. They play a fundamental role in reduction/oxidation (redox) metabolism through their contribution to the redox status of compounds, such as glutathione, thioredoxins and ascorbate (Noctor and Foyer 2016). In plant peroxisomes NADP-dependent reactions are catalyzed by enzymes of the oxidative pentose phosphate pathway, such as glucose-6-phosphate dehydrogenase and 6-phosphogluconate dehydrogenase, but also the peroxisomal isocitrate dehydrogenase depends on NADP (Meyer et al. 2011; Hölscher et al. 2014; Hölscher et al. 2016). All three enzymes are key components of the defense machinery against oxidative stress in plants. The only pathway for *de novo* synthesis of NADP and NADPH is the ATP-dependent phosphorylation of NAD and NADH, respectively. This reaction is catalyzed in *Arabidopsis* by members of the NAD(H) kinase family ATNADK1, AtNADK2 and AtNADK3. While AtNADK1 and AtNADK2 localize to the cytosol

and plastids, respectively, AtNADK3 was shown to reside in peroxisomes (Turner et al. 2004, Turner et al. 2005; Chai et al. 2006; Waller et al. 2010). In contrast to AtNADK1 and AtNADK2, AtNADK3 phosphorylates NADH, but has a lower affinity to NAD (Turner et al. 2005). This might prevent the intraperoxisomal phosphorylation of NAD, which is required for oxidative reactions like β -oxidation. NADPH produced by Arabidopsis NADK3 is not only used for the detoxification of the concomitantly generated H_2O_2 in the peroxisomal matrix. It is also required in plants to reduce unsaturated fatty acids (Behrends et al. 1988; Gurvitz et al. 1997; Hua et al. 2012) and the JA precursor OPDA for their conversion via β -oxidation (Schaller et al. 2000; Stintzi and Browse 2000). The depletion of peroxisomal NADP(H) in case of the Arabidopsis *nadk3* knockout led to impaired biotic and abiotic stress responses either directly linked to pathogen resistance or as part of the peroxisomal antioxidant machinery (Chai et al. 2006; Waller et al. 2010).

All of the above described peroxisomal reactions depend on the import of cytosolic ATP, since plant peroxisomes are unable to synthesize ATP by substrate-level phosphorylation. Because AtPNC1 and AtPNC2 are up to now the only known peroxisomal ATP import route in Arabidopsis, *pnc1/2* silencing plants should be deficient in more processes than just fatty acid β -oxidation. Thus, the generation of Arabidopsis null mutants for both PNC1 and PNC2, if vital, are required to explore the impact of ATP deficiency for other ATP-dependent processes in plant peroxisomes.

The peroxisomal NAD carrier

Peroxisomes require a specific carrier that mediates the import of NAD into the peroxisomal matrix to supply numerous peroxisomal redox reactions inside peroxisomes (Figure 1) (Noctor et al. 2006; Gakière et al. 2018). In plants, peroxisomal pathways such as β -oxidation, photorespiration and ROS detoxification are essential for peroxisome function and strictly require NAD as cofactor (Hu et al. 2012). To maintain the flux through these metabolic pathways, regeneration of reducing equivalents needs to be assured (Linka and Esser 2012; Linka and Theodoulou 2013). It is widely accepted that the peroxisomal malate/oxaloacetate shuttle is essential for the indirect exchange of the oxidized and reduced forms of NAD in plant peroxisomes (Pracharoenwattana et al. 2007; Pracharoenwattana et al. 2010). The peroxisomal malate dehydrogenase, which is part of this shuttle, produces either NAD or NADH by catalyzing the reversible reduction of oxaloacetate to malate. These dicarboxylates are exported to the cytosol for the re-conversion by cytosolic malate dehydrogenase and re-imported into peroxisomes via peroxisomal pore-forming channels (Antonenkov and Hiltunen 2011).

Since the *de novo* biosynthesis of NAD as well as salvage pathways are located in the cytosol in plants, NAD has to be imported into the peroxisomal lumen (Noctor et al. 2006;

Hashida et al. 2009). A peroxisomal NAD carrier has been discovered in Arabidopsis (Bernhardt et al. 2012; Agrimi et al. 2012). This Arabidopsis carrier, called PXN, catalyzes the transport of NAD, NADH, AMP, ADP and CoA in a strict exchange mode *in vitro* using a liposome uptake system (Table 1) (Bernhardt et al. 2012; Agrimi et al. 2012). In contrast to previously characterized plastidial and mitochondrial NAD antiporters, AtPXN accepts NADH and CoA as substrates. Concentration-dependent CoA uptake experiments demonstrated that AtPXN had a lower affinity to CoA, catalyzing only marginal CoA uptake into liposomes even at high CoA concentrations (van Roermund et al. 2016). Since the cellular CoA levels are rather low in plants, a physiological role of AtPXN in supplying peroxisomes with CoA is unlikely. To elucidate whether AtPXN mediates the exchange of NAD/AMP or NAD/NADH in a living system, selected *S. cerevisiae* mutants were used (van Roermund et al. 2016). A yeast strain lacking the peroxisomal malate dehydrogenase 3 (ScMdh3p) led to yeast cells that were unable to metabolize fatty acids via peroxisomal β -oxidation, because NAD is completely reduced to NADH and cannot be re-oxidized (van Roermund et al. 1995). Under this condition the peroxisomal NADH pyrophosphatase 1 (Npy1p) from *S. cerevisiae* hydrolyzes NADH to AMP, preventing the accumulation of NADH in the peroxisomal matrix (Abdelraheim et al. 2001). Thus, in this mutant background mainly AMP would be available for AtPXN as internal substrate for the uptake of NAD into yeast peroxisomes. Furthermore, the gene encoding for ScNpy1p was deleted in the *mdh3 Δ* yeast background (van Roermund et al. 2016). It was expected that the elevated NADH pool in the peroxisomes of this double mutant supports the NAD import against peroxisomal NADH, mediated by the overexpressed AtPXN. However, AtPXN was able to enhance the fatty acid degradation activity in the *mdh3 Δ* yeast mutant, but not in the *mdh3/np1 Δ* yeast double mutant, indicating that the function of ScNpy1p is crucial for phenotype suppression (van Roermund et al. 2016). It is assumed that AtPXN catalyzes the influx of NAD into yeast peroxisomes versus AMP *in vivo*. As a consequence, how is net influx of NAD into peroxisomes guaranteed via such an antiport mechanism? To balance the loss of peroxisomal AMP, cytosolic AMP is re-imported into peroxisomes by an unknown peroxisomal carrier. An adenylate uniporter could refill the peroxisomal adenine nucleotide pool. In contrast, AMP as counter-exchange substrate for the NAD import is provided by the hydrolysis of NADH mediated by the peroxisomal nudix hydrolase NUDT19 in Arabidopsis (Ogawa et al. 2005; Ogawa et al. 2008; Reumann et al., 2009). The recombinant protein exhibits NADH hydrolysis activity and thus is a promising candidate catalyzing this enzymatic step.

To investigate whether Arabidopsis PXN provides peroxisomal reactions with NAD in plants, a loss-of-function would affect the action of NAD-dependent pathways, such as β -oxidation, photorespiration and ROS detoxification. Indeed, the mobilization rate of seed-stored fatty acids via β -oxidation is impaired in Arabidopsis *pxn* knockout plants (Bernhardt et

al. 2012). However, the degradation of fatty acid is not completely blocked, allowing a normal seedling establishment. The Arabidopsis T-DNA insertion lines for AtPXN displayed an obvious affect during plant development under standard growth conditions (personal communications), indicating that other peroxisomal NAD-dependent reactions are not restricted in plants. A photometric screen discovered a possible contribution of AtPXN to photorespiration under fluctuating and high light conditions (Li et al., 2018). This weak Arabidopsis *pxn* phenotype suggests alternative routes for the NAD uptake in plant peroxisomes (Bernhardt et al. 2012). Most likely a redundant carrier takes over the function of AtPXN in importing NAD into the plant peroxisomal matrix.

The peroxisomal CoA carrier

CoA is an essential acyl group carrier and carbonyl-activating group and it is utilized in the biosynthesis and catabolism of both primary and secondary metabolites; in plants, for example, for the citric acid cycle (mitochondria), fatty acid biosynthesis (plastids) and degradation (peroxisomes) (Coxon et al. 2005). The CoA biosynthesis is mainly localized to the cytosol in eukaryotes and starts with the condensation of pantoate to β -alanine to form pantothenate (vitamin B5) catalyzed by pantothenate synthase. Subsequent enzymatic steps lead to the production of dephospho-CoA that is finally phosphorylated by dephospho-CoA kinase to produce CoA (Tilton et al. 2006; Rubio et al. 2006; Rubio et al. 2008). To supply CoA dependent metabolic reactions in different organelles (cell compartments), the transfer of CoA across biological membranes is essential (Linka and Esser 2012; Linka and Theodoulou 2013). Members of the MCF have been shown to mediate this shuttle for an efficient subcellular distribution of this cofactor within the eukaryotic cell (Figure 1).

Leu5p and SLC25A42 represent mitochondrial CoA carriers in yeast and human, respectively (Prohl et al. 2001; Fiermonte et al. 2009). Based on sequence similarity, both mitochondrial CoA carriers from Arabidopsis AtCoAC1 and AtCoAC2 and their maize homologs have been identified (Zallot et al. 2013). All four proteins were able to functionally complement a ScLeu5 deficient yeast strain (Zallot et al. 2013). Yeast cells lacking LEU5 display retarded growth on rich media containing a non-fermentable carbon source, such as glycerol, and the CoA levels in intact *leu5* Δ mitochondria were strongly reduced (Prohl et al. 2001). Transport measurements in liposomes reconstituted with *E. coli* expressed human CoA carrier SLC25A42 demonstrated that this carrier transports, besides CoA, dephospho-CoA, adenosine 3',5'-diphosphate (PAP), and the adenine nucleotides by counter-exchange (Fiermonte et al. 2009).

In plants though, a peroxisomal CoA carrier (PCC) is still unknown (Figure 1). The peroxisomal NAD carrier PXN from Arabidopsis showed transport activities for CoA *in vitro* (Agrimi et al. 2012), but such a CoA import function is unlikely to occur under physiological

conditions (van Roermund et al. 2016). The only peroxisomal CoA carrier, characterized so far, is the human MCF member SLC25A17, which is also known as ANT1 or PMP34 (Agrimi et al. 2011). *In vitro* uptake assays revealed that the recombinant SLC25A17 protein - as its mitochondrial counterpart - also exhibits a broad substrate specificity (Agrimi et al. 2012). Notably, the human SLC25A17 is able to catalyze the flux of intermediates of the CoA biosynthesis and salvage pathway. In Arabidopsis, proteomic data imply that dephospho-CoA kinase is localized to peroxisomes, plastids and the cytosol (Reumann et al. 2009), thus giving the possibility that dephospho-CoA is transported in addition or instead of CoA. Transport function for PAP by the human SLC25A17 carrier gives rise to a potential CoA salvage pathway within peroxisomes in general. The yeast peroxisomal Pcd1p is a nudix hydrolase with specificity to CoA producing PAP and 4'-phosphopantetheine (4-PP) (Cartwright et al. 2000). NUDT7a and Y87G2A.14, the Pcd1p homologs in mouse and *C. elegans*, respectively, also show CoA hydrolase activity (Gasmi and McLennan 2001; AbdelRaheim and McLennan 2002; Reilly et al. 2008). While in Arabidopsis CoA hydrolysis activity of AtNUDT19 is almost undetectable (Ogawa et al. 2005; Ogawa et al. 2008), NUDT15 might be a better candidate catalyzing this reaction in Arabidopsis (Ito et al. 2012). AtNUDT15 has a splice variant NUDT15a with an early stop codon unveiling a putative peroxisomal targeting signal. Both variants have an N-terminal mitochondrial target peptide. Masking this domain results in a peroxisomal localization (Ito et al. 2012). The product of the CoA hydrolysis (PAP and 4-PP) might be used as counter-exchange substrates for the CoA import. 4-PP as a CoA precursor can then enter CoA biosynthesis pathway in the cytosol. Putative transport function of 4-PP by the peroxisomal CoA carrier in plants needs to be tested *in vitro*. As an alternative fate for PAP inside peroxisomes, it could be converted to AMP by an unknown peroxisomal hydrolase. The resulted AMP might function as exchange partner for CoA or NAD import (Table 1).

As a reminder, for the peroxisomal ABC transporter in Arabidopsis CTS it was demonstrated that during the transport process of acyl-CoA esters the CoA moiety is cleaved off. If the CoA molecule is released into the peroxisomal matrix, the need for a peroxisomal CoA importer would obliterate. In this scenario, the role of a peroxisomal CoA carrier in plants could be to regulate the peroxisomal CoA homeostasis by exporting CoA from the peroxisomes. For instance, in plants each glyoxylate cycle releases free CoA into the peroxisomal lumen. Still, due to the presence of the human peroxisomal CoA carrier it is most likely that in plants the CoA carrier is also a member of the MCF.

Peroxisomal pore-forming channels

Several reports provided evidences on pore-forming channels in membranes of peroxisomes from human, mammals, plant, yeast and *Trypanosoma brucei*, indicating that the existence of these channel proteins is highly conserved within the eukaryote lineage (Reumann et al. 1995; Reumann et al. 1996; Reumann et al. 1998; Rokka et al. 2009; Antonenkov et al. 2009; Gualdrón-López et al. 2012; Mindthoff et al. 2015). The detected channel activities in the peroxisomal membrane were studied using the lipid bilayer technique (Andreoli 1974; Ehrlich 1992). Integral proteins were detergent-solubilized from peroxisomal membranes and incorporated into the planar lipid bilayer (also called 'black membrane') which is formed over an aperture located in a septum separating two chambers. Each chamber is filled with buffered ionic solution, for example, with potassium chloride (KCl) solution as electrolyte (Andreoli 1974; Ehrlich 1992). This experimental set-up allows to record the facilitated diffusion of ions or various organic anions through the channel-forming pore. For a detailed overview of the lipid bilayer measurements describing peroxisomal channel activities we refer the reader to a review by Antonenkov et al. (2011).

Electrophysiological studies revealed that the peroxisomal channels mediate the transfer of solutes with a broad substrate specificity through the peroxisomal bilayer membrane. In different plant species, such as spinach and castor bean, only one peroxisomal channel protein with comparable characteristics has been investigated (Reumann et al. 1995; Reumann et al. 1996; Reumann et al. 1997; Reumann et al. 1998), whereas in other eukaryotes, such as mouse and yeast, more than one type of channel-forming proteins with distinct properties has been detected (Antonenkov et al. 2005; Grunau et al. 2009; Antonenkov et al. 2009; Gualdrón-López et al. 2012). In general, the activities of the peroxisomal channels from different eukaryotes are comparable to each other, but they differ in their properties from known β -barrel channels, *e.g.* porins of the gram-negative bacteria, voltage-dependent anion channel of the outer mitochondrial membrane (VDAC) and the outer envelope proteins of plastids (OEPs) (Zeth & Thein 2010). Candidates responsible of these peroxisomal pore-forming activities have been recently identified, such as PMP22 and PEX11, which are described in the next chapter.

The peroxisomal membrane protein of 22 kDa (PMP22)

The peroxisomal membrane protein of 22 kDa (PMP22) is one of the most abundant integral peroxisomal membrane proteins found in eukaryotes. It belongs to a small family of putative uncharacterized transport proteins, called MPV17/PMP22 family (Saier et al. 2009). This class of channels consists of two subgroups. One subgroup includes members that are found in mitochondria, named after the inner mitochondrial membrane in human (MPV17)

(Spinazzola et al. 2006), whereas the other subdivision contains peroxisomal members, like PMP22. Proteins of the MPV17/PMP22 family are multi-spanning membrane proteins with four putative α -helical transmembrane domains. They contain a conserved protein motif at the C-terminus (PF04117) and are predicted to form homotrimers. Several reports demonstrated that both the mitochondrial and peroxisomal members of this family are non-selective channels with similar basic properties (Rokka et al., 2009; Reinhold et al., 2012; Antonenkov et al. 2015). Since the MPV17/PMP22 members do not share sequence or structural similarities with known porin proteins or other channels, they represent a novel channel-type. Best-known mitochondrial members of this family are the mitochondrial inner membrane protein MPV17 in human (Spinazzola et al. 2006) and the stress-inducible yeast MPV17 homolog Sym1 (Trott & Morano 2004; Dallabona et al. 2010). The PMP22 members described so far are the peroxisomal membrane protein 2 in mouse (Pxmp2; Rokka et al. 2009; Vapola et al. 2014) and the peroxisomal membrane protein 22 kDa in Arabidopsis (PMP22) (Tugal et al. 1999; Murohy et al. 2003).

The channel activities of the human MPV17 and yeast Sym1p were investigated by lipid bilayer experiments using recombinant proteins (Reinhold et al. 2012; Antonenkov et al. 2015). Both channels form a membrane pore with a similar diameter (1.6-1.8 nm). The size of the pore is large enough to facilitate the transmembrane diffusion of nearly all mitochondrial solutes, including inorganic ions, different metabolites, and even ATP molecules. These non-selective channels were constitutively open at low and moderate voltages, but they are in the closed conformation at high voltages (± 100 mV) (Reinhold et al. 2012; Antonenkov et al. 2015). In case of the peroxisomal members of this MVP17/PMP22 channel family, the channel function of the mouse Pxmp2 protein has been verified (Rokka et al. 2009; Vapola et al. 2014). The recombinant protein also forms a relatively wide, water-filled pore with an estimated size diameter of 1.4 nm in an artificial lipid bilayer, allowing the passive diffusion of various organic acids with molecular masses up to 300 Da, such as glycolate, pyruvate, and 2-ketoglutarate (Table 1) (Rokka et al. 2009; Vapola et al. 2014). The basic characteristics of the channel activities of the recombinant Pxmp2 protein are comparable to those measured for the peroxisomal membrane preparations purified from mouse liver (Rokka et al. 2009; Vapola et al. 2014).

In Arabidopsis the peroxisomal member of this channel family, called PMP22, was identified as one of the first plant peroxisomal membrane proteins by subcellular fractionation (Tugal et al. 1999). Later immunofluorescence imaging (Murphy et al., 2003) and experimental proteomics (Eubel et al. 2008; Reumann et al. 2009) confirmed this finding. However, whether the Arabidopsis PMP22 functions as pore-forming channel, like the mouse Pxmp2 and contribute to the permeability of plant peroxisomes is so far unknown (Figure 1).

Both proteins are members of the same transport protein family and share 30% identity on protein sequence level (Saier et al., 2009).

The Peroxin 11 (PEX11)

Peroxin 11 (PEX11) is an integral membrane protein of the peroxisomal bilayer membrane with at least two predicted α -helical transmembrane domains and both termini exposed to the cytosol (Thoms & Erdmann 2005). PEX11 is considered a key player in peroxisomal proliferation, regulating peroxisome size and number in all eukaryotic organisms. The PEX11 protein family consists of three members in human and mammals (Pex11 α , Pex11 β , and Pex11 γ), five members in Arabidopsis (PEXa, PEXb, PEXc, PEXd, PEXe), and three members in yeast (Pex11, Pex25, and Pex27) (Abe & Fujiki 1998; Tanaka et al. 2003; Rottensteiner et al. 2003; Lingard & Trelease 2006). Unexpectedly, the yeast Pex11p also represents a non-selective channel responsible for transfer of solutes across peroxisomal membrane.

A small part of the PEX11 proteins (~ 100 aa) shares 40% sequence similarity to the transient receptor potential cation-selective channel (Mindthoff et al. 2015). Due to its relationship to the TRP channel family, the yeast PEX11 protein was recombinantly expressed and reconstituted into lipid bilayer to assess channel properties (Mindthoff et al. 2015). The electrophysiological experiments clearly demonstrated that ScPex11p exhibits channel-forming activities. A pore-diameter of around 0.6 nm was calculated, implying that molecules with up to 400 Da can pass the non-selective channel (Mindthoff et al. 2015). Comparative multi-channel analysis of Pex11-deficient yeast peroxisomes revealed pore-forming activities with different characteristics to those of the recombinant ScPex11p, indicating that the yeast peroxisomes possess more than one pore-forming channel (Mindthoff et al. 2015).

Ectopic overexpression of proteins of the PEX11 family from yeast, plants, mammals or humans induces peroxisome proliferation, leading to the formation of elongated peroxisomes (Abe & Fujiki 1998; Li & Gould 2002; Lingard & Trelease 2006; Orth et al. 2007; Nito et al., 2007; Koch et al. 2010). The deletion of PEX11 in yeast, however, results in fewer but giant peroxisomes in yeast (Erdmann & Blobel 1995). Arabidopsis has five paralogs of PEX11, which were subdivided into group 1 (AtPEX11a and AtPEX11b) and group 2 (AtPEX11c, ATPEX11d, and ATPEX11e). In Arabidopsis mutant plants in which single PEX11 genes were silenced the peroxisome number and size were reduced (Orth et al., 2007), whereas double and triple Arabidopsis knockdown mutants *pex11a/pex11b* and *pex11c/pex11d/pex11e* contain large peroxisomes in the cells of roots and leaves (Nito et al., 2007). Peroxisome proliferation is a multistep process including elongation, constriction and fission (Schrader et al. 2016). Based on the altered peroxisome morphology, it has been

implicated that PEX11 proteins directly participate in the first two steps. It enables membrane elongation by stabilizing peroxisomal membrane tubules and thus initiates the formation of constriction sites by recruiting the mitochondrial fission machinery to peroxisomes (Schrader et al. 2016).

Beside the peroxisome proliferation phenotype, yeast cells lacking Pex11p are unable to metabolize long- and medium-chain fatty acids, such as oleic acid (C18:1) and lauric acid (C12:0), as sole carbon and energy source (Table 1) (van Roermund et al. 2000). While the overexpression of ScPex11p led to enhanced β -oxidation activities in intact yeast cells (Mindthoff et al. 2015). This leads to the question how the peroxisomal fatty acid degradation is linked to the supposed role of PEX11. Changes in PEX11 as an essential regulator of peroxisome proliferation might indirectly lead to dysfunctional peroxisomes with an impaired metabolism. Alternatively, PEX11 as a solute channel mediating the import of medium- and long-chain fatty acids into peroxisomes, supplies peroxisomal β -oxidation with its substrates. The peroxisomal ABC transporter is essential for the import of very long-chain fatty acids, but the absence of a pore-forming protein might alter concentration and composition of solutes inside the peroxisomal lumen. This in turn could negatively influence the process of peroxisome proliferation. Enlarged peroxisomes have been reported for several *Arabidopsis* β -oxidation mutants, such as *kat2* (β -Ketothiolase; Germain et al. 2001), *mfp2* (Multifunctional protein; Rylott et al. 2006), and *pxn* (peroxisomal NAD carrier; Mano et al. 2011), assuming that a defective fatty acid degradation indirectly disturbs peroxisome proliferation.

Since other PEX11 orthologs from plants, mammals and humans are able to restore the inability of the *pex11* Δ yeast mutant to grow on oleic acid and rescue the peroxisome morphology phenotype, it remains to be solved how PEX11 proteins can fulfill two distinct functions in the eukaryotic cell - as a solute channel and as a factor required for peroxisome proliferation (Figure 1).

Conclusion

Peroxisomes have to exchange intermediates with other cell compartments to fulfill their role in cellular metabolism. For this functional interplay they rely on the peroxisomal transporters and channels described in this review. For a high-flux of solutes between two organelles, the membranes of both compartments need also to be in close proximity. Otherwise the slow diffusion of solutes to their cellular destination would rate-limit the metabolic flux through this pathway. Recently, protein complexes have been discovered that physically connect peroxisomes to mitochondria, for example, via membrane contact sites (MCSs) (Schrader et al., 2015). These membrane regions of tethered organelles are beneficial for rapid solute

channeling due to an enrichment of specific transporters and channels and the generation of concentration gradients of solutes at these sites. Further insights into the peroxisomal solute transport processes in respect to specificity and regulation, would be a great step towards using peroxisomes as synthetic organelles for heterologous pathway compartmentalization (Kessel-Vigelius et al., 2013).

An alternative mechanism for peroxisomes to exchange solutes is the transfer of vesicles from the ER or mitochondria, which both play an important role in peroxisome biogenesis. Peroxisomes derive *de novo* from vesicles from the ER and mitochondria and replicate by growth and division (Sugiura et al., 2017). Therefore, such a vesicular transport might provide peroxisomes with membrane proteins and enzymes, but also with lipids and other metabolites and cofactors.

Acknowledgements

The authors would like to thank members of the Weber Lab for helpful discussions and support. Special thanks to Dominik Brillhaus for reading the manuscript. This work was supported by the DFG grants LI1781/1-3 and LI1781/2-2.

Table and Figure

Table 1. Plant peroxisomal transport proteins described in this review, their predicted transport substrates and transport mode. Abbreviations: PNC, peroxisomal ATP carrier; PXN, peroxisomal NAD carrier; PCC, peroxisomal CoA carrier; PMP22, peroxisomal channel protein; PEX11, peroxisomal channel protein; CTS, peroxisomal ABC transporter; OAA, oxaloacetate; 2-OG, 2-oxoglutarate.

Transporter	Transport substrates	Transport mode
PNC	ATP _{in} / ADP _{out} ATP _{in} / AMP _{out}	passive transport down the chemical gradient in an antiport mechanism
PXN	NAD _{in} / AMP _{out}	passive transport down the chemical gradient in an antiport mechanism
PCC	CoA _{in} / AMP _{out} CoA _{in} / PAP _{out}	passive transport down the chemical gradient in an antiport mechanism
PMP22	Organic acids like Malate, OAA, 2-OG, glycolate succinate	passive transport down the chemical gradient in a uniport mechanism
PEX11	long-chain and medium-chain fatty acids	passive transport down the chemical gradient in a uniport mechanism
CTS	Acetyl-CoA	ATP-dependent active transport in a uniport mechanism

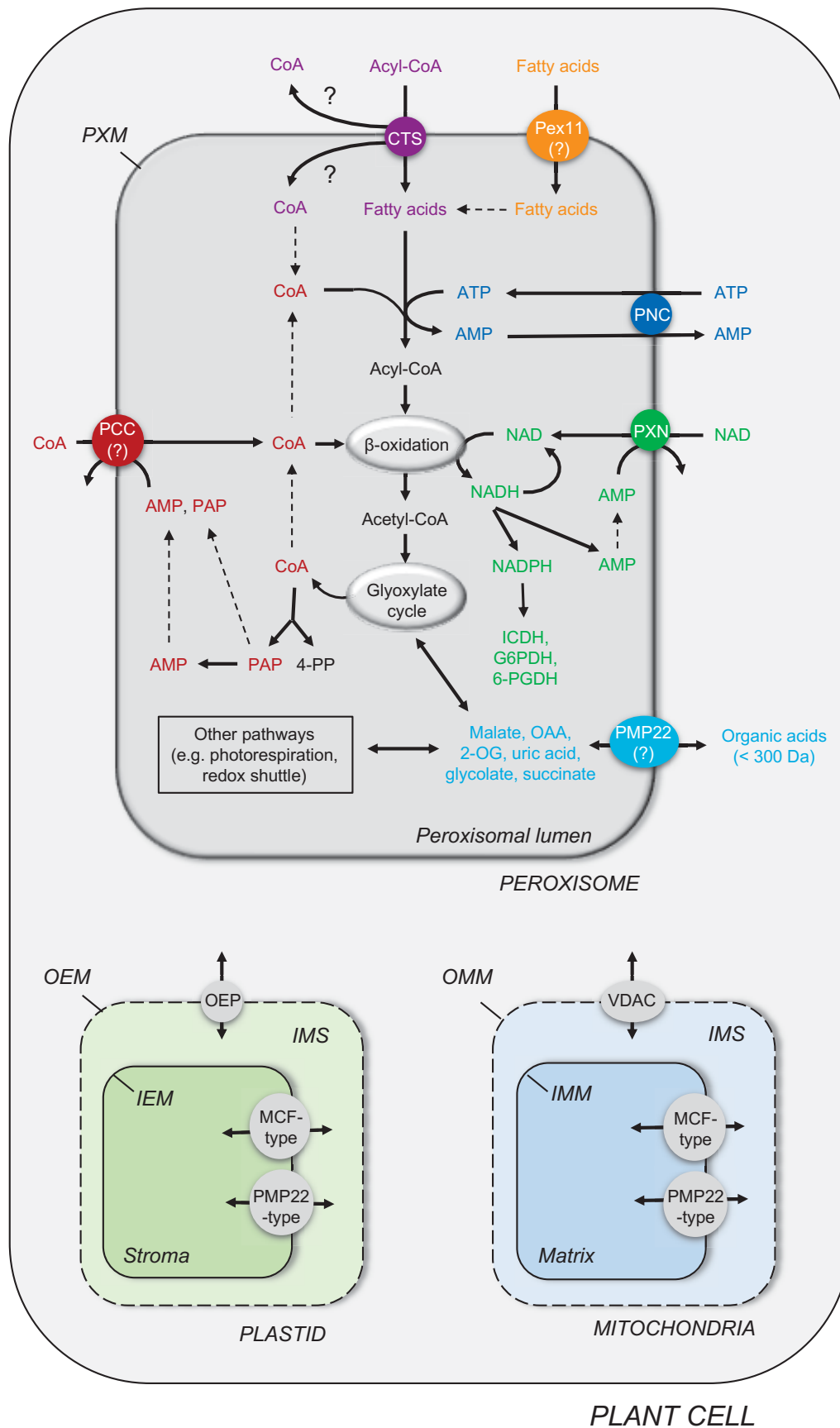


Figure 1. Scheme of a plant cell presenting the known peroxisomal transporter and channel proteins connecting peroxisomal metabolism with that of the cell. Based on the proposed transport mechanism, the peroxisomal ABC transporter CTS import acyl-CoA esters into the peroxisomes. During this import process, the substrates is hydrolyzed to fatty acids and CoA and released into the peroxisomal matrix. Such a transport mode requires the intra-peroxisomal ATP-dependent re-esterification to CoA for fatty acid activation. The peroxisomal ATP carrier PNC import cytosolic ATP in exchange with AMP, which is produced during fatty acid activation. ATP is also required for other ATP-dependent reaction inside peroxisomes, including auxin biosynthesis, protein phosphorylation and mevalonate pathway. NAD-dependent reactions inside peroxisomes, like fatty acid oxidation, depend on the import of NAD from the cytosol catalyzed by the peroxisomal NAD carrier PXN. The exchange partner for the NAD uptake is generated by peroxisomal NADH hydrolysis. NAD can be phosphorylated to NADPH, which is the cofactor for NADP-dependent ICDH and the OPPP enzymes G6PDH and 6-PGDH. In addition, peroxisomes require a peroxisomal CoA carrier (PCC) mediating the uptake of CoA., which has not been identified for plant peroxisomes. If the CoA is cleaved off at the cytosolic side of the peroxisomal membrane during the transport of acyl-CoA, the peroxisomal CoA carrier imports cytosolic CoA into peroxisomes required for fatty acid activation. Peroxisomal CoA is also used to remove acetyl-CoA from the fatty acyl chain in the last step of β -oxidation, whereas the glyoxylate cycle produces free CoA. To regulate CoA homeostasis, CoA can be hydrolyzed to PAP or 4-PP, which are suitable counter-exchange substrates for the CoA import. The further hydrolysis of PAP yields AMP, another putative export substrate for the peroxisomal CoA carrier. Other intermediates of the peroxisomal metabolism, such as organic acids, might be shuttled via the peroxisomal channel protein called PMP22 across the peroxisomal membrane. Pex11 as a second channel might be involved in the uptake of free fatty acids into the peroxisomes, as a redundant system to the peroxisomal ABC transporter. Other compartments of a plant cell, like plastids and mitochondria, possess a large variety of transporter and channel proteins for shuttling metabolites across their bilayer membranes, including the outer envelope proteins OEPs, plastidial MCF-type carriers, plastidial PMP22-type channels, voltage-dependent anion channels (VDACs), mitochondrial MCF carriers, and mitochondrial PMP22-type channels. Abbreviations: PAP, 3',5'-ADP; 4-PP, 4-Phosphopantetheine; OAA, oxaloacetate; 2-OG, 2-oxoglutarate; ICDH, isocitrate dehydrogenase; G6PDH, glucose-6-phosphate dehydrogenase; 6-PGDH, 6-phosphogluconate dehydrogenase; OEM, outer envelope membrane; IEM, inner envelope membrane; OMM, outer mitochondrial membrane; IMM, inner mitochondrial membrane; IMS, intermembrane space.

References

AbdelRaheim SR, Cartwright JL, Gasmi L, McLennan AG (2001) The NADH diphosphatase encoded by the *Saccharomyces cerevisiae* NPY1 nudix hydrolase gene is located in peroxisomes. **Arch Biochem Biophys** 388: 18–24

AbdelRaheim SR, McLennan AG (2002) The *Caenorhabditis elegans* Y87G2A.14 Nudix hydrolase is a peroxisomal coenzyme A diphosphatase. **BMC Biochem** 3: 5

Abe I, Fujiki Y (1998) cDNA cloning and characterization of a constitutively expressed isoform of the human peroxin Pex11p. **Biochem Biophys Res Commun** 252: 529–533

Agrimi G, Russo A, Scarcia P, Palmieri F (2011) The human gene SLC25A17 encodes a peroxisomal transporter of coenzyme A, FAD and NAD. **Biochem J** 443: 241–247

Agrimi G, Russo A, Pierri CL, Palmieri F (2012) The peroxisomal NAD carrier of *Arabidopsis thaliana* transports coenzyme A and its derivatives. **J Bioenerg Biomembr** 44: 333–340

Andreoli TE (1974) Planar lipid bilayer membranes. **Meth Enzymol** 32: 513–539

Antonenkov VD, Rokka A, Sormunen RT, Benz R, Hiltunen JK (2005) Solute traffic across mammalian peroxisomal membrane - single channel conductance monitoring reveals pore-forming activities in peroxisomes. **Cell Mol Life Sci** 62: 2886–2895

Antonenkov VD, Mindthoff S, Grunau S, Erdmann R, Hiltunen JK (2009) An involvement of yeast peroxisomal channels in transmembrane transfer of glyoxylate cycle intermediates. **Int J Biochem Cell Biol** 41: 2546-2554

Antonenkov VD, Hiltunen JK (2011) Transfer of metabolites across the peroxisomal membrane. **Biochim Biophys Acta** 1822: 1374-1386

Antonenkov VD, Isomursu A, Mennerich D, Vapola MH, Weiher H, Kietzmann T, Hiltunen JK (2015) The human mitochondrial DNA depletion syndrome gene MPV17 encodes a non-selective channel that modulates membrane potential. **J Biol Chem** 290: 13840–13861

Arai Y, Hayashi M, Nishimura M, Nishimura M (2008) Proteomic identification and characterization of a novel peroxisomal adenine nucleotide transporter supplying ATP for fatty acid β -oxidation in soybean and *Arabidopsis*. **Plant Cell** 20: 3227–3240

Baker A, Carrier DJ, Schaedler T, Waterham HR, van Roermund CWT, Theodoulou FL (2015) Peroxisomal ABC transporters: functions and mechanism. **Biochem Soc Trans** 43: 959–965

Behrends W, Thieringer R, Engeland K, Kunau WH, Kindl H (1988) The glyoxysomal β -oxidation system in cucumber seedlings: identification of enzymes required for the degradation of unsaturated fatty acids. **Arch Biochem Biophys** 263: 170–177.

Bernhardt K, Wilkinson S, Weber APM, Linka N (2012) A peroxisomal carrier delivers NAD and contributes to optimal fatty acid degradation during storage oil mobilization. **Plant J** 69: 1–13

Block A, Widhalm JR, Fatihi A, Cahoon RE, Wamboldt Y, Elowsky C, Mackenzie SA, Cahoon EB, Chapple C, Dudareva N, Basset GJ (2014) The origin and biosynthesis of the benzenoid moiety of ubiquinone (Coenzyme Q) in Arabidopsis. **Plant Cell** 26: 1938–1948

Bussell JD, Reichelt M, Wiszniewski AAG, Gershenzon J, Smith SM (2014) Peroxisomal ATP-binding cassette transporter COMATOSE and the multifunctional protein ABNORMAL INFLORESCENCE MERISTEM are required for the production of benzoylated metabolites in Arabidopsis seeds. **Plant Physiol** 164: 48–54

Cartwright JL, Gasmi L, Spiller DG, McLennan AG (2000) The *Saccharomyces cerevisiae* PCD1 gene encodes a peroxisomal nudix hydrolase active toward coenzyme A and its derivatives. **J Biol Chem** 275: 32925–32930

Cassin-Ross G, Hu J (2014a) Systematic phenotypic screen of Arabidopsis peroxisomal mutants identifies proteins involved in β -oxidation. **Plant Physiol** 166: 1546–1559

Cassin-Ross G, Hu J (2014b) A simple assay to identify peroxisomal proteins involved in 12-oxo-phytodienoic acid metabolism. **Plant Signal Behav** 9: e29464.

Chai MF, Wei, PC, Chen QJ, An R, Chen J, Yang S, Wang XC (2006) NADK3, a novel cytoplasmic source of NADPH, is required under conditions of oxidative stress and modulates abscisic acid responses in Arabidopsis. **Plant J** 47: 665–674

Chuang CY, Chen LY, Fu RH, Chen SM, Ho MH, Huang JM, Hsu CC, Wang CC, Chen MS, Tsai RT (2014) Involvement of the carboxyl-terminal region of the yeast peroxisomal half ABC transporter Pxa2p in its interaction with Pxa1p and in transporter function. **PLoS One** 9: e104892

Coca M, San Segundo B (2010) AtCPK1 calcium-dependent protein kinase mediates pathogen resistance in Arabidopsis. **Plant J** 2010:18

Cohen P (2000) The regulation of protein function by multisite phosphorylation – a 25 year update. **Trends Biochem Sci** 25: 596–601

Coxon KM, Chakauya E, Ottenhof HH, Whitney HM, Blundell TL, Abell C, Smith AG (2005) Pantothenate biosynthesis in higher plants. **Biochem Soc Trans** 33: 743–746

Dallabona C, Marsano RM, Arzuffi P, Ghezzi D, Mancini P, Zeviani M, Ferrero I, Donnini C (2010) Sym1, the yeast ortholog of the MPV17 human disease protein, is a stress-induced bioenergetic and morphogenetic mitochondrial modulator. *Human Mol Gen* 19: 1098–1107

Dave A, Hernandez ML, He Z, Andriotis VM, Vaistij FE, Larson TR, Graham IA (2011) 12-oxo-phytodienoic acid accumulation during seed development represses seed germination in Arabidopsis. **Plant Cell** 23: 583–599

De Marcos Lousa C, van Roermund CWT, Postis VLG, Dietrich D, Kerr ID, Wanders RJA, Baldwin SA, Baker A, Theodoulou FL (2013) Intrinsic acyl-CoA thioesterase activity of a peroxisomal ATP binding cassette transporter is required for transport and metabolism of fatty acids. **Proc Natl Acad Sci USA** 110: 1279–1284

De Rybel B, Audenaert D, Xuan W, Overvoorde P, Strader LC, Kepinski S, Hoye R, Brisbois R, Parizot B, Vanneste S, Liu X, Gilday A, Graham IA, Nguyen L, Jansen L, Nijo MF, Inze D, Bartel B, Beeckman T (2012) A role for the root cap in root branching revealed by the non-auxin probe naxillin. **Nat Chem Biol** 8: 798–805

Dietrich D, Schmuths H, De Marcos Lousa C, Baldwin JM, Baldwin SA, Baker A, Theodoulou FL, Holdsworth MJ (2009) Mutations in the Arabidopsis peroxisomal ABC transporter COMATOSE allow differentiation between multiple functions in planta: insights from an allelic series. **Mol Biol Cell** 20: 530–543

Ehrlich BE (1992) Planar lipid bilayers on patch pipettes: bilayer formation and ion channel incorporation. **Meth Enzymol** 207: 463–470

Erdmann R, Blobel G (1995) Giant peroxisomes in oleic acid-induced *Saccharomyces cerevisiae* lacking the peroxisomal membrane protein Pmp27p. **J Cell Biol** 128: 509–523

Eubel H, Meyer EH, Taylor NL, Bussell JD, O'Toole N, Heazlewood JL, Castleden I, Small ID, Smith SM, Millar AH (2008) Novel proteins, putative membrane transporters, and an integrated metabolic network are revealed by quantitative proteomic analysis of Arabidopsis cell culture peroxisomes. **Plant Physiol** 148: 1809–1829

Ferdinandusse S, Jimenez-Sanchez G, Koster J, Denis S, van Roermund CWT, Silva-Zolezzi I, Moser AB, Visser WF, Gulluoglu M, Durmaz O, Demirkel M, Waterham HR, Gökçay G, Wanders RJA, Valle D (2015) A novel bile acid biosynthesis defect due to a deficiency of peroxisomal ABCD3. **Human Mol Gen** 24: 361–370

Fiermonte G, Paradies E, Todisco S, Marobbio CMT, Palmieri F (2009) A novel member of solute carrier family 25 (SLC25A42) is a transporter of coenzyme A and adenosine 3',5'-diphosphate in human mitochondria. **J Biol Chem** 284: 18152–18159

Footitt S, Slocombe SP, Lerner V, Kurup S, Wu Y, Larson T, Graham IA, Baker A, Holdsworth M (2002) Control of germination and lipid mobilization by COMATOSE, the Arabidopsis homologue of human ALDP. **EMBO J** 21: 2912–2922

Friso G, van Wijk KJ (2015) Update: Post-translational protein modifications in plant metabolism. **Plant Physiol** 169: 1469–1487

Fukao Y, Hayashi M, Hara-Nishimura I, Nishimura M (2003) Novel glyoxysomal protein kinase, GPK1, identified by proteomic analysis of glyoxysomes in etiolated cotyledons of *Arabidopsis thaliana*. **Plant Cell Physiol** 44: 1002–1012

Fulda M, Schnurr J, Abbadi A, Heinz E, Browse J (2004) Peroxisomal Acyl-CoA synthetase activity is essential for seedling development in *Arabidopsis thaliana*. **Plant Cell** 16: 394–405

Gakière B, Fernie AR, Pétriacq P (2018) More to NAD than meets the eye: A regulator of metabolic pools and gene expression in Arabidopsis. **Free Radic Biol Med** 122: 86–95

Gasmi L, McLennan AG (2001) The mouse Nudt7 gene encodes a peroxisomal nudix hydrolase specific for coenzyme A and its derivatives. **Biochem J** 357: 33–38

Geillon F, Gondcaille C, Raas Q, Dias AMM, Pecqueur D, Truntzer C, Lucchi G, Ducoroy P, Falson P, Savary S, Trompier D (2017) Peroxisomal ATP-binding cassette transporters form mainly tetramers. **J Biol Chem** 292: 6965–6977

Goepfert S, Poirier Y (2007) β -oxidation in fatty acid degradation and beyond. **Curr Opin Plant Biol** 10: 245–251

Germain V, Rylott EL, Larson TR, Sherson SM, Bechtold N, Carde JP, Bryce JH, Graham IA, Smith SM (2001) Requirement for 3-ketoacyl-CoA thiolase-2 in peroxisome development, fatty acid β -oxidation and breakdown of triacylglycerol in lipid bodies of Arabidopsis seedlings. *Plant J* 28: 1–12

Graham IA (2008) Seed storage oil mobilization. **Annu Rev Plant Biol** 59: 115–142

Grunau S, Mindthoff S, Rottensteiner H, Sormunen RT, Hiltunen JK, Erdmann R, Antonenkov VD (2009) Channel-forming activities of peroxisomal membrane proteins from the yeast *Saccharomyces cerevisiae*. **FEBS J** 276: 1698–1708

Gualdrón-López M, Vapola MH, Miinalainen IJ, Hiltunen JK, Michels PAM, Antonenkov VD (2012) Channel-forming activities in the glycosomal fraction from the bloodstream form of *Trypanosoma brucei*. **PLoS One** 7: e34530

Gurvitz A, Rottensteiner H, Kilpeläinen SH, Hartig A, Hiltunen JK, Binder M, Dawes IW, Hamilton B (1997) The *Saccharomyces cerevisiae* peroxisomal 2,4-dienoyl-CoA reductase is encoded by the oleate-inducible gene SPS19. **J Biol Chem** 272: 22140–22147

Haferkamp I, Schmitz-Esser S (2012) The plant mitochondrial carrier family: functional and evolutionary aspects. **Front Plant Sci** 3: 2

Haferkamp I (2007) The diverse members of the mitochondrial carrier family in plants. **FEBS Lett** 581: 2375–2379

Hashida SN, Takahashi H, Uchimiya H (2009) The role of NAD biosynthesis in plant development and stress responses. **Ann Bot** 103: 819–824

Hayashi M, Nito K, Takei-Hoshi R, Yagi M, Kondo M, Suenaga A, Yamaya T, Nishimura M, Nishimura M (2002) Ped3p is a peroxisomal ATP-binding cassette transporter that might supply substrates for fatty acid β -oxidation. **Plant Cell Physiol** 43: 1–11

Henry LK, Gutensohn M, Thomas ST, Noel JP, Doudareva N (2015) Orthologs of the archaeal isopentenyl phosphate kinase regulate terpenoid production in plants. **Proc Natl Acad Sci USA** 112: 10050–10055

Hemmerlin A, Harwood JL, Bach TJ (2012) A raison d'être for two distinct pathways in the early steps of plant isoprenoid biosynthesis? **Prog Lipid Res** 51: 95–148

Hettema EH, van Roermund CWT, Distel B, van den Berg M, Vilela C, Rodrigues-Pousada C, Wanders RJA, Tabak HF (1996) The ABC transporter proteins Pat1 and Pat2 are required for import of long-chain fatty acids into peroxisomes of *Saccharomyces cerevisiae*. **EMBO J** 15: 3813–3822

Higgins CF (1992) ABC transporters: from microorganisms to man. **Annu Rev Cell Biol** 8: 67–113

Hodges M, Jossier M, Boex-Fontvieille E, Tcherkez G (2013) Protein phosphorylation and photorespiration. **Plant Biol J** 15: 694–706

Hooks MA, Turner JE, Murphy EC, Graham IA (2004) Acetate non-utilizing mutants of *Arabidopsis*: evidence that organic acids influence carbohydrate perception in germinating seedlings. **Mol Genet Genomics** 271: 249–256

Hölscher C, Meyer T, Schaewen von A (2014) Dual-Targeting of *Arabidopsis* 6-Phosphogluconolactonase 3 (PGL3) to Chloroplasts and Peroxisomes Involves Interaction with Trx m2 in the Cytosol. **Mol Plant** 7: 252–255

Hölscher C, Lutterbey M-C, Lansing H, Meyer T, Fischer K, Schaewen von A (2016) Defects in peroxisomal 6-phosphogluconate dehydrogenase isoform PGD2 prevent gametophytic interaction in *Arabidopsis thaliana*. **Plant Physiol** 171: 192–205

Hu J, Baker A, Bartel B, Linka N, Mullen RT, Reumann S, Zolman BK (2012) Plant peroxisomes: biogenesis and function. **Plant Cell** 24: 2279–2303

Hua T, Wu D, Ding W, Wang J, Shaw N, Liu Z-J (2012) Studies of human 2,4-dienoyl-CoA reductase shed new light on peroxisomal β -oxidation of unsaturated fatty acids. **J Biol Chem** 287: 28956–28965

Ito D, Yoshimura K, Ishikawa K, Ogawa T, Maruta T, Shigeoka S (2012) A comparative analysis of the molecular characteristics of the Arabidopsis CoA pyrophosphohydrolases AtNUDX11, 15, and 15a. **Biosci Biotechnol Biochem** 76: 139–147

Kamijo K, Taketani S, Yokota S, Osumi T, Hashimoto T (1990) The 70-kDa peroxisomal membrane protein is a member of the Mdr (P-glycoprotein)-related ATP-binding protein superfamily. **J Biol Chem** 265: 4534–4540

Kataya ARA, Schei E, Lillo C (2015) Towards understanding peroxisomal phosphoregulation in *Arabidopsis thaliana*. **Planta** 243:699–701

Kessel-Vigeliuss, Wiese J, Schroers M, Wrobel T, Han F, Linka N (2013) An engineered plant peroxisomes and its application in biotechnology. *Plant Sci* 210: 232–240

Kienow L, Schneider K, Bartsch M, Stuible HP, Weng H, Miersch O, Wasternack C, Kombrink E (2008) Jasmonates meet fatty acids: functional analysis of a new acyl-coenzyme A synthetase family from *Arabidopsis thaliana*. **J Exp Bot** 59: 403–419

Koch J, Pranjić K, Huber A, Ellinger A, Hartig A, Kragler F, Brocard C (2010) PEX11 family members are membrane elongation factors that coordinate peroxisome proliferation and maintenance. **J Cell Sci** 123: 3389–3400

Koo AJ, Chung HS, Kobayashi Y, Howe GA (2006) Identification of a peroxisomal acyl-activating enzyme involved in the biosynthesis of jasmonic acid in *Arabidopsis*. **J Biol Chem** 281: 33511–33520

Korasick DA, Enders TA, Strader LC (2013) Auxin biosynthesis and storage forms. **J Exp Bot** 64: 2541–2555

Li J, Tietz S, Cruz JA, Strand DD, Xu Y, Chen J, Kramer DM, Hu J (2018) Photometric screens identified *Arabidopsis* peroxisome proteins that impact photosynthesis under dynamic light conditions. **Plant J** doi: 10.1111/tpj.14134

Lingard MJ, Trelease RN (2006) Five *Arabidopsis* peroxin 11 homologs individually promote peroxisome elongation, duplication or aggregation. **J Cell Sci** 119: 1961–1972

Linka N, Theodoulou FL, Haslam RP, Linka M, Napier JA, Neuhaus HE, Weber APM (2008) Peroxisomal ATP import is essential for seedling development in *Arabidopsis thaliana*. **Plant Cell** 20: 3241–3257

Linka N, Esser C (2012) Transport proteins regulate the flux of metabolites and cofactors across the membrane of plant peroxisomes. **Front Plant Sci** 3: 3

Linka N, Theodoulou FL (2013) Metabolite transporters of the plant peroxisomal membrane: known and unknown. **Subcell Biochem** 69: 169–194

Lombard-Platet G, Savary S, Sarde CO, Mandel JL, Chimini G (1996) A close relative of the adrenoleukodystrophy (ALD) gene codes for a peroxisomal protein with a specific expression pattern. **Proc Natl Acad Sci USA** 93: 1265–1269

Mano S, Nakamori C, Fukao Y, Araki M, Matsuda A, Kondo M, Nishimura M (2011) The defect of peroxisomal membrane protein 38 causes enlargement of peroxisomes. **Plant Cell Physiol** 52: 2157–2172

Meyer T, Hölscher C, Schwöppe C, Schaewen von A (2011) Alternative targeting of *Arabidopsis* plastidic glucose-6-phosphate dehydrogenase G6PD1 involves cysteine-dependent interaction with G6PD4 in the cytosol. **Plant J** 66: 745–758

Mindthoff S, Grunau S, Steinfort LL, Girzalsky W, Hiltunen JK, Erdmann R, Antonenkov VD (2015) Peroxisomal Pex11 is a pore-forming protein homologous to TRPM channels. **Biochim Biophys Acta** 1863: 271–283

Morita M, Imanaka T (2012) Peroxisomal ABC transporters: Structure, function and role in disease. **Biochim Biophys Acta** 1822: 1387–1396

Mosser J, Douar AM, Sarde CO, Kioschis P, Feil R, Moser H, Poustka AM, Mandel JL, Aubourg P (1993) Putative X-linked adrenoleukodystrophy gene shares unexpected homology with ABC transporters. **Nature** 361: 726–730

Nito K, Kamigaki A, Kondo M, Hayashi M, Nishimura M (2007) Functional classification of Arabidopsis peroxisome biogenesis factors proposed from analyses of knockout mutant. **Plant Cell Physiol** 48: 763–774.

Noctor G, Queval G, Gakiere B (2006) NAD(P) synthesis and pyridine nucleotide cycling in plants and their potential importance in stress conditions. **J Exp Bot** 57: 1603–1620

Noctor G, Foyer CH (2016) Intracellular redox compartmentation and ROS-related communication in regulation and signaling. **Plant Physiol** 171: 1581–1592

Nyathi Y, De Marcos Lousa C, van Roermund CWT, Wanders RJA, Johnson B, Baldwin SA, Theodoulou FL, Baker A (2010) The Arabidopsis peroxisomal ABC transporter, comatose, complements the *Saccharomyces cerevisiae* *pxa1/pxa2Δ* mutant for metabolism of long-chain fatty acids and exhibits fatty acyl-CoA-stimulated ATPase activity. **J Biol Chem** 285: 29892–29902

Ogawa T, Ueda Y, Yoshimura K, Shigeoka S (2005) Comprehensive analysis of cytosolic Nudix hydrolases in *Arabidopsis thaliana*. **J Biol Chem** 280: 25277–25283

Ogawa T, Yoshimura K, Miyake H, Ishikawa K, Ito D, Tanabe N, Shigeoka S (2008) Molecular characterization of organelle-type Nudix hydrolases in Arabidopsis. **Plant Physiol** 148: 1412–1424

Okamoto T, Kawaguchi K, Watanabe S, Agustina R, Ikejima T, Ikeda K, Nakano M, Morita M, Imanaka T (2018) Characterization of human ATP-binding cassette protein subfamily D reconstituted into proteoliposomes. **Biochem Biophys Res Commun** 496: 1122–1127

Orth T, Reumann S, Zhang X, Fan J, Wenzel D, Quan S, Hu J (2007) The PEROXIN11 protein family controls peroxisome proliferation in Arabidopsis. **Plant Cell** 19: 333–350

Palmieri L, Lasorsa FM, Vozza A, Agrimi G, Fiermonte G, Runswick MJ, Walker JE, Palmieri F (2000) Identification and functions of new transporters in yeast mitochondria. **Biochim Biophys Acta** 1459: 363–369

Palmieri L, Rottensteiner H, Girzalsky W, Scarcia P, Palmieri F, Erdmann R (2001) Identification and functional reconstitution of the yeast peroxisomal adenine nucleotide transporter. **EMBO J** 20: 5049–5059

Palmieri F, Agrimi G, Blanco E, Castegna A, Di Noia MA, Iacobazzi V, Lasorsa FM, Marobbio CMT, Palmieri L, Scarcia P, Todisco S, Vozza A, Walker J (2006) Identification of mitochondrial carriers in *Saccharomyces cerevisiae* by transport assay of reconstituted recombinant proteins. **Biochim Biophys Acta** 1757: 1249–1262

Palmieri F, Pierri CL, De Grassi A, Nunes-Nesi A, Fernie AR (2011) Evolution, structure and function of mitochondrial carriers: a review with new insights. **Plant J** 66: 161–181

Palmieri F (2014) Mitochondrial transporters of the SLC25 family and associated diseases: a review. **J Inherit Metab Dis** 37: 565–575

Pollak N, Dölle C, Ziegler M (2007) The power to reduce: pyridine nucleotides--small molecules with a multitude of functions. **Biochem J** 402: 205–218

Pracharoenwattana I, Cornah JE, Smith SM (2007) Arabidopsis peroxisomal malate dehydrogenase functions in β -oxidation but not in the glyoxylate cycle. **Plant J** 50: 381–390

Pracharoenwattana I, Zhou W, Smith SM (2010) Fatty acid β -oxidation in germinating Arabidopsis seeds is supported by peroxisomal hydroxypyruvate reductase when malate dehydrogenase is absent. **Plant Mol Biol** 72: 101–109

Prohl C, Pelzer W, Diekert K, Kmita H, Bedekovics T, Kispal G, Lill R (2001) The yeast mitochondrial carrier Leu5p and its human homologue Graves' disease protein are required for accumulation of coenzyme A in the matrix. **Mol Cell Biol** 21: 1089–1097

Rees DC, Johnson E, Lewinson O (2009) ABC transporters: the power to change. **Nat Rev Mol Cell Biol** 10: 218–227

Reilly SJ, Tillander V, Ofman R, Alexson SE, Hunt MC (2008) The nudix hydrolase 7 is an Acyl-CoA diphosphatase involved in regulating peroxisomal coenzyme A homeostasis. **J Biochem** 144: 655–663

Reinhold R, Krüger V, Meinecke M, Schulz C, Schmidt B, Grunau SD, Guiard B, Wiedemann N, van der Laan M, Wagner R, Rehling P, Dudek J (2012) The channel-forming Sym1 protein is transported by the TIM23 complex in a pre-sequence-independent manner. **Mol Cell Biol** 32: 5009–5021

Reumann S, Maier E, Benz R, Heldt HW (1995) The membrane of leaf peroxisomes contains a porin-like channel. **J Biol Chem** 270: 17559–17565

Reumann S, Maier E, Benz R, Heldt HW (1996) A specific porin is involved in the malate shuttle of leaf peroxisomes. **Biochem Soc Trans** 24: 754–757

Reumann S, Bettermann M, Benz R, Heldt HW (1997) Evidence for the presence of a porin in the membrane of glyoxysomes of castor bean. **Plant Physiol** 115: 891–899

Reumann S, Maier E, Heldt HW, Benz R (1998) Permeability properties of the porin of spinach leaf peroxisomes. **Eur J Biochem** 251: 359–366

Reumann S, Quan S, Aung K, Yang P, Manandhar-Shrestha K, Holbrook D, Linka N, Switzenberg R, Wilkerson CG, Weber APM, Olsen LJ, Hu J (2009) In-depth proteome analysis of Arabidopsis leaf peroxisomes combined with in vivo subcellular targeting verification indicates novel metabolic and regulatory functions of peroxisomes. **Plant Physiol** 150: 125–143

Reumann S, Buchwald D, Lingner T (2012) PredPlantPTS1: A web server for the prediction of plant peroxisomal proteins. **Front Plant Sci** 3: 194

Rodríguez-Concepción M, Boronat A (2015) Breaking new ground in the regulation of the early steps of plant isoprenoid biosynthesis. **Curr Opin Plant Biol** 25: 17–22

Rokka A, Antonenkov VD, Soininen R, Immonen HL, Pirilä PL, Bergmann U, Sormunen RT, Weckström M, Benz R, Hiltunen JK (2009) Pxmp2 is a channel-forming protein in mammalian peroxisomal membrane. **PLoS One** 4: e5090

Rottensteiner H, Stein K, Sonnenhol E, Erdmann R (2003) Conserved function of pex11p and the novel pex25p and pex27p in peroxisome biogenesis. **Mol Biol Cell** 14: 4316–4328

Rottensteiner H, Theodoulou FL (2006) The ins and outs of peroxisomes: co-ordination of membrane transport and peroxisomal metabolism. **Biochim Biophys Acta** 1763: 1527–1540

Rubio S, Larson TR, Gonzalez-Guzman M, Alejandro S, Graham IA, Serrano R, Rodriguez PL (2006) An Arabidopsis mutant impaired in coenzyme A biosynthesis is sugar dependent for seedling establishment. **Plant Physiol** 140: 830–843

Rubio S, Whitehead L, Larson TR, Graham IA, Rodriguez PL (2008) The coenzyme a biosynthetic enzyme phosphopantetheine adenylyltransferase plays a crucial role in plant growth, salt/osmotic stress resistance, and seed lipid storage. **Plant Physiol** 148: 546–556

Rylott EL, Eastmond PJ, Gilday AD, Slocombe SP, Larson TR, Baker A, Graham IA (2006) The Arabidopsis thaliana multifunctional protein gene (MFP2) of peroxisomal beta-oxidation is essential for seedling establishment. **Plant J** 45: 930–941

Saier MH, Yen MR, Noto K, Tamang DG, Elkan C (2009) The transporter classification database: recent advances. **Nucleic Acids Res** 37: D274–8

Sapir-Mir M, Mett A, Belausov E, Tal-Meshulam S, Frydman A, Gidoni D, Eyal Y (2008) Peroxisomal localization of Arabidopsis isopentenyl diphosphate isomerases suggests that part of the plant isoprenoid mevalonic acid pathway is compartmentalized to peroxisomes. **Plant Physiol** 148: 1219–1228

Schaller F, Biesgen C, Müssig C, Altmann T, Weiler EW (2000) 12-Oxophytodienoate reductase 3 (OPR3) is the isoenzyme involved in jasmonate biosynthesis. **Planta** 210: 979–984

Schrader M, Godinho LF, Costello JL, Islinger M (2015) The different facets of organelle interplay – an overview of organelle interactions. **Front Cell Dev Biol** 3: 56

Schrader M, Costello JL, Godinho LF, Azadi AS, Islinger M (2016) Proliferation and fission of peroxisomes - An update. **Biochim Biophys Acta** 1863: 971–983

Shani N, Valle D (1996) A *Saccharomyces cerevisiae* homolog of the human adrenoleukodystrophy transporter is a heterodimer of two half ATP-binding cassette transporters. **Proc Natl Acad Sci USA** 93: 11901–11906

Simkin AJ, Guirimand G, Papon N, Courdavault V, Thabet I, Ginis O, Bouzid S, Giglioli-Guivarc'h N, Clastre M (2011) Peroxisomal localisation of the final steps of the mevalonic acid pathway in planta. **Planta** 234: 903–914

Spinazzola A, Viscomi C, Fernandez-Vizarra E, Carrara F, D'Adamo P, Calvo S, Marsano RM, Donnini C, Weiher H, Strisciuglio P, Parini R, Sarzi E, Chan A, DiMauro S, Rötig A, Gasparini P, Ferrero I, Mootha VK, Tiranti V, Zeviani M (2006) MPV17 encodes an inner mitochondrial membrane protein and is mutated in infantile hepatic mitochondrial DNA depletion. **Nat Genet** 38: 570–575

Sugiura A, Mattie S, Prudent J, and McBride HM (2017) Newly born peroxisomes are a hybrid of mitochondrial and ER-derived pre-peroxisomes. **Nature** doi:10.1038/nature21375.

Stintzi A, Browse J (2000) The Arabidopsis male-sterile mutant, *opr3*, lacks the 12-oxophytodienoic acid reductase required for jasmonate synthesis. **Proc Natl Acad Sci USA** 97: 10625–10630

Strader LC, Culler AH, Cohen JD, Bartel B (2010) Conversion of endogenous indole-3-butyric acid to indole-3-acetic acid drives cell expansion in Arabidopsis seedlings. **Plant Physiol** 153: 1577–1586

Strader LC, Wheeler DL, Christensen SE, Berens JC, Cohen JD, Rampey RA, Bartel B (2011) Multiple facets of Arabidopsis seedling development require indole-3-butyric acid-derived auxin. **Plant Cell** 23: 984–999

Tanaka A, Okumoto K, Fujiki Y (2003) cDNA cloning and characterization of the third isoform of human peroxin Pex11p. **Biochem Biophys Res Commun** 300: 819–823

Taylor EB (2017) Functional properties of the mitochondrial carrier system. **Trends Cell Biol** 27: 633–644

Theodoulou FL, Job K, Slocombe SP, Footitt S, Holdsworth M, Baker A, Larson TR, Graham IA (2005) Jasmonic acid levels are reduced in COMATOSE ATP-binding cassette transporter

mutants. Implications for transport of jasmonate precursors into peroxisomes. **Plant Physiol** 137: 835–840

Theodoulou FL, Kerr ID (2015) ABC transporter research: going strong 40 years on. **Biochem Soc Trans** 43: 1033–1040

Thoms S, Erdmann R (2005) Dynamin-related proteins and Pex11 proteins in peroxisome division and proliferation. **FEBS J** 272: 5169–5181

Tilton GB, Wedemeyer WJ, Browse J, Ohlrogge JB (2006) Plant coenzyme A biosynthesis: characterization of two pantothenate kinases from *Arabidopsis*. **Plant Mol Biol** 61: 629–642

Trott A, Morano KA (2004) SYM1 is the stress-induced *Saccharomyces cerevisiae* ortholog of the mammalian kidney disease gene Mpv17 and is required for ethanol metabolism and tolerance during heat shock. **Eukaryot Cell** 3: 620–631

Tugal HB, Pool M, Baker A (1999) *Arabidopsis* 22-kilodalton peroxisomal membrane protein. Nucleotide sequence analysis and biochemical characterization. **Plant Physiol** 120: 309–320

Turner WL, Waller JC, Vanderbeld B, Snedden WA (2004) Cloning and characterization of two NAD kinases from *Arabidopsis*. identification of a calmodulin binding isoform. **Plant Physiol** 135: 1243–1255

Turner WL, Waller JC, Snedden WA (2005) Identification, molecular cloning and functional characterization of a novel NADH kinase from *Arabidopsis thaliana* (thale cress). **Biochem J** 385: 217–223

van Roermund CWT, Elgersma Y, Singh N, Wanders RJA, Tabak HF (1995) The membrane of peroxisomes in *Saccharomyces cerevisiae* is impermeable to NAD(H) and acetyl-CoA under *in vivo* conditions. **EMBO J** 14: 3480–3486

van Roermund CWT, Tabak HF, van den Berg M, Wanders RJA, Hettema EH (2000) Pex11p plays a primary role in medium-chain fatty acid oxidation, a process that affects peroxisome number and size in *Saccharomyces cerevisiae*. *J Cell Biol* 150: 489–498

van Roermund CWT, Drissen R, van den Berg M, Ijlst L, Hetteema EH, Tabak HF, Waterham HR, Wanders RJA (2001) Identification of a peroxisomal ATP carrier required for medium-chain fatty acid β -oxidation and normal peroxisome proliferation in *Saccharomyces cerevisiae*. **Mol Cell Biol** 21: 4321–4329

van Roermund CWT, Waterham HR, Ijlst L, Wanders RJA (2003) Fatty acid metabolism in *Saccharomyces cerevisiae*. **Cell Mol Life Sci** 60: 1838–1851

van Roermund CWT, Visser WF, Ijlst L, van Cruchten A, Boek M, Kulik W, Waterham HR, Wanders RJA (2008) The human peroxisomal ABC half transporter ALDP functions as a homodimer and accepts acyl-CoA esters. **FASEB J** 22: 4201–4208

van Roermund CWT, Visser WF, Ijlst L, Waterham HR, Wanders RJA (2011) Differential substrate specificities of human ABCD1 and ABCD2 in peroxisomal fatty acid β -oxidation. **Biochim Biophys Acta** 1811: 148–152

van Roermund CWT, Ijlst L, Majczak W, Waterham HR, Folkerts H, Wanders RJA, Hellingwerf KJ (2012) Peroxisomal fatty acid uptake mechanism in *Saccharomyces cerevisiae*. **J Biol Chem** 287: 20144–20153

van Roermund CWT, Ijlst L, Wagemans T, Wanders RJA, Waterham HR (2014) A role for the human peroxisomal half-transporter ABCD3 in the oxidation of dicarboxylic acids. **Biochim Biophys Acta** 1841: 563–568

van Roermund CWT, Schroers MG, Wiese J, Facchinelli F, Kurz S, Wilkinson S, Charton L, Wanders RJA, Waterham HR, Weber APM, Linka N (2016) The peroxisomal NAD carrier from *Arabidopsis* imports NAD in exchange with AMP. **Plant Physiol** 171: 2127–2139

Vapola MH, Rokka A, Sormunen RT, Alhonen L, Schmitz W, Conzelmann E, Wärri A, Grunau S, Antonenkov VD, Hiltunen JK (2014) Peroxisomal membrane channel Pxmp2 in the mammary fat pad is essential for stromal lipid homeostasis and for development of mammary gland epithelium in mice. **Dev Biol** 391: 66–80

Verleur N, Hetteema EH, van Roermund CWT, Tabak HF, Wanders RJA (1997) Transport of activated fatty acids by the peroxisomal ATP-binding-cassette transporter Pxa2 in a semi-intact yeast cell system. **Eur J Biochem** 249: 657–661

Visser WF, van Roermund CWT, Waterham HR, Wanders RJA (2002) Identification of human PMP34 as a peroxisomal ATP transporter. **Biochem Biophys Res Commun** 299: 494–497

Visser WF, van Roermund CWT, Ijlst L, Hellingwerf KJ, Wanders RJA, Waterham HR (2005) Demonstration and characterization of phosphate transport in mammalian peroxisomes. **Biochem J** 389: 717–722

Waller JC, Dhanoa PK, Schumann U, Mullen RT, Snedden WA (2010) Subcellular and tissue localization of NAD kinases from Arabidopsis: compartmentalization of *de novo* NADP biosynthesis. **Planta** 231: 305–317

Wasternack C, Strnad M (2017) Jasmonates are signals in the biosynthesis of secondary metabolites - Pathways, transcription factors and applied aspects - A brief review. **N Biotechnol** doi: 10.1016/j.nbt.2017.09.007

Wasternack C, Feussner I (2018) The oxylipin pathways: Biochemistry and function. **Annu Rev Plant Biol** 69: 363–386

Wiesinger C, Kunze M, Regelsberger G, Forss-Petter S, Berger J (2013) Impaired very long-chain acyl-CoA β -oxidation in human X-linked adrenoleukodystrophy fibroblasts is a direct consequence of ABCD1 transporter dysfunction. **J Biol Chem** 288: 19269–19279

Zallot R, Agrimi G, Lerma-Ortiz C, Teresinski HJ, Frelin O, Ellens KW, Castegna A, Russo A, de Crécy-Lagard V, Mullen RT, Palmieri F, Hanson AD (2013) Identification of mitochondrial coenzyme a transporters from maize and Arabidopsis. **Plant Physiol** 162: 581–588

Vapola MH, Rokka A, Sormunen RT, Alhonen L, Schmitz W, Conzelmann E, Wärri A, Grunau S, Antonenkov VD, Hiltunen JK (2014) Peroxisomal membrane channel Pxmp2 in the mammary fat pad is essential for stromal lipid homeostasis and for development of mammary gland epithelium in mice. **Dev Biol** 391: 66–80

Zeth K, Thein M (2010) Porins in prokaryotes and eukaryotes: common themes and variations. **Biochem J** 431: 13–22

Zolman BK, Silva ID, Bartel B (2001) The Arabidopsis *pxa1* mutant is defective in an ATP-binding cassette transporter-like protein required for peroxisomal fatty acid β -oxidation. *Plant Physiol* 127: 1266–1278

Author contribution

Ana Plett wrote the part about ABC-transporter. Nicole Linka wrote the conclusion, the part about peroxisomal pore-forming channels and designed the figure and table. Lennart Charton wrote the introduction and the part about peroxisomal MCF carrier.

IV. Published Manuscripts

IV.II Published Manuscript 2

The mitochondrial NAD⁺ transporter (NDT1) plays important roles in cellular NAD⁺ homeostasis in *Arabidopsis thaliana*

Isabel de Souza Chaves¹, Elias Feitosa Araújo¹, Alexandra Florian², David Barbosa Medeiros¹, Paula da Fonseca-Pereira¹, Lennart Charton³, Elmién Heyneke², Jorge Alberto Condori Apfata¹, Marcel Viana Pires¹, Tabea Mettler-Altmann³, Wagner L. Araújo¹, H. Ekkehard Neuhaus⁴, Ferdinando Palmieri⁵, Toshihiro Obata², Andreas P.M. Weber³, Nicole Linka³, Alisdair R. Fernie^{2*}, Adriano Nunes-Nesi^{1*}

¹ Max Planck Partner Group, Departamento de Biologia Vegetal, Universidade Federal de Viçosa, 36570-900 Viçosa, Minas Gerais, Brazil


² Max-Planck-Institute of Molecular Plant Physiology Am Mühlenberg 1, 14476 Potsdam-Golm, Germany

³ Department of Plant Biochemistry, Heinrich Heine University Düsseldorf, 40225, Düsseldorf, Germany

⁴ Department of Plant Physiology, University of Kaiserslautern, D-67663 Kaiserslautern, Germany

⁵ Department of Biosciences, Biotechnology and Biopharmaceutics, University of Bari, 70125 Bari, Italy

The mitochondrial NAD⁺ transporter (NDT1) plays important roles in cellular NAD⁺ homeostasis in *Arabidopsis thaliana*

Ízabel de Souza Chaves¹, Elías Feitosa-Araújo¹, Alexandra Florian², David B. Medeiros¹, Paula da Fonseca-Pereira¹, Lennart Charton³, Elmién Heyneke², Jorge A.C. Apfata¹, Marcel V. Pires¹, Tabea Mettler-Altmann³, Wagner L. Araújo¹, H. Ekkehard Neuhaus⁴, Ferdinando Palmieri⁵, Toshihiro Obata², Andreas P.M. Weber³, Nicole Linka³, Alisdair R. Fernie^{2,*} and Adriano Nunes-Nesi^{1,2,*} 

¹Max Planck Partner Group, Departamento de Biologia Vegetal, Universidade Federal de Viçosa, 36570-900 Viçosa, Minas Gerais, Brazil,

²Max-Planck-Institute of Molecular Plant Physiology Am Mühlenberg 1, 14476 Potsdam-Golm, Germany,

³Department of Plant Biochemistry, Heinrich Heine University Düsseldorf, 40225 Düsseldorf, Germany,

⁴Department of Plant Physiology, University of Kaiserslautern, D-67663 Kaiserslautern, Germany, and

⁵Department of Biosciences, Biotechnology and Biopharmaceutics, University of Bari, 70125 Bari, Italy

Received 25 August 2017; revised 14 June 2019; accepted 26 June 2019; published online 6 July 2019.

*For correspondence (e-mails fernie@mpimp-golm.mpg.de and nunesnesi@ufv.br).

SUMMARY

Nicotinamide adenine dinucleotide (NAD⁺) is an essential coenzyme required for all living organisms. In eukaryotic cells, the final step of NAD⁺ biosynthesis is exclusively cytosolic. Hence, NAD⁺ must be imported into organelles to support their metabolic functions. Three NAD⁺ transporters belonging to the mitochondrial carrier family (MCF) have been biochemically characterized in plants. *At*NDT1 (*At*2g47490), focus of the current study, *At*NDT2 (*At*1g25380), targeted to the inner mitochondrial membrane, and *At*PXN (*At*2g39970), located in the peroxisomal membrane. Although *At*NDT1 was presumed to reside in the chloroplast membrane, subcellular localization experiments with green fluorescent protein (GFP) fusions revealed that *At*NDT1 locates exclusively in the mitochondrial membrane in stably transformed *Arabidopsis* plants. To understand the biological function of *At*NDT1 in *Arabidopsis*, three transgenic lines containing an antisense construct of *At*NDT1 under the control of the 35S promoter alongside a T-DNA insertional line were evaluated. Plants with reduced *At*NDT1 expression displayed lower pollen viability, silique length, and higher rate of seed abortion. Furthermore, these plants also exhibited an increased leaf number and leaf area concomitant with higher photosynthetic rates and higher levels of sucrose and starch. Therefore, lower expression of *At*NDT1 was associated with enhanced vegetative growth but severe impairment of the reproductive stage. These results are discussed in the context of the mitochondrial localization of *At*NDT1 and its important role in the cellular NAD⁺ homeostasis for both metabolic and developmental processes in plants.

Keywords: *Arabidopsis thaliana*, nicotinamide adenine dinucleotide, transporter, pollen viability, starch metabolism.

INTRODUCTION

Nicotinamide adenine dinucleotide (NAD⁺) and its phosphorylated derivative (NADP⁺) are central coenzymes implicated in cellular homeostasis. Alteration in the balance of the anabolism and catabolism of these nucleotides does not only affect metabolism but also the redox poise of the entire cell, thereby strongly impacting plant growth and development (Noctor *et al.*, 2006; Hashida *et al.*, 2009, 2010; Gakière *et al.*, 2018). Along with its derivative forms, NAD⁺ participates in several biological reactions in glycolysis, the tricarboxylic acid (TCA) cycle, glycine decarboxylation,

the Calvin–Benson cycle, and the β -oxidation in peroxisomes (Bernhardt *et al.*, 2012; Geigenberger and Fernie, 2014).

NAD⁺ is widely used as coenzyme for reductive/oxidative processes, playing important roles in the operation of a range of dehydrogenase activities (Selinski *et al.*, 2014). In addition, an important role for NAD⁺ metabolism has been demonstrated in pollen maturation and germination (Hashida *et al.*, 2013) and for the energy generation during pollen germination and tube growth (Cárdenas *et al.*, 2006; Selinski and Scheibe, 2014). The NADPH generated in

© 2019 The Authors

The Plant Journal published by Society for Experimental Biology and John Wiley & Sons Ltd

This is an open access article under the terms of the Creative Commons Attribution License, which permits use, distribution and reproduction in any medium, provided the original work is properly cited.

487

488 *Izabel de Souza Chaves et al.*

heterotrophic plastids by the oxidative pentose phosphate pathway (OPPP) provides the reducing power required for several pathways, such as fatty acid biosynthesis (Neuhaus and Emes, 2000), as well as nitrogen assimilation (Bowsher *et al.*, 2007) and amino acid biosynthesis. Moreover, both NAD⁺ and NADP⁺ play an essential role in signalling pathways through their interaction with reactive oxygen species (ROS) (Hashida *et al.*, 2010). Consequently, it is assumed that these two coenzymes are involved in the acclimation to environmental stresses such as UV radiation, salinity, temperature, and drought (De Block *et al.*, 2005). Over and above this, it has been proposed that pyridine nucleotide metabolism is important for seed germination (Hunt *et al.*, 2007), stomatal movement (Hashida *et al.*, 2010), bolting (Liu *et al.*, 2009), development (Hashida *et al.*, 2009), senescence (Schippers *et al.*, 2008), and nitrogen assimilation (Takahashi *et al.*, 2009).

NAD⁺ biosynthesis in plants occurs via either the *de novo* or the salvage pathway (Noctor *et al.*, 2006; Hashida *et al.*, 2009). The *de novo* pathway starts in plastids using aspartate or tryptophan as precursors, while the salvage pathway starts with nicotinamide (NAM) or nicotinic acid (NA). Both metabolic fluxes converge in the formation of nicotinic acid mononucleotide (NAMN), which in turn gives rise to NAD⁺. Furthermore NAD⁺ kinases can synthesize NADP⁺ from NAD⁺ and ATP in the cytosol (NADK1; Berrin *et al.*, 2005; Waller *et al.*, 2010) and in the chloroplasts (NADK2; Chai *et al.*, 2005, 2006). In addition, peroxisomal NADH kinase, which uses NADH rather than NAD⁺ as substrate to produce NADPH, has been found in *Arabidopsis thaliana* (NADK3; Turner *et al.*, 2005; Waller *et al.*, 2010). Since the last step of NAD⁺ synthesis takes place in the cytosol, NAD⁺ must be imported into the cell organelles to allow proper metabolism (Noctor *et al.*, 2006).

In yeast, two carrier proteins called ScNDT1 and ScNDT2 (NDT: NAD⁺ transporter), which are capable of transporting NAD⁺, have been identified (Todisco *et al.*, 2006). The characterization of ScNDT1 protein revealed its location in the inner mitochondrial membrane and its high NAD⁺ transport activity in exchange with ADP and AMP *in vitro* (Todisco *et al.*, 2006). The lack of both ScNDT proteins in yeast assigns a function for supplying NAD⁺ to the mitochondrial matrix (Todisco *et al.*, 2006). Three genes encoding proteins capable of NAD⁺ transport have been identified in Arabidopsis. *AtNDT2* is located in the inner mitochondrial membrane (Palmieri *et al.*, 2009) and *AtPXN* resides in the peroxisomal membrane (Agrimi *et al.*, 2012; Bernhardt *et al.*, 2012). Moreover, re-evaluation of the subcellular localization of *AtNDT1*, previously reported to encode a protein targeted to the inner membrane of the chloroplast (Palmieri *et al.*, 2009), revealed the exclusive mitochondrial localization of this carrier (the present work). Interestingly, the two mitochondrial NAD⁺ carrier proteins found in Arabidopsis, *AtNDT1* and *AtNDT2*, have similar substrate specificity, importing NAD⁺, but not

NADH, nicotinamide, nicotinic acid, NADP⁺ or NADPH, against ADP or AMP (Palmieri *et al.*, 2009). In contrast, the *AtPXN* transporter has a versatile transport function *in vitro*, also using NADH and CoA as substrates (Agrimi *et al.*, 2012; Bernhardt *et al.*, 2012). Yeast complementation studies revealed that *AtPXN* favours the import of NAD⁺ in exchange for AMP in intact yeast cells (van Roermund *et al.*, 2016). Furthermore, expression of either *AtNDT1* or *AtNDT2* is able to complement the phenotype of *S. cerevisiae* cells lacking their NAD⁺ mitochondrial transporters and increase the mitochondrial NAD⁺ content of the double mutant strain devoid of their two NAD⁺ mitochondrial transporters (Palmieri *et al.*, 2009). In addition, the expression of either *AtNDT2* or *ScNDT1* in human cells increases the NAD⁺ content within the mitochondria (VanLinden *et al.*, 2015). Together, these studies provide evidence that *AtNDT1*, like *AtNDT2*, catalyzes the import of NAD⁺ into the mitochondria under *in vivo* conditions.

Analysis of *Atndt1*- and *Atndt2*-promoter-GUS plants showed that both genes are strongly expressed in developing tissues, mainly in highly metabolically active cells, which is in line with their mitochondrial localization. However, these transporters have only been characterised at the biochemical and molecular level, while their physiological function remains unclear. For this reason, we aimed to investigate the impact of decreased *AtNDT1* expression on plant development and performance. Given the importance of NAD⁺ in plant metabolism, we would expect that the deficiency of *AtNDT1* transport would impact the redox balance of the cells in different plant tissues. This impact on the redox balance could influence plant growth and development under both optimal and stress situations. In addition, evaluation of the *AtNDT1* protein function is critical for a better understanding of mitochondrial processes and their regulation. To test this hypothesis, we analysed the corresponding Arabidopsis mutants showing reduced expression of *AtNDT1* to understand how and at what level changes in the mitochondrial NAD⁺ transport can affect cell metabolism and plant development. We focused our attention on the impact of reduced *AtNDT1* expression in reproductive tissues and on the importance of this carrier in illuminated leaves.

RESULTS

AtNDT1 is highly expressed in the pollen grain

The need for NAD⁺ for multiple essential functions in cellular organelles is met by specialized NAD⁺ transport proteins. We therefore expect the presence of these carrier proteins in various tissues and at several developmental stages in Arabidopsis. To investigate the *AtNDT1* gene expression, we determined their transcript levels in different organs of young and mature Arabidopsis plants by quantitative real-time PCR (qRT-PCR) analysis (Supporting

Information Figure S1). In agreement with information in publicly available gene expression databases (<http://bar.utoronto.ca>), but slightly in contrast to that observed in our previous promoter GUS study (Palmieri *et al.*, 2009), *AtNDT1* was strongly expressed in the pollen grain. It also displayed considerable expression in seeds, seedlings, mature leaves and flowers. This suggest that *AtNDT1* transcript is ubiquitously expressed in Arabidopsis, but mainly found in pollen grain. This implies a role in sink and source tissues at any phase of the plant life cycle.

Generation of Arabidopsis plants with reduced expression of *AtNDT1*

To investigate the physiological role of the *AtNDT1* transporter in Arabidopsis, a T-DNA insertion line (GK-241G12) was isolated and three independent antisense lines were selected in the Col-0 ecotype (Figure 1a). The T-DNA was inserted in the ninth exon of the *AtNDT1* gene. Due to the presence of the T-DNA insertion, the homozygous T-DNA insertion plant *ndt1⁻:ndt1⁻* contained only 13% of the wild type (WT) *AtNDT1* transcript level in leaves (Figure 1b). The *AtNDT1* antisense lines were generated by ectopic repression of the *AtNDT1* transcription. The *AtNDT1* mRNA levels of the three antisense lines *as-1-ndt1*, *as-2-ndt1* and *as-3-ndt1* were reduced to 28, 34, and 49%, respectively, compared with those in WT leaves (Figure 1b). These independent mutant lines were used for further analyses to investigate the *in planta* function of *AtNDT1*.

Plants with reduced expression of *AtNDT1* display alterations in the expression of genes involved in NAD⁺ metabolism

To provide further insight into the physiological role of *AtNDT1*, we analysed the expression levels of *AtNDT1*,

AtNDT2, and *AtPXN* in WT and *ndt1⁻:ndt1⁻* plants by qRT-PCR using RNA isolated from dry seeds, leaves, flowers and pollen grains. The analysis revealed a significant reduction in the *AtNDT2* transcripts in flowers and pollen grains coupled with increases in the seeds of the *ndt1⁻:ndt1⁻* mutant compared with their WT counterparts (Figure S2). Moreover, a strong reduction in the expression of *AtPXN* was observed in the *ndt1⁻:ndt1⁻* pollen grains (Figure S2), while *AtPXN* expression levels were not significantly altered in seeds, leaves and flowers. These data therefore indicated that a reduced *AtNDT1* expression in the *ndt1⁻:ndt1⁻* is associated with changes in the expression levels of *AtNDT2* and *AtPXN*.

To further characterize the plants with reduced *AtNDT1* expression, the expression of genes encoding NAD⁺ biosynthetic enzymes and NAD kinases was evaluated by qRT-PCR using RNA isolated from seeds after 48 h of imbibition and leaves from 28-day-old rosette (Figure S3). The expression of genes encoding the NAD⁺ biosynthetic enzymes QPRT (quinolinate phosphoribosyltransferase) and NMNAT (nicotinate/nicotinamide mononucleotide adenylyltransferase), as well as the genes encoding cytosolic (NADK1) and plastidic (NADK2) isoforms of NAD kinases in Arabidopsis was significantly higher in *ndt1⁻:ndt1⁻* seeds. These results suggested that, especially in imbibed seeds, the expression of genes related to the biosynthetic pathway of NAD⁺ is upregulated presumably in an attempt to compensate for the lower *AtNDT1* expression. Conversely, expression of the genes encoding enzymes from NAD⁺ metabolism was only slightly lower in *ndt1⁻:ndt1⁻* mutant leaves (significantly only for the plastidic quinolinate synthase, QS) (Figure S3), which might have occurred as a consequence of different energetic requirements exhibited by seeds and leaves.

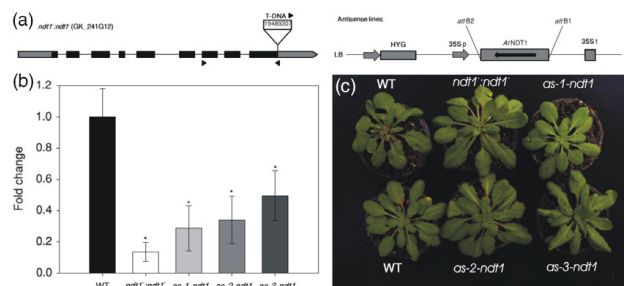


Figure 1. Isolation and characterization of *Arabidopsis thaliana* genotypes deficient in the expression of the mitochondrial NAD⁺ transporter (NDT1). (a) Schematic representation of the gene *AtNDT1* (At2g47490) showing the T-DNA insertion site. The T-DNA insert, approximately 4.5 kb, is not to scale. Boxes represent gene exons, and arrows on T-DNA denote primer positions used for population screening. The antisense construct includes the hygromycin resistance gene (*HYG*), the 35S promoter, the gene *NDT1* in antisense position and the 35S terminator. (b) Expression by quantitative real-time PCR analysis of *NDT1* in mature leaves of the *A. thaliana* mutants and wild-type plants (WT). The values were calculated relative to the WT in rosette leaves of 28-day-old plants. Values are presented as mean \pm SE of six individual plants per line; an asterisk indicates values that were determined by Student's *t*-test to be significantly different ($P < 0.05$) from the WT. (c) Phenotypic characterization of 4-week-old short-day grown Arabidopsis genotypes deficient in the expression of the plastidic NAD⁺ transporter (NDT1) and WT plants.

490 Izabel de Souza Chaves et al.

Effects of reduction in *AtNDT1* expression on seed development and seed filling

As *AtNDT1* is expressed in seeds and seedlings, we investigated whether *AtNDT1* plays a role in seed development or seed filling. We observed that the silique size (Figures 2a,b and S4a) and the number of seeds per silique were lower for *ndt1⁻:ndt1⁻*, *as-1-ndt1* and *as-2-ndt1* lines (Figure 2c). Similarly, the total number of seeds per plant was also decreased in the mutant *ndt1⁻:ndt1⁻* line (Figure 2h), while seed size increased in these lines compared with WT (Figures 2d–f, and S4b). Moreover, the weight of one thousand seeds from these plants was also higher (Figure 2g), although the total seed weight per plant did not differ among the lines (Figure S4c).

To analyse the accumulation of storage compounds, we also determined lipid, carbohydrate, and protein contents in seeds. *ndt1⁻:ndt1⁻* mutant line displayed higher amounts of lipids in mature seeds (Figure S5a) and, after imbibition, significantly at 4 days post-imbibition (Figure S5b). The starch content was also higher in *ndt1⁻:ndt1⁻* mature seeds (Figure S5c), while similar amounts of proteins (Figure S5d) was observed when compared with WT seeds.

Given the importance of NAD(P)H as a reducing power source for fatty acid biosynthesis, we further analysed how the reduction in the *AtNDT1* expression impacts fatty acid profile in mature seeds (Figure S6). We detected a 2.7-fold increase of the 14:0 fatty acid in the mutant line compared with WT (Figure S6a), suggesting that NAD⁺ import by *AtNDT1* is required for the metabolism of fatty acids in seeds.

Effects of reduction in *AtNDT1* expression on seed germination and seedling establishment

To investigate if the increased levels on the storage reserves in the *ndt1⁻:ndt1⁻* mature seeds have an effect on seed germination and seedling establishment, we evaluated the percentage of seed germination and number of abnormal seedlings. These analyses revealed that germination as well as the percentage of normal developing seedlings were reduced in the *ndt1⁻:ndt1⁻* line in comparison with WT (Figure S5g,h). In addition, the germination speed index (GSI) and emergence speed index (ESI) were significantly reduced in the *ndt1⁻:ndt1⁻* line (Figure S5e,f), indicating that *AtNDT1* is an important component affecting seed germination and seedling development.

As NAD⁺ is necessary for the conversion of fatty acids into carbohydrates during storage lipid mobilization to drive seedling establishment (Bernhardt *et al.*, 2012), we further evaluated the fatty acids profile in seedlings at 2, 4, and 6 days after imbibition. The TAG marker fatty acid in Arabidopsis is eicosenoic acid C20:1. Interestingly, we observed elevated C20:1 levels in 2-day-old, 4-day-old and 6-day-old mutant seedlings compared with WT, indicating

that the repression of *AtNDT1* led to an impaired storage oil mobilization during seedling establishment. Our data also demonstrated that the mutant is able to degrade C20:1, but the degradation rate is slowed down. The amounts of 20:2, 24:0, and 24:1 fatty acids were increased in 2-day-old *ndt1⁻:ndt1⁻* seedlings (Figure S6b). At 4 days after stratification, the fatty acids 14:0 and 20:1a were higher in the mutant seedlings (Figure S6c). In 6-day-old seedlings, higher levels of 14:0, 16:2, 16:3, 18:2, 18:3, 20:2, and 20:1a were observed for *ndt1⁻:ndt1⁻* line compared with WT (Figure S6d). These results suggested that the mobilization of the storage reserves for seed germination rate and seedling establishment is impaired in the mutant plants.

Effects of reduction in *AtNDT1* expression in pollen

Considering the observed reduction in seed number per silique and the higher expression of *AtNDT1* in the pollen, we evaluated if this phenotype could be a consequence of lower pollen viability, pollen tube growth, effects of lower expression of *AtNDT1* on maternal tissues or impaired embryo development. Comparing WT, *ndt1⁻:ndt1⁻*, *as-1-ndt1*, and *as-2-ndt1* pollen grains by stereomicroscopy revealed lower pollen grain viability in plants with reduced *AtNDT1* expression reaching only 50, 64, and 89% of the WT values for the *ndt1⁻:ndt1⁻*, *as-1-ndt1*, and *as-2-ndt1* lines, respectively (Figures 3a and S7). Further analysis revealed that pollen germination and tube growth were also affected in the *ndt1⁻:ndt1⁻* line (Figure S8). In agreement with these results, *in silico* analysis of the *AtNDT1* gene expression pattern by using the Arabidopsis eFP Browser (Winter *et al.*, 2007; <http://bar.utoronto.ca/efp/cgi-bin/efpWeb.cgi>), indicated that *AtNDT1* is highly expressed in the later stages of pollen development and following germination (Figure S9a,b).

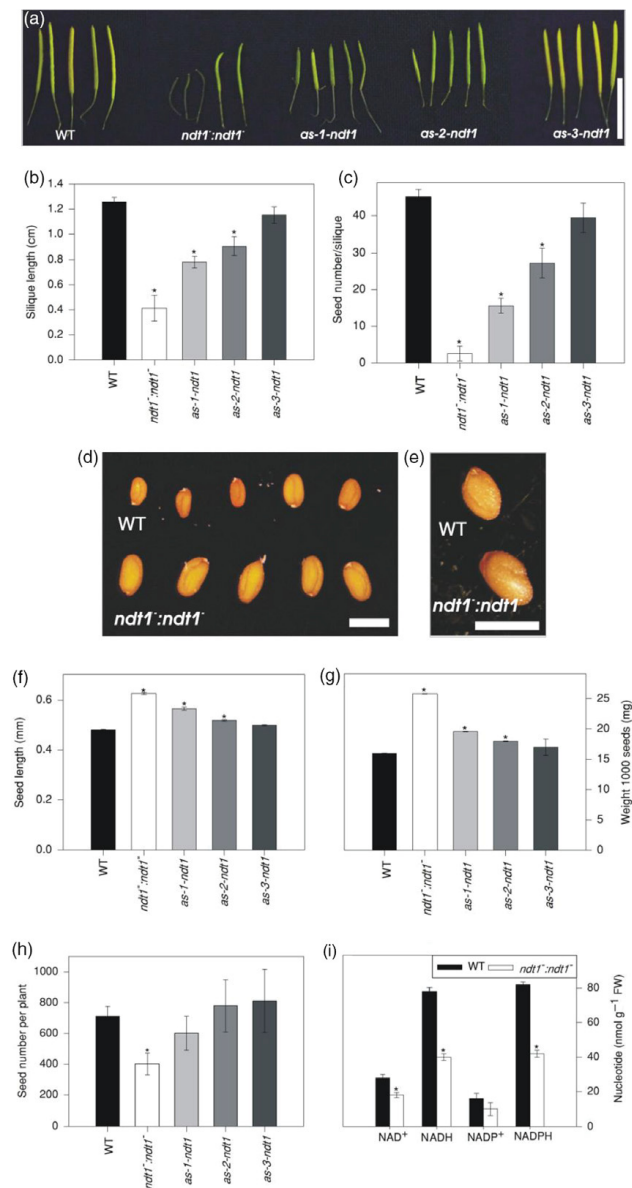
To better understand the reasons underlying the *ndt1⁻:ndt1⁻* seed phenotype, we pollinated *ndt1⁻:ndt1⁻* mutants using WT pollen (Figure 3b). Manual pollination of WT (female donor) with *ndt1⁻:ndt1⁻* pollen (male donor) gave rise to shorter siliques (Figure 3d), while siliques developing on plants in which WT pollen served as male donor used to pollinate *ndt1⁻:ndt1⁻* (female donor) had no discernible difference in length compared with WT plants (Figure 3c). Therefore, the complementation of *ndt1⁻:ndt1⁻* stigmas with WT pollen suggested that male gametophyte and pollen development are sensitive to the reduced *AtNDT1* transport activity. Collectively, our results supported the important contribution of *AtNDT1* to pollen viability.

AtNDT1 repression enhanced growth and photosynthesis in Arabidopsis plants

The general impact of the reduced expression of *AtNDT1* on vegetative plant growth was studied in detail regarding leaf morphology and photosynthesis. *AtNDT1* T-DNA

The role of mitochondrial NAD⁺ transporter in plants 491

Figure 2. Phenotypic analysis of *Arabidopsis thaliana* genotypes deficient in the expression of the mitochondrial NAD⁺ transporter (NDT1) and wild type (WT) plants. (a) Siliques of all lines. (b) Silique length. (c) Seed number per silique. (d) Seeds of WT and *ndt1:ndt1* showing length differences. (e) Detail of WT and *ndt1:ndt1* seeds. (f) Seed length. (g) Weight 1000 seeds. (h) Seed number per plant. (i) Nucleotide levels in mature siliques. Values are presented as mean \pm SE of six individual plants per line; an asterisk indicates values that were determined by *t*-test to be significantly different ($P < 0.05$) from the WT. FW: fresh weight. Bar in (a) represents 1 cm; and in (d, e), and represent 1 mm.



insertion and antisense lines were grown under short-day conditions side by side with WT plants. No differences in the visible phenotype could be identified in 4-week-old

plants with reduced *AtNDT1* expression (Figure 1c). However, a detailed analysis of the growth parameters revealed significant differences between the transgenic lines when

492 Izabel de Souza Chaves et al.

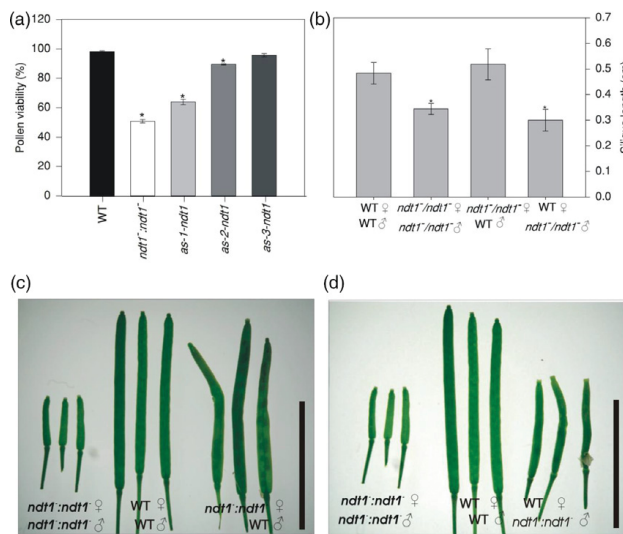


Figure 3. Pollen viability and crossing mutants analyses for phenotypic reestablishment of *Arabidopsis thaliana* genotypes deficient in the expression of the mitochondrial NAD⁺ transporter (NDT1) and wild type (WT) plants. (a) Pollen viability. (b) Silique length in different crossings. (c) Crossing with *ndt1:ndt1* female donor and WT pollen grain donor and controls. (d) Crossing with WT female donor and *ndt1:ndt1* pollen grain donor and controls. Eight crossings were done for each combination and asterisk indicates values that were determined by Student's *t*-test to be significantly different ($P < 0.05$) comparing WT female donor and WT pollen grain donor with the others crossing. Bars represents 1 cm.

compared with WT (Table 1). The *ndt1:ndt1* and *as-1-ndt1*, the antisense lines with the strongest reduction in *AtNDT1* expression, displayed a higher leaf number (LN) along with increases in the total leaf area (TLA), specific leaf area (SLA), rosette leaf area (RLA), and root system dry weight (RDW). For *ndt1:ndt1*, the specific rosette area (SRA) was also significantly increased compared with WT. For the two other genotypes, representing a lesser reduction in *AtNDT1* transcript, only LN (*as-2-ndt1*, *as-3-ndt1*) and SLA (*as-2-ndt1*) were increased compared with WT.

To investigate if the repression of *AtNDT1* affects photosynthesis, several photosynthetic parameters were measured in the mutant plants. A reduced *AtNDT1* expression did not alter CO₂ assimilation rates at 400 $\mu\text{mol photons m}^{-2} \text{sec}^{-1}$ (Figure 4a), or at 100 $\mu\text{mol photons m}^{-2} \text{sec}^{-1}$ (Figure S10a,b). The parameters obtained from the light response curves (Figure S10a) were similar to WT when calculated as per unit of leaf area (Table S1). We further normalised the photosynthetic rates to be expressed per unit of mass, taking the leaf mass and thickness into account, as increased SLA was observed in the mutant lines (Table 1). Interestingly, photosynthetic rates increased significantly in the *ndt1:ndt1* and *as-1-ndt1* plants (Figure 4b), whereas stomatal conductance (g_s), internal CO₂ concentration (C_i), transpiration (E), photorespiration (R_p), and stomatal density decreased in the NDT1 deficient plants (Figure 4c–f). Furthermore, non-photochemical quenching (NPQ) increased in *ndt1:ndt1*, *as-1-ndt1*, *as-2-ndt1* and *as-3-ndt1* plants relative to WT plants

under 400 $\mu\text{mol photons m}^{-2} \text{sec}^{-1}$ and higher light intensities (Figure 4g; Figure S11). In contrast, the electron transport rate (ETR), maximum quantum efficiency of photosystem II (F_v/F_m), the instantaneous water use efficiency (A/E), and intrinsic water use efficiency (A/g_s) did not change significantly compared with WT (Figure S10c–f). These results indicated that the enhanced growth of the *ndt1* mutant plants is linked with an increased photosynthetic activity.

Reduction of *AtNDT1* expression affected starch and sugar accumulation and altered cellular redox poise in leaves

To evaluate the putative metabolic changes caused by *AtNDT1* silencing in fully expanded leaves, compounds related to carbon and nitrogen metabolism were measured throughout the diurnal cycle. Plants with reduced *AtNDT1* transcript levels accumulated more starch at the end of the light period (Figure 5a). Accordingly, increased starch synthesis and starch degradation rates were observed for the mutant plants (Figure 5b,d). Glucose and sucrose levels were higher in the *ndt1:ndt1* mutant plants in the middle and in the end of the light period (Figure 5c,f), while fructose levels remained unaltered (Figure 5e). Interestingly, malate and fumarate contents also increased throughout the day in the *ndt1:ndt1*, *as-1-ndt1*, and *as-2-ndt1* plants (Figure 5g,h). Protein content was increased in the *ndt1:ndt1* line at the end of the light period (Figure S12), whereas plants with low *AtNDT1* expression levels did not display altered chlorophyll levels (Figure S13).

Table 1 Growth parameters of 4-week-old Arabidopsis genotypes deficient in the expression of the mitochondrial NAD⁺ transporter (NDT1) and wild type (WT) plants

Parameter	WT	<i>ndt1⁻:ndt1⁻</i>	<i>as-1-ndt1</i>	<i>as-2-ndt1</i>	<i>as-3-ndt1</i>
RDW	50.0 ± 3.0	90.0 ± 3.0	80.0 ± 3.0	60.0 ± 8.0	60.0 ± 4.0
RSDW	10.0 ± 3.0	20.0 ± 3.0	20.0 ± 4.0	10.0 ± 4.0	10.0 ± 3.0
RRS	0.17 ± 0.02	0.18 ± 0.02	0.20 ± 0.01	0.17 ± 0.01	0.19 ± 0.01
LN	13.7 ± 1.4	19.2 ± 1.5	23.0 ± 0.3	21.0 ± 1.5	19.8 ± 1.3
TLA	14.64 ± 1.4	27.27 ± 1.5	20.42 ± 0.8	19.95 ± 2.2	18.65 ± 1.3
SLA	241 ± 24	320 ± 14	306 ± 9	331 ± 17	269 ± 15
RLA	12.8 ± 1.6	25.7 ± 1.2	19.5 ± 0.6	16.7 ± 1.9	16.8 ± 0.6
SRA	225 ± 51	303 ± 11	266 ± 5	279 ± 25	252 ± 12
Stomatal density	138.4 ± 4.8	117.9 ± 3.3	117.9 ± 2.4	121.9 ± 5.2	136.6 ± 10.1

RDW, rosette dry weight (mg); RSDW, root system dry weight (mg); RRS, root/shoot ratio; LN, leaf number; TLA, total leaf area (cm²); SLA, specific leaf area (cm² g⁻¹); RLA, rosette leaf area (cm²); SRA, specific rosette area (cm² g⁻¹) and stomata density (stomatal number mm⁻²). Values are presented as means ± SE of determinations on six individual plants per line; bold type values were determined using Student's *t*-test to be significantly different (*P* < 0.05) from the WT.

A non-targeted metabolic profile analysis identified additional effects in leaf samples harvested in the middle of the light period (Table S2). Among the successfully annotated metabolites, sugars and related compounds differed markedly in the lines with low *AtNDT1* expression. *AtNDT1* silencing led to elevated levels of glucose (significantly in all lines), fructose (significantly in *ndt1⁻:ndt1⁻* and *as-3-ndt1* lines), and galactinol (significantly in *ndt1⁻:ndt1⁻*, *as-2-ndt1* and *as-3-ndt1* lines). Additionally, glutamate (significantly in *ndt1⁻:ndt1⁻* and *as-1-ndt1* lines), leucine (significantly in *ndt1⁻:ndt1⁻* line), sorbose (significantly in *ndt1⁻:ndt1⁻* line), erythritol (significantly in *ndt1⁻:ndt1⁻* line), and myo-inositol (significantly in *ndt1⁻:ndt1⁻* and *as-3-ndt1* lines) levels were elevated in the *AtNDT1* silencing lines. Furthermore, the levels of ascorbate were also increased in leaves of *ndt1⁻:ndt1⁻* and *as-1-ndt1* lines.

An analysis of the pyrimidine nucleotide pools in leaves (Figure 6) revealed a significant decrease in the contents of NAD⁺ in *ndt1⁻:ndt1⁻*, *as-1-ndt1*, and *as-2-ndt1* lines (Figure 6a), while the levels of NADP⁺, NADH and NADPH increased in the same lines compared with WT (Figure 6b–d). Furthermore, the sum of NAD⁺ and NADH decreased, while the NADP⁺ plus NADPH increased significantly in *ndt1⁻:ndt1⁻*, *as-1-ndt1*, and *as-2-ndt1* (Figure 6e–f). Interestingly, a higher NADH/NAD⁺ ratio was observed in these lines compared with WT (Figure 6g), while the NADPH/NADP⁺ ratio was not significantly altered (Figure 6h). To confirm changes in the cellular redox state in the mutant plants, we evaluated the activation state of NADP-dependent malate dehydrogenase (NADP-MDH) (Table 2), a key redox-regulated enzyme controlling the malate valve, which exports reducing equivalents indirectly from chloroplasts. We observed an increase in the NADP-MDH activation state in mutant leaves, which was significantly different for *ndt1⁻:ndt1⁻* and *as-1-ndt1*. The significant increase in the maximal NADP-MDH activity corroborated

well with the increased NADPH (Figure 6d) and malate levels (Figure 5g) found in plants with reduced expression of *AtNDT1*. Altogether, these results suggested that the cellular redox state is changed as a consequence of the reduced expression of *AtNDT1*.

Subcellular localization of AtNDT1-GFP revealed its mitochondrial localization

AtNDT1 was presumed to exclusively reside in the chloroplast membrane (Palmieri *et al.*, 2009). However, this protein was recently found in mitochondrial membranes in proteome studies (Senkler *et al.*, 2017) and a previous GFP-tagging and immunolocalization study was not able to find *AtNDT1* targeted to chloroplast membranes (Bedhomme *et al.*, 2005). In addition, many phenotypic changes (described above) caused by *AtNDT1* downregulation did not directly support that *AtNDT1* functions in the chloroplast but rather suggested an increase in chloroplast import of NAD⁺ at the expense of deficient mitochondria import. Considering these facts, we decided to re-evaluate the subcellular localization of *AtNDT1*. To provide experimental evidence on the subcellular localization of *AtNDT1* and *AtNDT2*, we generated corresponding GFP fusions under the control of the ubiquitin 10 promoter (Grefen *et al.*, 2010) and expressed the recombinant proteins in Arabidopsis seedlings. Both *AtNDT1*- and *AtNDT2*-GFP fusion proteins were exclusively localized in the mitochondria (Figure 7), indicating their mitochondrial localization.

DISCUSSION

AtNDT1 has a mitochondrial localization in Arabidopsis

It has been previously described that *AtNDT1* protein resides in the chloroplast membrane (Palmieri *et al.*, 2009). Intriguingly, however, both *AtNDT1* and *AtNDT2* have been found in mitochondria by a recent proteome study (Senkler

494 Izabel de Souza Chaves et al.

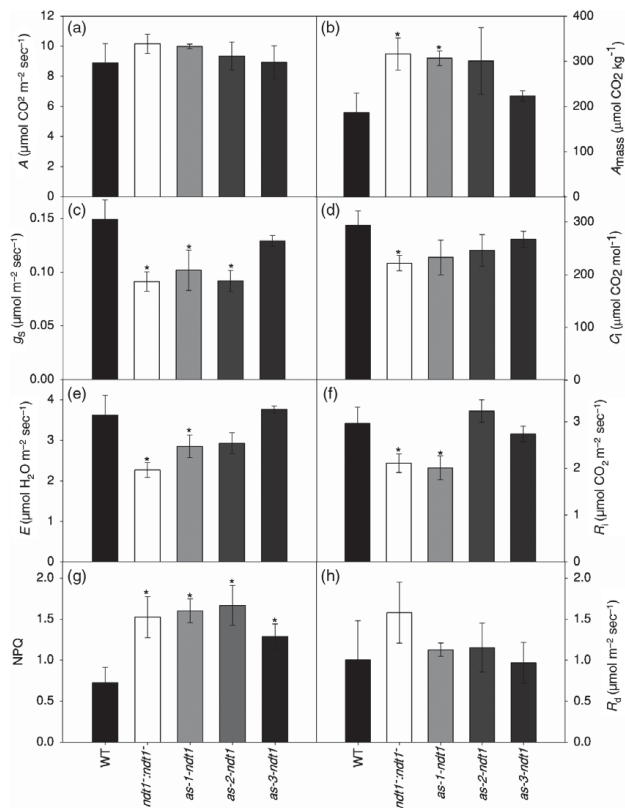


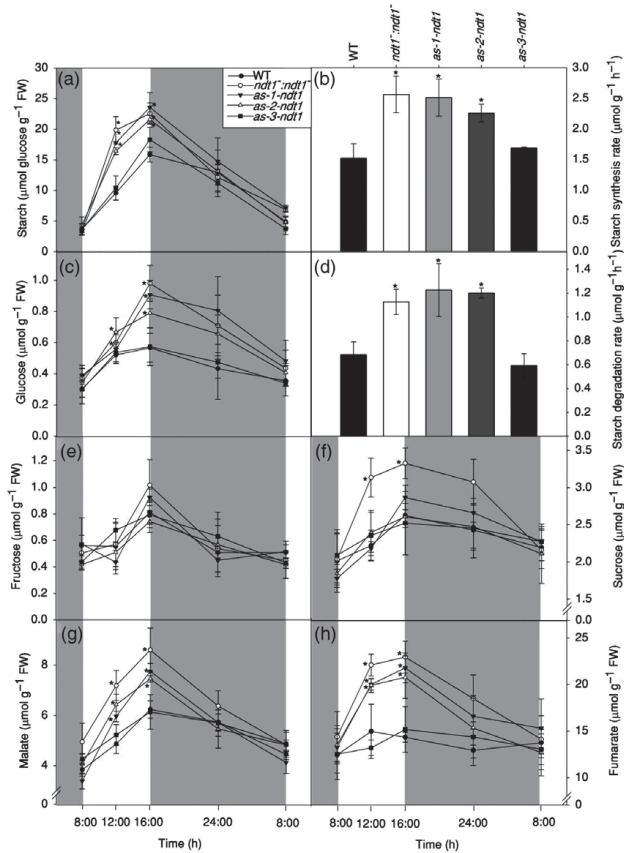
Figure 4. Gas exchange and chlorophyll *a* fluorescence parameters in 4-week-old *Arabidopsis thaliana* genotypes deficient in the expression of the mitochondrial NAD⁺ transporter (NDT1) and wild type (WT) plants. (a) Assimilation rate (*A*) per area unit at 400 µmol photons m⁻² s⁻¹. (b) Assimilation rate (*A*_{mass}) per mass unit at 400 µmol photons m⁻² s⁻¹. (c) Stomatal conductance (*g*_s). (d) Internal CO₂ concentration (*C*_i). (e) Transpiration (*E*). (f) Photorespiration (*R*_i). (g) Nonphotochemical quenching (NPQ). (h) Dark respiration (*R*_d). Values are presented as mean ± SE of six individual plants per line; an asterisk indicates values that were determined by *t*-test to be significantly different (*P* < 0.05) from the WT.

et al., 2017) and could not be localized to plastids by earlier GFP-tagging and/or immunolocalization studies (Bedhomme *et al.*, 2005). Moreover, our results revealed unexpected physiological features exhibited by *AtNDT1* downregulated lines that are not consistent with the proposed chloroplastic localization of *AtNDT1*. For instance, the higher photosynthetic rates (Figure 4), the increased NADP⁺ and NADPH contents in leaves (Figure 6), and the higher accumulation of sugar and starch at the end of the light period in the mutants (Figure 5) in comparison with their WT counterparts implicated an increase in the chloroplast import of NAD⁺. The observed increase in the activation state of the plastidic NADP-MDH (Table 2) also contradicted the proposed chloroplastic localization of *AtNDT1*.

Given that the information on correct subcellular localization is essential to deduce the effect of a protein on metabolism (Kirchberger *et al.*, 2008), we re-investigated the question in which membrane *AtNDT1* resides.

Considering the similarities in the biochemical properties of *AtNDT1* and *AtNDT2*, *Arabidopsis* plants were stably transformed with C-terminal GFP fusions of either *AtNDT1* or *AtNDT2*. Both *AtNDT1*- and *AtNDT2*-GFP fusion proteins were found to exclusively localize in the mitochondria (Figure 7). Considering the discrepancy with some of the earlier work on this protein, we can only speculate the possible reasons why previous studies (Palmieri *et al.*, 2009) failed to detect *NDT1* proteins in the mitochondrial compartment. The fact that the previously published chloroplast membrane location of *AtNDT1* was deduced from interpretation of the location of an *AtNDT1*-GFP fusion protein transiently expressed in tobacco leaf protoplasts (Palmieri *et al.*, 2009) and not in *Arabidopsis* plants may possibly explain why previous investigations failed to detect the mitochondrial localization of *AtNDT1*-GFP proteins. Based on these findings, we proposed to re-evaluate the physiological roles of *AtNDT1* within plant cells and its connection to metabolic and redox-mediated control of

Figure 5. Leaf metabolite levels of 4-week-old *Arabidopsis thaliana* genotypes deficient in the expression of the mitochondrial NAD⁺ transporter (NDT1) and wild type (WT) plants. (a) Starch. (b) Starch synthesis rate. (c) Glucose. (d) Starch degradation rate. (e) Fructose. (f) Sucrose. (g) Malate. (h) Fumarate. Values are presented as mean \pm SE of six individual plants per line; an asterisk indicates values that were determined by *t*-test to be significantly different ($P < 0.05$) from the WT. Grey areas represent the dark period. FW: fresh weight.



cellular processes in light of its newly found mitochondrial localization.

AtNDT1 is involved in the cellular NAD⁺ homeostasis

The fact that the pyridine pools are to some extent interdependent (Agledeal *et al.*, 2010) raises the question of the very large range of possible consequences of the decreased NAD⁺ import into mitochondria. Therefore, to investigate the role of the mitochondrial NAD⁺ carrier AtNDT1, we analyzed the phenotypes of corresponding *Arabidopsis* mutant and antisense plants. Here, we show that plants with lower expression of the *AtNDT1* displayed reductions in the NAD⁺ levels in leaves (Figure 6a) and in siliques (Figure 2i), whereas the levels of NADH, NADP⁺ and NADPH were increased (Figure 6b–d, respectively). Furthermore, the ratio NADH/NAD⁺ was shown to be augmented in plants that carried reductions in *AtNDT1*

expression, leading these plants to a more reduced state (Figure 6g). That said, the observed reduction in the levels of NAD⁺ may also be associated with changes in the rate of NAD⁺ biosynthesis in the plants with reduced *AtNDT1* expression. In bacteria, regulation of NAD⁺ levels occurs at the level of transcription (Penfound and Foster, 1999). These organisms contain genes belonging to NAD⁺ biosynthesis organized in *operons* and the content of NAD⁺ regulates their expression (Penfound and Foster, 1999). However, little information is known about the regulation of NAD⁺ content at the level of gene expression in plants. Therefore, to test whether altered NAD⁺ content in plants with decreased expression of *AtNDT1* would influence gene expression, we quantified the expression levels of genes that encoded enzymes belonging to NAD⁺ salvage and *de novo* pathways (Figure S3). This analysis revealed that *ndt1::ndt1* plants displayed differential expression of

496 Izabel de Souza Chaves et al.

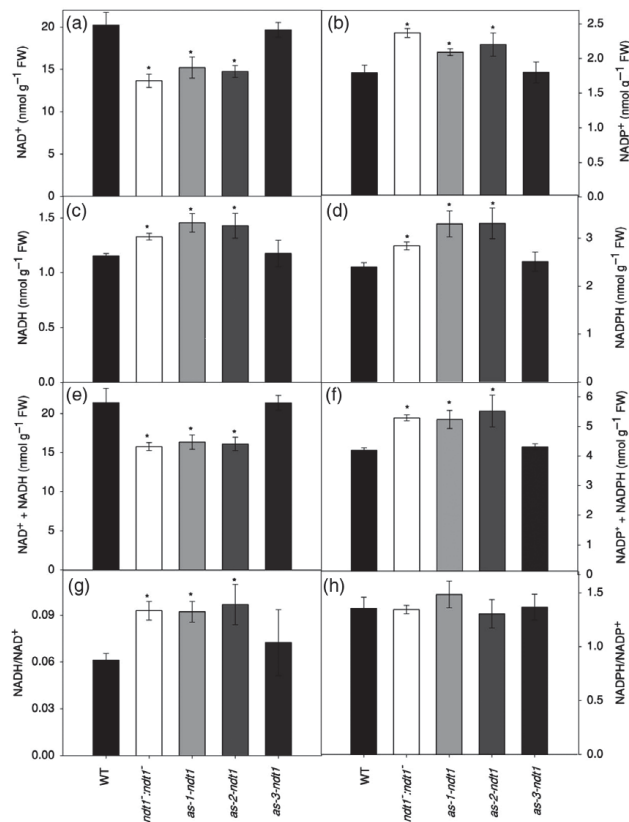


Figure 6. Changes in nucleotide levels in fully expanded leaves of 4-week-old *Arabidopsis thaliana* genotypes deficient in the expression of the mitochondrial NAD^+ transporter (NDT1) and wild type (WT) plants, collected at midday. (a) NAD^+ . (b) NADP^+ . (c) NADPH. (d) NADPH. (e) NADH/NAD^+ ratio. (f) $\text{NADPH}/\text{NADP}^+$ ratio. Values are presented as mean \pm SE of six individual plants per line; an asterisk indicates values that were determined by t-test to be significantly different ($P < 0.05$) from the WT. FW: fresh weight.

Table 2 NADP-dependent malate dehydrogenase (NADP-MDH) of 4-week-old *Arabidopsis* mutants deficient in the expression of the mitochondrial NAD^+ transporter (NDT1) and wild type (WT) plants

Enzymes	WT	<i>ndt1:ndt1</i>	<i>as-1-ndt1</i>	<i>as-2-ndt1</i>	<i>as-3-ndt1</i>
NADP-MDH initial ^a	12.7 \pm 0.2	13.5 \pm 0.2	12.8 \pm 0.7	13.2 \pm 0.5	12.8 \pm 0.4
NADP-MDH total ^a	16.0 \pm 0.5	14.8 \pm 0.3	14.3 \pm 0.7	15.6 \pm 1.0	14.7 \pm 0.9
NADP-MDH activation state ^b	79.7 \pm 2.0	91.2 \pm 1.4	89.6 \pm 3.6	85.2 \pm 3.2	87.6 \pm 2.9

Activities were determined in whole rosettes harvested at the middle of the photoperiod. Values are presented as mean \pm SE ($n = 6$); values in bold type in mutant plants were determined by using Student's t-test to be significantly different ($P < 0.05$) from the WT.

FW, fresh weight.

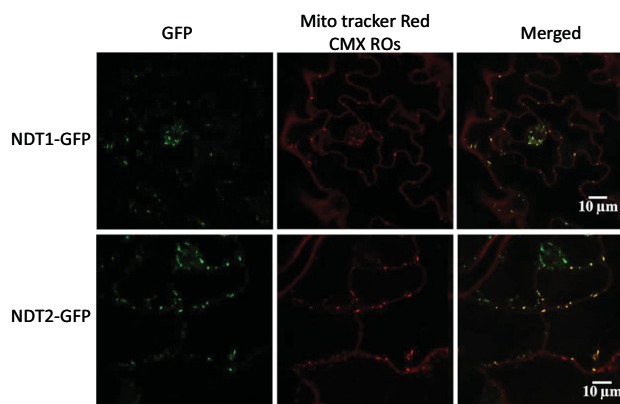
^a $\mu\text{mol min}^{-1} \text{g}^{-1}$ FW.

^bPercentage of NADP-MDH total.

genes encoding the NAD^+ biosynthetic pathway; *QPR1* and *NMNAT* showed higher expression in imbibed seeds, while *QS* expression was reduced in *ndt1:ndt1* leaves. Furthermore, higher expression of *AtNDT2* in imbibed seeds and a minor increase in leaves (Figure S2) of *ndt1:*

ndt1 line, was observed. Higher *AtNDT2* expression may be acting as a compensatory mechanism for NAD^+ import into mitochondria in plants carrying reduced *AtNDT1* expression; which implied that *AtNDT1* and *AtNDT2* may have overlapping functions in the NAD^+ transport in seeds

Figure 7. Localization of AtNDT1 and AtNDT2 by confocal laser scanning microscopy (CLSM). Arabidopsis plants were stable transformed with C-terminal GFP fusions of NDT1 (upper panel) and NDT2 (lower panel), respectively. Whole seedlings were analyzed by CLSM. The left panel shows the GFP-specific fluorescence signal (green) while the middle panel shows the localization of the mitochondrial Mito tracker Red CMX ROs (red). The right panel represents the merged image of both channels revealing an overlay of the fluorescent signals (yellow) indicating a mitochondrial localization of NDT1 and NDT2.



and leaves. Moreover, these results suggested that NAD⁺ metabolism and transport in the mitochondrion and peroxisome were modified in those plants. Interestingly, NADP⁺ and NADPH levels were increased with decrease in the sum of NAD⁺ and NADH (Figure 4), indicating that NAD⁺ phosphorylation is likely to be promoted by *AtNDT1* downregulation. Given that we found no changes in the expression of the NAD kinases (NADK1-3) in leaves (Figure S3b), and considering the mild increase of *AtNDT2* expression (which was strongly expressed in *NDT1* mutant seeds), it can be presumed that the compensatory increased expression of the mitochondrial NAD⁺ carrier *AtNDT2* is mainly responsible for the observed rise in the NADH/NAD⁺ ratio in the leaves of *AtNDT1* mutants. Taken together, these results suggested that *AtNDT1* is likely to play an important role in the cellular NAD⁺ homeostasis in plants by linking pyridine nucleotide pools in different subcellular compartments. Therefore, as a consequence of *AtNDT1* downregulation, whole NAD⁺ metabolism and transport could be re-balanced.

Reduced *AtNDT1* expression impacts carbon metabolism turnover in the light and photosynthesis

Here, we show that the reduction in *AtNDT1* expression influenced processes that take place in chloroplasts, suggesting that there is a precise communication between organelles regarding NAD⁺ levels in subcompartments. We demonstrated that the downregulation of *AtNDT1* increased the photosynthetic rate per unit of mass (Figure 4b), impacted leaf carbon metabolism (Figure 5), and enhanced plant growth (Table 1). Moreover, NPQ was increased in *ndt1⁻ndt1⁻*, *as-1-ndt1*, *as-2-ndt1* and *as-3-ndt1* plants under high light (400–1200 μmol photons m⁻² sec⁻¹) (Figure S10), which would imply a decrease in chloroplastic NADP⁺ levels under these conditions

(Takahashi *et al.*, 2006). This finding is in line with the observed increase in the activation state of the plastidic NADP-MDH (Table 2), as this enzyme uses excess NADPH to regenerate the electron acceptor NADP⁺ and is inhibited by the product NADP⁺ (Scheibe, 2004). In support of this hypothesis, plants with reduced *AtNDT1* expression exhibited a higher NADH/NAD⁺ ratio (Figure 6a) and increase in NADPH in leaves (Figure 6d).

Redox regulation is the preferred strategy for plastidic enzymes to regulate a range of metabolic processes such as carbon fixation, starch metabolism, lipid synthesis and amino acid synthesis (Geigenberger *et al.*, 2005). The time course analysis provided here clearly demonstrated a pronounced accumulation of glucose, starch, fumarate, and malate during the day, but not at night, in leaves of the mutants with reduced *AtNDT1* expression (Figure 5). Taking into account that NADP-MDH is a redox-controlled enzyme only active in the light, these results reinforced the hypothesis that the malate valve is being used by the mutants to balance cellular energy supply (Scheibe, 2004). Furthermore, the increase in the activation of NADP-MDH and in NPQ values indicated that low *AtNDT1* expression led to a energetic reduced state of the chloroplast that could be associated with the increase in starch biosynthesis (Figure 5b) and photosynthesis per mass unit (Figure 4b).

Photosynthetic capacity may be limited either by biochemical or diffusive processes. The first refers to CO₂ fixation by RuBisCO and the second to stomatal and mesophyll resistances that CO₂ can encounter during its diffusion from the atmosphere to the carboxylation sites in the chloroplasts (Flexas *et al.*, 2008). The reverse of stomatal resistance is *g_s* and changes in this parameter may occur in parallel with changes in stomatal density (Tanaka *et al.*, 2013). Despite decreases in stomatal density

498 *Izabel de Souza Chaves et al.*

(Table 1) and g_s (Figure 4c) in the mutant lines, the increases in photosynthesis demonstrated that the mutant plants maintained the synthesis of NADP^+ required for photochemical reactions that might be explained by the indirect transfer of redox equivalents by redox shuttles from the cytosol across the chloroplast membrane. Curiously, reduced *AtNDT2* expression negatively affected photosynthetic efficiency as a result of a lowered stomatal density and conductance (unpublished work). This apparent contradiction can be explained by the fact that *AtNDT1* expression is much higher than *AtNDT2* in leaves (Figure S2). Therefore, the entire NAD^+ metabolism and transport seems to be reorganized in *AtNDT1* downregulated lines in a more extended way than that in *AtNDT2* mutant lines, in a manner that enables greater transfer of redox power for photochemical reactions, therefore compensating lower stomatal conductance and density in leaves of *AtNDT1* downregulated lines.

AtNDT1 was highly expressed in guard cells (Figure S9c); this finding is in line with the lower stomatal conductance observed in *ndt1:ndt1* plants in our study (Figure 4c). It has been shown that NAD^+ levels are reduced in response to the generation of ROS induced by abscisic acid (ABA), which acts as a signal for stomatal closure (Hashida *et al.*, 2010). Therefore, considering the association of NAD^+ metabolism to stomatal function, the results presented here suggested that NAD^+ is important not only for stomatal movements, but that NAD^+ transport also acts in regulating guard cell biogenesis.

Repression of *AtNDT1* affects pollen viability

It has been demonstrated that pollen maturation and tube growth are dependent on energy produced by mitochondrial respiration and plastid glycolysis (Selinski and Scheibe, 2014). Recently, it has been shown that NADPH provision via the OPPP in peroxisomes is also needed for gametophytic interaction during pollen tube guidance to ovules (Hölscher *et al.*, 2016). Therefore, it is clear that energy metabolism during pollen maturation and tube growth is highly complex and involves different pathways and cell compartments and, as NAD^+ supply is essential for reduction related reactions, NAD^+ transport is necessary. For example, deficiency in the plastidic glycolytic glyceraldehyde-3-phosphate dehydrogenase, an enzyme that reversibly converts the glyceraldehyde-3-phosphate to 1,3-bisphosphoglycerate, with the reduction of NAD^+ to NADH , displays male sterility in Arabidopsis, due to a disorganized tapetum cell layer (Muñoz-Bertomeu *et al.*, 2010). Furthermore, NAD(P)H accumulation during the growth of the pollen tube is directly coupled to ATP generation, which is used to enable a variety of energy-dependent processes localized in the pollen tube tip (Cárdenas *et al.*, 2006).

Recent studies using mutants deficient in NAD^+ biosynthesis demonstrated a functional importance of NAD^+ in

reproductive tissues such as pollen, floral meristem, siliques and seeds (Hashida *et al.*, 2007, 2013; Hunt *et al.*, 2007; Liu *et al.*, 2009). Here, we demonstrated that *AtNDT1* silencing promoted a decrease in pollen viability and pollen tube growth (Figures 3a, S7 and S8). Cumulative evidence supports the importance of NAD^+ metabolism in pollen grain formation and pollen tube growth (Berrin *et al.*, 2005; Chai *et al.*, 2005, 2006; Cárdenas *et al.*, 2006; Hashida *et al.*, 2009). In freshly harvested dry pollen, NAD^+ is accumulated, whereas it dramatically decreased immediately after water contact (Hashida *et al.*, 2013). Furthermore, several metabolic pathways, which operate during maturation of pollen grains and pollen tube growth such as the biosynthesis of lipids, components of cell walls, and amino acids, are highly dependent on NAD^+ levels (Hashida *et al.*, 2009). At the same time, the occurrence of high NAD^+ levels can maintain dormant pollen grains by competitive inhibition of NADH -dependent redox reactions that are essential for the formation of the pollen tube (Hashida *et al.*, 2013). Accordingly, the formation of non-viable pollen as found in our study and the strong expression of *AtNDT1* in pollen during the later stages of development and following germination (Figure S9) confirmed that *AtNDT1* is of fundamental importance for pollen formation and germination.

In this study, we have shown that decreased *AtNDT1* expression also resulted in reduced expression of *AtPXN* and *AtNDT2* in pollen grains (Figure S2). This result indicated that reduction in NAD^+ import by *AtNDT1* may also impact the NAD^+ import by *AtNDT2* and *AtPXN* and this may possibly disturb the whole cell NAD^+ balance in pollen. It deserves special mention that *AtNDT2* expression is dramatically lower than *AtNDT1* in the pollen of WT Arabidopsis (Figure S2), meaning that emerging phenotypes in pollen could directly result from *AtNDT1* downregulation.

Seed germination and seedling establishment are impaired due to *AtNDT1* repression

The decreased viability of pollen grains observed in plants with low *AtNDT1* expression probably contributed to the significant reduction in the number of seeds and the resulting reduction in siliques filling and lower length and diameter of the siliques (Figures 2 and S4). The production of shorter siliques can be ascribed to dysfunctional male gametophytes (Hashida *et al.*, 2013). It was recently found that mutant plants deficient in the expression of nicotinamide mononucleotide adenylyltransferase (NMNAT), an important enzyme in NAD^+ biosynthesis, produced non-viable pollen grains, shortened siliques, and smaller numbers of seeds per plant (Hashida *et al.*, 2013). These authors did not comment on the mechanism that led to the shortening of siliques, although, consistent with our observations, they showed that it may be a result of pollen germination and malformation of the pollen tube, due to the lower concentration of NAD^+ found in the mutants.

The lower number of seeds in *ndt1⁻:ndt1⁻* plants suggested that, in addition to NAD⁺ metabolism, mitochondrial NAD⁺ transport is also important during embryonic development. As the concentration of nucleotides decreased in mature siliques (Figure 2i), we may assume that resources allocated to the zygote were impaired. As a result, fewer seeds were generated, however the seeds produced received a greater amount of carbohydrates, explaining the larger seed size in *ndt1⁻:ndt1⁻*, *as-1-ndt1* and *as-2-ndt1* plants (Figures 2 and S4b).

Interestingly, the repression of *AtNDT1* expression was associated with a higher amount of lipids per seed (Figure S5a). It is well known that Arabidopsis seeds have high fatty acid content (~35% by weight; Baud *et al.*, 2002), which serve as a carbon and energy reserve. Accordingly, the increase in lipid content per seed was followed by a mild but non-significant increase in starch contents in *ndt1⁻:ndt1⁻* seeds, without changes in the protein level (Figure S5c,d). Taken together, these results suggested that the remaining seeds apparently exerted a higher sink strength and therefore accumulated a higher amount of storage compounds when the *AtNDT1* expression was reduced. Additionally, the relative concentration of fatty acids alongside seedling development was generally higher in the *ndt1⁻:ndt1⁻* line (Figure S6). As NAD⁺ is required for β -oxidation during lipid mobilization and seedling development (Bernhardt *et al.*, 2012), it is suggested that NDT1 mutant seeds fail to mobilize lipids possibly as a consequence of an impaired fatty acid β -oxidation. Therefore, the delay in seed germination and impaired fatty acid degradation (β -oxidation) may also indicate changes in the peroxisomal NAD⁺ status in the *ndt1⁻:ndt1⁻* line. Additionally, given that seed dormancy may be regulated by the relative levels of pyridine nucleotides (Hunt and Gray, 2009), it is possible that the reduced germination rates observed (Figure S5) are related to alterations in the levels of NAD(P)(H) in the mutant siliques (Figure 2i).

***AtNDT1* and *AtNDT2* show varying degrees of redundancy and specialization**

The demonstration that both NDT1 and NDT2 are localized in the mitochondria of Arabidopsis raises questions about their exact roles *in vivo*. Therefore, to ascertain the individual contributions of *AtNDT1* and *AtNDT2* to metabolism, it is important to reconsider previously reported biochemical features of the two carriers (Palmieri *et al.*, 2009). First, *AtNDT1* and *AtNDT2* genes exhibited high structural similarities and their encoded proteins shared a number of similar transport properties, with both accepting AMP and ADP as highly efficient counter-exchange substrates for NAD⁺. Second, it is assumed that they derive from a common evolutionary ancestor; this assumption could explain similarities in their biochemical properties (Palmieri *et al.*, 2009). Third, in spite of these functional similarities, *AtNDT1* and *AtNDT2* have different kinetic

constants, with different levels of activity and affinities for NAD⁺ (Palmieri *et al.*, 2009). In addition, it should be recalled that *AtNDT1* and *AtNDT2* display distinct tissue-specific expression patterns. For instance, gene expression analysis of *AtNDT1* and *AtNDT2* by qRT-PCR (Figure S2) demonstrated much higher expression of *AtNDT1* than *AtNDT2* in seeds, leaves, flowers and pollen, therefore suggesting that *AtNDT1* is the dominant NDT isoform in *A. thaliana* in these tissues. In addition, gene expression analysis of *AtNDT1* and *AtNDT2* (Figure S2), and depicted by the publicly available data in Arabidopsis eFP Browser, demonstrated that the highest expression of *AtNDT1* occurs in pollen grains in comparison with its expression in seeds, leaves and flowers. Another aspect to be pointed out is that the T-DNA insertion lines for *AtNDT1* and *AtNDT2* showed reductions in pollen grain viability of approximately 50% and 13%, respectively, in relation to the corresponding WT. Altogether, these data suggested that the formation of non-viable pollen in *AtNDT1* downregulated lines is mainly a result of *AtNDT1* downregulation. Moreover, given that decreased *AtNDT1* expression also resulted in lower expression of *AtNDT2* in pollen grains (Figure S2), it seems that, at least in pollen, *AtNDT2* does not compensate for *AtNDT1* deficiency. Notwithstanding, the mutant plants for either *AtNDT1* or *AtNDT2* exhibited reductions in pollen viability, seed germination, stomatal density and conductance, indicating that the activities of both *AtNDT1* and *AtNDT2* are important for NAD⁺ metabolism in these tissues (unpublished work and the current study). In spite of these similarities, mutant plants for *AtNDT1* and *AtNDT2* displayed opposite phenotypes regarding their photosynthetic performance, having higher and lower photosynthetic rates, respectively, than the corresponding WT plants. In conjunction, this information demonstrated that, even though *AtNDT1* and *AtNDT2* cooperatively participate in NAD⁺ import into mitochondria, both proteins have varying degrees of specialization which probably took place alongside their independent cellular evolution and that have allowed the development of their individual properties such as the different transport properties and gene expression patterns.

In summary, the present study revealed that *AtNDT1* is targeted to the inner mitochondrial membrane and that this transport protein appears to play an important role in cellular NAD⁺ homeostasis in leaves. As a consequence of *AtNDT1* downregulation, NAD⁺ metabolism and transport seems to be reorganized, leading to metabolic shifts, which results in increases in photosynthesis, starch accumulation and in the activation state of the stromal NADP-MDH. In addition, impaired *AtNDT1* transport results in reduced pollen grain viability, tube growth, and seed filling, demonstrating the important role of *AtNDT1* in reproductive tissues. Furthermore, we demonstrated a possible function for NAD⁺ transport during seed germination and seedling establishment that appears to be linked to the need of NAD⁺ during lipid

500 *Izabel de Souza Chaves et al.*

metabolism and related processes. In the future, we are interested in identifying to what extent, *AtNDT1* and *AtNDT2* have overlapping functions in NAD^+ transport in different tissues and conditions. It will also be interesting to determine whether specific stress situations characterized by differential expression patterns of *AtNDT1* and *AtNDT2* correlated with the establishment or alteration of the mitochondrial pyridine nucleotide pool. It seems reasonable to assume that the generation of multiple mutants for NAD^+ transport proteins will be needed to gain precise mechanistic insight into these phenotypes. Moreover, the determination of NAD^+ and NADP^+ levels at tissue-specific and subcellular levels in these mutants is likely to enhance our knowledge of the specificities and redundancies of these different albeit partially complementary transport proteins allowing us to truly understand the physiological hierarchy under which they operate.

EXPERIMENTAL PROCEDURES

Plant material

The *ndt1⁻:ndt1⁻* line, previously named GK-241G12, was obtained from the GABI-KAT collection. This mutant line harbours a T-DNA insertion in the ninth exon of *AtNDT1* (At2g47490) (Figure 1a). The mutant line was selected on medium containing sulfadiazine (<https://www.sigmaaldrich.com>) and the insertion of T-DNA and homozygous plants were confirmed by PCR using specific primers for the gene that confers resistance to sulfadiazine (forward 5'-GCACGAGGTACAAACCTCTACTCT-3', reverse 5'-GTCTCTCAAGTTTCAACCCATTCT-3' and T-DNA 5'-ATATTGAC-CATCATACTCATTGC-3').

In addition, transgenic plants were generated by insertion of an antisense construct, under the control of the 35S promoter, produced using the Gateway system (Landy, 1989). For this purpose, primers were designed (forward 5'-CCACCATGTCCGCTAATTCT-CATCCTC-3' and reverse 5'-CTTAAAGTATAGAGCTTGCTCA-GAAGG-3') from a cDNA library, for amplification of the 939-bp *AtNDT1* cDNA fragment. The PCR product was recombined with the vector donor pDONR207 generating an entry clone in *Escherichia coli* (DH5 α strain). A second recombination was performed in pK2WG7 and transformed into *E. coli*. Subsequently, the selected colonies were used to transform *A. tumefaciens* (strain GV3101), which was then used for insertion in *Arabidopsis* plants, ecotype Columbia-0, in which the transgene expression was driven by the constitutive 35S promoter (Bechtold *et al.*, 1993). The cassette contained a marker gene, conferring resistance to hygromycin (<https://www.thermofisher.com>) driven by the *nos* promoter and *nos* terminator.

Growth conditions

Seeds were surface sterilized and germinated on half-strength Murashige and Skoog ($\frac{1}{2}$ MS) medium (Murashige and Skoog, 1962), supplemented with 1% sucrose (w/v) and the selective agent corresponding to the genotype used. Seeds were stratified for 4 days at 4°C in the darkness and then kept in a growth chamber at 22 \pm 2°C, 60% relative humidity, irradiance of 150 $\mu\text{mol photons m}^{-2} \text{sec}^{-1}$ and a photoperiod of 8 h light and 16 h dark for 10 days. After, seedlings were transferred to pots containing 0.08 dm³ of commercial substrate, Tropstrato HT[®], and

maintained under the same conditions. During the 4th week after transplanting, physiological assessments and harvesting of samples in liquid nitrogen for biochemical analyses were performed.

For the analyses involving heterotrophic tissues, plates were kept in an air-conditioned growth room at 22 \pm 2°C, relative humidity 60%, and an irradiance of 150 $\mu\text{mol photons m}^{-2} \text{sec}^{-1}$, with a photoperiod of 8 h light and 16 h dark for 10 days. Then, the seedlings were also transferred to commercial substrate and evaluated for seed production.

Subcellular localization of NDT1 and NDT2 by confocal laser scanning microscopy (CLSM)

Arabidopsis plants were stable transformed by *Agrobacterium*-mediated transformation with NDT1 or NDT2 fused to a C-terminal GFP tag under the control of the ubiquitin 10 promoter (Grefen *et al.*, 2010). Five-day-old transformed seedlings were incubated in 200 nM Mito tracker Red CMX ROs in $\frac{1}{2}$ MS medium for 1 h in the dark. Afterwards, seedlings were washed with $\frac{1}{2}$ MS medium to remove the Mito tracker solution and analyzed by a CLSM (Zeiss LSM 780) and Zeiss Zen software. Excitation and emission ranges of GFP (488 nm/490–550 nm) and Mito tracker Red CMX ROs (561 nm/580–625 nm) were measured in two tracks. Image processing was performed using Fiji as previously described (Schindelin *et al.*, 2012).

Gene expression analysis

Gene expression analysis was performed in leaves, flowers, pollen, and imbibed seeds using quantitative real-time PCR (qRT-PCR). Total RNA was extracted from leaves and flowers using TRIzol[®] reagent (<https://www.thermofisher.com>) according to the manufacturer's instructions. Then total RNA was treated with DNase/RNase-free (<https://www.thermofisher.com>) and quantified spectrophotometrically at 260 nm. Approximately 2 μg of isolated RNA were used to synthesize the complementary strand of DNA (cDNA) using an ImProm-II[™] Reverse Transcription System (Promega, Madison, WI, USA, <https://www.promega.com>) and oligo (dT)₁₅, following the manufacturer's recommendations.

The pollen isolation was made using a liquid pollen collection method as described previously (Hicks *et al.*, 2004), with some modifications. Briefly, 50 inflorescences were collected into cold pollen growth medium (PGM) 17% sucrose, 2 mM CaCl₂, 1.625 mM boric acid pH adjusted to 7.5 with KOH. The pollen was released by agitating with gloved hands. After removing all green plant material the PGM was filtered in a nylon membrane (80 μm mesh size). Finally, after centrifugation at 5000 *g* for 10 min the pellet containing the pollen was immediately frozen until RNA extraction.

Total RNA from pollen and 48 h imbibed seeds were both isolated using the SV Total RNA Isolation System (Promega, <https://www.promega.com>) following the manufacturer's manual. The integrity of the RNA was checked on 1% (w/v) agarose gels, and the concentration was measured using the QIAxpert system (QIAGEN, <https://www.qiagen.com>). Subsequently, total RNA was reverse transcribed into cDNA using the Universal RiboClone[®] cDNA Synthesis System (Promega) according to the manufacturer's protocol.

Quantitative RT-PCRs were performed using a 7300 Real-Time System (Applied Biosystems, Foster City, CA, USA, <https://www.thermofisher.com>) and Power SYBR[®] Green PCR Master Mix (<https://www.thermofisher.com>), following the manufacturer's recommendations. The relative expression levels were normalized using housekeeping genes (Table S3) and calculated using the $\Delta\Delta\text{Ct}$ method. All primers used for qRT-PCR were designed using the QuantPrime software (Messinger *et al.*, 2006) and are listed in

Table S3. qRT-PCR cycles were set up as follows: 94°C for 10 min, 40 cycles of 94°C for 15 sec, 58°C for 15 sec and 72°C for 15 sec.

Gas-exchange and chlorophyll *a* fluorescence parameters

Gas-exchange and chlorophyll *a* fluorescence parameters were evaluated 1 h after the onset of the light period by an infrared gas analyzer (IRGA) LI 6400XT (LI-COR, Lincoln, NE, USA, <https://www.licor.com/>) with coupled fluorometer (6400-40 LI-LI-COR Inc.). Light response curves of net CO₂ assimilation were obtained using a 2 cm² foliar chamber, 25°C temperature, CO₂ concentration (*C_a*) of 400 μmol CO₂ mol⁻¹ and irradiances (PPFD) of 0, 10, 25, 50, 100, 200, 400, 800, 1000 and 1200 μmol photons m⁻² sec⁻¹. The variables derived from the curves *A*/PPFD, such as compensation irradiance (*I_c*), saturation irradiance (*I_s*), light use efficiency (1/*φ*), and CO₂ assimilation rate saturated by light (*A_{RFA}*) were estimated from response curve settings to light by the non-rectangular hyperbolic model (von Caemmerer, 2000).

Gas-exchange parameters were evaluated at saturation, i.e. 400 μmol photons m⁻² sec⁻¹ (Figure S10). Photosynthesis per mass unit was estimated based on SLA and LN.

The photorespiration rate (*R_i*) was estimated as: $R_i = ((1/12) \times (J_{H_2O} - (4 \times (A + R_d))))$ where *J_{H₂O}* equivalent to ETR estimated by fluorescence parameters (Valentini *et al.*, 1995). The instantaneous water use efficiency (*A/E*) and intrinsic water use efficiency (*A/g_s*), where *E* stands for transpiration and *g_s* for stomatal conductance, were also calculated.

Dark respiration (*R_d*) was determined after 1 h dark acclimation using the same IRGA system described above. The maximum quantum efficiency of photosystem II (*F_v/F_m*) was evaluated. After 1 h of dark acclimation, an irradiance of 0.03 μmol photons m⁻² sec⁻¹ was applied to determine the initial fluorescence (*F₀*). To obtain maximal fluorescence (*F_m*), a saturating pulse of 6000 μmol photons m⁻² sec⁻¹ was applied for 0.8 sec. The *F_v/F_m* was then calculated as (*F_m* - *F₀*)/*F_m*. Furthermore, NPQ and ETR were estimated as described by DaMatta *et al.* (2002) and Lima *et al.* (2002).

Biometric analysis

Following measurement of gas exchange and fluorescence, the whole plant was harvested and the following growth parameters were evaluated: rosette dry weight (RDW), RSDW, root/shoot ratio (RRS), RLA, SRA, LN, TLA, and SLA. RLA and TLA were determined using a digital image, in which the leaves were scanned (Hewlett Packard Scanjet G2410, Palo Alto, CA, USA) and the obtained images were processed with the aid of Rosette Tracker software (De Vylder *et al.*, 2012). SRA and SLA were estimated using the formula: SRA (or SLA) = RLA (or TLA)/RDW.

Stomatal density

The stomatal density was determined using epidermal prints, from the abaxial surface of fully expanded leaves according to von Groll *et al.* (2002). Six plants per genotype were printed and, for each epidermal print, 10 different regions were evaluated.

Biochemical analyses

Six whole rosettes of each line were collected from 5-week-old plants and snap frozen in liquid nitrogen at 8, 12 or 16 h corresponding to the beginning, middle and end of the light period and 24 h and 8 h representing the middle and end of the dark period, respectively. Subsequently, samples were homogenized, and subjected to ethanol extraction as described by Gibon *et al.* (2004). Chlorophyll, nitrate, glucose, fructose and sucrose contents were

quantified according to Sulpice *et al.* (2009) and Fernie *et al.* (2001), soluble amino acids as described by Gibon *et al.* (2004) and malate and fumarate as detailed by Nunes-Nesi *et al.* (2007). In the insoluble fraction, the levels of starch and protein were determined according to Cross *et al.* (2006). The rates of starch biosynthesis ((starch concentration at the end of the light period - starch concentration at the beginning of the light period)/the number of hours of light) and starch degradation ((starch concentration at the end of the light period - concentration starch at the end of the dark period)/number of dark hours) were calculated. In addition, aliquots of approximately 25 mg of leaf samples were collected in the middle of the light period for the quantification of nucleotide NAD⁺, NADH, NADP⁺ and NADPH according to the protocol described by Schippers *et al.* (2008).

The metabolic profile was determined by gas chromatography time-of-flight mass spectrometry (GC-TOF MS) according to the protocol described by Lisec *et al.* (2006). Metabolites were manually identified using the reference library mass spectra and retention indices from the Golm Metabolome Database (<http://gmd.mpimp-golm.mpg.de>; Kopka *et al.*, 2005). Metabolite profiling data are reported following recommendations (Fernie *et al.*, 2011).

Fatty acids of mature dried seeds and seedlings at 2, 4 or 6 days old were extracted and derivatized as described by Browse *et al.* (1986), and analyzed as methyl esters (FAMES). The fatty acid profile was analyzed by GC-TOF MS. Before derivatization, fatty acid 17:0 was added as an internal standard to enable quantification. The identification of compounds was based on retention time and comparison of the mass spectra with reference spectra available on the NIST 08 and NIST 08s library database (National Institute of Standards and Technology, Babushok *et al.*, 2007). The quantification was performed automatically by integrating the chromatographic peaks obtained (Bernhardt *et al.*, 2012). The amounts of the 17:0 standard was used for the correction of inter-sample variation and absolute quantification of fatty acids according to Hielscher *et al.* (2017). The percentage of each fatty acid was calculated relative to the total of all fatty acids for each line per time point.

Morphological analysis

The viability of pollen grain was evaluated as described by Lorenzon and Almeida (1996). For this, dehiscent anthers of different genotypes were gently dipped onto the surface of the microscope slide and the pollen grains released were transferred to the dye and evaluated under a light microscope. Six flowers from six plants from each line were analyzed, with unstained or deformed pollen grains being considered non-viable. We additionally determined the length and diameter of siliques using a stereomicroscope. Six siliques from six plants of each line were photographed and measured and the length, diameter and number of seeds in each silique were determined. In addition, the 1000-seed weight was also determined.

Seed germination and seedling development

Seeds of *ndt1⁻:ndt1⁻* and WT plants were surface sterilized and germinated as described above. After 48 h in the light, the percentage of germination, GSI, percentage of normal and abnormal seedlings (including albino seedlings) and the ESI was determined. GSI and ESI were calculated by the sum of the number of germinated seeds (or normal seedlings) each day, divided by the number of days between sowing and germination, according to Maguire (1962). Six replicates of 50 seeds each were used for this evaluation.

502 *Izabel de Souza Chaves et al.*

Statistical analysis

All the data are expressed as the mean \pm standard error. Data were tested for significant differences ($P \leq 0.05$) using Student's *t* test. All the statistical analyses were performed using the algorithm embedded into Microsoft Excel[®] (Microsoft, Seattle).

ACCESSION NUMBERS

AtNDT1 (At2g47490); *AtNDT2* (At1g25380); *AtPXN* (At2g39970); *COBL11* (At4g27110); F-box family protein (At5g15710); *AtNADK1* (At3g21070); *AtNADK2* (At1G21640); *AtNADK3* (At1G78590); *AtACTIN* (At2g37620); *AtPARP1* (At2g31320); *AtPARP2* (At4g02390); *AtNUDIX7* (At4g12720); *AtNIC1* (At2G22570); *AtNIC4* (At3g16190); *AtNAPRT1* (At4g36940); *AtNAPRT2* (At2g23420); *AtNADS* (At1g55090); *AtNMNAT* (At5g55810); *AtQPT* (At2g01350); *AtQS* (At5g50210); *AtAO* (At5g14760).

DATA STATEMENT

All data used for the analyses are available upon request or as Supporting Information and may be found in the online version of this article.

ACKNOWLEDGEMENTS

Financial support was provided by Conselho Nacional de Desenvolvimento Científico e Tecnológico (CNPq) (Grant 402511/2016-6 to WLA), Fundação de Amparo à Pesquisa do Estado de Minas Gerais (FAPEMIG) [Grant CRA – APQ-01713-13, CBB – APQ-02548-13, CEX – APQ-02985-14 and CRA – RED-00053-16] and Max Planck Society to ANN and WLA. HEN and ARF acknowledge the support of the Deutsche Forschungsgemeinschaft in the framework of the trans-regional collaborative research centre TRR175. APMW acknowledges funding by the Deutsche Forschungsgemeinschaft (DFG, German Research Foundation) under Germany's Excellence Strategy – EXC-2048/1 – Project ID: 390686111. Research fellowships granted by CNPq to ANN and WLA, Coordenação de Aperfeiçoamento de Pessoal de Nível Superior (CAPES) and FAPEMIG to ISC and DBM are also gratefully acknowledged. The authors wish to thank the NUBIOMOL-UFV for providing the facilities for the analysis of this work.

CONFLICT OF INTEREST

The authors declare no conflict of interest.

AUTHOR CONTRIBUTIONS

AF and ANN screened and genotyped the mutant line. MVP performed the cloning and plant transformation under supervision of TO; ISC screened the transgenic lines and performed most of the experiments under supervision of ANN; DBM, PFP, LC, EH and JACA performed complementary experiments and analyses; NL and TM-A supervised ISC in the lipid analysis and LC in protein localization analysis; ANN and ISC designed the experiments and analyzed the data; ARF and ANN conceived the project and wrote the article with contributions of all the authors; PFP, HEN, FP, WLA, NL and APMW complemented the writing.

SUPPORTING INFORMATION

Additional Supporting Information may be found in the online version of this article.

Figure S1. Gene expression analysis of the *NDT1* gene in different organs of *Arabidopsis thaliana* wild type plants.

Figure S2. Gene expression analysis of genes encoding NAD^+ carriers (*NDT1*, *NDT2* and *PXN*) in different organs of *Arabidopsis thaliana* wild type and *ndt1::ndt1* plants.

Figure S3. Gene expression analysis of genes encoding enzymes related to NAD^+ metabolism in imbibed seeds and leaves of *Arabidopsis thaliana* mutants deficient in the expression of the mitochondrial NAD^+ transporter (*NDT1*) and wild type (WT) plants.

Figure S4. Phenotypic analysis of *Arabidopsis thaliana* lines deficient in the expression of the mitochondrial NAD^+ transporter (*NDT1*) and wild type (WT) plants.

Figure S5. Seed, seedling, germination and seedling establishment characterization of *Arabidopsis thaliana* mutant line deficient in the expression of the mitochondrial NAD^+ transporter (*NDT1*) and wild type (WT) plants.

Figure S6. Fatty acid composition in seeds and seedling of *Arabidopsis thaliana* mutants deficient in the expression of the mitochondrial NAD^+ transporter (*NDT1*) and wild type (WT) plants.

Figure S7. Phenotypic analysis of pollen grains stained with acetic carmine from *Arabidopsis thaliana* genotypes deficient in the expression of the mitochondrial NAD^+ transporter (*NDT1*) and wild type plants.

Figure S8. Germination rate and tube growth of pollen grains from *Arabidopsis thaliana* genotype deficient in the expression of the mitochondrial NAD^+ transporter (*NDT1*) and wild type (WT) plants.

Figure S9. eFP display of transcript accumulation patterns across a variety of *Arabidopsis* organs and treatments.

Figure S10. Gas-exchange and chlorophyll *a* fluorescence parameters in leaves of 4-week-old *Arabidopsis thaliana* genotypes deficient in the expression of the mitochondrial NAD^+ transporter (*NDT1*) and wild type (WT) plants.

Figure S11. Non-photochemical quenching (NPQ) of 4-week-old *Arabidopsis thaliana* genotypes deficient in the expression of the mitochondrial NAD^+ transporter (*NDT1*) and wild type (WT) plants under various light intensities.

Figure S12. Changes in the main nitrogen metabolites in leaves of 4-week-old *Arabidopsis thaliana* genotypes deficient in the expression of the mitochondrial NAD^+ transporter (*NDT1*) and wild type (WT) plants.

Figure S13. Changes in chlorophyll content in leaves of 4-week-old *Arabidopsis thaliana* genotypes deficient in the expression of the mitochondrial NAD^+ transporter (*NDT1*) and wild type (WT) plants.

Table S1. Parameters derived from photosynthetic light curve response (Figure S4a) of 4-week-old, short-day grown *Arabidopsis thaliana* genotypes deficient in the expression of the mitochondrial NAD^+ transporter (*NDT1*).

Table S2. Relative metabolite levels in leaves of 4-week-old, short-day grown, *Arabidopsis thaliana* genotypes deficient in the expression of the mitochondrial NAD^+ transporter (*NDT1*) and wild type (WT) plants.

Table S3. List of primers used in this work to perform qPCR analysis.

REFERENCES

Agledal, L., Niere, M. and Ziegler, M. (2010) The phosphate makes a difference: cellular functions of NADP. *Redox Rep.* **15**, 2–10. <https://doi.org/10.1179/174329210x12650506623122>

The role of mitochondrial NAD⁺ transporter in plants 503

- Agrimi, G., Russo, A., Pierri, C.L. and Palmieri, F. (2012) The peroxisomal NAD⁺ carrier of *Arabidopsis thaliana* transports coenzyme A and its derivatives. *J. Bioenerg. Biomembr.* **44**, 333–340. <https://doi.org/10.1007/s10863-012-9445-0>
- Babushok, V.I., Linstrom, P.J., Reed, J.J., Zenkevich, I.G., Brown, R.L., Mallard, W.G. and Stein, S.E. (2007) Development of a database of gas chromatographic retention properties of organic compounds. *J. Chromatogr. A*, **1157**, 414–421. <https://doi.org/10.1016/j.chroma.2007.05.044>
- Baud, S., Boutin, J.P., Miquel, M., Lepiniec, L. and Rochat, C. (2002) An integrated overview of seed development in *Arabidopsis thaliana* ecotype WS. *Plant Physiol. Biochem.* **40**, 151–160. [https://doi.org/10.1016/s0981-9428\(01\)01350-x](https://doi.org/10.1016/s0981-9428(01)01350-x)
- Bechtold, N., Ellis, J. and Pelletier, G. (1993) In planta *Agrobacterium* mediated gene transfer by infiltration of adult *Arabidopsis thaliana* plants. *C. R. Acad. III*, **316**, 1194–1199. https://doi.org/10.1007/978-3-642-79247-2_3
- Bedhomme, M., Hoffmann, M., McCarthy, E.A., Gambonnet, B., Moran, R.G., Rébellé, F. and Ravanel, S. (2005) Folate metabolism in plants: an Arabidopsis homolog of the mammalian mitochondrial folate transporter mediates folate import into chloroplasts. *J. Biol. Chem.* **280**, 34823–34831.
- Bernhardt, K., Wilkinson, S., Weber, A.P.M. and Linka, N. (2012) A peroxisomal carrier delivers NAD⁺ and contributes to optimal fatty acid degradation during storage oil mobilization. *Plant J.* **69**, 1–13. <https://doi.org/10.1111/j.1365-3113x.2011.04775.x>
- Berrin, J.-G., Pierrugues, O., Brutesco, C., Alonso, B., Montillet, J.-L., Roby, D. and Kazmaier, M. (2005) Stress induces the expression of AtNADK-1, a gene encoding a NAD(H) kinase in *Arabidopsis thaliana*. *Mol. Genet. Genomics*, **273**, 10–19. <https://doi.org/10.1007/s00438-005-1113-1>
- Bowsher, C.G., Lacey, A.E., Hanke, G.T., Clarkson, D.T., Saker, L.R., Stulen, I. and Emes, M.J. (2007) The effect of Glc6P uptake and its subsequent oxidation within pea root plastids on nitrite reduction and glutamate synthesis. *J. Exp. Bot.* **58**, 1109–1118. <https://doi.org/10.1093/jxb/erl269>
- Browse, J., McCourt, P.J. and Somerville, C.R. (1986) Fatty acid composition of leaf lipids determined after combined digestion and fatty acid methyl ester formation from fresh tissue. *Anal. Biochem.* **152**, 141–145. [https://doi.org/10.1016/0003-2697\(86\)90132-6](https://doi.org/10.1016/0003-2697(86)90132-6)
- Cárdenas, L., McKenna, S.T., Kunkel, J.G. and Hepler, P.K. (2006) NAD(P)H oscillates in pollen tubes and is correlated with tip growth. *Plant Physiol.* **142**, 1460–1468. <https://doi.org/10.1104/pp.109.150458>
- Chai, M.F., Chen, Q.J., An, R., Chen, Y.M., Chen, J. and Wang, X.C. (2005) NADK2, an Arabidopsis chloroplastic NAD kinase, plays a vital role in both chlorophyll synthesis and chloroplast protection. *Plant Mol. Biol.* **59**, 553–564. <https://doi.org/10.1007/s11103-005-6802-y>
- Chai, M.F., Wei, P.C., Chen, Q.J., An, R., Chen, J., Yang, S. and Wang, X.C. (2006) NADK3, a novel cytoplasmic source of NADPH, is required under conditions of oxidative stress and modulates abscisic acid responses in Arabidopsis. *Plant J.* **47**, 665–674. <https://doi.org/10.1111/j.1365-3113x.2006.02816.x>
- Cross, J.M., von Korff, M., Altmann, T., Bartzetko, L., Sulpcie, R., Gibon, Y., Palacios, N. and Stitt, M. (2006) Variation of enzyme activities and metabolite levels in 24 Arabidopsis accessions growing in carbon-limited conditions. *Plant Physiol.* **142**, 1574–1588. <https://doi.org/10.1104/pp.106.086629>
- DaMatta, F.M., Loos, R.A., Silva, E.A. and Loureiro, M.E. (2002) Limitations to photosynthesis in *Coffea canephora* as a result of nitrogen and water availability. *J. Plant Physiol.* **159**, 975–981. <https://doi.org/10.1078/0176-1617-00807>
- De Block, M., Verduyn, C., De Brouwer, D. and Cornelissen, M. (2005) Poly (ADP-ribose) polymerase in plants affects energy homeostasis, cell death and stress tolerance. *Plant J.* **41**, 95–106. <https://doi.org/10.1111/j.1365-3113x.2004.02277.x>
- De Vylder, J., Vandenbussche, F., Hu, Y., Philips, W. and Van Der Straeten, D. (2012) Rosette Tracker: an open source image analysis tool for automatic quantification of genotype effects. *Plant Physiol.* **160**, 1149–1159. <https://doi.org/10.1104/pp.112.202762>
- Fernie, A.R., Roscher, A., Ratcliffe, R.G. and Kruger, N.J. (2001) Fructose 2,6-bisphosphate activates pyrophosphate: fructose 6 phosphate 1-phosphotransferase and increases triose phosphate to hexose phosphate cycling in heterotrophic cells. *Planta*, **212**, 250–263. <https://doi.org/10.1007/s00425000386>
- Fernie, A.R., Aharoni, A., Willmitzer, L., Stitt, M., Tohge, T., Kopka, J., Carroll, A.J., Saito, K., Fraser, P.D. and de Luca, V. (2011) Recommendations for reporting metabolite data. *Plant Cell*, **23**, 2477–2482. <https://doi.org/10.1105/tpc.111.086272>
- Flexas, J., Ribas-Carbó, M., Diaz-Espejo, A., Galmés, J. and Medrano, H. (2008) Mesophyll conductance to CO₂: current knowledge and future prospects. *Plant Cell Environ.* **31**, 602–621. <https://doi.org/10.1111/j.1365-3040.2007.01757.x>
- Gakière, B., Fernie, A.R. and Pétriacq, P. (2018) More to NAD⁺ than meets the eye: A regulator of metabolic pools and gene expression in Arabidopsis. *Free Radical Biology and Medicine*, **122**, 86–95. <https://doi.org/10.1016/j.freeradbiomed.2018.01.003>
- Geigenberger, P. and Fernie, A.R. (2014) Metabolic control of redox and redox control of metabolism in plants. *Antioxid. Redox Signal.* **21**, 1389–1421. <https://doi.org/10.1089/ars.2014.6018>
- Geigenberger, P., Kolbe, A. and Tiessen, A. (2005) Redox regulation of carbon storage and partitioning in response to light and sugars. *J. Exp. Bot.* **56**, 1469–1479. <https://doi.org/10.1093/jxb/eri178>
- Gibon, Y., Blaesing, O.E., Hannemann, J., Carillo, P., Hohne, M., Hendriks, J.H.M., Palacios, N., Cross, J., Selbig, J. and Stitt, M. (2004) A robot-based platform to measure multiple enzyme activities in Arabidopsis using a set of cycling assays: comparison of changes of enzyme activities and transcript levels during diurnal cycles and prolonged darkness. *Plant Cell*, **16**, 3304–3325. <https://doi.org/10.1105/tpc.104.025973>
- Grefen, C., Donald, N., Hashimoto, K., Kudla, J., Schumacher, K. and Blatt, M.R. (2010) A ubiquitin-10 promoter-based vector set for fluorescent protein tagging facilitates temporal stability and native protein distribution in transient and stable expression studies. *The Plant Journal*, **64**(2), 355–365. <https://doi.org/10.1111/j.1365-3113x.2010.04322.x>
- Hashida, S.N., Takahashi, H., Kawai-Yamada, M. and Uchimiya, H. (2007) Arabidopsis thaliana nicotinate/nicotinamide mononucleotide adenyltransferase (AtNMNAT) is required for pollen tube growth. *Plant J.* **49**, 694–703. <https://doi.org/10.1111/j.1365-3113x.2006.02989.x>
- Hashida, S.N., Takahashi, H. and Uchimiya, H. (2009) The role of NAD biosynthesis in plant development and stress responses. *Ann. Bot.* **103**, 819–824. <https://doi.org/10.1093/aob/mcp019>
- Hashida, S.N., Itami, T., Takahashi, H., Takahara, K., Nagano, M., Kawai-Yamada, M., Shoji, K., Goto, F., Yoshihara, T. and Uchimiya, H. (2010) Nicotinate/nicotinamide mononucleotide adenyltransferase-mediated regulation of NAD biosynthesis protects guard cells from reactive oxygen species in ABA-mediated stomatal movement in Arabidopsis. *J. Exp. Bot.* **61**, 3813–3825. <https://doi.org/10.1093/jxb/erq190>
- Hashida, S.N., Takahashi, H., Takahara, K., Kawai-Yamada, M., Kitazaki, K., Shoji, K., Goto, F., Yoshihara, T. and Uchimiya, H. (2013) NAD⁺ accumulation during pollen maturation in Arabidopsis regulating onset of germination. *Mol. Plant*, **6**, 216–225. <https://doi.org/10.1093/mp/sss071>
- Hicks, G.R., Rojo, E., Hong, S., Carter, D.G. and Raikhel, N.V. (2004) Germinating pollen has tubular vacuoles, displays highly dynamic vacuole biogenesis, and requires VACUOLESS1 for proper function. *Plant Physiol.* **134**, 1227–1239. <https://doi.org/10.1104/pp.103.037382>
- Hielscher, B., Charton, L., Mettler-Altmann, T. and Linka, N. (2017) Analysis of Peroxisomal beta-oxidation during storage oil mobilization in Arabidopsis thaliana seedlings. *Methods Mol. Biol.* **1595**, 291–304. https://doi.org/10.1007/978-1-4939-6937-1_27
- Hölscher, C., Lutterbey, M.C., Lansing, H., Meyer, T., Fischer, K. and von Schaewen, A. (2016) Defects in peroxisomal 6-phosphogluconate dehydrogenase isoform PGD2 prevent gametophytic interaction in Arabidopsis thaliana. *Plant Physiol.* **171**, 192–205. <https://doi.org/10.1104/pp.15.01301>
- Hunt, L. and Gray, J.E. (2009) The relationship between pyridine nucleotides and seed dormancy. *New Phytol.* **181**, 62–70. <https://doi.org/10.1111/j.1469-8137.2008.02641.x>
- Hunt, L., Holdsworth, M.J. and Gray, J.E. (2007) Nicotinamide activity is important for germination. *Plant J.* **51**, 341–351. <https://doi.org/10.1111/j.1365-3113x.2007.03151.x>
- Kirchberger, S., Tjaden, J. and Neuhaus, H.E. (2008) Characterization of the Arabidopsis Brittle1 transport protein and impact of reduced activity on plant metabolism. *Plant J.* **56**, 51–63. <https://doi.org/10.1111/j.1365-3113x.2008.03583.x>
- Kopka, J., Schauer, N., Krueger, S. et al. (2005) GMD@CSB.DB: the Golm Metabolome Database. *Bioinformatics*, **21**, 1635–1638. <https://doi.org/10.1093/bioinformatics/bti236>

504 *Izabel de Souza Chaves et al.*

- Landy, A. (1989) Dynamic, structural, and regulatory aspects of Lambda site specific recombination. *Ann. Rev. Biochem.* **58**, 913–949. <https://doi.org/10.1146/annurev.bi.58.070189.004405>
- Lima, A.L.S., DaMatta, F.M., Pinheiro, H.A., Totola, M.R. and Loureiro, M.E. (2002) Photochemical responses and oxidative stress in two clones of *Coffea canephora* under water deficit conditions. *Environ. Exp. Bot.* **47**, 239–247. [https://doi.org/10.1016/s0098-8472\(01\)00130-7](https://doi.org/10.1016/s0098-8472(01)00130-7)
- Lisec, J., Schauer, N., Kopka, J., Willmitzer, L. and Fernie, A.R. (2006) Gas chromatography mass spectrometry-based metabolite profiling in plants. *Nat. Protoc.* **1**, 387–396. <https://doi.org/10.1038/nprot.2006.59>
- Liu, Y.-J., Nunes-Nesi, A., Wallström, S.V., Lager, I., Michalecka, A.M., Norberg, F.E.B., Widell, S., Fredlund, K.M., Fernie, A.R. and Rasmussen, A.G. (2009) A redox-mediated modulation of stem bolting in transgenic nicotiana sylvestris differentially expressing the external mitochondrial NADPH dehydrogenase. *Plant Physiol.* **150**, 1248–1259. <https://doi.org/10.1104/pp.109.136242>
- Lorenzon, M.C.A. and Almeida, E.C. (1996) Viabilidade e germinação do pólen de linhagens parentais de cebola híbrida. *Pesqui. Agropec. Bras.* **32**, 345–349
- Maguire, J.D. (1962) Speed of germination aid in selection and evaluation for seedling emergence and vigor. *Crop Sci.* **2**, 176–177. <https://doi.org/10.2135/cropsci1962.0011183x0002000200033x>
- Messinger, S.M., Buckley, T.N. and Mott, K.A. (2006) Evidence for involvement of photosynthetic processes in the stomatal response to CO₂. *Plant Physiol.* **140**, 771–778. <https://doi.org/10.1104/pp.105.073676>
- Munoz-Bertomeu, J., Cascales-Minana, B., Iriés-Segura, A., Mateu, I., Nunes-Nesi, A., Fernie, A.R., Segura, J. and Ros, R. (2010) The plastidial glyceraldehyde-3-phosphate dehydrogenase is critical for viable pollen development in Arabidopsis. *Plant Physiol.* **152**, 1830–1841
- Murashige, T. and Skoog, F. (1962) A revised medium for rapid growth and bioassay with tobacco tissue cultures. *Physiol. Plant.* **15**, 473–497. <https://doi.org/10.1111/j.1399-3054.1962.tb08052.x>
- Neuhaus, H.E. and Emes, M.J. (2000) Nonphotosynthetic metabolism in plastids. *Annu. Rev. Plant Physiol. Plant Mol. Biol.* **51**, 111–140. <https://doi.org/10.1146/annurev.arplant.51.1.111>
- Noctor, G., Queval, G. and Gakiere, B. (2006) NAD(P) synthesis and pyridine nucleotide cycling in plants and their potential importance in stress conditions. *J. Exp. Bot.* **57**, 1603–1620. <https://doi.org/10.1093/jxb/erj202>
- Nunes-Nesi, A., Carrari, F., Gibon, Y., Sulpice, R., Lytovchenko, A., Fisahn, J., Graham, J., Ratcliffe, R.G., Sweetlove, L.J. and Fernie, A.R. (2007) Deficiency of mitochondrial fumarate activity in tomato plants impairs photosynthesis via an effect on stomatal function. *Plant J.* **50**, 1093–1106. <https://doi.org/10.1111/j.1365-3113.2007.03115.x>
- Palmieri, F., Rieder, B., Ventrella, A. et al. (2009) Molecular identification and functional characterization of *Arabidopsis thaliana* mitochondrial and chloroplastic NAD⁺ carrier proteins. *J. Biol. Chem.* **284**, 31249–31259. <https://doi.org/10.1074/jbc.m109.041830>
- Penfound, T. and Foster, J.W. (1999) NAD-dependent DNA-binding activity of the bifunctional NadR regulator of *Salmonella typhimurium*. *J. Bacteriol.* **181**, 648–655.
- Scheibe, R. (2004) Malate valves to balance cellular energy supply. *Physiol. Plant.* **120**, 21–26. <https://doi.org/10.1111/j.0031-9317.2004.0222.x>
- Schippers, J.H.M., Nunes-Nesi, A., Apetrei, R., Hille, J., Fernie, A.R. and Dijkwel, P.P. (2008) The *Arabidopsis* onset of leaf death5 mutation of quinolinate synthase nicotinamide adenine dinucleotide biosynthesis and causes early ageing. *Plant Cell.* **20**, 2909–2925. <https://doi.org/10.1105/tpc.107.056341>
- Selinski, J. and Scheibe, R. (2014) Pollen tube growth: where does the energy come from? *Plant Signal. Behav.* **9**, e977200–e977209. <https://doi.org/10.4161/15592324.2014.977200>
- Selinski, J., König, N., Wellmeyer, B., Hanke, G.T., Linke, V., Neuhaus, H.E. and Scheibe, R. (2014) The plastid-localized NAD-dependent malate dehydrogenase is crucial for energy homeostasis in developing *Arabidopsis thaliana* seeds. *Mol. Plant.* **7**, 170–186
- Senkler, J., Senkler, M., Eubel, H., Hildebrandt, T., Lengwenus, C., Schertl, P., Schwarzländer, M., Wagner, S., Wittig, I. and Braun, H.P. (2017) The mitochondrial complexome of *Arabidopsis thaliana*. *Plant J.* **89**, 1079–1092. [Epub 2017 Feb 20]. <https://doi.org/10.1111/tpj.13448>
- Schindelin, J., Arganda-Carreras, I., Frise, E. et al. (2012) Fiji: an open-source platform for biological-image analysis. *Nat. Methods.* **9**, 676–682
- Sulpice, R., Pyl, E.T., Ishihara, H. et al. (2009) Starch as a major integrator in the regulation of plant growth. *Proc. Natl Acad. Sci. USA.* **106**, 10348–10353. <https://doi.org/10.1073/pnas.0903478106>
- Takahashi, H., Takahara, K., Hashida, S., Hirabayashi, T., Fujimori, T., Kawai-Yamada, M., Yamaya, T., Yanagisawa, S. and Uchimiya, H. (2009) Pleiotropic modulation of carbon and nitrogen metabolism in Arabidopsis plants overexpressing the *NAD kinase2* Gene. *Plant Physiol.* **151**, 100–113. <https://doi.org/10.1104/pp.109.140665>
- Takahashi, H., Watanabe, A., Tanaka, A., Hashida, S., Kawai-yamada, M., Sonoike, K. and Uchimiya, H. (2006) Chloroplast NAD Kinase is essential for energy transduction through the xanthophyll cycle in photosynthesis. *Plant Cell Physiol.* **47**, 1678–1682
- Tanaka, Y., Sugano, S.S., Shimada, T. and Hara-Nishimura, I. (2013) Enhancement of leaf photosynthetic capacity through increased stomatal density in Arabidopsis. *New Phytol.* **198**, 757–764. <https://doi.org/10.1111/nph.12186>
- Todisco, S., Agrimi, G., Castegna, A. and Palmieri, F. (2006) Identification of the mitochondrial NAD1 transporter in *Saccharomyces cerevisiae*. *J. Biol. Chem.* **281**, 1524–1531. <https://doi.org/10.1074/jbc.m510425200>
- Turner, W.L., Waller, J.C. and Snedden, W.A. (2005) Identification, molecular cloning and functional characterization of a novel NADH kinase from *Arabidopsis thaliana* (thale cress). *Biochem. J.* **385**, 217–223. <https://doi.org/10.1042/bj20040292>
- Valentini, R., Epron, D., De Angelis, P., Matteucci, G. and Dreyer, E. (1995) *In situ* estimation of net CO₂ assimilation, photosynthetic electron flow and photorespiration in Turkey oak (*Q. cerris* L.) leaves: diurnal cycles under different levels of water supply. *Plant Cell Environ.* **18**, 631–640. <https://doi.org/10.1111/j.1365-3040.1995.tb00564.x>
- VanLinden, M.R., Dölle, C., Pettersen, I.K. et al. (2015) Subcellular distribution of NAD⁺ between cytosol and mitochondria determines the metabolic profile of human cells. *J. Biol. Chem.* **290**, 27644–27659. <https://doi.org/10.1074/jbc.m115.654129>
- van Roermund, C.W., Schroers, M.G., Wiese, J. et al. (2016) The peroxisomal NAD carrier from Arabidopsis imports NAD in exchange with AMP. *Plant Physiol.* **171**, 2127–2139
- von, Caemmerer, S. (2000). *Biochemical Models of Leaf Photosynthesis*. Victoria: CSIRO Publishing.
- von Groll, U., Berger, D. and Altmann, T. (2002) The subtilisin-like serine protease SDD1 mediates cell-to-cell signaling during Arabidopsis stomatal development. *Plant Cell.* **14**, 1527–1539. <https://doi.org/10.1105/tpc.001016>
- Waller, J.C., Dhanoa, P.K., Schumann, U., Mullen, R.T. and Snedden, W.A. (2010) Subcellular and tissue localization of NAD kinases from Arabidopsis: compartmentalization of de novo NADP biosynthesis. *Planta*, **231**, 305–317. <https://doi.org/10.1007/s00425-009-1047-7>
- Winter, D., Vinegar, B., Nahal, H., Ammar, R., Wilson, G.V. and Provart, N.J. (2007) An “Electronic Fluorescent Pictograph” browser for exploring and analyzing large-scale biological data sets. *PLoS ONE*, **2**, e718

Author contribution

Lennart Charton performed the sub-cellular localization shown in Figure 7.

IV. Published Manuscripts

IV.III Published Manuscript 3

Slc25a17 acts as a peroxisomal coenzyme A transporter and regulates multiorgan development in zebrafish

Yong-Il Kim^{1*} In-Koo Nam^{1,2*} Dong-Kyu Lee³ Sushil Bhandari¹
Lennart Charton⁴ SeongAe Kwak⁵ Jae-Young Lim^{1,2} KwangHeum Hong¹
Se-Jin Kim² Joon No Lee² Sung Won Kwon³ Hong-Seob So¹ Nicole Linka⁴
Raekil Park² Seong-Kyu Choe^{1,6}

¹Department of Microbiology and Center for Metabolic Function Regulation, Wonkwang University School of Medicine, Iksan, South Korea

²Department of Biomedical Science and Engineering, Gwangju Institute of Science and Technology, Gwangju, South Korea

³College of Pharmacy and Research Institute of Pharmaceutical Sciences, Seoul National University, Seoul, South Korea

⁴Department of Plant Biochemistry, Heinrich-Heine University Düsseldorf, Düsseldorf, Germany

⁵Zoonosis Research Center, Wonkwang University School of Medicine, Iksan, South Korea

⁶Wonkwang Medical Institute, Wonkwang University School of Medicine, Iksan, South Korea


Received: 5 January 2019 | Revised: 23 May 2019 | Accepted: 24 May 2019

DOI: 10.1002/jcp.28954

ORIGINAL RESEARCH ARTICLE

Journal of
Cellular Physiology WILEY

Slc25a17 acts as a peroxisomal coenzyme A transporter and regulates multiorgan development in zebrafish

Yong-Il Kim^{1*} | In-Koo Nam^{1,2*} | Dong-Kyu Lee³ | Sushil Bhandari¹ |
Lennart Charton⁴ | SeongAe Kwak⁵ | Jae-Young Lim^{1,2} | KwangHeum Hong¹ |
Se-Jin Kim² | Joon No Lee² | Sung Won Kwon³ | Hong-Seob So¹ | Nicole Linka⁴ |
Raekil Park² | Seong-Kyu Choe^{1,6} ¹Department of Microbiology and Center for Metabolic Function Regulation, Wonkwang University School of Medicine, Iksan, South Korea²Department of Biomedical Science and Engineering, Gwangju Institute of Science and Technology, Gwangju, South Korea³College of Pharmacy and Research Institute of Pharmaceutical Sciences, Seoul National University, Seoul, South Korea⁴Department of Plant Biochemistry, Heinrich-Heine University Düsseldorf, Düsseldorf, Germany⁵Zoonosis Research Center, Wonkwang University School of Medicine, Iksan, South Korea⁶Wonkwang Medical Institute, Wonkwang University School of Medicine, Iksan, South Korea**Correspondence**Nicole Linka, Department of Plant Biochemistry, Heinrich-Heine University Düsseldorf, 40225 Düsseldorf, Germany.
Email: Nicole.Linka@uni-duesseldorf.deRaekil Park, Department of Biomedical Science and Engineering, Gwangju Institute of Science and Technology, Gwangju, South Korea.
Email: rkpark@gist.ac.krSeong-Kyu Choe, Department of Microbiology and Center for Metabolic Function Regulation, Wonkwang University School of Medicine, Iksan, Jeonbuk 54538, South Korea.
Email: seongkyu642@wku.ac.kr**Funding information**

Deutsche Forschungsgemeinschaft, Grant/Award Number: DFG1871/1-2; National Research Foundation of Korea, Grant/Award Numbers: NRF-2016R1A2B4009129, NRF-2014M3A9D8034463; Ministry of Oceans and Fisheries, Grant/Award Number: MOF-20180430

Abstract

Slc25a17 is known as a peroxisomal solute carrier, but the *in vivo* role of the protein has not been demonstrated. We found that the zebrafish genome contains two *slc25a17* genes that function redundantly, but additively. Notably, peroxisome function in *slc25a17* knockdown embryos is severely compromised, resulting in an altered lipid composition. Along the defects found in peroxisome-associated phenotypic presentations, we highlighted that development of the swim bladder is also highly dependent on Slc25a17 function. As Slc25a17 showed substrate specificity towards coenzyme A (CoA), injecting CoA, but not NAD⁺, rescued the defective swim bladder induced by *slc25a17* knockdown. These results indicated that Slc25a17 acts as a CoA transporter, involved in the maintenance of functional peroxisomes that are essential for the development of multiple organs during zebrafish embryogenesis. Given high homology in protein sequences, the role of zebrafish Slc25a17 may also be applicable to the mammalian system.

KEYWORDS

coenzyme A transporter, peroxisomes, solute carrier family 25 member 17, swim bladder, zebrafish

1 | INTRODUCTION

Peroxisomes are subcellular organelles containing various proteins that perform anabolic and catabolic reactions of fatty acids and decay of undesirable reactive oxygen species (ROS; Lodhi & Semenkovich,

2014; Wanders, 2014). Therefore, peroxisomal disorders due to defective single enzyme in peroxisomes, let alone the defective peroxisome biogenesis, are known to induce developmental abnormalities in humans that manifest a variety of symptoms, including growth retardation, neurological deficits, hypotonia, and liver dysfunction (Delille, Bonekamp, & Schrader, 2006; Fujiki, Yagita, & Matsuzaki, 2012; Vamecq, Cherkaoui-Malki, Andreoletti, & Latruffe,

*Yong-Il Kim and In-Koo Nam contributed equally to this study.

2014; Wanders, 2014; Waterham & Wanders, 2012). In particular, neurological abnormalities due to peroxisome dysfunction originate likely from aberrant development of neuronal systems, including, defective neuronal migration, altered axonal integrity, and myelin formation and maintenance (Berger, Dorninger, Forss-Petter, & Kunze, 2016). However, it needs further investigation which factor is responsible for neuropathology that was differentially observed between peroxisome-deficient patients and individuals with defective in a peroxisome-resident enzyme (Berger et al., 2016; Islinger, Voelkl, Fahimi, & Schrader, 2018). Given the known cellular roles of peroxisomes in regulating lipid metabolism and intracellular ROS levels, much work is needed to better understand the mechanistic aspects of peroxisome-resident proteins in vivo.

Zebrafish has evolved as an important model organism to study various aspects of biological sciences. In particular, zebrafish may serve as an ideal animal model to study a gene function in proper and the associated phenotypes upon its deficiency in vivo, as its embryonic development entirely relies on its yolk contents for the first 5 days post fertilization (dpf; Kim et al., 2014; Lieschke & Currie, 2007). Yolk absorption during early zebrafish embryogenesis has previously been reported in which yolk-metabolizing processes seem relatively simple, but may share fundamental similarities to lipid metabolism in human physiology (Miyares, de Rezende, & Farber, 2014). More recently, yolk absorption has been shown to be closely related to metabolic profiles of genes involved in metabolic dynamics (Huang & Linsen, 2015), further suggesting a tight link between yolk lipid utilization and metabolic organelles. The potential link between yolk lipid consumption and the roles of metabolic organelles during vertebrate development is not fully understood.

Members of the solute carrier protein family (SLC) transport various molecules across membranes, including charged and uncharged organic molecules, ions, metals, and other metabolites, and support basal cellular functions (Hediger, Clemençon, Burrier, & Bruford, 2013; Palmieri, 2013). Among the members of the mitochondrial SLC25 subfamily, SLC25A17, also known as PMP34, was originally reported as a peroxisomal membrane protein that transports adenosine triphosphate (ATP) across the peroxisomal membrane (Visser, van Roermund, Waterham, & Wanders, 2002). However, a recent study suggested that human SLC25A17 may act as a transporter for exchanging not only coenzyme A (CoA), flavin adenine dinucleotide (FAD), flavin mononucleotide (FMN), or adenosine monophosphate (AMP) across peroxisomal membranes, but also nicotinamide adenine dinucleotide (NAD⁺) or adenosine diphosphate (ADP; Agrimi, Russo, Scarzia, & Palmieri, 2012). Because the molecules listed above are necessary for the accomplishment of β -oxidation of very long-chain fatty acids, as well as synthesis of ether phospholipids in peroxisomes, SLC25A17 has been predicted to play a critical role in the functions of the peroxisome (Gutierrez-Aguilar & Baines, 2013; Visser, van Roermund, Ijlst, Waterham, & Wanders, 2007; Wylin et al., 1998). However, the in vivo role of SLC25A17 has not been demonstrated till date.

In this study, we report that there are two *slc25a17* genes in zebrafish, presumably due to genome duplication through evolution.

The two *Slc25a17* proteins (named as *Slc25a17* and *Slc25a17*-like [*Slc25a17l* in short]) are localized to peroxisomes in developing zebrafish embryos. By analyzing the developmental phenotypes associated with *slc25a17* gene knockdown, we show that *Slc25a17* acts as a CoA transporter, which is essentially required for multiple organ development, including swim bladder, during zebrafish embryogenesis.

2 | EXPERIMENTAL PROCEDURES

2.1 | Animal care and handling

Adult zebrafish and their embryos were handled and staged according to standard protocols (Kimmel, Ballard, Kimmel, Ullmann, & Schilling, 1995). A transgenic line, *Tg(lfabp:DsRED)* was provided by the Zebrafish Organogenesis and Mutant Bank in Korea. All experimental protocols were approved by the Committee for Ethics in Animal Experiments of the Wonkwang University (WKU15-127) and carried out according to the Guidelines for Animal Experiments.

2.2 | Constructs

The open reading frames (ORFs) of zebrafish *slc25a17* and *slc25a17l* were individually amplified from complementary DNAs (cDNAs); the total RNA was prepared from zebrafish embryos at 1 dpf. Primer sequences used in polymerase chain reactions (PCRs) are listed in Table 1. The amplified *slc25a17* and *slc25a17l* ORFs were cloned into pCRII-TOPO vector (Invitrogen, Carlsbad, CA). Final constructs were obtained by cloning the *slc25a17* and *slc25a17l* ORFs into pCS2 + vector or pCS2 + MYC vector using *EcoRI* and *XhoI* restriction enzymes (NEB, Ipswich, MA). The *mdh1aa* (malate dehydrogenase 1Aa) ORF was amplified by PCR, digested with *EcoRI* and *XhoI* enzymes and subsequently cloned in the same sites of pCS2 + MT vector. The peroxisomal targeting signal 1 (PTS-1) sequence was inserted by using the primer sets (listed in the supplemental table) in front of the stop codon. For heterologous protein expression using wheat-germ lysate, the ORFs of *slc25a17* and *slc25a17l* were cloned into pIVEX1.3 expression vector in frame with a C-terminal His₆-tag using the primers listed. Both coding sequences were inserted into pIVEX1.3 by using *NcoI* and *XhoI* (for *slc25a17*) or *NdeI* and *XmaI* (for *slc25a17l*) restriction enzymes.

2.3 | Microinjections

Morpholinos (MOs) for control, *slc25a17*, *slc25a17l*, and *CoA synthase* were purchased from Gene Tools, LLC (Philomath, OR). Morpholino sequences are listed in Table 1. A dosage curve was built for each MO to determine microinjection concentrations, and translation MO*slc25a17* (5 ng), splicing MO*slc25a17* (3 ng), translation MO*slc25a17l* (5 ng), splicing MO*slc25a17l* (5 ng), translation MO*CoA synthase* (5 ng), splicing MO*CoA synthase* (5 ng), or control MO (5 ng) was microinjected into one-cell stage

zebrafish embryos. For the rescue experiment, 25 mM NAD⁺ (Sigma-Aldrich, St. Louis, MO) or 2.5 mM CoA (Sigma-Aldrich) was injected either singly or together into the one-cell stage embryos with MOslc25a17, and the number of embryos with normal swim bladder was counted under a dissection microscope. For over-expression studies, in vitro synthesized slc25a17 or slc25a17i messenger RNA (mRNA; mMessage mMachine SP6, Ambion-Thermo Fisher, Pittsburgh, PA) was microinjected into the one-cell stage embryos, which were fixed at desired developmental stages and processed for in situ hybridization. All experiments were

repeated at least two times with the minimum of 30 embryos per condition.

2.4 | In situ hybridization, immunostaining, and imaging

Control, and slc25a17 or slc25a17i knockdown embryos were collected at various developmental stages, fixed in 4% paraformaldehyde, and processed for in situ hybridization or immunostaining as previously described (Kim et al., 2015). For immunostaining,

TABLE 1 Sequence information of morpholinos and primers

Name	Purpose	Sequence (5'–3')
acox1F	RT-PCR	CCTGGAACAACACTTCCATTG
acox1R		CGTTGCCATCATATCGTCCC
dbpF	RT-PCR	CGGTCTATCCTGGTCAGTCT
dbpR		TTTCCCCATCACCACCTCCA
scp2aF	RT-PCR	GGTGGTGGATGGAAGATGG
scp2aR		GGGAGCTGTGTTTCCACAGTT
agpsF	RT-PCR	GTCCTCCATATTCACCTCATT
agpsR		CACTCTTATTATCCTCTCCT
pex5F	RT-PCR	GGGAGAGAGAGAAAGAGAGT
pex5R		ACAGAGAGTGGCGAGAGAAA
Slc25a17RTF	RT-PCR	CCAGACTCCTGAACAGCCTG
Slc25a17RTR		CGTTTGACCCCCATGACCCTAA
Slc25a17likeRTF	RT-PCR	CGCCTTCTCTCAGATCATCGCT
Slc25a17likeRTR		ATTCCTCAGGCTGCCACCAG
slc25a17F	Cloning into pCRII-TOPO	CCGAATTCATGAAACTCATGGATGTCTTTCCGTAT
slc25a17R		GGCTCGAGTCAATGGGAGGTCATTGGTCTGTTT
slc25a17likeF	Cloning into pCRII-TOPO	CCGAATTCATGTCGGACAGCAGCGGCTC
slc25a17likeR		GGCTCGAGTCAGTCTTGTGTTTCTCTGAAGGCC
slc25a17F	Cloning into pIVEX1.3	CGCGGCCATGGGATCTACAGACATGAAACTC
slc25a17R		GACTGCCTCGAGATGGGAGTTCATTGGTCTTTGAC
slc25a17likeF	Cloning into pIVEX1.3	GACTATCATATGTCGGACAGCAGCGGCTCAGTCG
slc25a17likeR		GTAATCCCGGGTGTCTTGTGTTTCTCTGAAGGC
mdh1aaF	Cloning into pCS2+	GGGAATTCATGGCCGAACCGATCCGTGTTT
mdh1aaR		CCCTCGAGTCACGCTGAGAGGAAGGTGA
mdh1aa-SKLF	Cloning Into pCS2+	GGGAATTCATGGCCGAACCGATCCGTGTTT
mdh1aa-SKLR		CCCTCGAGTCAAAGTTTAGACGCTGAGAGG
MOctrl	Gene knockdown	AACATACATCAGTTTAATATATGTA
MOslc25a17transl	Gene knockdown	GACATCCATGAGTTTCATGTCTGTA
MOslc25a17spli		ATGGAGCCAACCTGGAGACAAAGAG
MOslc25a17liketransl	Gene knockdown	CTGAGCCGCTGCTGTCCGACATATT
MOslc25a17likespli		CAGGACGATAGAAATCTCACCTGA
MOcoasyltransl	Gene knockdown	CTGAACATGGACATGGTTGACAGCT
MOcoasyspli		ATGCATAAGCCTACCTGAGCGGCT

Abbreviation: RT-PCR, real-time polymerase chain reaction.

antibodies to detect acetylated tubulin (antiacetyl tubulin, 1:500, Sigma-Aldrich), peroxisomal PMP70 (anti-PMP70, 1:500, Abcam, Cambridge, United Kingdom), and secondary Alexa Fluor-conjugated antimouse antibodies (1:400, Invitrogen) or antirabbit (1:400, Invitrogen) antibodies were used. Images were taken using a Leica M165FC microscope equipped with Leica DFC500, or confocal microscope (Olympus IX81, Fluoview FV1000). For the observation of peroxisomes, RFP-positive embryos obtained from wild type outcross or from an outcross between wild type and *Tg(ef1α:RFP-SKL)* transgenic zebrafish were microinjected with either control MO or *MOslc25a17* and cryoprocessed to obtain sections for imaging using confocal microscopy.

2.5 | Cryosectioning

Control or MO-injected embryos were fixed in AB fix solution (1:1 ratio of 8% paraformaldehyde and 2X fix solution [8% sucrose, 30 μl 1 M CaCl₂ in 25 ml phosphate-buffered saline PBS]) overnight. The samples are washed once with PBS, and then mounted in 5% sucrose + 1.5% agarose. The blocks were kept in 30% sucrose at 4°C, overnight. To make frozen blocks, 2-methylbutane (Junsei Chemical, Tokyo, Japan) was used, and sectioning of sample blocks was performed using a cryomicrotome HX525 NX (Thermo Fisher Scientific, Waltham, MA).

2.6 | Quantitative RT-PCR

Control or MO-injected embryos were grown up to 3 dpf ($n = 10$ per condition, triplicates) and collected in the Trizol (Ambion-Thermo Fisher Scientific, Pittsburgh, PA) from which total RNAs were prepared. First strand cDNA was synthesized as previously described (Kim et al., 2015). Primer sequences used are listed in Table 1. The experiment was replicated to confirm data consistency and Student's *t* test in Microsoft Excel was used to determine statistical significance.

2.7 | Oil red-O staining

Control and MO-injected embryos were fixed with 4% paraformaldehyde overnight, washed three times with PBS, and depigmented with a bleaching solution (200 μl 1X saline sodium citrate [SSC]), 33.8 ml water, 2 ml formamide, and 4 ml hydrogen peroxide). The embryos were then washed three times with PBS, and preincubated in 60% isopropanol for 30 min. For staining, embryos were incubated in freshly prepared 0.3% oil red-O (Sigma-Aldrich) solution in 60% isopropanol for 3 hr, rinsed several times with PBS and photographed. Microscopic examination was used to quantify the number of embryos with positive oil red-O stain in the yolk. Student's *t* test in Microsoft Excel was used to determine statistical significance.

2.8 | Analysis of fatty acids and plasmalogens

Mild methanolysis was applied to simultaneously convert very long-chain fatty acids (VLCFA) and plasmalogens into methyl ester (ME) and dimethyl acetal (DMA) forms, respectively, which were subsequently volatilized and detected by the GC-MS system. For the reaction, 100 zebrafish larvae at the indicated days were collected and immersed into 1 ml of hydrolysis reagent containing methanol: 37% (w/w) hydrochloric acid (4:1) in a 4-ml glass vial. Methanolic derivatization was conducted at 100°C for 60 min, after which hydrophobic VLCFA methyl ester and DMA were extracted by adding 1 ml hexane three times for liquid-liquid extraction. The collected hexane layer was reconstituted into 100 μl hexane. Before methanolysis, 1 μg of tricostylic acid (C23:0; Sigma-Aldrich) was added as an internal standard for elimination any possible variations from the experimental procedure. Methyl docosanoate (C22:0 ME), methyl tetracosanoate (C24:0 ME), methyl hexacosanoate (C26:0 ME), 1,1-dimethoxyhexadecane (C16:0 DMA), 1,1-dimethoxyoctadecane (C18:0 DMA), and 1,1-dimethoxy-(9Z)octadecene (C18:1 DMA) were prepared (fatty acid methyl ester from Sigma-Aldrich and DMA from Avanti Polar Lipids, Alabaster, AL) for external standard and confirmation of the mass spectrum. Derivatized compounds were separated and detected using GC-MS (GCMS-QP2010, Shimadzu, Kyoto, Japan) system, where 1 μl of reconstituted sample was injected (split ratio 2:1) and volatilized at 300°C to be introduced into capillary column (HP-1, 30 m length, 0.32 mm ID, 0.25 μm film thickness; Agilent Technologies, Santa Clara, CA). Helium gas at a flow rate of 1 ml/min carried compounds that were separated by capillary column, with GC temperature program as follows: initial temperature was 100°C for 2 min, which increased at 10°C/min up to 150°C, at 5°C/min up to 300°C, and was held for 5 min. For mass spectrometry, the compounds were ionized by the electron impact ion source at 70 eV at 200°C source temperature. Detection range was from 50 to 500 m/z and detection was processed at 5 scan/s scan rate. For measuring the quantity, 74 m/z; [C₃H₆O₂]⁺ and 75 m/z; [C₃H₇O₂]⁺, McLafferty rearrangement ions of each VLCFA methyl ester and DMA structure, were chosen as a quantification ion. Extracted ion chromatograms (EIC) of both ions were used to integrate the peak area of every compound, after which all the areas were normalized to the response of the internal standard. External standard calibration was performed with normalized area and derived linear regression. Limit of detection and limit of quantification for the validation and concentration of each compound were calculated.

2.9 | Heterologous protein expression

Slc25a17 and *Slc25a17l* were heterologously expressed using the RTS Wheat Germ CECF kit (biotechrabbit) in the presence of 1% (w/v) L-α-phosphatidylcholine vesicles and 0.04% (w/v) Brij-35 as described by Bernhardt, Wilkinson, Weber, and Linka (2012). Cell-free expressed proteins were desalted using Nap-5 columns (GE-Healthcare) and 1 ml 10 mM Tricine-KOH, pH 7.2.

2.10 | Reconstitution of liposomes and in vitro uptake assay

Recombinant proteins were reconstituted into liposomes by freeze-thaw-sonication procedure (Kasahara & Hinkle, 1976). Therefore, 50 μ l of protein extract was added to 950 μ l 3% (w/v) L- α -phosphatidylcholine and frozen in liquid nitrogen. The in vitro uptake of 0.2 mM (α - 32 P)-AMP (6,000 Ci/mmol; Hartmann Analytic) was performed as described previously (Bernhardt et al., 2012). The transport reaction was terminated by passing through proteoliposomes over Dowex AG1-X8 anion-exchange columns (acetate form, 100-200 mesh, Bio-RAD). The proteoliposomes were eluted with 150 mM sodium acetate (pH 7.2). The nonincorporated AMP was removed by binding to the anion-exchange columns. The incorporated radiolabeled AMP was analyzed by liquid scintillation counting. Time-dependent uptake kinetics was fitted by nonlinear regression, based on one-phase exponential association using GraphPad Prism 5.0 software (GraphPad, www.graphpad.com). Background activities in the absence of recombinant proteins were subtracted. Calculated kinetic parameters were used to determine initial velocities using the equation: $slope = (Plateau - Y_0) \times k$, where Y_0 was set to 0. The values for the *plateau* and *k* were determined from the nonlinear regression analyses using a global fit from three technical replicates.

3 | RESULTS

3.1 | Slc25a17 is an evolutionarily conserved peroxisomal protein

We identified two *slc25a17* genes in zebrafish, *slc25a17* and *slc25a17l* (Figure 1). Sequence analysis suggested that the two predicted proteins shared ~65% identical amino acids, and that Slc25a17 was more closely related to human SLC25A17 (~73% between Slc25a17 and human SLC25A17 vs. ~67% between Slc25a17l and human SLC25A17). Furthermore, six predicted transmembrane domains of Slc25a17 were found to be highly conserved with those of human SLC25A17 (~80% on average show in the figure by highlighting), suggesting functional conservation of SLC25A17 between human and zebrafish, and the transmembrane nature of the proteins. Examination of *slc25a17* and *slc25a17l* expression by in situ hybridization indicated that both the genes are maternally deposited and thus ubiquitously expressed until early segmentation stages (Figure 2a). At 1 dpf, both genes are highly expressed in tissues that become brain and digestive organs, but also weakly expressed throughout the embryo body. Although the expression in the head region seems to decrease at 2 dpf, expression in the deep tissue layer between the embryo body and the yolk remains at least until 5 dpf when it is mostly found in the swim bladder.

Previous reports suggested that SLC25A17 is localized in peroxisomes (Agrimi et al., 2012; Visser et al., 2002). By performing immunostaining of embryos injected with MYC-*slc25a17* mRNA together with GFP-SKL mRNA at one-cell stage, we found that both MYC-Slc25a17 and GFP-SKL proteins are colocalized, implying Slc25a17 to be localized in the peroxisome where GFP is targeted by SKL, the C-terminal

peroxisomal targeting signal sequence (Figure 2b). A similar immunostaining confirmed that Slc25a17l is also peroxisomally targeted.

3.2 | Knockdown of slc25a17 alters the composition of body lipids metabolized in peroxisomes, and impairs embryonic development

To examine the role of Slc25a17 during animal development, we tried to generate a *slc25a17* gene knockout (KO) animal utilizing both the TALEN and CRISPR/CAS9 systems but failed to generate a KO allele. The effect of morpholinos (MOs) in comparison with the use of knockout animal model has reportedly been discussed; a MO is considered a valuable tool provided evidence for its specificity and solid rescue, especially under the condition that no corresponding gene KO animal is available (Stainier et al., 2017). We utilized MOs with *slc25a17* or *slc25a17l* to block the step of either mRNA maturation (splice-MO) or translation (transl-MO). We found that a splice-MO efficiently blocked mRNA maturation by interfering presumably with normal splicing event (Figure 3a). Microinjection of either splice-MO or transl-MO generated embryos with indistinguishable, but robust phenotypes, including short body length compared with control MO-injected embryos, suggesting that both MOs may specifically interfere with Slc25a17 function (Figure 3b). We noticed that *slc25a17* knockdown embryos could be recognized by their voluminous yolks for which we performed oil red-O stain to detect neutral lipids. On or before 3 dpf, oil red-O stain of control embryos was largely detected in the yolk and most embryonic tissues, including brain, heart, and blood vessels (Kim et al., 2014; Schlegel & Stainier, 2006). However, control embryos at 5 dpf consumed most of their yolk lipids and thus no or very low level of oil red-O staining was visible in the yolks (Figure 3b). At 6 dpf, almost all control embryos were completely devoid of yolk lipids and the staining was only detectable in the swim bladder and the head region (250/260 total embryos from three independent experiments). However, the pattern of oil red-O staining changed drastically, especially in the yolk, when MOslc25a17 was injected. A significant percent of the *slc25a17* knockdown embryos retained yolk lipids that could be detected at least at 6 dpf or later, indicating that *slc25a17* knockdown severely impaired the consumption of yolk lipids (45% in the total of 226 embryos from three independent experiments; Figure 3b). We noted that knockdown of *slc25a17l* generated phenotypes essentially the same as those with MOslc25a17 injection, and thus experiments using only MOslc25a17 will hereafter be described, unless indicated.

Given that Slc25a17 acts as a potential peroxisomal transporter of essential cofactors such as CoA, FAD, and NAD⁺, we reasoned that Slc25a17 might play a crucial role in peroxisome number and function. We found that the number of peroxisomes had not changed by *slc25a17* knockdown, as similar levels of the peroxisome-targeted RFP signals between control and MOslc25a17-injected *Tg(ef1a:RFP-SKL)* transgenic embryos were detected (Figure 3c; Kim et al., 2015). To examine peroxisome-dependent functions involved in the oxidation of very long-chain fatty acids and the synthesis of ether phospholipids (also known

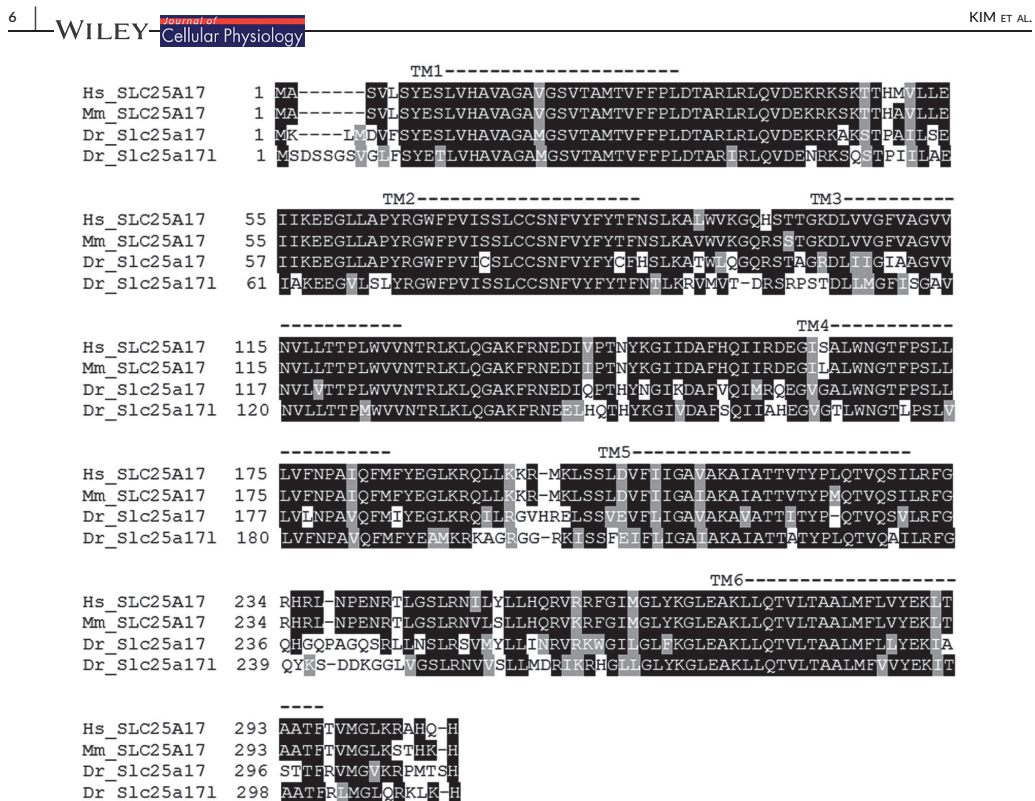


FIGURE 1 Sequence alignment of SLC25A17 orthologs at the amino acid level. SLC25A17 genes are highly conserved among different species in vertebrates. Aligned sequences are human (Hs), mouse (Mm) SLC25A17, zebrafish (Dr) Slc25a17, and Slc25a171 from the top. Amino acids corresponding to the expected six transmembrane domains (TM1-6) are marked by dotted lines at the top of the aligned sequences. Conserved amino acids are shaded in black, and amino acids with similar characteristic are shaded in gray

as plasmalogens), we analyzed the expression of genes involved in fatty acid oxidation or plasmalogen synthesis. Expression of these genes was significantly downregulated in *slc25a17* knockdown embryos compared with age-matched controls, suggesting that peroxisomes might be functionally impaired (Figure 3d).

Impaired expression of the genes involved in fatty acid oxidation and plasmalogen synthesis in peroxisomes was predicted to alter the lipid composition of the body. We found that the amounts of very long-chain fatty acids comprising equal or more than 24 carbons (C) (shown as the ratio of either C24/C22 or C26/C22 fatty acids at 3 dpf and 5 dpf) were significantly increased in *slc25a17* knockdown embryos, compared with those in the control (Figure 4a). Furthermore, the levels of C16, C18, and C18:1 plasmalogens at 2.5 dpf and 3.5 of MO*slc25a17*-injected embryos were significantly decreased as compared with those of control embryos (Figure 4b). These results indicated the involvement of peroxisomal Slc25a17 in the utilization of very long-chain fatty acids, as well as the synthesis of plasmalogens, which is necessary for normal embryonic growth.

In humans, peroxisomal dysfunction leading to metabolic abnormalities, such as accumulation of very long-chain fatty acids and defective plasmalogen synthesis, may induce various neurological abnormalities (Braverman et al., 2016; De Munter, Verheijden, Regal, & Baes, 2015). We found that knockdown of *slc25a17* severely impaired myelination of the peripheral nerves of the head and trunk (Figure 4c), suggesting a crucial role of Slc25a17 in the neuronal development during vertebrate embryogenesis. The role of Slc25a17 in the maturation of nervous system is consistent with the neuronal phenotypes associated with peroxisomal dysfunction in humans (Berger et al., 2016; De Munter et al., 2015; Verheijden, Beckers, De Munter, Van Veldhoven, & Baes, 2014).

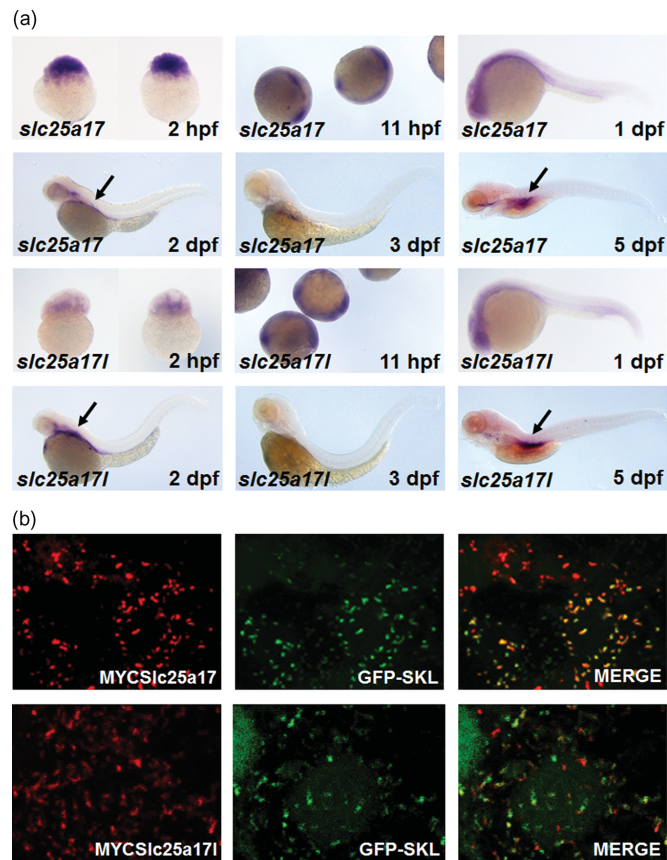
3.3 | Knockdown of *slc25a17* impairs development of multiorgans, including the swim bladder

While observing embryos injected with MO*slc25a17*, we noticed that they did not inflate the swim bladder. In spite of the functional

KIM ET AL.

Journal of
Cellular Physiology WILEY-L7

FIGURE 2 *Slc25a17* transcripts are maternally delivered and their proteins are localized in the peroxisomes. (a) Embryos were processed for whole-mount in situ hybridization to show expression of *slc25a17* or *slc25a17l*. Both genes were maternally expressed (as shown in embryos at 2 hpf) and detected ubiquitously until early segmentation stages (11 hpf) after which they became differentially expressed. At 1 day post fertilization (dpf), both genes were highly expressed in the head region and in cells that were in direct contact with the yolk. At 2 dpf and later, the expression becomes more restricted to the swim bladder (indicated by arrows). (b) In vitro synthesized GFP-SKL together with either MYC-*slc25a17* or MYC-*slc25a17l* mRNAs were microinjected at one-cell stage of zebrafish embryos and the resulting proteins were visualized by immunostaining with anti-MYC antibody (for Slc25a17), or directly by GFP fluorescent signal at 10 hr post fertilization. Merged images show that both Slc25a17 and Slc25a17l are colocalized with peroxisomal GFP-SKL. GFP, green fluorescent protein; mRNA, messenger RNA [Color figure can be viewed at wileyonlinelibrary.com]



difference, both zebrafish swim bladder and alveoli of human lung are composed of three layers of tissues, epithelium, mesenchyme, and mesothelium; and gene expression profiles of the both organs showed striking resemblance (Winata et al., 2009; Zheng et al., 2011). While the control embryos showed a discernible swim bladder, embryos injected with MO*slc25a17* did not inflate the swim bladder at 5 dpf, and even later during development (Figure 5a). To visualize the general morphology of the swim bladder along with its lipid contents, we first performed oil red-O staining and then resected the swim bladder for comparison between the control and MO*slc25a17*-injected embryos. Developing swim bladder at 3 dpf, and older contained neutral lipids that could be detected by the oil red-O stain (Kim et al., 2014; Schlegel & Stainier, 2006). As shown in Figure 5a, bilateral neutral lipids were found abundantly within the swim bladder of control embryos at 3 dpf, became dispersed at 4 dpf, and disappeared along with the inflation of the swim bladder at 5 dpf.

In contrast, *slc25a17* knockdown embryos developed a swim bladder that was similar in shape to the control at 3 dpf, but failed to inflate it at 5 dpf. Notably, *slc25a17*-knockdown embryos contained bilateral lipid droplets that remained even after 5 dpf at which swim bladders of the control embryos normally became inflated, suggesting a critical role for Slc25a17 in lipid metabolism related to swim bladder development.

To further examine the role of Slc25a17 in developing swim bladder, we performed in situ hybridization to analyze the expression of genes involved in swim bladder development. We found that *sox2*, an early marker gene expressed in the pneumatic duct and the epithelial layer of the developing swim bladder, was significantly downregulated upon knockdown of *slc25a17* (Figure 5b). In addition, genes expressed in different layers of the developing swim bladder (*hb9* in epithelium, *acta2* in mesenchyme, and *anxa5* and *hprt1* in outer mesothelium) (Winata et al., 2009) were also severely affected.

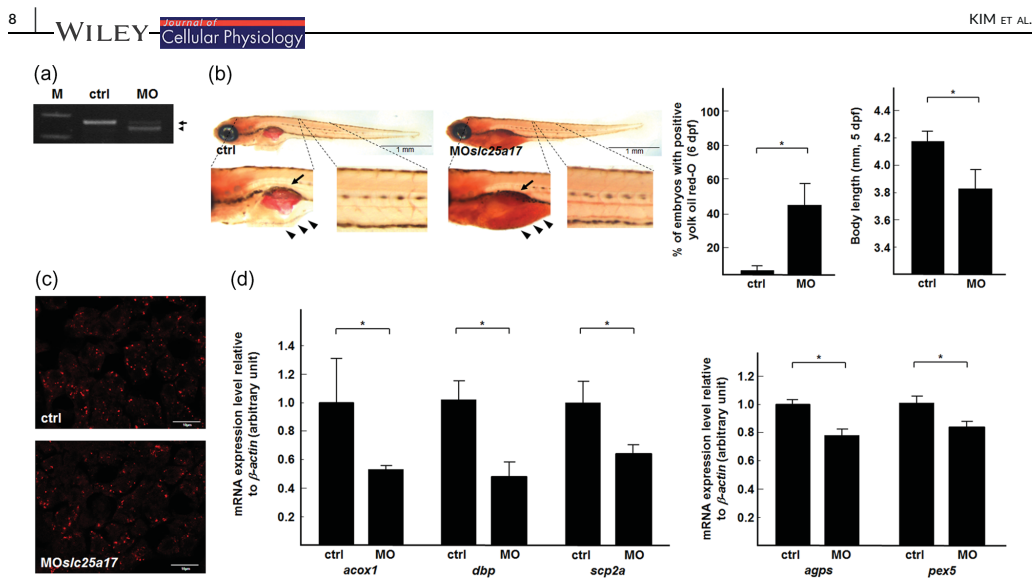


FIGURE 3 Knockdown of *slc25a17* impairs peroxisomal gene expression. (a) Morpholino efficiency test. A splicing morpholino to *slc25a17* was tested for its ability to block the splicing event. Arrow indicates the band with expected size, and arrowhead indicates a mis-spliced band. (b) Control and MOslc25a17-injected embryos were subjected to oil red-O staining at 5 dpf, and were shown laterally with anterior to the left. Arrows point to strongly oil red-O positive swim bladders, and arrowheads to yolk regions. Enlarged pictures are shown to clarify the differential staining between the control and the MOslc25a17-injected embryos. Size bar equals 1 mm. The percentage of the embryos at 6 dpf with positive oil red-O staining in the yolk is presented in a graph after quantification of the results from three independent experiments. The body lengths of embryos at 5 dpf were measured from three independent experiments and the result is presented in a graph. More than 30 experiments ($n > 40$ per condition per experiment) were performed and the phenotype of short body length was consistently observed throughout the study. The percentage of embryos displaying the phenotypes was consistently kept close to 50. (c) RFP signals from the liver samples of Tg(EF1α:RFP-SKL) embryos at 5 dpf injected with either control or MOslc25a17 are shown for comparison. Red puncta represent peroxisomes. Three independent experiments were performed to confirm the result. (d) Expression of peroxisomal genes quantified by qRT-PCR is highly decreased in MOslc25a17-injected embryos. Y-axis represents the mRNA expression levels of peroxisomal genes with reference to that of β-actin. Statistical significance was determined using Student's *t* test in Microsoft Excel, * indicates p value < .05. mRNA, messenger RNA; qRT-PCR, quantitative real-time polymerase chain reaction [Color figure can be viewed at wileyonlinelibrary.com]

Strikingly, the expression of prosaposin b, a member of saposin-like protein superfamily that includes surfactant protein B family, necessary for the integrity and function of the lung surfactant (Zheng et al., 2011), was almost completely abrogated. We noted that the expression of prosaposin b was not affected in other epithelial linings, such as in the kidney tubule, where *slc25a17* was not expressed. This observation indicated a specific role for Slc25a17 in regulating expression of genes involved in swim bladder development.

Since swim bladder is initially derived from cells of the endodermal origin, we asked whether knockdown of *slc25a17* impairs formation of other endodermal organs. We found that expression of *foxa3*, an early marker gene for endodermal organs, including liver, pancreas, and intestine, was significantly decreased in embryos injected with MOslc25a17 (Figure 5c). Consistent with the decreased *foxa3* expression, the size of the liver was also found to be significantly reduced when examined in a transgenic line, Tg(Ifabp:DsRED; Figure 5c). These results indicated the indispensable role of peroxisomal Slc25a17 in regulating genes involved in the

formation and/or growth of endoderm-derived organs, including swim bladder.

3.4 | Overexpression of *slc25a17* increases gene expression in the developing swim bladder

Impaired swim bladder development upon *slc25a17* knockdown prompted us to examine the effect upon *slc25a17* overexpression. Microinjection of in vitro synthesized *slc25a17* mRNA (up to 500 pg) into one-cell stage embryos did not produce any apparent morphological defect in developing embryos. However, we found that overexpression of *slc25a17* upregulated the expression of most swim bladder-related genes within their normal expression domains (Figure 6). One notable exception was the induction of *prosaposin b* whose expression was detected at a strikingly high level in the swim bladder, digestive tract, and the kidney tubule, implying a potential connection between the role of Slc25a17 and of the expression of *prosaposin b*. These results confirmed that Slc25a17 is indeed involved in swim bladder development at least in part by influencing expression of genes.

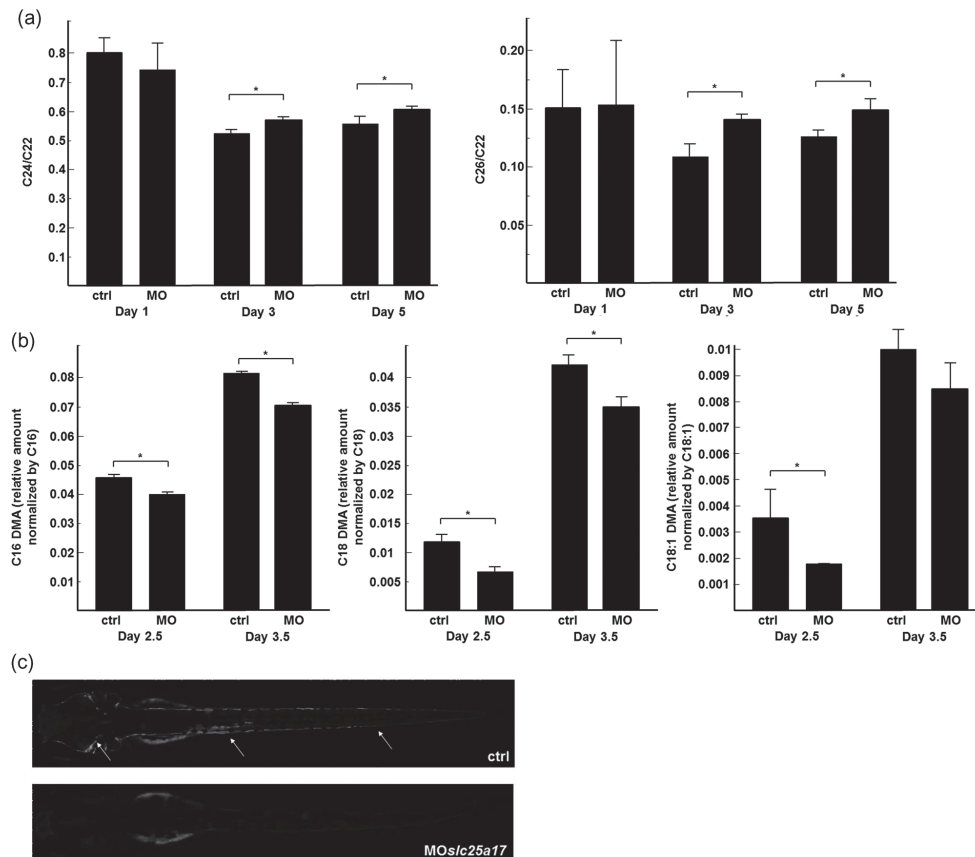


FIGURE 4 Knockdown of *slc25a17* alters the composition of body lipids and impairs nerve myelination. (a,b) The ratio of C24/C22 or C26/C22 very long-chain fatty acids was determined by analyzing total fatty acid extracts from embryos at 1-, 3-, and 5 dpf as indicated. *MOslc25a17*-injected groups at 3- and 5 dpf show accumulated levels of both C24 and C26 very long-chain fatty acids (a). The amounts of C16, C18, and C18:1 ether phospholipids normalized by those of C16, C18 and C18:1 fatty acids were compared between control and *MOslc25a17*-injected groups at 2.5 and 3.5 dpf, and presented in arbitrary units (b). Ether phospholipids analyzed are significantly decreased in *MOslc25a17*-injected groups as compared with those in control. Statistical significance was determined using Student's *t* test in Microsoft Excel, * indicates *p* value < .05. (c) Embryos from crosses of *Tg(mbp:eGFP)* were used to visualize myelination of peripheral nerves of head and trunk regions. Intense GFP signal shown in the control is almost absent in *MOslc25a17*-injected embryos. GFP, green fluorescent protein

3.5 | *Slc25a17* is a CoA transporter

A biochemical study has recently suggested that human SLC25A17 may transport CoA, FAD, and AMP, and potentially NAD^+ and ADP as well (Agrimi et al., 2012). We asked whether zebrafish *Slc25a17* proteins transport molecules similar to those by human orthologue. Liposomes reconstituted with His-tagged *Slc25a17* and *Slc25a17I*, produced using the wheat germ cell-free expression system, were preloaded with either NAD^+ , CoA, or AMP and analyzed for their ability to import radioactively labeled AMP. Both *Slc25a17* carriers mediated high AMP uptake activities against CoA in a time-dependent manner (Figure 7a), similar to the human SLC25A17. To

investigate the substrate specificity of *Slc25a17* and *Slc25a17I*, we determined the initial velocities of the AMP import versus the different internal substrates (Figure 7b). Relative to the AMP/AMP homo-exchange experiments, the highest AMP transport rates for both *Slc25a17* proteins were observed when liposomes were preloaded with CoA. In case of the other tested substrates, such as NAD^+ , ADP, and ATP, the exchange rates were minimal. This result suggested that zebrafish *Slc25a17* and *Slc25a17I* may transport AMP and CoA, but not NAD^+ , ADP, or ATP. This led us to test the possibility that CoA supplementation might rescue the swim bladder phenotype induced by knockdown of *slc25a17*. Indeed, we found that

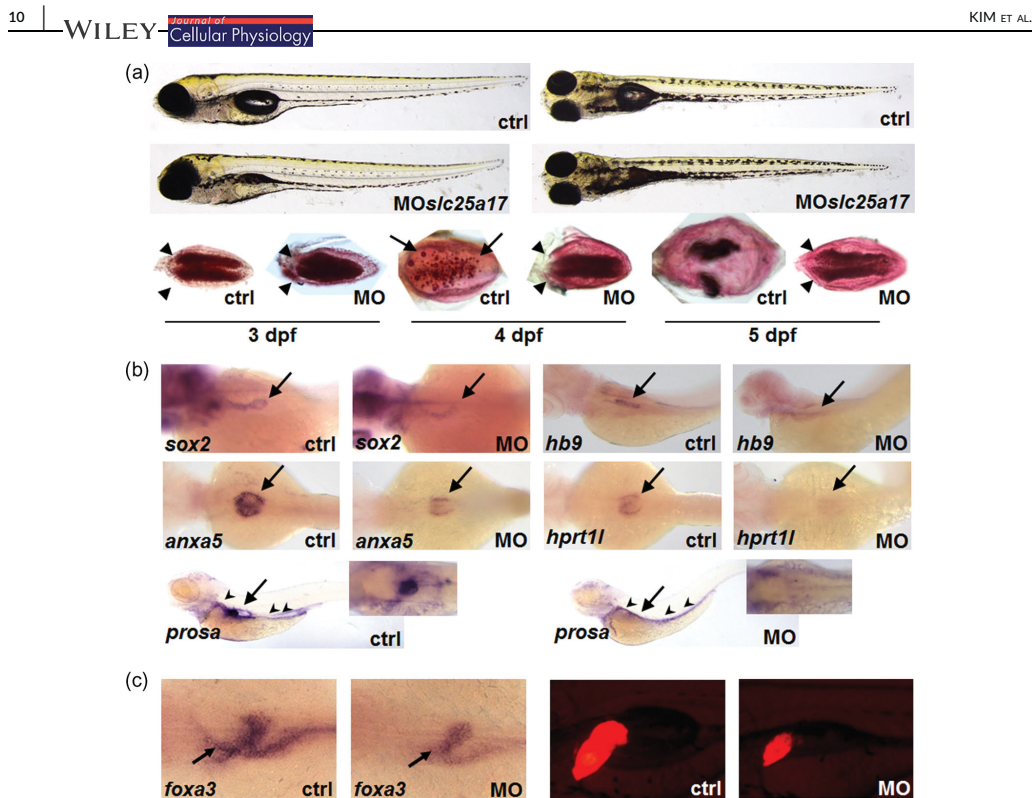


FIGURE 5 Knockdown of *slc25a17* impairs development of endoderm-derived organs including swim bladder. (a) Control and *MOslc25a17*-injected embryos were shown in lateral or ventral views. Note that embryos injected with *MOslc25a17* do not inflate swim bladder. To compare lipid contents of the swim bladder, control and *MOslc25a17*-injected embryos at 3–5 dpf were oil red-O stained and swim bladders were resected. Swim bladders in both control and *MOslc25a17*-injected embryo show bilaterally accumulated lipid droplets pointed by triangular arrowheads at 3 dpf. Lipids in the swim bladder of the control embryos started being dispersed at 4 dpf (indicated by arrows), and completely dissipated at 5 dpf. In contrast, *MOslc25a17*-injected embryos contained accumulated lipids bilaterally within the swim bladder until 5 dpf (marked by triangular arrowheads, 13 embryos out of 24 (54%)). (b) Control and *MOslc25a17*-injected embryos were subjected to in situ hybridization to detect expression of *sox2*, *hb9*, *anxa5*, *hprt1l*, and *prosa* at 36 hpf. Insets are dorsal views of the swim bladder region. Arrows indicate the swim bladder. Embryos were shown in lateral or dorsal views. Note that expression of genes outside of the swim bladder, for examples, *sox2* in pneumatic duct (arrowheads) and *prosa* in pronephric duct (arrowheads), is relatively normal in *MOslc25a17*-injected embryos. Thirty embryos per gene per condition were examined, and the experiment was repeated two times. The number of total affected embryos was between 25 to 39, which corresponds 42–65%. (c) Knockdown of *slc25a17* impairs development of endodermal organs. Embryos injected with *MOslc25a17* were processed with in situ hybridization using the *foxa3* probe that detects developing liver (arrow), pancreas (upper leaflet), and gut (posterior expression) at 36 hpf. Thirty one embryos out of 60 (52%) showed reduced *foxa3* expression. Similarly, transgenic embryos from *Tg(lfabp:DsRED)* were injected with *MOslc25a17* and developing livers were imaged at 3 dpf. About 19 embryos out of 44 (43%) showed reduced liver [Color figure can be viewed at wileyonlinelibrary.com]

coinjecting CoA together with either *MOslc25a17* or *MOslc25a17l* efficiently restored the swim bladder to its normal state (Figure 7c). Since it is plausible that the phenotypic rescue observed by CoA injection could result from an increased expression of either *slc25a17* or *slc25a17l* gene, rather than a transport of injected CoA into the peroxisome, we tested whether CoA injection regulates expression of *slc25a17* genes. Injecting CoA did not change the expression levels of both *slc25a17* and *slc25a17l* (Figure 7d). In addition, knockdown of CoA synthase did not alter the expression levels of both *slc25a17* and

slc25a17l (Figure 7e). Since a previous report suggested that NAD^+ is a potential solute to be transported by *Slc25a17*, we tested whether increasing NAD^+ levels could rescue the phenotype induced by *slc25a17* knockdown. However, we were unable to rescue phenotypes associated with *slc25a17* knockdown by coinjecting various concentrations of NAD^+ (Figure 7f). The existence of MDH1 in peroxisomes was recently reported through a proteomics study (Gronemeyer et al., 2013), and we reasoned that forced peroxisomal expression of MDH1a may re-establish normal NAD^+ levels in

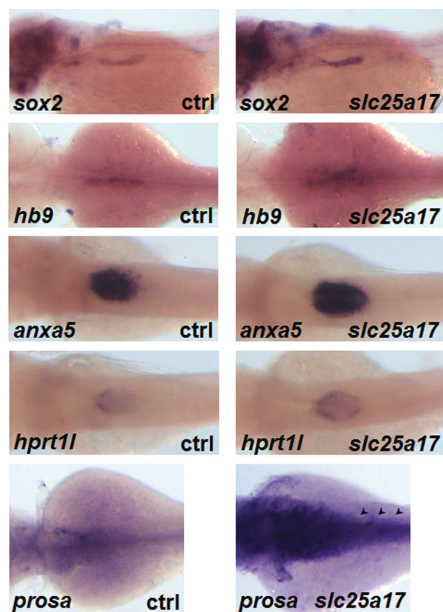


FIGURE 6 Overexpression of *slc25a17* upregulates genes expressed in developing swim bladder. Embryos injected with either GFP or *slc25a17* mRNA were subjected to in situ hybridization. Expression of genes in developing swim bladder, such as *sox2*, *hb9*, *anxa5*, *hpert1l*, and *prosapin b* (*prosa*) at 36 hpf is shown in lateral or dorsal views with anterior to the left. Note that expression of *prosapin b* is highly induced, not only in the swim bladder, but also in posterior pronephric duct (arrowheads). Thirty embryos per gene per condition were examined, and the experiment was repeated two times. The number of embryos with increased gene expression was all ranged between 55 and 60, which corresponds 92–100%. GFP, green fluorescent protein; mRNA, messenger RNA [Color figure can be viewed at wileyonlinelibrary.com]

peroxisomes upon *slc25a17* knockdown. However, we found that coinjection of *mdh1a*-SKL mRNA together with *MOslc25a17* also failed to rescue defective swim bladder in response to *slc25a17* knockdown (Figure 7). These results suggested that Slc25a17 acts as a peroxisomal CoA transporter with its expression being regulated independently of the subcellular CoA levels.

Since both *slc25a17* and *slc25a17l* induce indistinguishable embryonic phenotypes, we asked whether these genes act redundantly during zebrafish embryonic development by performing a mutual rescue experiment of microinjecting mRNA of one gene together with MO of the other. Combination of mRNA of one gene and MO of the other almost completely rescued the swim bladder phenotype (Figure 7g), suggesting that both genes act similarly to promote normal embryogenesis. Given that knockdown of either *slc25a17* or *slc25a17l* generated a phenotype, the amount of total Slc25a17 (Slc25a17 + Slc25a17l) might be an important determinant

to ensure proper functioning of peroxisomes in the swim bladder development during zebrafish embryogenesis.

4 | DISCUSSION

Peroxisomes are thought to participate in the control of cellular metabolism by assisting mitochondrial β -oxidation (Schrader, Costello, Godinho, & Islinger, 2015), influencing autophagy (Zhang et al., 2015), and generating and decaying ROS (Fransen, Lismont, & Walton, 2017), all of which may integrate into maintenance of the cellular homeostasis. These roles of the peroxisome are highlighted by human disorders related to defective peroxisome biogenesis or dysfunctional enzymes (Braverman et al., 2016; Fujiki et al., 2012). Although, the recent focus has been on elucidation of the roles of peroxisomes in cellular metabolism, incomplete understanding of an individual molecule located in the peroxisome often precludes further mechanistic insights into an interorganelle interaction, which may presumably be one of the most important factors determining cellular health and metabolic responses. In an effort to characterize the unidentified roles of *slc25a17* in vivo, we utilized the zebrafish as an animal model and examined its role during embryogenesis.

Slc25a17 was reported to localize in the peroxisomes, and belongs to the mitochondrial solute carriers that transport various molecules across the mitochondrial membranes (Berger et al., 2016). In agreement, a recent biochemical study suggested that human SLC25A17 transports CoA, NAD⁺, and FAD as primary solutes across the peroxisomal membrane (Palmieri, 2013). In this report, we identified duplicated zebrafish *slc25a17* genes and characterized their roles during vertebrate embryogenesis. Specifically, we found that knockdown of either *slc25a17* or *slc25a17l* gene impairs normal growth by interfering with lipid metabolism during embryogenesis. Consequently, knockdown of *slc25a17* resulted in increased levels of very long-chain fatty acids and reduced levels of ether phospholipids that serve as clinical hallmarks of Zellweger patients (Brown et al., 1982; Heymans, Schutgens, Tan, van den Bosch, & Borst, 1983). Either accumulation of very long-chain fatty acids (Hein, Schonfeld, Kahlert, & Reiser, 2008) or defective ether lipid synthesis (Dorninger, Forss-Petter, & Berger, 2017) has reportedly been a cause for hypomyelination and/or demyelination, and accordingly, we observed a profound defect in myelin deposition. In accordance with defective neural function, *MOslc25a17*-injected zebrafish prone to lie sideways without showing much swimming activity (not shown). However, *MOslc25a17*-injected zebrafish showed a touch-evoked escape response, and we tried to determine whether lack of swim bladder inflation is due to impaired swimming. We placed them in a dish containing very little water and let them swim to gulp air from the water–air interface, but failed to make them inflate their swim bladders. Deduced from defective gene expression involved in swim bladder development in *MOslc25a17*-injected zebrafish (Figure 5), we concluded that defective neural function has a minimal role in the failure of swim bladder inflation in *MOslc25a17*-injected zebrafish.

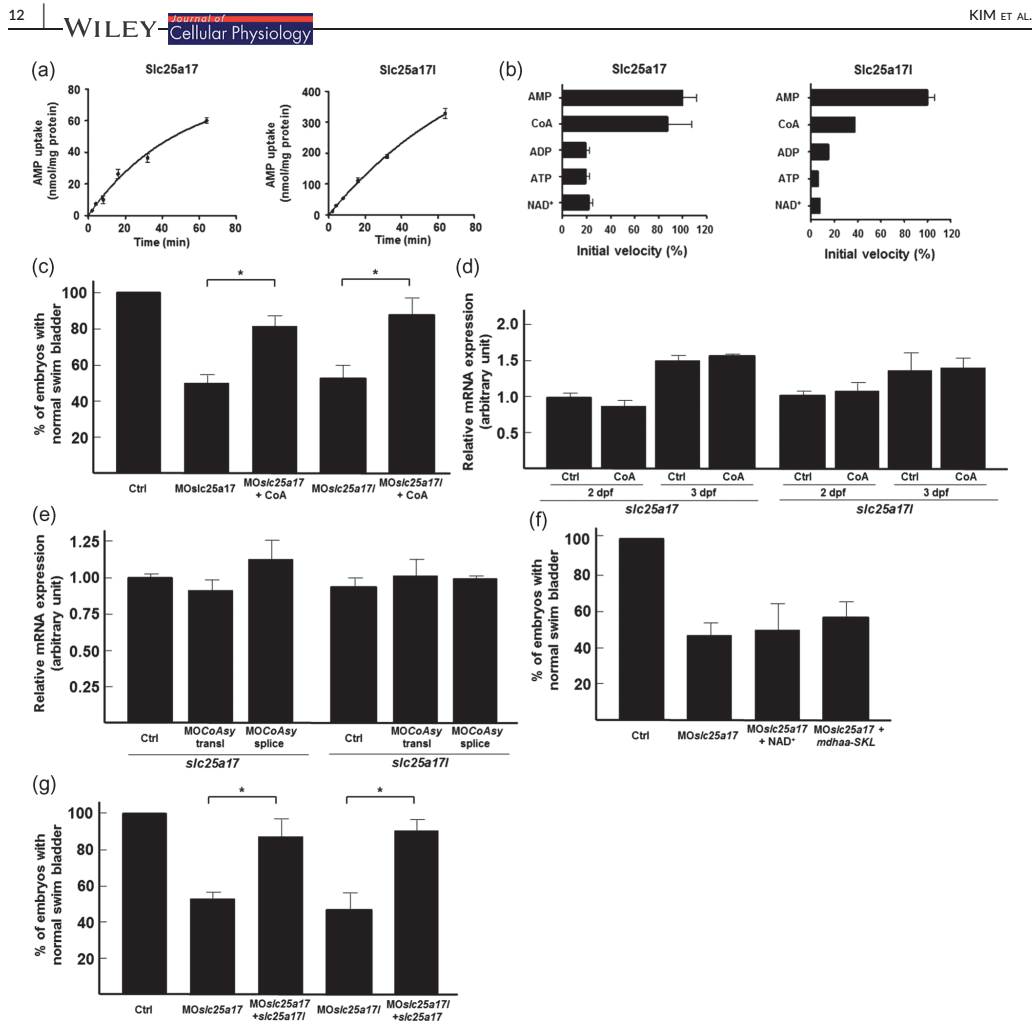


FIGURE 7 Slc25a17 carrier protein acts as a coenzyme A transporter. (a) Time-dependent uptake of radioactively labeled (α -³²P)-AMP (0.2 mM) was measured in liposomes reconstituted with His-tagged Slc25a17 (left panel) and Slc25a17i (right panel). Liposomes were preloaded with 10 mM CoA as counter-exchange substrate. Both graphs represent the arithmetic means \pm SEs of technical triplicates. (b) Initial velocities of SLC25A17 and Slc25a17i for the import of AMP against various exchange substrates. Liposomes were internally loaded with AMP, CoA, ADP, ATP, and NAD⁺ (10 mM). These liposomes were reconstituted with SLC25A17-His (left panel) or Slc25a17i-His (right panel). The time-dependent uptake of (α -³²P)-AMP (0.2 mM) into liposomes was measured. The initial velocity was determined by nonlinear regression analyses. The data shown here represent arithmetic means \pm SEs of technical triplicates. (c) Embryos injected with either MOslc25a17 or MOslc25a17i alone or together with CoA were counted for the presence of normal swim bladder, which was expressed as % of the total number of embryos injected. (d) Expression levels of *slc25a17* and *slc25a17i* in response to CoA injection were analyzed in 2- and 3 dpf and presented in arbitrary units with reference to those of β -actin. Statistical significance was determined using Student's *t* test in Microsoft Excel. (e) Expression of *slc25a17* and *slc25a17i* upon knockdown of CoA synthase in reference to that of β -actin was presented in arbitrary units. Statistical significance was determined using Student's *t* test in Microsoft Excel. (f) Embryos injected with either MOslc25a17 or together with either NAD⁺ or *mdh1aa-SKL* mRNA were counted for the presence of normal swim bladder, which was expressed as % of the total injected number of embryos. (g) Embryos injected with MOslc25a17 alone or together with *slc25a17i* mRNA were examined for the presence of their swim bladder, which was expressed as % of the total injected number of embryos. A reciprocal rescue experiment was also performed with MOslc25a17i together with *slc25a17*. Rescue experiments (c,f,g) were performed at least three times with the minimum of 40 embryos per condition per experiment. Statistical significance was determined using Student's *t* test in Microsoft Excel, *indicates *p* value < .05. ADP, adenosine diphosphate; AMP, adenosine monophosphate; ATP, adenosine triphosphate; CoA, coenzyme A; mRNA, messenger RNA; NAD⁺, nicotinamide adenine dinucleotide

Interestingly, disturbance in cellular lipid metabolism upon *slc25a17* knockdown may also induce changes in the expression of peroxisomal genes, although the exact mechanism awaits further investigation. One possibility is that dysregulated lipid metabolism and altered metabolites may perturb the transcriptional repertoire of the major metabolic genes, which in turn reduces peroxisomal gene expression. Such metabolic dynamics in response to partial yolk depletion in zebrafish has recently been reported (Huang & Linsen, 2015). Alternatively, it is also plausible that an impaired peroxisomal CoA transport may impact the activities of other intracellular organelles including mitochondria, endoplasmic reticulum, and lysosomes, which in turn alters transcriptional response. Consequences and importance of molecular interactions between intracellular organelles are being characterized (Islinger et al., 2018).

A number of factors may result in defective swim bladder upon the knockdown of *slc25a17*, and we reasoned that dysregulation of lipid metabolism may cause, at least in part, the *MOslc25a17*-mediated swim bladder defect. Although it was technically not suitable to analyze differential amounts of lipid components in developing swim bladders between normal and *slc25a17* knockdown embryos, dissected swim bladders after oil red-O stain of *MOslc25a17*-injected embryos showed a comparable level of lipid droplets in the control embryos during the initial phase of swim bladder development. However, the fact that the lipid droplets in *MOslc25a17*-injected embryos remained for a period long after inflation of swim bladder as opposed to those in control embryos suggested that lipid metabolism required for swim bladder development was hampered upon knockdown of *slc25a17*. Interestingly, we have recently reported that alterations in the lipid profiles of the body by knockdown of *elov1* (thus inhibiting the synthesis of long-chain fatty acids) also impaired swim bladder inflation (Bhandari et al., 2016). Moreover, the fact that the *elov1* genes are strongly expressed in the swim bladder suggests that balanced actions between fatty acid synthesis and degradation are critical for normal swim bladder development in zebrafish. In this regard, defective swim bladder inflation may, at least partially, be attributed to impaired yolk consumption observed in zebrafish embryos with *slc25a17* knockdown. It is reasonable that yolk consumption during early embryonic development in zebrafish involves not only lipoproteins and lipid-modifying enzymes to process yolk lipids (Miyares et al., 2014; Pickart et al., 2006; Schlegel & Stainier, 2006), but also enzymes involved in the oxidation of fatty acids. Indeed, we have reported that knockdown of D-bifunctional protein (*dbp*), a gene involved in peroxisomal fatty acid β -oxidation, generates a zebrafish embryo with delayed yolk consumption and impaired swim bladder inflation, a phenotype similar to that upon *slc25a17* knockdown (Kim et al., 2014). As oxidation of long-chain and very-long-chain fatty acids requires a concerted action between mitochondrial and peroxisomal enzymes, it will be interesting to examine whether mitochondrial fatty acid β -oxidation is also involved in yolk consumption and thus swim bladder development. In an evolutionary perspective, an interesting study

reported that swim bladder in zebrafish shares regulatory and molecular characteristics with the lungs in mammals (Zheng et al., 2011). Given the importance of lipid metabolism for proper alveolar functions such as synthesis of pulmonary surfactants and lipids (Perez-Gil, 2008; Torday & Rehan, 2016), detailed analysis on the *Slc25a17*-dependent regulatory mechanisms during swim bladder development may provide a clue to the pulmonary pathogenesis involving peroxisome dysfunction in humans.

Lastly, to determine the primary solute that *Slc25a17* transports across the peroxisomal membrane, we first performed an in vitro transport assay and found that *Slc25a17* transports CoA more effectively than NAD^+ . We then performed an in vivo rescue experiment, and found that exogenously supplied CoA efficiently rescued developmental defects, whereas increasing NAD^+ levels either exogenously or endogenously failed to rescue phenotypes associated with *slc25a17* knockdown. We proposed *Slc25a17* to be a major regulator of CoA levels in peroxisomes, but cannot completely rule out its minor role in transporting other solutes such as NAD^+ as previously suggested (Agrimi et al., 2012).

In humans, defective peroxisomes are closely linked to developmental delay and growth retardation (Baumgart et al., 2001; Kim et al., 2014; Schrader et al., 2015; Wanders, 2014). Although it is plausible that the well-known functions of peroxisomes, including β -oxidation, ether phospholipid synthesis and ROS decay, may be responsible for the clinical manifestations, recent studies suggested that the unidentified roles for peroxisomes may prove critical under different environments (Delmaghani et al., 2015; Zhang et al., 2015). The supporting role of peroxisomes as a signaling platform that links the ROS challenge to the cellular energy status has been reported (Zhang et al., 2013). Due to the paucity of developmental studies in vertebrates, from the view of cellular homeostasis associated with the peroxisomes, our effort to understand the molecular role of a peroxisomal protein during zebrafish embryogenesis may provide a unique opportunity to investigate the unappreciated roles of peroxisomes during animal development.

In conclusion, we have characterized the duplicated zebrafish *slc25a17* genes, both of which may act additively, yet similarly to promote the expression of genes necessary for the development of swim bladder, and also potentially for neuronal development and other internal organs. This is to our knowledge the first characterization of the in vivo role of *Slc25a17* as a peroxisomal CoA transporter, which helps in the maintenance of functional peroxisomes, and thus is essential for normal animal development.

ACKNOWLEDGMENTS

We thank Dr. Zhiyuan Gong for sharing constructs to synthesize in situ probes. We also thank members of Dr. S-K Choe laboratory for sharing materials and providing constructive comments on this project. This study was supported by the grants NRF-2016R1A2B4009129, NRF-2014M3A9D8034463, and MOF-20180430 given to S.-K.C., and DFG1871/1-2 to N.L. South Korea. Email: seongkyu642@wku.ac.kr.

CONFLICTS OF INTEREST

The authors declare that they have no conflict of interests.

AUTHOR CONTRIBUTIONS

S.-K. C. and R. P. conceived and designed the experiments; Y.-I. K., I.-K. N., D.-K. L., S. B., L. C., S. K., J.-Y. L., K. H., S.-J., and J. N. L. performed experiments; H.-S. S., N. L., and S.-K. C. analyzed data; N. L., R. P. and S.-K. C. wrote the manuscript.

ORCID

Seong-Kyu Choe  <http://orcid.org/0000-0002-2102-973X>

REFERENCES

- Agrimi, G., Russo, A., Scarcia, P., & Palmieri, F. (2012). The human gene SLC25A17 encodes a peroxisomal transporter of coenzyme A, FAD and NAD⁺. *Biochemical Journal*, 443(1), 241–247. <https://doi.org/10.1042/BJ20111420>
- Baumgart, E., Vanhorebeek, I., Grabenbauer, M., Borgers, M., Declercq, P. E., Fahimi, H. D., & Baes, M. (2001). Mitochondrial alterations caused by defective peroxisomal biogenesis in a mouse model for Zellweger syndrome (PEX5 knockout mouse). *American Journal of Pathology*, 159(4), 1477–1494. [https://doi.org/10.1016/S0002-9440\(10\)62534-5](https://doi.org/10.1016/S0002-9440(10)62534-5)
- Berger, J., Dorninger, F., Forss-Petter, S., & Kunze, M. (2016). Peroxisomes in brain development and function. *Biochimica Et Biophysica Acta-Molecular Cell Research*, 1863(5), 934–955. <https://doi.org/10.1016/j.bbamcr.2015.12.005>
- Bernhardt, K., Wilkinson, S., Weber, A. P. M., & Linka, N. (2012). A peroxisomal carrier delivers NAD plus and contributes to optimal fatty acid degradation during storage oil mobilization. *Plant Journal*, 69(1), 1–13. <https://doi.org/10.1111/j.1365-313X.2011.04775.x>doi:DOI
- Bhandari, S., Lee, J. N., Kim, Y. I., Nam, I. K., Kim, S. J., Kim, S. J., ... Park, R. (2016). The fatty acid chain elongase, Elov1, is required for kidney and swim bladder development during zebrafish embryogenesis. *Organogenesis*, 12(2), 78–93. <https://doi.org/10.1080/15476278.2016.1172164>
- Braverman, N. E., Raymond, G. V., Rizzo, W. B., Moser, A. B., Wilkinson, M. E., Stone, E. M., ... Bose, M. (2016). Peroxisome biogenesis disorders in the Zellweger spectrum: An overview of current diagnosis, clinical manifestations, and treatment guidelines. *Molecular Genetics and Metabolism*, 117(3), 313–321. <https://doi.org/10.1016/j.ymgme.2015.12.009>
- Brown, F. R., 3rd, McAdams, A. J., Cummins, J. W., Konkol, R., Singh, I., Moser, A. B., & Moser, H. W. (1982). Cerebro-hepato-renal (Zellweger) syndrome and neonatal adrenoleukodystrophy: Similarities in phenotype and accumulation of very long chain fatty acids. *Johns Hopkins Medical Journal*. *JHMJAX*, 151(6), 344–351 <http://www.ncbi.nlm.nih.gov/pubmed/7176294>
- Delille, H. K., Bonekamp, N. A., & Schrader, M. (2006). Peroxisomes and disease - an overview. *International Journal of Biomedical Science*, 2(4), 308–314 <http://www.ncbi.nlm.nih.gov/pubmed/23674998>
- Delmagnani, S., Defourny, J., Aghaie, A., Beurg, M., Dulon, D., Thelen, N., ... Petit, C. (2015). Hypervulnerability to sound exposure through impaired adaptive proliferation of peroxisomes. *Cell*, 163(4), 894–906. <https://doi.org/10.1016/j.cell.2015.10.023>
- Dorninger, F., Forss-Petter, S., & Berger, J. (2017). From peroxisomal disorders to common neurodegenerative diseases - the role of ether phospholipids in the nervous system. *FEBS Letters*, 591(18), 2761–2788. <https://doi.org/10.1002/1873-3468.12788>
- Fransen, M., Lismont, C., & Walton, P. (2017). The peroxisome-mitochondria connection: How and why? *International Journal of Molecular Sciences*, 18(6), 1126. <https://doi.org/10.3390/Ijms18061126doi:Artn 1126>
- Fujiki, Y., Yagita, Y., & Matsuzaki, T. (2012). Peroxisome biogenesis disorders: Molecular basis for impaired peroxisomal membrane assembly: In metabolic functions and biogenesis of peroxisomes in health and disease. *Biochimica et Biophysica Acta/General Subjects*, 1822(9), 1337–1342. <https://doi.org/10.1016/j.bbadis.2012.06.004>
- Gronemeyer, T., Wiese, S., Ofman, R., Bunse, C., Pawlas, M., Hayen, H., ... Warscheid, B. (2013). The Proteome of human liver peroxisomes: Identification of five new peroxisomal constituents by a label-free quantitative proteomics survey. *PLoS One*, 8(2), e57395. <https://doi.org/10.1371/journal.pone.0057395doi:ARTN e57395>
- Gutierrez-Aguilar, M., & Baines, C. P. (2013). Physiological and pathological roles of mitochondrial SLC25 carriers. *Biochemical Journal*, 454, 371–386. <https://doi.org/10.1042/BJ20121753>
- Hediger, M. A., Clemencón, B., Burrier, R. E., & Bruford, E. A. (2013). The ABCs of membrane transporters in health and disease (SLC series): Introduction. *Molecular Aspects of Medicine*, 34(2-3), 95–107. <https://doi.org/10.1016/j.mam.2012.12.009>
- Hein, S., Schonfeld, P., Kahlert, S., & Reiser, G. (2008). Toxic effects of X-linked adrenoleukodystrophy-associated, very long chain fatty acids on glial cells and neurons from rat hippocampus in culture. *Human Molecular Genetics*, 17(12), 1750–1761. <https://doi.org/10.1093/hmg/ddn066>
- Heymans, H. S., Schutgens, R. B., Tan, R., vanden Bosch, H., & Borst, P. (1983). Severe plasmalogen deficiency in tissues of infants without peroxisomes (Zellweger syndrome). *Nature*, 306(5938), 69–70 <http://www.ncbi.nlm.nih.gov/pubmed/6633659>
- Huang, Y., & Linsen, S. E. (2015). Partial depletion of yolk during zebrafish embryogenesis changes the dynamics of methionine cycle and metabolic genes. *BMC Genomics*, 16, 427. <https://doi.org/10.1186/s12864-015-1654-6>
- Islinger, M., Voelkl, A., Fahimi, H. D., & Schrader, M. (2018). The peroxisome: An update on mysteries 2.0. *Histochemistry and Cell Biology*, 150(5), 443–471. <https://doi.org/10.1007/s00418-018-1722-5>
- Kasahara, M., & Hinkle, P. C. (1976). Reconstitution of D-glucose transport catalyzed by a protein fraction from human erythrocytes in sonicated liposomes. *Proceedings of the National Academy of Sciences of the United States of America*, 73(2), 396–400 <http://www.ncbi.nlm.nih.gov/pubmed/1061142>
- Kim, Y. I., Bhandari, S., Lee, J. N., Yoo, K. W., Kim, S. J., Oh, G. S., ... Choe, S. K. (2014). Developmental roles of D-bifunctional protein-A Zebrafish model of peroxisome dysfunction. *Molecules and Cells*, 37(1), 74–80. <https://doi.org/10.14348/molcells.2014.2300>
- Kim, Y. I., Lee, J. N., Bhandari, S., Nam, I. K., Yoo, K. W., Kim, S. J., ... Park, R. (2015). Cartilage development requires the function of estrogen-related receptor alpha that directly regulates sox9 expression in zebrafish. *Scientific Reports*, 5, <https://doi.org/10.1038/Srep18011doi:Artn 18011>
- Kimmel, C. B., Ballard, W. W., Kimmel, S. R., Ullmann, B., & Schilling, T. F. (1995). Stages of embryonic development of the zebrafish. *Developmental Dynamics*, 203(3), 253–310. <https://doi.org/10.1002/aja.1002030302>
- Lieschke, G. J., & Currie, P. D. (2007). Animal models of human disease: Zebrafish swim into view. *Nature Reviews Genetics*, 8(5), 353–367. <https://doi.org/10.1038/nrg2091>
- Lodhi, I. J., & Semenkovich, C. F. (2014). Peroxisomes: A nexus for lipid metabolism and cellular signaling. *Cell Metabolism*, 19(3), 380–392. <https://doi.org/10.1016/j.cmet.2014.01.002>
- Miyares, R. L., deRezende, V. B., & Farber, S. A. (2014). Zebrafish yolk lipid processing: A tractable tool for the study of vertebrate lipid transport and metabolism. *Disease Models & Mechanisms*, 7(7), 915–927. <https://doi.org/10.1242/dmm.015800>
- DeMunter, S., Verheijden, S., Regal, L., & Baes, M. (2015). Peroxisomal disorders: A review on cerebellar pathologies. *Brain Pathology*, 25(6), 663–678. <https://doi.org/10.1111/bpa.12290>

- Palmieri, F. (2013). The mitochondrial transporter family SLC25: Identification, properties and physiopathology. *Molecular Aspects of Medicine*, 34(2-3), 465–484. <https://doi.org/10.1016/j.mam.2012.05.005>
- Perez-Gil, J. (2008). Structure of pulmonary surfactant membranes and films: The role of proteins and lipid-protein interactions. *Biochimica et Biophysica Acta-Biomembranes*, 1778(7-8), 1676–1695. <https://doi.org/10.1016/j.bbamem.2008.05.003>
- Pickart, M. A., Klee, E. W., Nielsen, A. L., Sivasubbu, S., Mendenhall, E. M., Bill, B. R., ... Ekker, S. C. (2006). Genome-wide reverse genetics framework to identify novel functions of the vertebrate secretome. *PLoS One*, 1, e104. <https://doi.org/10.1371/journal.pone.0000104>
- Schlegel, A., & Stainier, D. Y. R. (2006). Microsomal triglyceride transfer protein is required for yolk lipid utilization and absorption of dietary lipids in zebrafish larvae. *Biochemistry*, 45(51), 15179–15187. <https://doi.org/10.1021/bi0619268>
- Schrader, M., Costello, J., Godinho, L. F., & Islinger, M. (2015). Peroxisome-mitochondria interplay and disease. *Journal of Inherited Metabolic Disease*, 38(4), 681–702. <https://doi.org/10.1007/s10545-015-9819-7>
- Stainier, D. Y. R., Raz, E., Lawson, N. D., Ekker, S. C., Burdine, R. D., Eisen, J. S., ... Moens, C. B. (2017). Guidelines for morpholino use in zebrafish. *PLoS Genetics*, 13(10), e1007000. <https://doi.org/10.1371/journal.pgen.1007000>
- Torday, J. S., & Rehan, V. K. (2016). On the evolution of the pulmonary alveolar lipofibroblast. *Experimental Cell Research*, 340(2), 215–219. <https://doi.org/10.1016/j.yexcr.2015.12.004>
- Vamecq, J., Cherkaoui-Malki, M., Andreoletti, P., & Latruffe, N. (2014). The human peroxisome in health and disease: The story of an oddity becoming a vital organelle. *Biochimie*, 98, 4–15. <https://doi.org/10.1016/j.biochi.2013.09.019>
- Verheijden, S., Beckers, L., DeMunter, S., VanVeldhoven, P. P., & Baes, M. (2014). Central nervous system pathology in MFP2 deficiency: Insights from general and conditional knockout mouse models. *Biochimie*, 98, 119–126. <https://doi.org/10.1016/j.biochi.2013.08.009>
- Visser, W. F., vanRoermund, C. W. T., Ijst, L., Waterham, H. R., & Wanders, R. J. A. (2007). Metabolite transport across the peroxisomal membrane. *Biochemical Journal*, 401, 365–375. <https://doi.org/10.1042/Bj20061352>
- Visser, W. F., vanRoermund, C. W. T., Waterham, H. R., & Wanders, R. J. A. (2002). Identification of human PMP34 as a peroxisomal ATP transporter. *Biochemical and Biophysical Research Communications*, 299(3), 494–497. [https://doi.org/10.1016/S0006-291x\(02\)02663-3](https://doi.org/10.1016/S0006-291x(02)02663-3)
- Wanders, R. J. (2014). Metabolic functions of peroxisomes in health and disease. *Biochimie*, 98, 36–44. <https://doi.org/10.1016/j.biochi.2013.08.022>
- Waterham, H. R., & Wanders, R. J. (2012). Metabolic functions and biogenesis of peroxisomes in health and disease. *Biochimica et Biophysica Acta-General Subjects*, 1822(9), 1325. <https://doi.org/10.1016/j.bbadis.2012.06.001>
- Winata, C. L., Korzh, S., Kondrychyn, I., Zheng, W. L., Korzh, V., & Gong, Z. Y. (2009). Development of zebrafish swimbladder: The requirement of Hedgehog signaling in specification and organization of the three tissue layers. *Developmental Biology*, 331(2), 222–236. <https://doi.org/10.1016/j.ydbio.2009.04.035>
- Wyllin, T., Baes, M., Brees, C., Mannaerts, G. P., Fransen, M., & VanVeldhoven, P. P. (1998). Identification and characterization of human PMP34, a protein closely related to the peroxisomal integral membrane protein PMP47 of *Candida boydii*. *European Journal of Biochemistry*, 258(2), 332–338. <https://doi.org/10.1046/j.1432-1327.1998.2580332.x>
- Zhang, J. W., Kim, J., Alexander, A., Cai, S. L., Tripathi, D. N., Dere, R., ... Walker, C. L. (2013). A tuberous sclerosis complex signalling node at the peroxisome regulates mTORC1 and autophagy in response to ROS. *Nature Cell Biology*, 15(10), 1186–U1145. <https://doi.org/10.1038/ncb2822>
- Zhang, J. W., Tripathi, D. N., Jing, J., Alexander, A., Kim, J., Powell, R. T., ... Walker, C. L. (2015). ATM functions at the peroxisome to induce pexophagy in response to ROS. *Nature Cell Biology*, 17(10), 1259–1269. <https://doi.org/10.1038/ncb3230>
- Zheng, W. L., Wang, Z. Y., Collins, J. E., Andrews, R. M., Stemple, D., & Gong, Z. Y. (2011). Comparative transcriptome analyses indicate molecular homology of zebrafish swimbladder and mammalian lung. *PLoS One*, 6(8), e24019. <https://doi.org/10.1371/journal.pone.0024019>

How to cite this article: Kim Y-I, Nam I-K, Lee D-K, et al. Slc25a17 acts as a peroxisomal coenzyme A transporter and regulates multiorgan development in zebrafish. *J Cell Physiol.* 2019;1–15. <https://doi.org/10.1002/jcp.28954>

Author contribution

Lennart Charton did the cloning of Slc25a17 and Slc25a17l constructs for heterologous protein expression and conducted the protein expression followed by uptake experiments with determination of substrate specificity as shown in Figure 7a and 7b.

IV. Published Manuscripts

IV.IV Published Manuscript 4

Analysis of peroxisomal β -oxidation during storage oil mobilization in *Arabidopsis thaliana* seedlings

Björn Hielscher¹, Lennart Charton¹, Tabea Mettler-Altmann¹ and Nicole Linka^{1,2}

¹ Institute for Plant Biochemistry and Cluster of Excellence on Plant Sciences (CEPLAS), Heinrich Heine University, Universitätsstrasse 1, 40225 Düsseldorf, Germany.

² To whom correspondence should be addressed.

i. Summary

Peroxisomal β -oxidation in plants is essential for mobilization of storage oil in seed-oil storing plants, such as *Arabidopsis thaliana*. In plants, degradation of fatty acids occurs exclusively in peroxisomes via the β -oxidation, driving seedling growth and development upon germination. Thus, the determination of storage oil breakdown rates is a useful approach to investigate defects in peroxisomal β -oxidation. Here we describe an acid catalyzed derivatization process of fatty acids representing a fast and efficient procedure to generate high yields of fatty acid methyl esters (FAMES). The subsequent analysis by gas-chromatography coupled to mass spectrometry (GC-MS) allows the quantification of total fatty acid content. The results provide detailed information of the complete storage oil breakdown process via peroxisomal β -oxidation during seedling growth.

ii. Key Words

Plant seedling, storage oil mobilization, peroxisomes, fatty acid β -oxidation

1. Introduction

Plants accumulate storage molecules during seed maturation in order to provide energy for post-germinative heterotrophic seedling establishment [1]. Depending on the plant species, these molecules can be divided in three major classes: carbohydrates, oil and proteins. But the storage of oil in the form of triacylglyceroles (TAGs), sequestered in cytosolic oil bodies, is arguable the most widely distributed strategy in nature. In the model oilseed plant *Arabidopsis thaliana* (*Arabidopsis*) the amount of TAGs can account for up to 60 % of seed weight and their complete oxidation yields more than twice the energy of carbohydrates and proteins [2]. Thus,

Arabidopsis has been instrumental in investigating molecular mechanisms involved in lipid metabolism [3]. Storage oil reserves are degraded within the first days after imbibition, providing energy until the seedlings become photoautotrophic [4] (Fig. 1).

In contrast to mammals, peroxisomal β -oxidation is the sole site of fatty acid degradation in plants underlying the essential role of this organelle in early seedling development [5]. The process of storage oil mobilization starts with the hydrolysis of TAGs at the oil/water interface of cytosolic oil bodies. The released free fatty acids are subsequently transported into peroxisomes and degraded via β -oxidation. The produced acetyl CoA is further metabolized within the glyoxylate cycle to succinate and malate. These four-carbon compounds are further converted to sucrose via gluconeogenesis [6]. Sucrose represents the mobile form of reduced carbon transported through the cell and serves as an energy source for developing tissues [7].

Arabidopsis mutants deficient in β -oxidation are associated with compromised storage oil breakdown. These plants are impaired in post-germinative growth, which can be rescued by the exogenous supply of sucrose [1]. This sucrose-dependent phenotype is a suitable marker to detect mutants deficient in storage oil mobilization. However, some Arabidopsis mutants, such as the one for the peroxisomal NAD carrier PXN, exhibit wild type like growth in the absence of sucrose but analysis of the fatty acid amounts during seedling establishment revealed a reduced storage oil turnover [8]. This indicates that once a certain threshold of degraded fatty acids is achieved, there is no obvious seedling phenotype detectable. Thus, information on the ability to break down fatty acids are required to verify a defect in β -oxidation-associated storage oil breakdown.

The analysis of TAG breakdown products by gas chromatography-mass spectrometry (GC-MS) delivers absolute quantitative values and therefore is a

powerful tool to identify *Arabidopsis* mutants involved in peroxisomal β -oxidation [9]. In addition, the use of GC-MS facilitates the analysis of small amounts of tissue and provides complete information on fatty acid composition [9]. Beyond the broad spectrum of different *Arabidopsis* fatty acids, eicosenoic acid (C20:1) is found almost exclusively in TAGs and therefore can be used as a convenient marker to monitor storage oil degradation [10]. Fatty acid determination is usually performed after derivatization to the corresponding methyl ester by methylation or transmethylation [11]. Many methods have been described for the preparation of fatty acid methyl esters (FAMEs), but the acid catalyzed esterification using methanolic HCl is the most widely used procedure for the rapid isolation of high amounts of FAMEs [12,13,9]. Further, the addition of an internal standard prior extraction permits absolute quantification of the fatty acid content and allows correcting for technical variation, for example, due to slightly different efficiencies of the derivatization process.

Here we describe a fast and efficient isolation procedure of FAMEs from *Arabidopsis* ecotype Col-0 seeds and seedlings on sucrose containing medium to monitor not only the initial seed oil content but also the storage oil degradation rate. The chosen light regime was short day (8 h light / 16 h darkness), but other growth conditions, such as long day, continuous light or darkness, did not negatively influence fatty acid catabolism, but the rate of fatty acid turnover is elevated when day length is increased [8]. However, stratification of seeds is mandatory to assure simultaneous and efficient germination [14]. In contrast to that, the growth conditions of the parental generation can affect both seed quantity and quality in terms of germination and developmental efficiency, as well as general fatty acid content [9]. Therefore, the respective control and mutant plants have to be grown under equal conditions to yield comparable results. In consideration of the predominant sucrose dependency, it is

favorable to cultivate seedlings for fatty acid analysis on sucrose containing medium to avoid the influence of developmental deficiencies on the fatty acid breakdown rate. It is important to note that storage oil breakdown is decelerated but not inhibited in the presence of sucrose [15].

2. Materials

2.1 Components for plant growth, seed production and germination

1. Arabidopsis ecotype Col-0 seeds from Nottingham Arabidopsis Stock Center (NASC, <http://arabidopsis.info>, [16])
2. 1.5 mL reaction tubes
3. Commercial white peat-vermiculite soil mix including a starter nutrient charge
4. Autoclave
5. Ethanol, technical grade (70 %, 100 %), Ethanol (p.a. grade)
6. Filter paper (Whatman qualitative paper, Grade 1, 8.5 cm diameter)
7. Laminar flow cabinet
8. Half-strength Murashige and Skoog agar medium (0.5x MS agar) [17]: 2.2 g/L MS salts, 10 mL/L 0.5 M MES/KOH, pH 5.7, 8 g/L plant agar. Add 10 g/L sucrose if necessary for germination of plants impaired in β -oxidation. Autoclave at 121 °C for at least 15 min.
9. Petri dishes (8.5 cm diameter)
10. Programmable growth chamber
11. Surgical tape
12. Triton-X 100
13. Vortexer

2.2 Components for fatty acid extraction

1. 1 % (w/v) sodium chloride
2. Acetone
3. Analytical balance
4. Centrifuge (2.000 g, for glass reaction tubes)
5. Deep-freezer (-80 °C)
6. Detergent tablet
7. Distilled water
8. Electric water boiler
9. Freezer (-20 °C)
10. Glass GC vials
11. Glass Pasteur pipettes (New or cleaned with n-hexane; purity \geq 95 %)
12. Glass pipettes (cleaned with n-hexane; purity \geq 95 %)
13. Glass reaction tubes with screw-cap (Teflon)
14. Hamilton glass syringe (cleaned with n-hexane; purity \geq 95 %)
15. Heptadecanoic acid (C17:0; 1 mg/ml in n-hexane; purity \geq 99 %) as internal standard
16. Incubator (60 - 80 °C)
17. Liquid nitrogen
18. Methanolic HCl (3 N hydrochloric acid in methanol)
19. n-hexane (purity \geq 99 %) for fatty acid extraction and n-hexane (purity \geq 95 %) to clean pipets and syringes
20. Spoon or spatula
21. Thermoblock (90 °C, for glass reaction tubes)

3. Methods

3.1 Seed production and germination

Plant growth conditions and seed production

Photoperiod, temperature and humidity have a direct influence on seed production. Therefore, it is highly recommended to choose the most beneficial growth conditions for plants to produce seeds with comparable quality and quantity. Likewise, it is important to analyze seeds of the same age. To compare the β -oxidation rates of different Arabidopsis seedlings, maternal plants should be grown simultaneously.

1. Sterilize the surface of Arabidopsis seeds to minimize fungi contamination of half strength MS agar medium, especially when sucrose was added to the medium (Note 1). Transfer 2 mg of dried seeds (approx. 100 seeds) into 1.5 mL reaction tubes. Add 0.5 to 1 mL ethanol (70 %) and a droplet of detergent (e.g. Triton-X 100). Shake the tubes for 10 min at room temperature (RT) using a vortexer. Afterwards, remove all liquid with a pipette and add 0.5 to 1 mL ethanol (100 %) and shake again (Note 2). Make sure to thoroughly clean the seed surface with ethanol to remove all residual detergent. Remove all liquid and dry the seeds in a Laminar flow cabinet. Alternatively, seeds can also be sterilized via vapor-phase sterilization with chlorine. (Note 3).
2. Sow the Arabidopsis seeds on petri dishes filled with sterile 0.5x MS agar medium supplemented with 1 % (w/v) sucrose. In case of transgenic plants (e.g. T-DNA insertion lines), include appropriate antibiotics for selection. It is recommended to seal the dishes with surgical tape to allow airflow and high humidity, but prevent further contamination. The absorption of water by the dried seeds, called imbibition, is the first step of seed germination. Keep the plates with seeds in the dark at 4 °C for at least 3 days. This cold treatment

(stratification) improves germination rate and synchrony of seed germination (Note 4).

3. Transfer the *Arabidopsis* seeds to a controlled growth chamber (growth conditions, see below). Keep the seedlings on 0.5x MS agar medium until four leaves are visible (approx. after 2 weeks). Then transfer single seedlings to pots filled with soil mix (Note 5). Regardless of the growth medium, the following conditions should provide you with healthy plants with satisfactory yield.

Temperature: Optimal temperatures for flowering plants are at 22 - 23 °C (Note 6).

Light regime and photoperiod: Light intensities of 120 - 150 $\mu\text{mol} \cdot \text{m}^{-2} \cdot \text{s}^{-1}$ and long day conditions with 16 h light / 8 h darkness induce flowering with first flower buds after approx. 4 - 5 weeks (Note 7).

Humidity: Higher humidity is beneficial for seedlings especially during germination and after the transfer to soil. Set humidity to 60 - 80 %. Later growth on soil allows a subsequent decrease in humidity to 50 - 60 % and lower when siliques develop (Note 8).

Watering: It is not recommended to overwater *Arabidopsis* plants. Wait for the top layer of soil to be almost dry until the plants are watered again (Note 9). Stop watering when most of the siliques start to dry (see step 5).

4. 5 weeks after germination plants may need to be stabilized. Use wire or string to bind the shoot stems to a wooden stick.
5. 6 - 8 weeks after germination siliques start to dry and are ready to shatter. Harvest seeds by covering the upper part of the plant with a glassine sleeves for seed collection (Note 10).

6. After complete desiccation cut off the bag and sieve the seeds to remove any residues of siliques or other parts of the plant (Note 11).

Germination

Fatty acid degradation is a rapid process during the first days after germination. Hence, stratification is of great importance to achieve a uniform germination rate of the seeds. For β -oxidation related phenotypes the addition or omission of 1 % (w/v) sucrose to the growth agar medium is essential to detect differences in the capability of TAG breakdown via peroxisomal β -oxidation.

1. Degradation of storage fatty acids by β -oxidation will be observed over a time course of 6 days after imbibition (DAI). Plan your experiment in order to harvest enough material at the following stages (Fig. 1): Seeds (10 mg, approx. 500 seeds), 2 DAI (20 mg, approx. 200 seedlings), 4 DAI (20 mg, approx. 60-70 seedlings) and 6 DAI (20 mg, approx. 40-50 seedlings) (Note 12, 13). Collect a minimum of three biological replicates for each stage. Prepare and sterilize seeds as described before.
2. Prepare petri dishes with 0.5x MS agar medium with and without 1 % (w/v) sucrose. Place an autoclaved 8.5 mm filter paper on top of the agar plates (Note 14). Sow seeds on the soaked filter and seal the dishes with surgical tape. Stratify the seeds by keeping them in the dark at 4 °C for at least 3 days.
3. Transfer the seeds into a growth chamber with controlled growth conditions as listed before (Note 15).
4. Retrieve the seedlings after 2 DAI, 4 DAI and 6 DAI, preferably at the same time of day to assure good reproducibility between different sets of experiments.

3.2 Preparation of plant material and fatty acid extraction

Collecting plant material

For every step of the following protocol use metal or glassware if not stated otherwise.

Wearing gloves is mandatory to avoid contamination with fatty acids from skin.

1. Prepare a small spoon or spatula by cleaning it once with water, ethanol (70 %) and acetone, respectively, to remove any fatty acids.
2. Carefully scratch the seedlings from the filter using the spoon or spatula. Weigh 20 mg of plant material for each sample and transfer the plant material into pre-cooled 1.5 mL reaction tubes (Note 16). Directly freeze the tubes in liquid nitrogen. Record the exact weight of the plant material (Note 17). Store the samples frozen at -80 °C until further use.
3. Seeds can be directly taken from the seed stock. Weigh 10 mg of seed material and keep them at RT in already cleaned glass reaction tubes used for fatty acid extraction until further use (Note 18).

Fatty acid derivatization and extraction

The detection of fatty acids via GC-MS requires derivatization to fatty acid methyl esters (FAMES). Fatty acids will be extracted and derivatized with cleaned or n-hexane rinsed glassware. Again, wearing gloves is mandatory.

1. Thoroughly clean glass reaction tubes and screw caps to prevent fatty acid contamination. Transfer reaction tubes and screw caps into a heat-resistant glass beaker. Add boiling water (e.g. with an electric water boiler) and detergent (Note 19) to the beaker. Wait until water cooled down entirely. Remove the water and rinse the material with boiling water up to eight times. Air-dry the glassware at 60 to 80 °C in an incubator. Rinse the glass tubes with 1 mL

ethanol (puriss. p.a. grade) by vortexing, remove the liquid and dry at 60 - 80 °C. Afterwards, close the tubes.

2. Prepare a thermoblock at 90 °C.
3. Take the seedlings from the deep-freezer and keep them in liquid nitrogen. Still frozen, transfer the seedlings into the cleaned glass reaction tubes with a spatula. Likewise, transfer the seeds.
4. Immediately add 10 µl of the internal standard heptadecanoic acid (C17:0, 1 mg / mL) to all seedling samples and 100 µl to all seed samples with a Hamilton glass syringe (Note 20). Then add 1 mL 3 N methanolic HCl with a glass pipet (Note 21).
5. Close the reaction tubes tightly and incubate the samples in the thermoblock at 90 °C for 1 h (Note 22). Check if the screw caps are tightly closed during derivatization.
6. Cool down the reaction tubes to RT for 5 min.
7. Add 1 mL n-hexane (purity ≥ 99 %, Note 23) with a glass pipet and vortex for 10 s to trap the derivatization products.
8. Add 1 mL 1 % (w/v) sodium chloride and vortex again for 10 s. Sodium chloride will allow complete phase separation.
9. Centrifuge the reaction tubes for 5 min at 2000 g at RT for clear phase separation.
10. Transfer the resulting upper hexane phase (approx. 1 mL) with a glass Pasteur pipet into a GC vial without piercing through the lower methanolic HCl / sodium chloride phase or seeds and seedlings.
11. Dilute all seed samples (1:10 in n-hexane; purity ≥ 99 %). Store the samples at -20 °C until further analysis.

12. Store one sample of hexane (n-hexane; purity $\geq 99\%$) to be used a blank for the GC-MS analysis.

3.3 GC-MS analysis

FAME extracts are analyzed by GC-MS [17] using a 7200 GC-QTOF (Agilent Technologies, USA). Runs of hexane (blanks) are used to distinguish background from biologically meaningful peaks. The peak area is determined via peak integration using the Mass Hunter Software (Agilent Technologies, USA). Peak areas (hereafter referred to as response) are used for further calculations.

3.4 Viability tests

Calibration curve

The precise quantification of fatty acid content requires a linear dependency of concentration and response as can be seen in Fig. 2. With our equipment, quantities starting from 1 pg / μL up to a concentration on 150 pg / μL can be reliably detected for a variety of fatty acids present in Arabidopsis and for the internal standard C17:0. The slopes of the standard curves of the different tested FAMEs are comparable (less than 20 % SD). This means, together with the fact that C17:0 is not present naturally in plant material (see also below) that the amount of added C17:0 to the biological material can be used for absolute quantification of the different FAME species. The quantities of C20:1 FAMEs in extracts from seeds (using 10 mg, extracted in 1000 μl and 1 μl injected of a 1:10 dilution) and seedlings (using 20 mg, extracted in 1000 μl and 1 μl injected) normally ranges from 1.9 to 92.7 ng / μL and is within the linear range for quantities between 1 and 150 ng / μL (Fig. 2) (Note 24).

Recovery experiment

The quality of this method and the influence of plant material on the detection of FAMES can be verified with a recovery experiment (Equation A) [18]. This test identifies the recoverable amount of added fatty acid standards from plant material. Separate aliquots of collected plant material are processed as described before with or without the addition of fatty acid standards.

$$(A) \quad \% \text{ Recovery} = 100 \cdot \frac{\text{Conc}_{\text{Observed}} - \text{Conc}_{\text{Expected}}}{\text{Conc}_{\text{Expected}}} + 100$$

Here we added 10 μl of heptadecanoic acid (C17:0, 1 mg/mL) and derivatized samples with and without frozen plant material (4 DAI). Our results show a C17:0 recovery of 107 %, SD \pm 4.8 (N = 3 biological replicates), meaning that the derivatization is not limited by the presence of plant material. Additionally, plant material without the addition of C17:0 was analyzed and minor amounts of C17:0 was detected (138-fold less) making C17:0 a reliable internal standard.

3.5 Data analysis

Quantitation of fatty acid composition

Eicosenoic acid (C20:1) is a TAG-specific fatty acid in Arabidopsis seeds. It is represented by the 13-eicosenoic (C20:1 Δ^{13}) and 11-eicosenoic (C20:1 Δ^{11}) acid in the FAME mass chromatogram (see Fig. 3). The defined concentration of the internal standard heptadecanoic acid (C17:0) will allow calculating the amount of fatty acids of the seed/seedling extracts.

1. For the following calculations the response of C20:1 ($\text{Response}_{\text{FA}}$) equals the sum of responses of both detected eicosenoic acid forms. Equation (B)

determines the concentration of C20:1 in the transferred hexane phase. For this, use the internal standard C17:0 ($Response_{Standard}$) and its defined concentration ($Conc_{Standard}$).

$$(B) \quad FA \left[\frac{ng}{\mu L} \right] = \frac{Conc_{Standard} \left[\frac{ng}{\mu L} \right] \cdot Response_{FA}}{Response_{Standard}}$$

2. The total content of C20:1 in the collected plant sample can be calculated with equation (B). It includes the dilution factor (DF) of the sample (Seeds: 10, seedlings: 1) and the volume of hexane used for extraction (Vol_{Hexane}). For the content of C20:1 per seed, divide the result of equation (C) by the number of collected seeds/seedlings.

$$(C) \quad FA \left[\frac{ng}{total \text{ FW}} \right] = FA \left[\frac{ng}{total \text{ Vol}_{Hexane} [\mu L]} \right] = FA \left[\frac{ng}{\mu L} \right] \cdot Vol_{Hexane} [\mu L] \cdot DF$$

3. Determine the content of C20:1 per mg fresh weight (FW) with equation (D). A typical decrease of C20:1 in Arabidopsis during seedling establishment can be seen in Fig. 4.

$$(D) \quad FA \left[\frac{ng}{mg \text{ FW}} \right] = \frac{FA \left[\frac{ng}{total \text{ FW}} \right]}{FW [mg]}$$

4. Equation (E) determines the percentage of C20:1 compared to the sum of all present fatty acids detected in the plant material. Important: subtract the

response of the internal standard C17:0 ($Response_{Standard}$) from the sum of all fatty acid responses ($Response_{TotalFA}$).

$$(E) \% FA/Total FA = \frac{Response_{FA} \cdot 100}{Response_{TotalFA} - Response_{Standard}}$$

4. Notes

1. 1% (w/v) sucrose is required for Arabidopsis mutants defective in β -oxidation supporting seedling establishment. The addition of sucrose suppresses the mutant growth phenotype but also favors growth of fungi if seeds are not properly sterilized.
2. For more than 2 mg seeds repeat the washing steps with 1 mL ethanol (70 %) and detergent, as well as 1 mL ethanol (100 %).
3. Vapor-phase sterilization with chlorine is an alternative method to sterilize the surface of Arabidopsis seeds [19]. Fill 1 - 2 mg seeds into a 1.5 mL tube. Use a desiccator jar located in a fume hood and place the seeds into the jar. Fill a beaker with approx. 100 mL sodium hypochlorite solution (13 % active chlorite) and put it next to your seeds into the desiccator jar. Partly close the jar and add 3 mL concentrated HCl (37 %) to the beaker. Immediately close the jar and make sure it is sealed tightly. After 2 h of sterilization open the jar and let the chlorine fumes evaporate for 1 - 2 min. Close your seed containing reaction tubes and transfer them to a Laminar flow cabinet for complete evaporation of chlorine for 30 min.
4. Arabidopsis seeds need to be cold treated before they start to germinate (stratification). Physiological experiments require at least 3 days to induce simultaneous germination. This highly improves comparability between biological replicates.

5. Choose only healthy looking seedlings, preferably of equal size. Remove any residual agar sticking to the roots (e.g. by carefully washing the roots in water) to avoid the transfer of fungi contamination. Negative interaction between plant roots can be reduced as much as possible by keeping the plants separately in a pot or allow them to grow at least 5-6 cm apart from each other in one pot.
6. The preferred temperature range of *Arabidopsis* plants is 16 - 25 °C. Temperatures < 22 °C prolong the vegetative state. Higher temperatures induce heat stress and negatively affect growth and seed maturation.
7. Grown under short day conditions with < 12 h light per day cycle favor vegetative growth. Continuous light can be used when the majority of siliques start to dry (yellowish coat, 6 - 8 weeks after germination).
8. Germination on 0.5x MS agar medium provides enough humidity for seedlings, when they are in a covered petri dish. After the transfer to soil, plants should be covered, preferably with a plastic dome, for at least one week to protect plants from drying out.
9. Fertilize plants with fertilizers containing nitrogen, phosphorus, and potassium source on a weekly basis. Extensive watering promotes pests (e.g. insects, moss or fungi). Additional biological pest management should be considered (e.g. *Chrysoperla carnea*, *Hypoaspis miles*).
10. Glassine bags are permeable for air (when not entirely closed), light and water. This prevents fungi infection but allows silique maturation and speeds up seed collection.
11. Use a sieve with 450 µm mesh size to remove remnants of siliques and other plant parts.

12. Seeds can be directly used for fatty acid extraction without sterilization and stratification.
13. The total fatty acid content of Arabidopsis seeds largely exceeds the content of seedlings. 10 mg of seeds and 20 mg seedlings are sufficient (see also Note 20).
14. The filter facilitates the collection of seeds after germination without piercing through the agar. Wrap filters into aluminum foil to prevent damaging during autoclaving.
15. Short day (8 h light / 16 h darkness), normal day (12 h light / 12 h darkness), long day (16 h light / 8 h darkness) and continuous light do not influence germination or fatty acid catabolism.
16. Form a bale of seedlings. This facilitates the transfer to glass reaction tubes during fatty acid extraction and prevents loss of the frozen material (see also Note 17).
17. The exact weight of the plant material allows the calculation of the fatty acid content per mg of seedlings or seeds, respectively. If required, count the seedlings or seeds to determine the fatty acid content of single seedlings or seeds, respectively. Quantity of seeds: 1 mg equals approximately 50 Arabidopsis seeds.
18. Alternatively, Arabidopsis seeds can be stored in a thoroughly cleaned glass vial prior to fatty acid extraction. Do not use plastic tubes to avoid loss of material due to electrostatics.
19. Detergent tablets used for dishwashers work perfectly.
20. Heptadecanoic acid is not present in plants and can be used as internal standard for quantification. The tenfold amount of this standard is added for a consistent concentration between seedling and diluted seed extracts as the seed extracts are diluted tenfold prior measurement.

21. Add the internal standard, as well as methanolic HCl at the bottom of the reaction tube to avoid loss of the internal standard prior and during derivatization. Do not vortex.
22. Do not shake or vortex the glass reaction tube containing seeds and seedlings before incubation at 90 °C. The material easily sticks to the side of the tube and will not be processed. Return plant material into methanolic HCl with a thin spatula, thoroughly cleaned before.
23. Higher purity of hexane improves the quality of your samples and data.
24. FAMES in 6 DAI samples may be below detection limit (see Fig. 4). To measure those samples, FAMES can be extracted in a smaller hexane volume (< 1 mL). It is recommended to use at least 200 µL to allow an easy phase transfer. Alternatively, the 1 mL hexane phase can be evaporated at temperatures ≤ 50 °C after extraction and the FAMES can be resuspended in 100 µL n-hexane (purity ≥ 99 %). Note: Differences in concentrations have to be included into further calculations.

5. References

1. Graham IA (2008) Seed storage oil mobilization. *Annu Rev Plant Biol* 59:115-142.
2. Theodoulou FL, Eastmond PJ (2012) Seed storage oil catabolism: a story of give and take. *Curr Opin Plant Biol* 15 (3):322-328.
3. Graham IA, Eastmond PJ (2002) Pathways of straight and branched chain fatty acid catabolism in higher plants. *Prog Lipid Res* 41 (2):156-181.
4. Eastmond PJ, Graham IA (2001) Re-examining the role of the glyoxylate cycle in oilseeds. *Trends Plant Sci* 6 (2):72-78.

5. Kindl H (1993) Fatty acid degradation in plant peroxisomes: function and biosynthesis of the enzymes involved. *Biochimie* 75 (3-4):225-230.
6. Pracharoenwattana I, Smith SM (2008) When is a peroxisome not a peroxisome? *Trends Plant Sci* 13 (10):522-525.
7. Williams LE, Lemoine R, Sauer N (2000) Sugar transporters in higher plants--a diversity of roles and complex regulation. *Trends Plant Sci* 5 (7):283-290.
8. Bernhardt K, Wilkinson S, Weber AP, Linka N (2012) A peroxisomal carrier delivers NAD and contributes to optimal fatty acid degradation during storage oil mobilization. *Plant J* 69 (1):1-13.
9. Li Y, Beisson F, Pollard M, Ohlrogge J (2006) Oil content of *Arabidopsis* seeds: the influence of seed anatomy, light and plant-to-plant variation. *Phytochemistry* 67 (9):904-915.
10. Lemieux B, Miquel M, Somerville C, Browse J (1990) Mutants of *Arabidopsis* with alterations in seed lipid fatty acid composition. *Theor Appl Genet* 80 (2):234-240.
11. Garces R, Mancha M (1993) One-step lipid extraction and fatty acid methyl esters preparation from fresh plant tissues. *Anal Biochem* 211 (1):139-143.
12. Browse J, McCourt PJ, Somerville CR (1986) Fatty acid composition of leaf lipids determined after combined digestion and fatty acid methyl ester formation from fresh tissue. *Anal Biochem* 152 (1):141-145.
13. Ichihara K, Fukubayashi Y (2010) Preparation of fatty acid methyl esters for gas-liquid chromatography. *J Lipid Res* 51 (3):635-640.
14. Munir J, Dorn LA, Donohue K, Schmitt J (2001) The effect of maternal photoperiod on seasonal dormancy in *Arabidopsis thaliana* (Brassicaceae). *Am J Bot* 88 (7):1240-1249

15. Fulda M, Schnurr J, Abbadi A, Heinz E, Browse J (2004) Peroxisomal Acyl-CoA synthetase activity is essential for seedling development in *Arabidopsis thaliana*. *Plant Cell* 16 (2):394-405.
16. Scholl RL, May ST, Ware DH (2000) Seed and molecular resources for *Arabidopsis*. *Plant Physiol* 124 (4):1477-1480.
17. Murashige T, Skoog F (1962) A Revised Medium for Rapid Growth and Bio Assays with Tobacco Tissue Cultures. *Physiol Plantarum* 15 (3):473-497.
18. Fiehn O, Kind T (2007) Metabolite profiling in blood plasma. *Methods Mol Biol* 358:3-17
19. Buhrman DL, Price PI, Rudewiczcor PJ (1996) Quantitation of SR 27417 in human plasma using electrospray liquid chromatography-tandem mass spectrometry: A study of ion suppression. *J Am Soc Mass Spectrom* 7 (11):1099-1105.
20. Clough SJ, Bent AF (1998) Floral dip: a simplified method for *Agrobacterium*-mediated transformation of *Arabidopsis thaliana*. *Plant J* 16 (6):735-743.

Figure legends



Figure 1: Seedling growth stages of an *Arabidopsis* Col-0 seed within 6 days after imbibition. Expansion of root and cotyledons solely depends on the breakdown of TAGs until the first photosynthetic active leaves develop. Growth conditions: 8 h light / 16 h darkness. Bars = 1 mm.

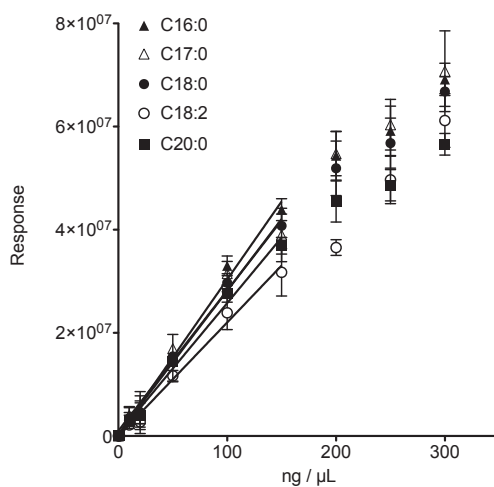


Figure 2. Calibration curve for selected fatty acids in *Arabidopsis*, palmitic acid (C16:0), stearic acid (C18:0), linoleic acid (C18:2), arachidic acid (C20:0) and the internal standard heptadecanoic acid (C17:0). Final concentrations: 0, 1, 10, 20, 50, 100, 150, 200, 250, 300 ng / μ L. Error bars indicate SD (N = 3 replicates; C16:0, slope = $302520 \pm 3.5\%$ SD, $R^2 = 0.98$; C17:0, slope = $272153 \pm 4.52\%$ SD, $R^2 = 0.96$; C18:0, slope = $278161 \pm 2.37\%$ SD, $R^2 = 0.99$; C18:2, slope = $220638 \pm 4.23\%$ SD, $R^2 = 0.97$; C20:0, slope = $254265 \pm 2.68\%$ SD, $R^2 = 0.99$).

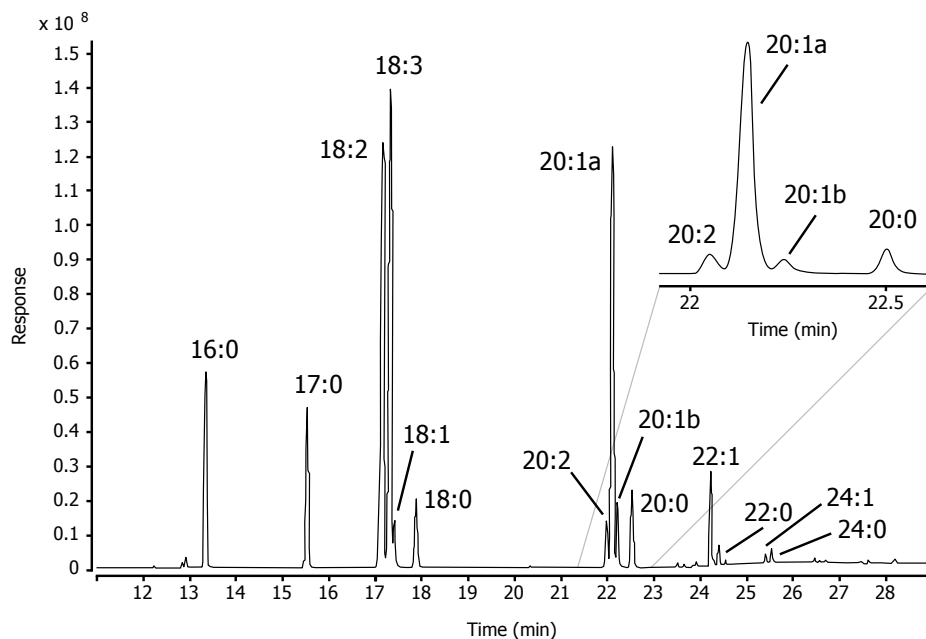


Figure 3. Typical chromatogram of fatty acid methyl esters of *Arabidopsis* seeds. 13-eicosenoic and 11-eicosenoic acid, two forms of eicosenoic acid in plants, are depicted as two separate peaks (20:1a and C20:1b). For fatty acid content calculation heptadecanoic acid (C17:0), which is not naturally present in *Arabidopsis*, is added to each sample as internal standard.

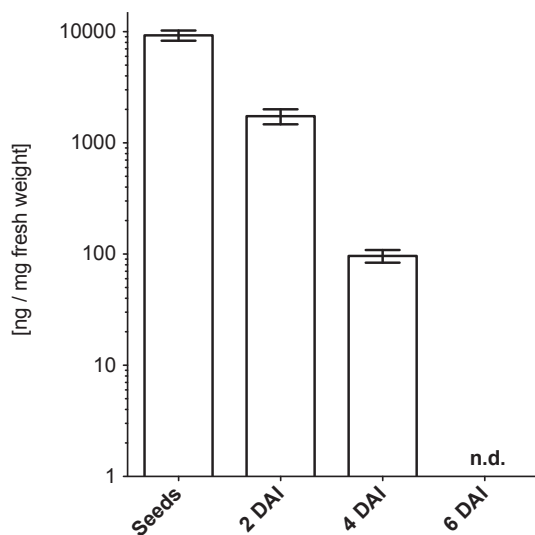


Figure 4. Breakdown of eicosenoic acid (C20:1) within 6 days after imbibition. Eicosenoic acid (C20:1) is used as a marker for TAG breakdown in *Arabidopsis*. C20:1 is highly abundant in seeds and rapidly degraded (note the logarithmic y-axis). Only approximately 100-fold less of this marker fatty acid is detectable after 4 days of germination. Growth conditions: 8 h light / 16 h darkness. Error bars indicate SD (N = 3 biological replicates). n. d.; not detected.

Acknowledgement

This work was supported by DFG-grant 1781/2-1 and GRK 1525. Authors thank Andreas P.M. Weber for stimulating discussion. We thank Elisabeth Klemp and Katrin Weber for technical assistance and Kirsten Abel for general assistance.

Author contribution

Björn Hielscher and Lennart Charton wrote the manuscript. Björn Hielscher performed all experiments and analyses. Nicole Linka and Tabea Mettler-Altmann participated in scientific discussions. Nicole Linka and Tabea Mettler-Altmann assisted in drafting this manuscript. Nicole Linka and Tabea Mettler-Altmann designed the experiments.

IV. Published Manuscripts

IV.V Published Manuscript 5

The Peroxisomal NAD Carrier from Arabidopsis Imports NAD in Exchange with AMP

Carlo W. T. van Roermund², Martin G. Schroers², Jan Wiese, Fabio Facchinelli, Samantha Kurz, Sabrina Wilkinson, Lennart Charton, Ronald J. A. Wanders, Hans R. Waterham, Andreas P. M. Weber and Nicole Link*

Laboratory Genetic Metabolic Diseases, Laboratory Division, Academic Medical Center, University of Amsterdam, 1105AZ Amsterdam, The Netherlands (C.W.T.v.R., R.J.A.W., H.R.W.); and Institute for Plant Biochemistry and Cluster of Excellence on Plant Sciences (CEPLAS), Heinrich Heine University, 40225 Düsseldorf, Germany (M.G.S., J.W., F.F., S.K., S.W., L.C., A.P.M.W., N.L.)

¹ This work was supported by Deutsche Forschungsgemeinschaft (grant nos. 1781/2-1 to N.L., GRK1525 to N.L., and EXC1028 to A.P.M.W.).

² These authors contributed equally to the article.

*Address correspondence to nicole.linka@hhu.de.

The Peroxisomal NAD Carrier from *Arabidopsis* Imports NAD in Exchange with AMP¹[OPEN]

Carlo W. T. van Roermund², Martin G. Schroers², Jan Wiese, Fabio Facchinelli, Samantha Kurz, Sabrina Wilkinson, Lennart Charton, Ronald J. A. Wanders, Hans R. Waterham, Andreas P. M. Weber, and Nicole Linka*

Laboratory Genetic Metabolic Diseases, Laboratory Division, Academic Medical Center, University of Amsterdam, 1105AZ Amsterdam, The Netherlands (C.W.T.v.R., R.J.A.W., H.R.W.); and Institute for Plant Biochemistry and Cluster of Excellence on Plant Sciences (CEPLAS), Heinrich Heine University, 40225 Düsseldorf, Germany (M.G.S., J.W., F.F., S.K., S.W., L.C., A.P.M.W., N.L.)

ORCID IDs: 0000-0001-5182-8076 (C.W.T.v.R.); 0000-0002-6853-1399 (S.K.); 0000-0003-0970-4672 (A.P.M.W.); 0000-0002-1400-717X (N.L.).

Cofactors such as NAD, AMP, and Coenzyme A (CoA) are essential for a diverse set of reactions and pathways in the cell. Specific carrier proteins are required to distribute these cofactors to different cell compartments, including peroxisomes. We previously identified a peroxisomal transport protein in *Arabidopsis thaliana* called the peroxisomal NAD carrier (PXN). When assayed *in vitro*, this carrier exhibits versatile transport functions, e.g. catalyzing the import of NAD or CoA, the exchange of NAD/NADH, and the export of CoA. These observations raise the question about the physiological function of PXN in plants. Here, we used *Saccharomyces cerevisiae* to address this question. First, we confirmed that PXN, when expressed in yeast, is active and targeted to yeast peroxisomes. Second, detailed uptake analyses revealed that the CoA transport function of PXN can be excluded under physiological conditions due to its low affinity for this substrate. Third, we expressed PXN in diverse mutant yeast strains and investigated the suppression of the mutant phenotypes. These studies provided strong evidences that PXN was not able to function as a CoA transporter or a redox shuttle by mediating a NAD/NADH exchange, but instead catalyzed the import of NAD into peroxisomes against AMP in intact yeast cells.

NAD is a ubiquitous biological molecule that participates in many fundamental processes within the living cell (Pollak et al., 2007; Houtkooper et al., 2010). NAD and its phosphorylated form act as electron acceptors and donors in numerous redox reactions, and it is also involved in the generation and scavenging of reactive oxygen species that serve as signaling molecules (Dröge, 2002; Mittler, 2002). Furthermore, NAD is also a precursor for cADP-ribose, which modulates the release of calcium as a second messenger (Pollak et al.,

2007; Houtkooper et al., 2010). Moreover, it also plays a role in transcription and post-translational modification through histone deacetylation and ADP ribosylation of proteins (Chang and Guarente, 2014; Bai et al., 2015).

Since NAD has multiple essential functions, its cellular levels need to be maintained either through *de novo* synthesis or salvage pathways, which involves recycling of NAD degradation products. In eukaryotic cells, both pathways take place in the cytosol, and thus NAD has to be always distributed to diverse cell compartments. As a consequence, transport proteins are required to shuttle NAD across intracellular membranes. In plants, humans, and fungi, members of the mitochondrial carrier family mediate the import of NAD into mitochondria, plastids, and peroxisomes (Todisco et al., 2006; Palmieri et al., 2009; Agrimi et al., 2012a, 2012b; Bernhardt et al., 2012). These transporters have been characterized by *in vitro* uptake assays using recombinant protein reconstituted into lipid vesicles (liposomes). Based on these biochemical data, the NAD carriers function as antiporters, importing NAD in a strict counter-exchange with another molecule (Todisco et al., 2006; Palmieri et al., 2009; Agrimi et al., 2012a, 2012b; Bernhardt et al., 2012).

In the case of plastids and mitochondria, the carriers catalyze the uptake of NAD in counter-exchange with AMP or ADP (Todisco et al., 2006; Palmieri et al., 2009). The efflux of adenine nucleotides is compensated by

¹ This work was supported by Deutsche Forschungsgemeinschaft (grant nos. 1781/2-1 to N.L., GRK1525 to N.L., and EXC1028 to A.P.M.W.).

² These authors contributed equally to the article.

*Address correspondence to nicole.linka@hhu.de.

The author responsible for distribution of materials integral to the findings presented in this article in accordance with the policy described in the Instructions for Authors (www.plantphysiol.org) is: Nicole Linka (nicole.linka@hhu.de).

C.W.T.v.R. and M.G.S. performed most of the experiments and analyzed the data; J.W. and F.F. conducted the subcellular localization in yeast; S.K. participated in the AMP uptake experiments; S.W. generated the *ndt1/ndt2Δ* double mutant and performed the suppression analysis; L.C. contributed the Ant1p uptake data; R.J.A.W., H.R.W., and A.P.M.W. helped in designing experiments; N.L. wrote the manuscript and designed the experiments; and all authors read and approved the final version of the article.

¹[OPEN] Articles can be viewed without a subscription.
www.plantphysiol.org/cgi/doi/10.1104/pp.16.00540

van Roermund et al.

their de novo synthesis in the stroma or unidirectional uptake into the matrix (Palmieri et al., 2008, 2009). The importance of such a NAD import system has been established in the yeast *Saccharomyces cerevisiae* (Todisco et al., 2006; Agrimi et al., 2011). Yeast cells lacking the mitochondrial NAD carrier proteins Ndt1p and Ndt2p were unable to grow on nonfermentable carbon sources, such as ethanol (Todisco et al., 2006). The utilization of ethanol requires the operation of the NAD-dependent tricarboxylic acid (Krebs) cycle and the mitochondrial respiratory chain. The *ndt1p/ndt2p* double mutant lacks mitochondrial NAD, which renders the two pathways inactive, thus explaining the mutant growth phenotype (Todisco et al., 2006; Agrimi et al., 2011). This finding indicates that mitochondrial NAD transport proteins are essential for providing NAD to mitochondria.

A peroxisomal NAD transporter from *Arabidopsis thaliana*, called peroxisomal NAD carrier

(PXN), has been previously identified (Agrimi et al., 2012a, 2012b; Bernhardt et al., 2012). In comparison to the plastidial and mitochondrial NAD carriers, PXN exhibits unique transport properties. The recombinant PXN protein accepts NADH and Coenzyme A (CoA) as suitable substrates in addition to NAD, AMP, and ADP (Agrimi et al., 2012a, 2012b; Bernhardt et al., 2012). Based on its broad substrate specificity, four transport functions can be postulated for PXN in plants (Fig. 1). In plants, NAD- and CoA-dependent processes play fundamental roles in peroxisomal metabolism. For example, fatty acid degradation via β -oxidation requires NAD and CoA as co-factor (Graham, 2008). Before fatty acids can enter β -oxidation, they need to be activated to the corresponding acyl-CoA esters, which occurs in the intraperoxisomal matrix (Fulda et al., 2004). Therefore, a specific transport protein is required to import CoA into plant peroxisomes. PXN might be a good candidate for catalyzing this transport step, since it accepts CoA as

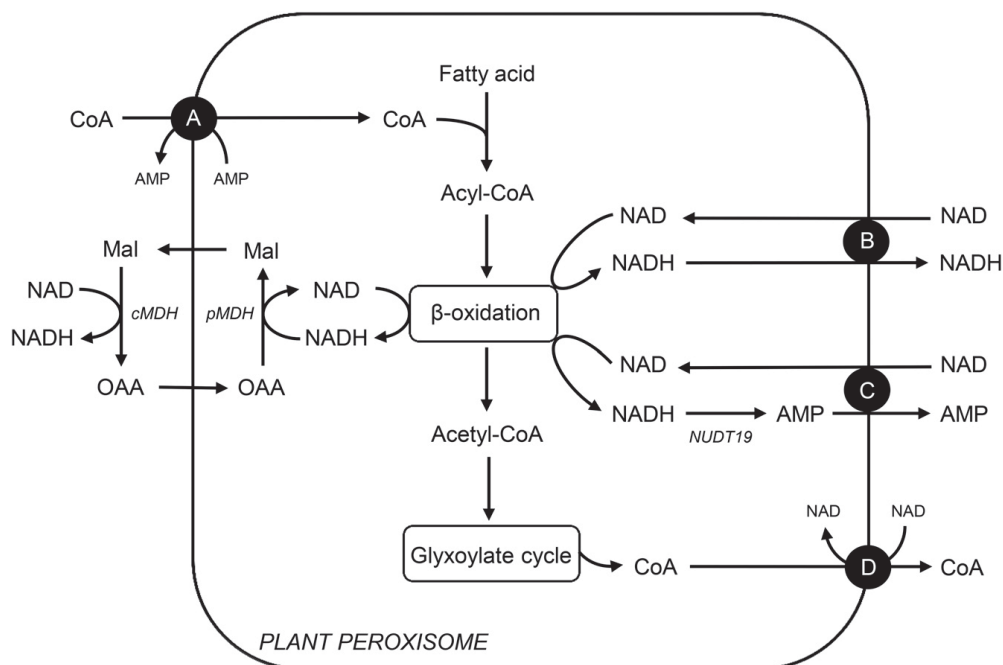


Figure 1. Possible transport functions in vivo for the peroxisomal NAD(H) or CoA carrier (PXN) in plants. A, PXN imports CoA against AMP to fuel fatty acid activation required for β -oxidation. B, PXN functions as redox shuttle by transferring NAD versus NADH across the peroxisomal membrane to regenerate NAD for β -oxidation, redundant to the malate/oxaloacetate shuttle via the peroxisomal and cytosolic malate dehydrogenases. C, PXN mediates the NAD uptake against AMP to provide β -oxidation with its cofactor. In *Arabidopsis*, the peroxisomal NADH pyrophosphatase NUDT19 might generate the counter-exchange substrate AMP for the PXN carrier via NADH hydrolysis. D, PXN exports CoA, which is released during the glyoxylate cycle to prevent an accumulation of CoA in the peroxisomal matrix. Mal, Malate; OAA, oxaloacetate; pMDH, peroxisomal malate dehydrogenase; cMDH, cytosolic malate dehydrogenase; NUDT19, a putative NADH pyrophosphatase in peroxisomes.

2128

Plant Physiol. Vol. 171, 2016

a substrate in vitro (Fig. 1A). During β -oxidation, NAD is reduced to NADH. To maintain the flux through this pathway, NAD has to be regenerated via the reversible reduction of oxaloacetate (Mettler and Beevers, 1980). The resulting malate is exported to the cytosol, where it is reoxidized to oxaloacetate, which in return is imported into peroxisomes (Fig. 1). Such a malate/oxaloacetate shuttle allows the indirect exchange of the oxidized and reduced forms of NAD with the cytosol (Mettler and Beevers, 1980). As a redundant system, PXN might catalyze the import of NAD in exchange with NADH. This leads to the transfer of reducing equivalents across the peroxisomal membrane (Fig. 1B). Alternatively, PXN imports NAD in exchange with AMP to supply β -oxidation system with NAD, as known for the plastidial and mitochondrial NAD transporters (Fig. 1C). The counter-exchange substrate for the NAD import might be generated via the hydrolysis of NADH to AMP catalyzed by the NADH pyrophosphatase NUDT19 (At5g20070) in Arabidopsis. This member of the NUDIX hydrolase family exhibits activity toward NADH and was shown to be targeted to peroxisomes (Ogawa et al., 2008; Lingner et al., 2011). An additional transport scenario for PXN is the export of CoA (Fig. 1D). High levels of CoA are released when acetyl-CoA, the end product of the β -oxidation, is further metabolized via the glyoxylate cycle (Graham, 2008). To maintain CoA homeostasis in peroxisomes and cytosol, PXN might mediate the CoA export. These predicted transport modes raise the question: what is the physiological function of PXN in living cells?

In this work, we used different deletion mutants from *S. cerevisiae* to explore the transport role of PXN. To this end, we functionally expressed the Arabidopsis carrier protein in yeast mutant strains and investigated the suppression of the mutant yeast phenotype in the presence of recombinant PXN. Our study demonstrated that PXN is required to supply peroxisomes with NAD by importing NAD in exchange with AMP.

RESULTS

PXN Protein Is Functional When Expressed in Yeast

In this study we used several deletion mutants from *S. cerevisiae* to dissect the physiological transport function of PXN. Our approach was to express PXN in the corresponding yeast mutant and analyze the suppression of the respective yeast mutant phenotype. To establish the feasibility of this approach, we first expressed recombinant PXN and assessed its functionality by analyzing the NAD uptake rates in yeast. Therefore, we expressed PXN with a C-terminal His affinity tag (His) in the *S. cerevisiae* wild-type strain FGY217 (Kota et al., 2007). The expression of PXN was driven by a Gal-inducible promoter 1 from *S. cerevisiae* (pGAL1) that led to sufficient amounts of recombinant protein to analyze its transport activity. We extracted membranes from yeast cells expressing PXN-His

(pMSU219) or transformed with the empty vector (pNL14) and separated the membrane proteins by sodium dodecyl-sulfate polyacrylamide gel electrophoresis (Fig. 2A, left panel). Proper expression of PXN-His, which has a calculated molecular mass of 37.1 kDa, was checked by immunoblot analysis with a His-tag antibody (Fig. 2A, right panel). Total yeast membranes containing recombinant PXN-His protein were reconstituted into lipid vesicles. The uptake of radioactively labeled [α - 32 P]-NAD into these liposomes was measured in the presence or absence of 10 mM NAD as counter-exchange substrate. We used total membrane fractions from yeast cells transformed with the empty vector as controls, to estimate the background activity of yeast endogenous NAD carriers. NAD import into liposomes reconstituted with yeast membranes from the control cells was below the detection limit of the

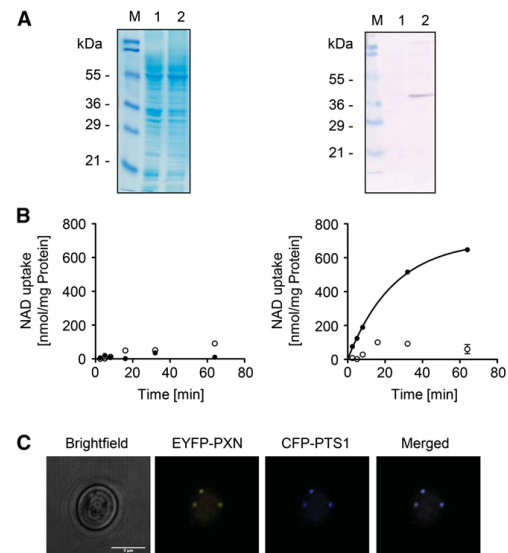


Figure 2. Functional expression of PXN in yeast. A, Gal-inducible expression of PXN-His (37.1 kDa) in FGY217 yeast cells. Left, Coomassie-stained sodium dodecyl-sulfate polyacrylamide gel electrophoresis gel; right, immunoblot analysis treated with His-tag antibody. Lane 1, Yeast membrane proteins isolated from yeast cells containing pNL14 vector; lane 2, yeast membrane proteins from yeast cells expressing PXN-His (pMSU219); M, protein marker. B, Time-dependent uptake of radioactively labeled [α - 32 P]-NAD (0.2 mM) was measured into liposomes reconstituted with total yeast membranes in the absence (left) or in the presence of PXN-His (right). The proteoliposomes were preloaded internally with 10 mM NAD (black symbols) or in the absence of NAD as counter-exchange substrate (white symbols). All graphs represent the arithmetic mean \pm SE of three technical replicates. C, PXN when expressed in yeast is targeted to peroxisomes. Confocal microscopic images were taken from yeast cells coexpressing EYFP-PXN and the peroxisomal marker CFP-PTS1. Scale bar = 5 μ m.

van Roermund et al.

employed assay system (Fig. 2B, left panel). In contrast, reconstituted PXN-His protein mediated rapid uptake of NAD into liposomes, but only when they were pre-loaded with NAD (Fig. 2B, right panel). The NAD/NAD exchange mediated by PXN-His followed first-order kinetics and reached a maximum uptake rate of 703 nmol/mg protein per minute. This finding confirmed that PXN functioned as an antiporter. Taken together, our *in vitro* activity experiments showed that PXN was functionally expressed in yeast cells.

In addition, we demonstrated that PXN fused at the N terminus to the enhanced yellow fluorescent marker (EYFP) was targeted to yeast peroxisomes. The expression of the EYFP-PXN protein (pMSU70) in the FGY217 yeast strain was driven by the constitutive promoter of the plasma membrane H^+ -ATPase from *S. cerevisiae* (pPMA1). These yeast cells were cotransformed with the pNL6 marker construct expressing the cyan fluorescent protein (CFP) tagged at the C terminus with the peroxisomal targeting signal 1 (PTS1) under the control of the alcohol dehydrogenase promoter from *S. cerevisiae* (pADH). This constitutive promoter was chosen to ensure the synthesis of PXN-EYFP in the presence of glycerol and fatty acids as carbon sources for the complementation studies. Furthermore, the proliferation of peroxisomes was found to be induced in yeast under those growth conditions (Gurvitz and Rottensteiner, 2006). Co-localization of EYFP-PXN and the peroxisomal fluorescent chimera (CFP-PTS1) was observed by fluorescence microscopy when both were expressed in yeast (Fig. 2C), indicating that Arabidopsis PXN was targeted to yeast peroxisomes.

Analysis of the PXN-Mediated CoA Transport Function

To investigate the physiological relevance of a CoA transport activity mediated by the PXN protein, we conducted concentration-dependent *in vitro* uptake assays into liposomes with yeast-expressed PXN-His protein (pMSU219), as described above. Therefore, we decreased stepwise the concentration of the internal exchange substrate from 10 mM to 2 mM, and finally 1 mM (NAD, CoA, or AMP) and kept the concentration of the radiolabeled uptake substrate constant at 0.2 mM: [α - 32 P]-NAD, [3 H]CoA, or [α - 32 P]-AMP (Fig. 3). The initial velocity of the NAD uptake against 10 mM NAD for PXN-His shown in Figure 2B was determined as 27.3 nmol/mg protein per min. We observed significant and similar initial rates of AMP uptake for PXN-His against the counter-exchange substrate NAD at all tested concentrations. In contrast, the velocity of AMP import into CoA-preloaded liposomes at time point zero had only a residual rate of 30% at the highest internal CoA concentration of 10 mM compared to 10 mM NAD. Furthermore, initial rates of AMP uptake drastically decreased to almost zero with 1 mM of internal CoA. In addition, neither 10 mM CoA nor 10 mM AMP as counter-exchange partner facilitated any uptake of

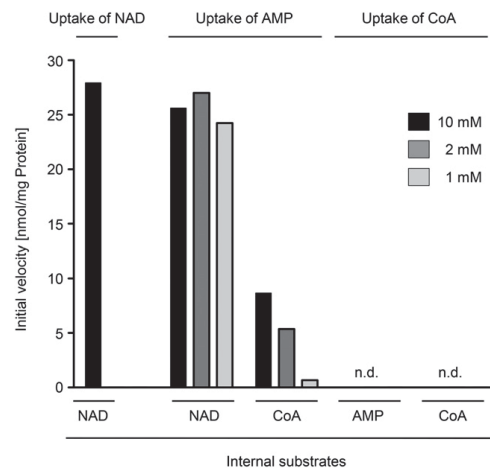


Figure 3. Initial velocities of PXN for the import of NAD, AMP, and CoA against various exchange partners in respect to internal concentrations. Time-dependent uptake of [α - 32 P]-NAD, [α - 32 P]-AMP, or [3 H]CoA (0.2 mM) into liposomes reconstituted with total yeast membranes containing recombinant PXN-His was measured. The proteoliposomes were preloaded internally with 10 mM, 2 mM, or 1 mM NAD, CoA, or AMP. Initial velocities of technical triplicates were determined using global fitting parameters extracted from nonlinear regression analyses. n.d., Not detectable.

labeled CoA (0.2 mM) into PXN-containing liposomes. Based on our findings, we concluded that PXN preferred AMP and NAD as substrates, leading to high AMP/NAD exchange activities even at low internal NAD levels. PXN had a lower affinity to CoA and showed a marginal CoA import even under very high nonphysiological CoA and AMP concentrations in the liposomes, thereby calling into question its *in vivo* relevance.

PXN Partially Restores the *mdh3Δ* Mutant Phenotype

Based on biochemical data PXN was able to catalyze NAD/NADH exchange in our liposome system (Agrimi et al., 2012a, 2012b; Bernhardt et al., 2012). We hypothesized that PXN transfers reducing equivalents across the peroxisomal membrane in addition to the peroxisomal malate/oxaloacetate shuttle (Pracharoenwattana et al., 2007; Fig. 1B). To test this hypothesis, we aimed for the complementation of a yeast mutant deficient in Mdh3p (peroxisomal malate dehydrogenase 3; van Roermund et al., 1995). This enzyme is part of the peroxisomal malate/oxaloacetate redox shuttle, which regenerates NAD in the peroxisomal matrix. Since NAD was required for fatty acid breakdown via peroxisomal β -oxidation, the loss of Mdh3p led to a yeast mutant that was unable to grow on oleate as sole carbon source (van Roermund et al., 1995).

2130

Plant Physiol. Vol. 171, 2016

We investigated whether PXN represented an alternative route for supplying peroxisomal β -oxidation with NAD in the *mdh3 Δ* mutant via a direct NAD/NADH exchange. To do so, we expressed the PXN protein (36.1 kDa) in this yeast mutant under the control of the oleate-inducible catalase promoter from *S. cerevisiae* (pCAT1). The presence of oleate as a sole carbon source results in the up-regulation of genes encoding β -oxidation enzymes (Gurvitz and Rottensteiner, 2006). Since the yeast mutant successfully expressed PXN (Fig. 4A), we analyzed the growth of *mdh3 Δ* cells transformed with *MDH3* (van Roermund et al., 1995), *PXN* (pHHU274), or an empty vector (pEL30) on oleate (C18:1) as sole carbon source. In addition, we used as a control the yeast mutant *fox1 Δ* , which lacks the acyl-CoA oxidase, the first enzyme in peroxisomal β -oxidation (Hiltunen et al., 1992). As expected, the *mdh3 Δ* cells transformed with the empty vector did not grow on oleate, whereas the complementation of *mdh3 Δ* mutant with *Mdh3p* led to complete growth recovery on oleate (van Roermund et al., 1995). Expression of

PXN in the *mdh3 Δ* mutant partially suppressed the mutant phenotype (Fig. 4B).

To examine whether the partial suppression of the *mdh3 Δ* mutant by *PXN* was associated with an increased rate of β -oxidation, we measured the rate of fatty acid oxidation (FAO) using octanoate (C8:0) as substrate in different mutant yeasts. Figure 4C shows the relative rates for C8:0 β -oxidation of mutant cells compared to the wild-type strain, which was set to 100%. In *fox1 Δ* cells lacking the acyl-CoA oxidase, the β -oxidation of octanoate was blocked, whereas deletion of the *MDH3* gene resulted in a decreased FAO rate (31%). Complementation with the endogenous *MDH3* led to a full recovery of β -oxidation function (94%). When *PXN* was expressed in the *mdh3 Δ* cells, we determined 73% of the wild-type FAO rates, and in comparison with β -oxidation activities in *mdh3 Δ* we measured a significant increase of 2.4-fold. These data strongly indicated that *PXN* was able to exchange NAD for NADH *in vivo*, which was required to suppress the *mdh3 Δ* growth defect and restore FAO function.

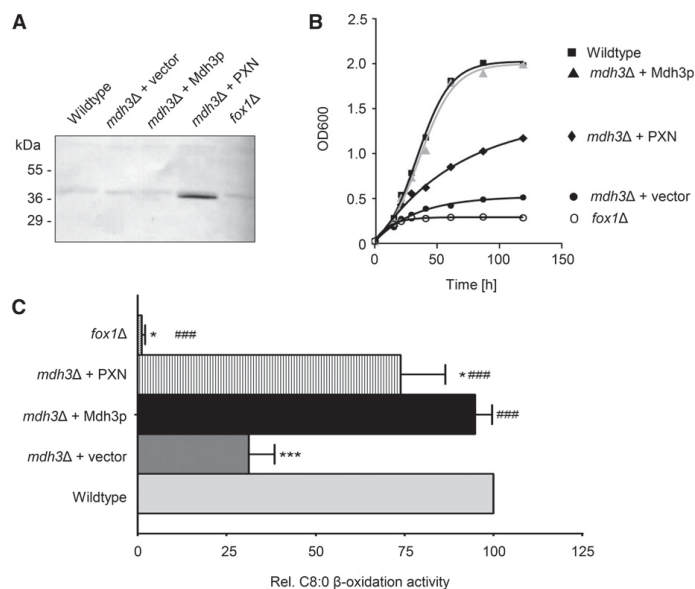


Figure 4. Partial rescue of FAO in *mdh3 Δ* mutant by *PXN*. A, Oleate-inducible expression of *PXN* (pHHU274; 36.1 kDa) in the *mdh3 Δ* mutant background was confirmed by immunoblot using *PXN*-specific antibody. Total yeast membrane proteins isolated from the wild type and different yeast mutants were analyzed. B, Growth curves of wild-type and mutant strains on oleate (C18:1) medium as sole carbon source. The strains shown are: wild-type cells (■), *mdh3 Δ* cells transformed with empty vector (●), *mdh3 Δ* cells expressing *Mdh3p* (▲ in gray), and *mdh3 Δ* cells expressing *PXN* (◆). As negative control *fox1 Δ* cells (○) were used. C, Wild-type and *mdh3 Δ* cells transformed with the empty vector or expressing *PXN* or *Mdh3p*, grown on oleate medium, were incubated with [14 C]-octanoate and β -oxidation activity was measured. The β -oxidation activity of wild-type cells was taken as reference (100%). Data are represented as arithmetic means \pm SD of two to five technical replicates. Asterisks indicate statistical differences to wild type with *** P < 0.001 as extremely significant and * P = 0.01 to 0.05 as significant. Hash tags indicate statistical differences to *mdh3 Δ* cells with ### P < 0.001 as extremely significant.

van Roermund et al.

Further Suppressor Analysis to Confirm PXN as Redox Shuttle Candidate

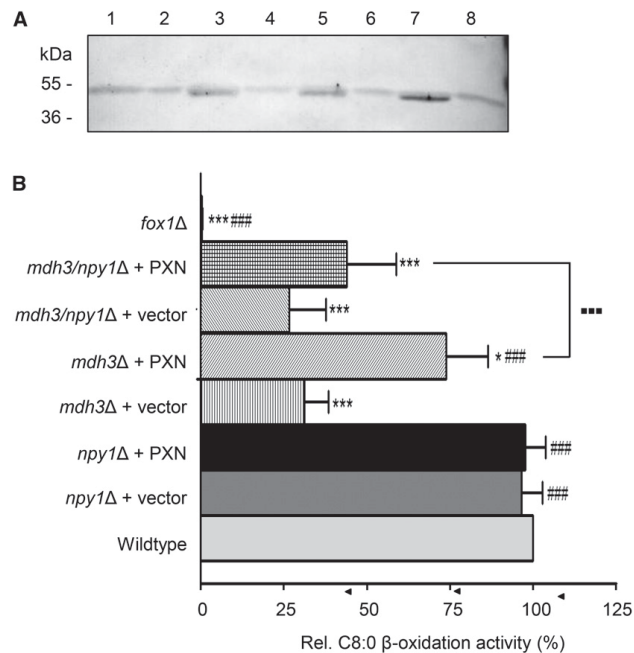
We performed an additional phenotype suppression analysis in yeast, to investigate the NAD/NADH exchange function of PXN. *S. cerevisiae* contains a peroxisomal NADH pyrophosphatase, called Npy1p (AbdelRaheim et al., 2001). This enzyme catalyzes the hydrolysis of NADH to AMP, as postulated for NUDT19 in Arabidopsis (see Fig. 1). Npy1p regulates NADH homeostasis, in particular when reducing equivalents accumulate inside the peroxisomal matrix (AbdelRaheim et al., 2001). Thus, the possibility exists that the loss of Mdh3p in the presence of oleate as a sole carbon source leads to high levels of NADH inside peroxisomes. As a consequence, Npy1p might reduce the peroxisomal NADH levels by converting it to AMP in the *mdh3Δ* mutant. As a second consequence, mainly AMP (and not NADH) might be available as transport substrate for PXN (see Fig. 1C).

To exclude a role of Npy1p in the conversion of NADH to AMP in the *mdh3Δ* mutant, we deleted the *NPY1* gene in this mutant background by PCR-mediated replacement of the *NPY1* gene with the antibiotic resistance gene cassette *BLE*. For the FAO analyses we compared wild type with the *mdh3Δ*, *npy1Δ*, and *mdh3/npy1Δ* mutants, which were transformed either with the empty vector (pEL30) or with the PXN expression construct (pHHU274), as described

above. We confirmed the expression of PXN (36.1 kDa) driven by the pCAT1 promoter in the yeast mutants under oleate growth conditions by immunoblot analysis using a PXN-specific antibody (Fig. 5A). Next we grew the corresponding yeast cells on oleate and measured octanoate FAO rates (Fig. 5B). The loss of Npy1p did not affect β -oxidation activities (96%). We measured comparable wild-type octanoate oxidation activities in *npy1Δ*, and also in *npy1Δ* cells with an overexpressed PXN protein (Fig. 5B; 97%). In the *mdh3Δ* and *mdh3/npy1Δ* double mutant, however, we observed reduced rates of octanoate oxidation (30% of the wild-type control; Fig. 5B). To test the PXN function as an NAD/NADH antiporter, we transformed *mdh3/npy1Δ* cells with PXN and measured octanoate β -oxidation. We observed that the expression of PXN did not restore, to the same extent, as the FAO phenotype when Npy1p is absent (Fig. 5B). The octanoate oxidation activities of the double mutant *mdh3/npy1Δ* with PXN were significantly decreased compared to *mdh3Δ* expressing PXN.

In summary, our results suggest that—due to the loss of Npy1p—the increased NADH levels in the peroxisomal matrix of *mdh3/npy1Δ* cells could not stimulate the NAD import required for higher FAO under these conditions. We assume that peroxisomes of the *mdh3Δ* single mutant contained less NADH and more AMP produced by the active Npy1p when compared to *mdh3Δ/npy1Δ* cells. Thus we hypothesize that PXN did

Figure 5. NPY1p regulates the peroxisomal NADH homeostasis in the *mdh3Δ* mutant. **A**, Constitutive expression of PXN (pHHU274; 36.1 kDa) in the *npy1Δ*, *mdh3Δ*, and *mdh3/npy1Δ* mutant was confirmed by immunoblot analysis using PXN-specific antibody. Arrowhead indicates the detected protein band for the recombinant PXN. Lane 1, Wild-type cells; lane 2, *npy1Δ* cells; lane 3, *npy1Δ* cells expressing PXN; lane 4, *mdh3Δ* cells; lane 5, *mdh3Δ* cells expressing PXN; lane 6, *mdh3/npy1Δ* cells; lane 7, *npy1Δ* cells expressing PXN; lane 8, *fox1Δ* cells. **B**, Octanoic acid β -oxidation activity in oleate-induced yeast wild-type and mutant cells. The strains shown are as follows: wild type, *mdh3Δ*, *npy1Δ*, and *mdh3/npy1Δ* transformed with empty vector or expressing PXN. Relative FAO rates were calculated, in which the activities in wild-type cells were taken as reference (100%). Data are represented as arithmetic means \pm SD of technical triplicates. Asterisks indicate statistical differences to the wild type with *** $P < 0.001$ as very significant and * $P < 0.05$ as significant. Hash tags indicate statistical differences to *mdh3Δ* cells with ### $P < 0.001$ as very significant. Large dots indicate statistical differences between *mdh3Δ* and *mdh3/npy1Δ* expressing PXN with **** $P < 0.001$ as very significant.



2132

Plant Physiol. Vol. 171, 2016

not function as a redox shuttle by exchanging NAD for NADH across the peroxisomal membrane in intact yeast cells, but was instead catalyzing the exchange of NAD with AMP.

PXN Catalyzes an NAD/AMP Exchange in Vivo

We used a yeast mutant lacking both mitochondrial NAD carriers Ndt1p and Ndt2p (Todisco et al., 2006) to verify the NAD/AMP exchange function of PXN in vivo. This double mutant displays a growth delay when ethanol is used as nonfermentable sole carbon source (Todisco et al., 2006). In this *ndt1/ndt2Δ* double mutant, the TCA cycle and mitochondrial respiration are inhibited due to the lack of mitochondrial NAD, which normally is imported by Ndt proteins in exchange for AMP (Todisco et al., 2006).

To be able to restore the impaired NAD uptake into the mitochondria of the *ndt1/ndt2Δ* double mutant, the peroxisomal PXN had to be targeted to mitochondria. To this end, the mitochondrial target peptide of the mitochondrial succinate/fumarate translocator from Arabidopsis was fused to the N terminus of PXN (Catoni et al., 2003). In addition, mt-PXN was tagged at

the C terminus with the EYFP. This reporter allowed visualization of the subcellular localization of the fusion protein. We expressed mt-PXN-EYFP driven by the constitutive pPMA1 promoter (pMSU388) in FGY217 yeast cells, which were stained with the mitochondria-specific dye MitoTracker Orange (see "Materials and Methods" for vendor information). Confocal microscopy revealed that the fluorescence pattern of EYFP matched with the distribution of the MitoTracker signal (Fig. 6A), confirming that PXN fused with a mitochondrial target signal was localized to mitochondria in yeast.

To show that the fusion with the mitochondrial target peptide did not affect the transport function of PXN, we conducted a Gal-inducible expression of mt-PXN-His (pMSU237) in FGY217 yeast cells. The mt-PXN-His protein was expressed in yeast with the expected calculated mass of 39.1 kDa visualized by immunoblot analysis using an His-tag antibody (Fig. 6B). We reconstituted lipid vesicles with yeast membranes containing mt-PXN-His fusion protein and measured the uptake of radioactively labeled [α - 32 P]-NAD (0.2 mM) in the absence or presence of internal NAD (10 mM). Reconstitution of the mt-PXN-His protein led to increased NAD transport activities at least when a counter-exchange

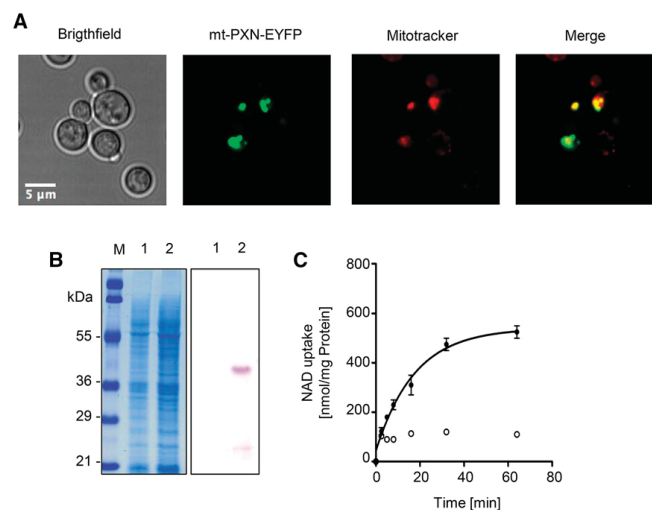


Figure 6. Mitochondrial targeted PXN protein is functional. A, Fusion of the mitochondrial target signal (mt) allows the localization of PXN to yeast mitochondria. The mt-PXN-EYFP fusion protein was constitutively expressed in BY4741 yeast cells (pMSU388). Localization study was analyzed by fluorescence microscopy. To visualize mitochondria, yeast cells were stained with MitoTracker Orange. Scale bar = 5 μ m. B, Gal-inducible expression of mt-PXN-His (39.1 kDa) in the FGY217 yeast strain. Left, Coomassie-stained SDS-PAGE gel. Right, Immunoblot blot treated with His-tag antibody. Lane 1, Yeast membrane proteins isolated from yeast cells containing empty vector pNL33; lane 2, yeast membrane proteins isolated from yeast cells expressing mt-PXN-His (pMSU237); M, protein marker. C, Time-dependent uptake of radioactively labeled [α - 32 P]-NAD (0.2 mM) was measured in liposomes reconstituted with total yeast membranes containing mt-PXN-His. The proteoliposomes were preloaded internally with 10 mM NAD (black symbols) or lack NAD as counter-exchange substrate (white symbols). Graphs represent the arithmetic mean \pm SE of three technical replicates.

van Roermund et al.

substrate was present (Fig. 6C), indicating that the recombinant fusion protein was active.

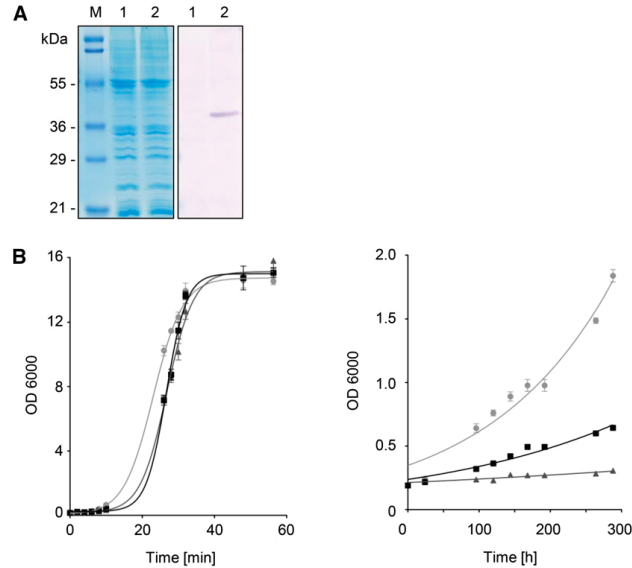
The *ndt1/ndt2Δ* double mutant was used to test the hypothesis that mt-PXN could complement NAD import into mitochondria in counter-exchange with AMP, as previously described for the yeast Ndt carriers (Todisco et al., 2006). Therefore, we expressed the mt-PXN-His fusion protein (39.1 kD) under the control of the constitutive pPMA1 promoter (pMSU377) in the double mutant (Fig. 7A). We grew the *ndt1/ndt2Δ* mutant carrying either the empty vector pNL24 or the mt-PXN-His expression plasmid on Glc or ethanol as sole carbon source at 28°C. Over time we monitored the growth of liquid yeast cultures by measuring the optical density at 600 nm (OD_{600}). In the presence of Glc no obvious growth difference of wild type, *ndt1/ndt2Δ*, or *ndt1/ndt2Δ* expressing mt-PXN was observed (Fig. 7B, left panel). In contrast, the growth rate on the non-fermentable carbon source ethanol was significantly reduced in the *ndt1/ndt2Δ* double mutant compared to wild type (Fig. 7B, right panel), in line with earlier results (Todisco et al., 2006). Expression of mt-PXN-His in this mutant background partially suppressed the growth defect on ethanol. From the resulting growth curves shown in Figure 7B (right panel), we calculated the growth rates. Compared to the exponential growth phase of wild-type cells with a doubling time of 121 h, *ndt1/ndt2Δ* cells were unable to grow on ethanol, indicated by the doubling time of 566 h. This severe phenotype was suppressed by the expression of mt-PXN-His as reflected in a doubling time of 182 h. These results suggested that mt-PXN-His partially compensated for the loss of both Ndt1p and Ndt2p

isoforms and supplied mitochondrial enzymes with NAD, which was essential for growth on ethanol. Since Ndt1p and Ndt2p catalyzed the import of NAD against AMP, we suggested that PXN mediated the same exchange.

DISCUSSION

Our knowledge of how peroxisomes are supplied with essential cofactors is still incomplete. In this study we elucidated the potential routes by which peroxisomes acquire NAD(H) and/or CoA. Like plastids and mitochondria, peroxisomes are absolutely dependent on supply with these cofactors from the cytoplasm (Linka and Esser, 2012). Since the last steps of NAD and CoA biosynthesis take place in the cytosol, these molecules must enter peroxisomes by specific transport proteins. The loss of the peroxisomal NAD carrier (PXN) compromises seedling growth in Arabidopsis (Bernhardt et al., 2012). This phenotype was explained by a delayed of storage lipid mobilization due to inefficient degradation of fatty acids via peroxisomal β -oxidation (Bernhardt et al., 2012). This previous work raised the question: How does PXN support FAO? Previous in vitro studies using artificial liposomes provided evidence that PXN is able to catalyze the following exchange modes: NAD/AMP, NAD/NADH, and AMP/CoA (Agrimi et al., 2012a, 2012b; Bernhardt et al., 2012). Consequently, several transport scenarios for a role of PXN in β -oxidation can be postulated as shown in Figure 1. Here, we performed analyses using baker's yeast to elucidate PXN function in a living system.

Figure 7. Rescue of ethanol growth by the mitochondrial-targeted Arabidopsis PXN in *ndt1/ndt2Δ*. A, Constitutive expression of mt-PXN-His (39.1 kD) in the *ndt1/ndt2Δ* double mutant. Left, Coomassie-stained SDS-PAGE gel; right, immunoblot treated with His-tag antibody. Lane 1, yeast membrane proteins isolated from yeast cells containing pNL24 vector; lane 2, yeast membrane proteins isolated from yeast cells expressing mt-PXN-His (pHHU377); M, protein marker. B, Suppression of the *ndt1/ndt2Δ* growth phenotype in the presence of mt-PXN-His: wild type transformed with empty vector (● in gray), *ndt1/ndt2Δ* transformed with the empty vector pDR195 (▲), and *ndt1/ndt2Δ* expressing mt-PXN (■) were inoculated in yeast nitrogen base-uracil medium supplemented with 2% (w/v) Glc (left panel) and 2% (v/v) ethanol (right panel). OD_{600} of liquid cultures were measured using a spectrophotometer. Data from a representative experiment are shown. Graphs represent the arithmetic mean \pm SD of three technical replicates. Similar results were obtained in three biological replicates.



2134

Plant Physiol. Vol. 171, 2016

First, we confirmed that PXN can be properly expressed in *S. cerevisiae* and that the protein is both functional and targeted to the correct organelle, the peroxisome (Fig. 2). The transport activity of PXN was analyzed in a reconstituted system. Measurement of the uptake of labeled substrate into lipid vesicles against a preloaded counter-exchange substrate led to high NAD exchange activities against NAD (Fig. 2B, right panel).

In the same experimental setup, we tested CoA as a putative substrate for PXN and compared the initial velocities of different CoA exchange combinations to the AMP/NAD exchange (Fig. 3). In contrast to the high uptake rates and high affinity for the AMP import against NAD, we detected only marginal CoA transport activities of PXN when CoA was offered at higher concentrations, indicating a lower affinity of PXN to this substrate. In context to the physiological situation, the free CoA levels are rather low. In animal tissue, the cytosolic and peroxisomal CoA concentrations are estimated between 0.02 and 0.14 mM and approximately 0.7 mM, respectively (Leonardi et al., 2005). Under our experimental conditions, we do not exhibit a significant CoA exchange with 10 mM of CoA or AMP. Therefore, a physiological role of PXN in supplying peroxisomes with CoA in plants is unlikely.

To address the *in vivo* transport function of PXN, we used different *S. cerevisiae* mutant strains. First, we analyzed a yeast strain deficient in the redox shuttle due to the deletion of the peroxisomal malate dehydrogenase. This mutant is unable to grow on fatty acids, because the NAD required for β -oxidation cannot be regenerated via the malate/oxaloacetate shuttle (van Roermund et al., 1995). Our complementation assay revealed that the growth on oleate and the activity of octanoate oxidation were partially restored in the presence of PXN (Fig. 4), indicating that PXN might catalyze a NAD/NADH exchange. When the peroxisomal enzyme Npy1p, which degrades NADH to AMP (thereby preventing NADH accumulation; AbdelRaheim et al., 2001), was deleted in the *mdh3* Δ mutant, PXN was unable to suppress the β -oxidation phenotype of the corresponding double mutant (Fig. 5). From this result, we conclude that PXN substitutes the loss of MDH3 via the import of cytosolic NAD in exchange with peroxisomal AMP, the latter being generated by Npy1-linked NADH degradation. This PXN-catalyzed transport mode allows β -oxidation with NAD even when the redox shuttle is compromised. We confirmed this hypothesis with a second independent yeast mutant. We artificially targeted PXN to yeast mitochondria (Fig. 5) and demonstrated that PXN was able to replace the endogenous NAD carriers Ndt1p and Ndt2p (Fig. 6). The successful suppression of *ndt1/ndt2* Δ mutant phenotype with PXN indicated that this carrier catalyzes the NAD/AMP exchange under *in vivo* conditions.

Our work provides strong evidence that the main function of PXN is to supply peroxisomes with NAD. In

other eukaryotic organisms, an analogous peroxisomal NAD import system has not yet been identified (Visser et al., 2007; Linka and Theodoulou, 2013). However, the loss of the MDH3 gene in *S. cerevisiae* did not fully abolish FAO activity. Indeed, in the *mdh3* Δ mutant we detected significant residual FAO activity that amounts to approximately 30% of wild type (Fig. 4). Thus, we assume that the impaired redox shuttle across the peroxisomal membrane is partially compensated by an alternative redox shuttle or/and endogenous NAD carriers of yeast peroxisomes. The abundance of this last protein is lower than the constitutively expressed PXN in the yeast mutant background. The higher import activity of the recombinant PXN protein led to a significant restoration of the mutant phenotype (Fig. 4). One prime candidate for mediating the NAD import into yeast peroxisomes is the peroxisomal ATP carrier Ant1p (Palmieri et al., 2001; van Roermund et al., 2001), which is the closest relative of PXN in yeast. Uptake studies using recombinant protein confined the substrate specificity of Ant1p to ATP, ADP, and AMP (Tumaney et al., 2004). However, only (desoxy) nucleotides were tested in this study (Palmieri et al., 2001). Thus, we investigated whether cell-free expressed Ant1p has a larger substrate spectrum (Supplemental Fig. S1). Based on our analysis, Ant1p is unable to transport NAD across the liposomal membrane, implying that other putative carrier proteins are involved in the uptake of NAD into yeast peroxisomes. Further yeast candidates for the peroxisomal NAD transport are the two mitochondrial Ndt proteins (Todisco et al., 2006). These carriers are able to specifically import NAD and might be dual-targeted to yeast peroxisomes, since several mitochondrial proteins have been also found in peroxisomes (Theodoulou et al., 2013; Ast et al., 2013; Carrie et al., 2009; Yogev and Pines, 2011). Ndt1p has been demonstrated by GFP fusion to be located to mitochondria (Todisco et al., 2006), whereas the mitochondrial localization of Ndt2p has not been experimentally validated. Alternative routes for supplying yeast peroxisomes with NAD are the glycerol 3-P shuttle or via vesicular traffic from the endoplasmic reticulum, but up to now there is no evidence for this route (Hoepfner et al., 2005).

In this work we showed that PXN did not mediate a CoA transport or NAD/NADH exchange under physiologically relevant conditions. Consequently, additional transport systems in the peroxisomal membrane must exist to mediate CoA transport or the redox shuttle in plants. In humans, a peroxisomal CoA carrier has been identified that belongs to the mitochondrial carrier family (MCF; Agrimi et al., 2012a), as is the case for PXN. Recently, two MCF transport proteins have been identified as mitochondrial CoA carriers in Arabidopsis (Zallot et al., 2013). Thus, one of the 58 MCF members encoded by the Arabidopsis genome might provide the peroxisomal β -oxidation with CoA (Haferkamp and Schmitz-Esser, 2012). An independent uptake route for this cofactor might be also the peroxisomal fatty acid transporter, called Comatose (also known as

van Roermund et al.

PXA1, PED3, ACN2, and AtABCD1 (Hu et al., 2012)). It has been suggested that this membrane protein has an additional intrinsic enzymatic function. During the import of activated fatty acids into plant peroxisomes, the thioesterase activity of Comatose releases the CoA moiety into the cytosol or in the peroxisomal lumen. In the latter case, the CoA release results in a net CoA uptake into peroxisomes (De Marcos Lousa et al., 2013).

A peroxisomal pore-forming channel (porin) has been proposed to mediate the exchange of malate and oxaloacetate, which acts as a redox shuttle that connects the cytosolic and peroxisomal NAD/NADH pools (Linka and Theodoulou, 2013). Such a porin has been characterized by electrophysiological experiments using spinach leaf peroxisomes and castor bean glyoxysomes (Reumann et al., 1995, 1996, 1997), but the identity of the corresponding proteins has remained elusive. The Arabidopsis ortholog of peroxisomal Pxmp2, which has been characterized as a channel-forming protein in mammals (Rokka et al., 2009), might represent a candidate protein for linking the peroxisomal and cytosolic pools of NAD(H) in plants (Linka and Theodoulou, 2013). A major challenge for the future will be to identify the genes responsible for the transport processes mentioned above, which are required to execute the great diversity of peroxisomal functions in plants.

CONCLUSION

We showed that PXN acts as a NAD/AMP transporter *in vivo* while other postulated transport functions for PXN could be excluded in physiologically relevant conditions. Thus, PXN imports cytosolic NAD into plant peroxisomes. The uptake of NAD by PXN occurs in a strict counter-exchange with peroxisomal AMP. Our yeast complementation studies revealed that the NAD transport into yeast peroxisomes is linked to a peroxisomal NADH pyrophosphatase. This enzyme maintains the NADH homeostasis by degrading NADH and thus preventing the accumulation of NADH, for example, during high flux of FAO. In Arabidopsis, NUDT19 might be responsible for hydrolysis of NADH to AMP. The resulting AMP might be used by PXN as a counter-exchange substrate for the NAD import. The exported AMP can be fed into the salvage pathway to synthesize NAD in the cytosol. Future studies are required to investigate whether the interplay between PXN and NUDT19 in Arabidopsis plays a role in regulating the NAD/NADH redox state as an ancillary system to the malate/oxaloacetate shuttle.

MATERIALS AND METHODS

Materials

Chemicals were purchased from Sigma-Aldrich (www.sigmaaldrich.com). Reagents and enzymes for recombinant DNA techniques were obtained from

New England Biolabs (www.neb.com), Qiagen (www.qiagen.com), ThermoFischer Scientific (www.thermoFischer.com), and Promega (www.promega.com). Anion-exchange resin was purchased from Bio-Rad Laboratories (www.bio-rad.com). Radiochemical [α - 32 P]-AMP, [α - 32 P]-NAD, and [3 H]CoA were obtained from Hartmann Analytic (www.hartmann-analytic.de) and Perkin Elmer (www.perkinelmer.de).

Cloning Procedures

In silico DNA sequences for cloning were retrieved from the Aramemnon database (aramemnon.uni-koeln.de) and the Saccharomyces Genome database (www.yeastgenome.org). Cloning was performed according to standard molecular techniques (Sambrook and Russell, 2001). Sequences were verified by DNA sequencing (Macrogen; dna.macrogen.com). Primers were synthesized by Sigma-Aldrich. The oligonucleotide sequences used in this study are listed in Supplemental Table S1. The coding DNA sequence (CDS) of PXN (At2g39970) was amplified via PCR using the cDNA clone pda.00682 provided by the Riken BioResource Center (www.en.brc.riken.jp) as a template.

For the *in vitro* uptake studies, the peroxisomal NAD carrier, PXN, was fused at the C terminus with a His-tag under the control of the Gal-inducible promoter pGAL1. The pYES2 vector (ThermoFischer Scientific) was chosen, in which a linker sequence (NL230/NL231) encoding for 6 His residues was introduced via *Bam*HI and *Xba*I, yielding pNL14. The gene-specific primers NL33 (*Hind*III) and NL34 (*Bam*HI) were used to clone the PXN CDS into the pNL14 expression vector, resulting in pMSU219.

To generate the constructs for the peroxisomal localization studies in yeast, PXN CDS was amplified using the primers NL7 (*Xho*I) and NL8 (*Bam*HI). The resulting PCR product was cloned into pDR195 (Rentsch et al., 1995). The primers NL9 and NL10 (*Xho*I) were used to clone EYFP CDS via *Xho*I into pDR195. The insertion of both DNA fragments led to pMSU70 expressing EYFP-PXN via the constitutive pMA1 promoter. The clone (a peroxisomal fluorescence marker protein, CFP-PTS1) and the sequence of the Ser-Lys-Leu motif were fused to the CFP sequence via the primers NL254/NL255. The CFP-PTS1 sequence was then inserted via *Hind*III into the expression vector pACTII (Clontech Laboratories; www.clontech.com) carrying the constitutive pADH promoter, yielding the pNL6 construct.

For the complementation of the *mdh3Δ* and *mdh3/nyp1Δ* mutants, the cells were transformed with the yeast expression vector pEL30 containing the PXN coding sequence. The primers NL631 and NL632 were used to clone PXN CDS into pEL30 via *Bam*HI and *Hind*III. The expression of PXN was under the control of the oleate-inducible catalase A promoter (pCTA1; Elgersma et al., 1993).

To complement the *ndt1/ndt2Δ* mutant with PXN, the transporter had to be targeted to yeast mitochondria. Therefore, the target sequence from the mitochondrial succinate/fumarate carrier from Arabidopsis (*Arabidopsis thaliana*; At5g01340) was fused to the N terminus of PXN. To do so, the mitochondrial target peptide (mt) was amplified from Arabidopsis cDNA using the primer (P75/P76) and introduced via *Hind*III and *Bam*HI into pYES2 (ThermoFischer Scientific). The inducible pGAL1 promoter was exchanged with the constitutive pPMA1 promoter from pDR195 (Rentsch et al., 1995). The EYFP CDS (amplified by NL350/NL351) was introduced via *Bam*HI and *Xba*I into pNL24. Finally, the PXN CDS (amplified by NL335/NL34) was cloned in frame with the mt and EYFP sequence via *Bam*HI, resulting pMSU388.

To investigate whether the mt-PXN fusion protein is functionally expressed in yeast, the mitochondrial target peptide was amplified as described above and introduced via *Hind*III and *Bam*HI into pNL14, leading to pNL33. The PXN CDS was amplified by NL335/NL34 and inserted into pNL33 via *Bam*HI. The resulting pMSU237 construct was used for the Gal-inducible expression of mt-PXN-His fusion protein in yeast, which was functionally analyzed by *in vitro* uptake studies.

The mt-PXN-His expressing construct was cloned for rescuing the *ndt1/ndt2Δ* yeast mutant phenotype. Therefore, the PXN CDS was amplified by NL335/NL34 and inserted into the frame with a mitochondrial target sequence of pNL24 via *Bam*HI, leading to the construct pMSU377. The synthesis of mt-PXN-His was driven by the constitutive pPMA1 promoter.

Yeast Strains and Culture Conditions

The *Saccharomyces cerevisiae* strain FGY217 (MAT α , ura3-52, lys2 Δ 201, pep4 Δ ; Kota et al., 2007) was used for PXN uptake studies and subcellular localization analyses of EYFP-PXN and mt-PXN-EYFP.

Peroxisomal NAD Carrier as NAD/AMP Exchanger

For complementing the *mdh3Δ* and *mdh3/npv1Δ* mutant phenotype, the BJ1991 yeast cells (*MATα*, *leu2*, *trp1*, *ura3-251*, *prb1-1122*, *pep4-3*, *gal2*) were used as a wild-type strain. The following derivatives of this strain, all impaired in β -oxidation, were used: *fox1Δ* and *mdh3Δ* (carrying a deletion of the acyl-CoA oxidase or peroxisomal malate dehydrogenase, respectively). These mutants were constructed from BJ1991 as described by van Roermund et al. (1995). The *mdh3/npv1Δ* double mutant was made by replacing the whole *NPY1* CDS from the *mdh3Δ:LEU* mutant by the *BLE* gene conferring resistance to Zeocin. The *NPY1* deletion construct was made by PCR using the pUG66 plasmid (Guedener et al., 2002) as a template and the CVR1 and CVR2 primers. *BLE+* transformants were selected for integration in the *NPY1* gene by PCR analysis. Yeast transformants were selected and grown in minimal medium containing 6.7 g/l yeast nitrogen base without amino acids, supplemented with 5 g/l Glc and amino acids (20 mg/l) if required. For the induction of peroxisome proliferation, cells were shifted to YPO medium containing 5 g/l potassium P buffer pH 6.0, 3 g/l yeast extract, 5 g/l peptone, 1.2 g/l oleate, and 2 g/l Tween-80. Prior to shifting to these media, the cells were grown in minimal 5 g/l Glc medium for at least 24 h.

For the generation of the *ndt1/ndt2Δ* double mutant, the *ndt1Δ* single mutant (BY4741; *MATα*, *his3Δ1*, *leu2Δ0*, *met15Δ0*, *ura3Δ0*; YIL006w::kanMX4) was obtained from the EUROSCARF collection (web.uni-frankfurt.de/fb15/mikro/euroscarf). The *NDT2* gene in *ndt1Δ* single mutant was disrupted by PCR-mediated gene replacement using the *LEU2* cassette, amplified from pUC73 (Guedener et al., 2002) with the primer set NL352/353. Transformed yeast cells that were able to grow in the absence of Leu were selected and the presence of the *LEU2* cassette was verified by PCR analysis.

Yeast cells were transformed according to standard protocols for lithium acetate/PEG transformation (Gietz and Schiestl, 2007). Yeast cells were selected on synthetic complete medium (SC; 0.67% [w/v] yeast nitrogen base supplemented with appropriate amino acids and bases for auxotrophy and a carbon source).

Heterologous Protein Expression in Yeast for Uptake Studies

For the heterologous expression, the FGY217 strain was transformed with the empty vectors pNL14 and pNL33 or the expression constructs pMSU219 (PXN-His) and pMSU237 (mt-PXN-His). Fifty milliliters of SC-Ura liquid medium supplemented with 2% (w/v) Glc were inoculated with an overnight culture and cultured to an OD_{600} of 0.4. The yeast cells were grown for 6 h aerobically at 30°C. Control cultures with the empty vectors were processed in parallel. Harvest and enrichment of total yeast membranes without and with heterologously expressed PXN proteins were achieved according to Linka et al. (2008).

Protein Biochemistry

Sodium dodecyl sulfate polyacrylamide gel electrophoresis and immunoblot analyses were conducted as described in Sambrook and Russell (2001). For immunodetection, either α -poly-His HRP-conjugated mouse IgG1 antibody (MACS Molecular; www.miltenyibiotec.com) or the PXN-specific antibody (Bernhardt et al., 2012) was used. No tagged PXN variants were visualized using anti-PXN-specific serum (Bernhardt et al., 2012) and AP-conjugated anti-rabbit IgG (Promega). PageRuler Prestained Protein Ladder (New England Biolabs) was used to estimate molecular masses. Protein concentrations were determined using a bicinchoninic acid assay (ThermoFischer Scientific).

Reconstitution of Transport Activities into Liposomes

Yeast membranes were reconstituted into 3% (w/v) 1- α -phosphatidylcholine by a freeze-thaw-sonication procedure for in vitro uptake studies, as described in Linka et al. (2008). Proteoliposomes were either preloaded with 10 mM NAD; 10 mM, 2 mM, or 1 mM AMP; 10 mM, 2 mM, or 1 mM CoA; or produced without preloading (negative control). Counter-exchange substrate, which was not incorporated into proteoliposomes, was removed by gel filtration on Sephadex G-25M columns (GE Healthcare; www.gehealthcare.com).

Transport assays were started via adding 0.2 mM [α - 32 P]-AMP (6000 Ci/mmol), [α - 32 P]-NAD (800 Ci/mmol), or [3 H]CoA (5 Ci/mmol). The uptake reaction was terminated via passing proteoliposomes over AG1-X8 Dowex anion-exchange columns (Merck Millipore; www.merckmillipore.com). The incorporated radiolabeled compounds were analyzed by liquid scintillation counting. Time-dependent uptake data were fitted using nonlinear regression

analysis based on one-phase exponential association using GraphPad Prism 5.0 software (GraphPad; www.graphpad.com). The background activities in the absence of PXN-His were subtracted. The initial velocity of uptakes were calculated using the equation $slope = (Plateau - Y_0) \times k$, whereas Y_0 was set to 0. The values for the *Plateau* and *k* were extracted from the nonlinear regression analyses using a global fit from three technical replicates.

Suppression Analysis of the *mdh3Δ* and *mdh3/npv1Δ* Mutant

PXN expression construct pHHU274 and empty pEL30 vector were transformed into the following strains: BJ1991 wild-type cells, *mdh3Δ* single mutant, *npv1Δ* single mutant, and *mdh3/npv1Δ* double mutant. Transformed yeast cells were selected accordingly to the yeast strain genotype and pEL30 autotrophy.

β -Oxidation Activity Measurements

β -oxidation assays in intact yeast cells were performed as described previously by van Roermund et al. (1995) and optimized for the pH and the amount of protein. Oleate-grown cells were washed in water and resuspended in 0.9% NaCl (OD = 0.5). Aliquots of 2 μ l of cell suspension were used for β -oxidation measurements in 200 μ l of 50 mM MES (pH 6.0) and 0.9% (w/v) NaCl supplemented with 10 μ M [14 C]-octanoate. Subsequently, [14 C]-CO₂ was trapped with 2 M NaOH and used to quantify the rate of FAO. Results are presented as percentage relative activity to the rate of oxidation of wild-type cells. In wild-type cells, the rates of octanoate oxidation is $7.84 \pm 1.09 \text{ nmol}^{-1} \text{ min}^{-1} \text{ OD cells}^{-1}$.

Suppression Analysis of the *ndt1/ndt2Δ* Double Mutant

Wild-type strain BY4741 and *ndt1/ndt2Δ* double mutant were transformed with the empty vector pNL24 and pMSU377 expressing mt-PXN-His. Yeast cells were grown on SC-Ura supplemented with either 2% (w/v) Glc or 2% (v/v) ethanol, as described in Todisco et al. (2006).

Fluorescence Microscopy

For peroxisomal localization studies in yeast, FGY217 cells were cotransformed with pMSU70 and pNL6 expressing EYFP-PXN or peroxisomal fluorescent chimera (CFP-PTS1), respectively. Both fluorescent proteins were synthesized under the control of the constitutive pPMA1 promoter. Yeast cells harboring both constructs were selected on SC agar medium with 2% (w/v) Glc in the absence of uracil (pMSU70) and Leu (pNL6). The selected yeast cells were grown overnight at 30°C in SC-Leu-Ura with 3% (w/v) glycerol, 0.1% (w/v) oleate, and 0.2% (w/v) Tween-80 to induce peroxisome proliferation. The expression of the EYFP-PXN and CFP-PTS1 was analyzed with a confocal laser scanning microscope model no. 510 Meta (Carl Zeiss www.zeiss.de). CFP fluorescence was excited at 405 nm; fluorescence emission was detected with a 470- to 500-nm band-pass filter. EYFP fluorescence was excited at 514 nm, and the emission was recorded with a 530- to 600-nm band-pass filter.

Targeting of mt-PXN to yeast mitochondria was validated by transforming FGY217 yeast cells with pMSU388 ensuring constitutive expression of the mt-PXN-EYFP fusion protein via the pPMA1 promoter. Yeast cells carrying pMSU388 were grown in liquid culture overnight in SC-Ura with 2% (w/v) Glc. Yeast cells were harvested by centrifugation for 5 min at 3000g, washed with 25 mM HEPES-KOH (pH 7.3) and 10 mM MgCl₂ and then stained with 50 μ M MitoTracker ORANGE CMTMRos (Life Technologies/Thermo Scientific) for 10 min at room temperature. Residual MitoTracker dye was removed by washing with wash buffer twice. Yeast cells were immobilized on poly-L-Lys coated microscope slides for confocal microscopy. Analysis of yeast cells was performed with a confocal laser scanning microscope model no. 510 Meta (Carl Zeiss). MitoTracker fluorescence was excited at 561 nm, fluorescence emission was detected with a 575- to 615-nm band-pass filter. EYFP fluorescence was excited at 514 nm and the emission was recorded with a 530- to 600-nm band-pass filter.

Accession Numbers

Sequence data from this article can be found in the GenBank/EMBL data libraries under accession numbers NP_181526.1.

van Roermund et al.

Supplemental Data

The following supplemental materials are available.

Supplemental Table S1. Primer used in this study; restriction sites (RS) are underlined.

Supplemental Figure S1. Substrate specificity of the peroxisomal ATP carrier An1p from *S. cerevisiae*.

ACKNOWLEDGMENTS

Authors thank Jeanine Schlebusch and Daniel Wrobel for assistance with obtaining yeast growth curves. For technical assistance, the authors acknowledge Kirsten Abel. We thank Dr. R. van der Bend from Saxion Hogeschool (Life Science, Engineering, and Design) in Deventer for assistance in generating the *np1Δ* and *mdh3/np1Δ* double mutants and grateful to Lodewijk IJlst for stimulating discussion.

Received April 2, 2016; accepted April 29, 2016; published May 2, 2016.

LITERATURE CITED

- AbdelRaheim SR, Cartwright JL, Gasmi L, McLennan AG (2001) The NADH diphosphatase encoded by the *Saccharomyces cerevisiae* NPY1 nudix hydrolase gene is located in peroxisomes. *Arch Biochem Biophys* 388: 18–24
- Agrimi G, Brambilla L, Frascotti G, Pisano I, Porro D, Vai M, Palmieri L (2011) Deletion or overexpression of mitochondrial NAD⁺ carriers in *Saccharomyces cerevisiae* alters cellular NAD and ATP contents and affects mitochondrial metabolism and the rate of glycolysis. *Appl Environ Microbiol* 77: 2239–2246
- Agrimi G, Russo A, Scarcia P, Palmieri F (2012a) The human gene SLC25A17 encodes a peroxisomal transporter of coenzyme A, FAD and NAD⁺. *Biochem J* 443: 241–247
- Agrimi G, Russo A, Pierri CL, Palmieri F (2012b) The peroxisomal NAD⁺ carrier of *Arabidopsis thaliana* transports coenzyme A and its derivatives. *J Bioenerg Biomembr* 44: 333–340
- Ast J, Stiebler AC, Freitag J, Bölker M (2013) Dual targeting of peroxisomal proteins. *Front Physiol* 4: 297
- Bai P, Nagy L, Fodor T, Liaudet L, Pacher P (2015) Poly(ADP-ribose) polymerases as modulators of mitochondrial activity. *Trends Endocrinol Metab* 26: 75–83
- Bernhardt K, Wilkinson S, Weber APM, Linka N (2012) A peroxisomal carrier delivers NAD⁺ and contributes to optimal fatty acid degradation during storage oil mobilization. *Plant J* 69: 1–13
- Carrie C, Kühn K, Murcha MW, Duncan O, Small ID, O'Toole N, Whelan J (2009) Approaches to defining dual-targeted proteins in *Arabidopsis*. *Plant J* 57: 1128–1139
- Catoni E, Schwab R, Hilpert M, Desimone M, Schwacke R, Flügge UI, Schumacher K, Frommer WB (2003) Identification of an *Arabidopsis* mitochondrial succinate-fumarate translocator. *FEBS Lett* 534: 87–92
- Chang HC, Guarente L (2014) SIRT1 and other sirtuins in metabolism. *Trends Endocrinol Metab* 25: 138–145
- De Marcos Lousa C, van Roermund CWT, Postis VLG, Dietrich D, Kerr ID, Wanders RJA, Baldwin SA, Baker A, Theodoulou FL (2013) Intrinsic acyl-CoA thioesterase activity of a peroxisomal ATP binding cassette transporter is required for transport and metabolism of fatty acids. *Proc Natl Acad Sci USA* 110: 1279–1284
- Dröge W (2002) Free radicals in the physiological control of cell function. *Physiol Rev* 82: 47–95
- Elgersma Y, van den Berg M, Tabak HF, Distel B (1993) An efficient positive selection procedure for the isolation of peroxisomal import and peroxisome assembly mutants of *Saccharomyces cerevisiae*. *Genetics* 135: 731–740
- Fulda M, Schnurr J, Abbadi A, Heinz E, Browse J (2004) Peroxisomal Acyl-CoA synthetase activity is essential for seedling development in *Arabidopsis thaliana*. *Plant Cell* 16: 394–405
- Gietz RD, Schiestl RH (2007) High-efficiency yeast transformation using the LiAc/SS carrier DNA/PEG method. *Nat Protoc* 2: 31–34
- Graham IA (2008) Seed storage oil mobilization. *Annu Rev Plant Biol* 59: 115–142
- Guedener U, Heinisch J, Koehler GJ, Voss D, Hegemann JH (2002) A second set of loxP marker cassettes for Cre-mediated multiple gene knockouts in budding yeast. *Nucleic Acids Res* 30: e23
- Gurvitz A, Rottensteiner H (2006) The biochemistry of oleate induction: transcriptional upregulation and peroxisome proliferation. *Biochim Biophys Acta* 1763: 1392–1402
- Haferkamp I, Schmitz-Esser S (2012) The plant mitochondrial carrier family: functional and evolutionary aspects. *Front Plant Sci* 3: 2
- Hiltunen JK, Wenzel B, Beyer A, Erdmann R, Fossá A, Kunau WH (1992) Peroxisomal multifunctional β -oxidation protein of *Saccharomyces cerevisiae*. Molecular analysis of the fox2 gene and gene product. *J Biol Chem* 267: 6646–6653
- Hoepfner D, Schildknecht D, Braakman I, Philippsen P, Tabak HF (2005) Contribution of the endoplasmic reticulum to peroxisome formation. *Cell* 122: 85–95
- Houtkooper RH, Cantó C, Wanders RJ, Auwerx J (2010) The secret life of NAD⁺: an old metabolite controlling new metabolic signaling pathways. *Endocr Rev* 31: 194–223
- Hu J, Baker A, Bartel B, Linka N, Mullen RT, Reumann S, Zolman BK (2012) Plant peroxisomes: biogenesis and function. *Plant Cell* 24: 2279–2303
- Kota J, Gilstring CF, Ljungdahl PO (2007) Membrane chaperone Shr3 assists in folding amino acid permeases preventing precocious ERAD. *J Cell Biol* 176: 617–628
- Leonardi R, Zhang YM, Rock CO, Jackowski S (2005) Coenzyme A: back in action. *Prog Lipid Res* 44: 125–153
- Lingner T, Kataya AR, Antonicelli GE, Benichou A, Nilssen K, Chen X-Y, Siemsen T, Morgenstern B, Meinicke P, Reumann S (2011) Identification of novel plant peroxisomal targeting signals by a combination of machine learning methods and in vivo subcellular targeting analyses. *Plant Cell* 23: 1556–1572
- Linka N, Esser C (2012) Transport proteins regulate the flux of metabolites and cofactors across the membrane of plant peroxisomes. *Front Plant Sci* 3: 3
- Linka N, Theodoulou FL (2013) Metabolite transporters of the plant peroxisomal membrane: known and unknown. *Subcell Biochem* 69: 169–194
- Linka N, Theodoulou FL, Haslam RP, Linka M, Napier JA, Neuhaus HE, Weber APM (2008) Peroxisomal ATP import is essential for seedling development in *Arabidopsis thaliana*. *Plant Cell* 20: 3241–3257
- Mettler JJ, Beevers H (1980) Oxidation of NADH in glyoxysomes by a malate-aspartate shuttle. *Plant Physiol* 66: 555–560
- Mittler R (2002) Oxidative stress, antioxidants and stress tolerance. *Trends Plant Sci* 7: 405–410
- Ogawa T, Yoshimura K, Miyake H, Ishikawa K, Ito D, Tanabe N, Shigeoka S (2008) Molecular characterization of organelle-type Nudix hydrolases in *Arabidopsis*. *Plant Physiol* 148: 1412–1424
- Palmieri F, Rieder B, Ventrella A, Blanco E, Do PT, Nunes-Nesi A, Trauth AU, Fiermonte G, Tjaden J, Agrimi G, et al (2009) Molecular identification and functional characterization of *Arabidopsis thaliana* mitochondrial and chloroplastic NAD⁺ carrier proteins. *J Biol Chem* 284: 31249–31259
- Palmieri L, Rottensteiner H, Girzalsky W, Scarcia P, Palmieri F, Erdmann R (2001) Identification and functional reconstitution of the yeast peroxisomal adenine nucleotide transporter. *EMBO J* 20: 5049–5059
- Palmieri L, Santoro A, Carrari F, Blanco E, Nunes-Nesi A, Arrigoni R, Genchi F, Fernie AR, Palmieri F (2008) Identification and characterization of ADNT1, a novel mitochondrial adenine nucleotide transporter from *Arabidopsis*. *Plant Physiol* 148: 1797–1808
- Pollak N, Dölle C, Ziegler M (2007) The power to reduce: pyridine nucleotides—small molecules with a multitude of functions. *Biochem J* 402: 205–218
- Pracharoenwattana I, Cornah JE, Smith SM (2007) *Arabidopsis* peroxisomal malate dehydrogenase functions in β -oxidation but not in the glyoxylate cycle. *Plant J* 50: 381–390
- Rentsch D, Laloi M, Rouhara I, Schmelzer E, Delrot S, Frommer WB (1995) NTR1 encodes a high affinity oligopeptide transporter in *Arabidopsis*. *FEBS Lett* 370: 264–268
- Reumann S, Bettermann M, Benz R, Heldt HW (1997) Evidence for the presence of a porin in the membrane of glyoxysomes of castor bean. *Plant Physiol* 115: 891–899

2138

Plant Physiol. Vol. 171, 2016

Peroxisomal NAD Carrier as NAD/AMP Exchanger

- Reumann S, Maier E, Benz R, Heldt HW (1996) A specific porin is involved in the malate shuttle of leaf peroxisomes. *Biochem Soc Trans* **24**: 754–757
- Reumann S, Maier E, Benz R, Heldt HW (1995) The membrane of leaf peroxisomes contains a porin-like channel. *J Biol Chem* **270**: 17559–17565
- Rokka A, Antonenkov VD, Soininen R, Immonen HL, Pirilä PL, Bergmann U, Sormunen RT, Weckström M, Benz R, Hiltunen JK (2009) Pxmp2 is a channel-forming protein in Mammalian peroxisomal membrane. *PLoS One* **4**: e5090
- Sambrook J, Russell DW (2001) *Molecular Cloning: A Laboratory Manual*. Cold Spring Harbor Laboratory Press, Cold Spring Harbor, NY
- Theodoulou FL, Bernhardt K, Linka N, Baker A (2013) Peroxisome membrane proteins: multiple trafficking routes and multiple functions? *Biochem J* **451**: 345–352
- Todisco S, Agrimi G, Castegna A, Palmieri F (2006) Identification of the mitochondrial NAD⁺ transporter in *Saccharomyces cerevisiae*. *J Biol Chem* **281**: 1524–1531
- Tumaney AW, Ohlrogge JB, Pollard M (2004) Acetyl coenzyme A concentrations in plant tissues. *J Plant Physiol* **161**: 485–488
- van Roermund CWT, Drissen R, van Den Berg M, Ijlst L, Hettema EH, Tabak HF, Waterham HR, Wanders RJA (2001) Identification of a peroxisomal ATP carrier required for medium-chain fatty acid β -oxidation and normal peroxisome proliferation in *Saccharomyces cerevisiae*. *Mol Cell Biol* **21**: 4321–4329
- van Roermund CWT, Elgersma Y, Singh N, Wanders RJA, Tabak HF (1995) The membrane of peroxisomes in *Saccharomyces cerevisiae* is impermeable to NAD(H) and acetyl-CoA under *in vivo* conditions. *EMBO J* **14**: 3480–3486
- Visser WF, van Roermund CWT, Ijlst L, Waterham HR, Wanders RJA (2007) Metabolite transport across the peroxisomal membrane. *Biochem J* **401**: 365–375
- Yogev O, Pines O (2011) Dual targeting of mitochondrial proteins: mechanism, regulation and function. *Biochim Biophys Acta* **1808**: 1012–1020
- Zallot R, Agrimi G, Lerma-Ortiz C, Teresinski HJ, Frelin O, Ellens KW, Castegna A, Russo A, de Crécy-Lagard V, Mullen RT, et al (2013) Identification of mitochondrial coenzyme A transporters from maize and Arabidopsis. *Plant Physiol* **162**: 581–588

Author contribution

Lennart Charton performed the heterologous protein expression and uptake experiments of Ant1p shown in Figure S1.

V. Submitted Manuscripts

V.I Submitted Manuscript 1

Evidence for dual targeting of Arabidopsis plastidial glucose-6-phosphate transporter GPT1 to peroxisomes via the ER

Marie-Christin Baune¹, Hannes Lansing¹, Kerstin Fischer¹, Tanja Meyer¹,
Lennart Charton², Nicole Linka² and Antje von Schaewen^{1*}

¹ Institut für Biologie und Biotechnologie der Pflanzen (IBBP), Westfälische Wilhelms-
Universität Münster, Münster, Germany

² Biochemie der Pflanzen, Heinrich-Heine-Universität Düsseldorf, Düsseldorf, Germany

* Corresponding author

Submitted to Plant Cell

43 **ABSTRACT** (200 words)

44

45 Former studies on Arabidopsis glucose-6-phosphate/phosphate translocator isoforms GPT1
46 and GPT2 reported viability of *gpt2* mutants, however an essential function for GPT1,
47 manifesting as a variety of *gpt1* defects in the heterozygous state during fertilization/seed
48 set. Among other functions, GPT1 is important for pollen and embryo-sac development.
49 Since previous work on enzymes of the oxidative pentose phosphate pathway (OPPP)
50 revealed comparable effects, we investigated whether GPT1 might dually localize to plastids
51 and peroxisomes. In reporter fusions, GPT2 was found at plastids, but GPT1 also at the
52 endoplasmic reticulum (ER) and around peroxisomes. GPT1 contacted oxidoreductases and
53 also peroxins that mediate import of peroxisomal membrane proteins from the ER, hinting at
54 dual localization. Reconstitution in yeast proteoliposomes revealed that GPT1 preferentially
55 exchanges glucose-6-phosphate for ribulose-5-phosphate. Complementation analyses of
56 heterozygous *gpt1* plants demonstrated that GPT2 is unable to compensate for GPT1 in
57 plastids, whereas genomic *GPT1* without transit peptide (enforcing ER/peroxisomal
58 localization) increased *gpt1* transmission significantly. Since OPPP activity in peroxisomes is
59 essential during fertilization, and immuno-blot analyses hinted at unprocessed GPT1-specific
60 bands, our findings suggest that GPT1 is indispensable at both plastids and peroxisomes.
61 Together with the G6P-Ru5P exchange preference, dual targeting explains why GPT1 exerts
62 functions distinct from GPT2 in Arabidopsis.

63

64 **INTRODUCTION** (1403 words)

65 In plant cells, the oxidative pentose phosphate pathway (OPPP) is found in plastids and the
66 cytosol (reviewed in Kruger and von Schaewen, 2003), but transiently also in peroxisomes
67 (Meyer et al., 2011; Hölscher et al., 2014; 2016). In each subcellular compartment, the OPPP
68 has distinctive functions and thus requires subcellular distribution of the corresponding enzymes
69 and their metabolites.

70 During the day, NADPH is provided by photosynthetic electron flow to ferredoxin-(Fd) NADP⁺
71 oxidoreductase (FNR; Palatnik et al., 2003), whereas at night, the OPPP is the main source of
72 NADPH in chloroplasts and in heterotrophic plastids of non-green tissues (Dennis et al., 1997).
73 The oxidation of 1 mole glucose-6-phosphate (G6P) to ribulose-5-phosphate (Ru5P) produces 2
74 moles of NADPH (at the expense of CO₂ release) in three enzymatic steps: i) glucose-6-
75 phosphate dehydrogenase (G6PD), ii) 6-phosphogluconolactonase (6PGL), and iii) 6-phospho-
76 gluconate dehydrogenase (6PGD). These irreversible reactions are followed by reversible OPPP
77 steps in the stroma, comprising transketolase (TK) and transaldolase (TA) that create a broad
78 range of phosphorylated intermediates. Since the reversible OPPP reactions share
79 intermediates with the Calvin cycle, they are essential for plant metabolism (reviewed in Kruger
80 and von Schaewen, 2003). In the cytosol of plant cells only the irreversible OPPP reactions
81 occur (Schnarrenberger et al., 1995), linked to the full cycle in plastids via epimerization of Ru5P
82 to Xu5P and import by the Xylulose-5-phosphate/phosphate translocator (XPT) in the inner
83 envelope (Eicks et al., 2002).

84 NADPH is the preferred reducing equivalent of anabolic reactions, both in plastids and the
85 cytosol, needed mostly for the biosynthesis of amino acids, fatty acids, and nucleotides
86 (Hutchings et al., 2005; Geigenberger et al., 2005). Furthermore, NADPH is important for redox
87 homeostasis of the glutathione pool (GSH/GSSG) via NADPH-dependent glutathione-disulfide
88 reductases (GRs). Arabidopsis GR1 dually localizes in the cytosol and peroxisomes (Marty et
89 al., 2009; Mhamdi et al., 2010; Kataya and Reumann, 2010) and GR2 in plastids and
90 mitochondria (Marty et al., 2019). Hence, OPPP reactions play an important role in plant cells
91 (Kruger and von Schaewen, 2003), particularly with the onset of stress or developmental
92 change. Such conditions are often linked to physiological sink states induced by pathogen
93 infection of leaves and related signaling. Resulting callose formation at plasmodesmata leads to
94 sugar accumulation in the cytosol that stimulates G6PDH activity/expression and NADPH
95 production via the OPPP (Hauschild and von Schaewen, 2003; Scharte et al., 2009; Stampfl et
96 al., 2016). Concomitantly activated NADPH oxidases at the plasma membrane (in plants called

129 To provide the peroxisomal OPPP reactions with substrate, we reasoned that one of the two
130 Arabidopsis GPT proteins may dually localize to peroxisomes, similar to originally plastid-
131 annotated OPPP isoforms G6PD1 (Meyer et al., 2011) and PGL3 (Kruger and von Schaewen,
132 2003; Reumann et al., 2004; Hölscher et al., 2014). GPT1 and GPT2 show 81% identity at the
133 amino-acid level and catalyze the import of G6P into heterotrophic plastids needed for starch
134 synthesis and NADPH provision via the stromal OPPP reactions (Kammerer et al., 1998). GPT2
135 expression is most abundant in heterotrophic tissues (senescing leaves, sepals, seeds) and can
136 be induced by high light in leaves (Athanasίου et al., 2010; Weise et al., 2019), whereas GPT1 is
137 ubiquitously expressed, with highest levels in reproductive tissues (Niewiadomski et al., 2005;
138 Kunz et al., 2010). Loss of GPT2 function reduced starch levels, but yielded vital plants
139 (Niewiadomski et al., 2005; Kunz et al., 2010; Athanasίου et al., 2010; Dyson et al., 2014; 2015).
140 However, lack of GPT1 was detrimental, leading to an early arrest of pollen and ovule develop-
141 ment. Resulting gametophyte and embryo lethality showed as incompletely filled siliques
142 (Niewiadomski et al., 2005; Andriotis et al., 2010; Flügge et al., 2011).

143 We noticed that GPT1 displays a canonical C-terminal peroxisomal targeting signal type 1
144 (PTS1 motif AKL) that matches the consensus (S/A)-(K/R)-(L/M/I) of soluble proteins (Gould et
145 al., 1989; Reumann, 2004; Platta and Erdmann, 2007; Reumann and Bartel, 2016). This
146 seemed odd, since peroxisomal membrane proteins (PMPs) exhibit independent mPTS motifs of
147 varying sequence (Rottensteiner et al., 2004). In general, two classes of PMPs are known.
148 Class-I PMPs are directly inserted into peroxisomal membranes (PerMs) from the cytosol, which
149 involves peroxins Pex3 and Pex19 (in some organisms also Pex16; Platta and Erdmann, 2007).
150 By contrast, class-II PMPs are first inserted into the endoplasmic reticulum (ER) via the Sec61
151 import pore and then transported to the peroxisomal ER (perER), from where peroxisomes are
152 formed *de novo* (Theodoulou et al., 2013; Reumann and Bartel, 2016; Kao et al., 2018). The
153 exact mechanism remains to be resolved, but involvement of Pex16 and Pex3 for ER
154 recruitment and sorting to peroxisomes is most likely (Aranovich et al., 2014). Interestingly,
155 mutation of Arabidopsis *PEX16* resulted in a shrunken seed phenotype (*sse1*) with impaired fatty
156 acid biosynthesis (Lin et al., 1999, 2004), reminiscent of some *gpt1* defects (Niewiadomski et al.,
157 2005), but no defects in pollen germination.

158 Here we report that both GPT1 and GPT2 may insert into the ER, but only the N-terminal part of
159 GPT1 is able to initiate ER targeting, a prerequisite shared with class-II PMPs. Co-expression of
160 various reporter fusions was used to analyze subcellular localization and protein interaction of
161 GPT1 in plant cells. GPT1 formed homodimers at plastids, but not readily at the ER, and
162 interacted with two cytosolic oxidoreductases listed by the Membrane-based Interactome

97 respiratory burst oxidase homologues, Rboh; Torres et al., 2002) use cytosolic NADPH for
98 extrusion of reactive oxygen species (ROS) into the apoplast. Superoxide (O_2^-) is converted to
99 hydrogen peroxide (H_2O_2) that enters the cell via aquaporins, leading to redox signaling in the
100 cytosol. H_2O_2 is dissipated by peroxiredoxins (Prx), which in turn retrieve electrons from
101 glutaredoxins (Grx) and thioredoxins (Trx), and the resulting dithiol-disulfide changes modulate
102 cognate target enzymes in a similar manner (reviewed in Noctor and Foyer, 2016; Waszczak et
103 al., 2018; Liebthal et al., 2018). This scenario also accompanies abiotic stress responses (e.g. to
104 drought or salt), together with phosphorylation cascades activated in parallel (Pitzschke et al.,
105 2006; dal Santo et al., 2012; Fancy et al., 2016; Landi et al., 2016).

106 OPPP enzymes were also found in purified plant peroxisomes (Corpas et al., 1998; del Río et
107 al., 2002; Reumann et al., 2007; Hölscher et al., 2016), where they may serve as NADPH source
108 to establish redox homeostasis via dual cytosolic/peroxisomal GR1 (Kataya and Reumann,
109 2010). Besides, NADPH is needed for metabolic reactions that occur exclusively in peroxisomes,
110 like removal of double bonds in unsaturated fatty acid/acyl chains prior to β -oxidation, which
111 includes final steps of auxin/jasmonic acid biosynthesis (Reumann et al., 2004). We previously
112 reported that dual targeting of *Arabidopsis thaliana* OPPP enzymes G6PD1 (At5g35790, OPPP
113 step 1) and PGL3 (At5g24400, OPPP step 2) to plastids and peroxisomes depends on the
114 cytosolic redox state (Meyer et al., 2011; Hölscher et al., 2014). Furthermore, plants
115 heterozygous for peroxisomal isoform PGD2 (At3g02360, OPPP step 3) failed to produce
116 homozygous offspring due to mutual sterility of the *pgd2* gametophytes. This indicated for the
117 first time an essential function of the OPPP in peroxisomes (Hölscher et al., 2016).

118 OPPP activity in organelles requires flux of intermediates across the corresponding membranes.
119 In *Arabidopsis*, G6P import into plastids involves G6P/phosphate translocator GPT1
120 (At5g54800) and GPT2 (At1g61800) in the inner envelope membrane (Kammerer et al., 1998;
121 Eicks et al., 2002; Knappe et al., 2003; Niewiadomski et al., 2005). In case of peroxisomes,
122 phosphorylated metabolites with a huge hydration shell are likely unable to pass the porin-like
123 channel described for malate and oxaloacetate (134 and 130 Da) first described in spinach
124 (Reumann et al., 1996). In mammalian cells, Rokka et al. (2009) measured that only molecules
125 below 200 Da are able to pass the pore-like channel of Pxmp2. G6P and Ru5P/Xu5P are larger
126 (258 Da and 230 Da), implying that they are unlikely transported via peroxisomal porins. Thus,
127 the issue of OPPP substrate and product transport across peroxisomal membranes remained
128 unclear so far.

163 Network Database (MIND) for Arabidopsis proteins with 38% confidence (Lalonde et al., 2010;
164 Chen et al., 2012; Jones et al., 2014). In addition, we found evidence for transient interaction of
165 GPT1 with early peroxins involved in PMP delivery via the ER. As rare event, GPT1-reporter
166 fusions were detected in membrane structures surrounding peroxisomes. Our main questions
167 were: 1) which protein parts confer dual targeting; 2) how this may be regulated; 3) which OPPP
168 metabolite leaves peroxisomes; and 4) whether some defects of heterozygous *gpt1* mutant
169 plants (Niewiadomski et al., 2005) may be related to missing transport across peroxisomal
170 membranes during fertilization.

171

172

173 **RESULTS** (2911 words)

174

175 **GPT1 dually targets plastids and the ER**

176 The alignment of GPT1 and GPT2 protein sequences from different *Brassicaceae*
177 (Supplemental Figure 1) revealed that the isoforms mostly diverge at their N-terminal ends,
178 whereas the central transmembrane regions (for substrate binding/transport) are highly
179 conserved. Subcellular targeting was studied with various N- and C-terminal reporter fusions of
180 the two Arabidopsis GPT isoforms and examined in transfected protoplasts (Arabidopsis or
181 tobacco) by confocal laser-scanning microscopy (CLSM).

182 All N-terminally masked/truncated GPT variants (Supplemental Figure 2A) localized at the ER
183 (Supplemental Figure 2B, green signals) as determined by co-expression with organelle markers
184 (magenta signals), i.e. G/OFP-ER (Rips et al., 2014) or peroxisome (Per) marker G/OFP-
185 PGL3_ *C-short* (formerly named G/OFP-PGL3(~50aa)-SKL; Meyer et al., 2011). Note that co-
186 localization of green and magenta signals appears white. Both GPT fusions occasionally formed
187 *Z membranes* (Supplemental Figure 2B, white patches), a term coined for overexpressed
188 integral membrane proteins (Gong et al., 1996). GPT1_ *C-full* labeled ring-like substructures of
189 the ER, approximately 3 μm in diameter (Supplemental Figure 2C, panel b), and interfered with
190 import of the peroxisome marker (Supplemental Figure 2B, panel n), which was never observed
191 for GPT2_ *C-full* (Supplemental Figure 2B, panel p). Mutagenesis of GPT1-AKL to -AKQ (or
192 GPT2-AKQ to -AKL) had no effect on localization of the fusion proteins (not shown).

193 Among the C-terminal reporter fusions, localization of GPT1 also differed from GPT2. The GPT1
194 *full-length* version (Figure 1A), with GFP pointing to the plastid stroma (or cytosol, when inserted
195 into the ER), was spotted at both plastids and the ER (Figure 1B, panels a,c, arrowheads), but

6

196 GPT2 only at plastids (Figure 1B, panels b,d, green signals; for single channel images, see
197 Supplemental Figure 3B). A region comprising the N-terminus plus first five membrane domains
198 (*N-5MD*, 1-240 amino acids) with OFP pointing to the intermembrane space (IMS), labeled the
199 plastid surface (Supplemental Figure 4B, panels a-d; green signals). The N-terminus plus first
200 two membrane domains (*N-2MD*, 1-155 amino acids) with GFP pointing to the stroma showed
201 patchy plastid labeling, indicative of partial reporter cleavage (Supplemental Figure 4B, panels e-
202 h), and in case of GPT1 also ER labeling (Figure 4B, panels e, and f, arrowheads), albeit to
203 varying extent (Supplemental Figure 4C, panels a-e). Again, small ring-like structures of
204 peroxisomal size were labeled by GFP, but without surrounding the peroxisome marker (Supple-
205 mental Figure 4C, panel e, single sections). With the N-terminal region (*N-term*, 1-91/92 amino
206 acids) fused to the reporter, stroma labeling was observed for both GPT proteins (Supplemental
207 Figure 4B, panels i-l). These results indicated that the region comprising the N-terminus plus first
208 two transmembrane GPT1 domains is important for alternative targeting to the ER.

209

210 **The first 155 amino acids of GPT1 are crucial for ER targeting**

211 To exclude localization artifacts by masking N- or C-terminal targeting signals, we also cloned
212 GPT-fusions with internal reporter at two different positions (Supplemental Figure 5A). Again, the
213 GPT1 versions (*GPT1_2MD:8MD* and *GPT1_5MD:5MD*) labeled both plastids and the ER
214 (Supplemental Figure 5B, panels a,b and e,f; arrowheads), whereas the GPT2 versions
215 (*GPT2_2MD:8MD* and *GPT2_5MD:5MD*) only plastids (Supplemental Figure 5B, panels c,d and
216 g,h). Protoplasts expressing the *GPT_2MD:8MD* fusions were additionally treated with Brefeldin
217 A (BFA), which interfered with delivery of peroxisomal ascorbate peroxidase (pxAPX) via the ER
218 (Mullen et al., 1999). BFA treatment abolished GPT1 signals at the ER, but not at plastids
219 (neither of GPT2; Supplemental Figure 6). This confirmed direct GPT targeting to plastids, and
220 that only GPT1 may insert into the ER.

221 Since alternative GPT1 localization seemed mediated by the soluble N-terminal part that
222 strongly differs from GPT2 (Figure S1), amino acid positions suspected to be subject to post-
223 translational modification were changed by site-directed mutagenesis in the medial
224 *GPT1_5MD:5MD* fusion (Figure 1C). However, neither S27 (listed by PhosPhAt 4.0; Zulawski et
225 al., 2013) changed to alanine (A, abolishing phosphorylation) or aspartate (D, mimicking
226 phosphorylation; Ackerley et al., 2003), nor single cysteine C65 changed to serine (S, precluding
227 redox modification) interfered with ER targeting. Domain swaps among the corresponding
228 unmodified *medial* reporter constructs (Figure 2A) resulted in dual localization of
229 *GPT1_2MD:8MD_GPT2* and *GPT1_5MD:5MD_GPT2* to plastids and the ER (Figure 2B, panels

7

230 a,b and e,f; arrowheads), but solely plastid localization of GPT2_2MD:8MD_GPT1 and
231 GPT2_5MD:5MD_GPT1 (Figure 2B, panels e,d and g,h; for single channel images, see
232 Supplemental Figure 7). These results proved that the GPT1 N-terminus (plus first two MDs) is
233 crucial for initiating alternative ER targeting.

234

235 **GPT1 dimer formation occurs at plastids and substructures of the ER**

236 In functional form, the plastidial phosphate translocators are dimers composed of two identical
237 subunits (Knappe et al., 2003). We therefore reasoned, if not necessary for ER targeting, amino
238 acids S27 and/or C65 may be important for preventing GPT1 dimerization prior to reaching the
239 final location(s). Therefore N- and C-terminal split YFP constructs of GPT1 were cloned and
240 above described amino-acid changes introduced. Arabidopsis protoplasts were transfected and
241 analyzed for GPT1-dimer formation (Figure 3) by bimolecular fluorescence complementation
242 (BiFC; Walter et al., 2004). Reconstitution of the GPT1-split YFP combinations was detected
243 only at plastids (Figure 3B, panels a-d), without effect of the indicated amino acid changes. In
244 case of the split YFP-GPT1 fusions (enforcing ER insertion), large signal accumulations in the
245 ER (including perinuclear structures) were observed for most variants. This signal did not
246 represent the usually observed ER pattern and even affected distribution of the ER marker (see
247 Figures 1 and 2). Among the amino acid changes analyzed, only C65S had an effect, resulting in
248 hollow spherical structures surrounding single peroxisomes (Figure 3C, arrowhead) compared to
249 the wild-type situation or S27 changes (Figure 3B, compare panels f-g to panel i, arrowhead; for
250 single channel images, see Supplemental Figure 8). Thus, ER insertion seems not to require
251 posttranslational modification, but sorting to PerMs may be negatively regulated by C65
252 modification.

253

254 **GPT1 recruitment to the ER involves redox transmitters**

255 To find potential interaction partners of GPT1, the Membrane-based Interactome Database
256 (MIND) of Arabidopsis proteins (based on split ubiquitin reconstitution in yeast; Lalonde et al.,
257 2010), was searched. Two cytosolic oxidoreductases, Thioredoxin *h7* (Trx_{h7}, At1g59730) and
258 Glutaredoxin *c1* (Grx_{c1}, At5g63030), were among the 21 candidates listed with highest score
259 (Supplemental Table 1). BiFC analyses in Arabidopsis protoplasts confirmed interaction of GPT1
260 with Trx_{h7} (Figure 4A) and Grx_{c1} (Figure 4B) at the ER and its substructures, but not at plastids
261 (Figure 4A, panel b), and more clearly when the N-terminus of GPT1 was masked (enforcing ER
262 insertion). Occasionally, ER-derived membranes around peroxisomes were labeled (Figure 4A,
263 panel b and d; Figure 4B, panel b, arrowheads), which was less obvious when the N-terminus of

8

264 Grx_{ct} was masked by split YFP (Figure 4B, panels c,d). To enhance interaction among the
265 Arabidopsis proteins, selected BiFC combinations were co-expressed with the other oxido-
266 reductase as OFP fusion in heterologous tobacco protoplasts. Similar results were obtained
267 (Figure 4C and D) and also smaller spherical structures (<3 μm) detected. Of note, in simple co-
268 expression studies, both Trx_{ht}-OFP and Grx_{ct}-OFP partially overlapped with the ER marker
269 (Supplemental Figure 9B, white signals), confirming predicted N-myristoylation, and co-localized
270 with GPT1_*N-2MD*-GFP at the ER (Supplemental Figure 9C). These results are consistent with
271 the two oxidoreductases assisting GPT1 insertion into the ER and/or sorting to peroxisomes.

272

273 **GPT1 contacts peroxins Pex3 and Pex16 at the ER**

274 While class-I PMPs are inserted into PerMs directly from the cytosol (involving Pex3 and Pex19),
275 class-II PMPs are first inserted into the ER (Platta and Erdmann, 2007). Since Pex3, Pex16, and
276 Pex19 play also central roles during ER insertion, sorting of peroxisomal membrane proteins,
277 and peroxisome biogenesis (Reumann and Bartel, 2016; Kao et al., 2018), we set out to analyze
278 potential interaction with GPT1. In Arabidopsis, two Pex3 genes, Pex3-1 (At3g18160) and
279 Pex3-2 (At1g48635; Hunt and Trelease, 2004), one Pex16 gene (At2g45690; Karnik and
280 Trelease, 2005) and two Pex19 genes, Pex19-1 (At3g03490) and Pex19-2 (At5g17550; Hadden
281 et al., 2006) exist. Analysis of N- and C-terminal reporter fusions in protoplasts revealed mainly
282 PerM labeling for the two Pex3 isoforms, ER and PerM labeling for Pex16 (see also Lansing et
283 al., 2019), and mostly cytosolic distribution for the two Pex19 isoforms (Supplemental Figure 10,
284 shown for one of the two Pex3 and Pex19 isoforms). OFP-Pex3-1 displayed weak signals in the
285 cytosol (not shown). BiFC analyses were conducted with Pex3-1, Pex16 and Pex19-1. GPT1
286 interaction with Pex3-1 and Pex16 was detected at PerMs, partially contiguous with the ER
287 (Figure 5A, panels a,b). By contrast, GPT1 interaction with Pex19 was mostly distributed across
288 the cytosol, but also labeled spherical structures (Figure 5A, panel d), when the C-terminal
289 farnesylation motif (McDonnell et al., 2016) was accessible. Again, Pex16-GPT1 interaction
290 interfered with import of the peroxisome (Per) marker (Figure 5A, panel b, magenta signals
291 largely cytosolic), as already observed for GFP-GPT1_*C-full* (Supplemental Figure 2, panel n).
292 Co-expression of GFP-GPT1_*C-full* with the OFP-based Pex fusions resulted in different
293 patterns (Figure 5B), suggesting that the Pex interactions are merely transient. Co-expression
294 with Pex3-1-OFP led in part to perinuclear localization of GFP-GPT1_*C-full*, reminiscent of the
295 BiFC data obtained for GPT1 homodimerization (Figure 5B, panel a compared to Figure 3,
296 panels f-i). Interestingly, Pex16 co-expression had visible effects on GPT1 localization,
297 promoting concentration/vesiculation at the ER (Figure 5B, panel b), similar to Pex16 alone, but

9

298 distinct from it (Supplemental Figure 10, compare B to C). In co-expression, Pex19-1 seemed to
299 have no impact on GPT1 localization (Figure 5B, panels c and d).

300 To make sure that the co-expression patterns obtained with Pex16 are no artifacts due to
301 expression from the strong constitutive CaMV 35S promoter (*Pro35S*), two N-terminally
302 truncated GPT1 versions (designated for stable plant transformation) were expressed also from
303 the own promoter (*ProGPT1*), which gave comparable results (Figure 5C, for single channel
304 images, see Supplemental Figure 11). Together with above BiFC analyses (Figure 5A), this
305 demonstrated that ER-inserted GPT1 can be dragged to PerMs, and thus behaves like a class-II
306 PMP that requires a special trigger to contact partner(s) (including Pex3 and Pex16) to reach
307 mature peroxisomes.

308

309 **GPT1 may be recruited to peroxisomes and preferentially exchanges G6P for** 310 **Ru5P**

311 After plastid import, the N-terminal transit peptide (TP) of the precursor proteins is usually
312 cleaved off (Schmidt et al., 1979; Chua and Schmidt, 1979). According to the recent elucidation
313 of the 3-dimensional structure of the Arabidopsis triose-phosphate/phosphate translocator (Lee
314 et al., 2017), both N- and C-terminal ends of GPT face the stroma. In case of GPT1 insertion into
315 the ER, both the unprocessed N-terminus and C-terminal end should point to the cytosol, which
316 was confirmed by topology analyses using *roGFP* (Supplemental Figure 12). To test whether N-
317 terminal modification or lack of transit-peptide processing might affect transport activity, we
318 fused an N-terminal His tag (or GFP) to the *full-length* and *mature* GPT1 versions (with *mature*
319 GPT2 as control) and measured metabolite exchange of the recombinant proteins in
320 reconstituted yeast proteoliposomes (Linka et al., 2008). For the physiological exchange of G6P
321 versus Pi using the mature versions (Figure 6A), His-matGPT1 reached about one third of the
322 His-matGPT2 rates (with comparable expression levels in yeast cells, not shown). N-terminal
323 modification by GFP did not affect the transport rates of GPT1, but presence of the transit
324 peptide (equivalent to localization at the ER/PerMs) reduced transport rates by about half (not
325 shown).

326 The *Pro35S:GFP-GPT1_C-mat* construct was stably introduced into heterozygous *gpt1-2* plants
327 by floral dip transformation (Clough and Bent, 1998). Similar immunoblot patterns were obtained
328 for the GFP-GPT1 proteins extracted from yeast or plant cells (Figure 6B, green arrowheads). In
329 leaf cells of soil-grown plants, ER labeling dominated, but also spherical structures ($\leq 3 \mu\text{m}$) were
330 detected (Figure 6C, top panels). Obviously, ER insertion of *mature* GPT1 occurs by default, but
331 sorting to PerMs requires a stimulus. When mesophyll protoplasts were prepared from

10

332 transgenic leaf material and transfected with the peroxisome (Per) marker (OFP-PGL3_*C-short*),
333 GFP-labeled structures resembling newly forming peroxisomes appeared (Figure 6C, bottom
334 panels; arrowheads).

335 If GPT1 imports G6P into peroxisomes, we wondered what might happen to Ru5P, the product
336 of the three irreversible OPPP reactions. Especially, since analyses of the ribulose-5-phosphate
337 epimerase (RPE) isoforms At1g63290 (cytosolic), At3g01850 (cytosolic), and At5g61410
338 (plastidic) (Kruger and Von Schaewen, 2003) did not give any hint on peroxisomal localization
339 (unpublished data). We therefore analyzed, whether the *mature* GPT versions (with N-terminal
340 His tag) may exchange G6P for Ru5P. As shown in Table 1, the relative velocity of matGPT1
341 was higher for G6P-Ru5P (112%) than for Pi-Ru5P exchange (59%), and differed from
342 matGPT2 (87% for G6P-Ru5P and 75% for Pi-Ru5P). Importantly, exchange rates for 6-
343 phosphogluconate (6PG <10%) were negligible.

344

345 **Stress and developmental stimuli enhance ER targeting of GPT1**

346 Since protoplast preparation (which is achieved by treating leaves with fungal enzymes) of stably
347 transformed leaves led to recruitment of GFP-GPT1_*C-mat* to peroxisomes, we tested whether
348 also treatment with a bacterial elicitor (flagellin) may affect GPT localization. Both, *GPT1*- and
349 *GPT2-N-full-GFP* constructs were co-transfected with peroxisome (Per) marker OFP-PGL3_*C-*
350 *short* in Arabidopsis protoplasts, samples were split in half, and analyzed after 24 h of mock or
351 flg22 treatment. The latter led to enhanced GPT1 recruitment to the ER (Figure 7A, arrow-
352 heads), without major effect on plastid localization (GPT2 was neither affected; for single
353 channel images, see Supplemental Figure 13).

354 In addition, His-tag versions of the GPT1 and GPT2 N-termini were cloned and (following over-
355 expression in *E. coli*) affinity-purified and used for raising polyclonal antisera in rabbits. The
356 obtained α -GPT1 antiserum specifically recognized the N-terminus of GPT1 but not GPT2
357 (Supplemental Figure 14). Immunoblot analyses of different Arabidopsis tissues detected
358 prominent high molecular weight bands in soluble fractions of flower, silique and seedling tissue
359 - but not leaf extracts (Figure 7B), with stronger labeling in *gpt2* (Niewiadomski et al., 2005) and
360 *xpt-2* (Hilgers et al., 2018), but not *tpt-5* mutant plants (Figure 7C). In total, four bands were
361 found in reproductive tissues/seedlings and three bands in leaves. The latter resembled those
362 reported for ³⁵S-labeled GPT upon import into isolated plastids, namely: precursor, weak
363 intermediate and processed *mature* forms (Kammerer et al., 1998). Intermediates are unlikely to
364 persist *in planta*. Thus, as deduced from the stronger labeled top bands in the *gpt2* mutants
365 compared to Col-0 wild-type, we suppose that weak bands ~39 kDa in leaf extracts represent a

11

366 minor share of active *mature* GPT1 in chloroplasts (Figure 7B, lower black arrowhead), migrating
367 between less active *mature* (estimated 36.8 kDa) and *full-length* (estimated 42.3 kDa) versions
368 (red arrowheads). Conversely, top bands in reproductive flower and silique tissue (black
369 arrowheads) would represent active GPT1 in the ER/peroxisomes (Figure 7B, compare Col to
370 *gpt2-2* and *gpt2-3*). This was also observed in seedling extracts, including other transporter
371 mutants (Figure 7C). Interestingly, the pattern of triose-phosphate/phosphate translocator
372 mutant *tpt-5* resembled wild-type (Ws, Col), whereas unprocessed (top) bands persisted in 4
373 week-old seedlings of OPPP-relevant mutants *xpt-2* and *gpt2-3*. However, additional treatments
374 prior to SDS-PAGE/immuno-detection (-/+Lambda Protein Phosphatase, extraction +/-
375 phosphatase inhibitors; Supplemental Figure 14 panels F-G) or use of 200 mM DTT for tissue
376 extraction and sample boiling (not shown), did not result in visible differences.

377

378 **GPT1 is required both at plastids and peroxisomes during fertilization**

379 Loss of the last OPPP step in peroxisomes prevented formation of homozygous offspring due to
380 mutual sterility of the *pgd2* gametophytes (Hölscher et al., 2016). In analogy to this, we set out to
381 rescue plastidial versus ER/peroxisomal defects by ectopic *GPT* expression in heterozygous
382 *gpt1* lines. First, the coding sequence of GPT2 was placed under control of the constitutive
383 mannopine synthase (*MAS*) promoter (Guevara-Garcia et al., 1993) or the *GPT1* promoter
384 (position -1958 to -1), and introduced into heterozygous *gpt1* plants by floral dip transformation.
385 The CaMV-35S promoter-driven *GFP-GPT1_C-mat* construct (targeting the ER/peroxisomes,
386 Figure 6C), was included for comparison (Supplemental Figure 15A). Obtained data showed that
387 ectopic *GPT2* expression merely rescued the *gpt1* defect of incompletely filled siliques
388 (Supplemental Figure 15B, panels a, b and f). When driven by the *GPT1* promoter, some
389 siliques of the *ProGPT1:GPT2* transformed plants were completely filled with seeds
390 (Supplemental Figure 15B, panel d), whereas most siliques of the same plant/line showed erratic
391 seed maturation (panel c) or seed abortion (panel e). The frequencies of unfertilized, aborted
392 ovules are compiled in Table 2. Compared to the untransformed heterozygous *gpt1-1* or *gpt1-2*
393 lines (~30%), a slight reduction was found for *::ProMAS:GPT2* (~27%), compared to
394 *::ProGPT1:GPT2* (~21%) and Ws wild-type (~7%), indicating some compensation by GPT2 on
395 the female side. Attempted ER/peroxisomal rescue by *::Pro35S:GFP-GPT1_C-mat* scored the
396 highest values with ~34% aborted ovules.

397 Despite occasionally filled siliques, analyses of the *ProGPT1:GPT2*-compensated lines revealed
398 no *gpt1* homozygous plants (Table 3). Therefore, *GPT1 gpt1-2::ProGPT1:GPT2* was reciprocally
399 crossed with ER/peroxisomal *GPT1 gpt1-2::Pro35S:GFP-GPT1_C-mat*, forming seeds only with

12

400 *::ProGPT1:GPT2* as mother plant (Table 3). Since again no homozygous *gpt1-2* alleles were
401 found in the F₂, several T₂ plants of *::ProGPT1:GPT2* (line 3 #6 with ~73% filled siliques;
402 Supplemental Figure 16A) were super-transformed with *ProGPT1:GPT1_N*-long mat
403 (ER/peroxisomal construct driven by the *GPT1* promoter; Supplemental Figure 16B), based on
404 OFP-Pex16 co-expression (Figure 5C) and GPT1-*roGFP* analyses (Supplemental Figure 12),
405 but lacking the reporter.

406 Surprisingly, siliques of heterozygous *gpt1* plants carrying *ProGPT1:GPT1_N*-long mat (T1)
407 were almost completely filled with seeds, irrespective of whether plastidial *ProGPT1:GPT2* was
408 present or not (Supplemental Figure 16C, compare top to bottom panels). This indicated a major
409 contribution by GPT1 in the ER/peroxisomes, as also corroborated by the *gpt1* transmission
410 rates (Table 3).

411 In summary, compared to the untransformed *GPT1 gpt1* lines (21-25%), heterozygous progeny
412 raised only slightly upon presence of *ProGPT1*-driven *GPT2* (29-32%), with highest values
413 scored for a *GPT1* construct lacking the transit peptide region (43%). Thus, substantial recovery
414 by GPT1 (solely targeting the ER/peroxisomes) was obtained without further contribution by
415 GPT2 (solely targeting plastids), expressed from the same promoter.

416

417

418 **DISCUSSION** (3196 words)

419

420 **GPT1 and GPT2 differ in several aspects**

421 Based on the concept that peroxisomes developed from the proto-endomembrane system of the
422 Archaeobacterial host in an early pre-eukaryote (Tabak et al., 2006; Cavalier-Smith, 2009; van
423 der Zand et al., 2010), and GPT1 developed a special role related to NADPH provision by the
424 OPPP in plastids during land plant evolution (Niewiadomski et al., 2005; Andriotis et al., 2010),
425 as opposed to GPT2 mainly contributing to starch biosynthesis (Athanasidou et al., 2010; Kunz et
426 al., 2010; Dyson et al., 2015), a preexisting role of GPT transporters in the secretory system is
427 conceivable. Further support for functional specialization is reflected by the late split of GPT1
428 from GPT2 sequences in dicots (Figure 8), and dichotomy of orthologous sequences in the
429 monocot species rice (*Oryza sativa*) and maize (*Zea mays*). In rice, ADP-Glc and not G6P was
430 shown to be imported by heterotrophic plastids as the precursor of starch biosynthesis (Cakir et
431 al., 2016), except for pollen tissue that imports G6P (Lee et al., 2016). Furthermore, the GPT1-
432 interacting oxidoreductase Grx_{c1} (Supplemental Table 1, listed by the MIND database also as
433 interaction partner of GPT2, albeit with lower score) is dicot-specific, while Grx_{c2} is present in all

13

434 seed plants (Riondet et al., 2012; Li, 2014). In Arabidopsis, *GPT2* is predominately expressed in
435 heterotrophic tissues, whereas *GPT1* is found ubiquitously (Niewiadomski et al., 2005), also in
436 leaves (Supplemental Figure 17). Thus, basal G6P exchange, needed to stabilize the Calvin
437 cycle in chloroplasts (Sharkey and Weise, 2016), should involve GPT1 rather than GPT2, which
438 may be additionally induced under stress, e.g. by light (Athanasίου et al., 2010; Preiser et al.,
439 2019).

440

441 **The GPT1 N-terminus mediates dual targeting**

442 Our analyses showed that the C-terminal PTS1 motif of GPT1 is inactive, although reporter-
443 GPT1 fusions interfered with import of the SKL-based peroxisome marker. As expected for
444 PMPs (Rottensteiner et al., 2004), alternative GPT1 targeting was driven by other sequence
445 motifs. The mPTS1 of class-I PMPs (directly imported into peroxisomes) comprises several
446 positively charged amino acids on the matrix side adjacent to a transmembrane domain (Mullen
447 and Trelease, 2006), besides a cytosolic Pex19-binding site (Rottensteiner et al., 2004; Platta
448 and Erdmann, 2007), whereas for class-II PMPs it is only known that they exhibit an ER sorting
449 signal (Mullen and Trelease, 2006; Eubel et al., 2008). Although the exact motif mediating ER
450 import of GPT1 was not determined, domain swapping with GPT2 showed that the sequence
451 must lie within the first 155 amino acids (N-terminus plus first two MDs). Since the *GPT1_N-long*
452 *mat* version (without TP) was inserted into the ER, the region between K48 and the first MD
453 (A92) is probably crucial, partly lacking and strongly differing from GPT2 (Supplemental Figure
454 1).

455 To exclude that GPT1 and GPT2 might be inserted into the ER prior to plastid import (Baslam et
456 al., 2016) we tested Brefeldin A (BFA), a fungal toxin that inhibits the formation of ER-derived
457 coated vesicles (Orcl et al., 1991; Klausner et al., 1992). Although BFA compartments of merged
458 ER and Golgi vesicles were formed, GPT1 and GPT2 still localized to plastids. Furthermore, all
459 *medial* swap constructs headed by GPT2 targeted plastids. Thus, in case of dually-targeted
460 GPT1, threading into the plastidial Toc/Tic complex should prevent binding of the signal
461 recognition particle (SRP) that directs proteins to the Sec61 import pore in the ER membrane
462 (Figure 9A). Alternatively, an ER-targeting suppressor (ETS) region may be exposed by default,
463 preventing SRP binding, as shown for human PMP70 (Sakaue et al., 2016).

464 How dual targeting to secretory versus endosymbiotic compartments may be regulated was
465 discussed by Porter et al. (2015). N-terminal phosphorylation might influence competition
466 between chloroplast import and SRP binding (as in case of protein disulfide isomerase RB60
467 from *Chlamydomonas reinhardtii*). GPT1 exhibits only one potentially phosphorylated serine

14

468 residue in the N-terminus (S27; Supplemental Figure 1) that is conserved among all GPT
469 sequences, albeit not listed with high score by the PhosPhAt 4.0 database (Heazlewood et al.,
470 2008; Durek et al., 2009; Zulawski et al., 2013). Phosphomimic/preclusion of phosphorylation
471 had no influence on dual targeting of GPT1, and neither change of the single cysteine (C65,
472 Figure 9). On the other hand, enforced interaction of GPT1 monomers (visualized by YFP
473 reconstitution) resulted in labeling of specific ER substructures, and the C65S change enabled
474 detection at PerMs – as rare event (Figure 3B, panel i and 3C). However, C65 is not present in
475 all Brassica isoforms (Supplemental Figure 1) nor in GFP-GPT1_*C-mature*, which was detected
476 around peroxisomes upon elicitation (Figure 6C). Thus, C65 is not essential for reaching
477 peroxisomes, but might play a role in negative regulation of GPT1 transfer from the ER to
478 peroxisomes.

479 In this respect, GPT1 release to peroxisomes may require interaction with Grx_{c1} (and Trx_{N7}),
480 known to engage in monothiol-dithiol mechanisms, including glutathionylation (Riondet et al.,
481 2012; Ukuwela et al., 2018). The latter is known to be triggered by oxidative transients that
482 accompany stress signaling and developmental change (2GSH→GSSG). Sensible cysteine
483 residues (-S⁻ at physiological pH) may become sulfenylated (-S-OH in the presence of H₂O₂) or
484 glutathionylated (-S-SG), which protects from over-oxidation (reviewed in Zaffagnini et al., 2019).
485 Reversion (de-glutathionylation) by GSH alone is slow, but fast together with Grx and Trx (as
486 recently shown for plastidial Amy3; Gurrieri et al., 2019). Perhaps this mechanism regulates
487 GPT1 interaction with Pex16 and/or Pex3, given that biochemically distinct ER vesicles were
488 shown to fuse and form new peroxisomes (Van Der Zand et al., 2012). In any case, GPT1
489 transport in monomeric form within the ER makes sense, since a potentially active translocator -
490 still *en route* to its final destination - is likely not tolerated. This idea is supported by aberrant ER
491 structure in analyses with enforced GPT1-dimer formation (Figure 3).

492

493 **Evidence for redox transmitters in GPT1 recruitment to the ER/peroxisomes**

494 For indirect delivery of PMPs via the ER, it is still unclear how the processes of ER targeting and
495 sorting to newly forming peroxisomes are regulated. For Pex3 it was suggested that cytosolic
496 chaperons may guide the protein to the Sec61 translocon (Kim and Hettema, 2015), and for
497 Pex16 that the protein may recruit Pex3 and other PMPs to the ER (Hua et al., 2015). We
498 already published on the importance of thioredoxins as redox-dependent targeting regulators for
499 OPPP enzymes before. Since Trx co-chaperon function (*holdase* versus *foldase*) depends on
500 the local redox state, dual targeting of Arabidopsis G6PD1 and PGL3 is regulated by either
501 preventing folding, allowing plastid import, or supporting folding, as pre-requisite for peroxisome

15

502 import (Meyer et al., 2011; Hölscher et al., 2014). Here we show that co-expression of GPT1
503 with the cytosolic oxidoreductases Trx_{h7} or Grx_{c1} enhanced ER localization. Moreover, GPT1
504 interaction with both oxidoreductases was spotted at structures reminiscent of PerMs.

505 Thioredoxins and glutaredoxins were previously reported to promote protein folding directly, via
506 protein-disulfide reduction or disulfide-bond formation (Berndt et al., 2008), besides enhancing
507 co-chaperon activities in a redox state-dependent manner. Both, *foldase* function of the
508 monomeric thioredoxin and *holdase* function in the oligomeric state, prevented
509 folding/aggregation of client proteins, as demonstrated for Trx *h* and *m* types (Park et al., 2009;
510 Sanz-Barrio et al., 2012). The oligomerization state of Grx_{c1} was also shown to be influenced by
511 the surrounding redox medium, and conversely activated under oxidizing conditions, implying a
512 function as cytosolic redox sensor (Riondet et al., 2012; Ströher and Millar, 2012). Considering
513 that Grx and Trx serve as electron donors for peroxiredoxins that detoxify H₂O₂ directly (Dietz,
514 2011), and regulation of *h*-type Trx via Grx_{c1} was demonstrated previously (Meng et al., 2010;
515 Rouhier, 2010), a complex co-regulation of the two protein classes exists in plant cells.
516 Furthermore, Trx_{h7} and Grx_{c1} were found to be N-myristoylated *in planta* (Meng et al., 2010;
517 Riondet et al., 2012; Traverso et al., 2013; Majeran et al., 2018). For Grx_{c1}, which had been
518 detected in the cytosol and nucleus before (Riondet et al., 2012), our results show that the
519 protein partially resides at the ER. Grx_{c1} promoted ER targeting of GPT1, also without N-
520 myristoylation motif (G2A) in *grx_{c1}* mutant protoplasts (not shown), indicating functional
521 redundancy with (an)other isoform/member(s) of the Grx/Trx superfamily. Interestingly, GPT1 is
522 listed as palmitoylation candidate by the plant membrane protein database Aramemnon
523 (<http://aramemnon.uni-koeln.de>) with high score. Protein S-acylation (via cysteine residues) is
524 still a poorly understood posttranslational process that is usually preceded by N-myristoylation,
525 to promote membrane association, targeting, and/or partitioning into membrane subdomains
526 (Aicart-Ramos et al., 2011; Hemsley, 2015). A potential role of Grx/Trx N-myristoylation for
527 putative S-palmitoylation of GPT1 will have to be analyzed by a complex experimental setup, a
528 difficult task considering partial redundancy among cytosolic Trx *h2*, *h7*, *h8*, *h9* as well as Grx *c1*
529 and *c2* isoforms (Riondet et al., 2012; Traverso et al., 2013; Majeran et al., 2018). Clearly, GPT1
530 is inserted into the ER membrane in monomeric form, and may be modified at C65 (Figure 9A,
531 question mark) for retention. Dimer formation beyond the perER would occur after de-protection,
532 likely triggered by cytosolic redox signaling that accompanies *a/biotic* stress responses
533 (Vandenabeele et al., 2004; Foyer et al., 2009) or specific developmental stages, like pollen tube
534 elongation (Considine and Foyer, 2014) and navigation to ovules (Hölscher et al., 2016).

535

536 **GPT1 behaves like a class-II PMP**

16

537 Our BiFC data suggested that GPT1 contacts at least two of the three early peroxins (Kim and
538 Mullen, 2013). Interaction with Pex3 and Pex16 was detected at the ER and PerMs, whereas
539 interaction with Pex19 was mostly distributed across the cytosol, reflecting its function as
540 cytosolic cargo receptor (Hadden et al., 2006). Since simple co-expression with Pex19-reporter
541 fusions did not show any change in GPT1 localization, dot-like structures labeled by GPT1-
542 Pex19 BiFC analyses might be a false-positive result. This would be in line with Pex19 being
543 mainly involved in targeting of class I, but not class II PMPs. Focal localization of GPT1 at the
544 ER, previously described for Pex3 in yeast and for pxAPX in cottonseed/APX3 in Arabidopsis
545 (Lisenbee et al., 2003; Narendra et al., 2006), was mainly seen upon BiFC, indicating that
546 dimerization occurs beyond the perER. GPT1 dimers may therefore represent a forced
547 interaction at the ER, which does not (yet) occur under physiological conditions. As a side note,
548 Pex3 of plant cells had not been detected at the ER before (Hunt and Trelease, 2004).

549 Usually, GPT1 distributed evenly across the ER, unless co-expressed with Pex16 that coexists
550 at both the ER and PerMs (Lin et al., 2004; Karnik and Trelease, 2005). Interestingly, presence
551 of Pex16 influenced GPT1 localization at the ER, resulting in a similar but distinct pattern – also
552 when driven by the own promoter (dark incubation in the presence of sugars activates *GPT1*
553 mRNA expression, Supplemental Figure 18). Considering that BiFC is not dynamic, and fluores-
554 cent signals persist once the split YFP halves are reconstituted (Robida and Kerppola, 2009),
555 GPT1 was likely dragged to PerMs upon (otherwise transient) interaction with the peroxins. In
556 any case, this demonstrated that GPT1 can reach PerMs (although not detected there, unless
557 triggered), wherefore the transporter may first interact with Pex16 (for ER insertion/transport to
558 the perER; Hua et al., 2015), and then Pex3 (and possibly Pex19, during sorting to PerMs). By
559 contrast to APX3, GPT1 is only needed at peroxisomes when the OPPP is required (Meyer et
560 al., 2011; Hölscher et al., 2014; Lansing et al., 2019). Of note, aside from continuously imported
561 PGD2, no other OPPP enzyme has been found by peroxisomal proteomics so far (see Hölscher
562 et al., 2016; Lansing et al., 2019 and references cited therein).

563

564 **GPT1 transport preference differs from GPT2**

565 After plastid import, TP sequences are cleaved off by the essential stromal processing peptidase
566 (SPP), which is usually important for maturation, stabilization, and activation of the proteins (van
567 Wijk, 2015). Here we show that also unprocessed GPT1 is an active transporter. Addition of a
568 small tag or large reporter did not influence transport activity. Furthermore, topology analyses of
569 *roGFP* fusions indicated that upon ER insertion, both N- and C-termini of GPT1 face the cytosol
570 (Supplemental Figure 12), similar to Arabidopsis PMP22 (Murphy et al., 2003) and the human

571 glucose transporter (Mueckler and Lodish, 1986). These findings support the theory of Shao and
572 Hegde (2011) that during post-translational ER import of membrane proteins, type-I topology (N-
573 terminus facing the lumen) is strongly disfavored. This leads to obligate type-II topology (N-
574 terminus facing the cytosol), and integration of the following MDs owing to the 'positive inside
575 rule' (von Heijne, 1986; Goder et al., 2004) for the cytosolic hinge regions. The latter is not
576 entirely true for the GPT proteins (marked red in Supplemental Figure 1 and the topology
577 models), which may facilitate posttranslational ER insertion.

578 The phosphate translocator family is known to form dimers that mediate strict counter-exchange
579 of various phosphorylated metabolites with inorganic phosphate (Pi). The ability to transport
580 other OPPP intermediates, although possible (e.g. triose-phosphates), is usually disfavored due
581 to the prevailing metabolite concentrations or competition with the preferred substrate (Flügge,
582 1999; Eicks et al., 2002). Here we show that GPT1 and GPT2 can exchange G6P for Ru5P, but
583 GPT1 has a stronger preference for Ru5P. Thus, import of the OPPP substrate and export of its
584 product is warranted across PerMs (Figure 9B). Moreover, poor rates obtained with 6-phospho-
585 gluconate (6PG) as counter-exchange substrate strongly suggest that sugar-derived NADPH
586 production occurs by all three OPPP steps (Meyer et al., 2011; Hölscher et al., 2014; Lansing et
587 al., 2019), making a short-cut via solely Arabidopsis PGD2, catalyzing the last OPPP step in
588 peroxisomes (Fernández-Fernández and Corpas, 2016; Hölscher et al., 2016), unlikely.

589 In principle, the discovered transport preference should also apply to metabolite exchange at
590 plastids. This may explain why Arabidopsis *tpt xpt* double mutants are viable (although strongly
591 growth-compromised; Hilgers et al., 2018) and why *rpi2* mutants, lacking one of the two cytosolic
592 ribose-phosphate isomerase (RPI) isoforms form less starch in leaves (Xiong et al., 2009).
593 Minute amounts of active GPT1 could drain G6P from chloroplasts due to preferred exchange
594 with Ru5P, likely more abundant in *rpi2* mutants (Supplemental Figure 19). Besides G6P
595 exchange needed to stabilize the Calvin cycle (Sharkey and Weise, 2016), this argues for a role
596 of ubiquitously expressed GPT1, considering that GPT2 is absent from unstressed leaves
597 (Supplemental Figure 14F). On the other hand, lower transport capacity of GPT1 compared to
598 GPT2 is not surprising, since our data confirm a specialization of the two transporters. For
599 GPT1's function, flux rates are not necessarily a limiting parameter, but substrate specificity
600 obviously is. This is in line with our complementation analyses, demonstrating that GPT2 cannot
601 compensate for the absence of GPT1.

602

603 **Dual targeting of GPT1 is essential during fertilization**

604 Niewiadowski et al. (2005) and Andriotis et al. (2010) found that loss of GPT1 function in
605 plastids strongly affects pollen maturation and embryo-sac development, resulting in aberrant
606 morphological changes. Interestingly, in plants with reduced GPT1 levels, embryo development
607 is normal up to the globular stage, but then embryos fail to differentiate further and accumulate
608 starch (Andriotis et al., 2010; Andriotis and Smith, 2019). According to the Arabidopsis eFP
609 Browser (Winter et al., 2007), in this stage mRNA expression of *GPT2* is up to 3.5-fold higher
610 than of *GPT1* (Supplemental Figure 17), which can explain the observed starch accumulation
611 upon GPT1 loss.

612 In accordance with these premises, we suspected that ectopic *GPT2* expression may rescue
613 some plastidial functions, but not all phenotypes of the mutant *gpt1* alleles, because swap
614 constructs headed by GPT2 were never detected at the ER. For heterozygous *gpt1-2*
615 transformed with *GPT2* (driven by the *GPT1* promoter), filled siliques with green, non-aborted
616 embryos, and fertilized, but later aborted brownish embryos were observed. Plants homozygous
617 for the *gpt1-2* T-DNA were absent from the progeny of this line and also from ER/peroxisomal
618 compensated *Pro35S:GFP-GPT1_C-mat*.

619 Upon reciprocal crossing of these two lines, only one direction worked (Table 3), indicating that
620 besides partial rescue of the female *gpt1* defects (showing as filled siliques), plastid-confined
621 GPT2 was unable to fully rescue GPT1's functions during pollen maturation/tube growth. Pollen
622 grains appeared normal, but no homozygous *gpt1-2* plants were found among the progeny of
623 combined complementation constructs. This suggested that the remaining defects result mainly
624 from absence of GPT1 from plastids, due to a unique function GPT2 cannot fulfill. Furthermore,
625 GPT1 transfer from the ER to peroxisomes might be impeded by artificial construct composition.
626 Of note, *Pro35S:GFP-GPT1_C-mat* (transport-competent ER/PerM control) did not rescue ovule
627 abortion (Table 2), but led to a substantial increase in heterozygous offspring compared to the
628 parental line (Table 3). This may be even an underestimation, since the CaMV-35S promoter is
629 not well expressed in pollen, and generally fluctuates in floral tissues (Wilkinson et al., 1997). By
630 contrast, the *ProGPT1*-driven *GPT1_N-long mat* construct (without TP) rescued seed set and
631 raised *gpt1* transmission up to 43%, independent of additional GPT2 in plastids. Thus, together
632 with the pollination defect (mentioned above) and complementation by a genomic *GPT1*
633 construct (Niewiadowski et al., 2005), our results indicate that for full rescue GPT1 is additionally
634 needed in plastids, where the OPPP is mainly required for Ru5P provision to nucleotide bio-
635 synthesis (Figure 9B), as recently shown by Andriotis and Smith (2019).

636 The findings nicely support our previous analyses that loss of Ru5P formation in peroxisomes
637 (by missing PGD2 activity; Hölscher et al., 2016) prevents homozygous offspring due to mutual
638 sterility of the male and female *pgd2* gametophytes. Moreover, the low transport rates for 6PG

639 and redundancy at the PGL step in Arabidopsis (Lansing et al., 2019) suggest that no other
640 OPPP intermediate is transported across PerMs. Transport preference for Ru5P may also
641 explain why GPT1 is indispensable in heterotrophic plastids (Figure 9B), probably accepting Pi
642 released by GPT2-driven starch synthesis as counter-exchange substrate. Finally, dual targeting
643 is supported by immuno-detection of unprocessed (ER/peroxisomal) GPT1 in flower/silique and
644 seedling tissues. In the latter, a shift in the GPT1 pattern seems to reflect gradual adaptation to
645 the photoautotrophic state. Besides, relative mobility and band intensities in wild-type versus
646 *gpt2* (and other transporter mutants) indicates that GPT1 transport activity may be regulated by
647 post-translational modification at both locations, perhaps phosphorylation of the mature protein
648 part (up to 5 sites; Supplemental Figure 1, blue frames). Potential glutathionylation (300 Da) of
649 the single cysteine in the GPT1 N-terminus (C65; Figure 9A) cannot explain the observed size
650 shifts, rather palmitoylation (Greaves et al., 2008). Of note, S-palmitoylation is usually preceded
651 by N-myristoylation (Wang et al., 1999), and both *Grx_{c1}* and *Trx_{h7}* were found to be N-
652 myristoylated *in planta* (Majeran et al., 2018). For sure Grx isoforms are important during
653 fertilization, since *grx_{c1} grx_{c2}* double mutants exhibited a lethal phenotype early after pollination
654 (Riondet et al., 2012). Together, this may add to the recently discovered role of palmitoylation
655 during male and female gametogenesis in Arabidopsis (Li et al., 2019). However, a definite link
656 of these aspects to dual targeting of GPT1 will require more detailed studies.

657

658 In summary, our data present compelling evidence for dual targeting of GPT1 to both plastids
659 and peroxisomes. Imported G6P is converted by the oxidative OPPP part to NADPH and Ru5P,
660 which is the preferred exchange substrate (likely at both locations), thus contributing to
661 gametophyte and embryo development as well as pollen-tube guidance to ovules. Since the
662 latter dominates the reproductive success, further analyses are required to determine the exact
663 physiological context of GPT1's presence at the ER/peroxisomes.

664

665

666 **MATERIALS AND METHODS** (1704 words)

667

668 **Bioinformatics**

669 For general information about *Arabidopsis thaliana*, the TAIR website (www.arabidopsis.org),
670 Araport (www.araport.org/), PhosPhAt 4.0 (<http://phosphat.uni-hohenheim.de/>), and the National
671 Center for Biotechnology Information (NCBI) (www.ncbi.nlm.nih.gov) were consulted. Routine
672 analyses were performed with programs of the ExPASy proteomics server (www.expasy.ch) and

20

673 Clustal Omega (www.ebi.ac.uk). For the phylogenetic tree, sequence information on different
 674 higher plant clades was retrieved from the National Center for Biotechnology Information (NCBI;
 675 www.ncbi.nlm.nih.gov), and for the moss *Physcomitrella patens* from www.cosmoss.org.
 676 Sequence alignments and phylogenetic analyses were performed in MEGA7 (Jones et al., 1992;
 677 Kumar et al., 2016) using the Maximum Likelihood method based on the JTT matrix-based
 678 model (Jones et al., 1992).

679

680 Cloning of Fluorescent Reporter Fusions

681 Open reading frames of candidate genes were obtained by RT-PCR using Arabidopsis total leaf
 682 RNA as described in Hölscher et al. (2016), except for *Trx_{h7}* which was amplified from genomic
 683 DNA. Appropriate oligonucleotide primers are listed in Supplemental Table 2. Reporter
 684 constructs were cloned in plant expression vectors as described before (Meyer et al., 2011;
 685 Hölscher et al., 2016) and indicated in the table below.

686

Reporter vector	Sites for N-terminal fusions	Sites for C-terminal fusions
pGFP2*	XbaI (SpeI), Acc65I	[not used]
pGFP2-ΔNcoI*	XbaI, Acc65I	[not used]
pOFP-ΔNcoI* (pSY526)	EcoRI, NcoI	SpeI, BamHI
pGFP2-SDM*	XbaI, Acc65I	SpeI, BamHI
pG/OFP-NX*	XbaI, NcoI, Acc65I	SpeI, BamHI
pUC-SPYNE pUC-SPYCE(M)	SpeI, Acc65I, BamHI	[not used]
pUC-SPYNE(R) pUC-SPYCE(MR)	[not used]	SpeI, BamHI

687 *For vector details see (Meyer et al., 2011; Hölscher et al., 2016); split YFP vectors (Walter et al., 2004)

688

689 Site-directed Mutagenesis

690 Single base changes, for destroying restriction sites or changing amino acids, were introduced
 691 by the Quick-Change PCR mutagenesis kit protocol (Stratagene), using the primer combinations
 692 listed in Supplemental Table 2 and Phusion™ High-Fidelity DNA Polymerase (Finnzymes). All
 693 base changes were confirmed by sequencing.

694

695 Heterologous Protein Expression in Yeast Cells

696 For in vitro-uptake studies, *full-length* or *mature* GPT1 and GPT2 versions were amplified with
 697 the corresponding primers from cDNA and inserted into yeast vectors pYES2 or pYES-NTa via

21

698 Acc65I (KpnI)/BamHI sites (Thermo Scientific). For *full-length* GPT1, primer combinations were
699 GPT1_Acc65I_s with GPT1+S_BamHI_as; for *mature* GPT1, GPT1_C-mat_Acc65I_s with
700 GPT1+S_BamHI_as; and for *mature* GPT2, GPT2_C-mat_Acc65I_s with GPT2+S_BamHI_as
701 (Supplemental Table 2). For the GFP-GPT1_C-mat version, PCR fragments (primers: GPT1_C-
702 mat_SpeI_s and GPT1+S_BamHI_as) were first inserted into pGFP2-SDM via SpeI/BamHI
703 sites, released with KpnI/BamHI, and cloned in pYES2. The resulting constructs were
704 transformed into strain INVSc1 (MATa, his3 Δ 1, leu2, trp1-289, ura3-52/MAT α , his3 Δ 1, leu2, trp1-
705 289, ura3-52) using the lithium acetate/PEG method (Gietz and Schiestl, 2007). Yeast cells were
706 selected on synthetic complete medium (SC-Ura; 0.67% (w/v) YNB supplemented with
707 appropriate amino acids and bases for uracil auxotrophy and 2% (w/v) glucose as carbon
708 source). Since protein expression is under control of the galactose-inducible promoter pGAL1,
709 yeast cells were grown aerobically in SC-Ura supplemented with 2% (w/v) galactose for 6 h at
710 30°C. Harvest and enrichment of total yeast membranes without and with recombinant GPT
711 proteins was performed according to Linka et al. (2008).

712

713 Uptake Studies Using Proteoliposomes

714 Yeast membranes were reconstituted into 3% (w/v) L- α -phosphatidylcholine by a freeze-thaw-
715 sonication procedure for in vitro-uptake studies as described in Linka et al. (2008). Proteolipo-
716 somes were either preloaded with 10 mM KPi, G6P, Ru5P, 6PG or produced without pre-loading
717 (negative control). Counter-exchange substrate not incorporated into proteoliposomes was
718 removed via gel filtration on Sephadex G-25M columns (GE Healthcare). Transport assays were
719 started either by adding 0.2 mM [α -³²P]-phosphoric acid (6,000 Ci/mmol) or 0.2 mM [¹⁴C]-
720 glucose-6-phosphate (290 mCi/mmol). The uptake reaction was terminated by passing
721 proteoliposomes over Dowex AG1-X8 anion-exchange columns. The incorporated radiolabeled
722 compounds were analyzed by liquid scintillation counting. Time-dependent uptake data were
723 fitted using nonlinear regression analysis based on one-phase exponential association using
724 GraphPad Prism 5.0 software (GraphPad, www.graphpad.com). The initial uptake velocities
725 were calculated using the equation slope = (Plateau - Y0)*k, whereas Y0 was set to 0. The
726 values for the plateau and k were extracted from the non-linear regression analyses using a
727 global fit from three technical replicates.

728

729 Arabidopsis Mutants

730 Heterozygous *gpt1-1* and *gpt1-2* lines (Arabidopsis ecotype Wassilewskia, Ws-2) were kindly
731 provided by Anja Schneider (LMU Munich) and analyzed via PCR amplification from genomic

22

732 DNA as suggested for the two T-DNA alleles (Niewiadomski et al., 2005). All oligonucleotide
733 primers are listed in Supplemental Table 2. For the Feldman line, primers
734 GPT1_EcoRI_s/GPT1-R5 were used for the wild-type allele, and F-RB/GPT1-R5 (Niewiadomski
735 et al., 2005) for the *gpt1-1* T-DNA allele. For the Arabidopsis Knockout Facility (AKF) line,
736 primers GPT1-F3/GPT1-R3 were used for the wild-type allele, and GPT1-F3/JL-202
737 (Niewiadomski et al., 2005) for the *gpt1-2* T-DNA allele. To improve PCR analyses, GPT1-F3
738 was later replaced by primer *gpt1-2_WT_s*. Further mutants used were *gpt2-2* (GK-950D09),
739 *gpt2-3* (GK-780F12), and *xpt-2* (SAIL_378C01) in the Columbia (Col) background, and *tpt-5*
740 (FLAG_124C02) in the Ws background. Mutant plants were identified by genomic PCR using the
741 suggested gene-specific and T-DNA-specific primer combinations (Supplemental Table 2).

742

743 **Plant Growth**

744 Arabidopsis seeds were surface-sterilized by ethanol washes (vortexed for 5 s each in 70%
745 EtOH, EtOH absolute, 70% EtOH), dried on sterile filter paper, and spread on sterile germination
746 medium (0.5 Murashige & Skoog salt mixture with vitamins, pH 5.7-5.8, 0.8% agar; Duchefa,
747 Haarlem, NL) supplemented with 1% sucrose and stratified for 2-3 days at 4°C. After
748 propagation in growth chambers for one week (short day regime: 8 h light 21°C, 16 h dark 19°C)
749 seedlings were transferred to sterile Magenta vessels (Sigma) and grown for 4-5 weeks until
750 harvesting rosette leaves for protoplast isolation. Alternatively, seedlings were transferred to
751 fertilized soil mix at the 4-leaf stage and grown in short day regime, prior to transfer to long day
752 regime (16 h light 21°C, 8 h dark 19°C) to promote flowering. In case of tobacco (*Nicotiana*
753 *tabacum* var. Xanthi), sterile apical cuttings were cultivated on MS agar supplemented with 2%
754 sucrose. The top leaves of four week-old plants were used for protoplast isolation.

755

756 **Protoplast Transfection and Microscopy**

757 Localization of fluorescent reporter fusions (all constructs driven by the CaMV-35S promoter, if
758 not indicated otherwise) was determined by confocal laser scanning microscopy (CLSM) in
759 freshly transfected mesophyll protoplasts (Meyer et al., 2011). For co-expression analyses,
760 25 µg of test DNA (BiFC: 20 µg of each plasmid) was pre-mixed with 5 µg of a reporter construct
761 (20 µg in case of Pex16-OFP) prior to PEG transfection. After cultivation for 12 to 48 h at 21-
762 25°C in the dark (without or with the drug/elicitor indicated), fluorescent signals were recorded
763 using a Leica TCS SP5 microscope with excitation/emission wavelengths of 405 vs. 488/490-
764 520 nm for roGFP, 488/490-520 nm for GFP, 514/520-550 nm for YFP, and 561/590-620 nm for
765 OFP (*mRFP*).

23

766

767 Immunoblot analyses

768 Arabidopsis tissues were harvested from plants grown in soil, or seedlings growing on
769 germination plates (1% sucrose) after different time points. Our standard protein-extraction
770 buffer was 50 mM HEPES-NaOH pH 7.5, 2 mM sodium pyrosulfite ($\text{Na}_2\text{S}_2\text{O}_5$), 1 mM Pefabloc
771 SC, Protease Inhibitor Cocktail (1:100) for use with plant extracts (Sigma), and 280 mM
772 β -mercaptoethanol (β -ME) - if not stated otherwise. Immunoblot analyses were conducted as
773 described previously (Meyer et al., 2011; Hölscher et al. 2016; Lansing et al., 2019) using 10%
774 separating gels with 10% glycerol. Polyclonal rabbit antisera were obtained from Eurogentec
775 (Seraing, B), raised against the N-terminal GPT sequences (91 amino acids of GPT1 or 92
776 amino acids of GPT2) with His tag as antigen (His-N1, His-N2) after overexpression in *E. coli*
777 BL21 from pET16b-based plasmids and affinity purification via Ni-NTA (Qiagen), followed by
778 specificity tests (Supplemental Figure 14).

779

780 GPT Constructs for Rescue Analyses

781 For one of the plastidial rescue lines, expression from the Mannopine synthase promoter was
782 used (pBSK-pMAS-T35S, Supplemental Figure 20). The ORF of GPT2 was amplified from
783 cDNA with primer combination GPT2_s_EcoRI/GPT2_as_PstI (all primers are listed in
784 Supplemental Table 2) and inserted into pBSK-pMAS-T35S via EcoRI/PstI sites (pBSK-
785 pMAS:GPT2). The entire expression cassette (pMAS:GPT2-T35S) was released with Sall/XbaI
786 and inserted into binary vector pGSC1704-HygR (*ProMAS:GPT2*). For *GPT1* promoter-driven
787 *GPT2*, the 5' upstream sequence of *GPT1* (position -1 to -1958) was amplified from genomic
788 DNA using Phusion™ High-Fidelity DNA Polymerase (Finnzymes) and inserted blunt end into
789 pBSK via EcoRV (orientation was confirmed by sequencing). The GPT2-T35S part was
790 amplified with primers GPT2_NdeI_s/T35S_Sall_as from pBSK-pMAS:GPT2 and inserted
791 downstream of the *GPT1* promoter via NdeI/Sall in pBSK. The final expression cassette
792 (*ProGPT1:GPT2-T35S*), amplified with primers pGPT1_s/T35S_Sall_as, was digested with Sall,
793 and inserted into pGSC1704-HygR via SnaBI/Sall sites.

794 For the CaMV promoter-driven *35S:GFP-GPT1_C*-mat construct, the expression cassette was
795 released from vector pGFP2-SDM with PstI/EcoRI, the EcoRI site filled (using Klenow Fragment,
796 Thermo Fisher) and inserted into binary vector pGSC1704-HygR via SdaI/SnaBI sites. For
797 *GPT1_N*-long mat (also driven by the *GPT1* promoter), fragments were amplified with primers
798 GPT1_long mat-s and G6P_peroxi_Trans_full_BamHI from existing cDNA clones upon insertion
799 into the pGFP-NX backbone via XbaI and BamHI (removing GFP). The *GPT1* promoter was

24

800 then amplified with primers P_GPT1_s and P_GPT1_as and inserted via PstI/SpeI into PstI/XbaI
801 in the target plasmid, replacing the CaMV-35S promoter. The resulting cassette with *GPT1*
802 promoter, *GPT1_N*-long mat and *NOS* terminator was then amplified via primers P_GPT1_s and
803 NosT_as upon Sall digestion and insertion into Sall and SnaBI-opened binary vector pDE1001
804 (Ghent University, B).

805 All binary constructs were transformed into *Agrobacterium* strain GV2260 (Scharte et al., 2009).
806 Floral dip transformation of heterozygous *gpt1* plants was conducted as described by Clough
807 and Bent (1998). Seeds were selected on germination medium containing 15 µg ml⁻¹ Hygromycin
808 B (Roche) or 50 µg ml⁻¹ Kanamycin (*ProGPT1-GPT1_N*-long mat) including 125 µg ml⁻¹ Beta-
809 lactyl (SmithKline Beecham), and transferred to soil at the 4-leaf stage. After three weeks, wild-
810 type and T-DNA alleles were genotyped as described above. *ProMAS:GPT2* and
811 *ProGPT1:GPT2* constructs were amplified from genomic DNA using primers GPT2_C-
812 4MD_SpeI_s and T35S_Sall_as. For testing presence of *Pro35S:GFP-GPT1_C*-mat, primer
813 combinations P35S_s and GPT1_EcoRI_as or NosT_as were used. Presence of
814 *ProGPT1:GPT2* was detected with primers GPT2_XbaI_s and GPT2-Stop_BHI_as
815 (discrimination between the cDNA-based complementation construct and wild-type sequence is
816 based on size, i.e. absence or presence of introns), while *GPT1_N*-long mat was detected with
817 primers GPT1_long mat_s and NosT_as".

818

819 **Determination of Ovule-Abortion Frequencies**

820 Siliques number 10 to 12 of the main inflorescence (counted from the top) were harvested and
821 incubated in 8 M NaOH overnight. Images of bleached and unbleached siliques were recorded
822 with transmitting light using a Leica MZ16 F stereo microscope connected to a Leica DFC420 C
823 camera. Aborted ovules were counted and frequencies were calculated.

824

825 **Acknowledgements** (135 words)

826 The authors thank Anja Schneider (LMU Munich) for providing the heterozygous *gpt1* lines, and
827 the Arabidopsis Stock Centers (NASC, INRA) for the other mutant lines. Andreas Meyer (INRES,
828 University of Bonn) donated the *roGFP2* plasmid, and Robert Marschall (IBBP) helped with
829 ratiometric analyses in ImageJ. Stephan Rips gave advice on CLSM imaging, Olessia Becker
830 was involved in GPT antigen production/antibody testing, Sebastian Hassa cloned expression
831 vector pBSK:pMAS-T35S, Lennart Doering finished the GPT1-C65S split YFP constructs, and
832 Wiltrud Krüger helped with routine lab work. Several Bachelor students contributed by their
833 thesis projects: Jan Wiese by ribose-phosphate epimerase (RPE) isoform analyses, Margareta

25

834 Westphalen to BiFC interaction analyses, and Hinrik Plaggenborg to *roGFP* topology analyses.
835 This work was in part funded by the German Research Foundation (DFG) via grants SCHA
836 541/12 (to AvS) and LI 1781/1-3 (to NL).

837

838 **Author contributions**

839 M-CB, HL, KF, TM, LC, and NL performed the experiments; AvS, M-CB, HL, and NL designed
840 experiments and analyzed the data; M-CB, HL, and AvS wrote the manuscript; all authors read
841 and approved the final version of the article.

842

843 **Conflict of interest**

844 The authors declare no conflict of interest.

845

846

847 **Supplemental Data**

848 The following supplemental materials are available online.

849

850 **Supplemental Tables**

851 **Supplemental Table 1.** GPT1 search results of the Membrane-based Interactome Network Database
852 (MIND).

853 **Supplemental Table 2.** Oligonucleotide primers used in this study.

854 **Supplemental Table 3.** Protein sequences used for calculating the phylogenetic tree.

855

856 **Supplemental Figures**

857 **Supplemental Figure 1.** Alignment of GPT1 and GPT2 polypeptide sequences from six
858 *Brassicaceae*.

859 **Supplemental Figure 2.** Localization of N-terminally truncated and full-length reporter-GPT
860 fusions.

861 **Supplemental Figure 3.** Single channel images of Figure 1.

862 **Supplemental Figure 4.** Localization of C-terminally truncated GPT-reporter fusions.

863 **Supplemental Figure 5.** Localization of two different GPT1 and GPT2 *medial* reporter fusions.

864 **Supplemental Figure 6.** Brefeldin-A treatment of the *medial* GPT_2MD:8MD fusions.

865 **Supplemental Figure 7.** Single channel images of Figure 2.

866 **Supplemental Figure 8.** Single channel images of Figure 3.

867 **Supplemental Figure 9.** Trx_{h7} and Grx_{c1} partially localize at the ER (together with GPT1).

26

868 **Supplemental Figure 10.** OFP fusions of Pex3-1, Pex16, Pex19-1 and co-expression with
869 GFP-GPT1.

870 **Supplemental Figure 11.** Single channel images of Figure 5C (*Pro35S* vs. *ProGPT1* promoter).

871 **Supplemental Figure 12.** Ratiometric topology analysis of GPT1 at the ER using *roGFP*.

872 **Supplemental Figure 13.** Single channel images of Figure 7A.

873 **Supplemental Figure 14.** Generation and test of the polyclonal rabbit GPT1 antiserum.

874 **Supplemental Figure 15.** Ectopic *GPT2* expression for plastidial rescue in heterozygous *gpt1* lines.

875 **Supplemental Figure 16.** ER/peroxisomal rescue of GPT1 function in heterozygous *gpt1-2*.

876 **Supplemental Figure 17.** Relative mRNA-expression levels of Arabidopsis *GPT1* and *GPT2*.

877 **Supplemental Figure 18.** *GPT1* mRNA expression is induced by sucrose in low light/darkness.

878 **Supplemental Figure 19.** Possible consequences of G6P-Ru5P exchange by GPT1 at
879 chloroplasts.

880 **Supplemental Figure 20.** Vector map of pBSK-pMAS-T35S.

881

882

883

884 **Tables** (601 words)

885

886 **Table 1. Initial velocities of Pi or G6P import for various exchange substrates.**

887 Time-dependent uptake of [³²P]-Pi or [¹⁴C]-G6P (0.2 mM) into liposomes reconstituted with total
 888 yeast membranes of cells expressing the indicated *mature* GPT versions (nmol mg⁻¹ total
 889 protein). Proteoliposomes were preloaded with 10 mM G6P, Ru5P, 6PG, or Pi. Relative
 890 velocities given in brackets were compared to the counter-exchange experiment Pi/G6P or
 891 G6P/Pi, which was set to 100%.

892

		His-matGPT1	His-matGPT2
Pi versus	G6P	9.9 (100 %)	19.3 (100 %)
	Ru5P	5.8 (59 %)	14.4 (75 %)
	6PG	0.8 (8 %)	1.2 (6 %)
G6P versus	Pi	10.5 (100 %)	32.6 (100 %)
	Ru5P	12.2 (116 %)	28.3 (87 %)
	6PG	0.9 (9 %)	3.1 (10 %)

893

894

895

896

897 **Table 2. Seeds and aborted ovules without and upon ectopic *GPT* expression.**
 898 *Arabidopsis thaliana* ecotype *Ws-2* and heterozygous *gpt1-1* and *gpt1-2* T-DNA lines compared
 899 to plastid compensated *GPT1 gpt1-2::ProMAS:GPT2* or *::ProGPT1:GPT2* lines (T2 generation),
 900 and ER/peroxisomal compensated line *::Pro35S:GFP-GPT1_C-mat* (T3 generation).
 901 Transformed progeny was initially selected on Hygromycin B. SD, standard deviation.

Genotype	Normal seeds	Aborted ovules	Frequency (% ± SD)
<i>GPT1 GPT1</i> (<i>Ws-2</i>)	439	39	8.3 ± 4.3
<i>GPT1 GPT1*</i>	755	53	6.6
<i>GPT1 gpt1-1</i>	86	26	30.2 (mean)
<i>GPT1 gpt1-1*</i>	507	236	32.0
<i>GPT1 gpt1-1::ProMAS:GPT2</i> (line 3)	1195	495	28.8 ± 7.2
<i>GPT1 gpt1-1::ProMAS:GPT2</i> (line 7)	1587	585	27.2 ± 8.8
<i>GPT1 gpt1-2</i>	371	164	29.4 ± 6.9
<i>GPT1 gpt1-2*</i>	1357	530	28.0
<i>GPT1 gpt1-2::ProGPT1:GPT2</i> (line 3)	2082	529	20.6 ± 8.9
<i>GPT1 gpt1-2::Pro35S:GFP-GPT1_C-mat</i> (line 14.5)	1412	690	33.8 ± 9.8
<i>gpt1-2 gpt1-2::gGPT1-3.10*</i>	1461	104	6.6

902 *Data of Niewiadomski et al. (2005) for comparison; n.d., not determined.

903

904

905 **Table 3. Transmission of the *gpt1* alleles with and without ectopic *GPT* expression.**

906 Segregation analysis of heterozygous *gpt1-1* and *gpt1-2* lines upon selfing or transformation
 907 with the indicated *GPT* rescue constructs: *GPT2* cDNA was driven either by the constitutive
 908 *ProMAS* (T2 generation) or the *GPT1* promoter (T2 and T3 generation). ER/peroxisomal
 909 *Pro35S:GFP-GPT1_C-mat* was analyzed in parallel (transformed plants were selected on
 910 Hygromycin). No homozygous *gpt1* plants were found. Therefore plastid-compensated *GPT1*
 911 *gpt1-2::ProGPT1:GPT2* was reciprocally crossed with ER/peroxisomal rescue construct *GPT1*
 912 *gpt1-2::Pro35S:GFP-GPT1_C-mat*. Only one combination set seeds, indicating that *GPT2* is
 913 unable to rescue *GPT1* function during pollen maturation. Still no homozygous *gpt1* plants were
 914 found. Thus, *GPT1 gpt1-2::ProGPT1:GPT2* was super-transformed with ER/peroxisomal rescue
 915 construct *ProGPT1:GPT1_N-long mat* (lacking the TP region) and selected on Kanamycin.
 916 Among the progeny of individuals carrying all three T-DNA alleles, *gpt1-2* transmission markedly
 917 improved, although no homozygous plants were found. Of note, this was also true for lines
 918 devoid of *ProGPT1:GPT2*. Values are given in percent with number (n) of plants analyzed.

Genotype	<i>GPT1 GPT1</i> +/+	<i>GPT1 gpt1</i> +/-	<i>gpt1 gpt1</i> -/-
<i>GPT1 gpt1-1</i>	79.3 (wt = 184)	20.7 (he = 48)	0 (n = 232)
<i>GPT1 gpt1-1::ProMAS:GPT2</i> (lines 3 & 7, T2)	67.8 (wt = 214)	32.2 (he = 102)	0 (n = 316)
<i>GPT1 gpt1-2</i>	74.8 (wt = 95)	25.2 (he = 32)	0 (n = 127)
<i>GPT1 gpt1-2::ProGPT1:GPT2</i> (line 3, T2)	71.0 (wt = 115)	29.0 (he = 47)	0 (n = 162)
<i>GPT1 gpt1-2::Pro35S:GFP-GPT1_C-mat</i> (T3)	65.8 (wt = 100)	34.2 (he = 51)	0 (n = 151)
<i>GPT1 gpt1-2::ProGPT1:GPT2</i> (♀) x <i>GPT1 gpt1-2::Pro35S:GFP-GPT1_C-mat</i> (F2)*	80.0 (wt = 152)	20.0 (he = 38)	0 (n = 190)
<i>GPT1 gpt1-2::ProGPT1:GPT2</i> (line 3, T3) <i>::ProGPT1:GPT1_N-long mat</i> (T2)*	56.1 (wt = 184)	43.9 (he = 144)	0 (n = 328)
<i>GPT1 gpt1-2::ProGPT1:GPT1_N-long mat</i> (T2)	56.5 (wt = 48)	43.5 (he = 37)	0 (n = 85)

919 *progeny of plants containing all three T-DNAs; wt, wildtype; he, heterozygous; n, number analyzed; n.d., not
 920 determined

921
 922

1104

1105 **REFERENCES**

1106

1107 Ackerley, S., Thornhill, P., Grierson, A.J., Brownlees, J., Anderton, B.H., Leigh, P.N., Shaw,

1108 C.E., and Miller, C.C.J. (2003). Neurofilament heavy chain side arm phosphorylation

1109 regulates axonal transport of neurofilaments. *J. Cell Biol.* 161: 489–495.

1110 Aicart-Ramos, C., Valero, R.A., and Rodriguez-Crespo, I. (2011). Protein palmitoylation and

1111 subcellular trafficking. *Biochim. Biophys. Acta* 1808: 2981–2994.

1112 Andriotis, V.M.E., Pike, M.J., Bunnewell, S., Hills, M.J., and Smith, A.M. (2010). The plastidial

1113 glucose-6-phosphate/phosphate antiporter GPT1 is essential for morphogenesis in

1114 *Arabidopsis* embryos. *Plant J.* 64: 128–139.

1115 Andriotis, V.M.E. and Smith, A.M. (2019). The plastidial pentose phosphate pathway is essential

1116 for postglobular embryo development in *Arabidopsis*. *Proc. Natl. Acad. Sci. U. S. A.* 116:

1117 15297–15306.

36

- 1118 Aranovich, A., Hua, R., Rutenberg, A.D., and Kim, P.K. (2014). PEX16 contributes to
1119 peroxisome maintenance by constantly trafficking PEX3 via the ER. *J. Cell Sci.* 127: 3675–
1120 3686.
- 1121 Athanasiou, K., Dyson, B.C., Webster, R.E., and Johnson, G.N. (2010). Dynamic Acclimation of
1122 Photosynthesis Increases Plant Fitness in Changing Environments. *Plant Physiol.* 152:
1123 366–373.
- 1124 Baslam, M., Oikawa, K., Kitajima-Koga, A., Kaneko, K., and Mitsui, T. (2016). Golgi-to-plastid
1125 trafficking of proteins through secretory pathway: Insights into vesicle-mediated import
1126 toward the plastids. *Plant Signal. Behav.* 11: e1221558 (5 pages).
- 1127 Berndt, C., Lillig, C.H., and Holmgren, A. (2008). Thioredoxins and glutaredoxins as facilitators
1128 of protein folding. *Biochim. Biophys. Acta - Mol. Cell Res.* 1783: 641–650.
- 1129 Cakir, B., Shiraishi, S., Tuncel, A., Matsusaka, H., Satoh, R., Singh, S., Crofts, N., Hosaka, Y.,
1130 Fujita, N., Hwang, S.-K., Satoh, H., and Okita, T.W. (2016). Analysis of the Rice ADP-
1131 Glucose Transporter (OsBT1) Indicates the Presence of Regulatory Processes in the
1132 Amyloplast Stroma That Control ADP-Glucose Flux into Starch. *Plant Physiol.* 170: 1271–
1133 1283.
- 1134 Cavalier-Smith, T. (2009). Predation and eukaryote cell origins: A coevolutionary perspective.
1135 *Int. J. Biochem. Cell Biol.* 41: 307–322.
- 1136 Chen, J., Lalonde, S., Obrdlik, P., Noorani Vatani, A., Parsa, S.A., Vilarino, C., Revuelta, J.L.,
1137 Frommer, W.B., and Rhee, S.Y. (2012). Uncovering Arabidopsis Membrane Protein
1138 Interactome Enriched in Transporters Using Mating-Based Split Ubiquitin Assays and
1139 Classification Models. *Front. Plant Sci.* 3: 1–14.
- 1140 Chua, N.-H. and Schmidt, G.W. (1979). Transport of Proteins into Mitochondria and
1141 Chloroplasts. *J. Cell Biol.* 81: 461–483.
- 1142 Clough, S.J. and Bent, A.F. (1998). Floral dip: a simplified method for *Agrobacterium*-mediated
1143 transformation of *Arabidopsis thaliana*. *Plant J.* 16: 735–743.
- 1144 Considine, M.J. and Foyer, C.H. (2014). Redox Regulation of Plant Development. *Antioxid.*
1145 *Redox Signal.* 21: 1305–1326.
- 1146 Corpas, F.J., Barroso, J.B., Sandalio, L.M., Distefano, S., Palma, J.M., Lupiáñez, J.A., and del
1147 Río, L.A. (1998). A dehydrogenase-mediated recycling system of NADPH in plant
1148 peroxisomes. *Biochem. J.* 330: 777–784.
- 1149 dal Santo, S., Stampfl, H., Krasensky, J., Kempa, S., Gibon, Y., Petutschnig, E., Rozhon, W.,
1150 Heuck, A., Clausen, T., and Jonak, C. (2012). Stress-Induced GSK3 Regulates the Redox
1151 Stress Response by Phosphorylating Glucose-6-Phosphate Dehydrogenase in
1152 *Arabidopsis*. *Plant Cell* 24: 3380–3392.
- 1153 Dennis, D.T., Layzell, D.B., Lefebvre, D.D., and Turpin, D.H. (1997). *Plant metabolism 2nd*
1154 *editio*. D.T. Dennis, D.B. Layzell, D.D. Lefebvre, and D.H. Turpin, eds (Prentice Hall
1155 College Div, Prentice Hall Inc., New Jersey).
- 1156 Dietz, K.-J. (2011). Peroxiredoxins in plants and cyanobacteria. *Antioxid. Redox Signal.* 15:
1157 1129–1159.
- 1158 Durek, P., Schmidt, R., Heazlewood, J.L., Jones, A., MacLean, D., Nagel, A., Kersten, B., and
1159 Schulze, W.X. (2009). PhosPhAt: The *Arabidopsis thaliana* phosphorylation site database.
1160 An update. *Nucleic Acids Res.* 38: 828–834.
- 1161 Dyson, B.C., Allwood, J.W., Feil, R., Xu, Y., Miller, M., Bowsher, C.G., Goodacre, R., Lunn, J.E.,
1162 and Johnson, G.N. (2015). Acclimation of metabolism to light in *Arabidopsis thaliana*: The

- 1163 glucose 6-phosphate/phosphate translocator GPT2 directs metabolic acclimation. *Plant*,
1164 *Cell Environ.* 38: 1404–1417.
- 1165 Dyson, B.C., Webster, R.E., and Johnson, G.N. (2014). GPT2: A glucose 6-
1166 phosphate/phosphate translocator with a novel role in the regulation of sugar signalling
1167 during seedling development. *Ann. Bot.* 113: 643–652.
- 1168 Eicks, M., Maurino, V., Knappe, S., Flügge, U.-I., and Fischer, K. (2002). The plastidic pentose
1169 phosphate translocator represents a link between the cytosolic and the plastidic pentose
1170 phosphate pathways in plants. *Plant Physiol.* 128: 512–522.
- 1171 Eubel, H., Meyer, E.H., Taylor, N.L., Bussell, J.D., O’Toole, N., Heazlewood, J.L., Castleden, I.,
1172 Small, I.D., Smith, S.M., and Millar, a H. (2008). Novel proteins, putative membrane
1173 transporters, and an integrated metabolic network are revealed by quantitative proteomic
1174 analysis of Arabidopsis cell culture peroxisomes. *Plant Physiol.* 148: 1809–29.
- 1175 Fancy, N.N., Bahlmann, A.-K., and Loake, G.J. (2016). Nitric oxide function in plant abiotic
1176 stress. *Plant. Cell Environ.*: 1–11.
- 1177 Fernández-Fernández, Á.D. and Corpas, F.J. (2016). In Silico Analysis of Arabidopsis thaliana
1178 Peroxisomal 6-Phosphogluconate Dehydrogenase. *Scientifica (Cairo)*. 2016.
- 1179 Flügge, U.-I. (1999). Phosphate Translocators in Plastids. *Annu. Rev. Plant Physiol. Plant Mol.*
1180 *Biol.* 50: 27–45.
- 1181 Flügge, U.-I., Häusler, R.E., Ludewig, F., and Gierth, M. (2011). The role of transporters in
1182 supplying energy to plant plastids. *J. Exp. Bot.* 62: 2381–2392.
- 1183 Foyer, C.H., Bloom, A.J., Queval, G., and Noctor, G. (2009). Photorespiratory metabolism:
1184 genes, mutants, energetics, and redox signaling. *Annu. Rev. Plant Biol.* 60: 455–484.
- 1185 Geigenberger, P., Kolbe, A., and Tiessen, A. (2005). Redox regulation of carbon storage and
1186 partitioning in response to light and sugars. *J. Exp. Bot.* 56: 1469–1479.
- 1187 Gietz, R.D. and Schiestl, R.H. (2007). High-efficiency yeast transformation using the LiAc/SS
1188 carrier DNA/PEG method. *Nat. Protoc.* 2: 31–34.
- 1189 Goder, V., Junne, T., and Spiess, M. (2004). Sec61p Contributes to Signal Sequence
1190 Orientation According to the Positive-Inside Rule. *Mol. Biol. Cell* 15: 1470–1478.
- 1191 Gong, F.-C., Giddings, T.H., Meehl, J.B., Staehelin, L.A., and Galbraith, D.W. (1996). Z-
1192 membranes: artificial organelles for overexpressing recombinant integral membrane
1193 proteins. *Proc. Natl. Acad. Sci. U. S. A.* 93: 2219–2223.
- 1194 Gould, S.J., Keller, G.-A., Hosken, N., Wilkinson, J., and Subramani, S. (1989). A Conserved
1195 Tripeptide Sorts Proteins to Peroxisomes. *J. Cell Biol.* 108: 1657–1664.
- 1196 Greaves, J., Salaun, C., Fukata, Y., Fukata, M., and Chamberlain, L.H. (2008). Palmitoylation
1197 and membrane interactions of the neuroprotective chaperone cysteine-string protein. *J.*
1198 *Biol. Chem.* 283: 25014–25026.
- 1199 Guevara-Garcia, A., Mosqueda-Cano, G., Argüello-Astorga, G., Simpson, J., and Herrera-
1200 Estrella, L. (1993). Tissue-specific and wound-inducible pattern of expression of the
1201 mannopine synthase promoter is determined by the interaction between positive and
1202 negative cis-regulatory elements. *Plant J.* 4: 495–505.
- 1203 Gurrieri, L., Distefano, L., Pirone, C., Horrer, D., Seung, D., Zaffagnini, M., Rouhier, N., Trost, P.,
1204 Santelia, D., and Sparla, F. (2019). The Thioredoxin-Regulated α -Amylase 3 of
1205 Arabidopsis thaliana Is a Target of S-Glutathionylation. *Front. Plant Sci.* 10: 993.

- 1206 Hadden, D. a, Phillipson, B. a, Johnston, K. a, Brown, L.-A., Manfield, I.W., El-Shami, M.,
1207 Sparkes, I. a, and Baker, A. (2006). Arabidopsis PEX19 is a dimeric protein that binds the
1208 peroxin PEX10. *Mol. Membr. Biol.* 23: 325–236.
- 1209 Hauschild, R. and von Schaewen, A. (2003). Differential regulation of glucose-6-phosphate
1210 dehydrogenase isoenzyme activities in potato. *Plant Physiol.* 133: 47–62.
- 1211 Heazlewood, J.I., Durek, P., Hummel, J., Selbig, J., Weckwerth, W., Walther, D., and Schulze,
1212 W.X. (2008). PhosPhAt : A database of phosphorylation sites in Arabidopsis thaliana and a
1213 plant-specific phosphorylation site predictor. *Nucleic Acids Res.* 36: 1015–1021.
- 1214 von Heijne, G. (1986). Net N-C charge imbalance may be important for signal sequence function
1215 in bacteria. *J. Mol. Biol.* 192: 287–290.
- 1216 Hemsley, P.A. (2015). The importance of lipid modified proteins in plants. *New Phytol.* 205: 476–
1217 489.
- 1218 Hilgers, E.J.A., Schöttler, M.A., Mettler-Altman, T., Krueger, S., Dörmann, P., Eicks, M.,
1219 Flügge, U.I., and Häusler, R.E. (2018). The combined loss of triose phosphate and
1220 xylulose 5-phosphate/phosphate translocators leads to severe growth retardation and
1221 impaired photosynthesis in arabidopsis thaliana tpt/xpt double mutants. *Front. Plant Sci.* 9.
- 1222 Hölscher, C., Lutterbey, M.-C., Lansing, H., Meyer, T., Fischer, K., and von Schaewen, A.
1223 (2016). Defects in peroxisomal 6-phosphogluconate dehydrogenase isoform PGD2
1224 prevent gametophytic interaction in Arabidopsis thaliana. *Plant Physiol.*: pp.15.01301-.
- 1225 Hölscher, C., Meyer, T., and Von Schaewen, A. (2014). Dual-targeting of arabidopsis 6-
1226 phosphogluconolactonase 3 (PGL3) to chloroplasts and peroxisomes involves interaction
1227 with Trx m2 in the cytosol. *Mol. Plant* 7: 252–255.
- 1228 Hua, R., Gidda, S.K., Aranovich, A., Mullen, R.T., and Kim, P.K. (2015). Multiple Domains in
1229 PEX16 Mediate Its Trafficking and Recruitment of Peroxisomal Proteins to the ER. *Traffic:*
1230 *n/a-n/a*.
- 1231 Hunt, J.E. and Trelease, R.N. (2004). Sorting pathway and molecular targeting signals for the
1232 Arabidopsis peroxin 3. *Biochem. Biophys. Res. Commun.* 314: 586–596.
- 1233 Hutchings, D., Rawsthorne, S., and Emes, M.J. (2005). Fatty acid synthesis and the oxidative
1234 pentose phosphate pathway in developing embryos of oilseed rape (*Brassica napus* L.). *J.*
1235 *Exp. Bot.* 56: 577–585.
- 1236 Jones, A.M. et al. (2014). Border Control - A Membrane-Linked Interactome of Arabidopsis.
1237 *Science* (80-.). 344: 711–716.
- 1238 Jones, D.T., Taylor, W.R., and Thornton, J.M. (1992). The rapid generation of mutation data
1239 matrices from protein sequences. *Comput. Appl. Biosci.* 8: 275–282.
- 1240 Kammerer, B., Fischer, K., Hilpert, B., Schubert, S., Gutensohn, M., Weber, A., and Flügge,
1241 U.-I. (1998). Molecular Characterization of a Carbon Transporter in Plastids from
1242 Heterotrophic Tissues: The Glucose 6-Phosphate/Phosphate Antiporter. *Plant Cell* 10:
1243 105–117.
- 1244 Kao, Y.T., Gonzalez, K.L., and Bartel, B. (2018). Peroxisome function, biogenesis, and dynamics
1245 in plants. *Plant Physiol.* 176: 162–177.
- 1246 Karnik, S.K. and Trelease, R.N. (2005). Arabidopsis peroxin 16 coexists at steady state in
1247 peroxisomes and endoplasmic reticulum. *Plant Physiol.* 138: 1967–1981.
- 1248 Kataya, A. and Reumann, S. (2010). Arabidopsis glutathione reductase 1 is dually targeted to
1249 peroxisomes and the cytosol. *Plant Signal. Behav.* 5: 171–175.

- 1250 Kim, P.K. and Hettema, E.H. (2015). Multiple Pathways for Protein Transport to Peroxisomes. *J.*
1251 *Mol. Biol.* 427: 1176–1190.
- 1252 Kim, P.K. and Mullen, R.T. (2013). PEX16: a multifaceted regulator of peroxisome biogenesis.
1253 *Front. Physiol.* 4: 1–6.
- 1254 Klausner, R.D., Donaldson, J.G., and Lippincott-Schwartz, J. (1992). Brefeldin A: Insights into
1255 the control of membrane traffic and organelle structure. *J. Cell Biol.* 116: 1071–1080.
- 1256 Knappe, S., Flügge, U.-I., and Fischer, K. (2003). Analysis of the plastidic phosphate
1257 translocator gene family in Arabidopsis and identification of new phosphate translocator-
1258 homologous transporters, classified by their putative substrate-binding site. *Plant Physiol.*
1259 131: 1178–1190.
- 1260 Kruger, N.J. and Von Schaewen, A. (2003). The oxidative pentose phosphate pathway:
1261 Structure and organisation. *Curr. Opin. Plant Biol.* 6: 236–246.
- 1262 Kumar, S., Stecher, G., and Tamura, K. (2016). MEGA7: Molecular Evolutionary Genetics
1263 Analysis Version 7.0 for Bigger Datasets. *Mol. Biol. Evol.* 33: 1870–1874.
- 1264 Kunz, H.-H., Häusler, R.E., Fettke, J., Herbst, K., Niewiadomski, P., Gierth, M., Bell, K., Steup,
1265 M., Flügge, U.-I., and Schneider, A. (2010). The role of plastidial glucose-6-
1266 phosphate/phosphate translocators in vegetative tissues of Arabidopsis thaliana mutants
1267 impaired in starch biosynthesis. *Plant Biol.* 12: 115–128.
- 1268 Lalonde, S. et al. (2010). A membrane protein / signaling protein interaction network for
1269 Arabidopsis version AMPv2. *Front. Physiol.* 1: 1–14.
- 1270 Landi, S., Nurcato, R., De Lillo, A., Lentini, M., Grillo, S., and Esposito, S. (2016). Glucose-6-
1271 phosphate dehydrogenase plays a central role in the response of tomato (*Solanum*
1272 *lycopersicum*) plants to short and long-term drought. *Plant Physiol. Biochem.* 105: 79–89.
- 1273 Lansing, H., Doering, L., Fischer, K., Baune, M.-C., and von Schaewen, A. (2019). Analysis of
1274 potential redundancy among Arabidopsis 6-phosphogluconolactonase (PGL) isoforms in
1275 peroxisomes. *J. Exp. Bot.*
- 1276 Lee, S.K., Eom, J.S., Hwang, S.K., Shin, D., An, G., Okita, T.W., and Jeon, J.S. (2016). Plastidic
1277 phosphoglucomutase and ADP-glucose pyrophosphorylase mutants impair starch
1278 synthesis in rice pollen grains and cause male sterility. *J. Exp. Bot.* 67: 5557–5569.
- 1279 Lee, Y., Nishizawa, T., Takemoto, M., Kumazaki, K., Yamashita, K., Hirata, K., Minoda, A.,
1280 Nagatoishi, S., Tsumoto, K., Ishitani, R., and Nureki, O. (2017). Structure of the triose-
1281 phosphate/phosphate translocator reveals the basis of substrate specificity. *Nat. Plants* 3:
1282 825–832.
- 1283 Li, S. (2014). Redox Modulation Matters: Emerging Functions for Glutaredoxins in Plant
1284 Development and Stress Responses. *Plants* 3: 559–582.
- 1285 Li, Y., Li, H., Morgan, C., Bomblies, K., Yang, W., and Qi, B. (2019). Both male and female
1286 gametogenesis require a fully functional protein S- acyl transferase 21 in Arabidopsis
1287 thaliana . *Plant J.*
- 1288 Liebthal, M., Maynard, D., and Dietz, K.-J. (2018). Peroxiredoxins and Redox Signaling in
1289 Plants. *Antioxid. Redox Signal.* 28: 609–624.
- 1290 Lin, Y., Cluette-brown, J.E., and Goodman, H.M. (2004). The Peroxisome Deficient Arabidopsis
1291 Mutant sse1 Exhibits Impaired Fatty Acid Synthesis 1 [w]. 135: 814–827.
- 1292 Lin, Y., Sun, L., Nguyen, L. V, Rachubinski, R.A., and Goodman, H.M. (1999). The Pex16p
1293 homolog SSE1 and storage organelle formation in Arabidopsis seeds. *Science* 284: 328–
1294 30.

- 1295 Linka, N., Theodoulou, F.L., Haslam, R.P., Linka, M., Napier, J. a, Neuhaus, H.E., and Weber,
1296 A.P.M. (2008). Peroxisomal ATP import is essential for seedling development in
1297 *Arabidopsis thaliana*. *Plant Cell* 20: 3241–3257.
- 1298 Lisenbee, C.S., Karnik, S.K., and Trelease, R.N. (2003). Overexpression and Mislocalization of a
1299 Tail-Anchored GFP Redefines the Identity of Peroxisomal ER. *Traffic* 4: 491–501.
- 1300 Majeran, W., Le Caer, J.P., Ponnala, L., Meinel, T., and Giglione, C. (2018). Targeted profiling
1301 of *Arabidopsis thaliana* subproteomes illuminates co- and posttranslationally N-terminal
1302 myristoylated proteins. *Plant Cell* 30: 543–562.
- 1303 Marty, L. et al. (2019). *Arabidopsis* glutathione reductase 2 is indispensable in plastids, while
1304 mitochondrial glutathione is safeguarded by additional reduction and transport systems.
1305 *New Phytol.*
- 1306 Marty, L., Siala, W., Schwarzländer, M., Fricker, M.D., Wirtz, M., Sweetlove, L.J., Meyer, Y.,
1307 Meyer, A.J., Reichheld, J.-P., and Hell, R. (2009). The NADPH-dependent thioredoxin
1308 system constitutes a functional backup for cytosolic glutathione reductase in *Arabidopsis*.
1309 *Proc. Natl. Acad. Sci. U. S. A.* 106: 9109–9114.
- 1310 McDonnell, M.M., Burkhart, S.E., Stoddard, J.M., Wright, Z.J., Strader, L.C., and Bartel, B.
1311 (2016). The early-acting peroxin PEX19 is redundantly encoded, farnesylated, and
1312 essential for viability in *Arabidopsis thaliana*. *PLoS One* 11: 1–19.
- 1313 Meng, L., Wong, J.H., Feldman, L.J., Lemaux, P.G., and Buchanan, B.B. (2010). A membrane-
1314 associated thioredoxin required for plant growth moves from cell to cell, suggestive of a
1315 role in intercellular communication. *Proc. Natl. Acad. Sci. U. S. A.* 107: 3900–3905.
- 1316 Meyer, T., Hölscher, C., Schwöppe, C., and von Schaewen, A. (2011). Alternative targeting of
1317 *Arabidopsis* plastidic glucose-6-phosphate dehydrogenase G6PD1 involves cysteine-
1318 dependent interaction with G6PD4 in the cytosol. *Plant J.* 66: 745–758.
- 1319 Mhamdi, A., Mauve, C., Gouia, H., Saindrenan, P., Hodges, M., and Noctor, G. (2010). Cytosolic
1320 NADP-dependent isocitrate dehydrogenase contributes to redox homeostasis and the
1321 regulation of pathogen responses in *Arabidopsis* leaves. *Plant, Cell Environ.* 33: 1112–
1322 1123.
- 1323 Mueckler, M. and Lodish, H.F. (1986). The human glucose transporter can insert
1324 posttranslationally into microsomes. *Cell* 44: 629–637.
- 1325 Mullen, R.T., Lisenbee, C.S., Miernyk, J. a, and Trelease, R.N. (1999). Peroxisomal membrane
1326 ascorbate peroxidase is sorted to a membranous network that resembles a subdomain of
1327 the endoplasmic reticulum. *Plant Cell* 11: 2167–2185.
- 1328 Mullen, R.T. and Trelease, R.N. (2006). The ER-peroxisome connection in plants: development
1329 of the “ER semi-autonomous peroxisome maturation and replication” model for plant
1330 peroxisome biogenesis. *Biochim. Biophys. Acta* 1763: 1655–1668.
- 1331 Murphy, M.A., Phillipson, B.A., Baker, A., and Mullen, R.T. (2003). Characterization of the
1332 Targeting Signal of the *Arabidopsis* 22-kD Integral Peroxisomal Membrane Protein 1. *Plant*
1333 *Physiol.* 133: 813–828.
- 1334 Niewiadomski, P., Knappe, S., Geimer, S., Fischer, K., Schulz, B., Unte, U.S., Rosso, M.G.,
1335 Ache, P., Flügge, U.-I., and Schneider, A. (2005). The *Arabidopsis* plastidic glucose 6-
1336 phosphate/phosphate translocator GPT1 is essential for pollen maturation and embryo sac
1337 development. *Plant Cell* 17: 760–775.
- 1338 Noctor, G. and Foyer, C.H. (2016). Intracellular redox compartmentation and ROS-related
1339 communication in regulation and signaling. *Plant Physiol.* 171: 1581–1592.

- 1340 Nozawa, A., Nanamiya, H., Miyata, T., Linka, N., Endo, Y., Weber, A.P.M., and Tozawa, Y.
1341 (2007). A cell-free translation and proteoliposome reconstitution system for functional
1342 analysis of plant solute transporters. *Plant Cell Physiol.* 48: 1815–1820.
- 1343 Orcl, L., Tagaya, M., Amherdt, M., Perrelet, A., Donaldson, J.G., Lippincott-Schwartz, J.,
1344 Klausner, R.D., and Rothman, J.E. (1991). Brefeldin A, a drug that blocks secretion,
1345 prevents the assembly of non-clathrin-coated buds on Golgi cisternae. *Cell* 64: 1183–
1346 1195.
- 1347 Palatnik, J.F., Tognetti, V.B., Poli, H.O., Rodríguez, R.E., Blanco, N., Gattuso, M., Hajirezaei,
1348 M.R., Sonnewald, U., Valle, E.M., and Carrillo, N. (2003). Transgenic tobacco plants
1349 expressing antisense ferredoxin-NADP(H) reductase transcripts display increased
1350 susceptibility to photo-oxidative damage. *Plant J.* 35: 332–341.
- 1351 Park, S.K. et al. (2009). Heat-shock and redox-dependent functional switching of an h-type
1352 Arabidopsis thioredoxin from a disulfide reductase to a molecular chaperone. *Plant*
1353 *Physiol.* 150: 552–561.
- 1354 Pitzschke, A., Forzani, C., and Hirt, H. (2006). Reactive oxygen species signaling in plants.
1355 *Antioxidants & Redox Signaling* 8: 1757–1764.
- 1356 Platta, H.W. and Erdmann, R. (2007). Peroxisomal dynamics. *Trends Cell Biol.* 17: 474–484.
- 1357 Porter, B.W., Yuen, C.Y.L., and Christopher, D.A. (2015). Dual protein trafficking to secretory
1358 and non-secretory cell compartments: Clear or double vision? *Plant Sci.* 234: 174–179.
- 1359 Preiser, A.L., Fisher, N., Banerjee, A., and Sharkey, T.D. (2019). Plastidic glucose-6-phosphate
1360 dehydrogenases are regulated to maintain activity in the light. *Biochem. J.* 476: 1539–
1361 1551.
- 1362 Reumann, S. (2004). Specification of the peroxisome targeting signals type 1 and type 2 of plant
1363 peroxisomes by bioinformatics analyses. *Plant Physiol.* 135: 783–800.
- 1364 Reumann, S., Babujee, L., Ma, C., Wienkoop, S., Siemsen, T., Antonicelli, G.E., Rasche, N.,
1365 Lüder, F., Weckwerth, W., and Jahn, O. (2007). Proteome analysis of Arabidopsis leaf
1366 peroxisomes reveals novel targeting peptides, metabolic pathways, and defense
1367 mechanisms. *Plant Cell* 19: 3170–3193.
- 1368 Reumann, S. and Bartel, B. (2016). Plant peroxisomes: recent discoveries in functional
1369 complexity, organelle homeostasis, and morphological dynamics. *Curr. Opin. Plant Biol.*
1370 34: 17–26.
- 1371 Reumann, S., Ma, C., Lemke, S., and Babujee, L. (2004). AraPeroX. A database of putative
1372 Arabidopsis proteins from plant peroxisomes. *Plant Physiol.* 136: 2587–2608.
- 1373 Reumann, S., Maier, E., Benz, R., and Heldt, H.W. (1996). A specific porin is involved in the
1374 malate shuttle of leaf peroxisomes. *Biochem. Soc. Trans.* 24: 754–757.
- 1375 del Río, L.A., Corpas, F.J., Sandalio, L.M., Palma, J.M., Gómez, M., and Barroso, J.B. (2002).
1376 Reactive oxygen species, antioxidant systems and nitric oxide in peroxisomes. *J. Exp. Bot.*
1377 53: 1255–1272.
- 1378 Riondet, C., Desouris, J.P., Montoya, J.G., Chartier, Y., Meyer, Y., and Reichheld, J.P. (2012). A
1379 dicotyledon-specific glutaredoxin GRXC1 family with dimer-dependent redox regulation is
1380 functionally redundant with GRXC2. *Plant, Cell Environ.* 35: 360–373.
- 1381 Rips, S., Bentley, N., Jeong, I.S., Welch, J.L., von Schaewen, A., and Koiwa, H. (2014). Multiple
1382 N-Glycans Cooperate in the Subcellular Targeting and Functioning of Arabidopsis
1383 KORRIGAN1. *Plant Cell* 26: 3792–3808.

- 1384 Robida, A.M. and Kerppola, T.K. (2009). Bimolecular fluorescence complementation analysis of
1385 inducible protein interactions: effects of factors affecting protein folding on fluorescent
1386 protein fragment association. *J. Mol. Biol.* 394: 391–409.
- 1387 Rokka, A., Antonenkov, V.D., Soininen, R., Immonen, H.L., Pirilä, P.L., Bergmann, U.,
1388 Sormunen, R.T., Weckström, M., Benz, R., and Hiltunen, J.K. (2009). Pxm2 is a channel-
1389 forming protein in mammalian peroxisomal membrane. *PLoS One* 4: 1–15.
- 1390 Rottensteiner, H., Kramer, A., Lorenzen, S., Stein, K., Landgraf, C., Volkmer-Engert, R., and
1391 Erdmann, R. (2004). Peroxisomal membrane proteins contain common Pex19p-binding
1392 sites that are an integral part of their targeting signals. *Mol. Biol. Cell* 15: 3406–3417.
- 1393 Rouhier, N. (2010). Plant glutaredoxins: Pivotal players in redox biology and iron-sulphur centre
1394 assembly. *New Phytol.* 186: 365–372.
- 1395 Sakaue, H., Iwashita, S., Yamashita, Y., Kida, Y., and Sakaguchi, M. (2016). The N-terminal
1396 motif of PMP70 suppresses cotranslational targeting to the endoplasmic reticulum. *J.*
1397 *Biochem.* 159: 539–551.
- 1398 Sanz-Barrio, R., Fernández-San Millán, A., Carballeda, J., Corral-Martínez, P., Seguí-Simarro,
1399 J.M., and Farran, I. (2012). Chaperone-like properties of tobacco plastid thioredoxins f and
1400 m. *J. Exp. Bot.* 63: 365–379.
- 1401 Scharfe, J., Schön, H., Tjaden, Z., Weis, E., and von Schaewen, A. (2009). Isoenzyme
1402 replacement of glucose-6-phosphate dehydrogenase in the cytosol improves stress
1403 tolerance in plants. *Proc. Natl. Acad. Sci. U. S. A.* 106: 8061–6.
- 1404 Schmidt, G.W., Devillers-Thiery, A., Desruisseaux, H., Blobel, G., and Chua, N.-H. (1979). NH2-
1405 Terminal Amino Acid Sequences of Precursor and Mature Forms of the Ribulose-1,5-
1406 Bisphosphate Carboxylase Small Subunit From *Chlamydomonas Reinhardtii*. *J. Cell Biol.*
1407 83: 615–622.
- 1408 Schnarrenberger, C., Flechner, A., and Martin, W. (1995). Enzymatic Evidence for a Complete
1409 Oxidative Pentose Phosphate Pathway in Chloroplasts and an Incomplete Pathway in the
1410 Cytosol of Spinach Leaves. *Plant Physiol.* 108: 609–614.
- 1411 Shao, S. and Hegde, R.S. (2011). Membrane protein insertion at the endoplasmic reticulum.
1412 *Annu. Rev. Cell Dev. Biol.* 27: 25–56.
- 1413 Sharkey, T.D. and Weise, S.E. (2016). The glucose 6-phosphate shunt around the Calvin-
1414 Benson cycle. *J. Exp. Bot.* 67: 4067–4077.
- 1415 Stampfl, H., Fritz, M., Dal Santo, S., and Jonak, C. (2016). The GSK3/Shaggy-like kinase ASKα
1416 contributes to pattern-triggered immunity in *Arabidopsis thaliana*. *Plant Physiol.* 171:
1417 pp.01741.2015.
- 1418 Tabak, H.F., Hoepfner, D., van der Zand, A., Geuze, H.J., Braakman, I., and Huynen, M.A.
1419 (2006). Formation of peroxisomes: Present and past. *Biochim. Biophys. Acta* 1763: 1647–
1420 1654.
- 1421 Theodoulou, F.L., Bernhardt, K., Linka, N., and Baker, A. (2013). Peroxisome membrane
1422 proteins: multiple trafficking routes and multiple functions? *Biochem. J.* 451: 345–352.
- 1423 Torres, M.A., Dangl, J.L., and Jones, J.D.G. (2002). *Arabidopsis* gp91phox homologues AtrbohD
1424 and AtrbohF are required for accumulation of reactive oxygen intermediates in the plant
1425 defense response. *Proc. Natl. Acad. Sci. U. S. A.* 99: 517–522.
- 1426 Traverso, J.A., Pulido, A., Rodríguez-García, M.I., and Alché, J.D. (2013). Thiol-based redox
1427 regulation in sexual plant reproduction: new insights and perspectives. *Front. Plant Sci.* 4:
1428 1–14.

- 1429 Ukuwela, A.A., Bush, A.I., Wedd, A.G., and Xiao, Z. (2018). Glutaredoxins employ parallel
1430 monothiol-dithiol mechanisms to catalyze thiol-disulfide exchanges with protein disulfides.
1431 Chem. Sci. 9: 1173–1183.
- 1432 Vandenaabeele, S., Vanderauwera, S., Vuylsteke, M., Rombauts, S., Langebartels, C., Seidlitz,
1433 H.K., Zabeau, M., Van Montagu, M., Inzé, D., and Van Breusegem, F. (2004). Catalase
1434 deficiency drastically affects gene expression induced by high light in *Arabidopsis thaliana*.
1435 Plant J. 39: 45–58.
- 1436 Walter, M., Chaban, C., Schütze, K., Batistic, O., Weckermann, K., Näke, C., Blazevic, D.,
1437 Grefen, C., Schumacher, K., Oecking, C., Harter, K., and Kudla, J. (2004). Visualization of
1438 protein interactions in living plant cells using bimolecular fluorescence complementation.
1439 Plant J. 40: 428–438.
- 1440 Wang, Y., Windh, R.T., Chen, C.A., and Manning, D.R. (1999). N-myristoylation and $\beta\gamma$ play
1441 roles beyond anchorage in the palmitoylation of the G protein $\alpha(o)$ subunit. J. Biol. Chem.
1442 274: 37435–37442.
- 1443 Waszczak, C., Carmody, M., and Kangasjärvi, J. (2018). Reactive Oxygen Species in Plant
1444 Signaling. Annu. Rev. Plant Biol. 69: 209–236.
- 1445 Weise, S.E., Liu, T., Childs, K.L., Preiser, A.L., Katulski, H.M., Perrin-Porzondek, C., and
1446 Sharkey, T.D. (2019). Transcriptional regulation of the glucose-6-phosphate/phosphate
1447 translocator 2 is related to carbon exchange across the chloroplast envelope. Front. Plant
1448 Sci. 10.
- 1449 van Wijk, K.J. (2015). Protein maturation and proteolysis in plant plastids, mitochondria, and
1450 peroxisomes. Annu Rev Plant Biol 66: 75–111.
- 1451 Wilkinson, J.E., Twell, D., and Lindsey, K. (1997). Activities of CaMV 35S and nos promoters in
1452 pollen: Implications for field release of transgenic plants. J. Exp. Bot. 48: 265–275.
- 1453 Winter, D. et al. (2007). An “Electronic Fluorescent Pictograph” Browser for Exploring and
1454 Analyzing Large-Scale Biological Data Sets. PLoS One e718: 1–12.
- 1455 Xiong, Y., Defraia, C., Williams, D., Zhang, X., and Mou, Z. (2009). Deficiency in a cytosolic
1456 ribose-5-phosphate isomerase causes chloroplast dysfunction, late flowering and
1457 premature cell death in *Arabidopsis*. Physiol. Plant. 137: 249–263.
- 1458 Zaffagnini, M., Fermani, S., Marchand, C.H., Costa, A., Sparla, F., Rouhier, N., Geigenberger,
1459 P., Lemaire, S.D., and Trost, P. (2019). Redox Homeostasis in Photosynthetic Organisms:
1460 Novel and Established Thiol-Based Molecular Mechanisms. Antioxid. Redox Signal. 31:
1461 155–210.
- 1462 van der Zand, A., Braakman, I., and Tabak, H.F. (2010). Peroxisomal Membrane Proteins Insert
1463 into the Endoplasmic Reticulum. Mol. Biol. Cell 21: 2057–2065.
- 1464 van der Zand, A., Gent, J., Braakman, I., and Tabak, H.F. (2012). Biochemically distinct vesicles
1465 from the endoplasmic reticulum fuse to form peroxisomes. Cell 149: 397–409.
- 1466 Zulawski, M., Braginets, R., and Schulze, W.X. (2013). PhosPhAt goes kinases-searchable
1467 protein kinase target information in the plant phosphorylation site database PhosPhAt.
1468 Nucleic Acids Res. 41: 1176–1184.
- 1469
1470

bioRxiv preprint first posted online Dec. 12, 2019; doi: <http://dx.doi.org/10.1101/2019.12.11.873000>. The copyright holder for this preprint (which was not peer-reviewed) is the author/funder, who has granted bioRxiv a license to display the preprint in perpetuity.
All rights reserved. No reuse allowed without permission.

Baune et al.

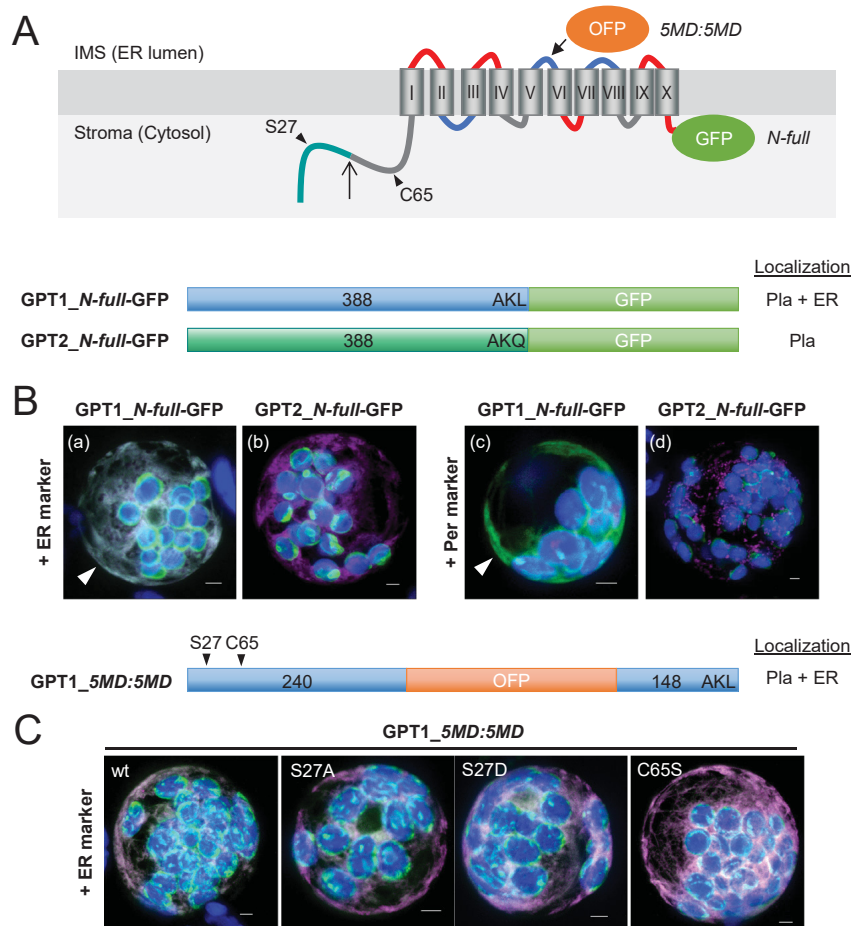


Figure 1. GPT1 reporter fusions dually localize to plastids and the ER.

A, Topology model of Arabidopsis glucose-6-phosphate/phosphate translocator (GPT) isoforms with 10 membrane domains (MD) depicted as barrels (roman numbering), connected by hinge regions (red, positive; blue, negative; grey, neutral net charge), and both N-/C-terminal ends facing the stroma (Lee et al. 2017). Relevant positions are indicated: Plastidic transit peptide (TP, green), TP processing site (upward arrow), N-terminal amino acids potentially modified/regulatory in GPT1 (arrowheads), medial OFF insertion (5MD:5MD) and C-terminal GFP fusion (N-full). ER, endoplasmic reticulum; IMS, intermembrane space. **B-C**, Localization of the depicted GPT-reporter fusions upon transient expression in Arabidopsis protoplasts (24-48 h post transfection). **B**, With free N-terminus, GPT1 targets both plastids and the ER (panels a and c, arrowheads), but GPT2 only plastids (Pla; panels b and d). **C**, The medial GPT1_5MD:5MD construct (wt, wildtype) was used for analyzing potential effects of single amino acid changes in the N-terminus: S27A (abolishing phosphorylation), S27D (phospho-mimic) and C65S (precluding S modification). All images show maximal projections of approximately 30 optical sections (Merge, for single channel images, see Supplemental Figure 5). Candidate fusions in green, ER marker (panel B, OFF-ER; panel C, GFP-ER) or peroxisome marker (Per; OFF-PGL3_C-short) in magenta, and chlorophyll fluorescence in blue. Co-localization of green and magenta (or very close signals less than 200 nm) appear white in the Merge of all channels. Bars = 3 μ m.

bioRxiv preprint first posted online Dec. 12, 2019; doi: <http://dx.doi.org/10.1101/2019.12.11.873000>. The copyright holder for this preprint (which was not peer-reviewed) is the author/funder, who has granted bioRxiv a license to display the preprint in perpetuity.
All rights reserved. No reuse allowed without permission.

Baune et al.

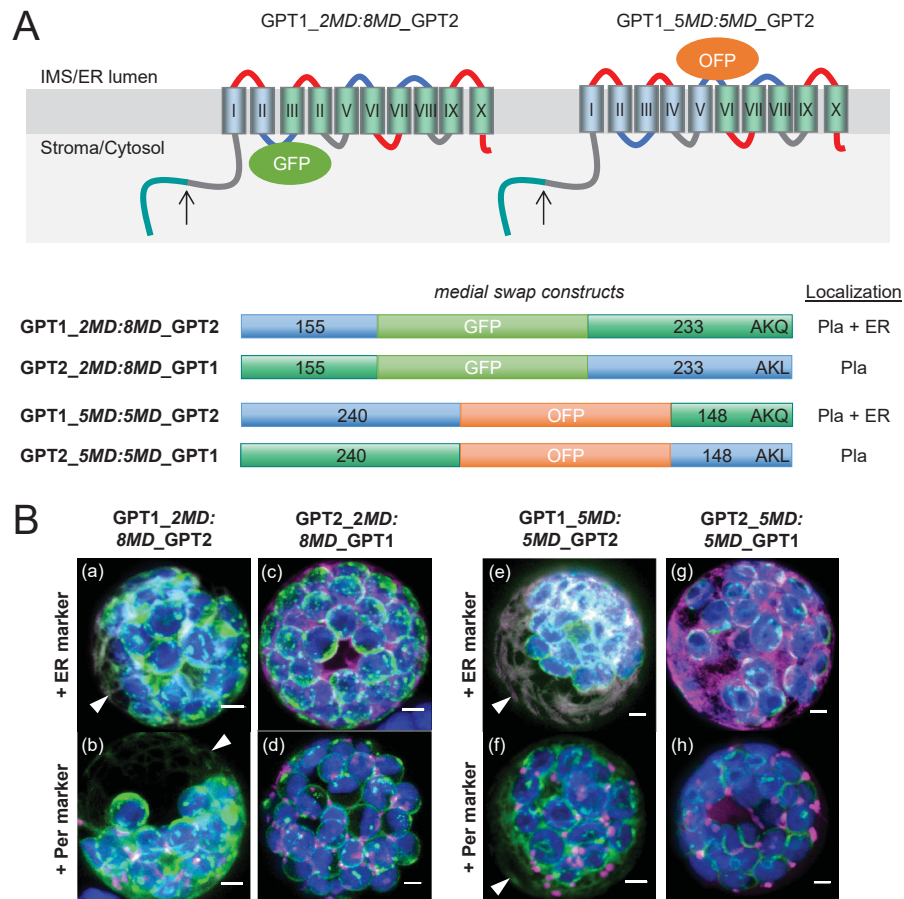


Figure 2. Domain swaps demonstrate that the N-terminus of GPT1 confers ER targeting.

A, Topology models of the GPT *medial* swap constructs, with orientation of the inserted reporters: GFP facing the stroma/cytosol and OFP the intermembrane space (IMS)/lumen of the endoplasmic reticulum (ER). Membrane domains (depicted as barrels, roman numbering) of GPT1 in blue and of GPT2 in green. The upward arrows indicate transit peptide cleavage sites (plastid stroma). **B**, Localization of the indicated medial swap constructs in Arabidopsis protoplasts (24-48 h post transfection). When headed by GPT1 (GPT1_2MD:8MD_GPT2 or GPT1_5MD:5MD_GPT2), plastids and the ER (arrowheads) are labeled (panels a,b and e,f); when headed by GPT2 (GPT2_2MD:8MD_GPT1 or GPT2_5MD:5MD_GPT1), only plastids (Pla) are labeled (panels c,d and g,h). All images show maximal projections of approximately 30 optical sections (Merge, for single channel images, see Supplemental Figure 7). Candidate fusions in green, ER marker (G/OFP-ER) or peroxisome marker (Per; G/OFP-PGL3_C-short) in magenta, and chlorophyll fluorescence in blue. Co-localization of green and magenta (and very close signals less than 200 nm) appear white in the Merge of all channels. Bars = 3 μ m.

bioRxiv preprint first posted online Dec. 12, 2019; doi: <http://dx.doi.org/10.1101/2019.12.11.873000>. The copyright holder for this preprint (which was not peer-reviewed) is the author/funder, who has granted bioRxiv a license to display the preprint in perpetuity.
All rights reserved. No reuse allowed without permission.

Baune et al.

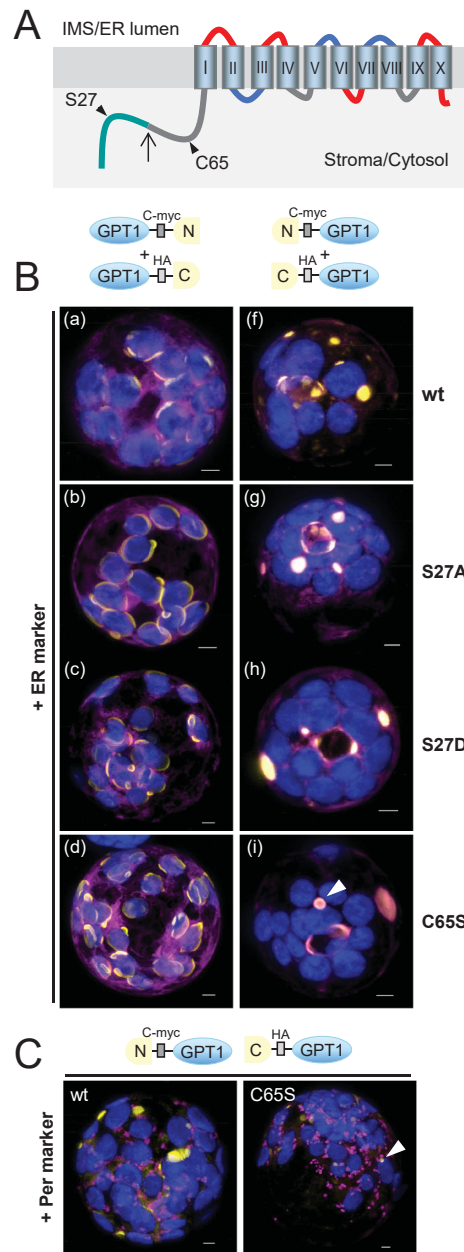


Figure 3. GPT1 dimer formation occurs at plastids and ER substructures.

A, Topology model of GPT1 with N-terminal transit peptide (green) and cleavage site (upward arrow) plus position of amino acids S27 and C65 (arrowheads). The membrane domains are depicted as barrels (roman numbering) connected by hinge regions of different net charge (red, positive; blue, negative; grey, neutral). **B**, Localization of yellow BiFC signals (reconstituted split YFP, N+C halves) due to interaction of the GPT1 parts in Arabidopsis protoplasts (24-48 h post transfection). With unmasked N-terminus, GPT1 may label plastids and the ER (left panels), but with masked N-terminus only the ER (right panels). In addition to unmodified GPT1 wild-type (wt), mutant combinations S27A (non-phosphorylated), S27D (phosphomimic) and C65S (precluding S modification) were analyzed. GPT1 dimer formation occurred at plastid rims (left panels) or ER substructures (right panels), with little impact of the S27 changes, but visible effect of C65S (hollow sphere in panel i; surrounding a peroxisome in C, arrowheads). Note that structures with BiFC signals on the right (panels f-i) are also labeled by the ER marker (most obvious in panel g). **C**, Localization of the indicated split YFP combinations in co-expression with the peroxisome (Per) marker. Note that in case of C65S, the ring-like BiFC signal surrounds a peroxisome (arrowhead). All images show maximal projections of approximately 30 optical sections (Merge; for single channel images, see Supplemental Figure 8). Organelle markers (OFP-ER or OFP-PGL3_C-short) in magenta chlorophyll fluorescence in blue. Co-localization of yellow and magenta (or very close signals less than 200 nm) appear whitish in the Merge of all channels. Bars = 3 μ m.

bioRxiv preprint first posted online Dec. 12, 2019; doi: <http://dx.doi.org/10.1101/2019.12.11.873000>. The copyright holder for this preprint (which was not peer-reviewed) is the author/funder, who has granted bioRxiv a license to display the preprint in perpetuity.
All rights reserved. No reuse allowed without permission.

Baune et al.

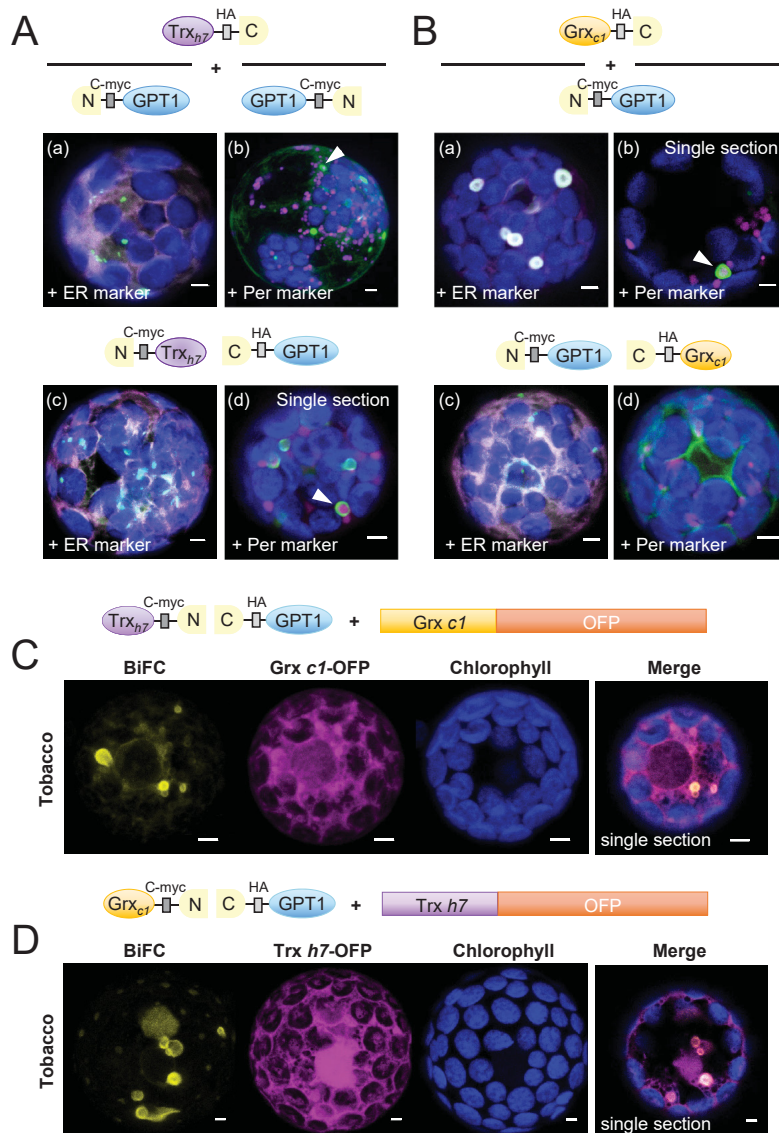


Figure 4. GPT1 interacts with cytosolic oxidoreductases Trx_{h7} and Grx_{c1} at the ER.

A-B, Localization of GPT1 upon interaction with Trx h7 or Grx c1 in Arabidopsis protoplasts (24-48 h post transfection). The schemes illustrate different orientation of the candidate proteins with respect to free N- and C-terminal ends. GPT1 interacts with both oxidoreductases (green signals) at the endoplasmic reticulum (ER) and its spherical sub-structures (arrowheads), except when the N-terminus of Grx c1 is masked (B, panels c and d). Note that these substructures differ from those labelled in Figure 3B. Merge of BiFC signals (green) with ER marker (OFP-ER) or peroxisome marker (Per, OFP-PGL3_C-short) in magenta, and chlorophyll fluorescence in blue. **C-D**, Localization of split YFP reconstitution (BiFC, yellow signals) in heterologous tobacco protoplasts (24-48 h post transfection), testing a potential effect of the other oxidoreductase (co-expressed as OFP fusion, magenta). Note that similar ER substructures are labelled (Merge, single sections). All other images show maximal projections of approximately 30 optical sections. Chlorophyll fluorescence in blue. Co-localization and very close signals (less than 200 nm) appear white in the Merge of all channels. Bars = 3 µm.

bioRxiv preprint first posted online Dec. 12, 2019; doi: <http://dx.doi.org/10.1101/2019.12.11.873000>. The copyright holder for this preprint (which was not peer-reviewed) is the author/funder, who has granted bioRxiv a license to display the preprint in perpetuity.
All rights reserved. No reuse allowed without permission.

Baune et al.

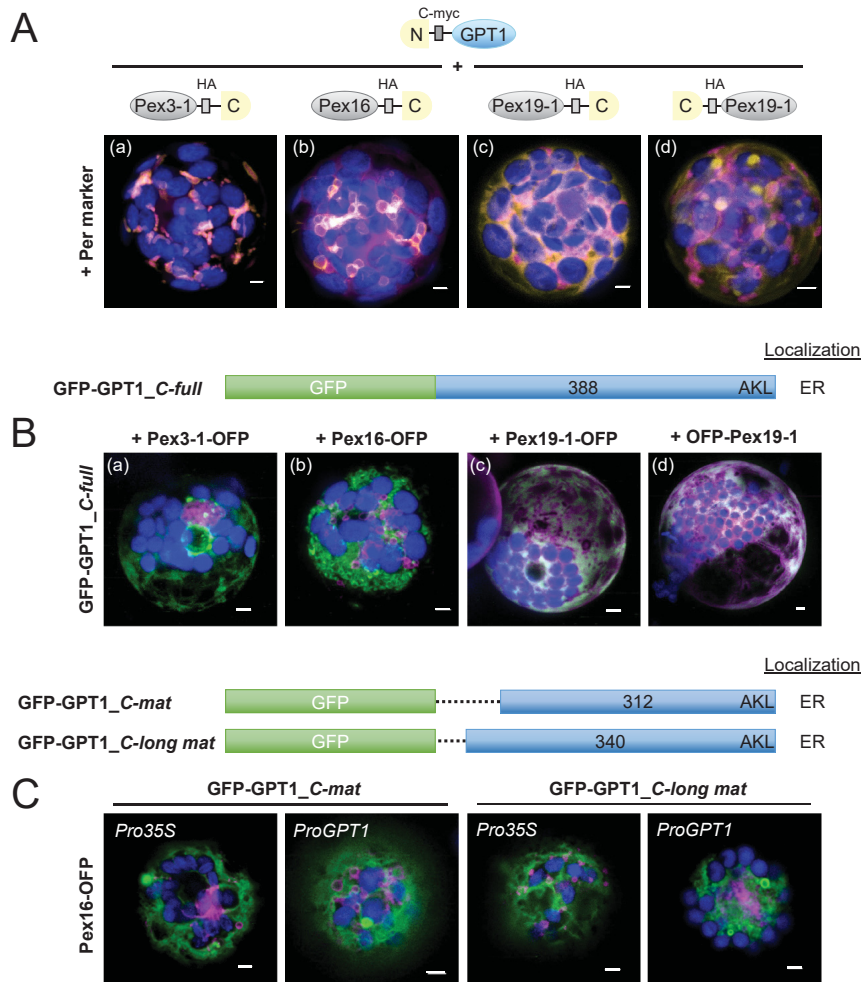
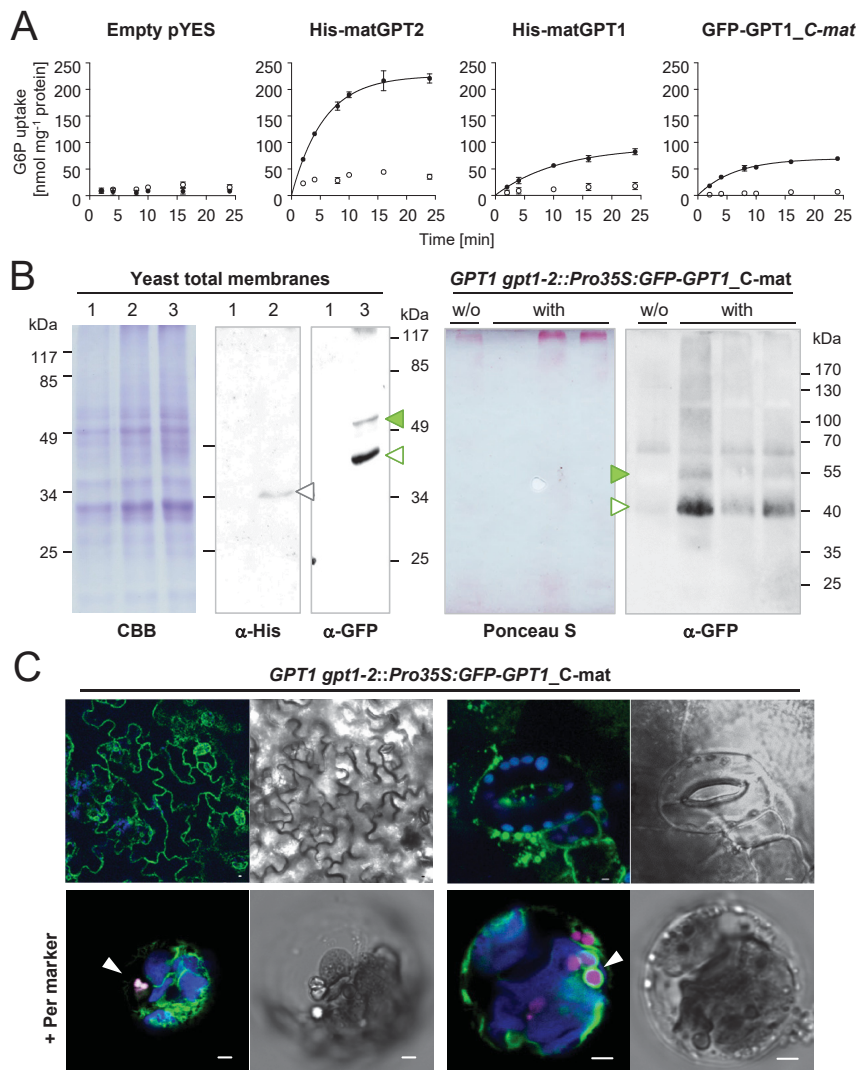


Figure 5. Interaction versus co-localization of GPT1 with Pex factors at the ER.

A, Localization of the indicated split YFP combinations (yellow BiFC signals) in Arabidopsis protoplasts (24-48 h post transfection). Pex3, Pex16, and Pex19 are important for sorting a class of peroxisomal membrane proteins via the ER to peroxisomes. Per; soluble peroxisome marker (OFP-PGL3_C-short) in magenta. **B**, Co-expression of GFP-GPT1 and the corresponding Pex-OFP fusions indicates that interaction with the Pex factors is transient (isoforms Pex3-2 = At1g48635 and Pex19-2 = At5g17550 gave comparable results, not shown). Note that Pex16 co-expression has a vesiculating effect on GPT1 at the ER (Merge; for single channel images, see Supplemental Figure 10C). **A-B**, Maximal projections of approximately 30 optical sections. **C**, Co-expression of the indicated GFP-GPT1 fusions with Pex16-OFP in Arabidopsis protoplasts (72 h post transfection). The *C_mat* version lacks the entire N-terminal part (including C65), whereas *C_long mat* version lacks only the transit peptide (Supplemental Figure 1). Besides the 35S promoter (*Pro35S*), these GFP fusions were also expressed from the *GPT1* promoter (*ProGPT1*), with similar results. Images show single optical sections (Merge; for single channel images, see Supplemental Figure 11). GFP fusions in green, Pex16-OFP in magenta and chlorophyll fluorescence in blue. Co-localization of green and magenta (or very close signals less than 200 nm) appear white in the Merge of all channels. Bars = 3 μ m.

bioRxiv preprint first posted online Dec. 12, 2019; doi: <http://dx.doi.org/10.1101/2019.12.11.873000>. The copyright holder for this preprint (which was not peer-reviewed) is the author/funder, who has granted bioRxiv a license to display the preprint in perpetuity.
All rights reserved. No reuse allowed without permission.



Baune et al.

Figure 6. Transport activity and localization of mature GPT1 in yeast and plant cells.

A, Time-dependent uptake of radioactively labeled [^{14}C]-G6P (0.2 mM) into reconstituted proteoliposomes preloaded with 10 mM Pi (closed symbols) or without exchange substrate (open symbols) prepared from yeast cells harboring the empty vector (pYES) or the indicated GPT constructs. Note that transport rates of GPT1 are not influenced by the N-terminal tag (compare His-matGPT1 to GFP-matGPT1). In all graphs, the arithmetic mean of 3 technical replicates (\pm SD) was plotted against time (see Table 1 for substrate specificities). **B**, Immunoblot analysis upon expression in yeast and plant cells. Left, SDS gel of total yeast membrane fractions, stained with Coomassie brilliant blue (CBB) or blot detection by anti-His (α -His) or anti-GFP (α -GFP) antibodies: 1, empty vector; 2, His-matGPT1 (grey open triangle); 3, GFP-matGPT1 (green closed and open triangles). Right, blotted pellet fractions of leaf extracts (without detergent) prepared from Arabidopsis *GPT1 gpt1-2::Pro35S:GFP-GPT1_C-mat* plants (T2 progeny without (w/o) or with the transgene) developed with anti-GFP (α -GFP) antibodies. The Ponceau S-stained blot serves as loading reference. Note that GFP-GPT1 (closed green and open triangles) extracted from yeast or plant membranes migrate similarly. Bands of molecular masses are indicated (kDa). **C**, Localization of GFP-GPT1_C-mat in heterozygous *GPT1 gpt1-2* plants. Top, Green net-like structures (ER) in leaf epidermal cells (left), and spherical structures in seedlings (right); bars = 10 μm . Bottom, Pattern upon protoplast preparation and transfection with the peroxisome marker (Per; OFP-PGL3_C-short, magenta) in membranes surrounding peroxisomes (arrowheads). Chlorophyll fluorescence in blue. All images show single optical sections. Co-localization (and very close signals less than 200 nm) appear white in the Merge of all channels (bright field images shown as reference). Bars = 3 μm .

bioRxiv preprint first posted online Dec. 12, 2019; doi: <http://dx.doi.org/10.1101/2019.12.11.873000>. The copyright holder for this preprint (which was not peer-reviewed) is the author/funder, who has granted bioRxiv a license to display the preprint in perpetuity.
All rights reserved. No reuse allowed without permission.

Baune et al.

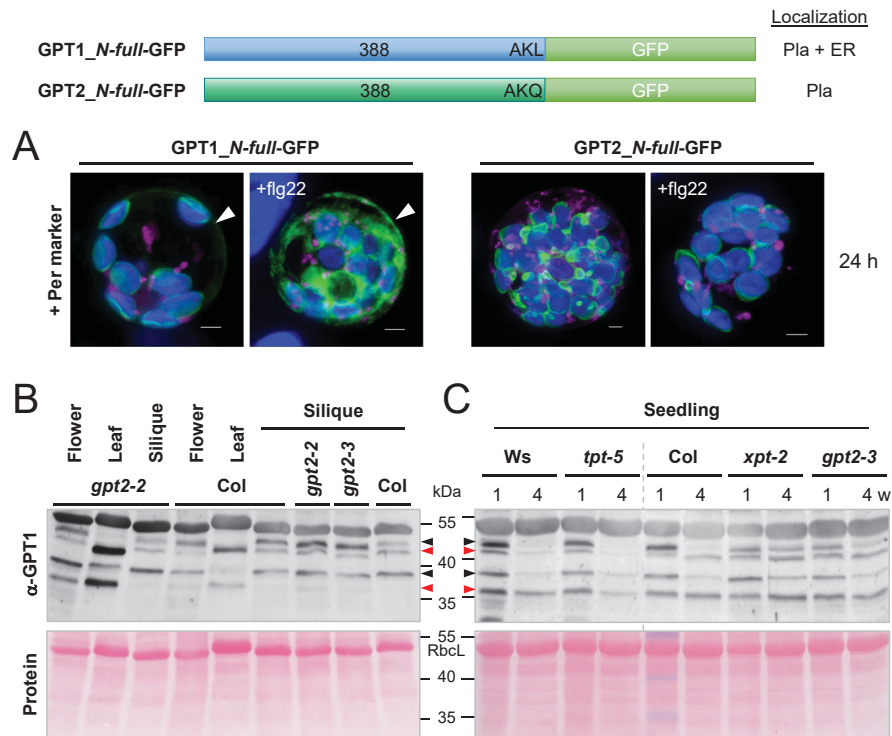


Figure 7. GPT1 detection at the ER is increased by stress treatment and in reproductive Arabidopsis tissues.

A, Arabidopsis protoplasts were co-transfected with the indicated GPT-GFP fusions and the peroxisome marker (Per, OPG-PGL3_C-short), samples were split in half, one was treated with 0.2 μ M flagellin peptide (+flg22), and the other mock-incubated for 24 h. Note that flg22 treatment did not change GPT localization to plastids, but enhanced the ER fraction of GPT1-GFP (arrowheads). All images show maximal projections of approximately 30 single sections (Merge; for single channel images, see Supplemental Figure S13). GFP fusions in green, peroxisome marker in magenta, and chlorophyll fluorescence in blue. Co-localization of magenta and green or very close signals (less than 200 nm) appear white in the Merge of all channels. Bars = 3 μ m. **B-C**, Protein extracts (without detergent) of flower, leaf, and (green) silique tissue were prepared from wild-type plants (Col, Ws) and the indicated homozygous mutant lines. Supernatant fractions were separated on 10% SDS gels and blotted to nitrocellulose. After Ponceau-S staining, the blots were developed with GPT1-specific antibodies (α -GPT1) raised against the N-terminus with His-tag (Supplemental Figure S14). Arrowheads mark double bands of full-length GPT1 (predicted size: 42.3 kDa) and mature GPT1 (ca. 37-39 kDa, depending on TP processing). Red arrowheads point to bands suspected to represent a largely 'off' situation and black arrowheads the corresponding 'on' situation at either location (as deduced from comparison of leaf to silique tissue), likely due to protein modification. **C**, Immunoblot of seedlings harvested from germination plates (1% sucrose) after 1- or 4-week (w) growth in short-day regime. Included mutant alleles: *gpt2-2* (GK-950D09, T-DNA intron 2/exon 3), *gpt2-3* (GK-780F12, T-DNA in exon 4), *tpt-5* (FLAG_124C02, T-DNA in exon 9), and *xpt-2* (SAIL_378C01, single exon; Hilgers et al., 2018). Note that the band pattern differs in OPPP-relevant *gpt2* and *xpt* transporter mutants compared to Col wildtype and *tpt-5* (Ws wildtype corresponds to *tpt-5*, grey dashed line). Ponceau S-stained blots (protein) are shown as loading reference; Rbcl, large subunit of RubisCO. Molecular masses are indicated in kDa (PageRuler Prestained Protein Ladder, Fermentas).

bioRxiv preprint first posted online Dec. 12, 2019; doi: <http://dx.doi.org/10.1101/2019.12.11.873000>. The copyright holder for this preprint (which was not peer-reviewed) is the author/funder, who has granted bioRxiv a license to display the preprint in perpetuity.
All rights reserved. No reuse allowed without permission.

Baune et al.

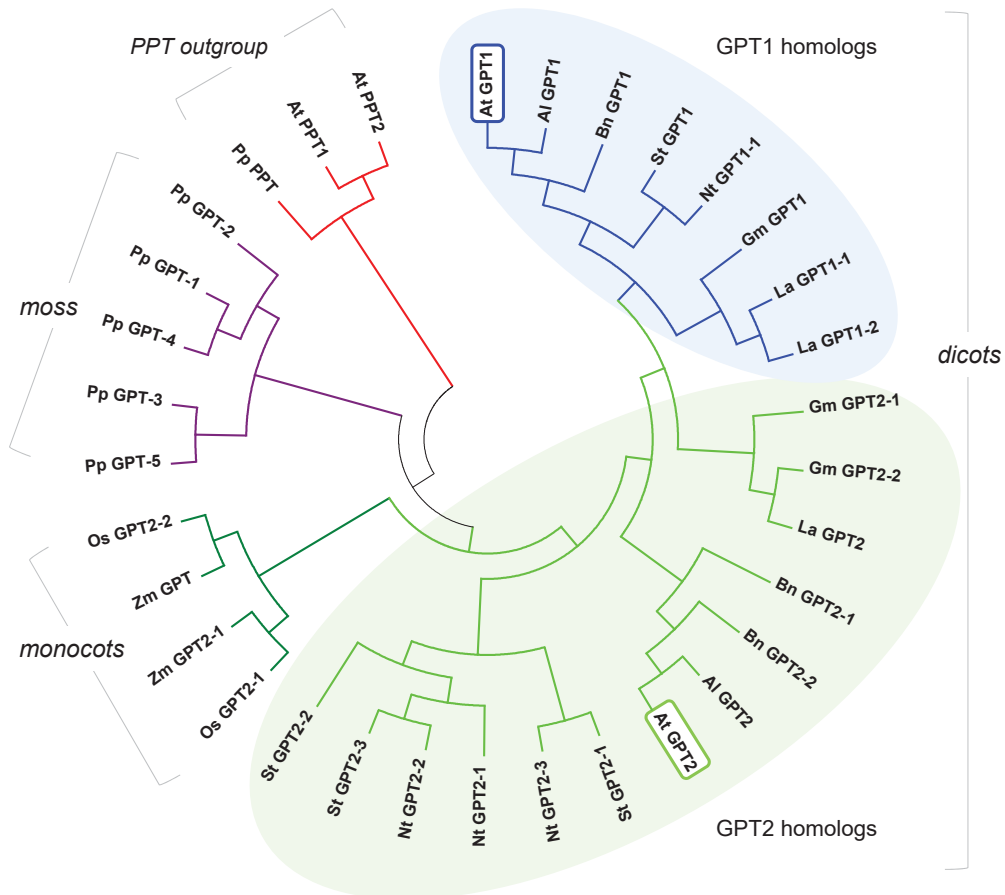


Figure 8. Phylogenetic analysis of GPT sequences from different plant clades.

Selected GPT isoforms of the *Brassicaceae*, *Fabaceae*, *Solanaceae* and *Poaceae* in comparison to the moss *Physcomitrella patens*. The phosphoenolpyruvate/phosphate translocator (PPT) accessions serve as outgroup (red). Glucose-6-phosphate/phosphate translocators (GPT) of *Physcomitrella patens* (Pp, violet) form the base of the phylogenetic tree. GPT2 accessions (green) of monocotyledonous plants split off early (monocots, dark green), whereas the GPT1 accessions (blue) split much later from the GPT2 accessions (light green) in the dicotyledonous branch (dicots, right). For sequence identifications see Table S3. Abbreviations: *Al*: *Arabidopsis lyrata* subsp. *lyrata*; *At*: *Arabidopsis thaliana*; *Bn*: *Brassica napus*; *Gm*: *Glycine max*; *La*: *Lupinus angustifolius*; *Nt*: *Nicotiana tabacum*; *Os*: *Oryza sativa*; *St*: *Solanum tuberosum*; *Zm*: *Zea mays*. Evolutionary history was inferred by using the Maximum Likelihood method based on the JTT matrix-based model (Jones et al., 1992). The tree with highest log likelihood (-5414.98) is shown. Initial tree(s) for the heuristic search were obtained automatically by applying Neighbor-Join and BioNJ algorithms to a matrix of pairwise distances estimated using a JTT model, and then selecting the topology with superior log likelihood value. The tree is drawn to scale, with branch lengths measured in the number of substitutions per site. The analysis involved 34 amino acid sequences (Supplemental Table 3). All positions containing gaps and missing data were eliminated. There were a total of 252 positions in the final dataset. Evolutionary analyses were conducted in MEGA7 (Kumar et al., 2016).

bioRxiv preprint first posted online Dec. 12, 2019; doi: <http://dx.doi.org/10.1101/2019.12.11.873000>. The copyright holder for this preprint (which was not peer-reviewed) is the author/funder, who has granted bioRxiv a license to display the preprint in perpetuity.
All rights reserved. No reuse allowed without permission.

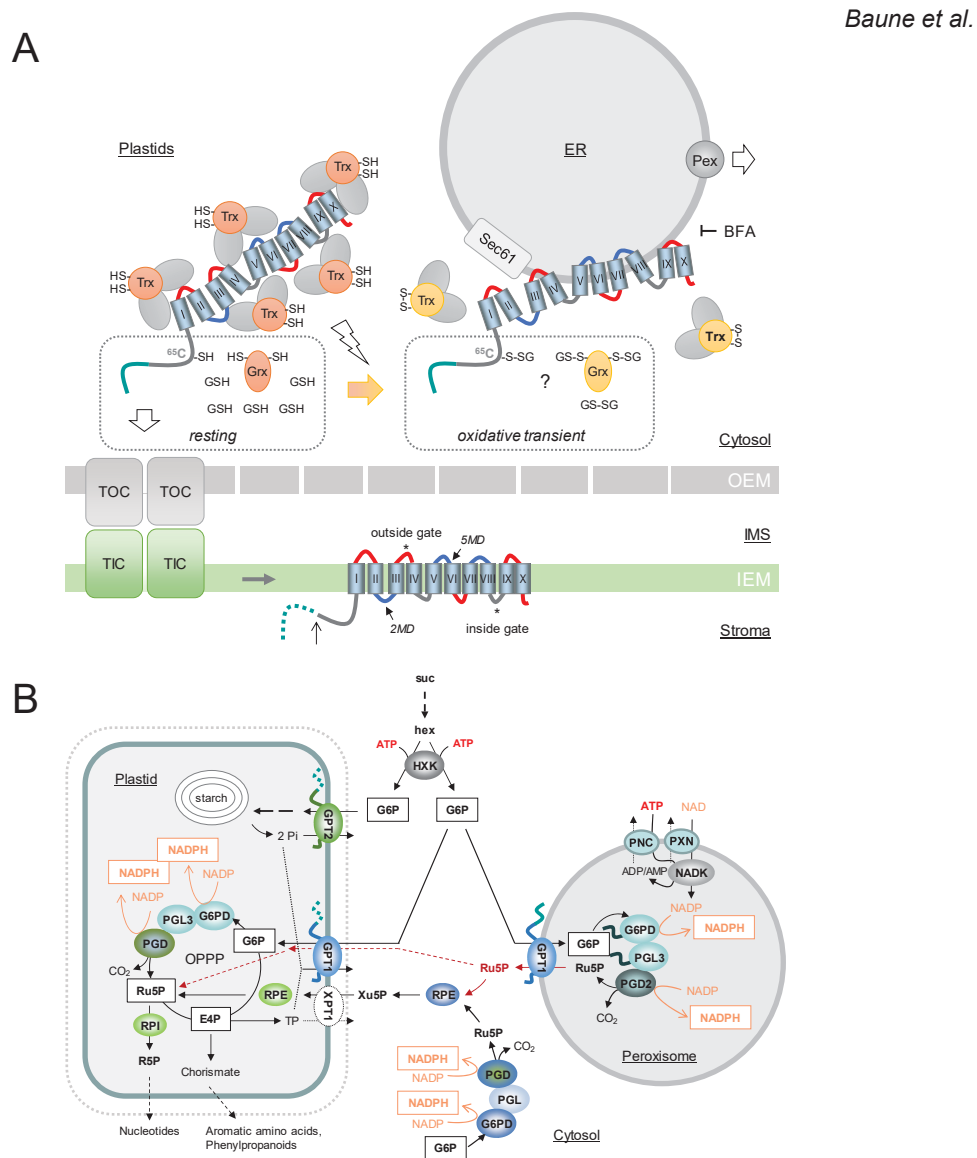


Figure 9. Model of dual GPT1 targeting for OPPP function in plastids and peroxisomes.

A. GPT1 precursors in the cytosol are covered with chaperons (grey spheres) and co-chaperons Trx₇₇ and Grx_{c1} as putative redox sensors/transmitters (orange = reduced state, -SH; yellow = oxidized state, -S-S-). The hydrophobic membrane domains (barrels) of GPT1 are labeled with roman numerals. Hinge regions of negative net charge (blue) may facilitate ER insertion. Left, In largely reduced state of the cytosolic glutathione pool (GSH), the N-terminus of GPT1 (green) enters the TOC/TIC complex (translocan of the outer/inner chloroplast envelope), the membrane domains (MDs) integrate into the inner envelope membrane (IEM), and the transit peptide is processed (open arrow)/degraded in the stroma (dotted line). Local oxidation (flash sign) of the cytosolic glutathione pool (GSSG) likely retains GPT1 in the cytosol by a functional change in the bound redox transmitters (Grx_{c1} and Trx₇₇). Whether this involves ⁶⁵C in the GPT1 N-terminus is unclear (question mark). ER insertion involves Sec61 and sorting to peroxisomal membranes specific peroxins (Pex). Brefeldin A (BFA) blocked ER import of GPT1. **B.** Scheme of sugar metabolism in a physiological sink state. Sucrose (suc) is cleaved by cytosolic invertase yielding two hexoses (hex) that are activated by hexokinase (HXK), consuming ATP provided by glycolysis and mitochondrial respiration (not shown). By contrast to GPT2, GPT1 imports G6P into both plastids (in exchange for Pi released by GPT2-driven starch synthesis) and peroxisomes (in exchange for Ru5P that may also enter plastids via GPT1, dashed red arrows), yielding 2 moles of NADPH in the oxidative part of the OPPP. NADP inside peroxisomes is formed by NAD kinase (NADK3) that relies on ATP and NAD imported into peroxisomes via PNC (At3g05290; At5g27520) and PXN (At2g39970). The cytosolic OPPP reactions are usually linked via RPE and XPT to the complete pathway in the plastid stroma. Abbreviations: G6PD, glucose-6-phosphate dehydrogenase; PGL, 6-phosphogluconolactonase; PGD, 6-phosphogluconate dehydrogenase; RPE, ribulosephosphate-3-epimerase; RPI, ribose-5-phosphate isomerase.

Author contribution

Lennart Charton did the heterologous protein expression and uptake experiments shown in Figure 6a, 6b as well as calculation of initial velocities depicted in Table 1.

V. Submitted Manuscripts

V.II Submitted Manuscript 2

Biochemical and Functional Characterization of a Mitochondrial Citrate Carrier in *Arabidopsis thaliana*

Danielle S. Britoa[#], Gennaro Agrimib[#], Lennart Charton^c, Dominik Brillhaus^c, Maria Gabriella Bitetto^b, Carolina P. Nascimento^a, Jaciara Lana-Costa^a, Elias Feitosa Araújo^a, Marcel Viana Pires^a, Jorge Luis Pérez-Díaz^a, Toshihiro Obata^d, Vito Porcelli^b, Luigi Palmieri^b, Wagner L. Araújo^a, Andreas P.M. Weber^c, Nicole Linka^c, Alisdair R. Fernie^d, Ferdinando Palmieri^{b*} and Adriano Nunes-Nesi^{a*}

^a Departamento de Biologia Vegetal, Universidade Federal de Viçosa, 36570-900, Viçosa, Minas Gerais, Brazil

^b Department of Biosciences, Biotechnology and Biopharmaceutics, Laboratory of Biochemistry and Molecular Biology, University of Bari, 70125 Bari, Italy

^c Institute of Plant Biochemistry, Cluster of Excellence on Plant Science (CEPLAS), Heinrich-Heine-Universität, Universitätsstraße 1, 40225 Düsseldorf, Germany.

^d Max-Planck-Institute of Molecular Plant Physiology, Am Mühlenberg 1, 14476 Potsdam-Golm, Germany.

[#] Equally contributing authors

Submitted to Bochemical Journey

57 **ABSTRACT**

58

59 A homologue of the mitochondrial succinate/fumarate carrier from yeast (Sfc1p)
60 has been found in the Arabidopsis genome, named *AtSFC1*. The *AtSFC1* gene
61 was expressed in *Escherichia coli*, and the gene product was purified and
62 reconstituted in liposomes. Its transport properties and kinetic parameters
63 demonstrated that *AtSFC1* transports citrate, isocitrate and aconitate and, to a
64 lesser extent, succinate and fumarate. This carrier catalyzes a fast counter-
65 exchange transport as well as a low uniport of substrates, exhibits a higher
66 transport affinity for tricarboxylates than dicarboxylates, and is inhibited by
67 pyridoxal 5'-phosphate and other inhibitors of mitochondrial carriers to various
68 degrees. Gene expression analysis indicated that the *AtSFC1* transcript is
69 mainly present in heterotrophic tissues and, fusion with a green-fluorescent
70 protein localized *AtSFC1* to the mitochondria. Furthermore, 35S-*AtSFC1*
71 antisense lines were generated and characterized at metabolic and
72 physiological levels in different organs and at various developmental stages.
73 Lower expression of *AtSFC1* reduced seed germination and impaired radicle
74 growth, a phenotype that was related with reduced respiration rate. These
75 findings suggest that *AtSFC1* is involved in storage oil mobilization at early
76 stages of seedling growth and in nitrogen assimilation in root tissue by
77 catalyzing citrate/isocitrate or citrate/succinate exchanges.

78

79

80

81

82

83

84

85

86

87

88

89

90

91 **INTRODUCTION**

92

93 Mobilization of seed oil reserves during germination of *Arabidopsis*
94 seedlings requires the conversion of lipids into sucrose via beta-oxidation and
95 gluconeogenesis. This process entails the transport of di- and tricarboxylic acids
96 from peroxisomes into mitochondria. Despite of the importance, the transporters
97 involved in this process are largely unknown. However, in *Arabidopsis thaliana*
98 a homolog of the mitochondrial succinate/fumarate carrier from *Saccharomyces*
99 *cerevisiae* (Sfc1p) has been identified, cloned and named AtSFC1 [1,2]. Both
100 proteins, Sfc1p and AtSFC1, belong to a family of mitochondrial carrier proteins
101 (MCF) that are widespread in eukaryotes and involved in numerous metabolic
102 pathways and cell functions [3,4]. All members of this family have a common
103 structural feature which consists of three tandemly repeated homologous
104 domains about 100 amino acids in length [5,6]. The great majority of the MCF
105 members have a molecular mass between 30-34 kDa and catalyze the
106 transport of a wide range of molecules, such as nucleotides, amino acids,
107 carboxylates, cofactors, phosphate and sulfate [7–10].

108 In functional complementation studies, AtSFC1 expressed in yeast
109 mutants lacking the *SFC1* gene restored their growth phenotype on ethanol or
110 acetate as carbon sources [2]. This finding suggested that AtSFC1 has the
111 same transport properties observed for the yeast carrier, catalyzing the
112 exchange of cytosolic succinate against mitochondrial fumarate [1]. Based on
113 this transport mode, AtSFC1 might link in plants the glyoxylate cycle with the
114 tricarboxylic acid (TCA) cycle during fatty acid mobilization, providing the carbon
115 necessary for seedling establishment [11,12].

116 In plants, the importance of a succinate/fumarate carrier is not clear in
117 germinating seedlings during storage oil mobilization. Even that the *SFC1* gene
118 is expressed in young heterotrophic tissues in seedlings [2], promoting the
119 import of succinate into the mitochondrion, the exchange for fumarate cannot be
120 essential. It has been reported in *A. thaliana* that a cytosolic fumarase, which
121 interconverts malate and fumarate, is not required for plant growth, but is vital
122 for nitrogen assimilation in leaves and growth on high nitrogen condition [13].
123 Furthermore, it has been shown that this fumarase isoform is necessary for cold
124 acclimation in *Arabidopsis* [14]. Thus, the import of succinate can be essential

4

125 in seedlings, but not the export of fumarate, since cytosolic fumarase is not
126 required for fatty acid oxidation, glyoxylate cycle, or gluconeogenesis [13].
127 Thus, important questions should be addressed regarding the role of
128 mitochondrial *AtSFC1* transport in Arabidopsis seedlings and the transported
129 substrates by *AtSFC1* protein. So far, the direct transport function of *AtSFC1* for
130 succinate and fumarate has not been confirmed, meaning that the biochemical
131 evidence in favour of succinate/fumarate transport is still lacking. For the yeast
132 succinate/fumarate carrier is known that Sfc1p transports oxoglutarate and
133 oxaloacetate much less efficiently than succinate and fumarate, and malate,
134 citrate, isocitrate and aconitate even more so (1). Therefore, it is likely that
135 *AtSFC1* transports other substrates besides succinate and fumarate and thus
136 has additional functions in plants.

137 Taken together the reported information regarding the function of *SFC1*
138 in plants is scarce. Biochemical analyses of the transporter protein and
139 physiological studies of plants with reduced transporter activity are required to
140 understand the role of *AtSFC1* carrier at different developmental plant stages or
141 in various plant organs. For these reasons, in this study we investigated first the
142 biochemical properties of heterologous expressed *AtSFC1* protein using
143 reconstituted liposomes. Secondly, we performed a detailed gene expression
144 analysis of *AtSFC1* in Arabidopsis. Thirdly, we analyzed the phenotype of
145 Arabidopsis *AtSFC1* antisense plants. Our obtained results allowed us to
146 predict diverse functions for *AtSFC1* in plants. We confirmed that *AtSFC1* is
147 highly expressed in young heterotrophic seedlings, flower, and young, mature
148 and senescent leaves, and found that the reduced expression of *AtSFC1*
149 impacts germination, root growth and leaf metabolism. The results are
150 discussed in the context of current models of lipid mobilization during seedling
151 establishment concentrating on aspects that have been discovered in plant
152 peroxisomes and highlighting other aspects, which are yet to be understood.

153

154

155

156

157

158 **MATERIAL AND METHODS**

159

160 **Sequence search and analysis**

161 Protein databases for fungi, plants and metazoa were screened with the
162 protein sequence of AtSFC1 using BLASTP. Multiple sequence alignments
163 were made with ClustalW. The maximum likelihood phylogenetic tree was built
164 in seaview4 using the Whelan and Goldman substitutional matrix from a Muscle
165 multiple-sequence alignment and drawn in FigTree v1.4.2. Bootstraps values
166 are indicated by the numbers at the nodes and branch lengths by the scale bar.

167

168 **Bacterial expression and purification of AtSFC1**

169 AtSFC1 was overexpressed as inclusion bodies in the cytosol of *E. coli*
170 C0214 (DE3) as described previously [43–45]. Control cultures with the empty
171 vector were processed in parallel. Inclusion bodies were purified on a sucrose
172 density gradient and washed at 4 °C, first with TE buffer (10 mM Tris-HCl and 1
173 mM EDTA, pH 7.0), then twice with a buffer containing 3% Triton X-114 (w/v), 1
174 mM EDTA and 10 mM PIPES pH 7.0, and finally once with TE buffer [46,47].
175 Proteins were analyzed by SDS-PAGE on 17.5% gels and stained with
176 Coomassie Blue dye. The identity of purified AtSFC1 was confirmed by matrix-
177 assisted laser desorption/ionization-time-of-flight (MALDI-TOF) mass
178 spectrometry of trypsin digests of the corresponding band excised from
179 Coomassie-stained gels [48,49]. The amount of purified AtSFC1 was estimated
180 by laser densitometry of stained samples using carbonic anhydrase as protein
181 standard [50,51]. The amount of protein incorporated into liposome was
182 measured as described [52] and about 12% of protein was added to the
183 reconstitution mixture.

184

185 **Reconstitution of AtSFC1 into liposomes**

186 Purified AtSFC1 was solubilized in 1.45% (w/v) sarkosyl
187 (dodecanoylsarcosine), 10 mM PIPES pH 7.0 and 3% Triton X-114, and
188 unsolubilized material was removed by centrifugation (15 300 x *g* for 10 min).

6

189 The solubilized recombinant protein was diluted 6-fold with a buffer containing
190 20 mM Na₂SO₄ and 10 mM PIPES, pH 7.0, and reconstituted into liposomes by
191 cyclic removal of the detergent with a hydrophobic column of amberlite beads
192 (Bio-Beads SM-2, Bio-Rad) as described [20,53,54]. The reconstitution mixture
193 contained the solubilized protein (about 6 µg), 1% Triton X-114, 1.4% egg yolk
194 phospholipids (L-α-phosphatidylcholine from dried egg yolk, Sigma-Aldrich) in
195 the form of sonicated liposomes [55], 10 mM substrate (except where otherwise
196 indicated), 20 mM PIPES pH 7.0, 1 mg cardiolipin (a mitochondrial inner
197 membrane lipid, which is required for the function of many MCs) [44,56,57] and
198 water to a final volume of 700 µl. These components were mixed thoroughly,
199 and the mixture was recycled 13 times through the amberlite column pre-
200 equilibrated with a buffer containing 10 mM PIPES pH 7.0 and the substrate at
201 the same concentration used in the starting mixture. All operations were
202 performed at 4°C, except for the passages through Amberlite, which were
203 carried out at room temperature.

204

205 **Transport assays**

206 External substrate was removed from proteoliposomes on Sephadex G-
207 75 columns pre-equilibrated with buffer A (10 mM PIPES and 50 mM NaCl pH
208 7.0). Transport at 25°C was initiated by adding [¹⁴C]citrate (NEN Life Science
209 Products), [¹⁴C]succinate (Scopus) or other indicated labeled compounds to
210 eluted proteoliposomes. The reaction was terminated by adding a mixture of 30
211 mM pyridoxal 5'-phosphate and 25 mM bathophenanthroline, which inhibit the
212 activity of several MCs completely and rapidly [58–60]. In controls, the inhibitors
213 were added simultaneously to the labeled substrate according to the “inhibitor-
214 stop” method [20]. Finally, the external radioactivity was removed on Sephadex
215 G-75 and the radioactivity in the proteoliposomes was measured. The
216 experimental values were corrected by subtracting the control values. The initial
217 transport rates were calculated from the radioactivity incorporated into
218 proteoliposomes after 1 min i. e. in the initial linear range of substrate transport
219 [61,62]. For efflux measurements, proteoliposomes containing 2 mM internal
220 citrate were loaded with 5 µM [¹⁴C]citrate by carrier-mediated exchange

7

221 equilibrium [49,63]. After 50 min incubation, the external radioactivity was
222 removed by passing the proteoliposomes through Sephadex G-75 columns pre-
223 equilibrated with buffer A. Efflux was started by adding unlabeled external
224 substrate or buffer alone and terminated by adding the inhibitors indicated
225 above.

226

227 **Subcellular localization of AtSFC1**

228

229 *AtSFC1* was amplified by PCR on an Arabidopsis cDNA mix from
230 different tissues using the following set of primers: *AtSFC1Fw* (3'-
231 CACCATGGCGACGAGAACGGAATC-5') and *AtSFC1Rv* (3'-
232 TAAAGGAGCATTCCGAAGATATCTCA-5'). The fragment containing the 927-
233 bp region upstream of the start codon of *AtSFC1* gene sequence without the
234 stop codon was amplified by using a *Pfu* polymerase (Fermentas), purified and
235 subcloned into a pENTR™/D-TOPO® vector by directional TOPO® cloning
236 (Life Technologies, Carlsbad, CA, USA). The gene was sequenced
237 (macrogen, Korea) and then this entry vector was used for Gateway® LR
238 reaction (Life Technologies) with pGWB505 (35S promoter::*AtSFC1*-GFP) [64].
239 This construct was used to transform *Agrobacterium tumefaciens* (strain
240 GV3101). *Nicotiana benthamiana* leaves were co-infiltrated with Agrobacteria
241 containing *AtSFC1*-GFP and IVD-eqFP611, respectively. The latter is a fusion
242 of the mitochondrial isovaleryl-CoA-dehydrogenase with a red fluorescence
243 protein (RFP) [65]. After three days of transient expression, leaf protoplasts
244 were isolated and analyzed by confocal laser scanning microscopy (Zeiss
245 LSM780, Germany). Excitation and emission for GFP and eqFP611 were set to
246 488 nm / 490-550 nm and 561 nm / 580 – 625 nm, respectively. Image
247 processing was performed with FIJI image analysis software [66].

248

249 **Plant material and growth conditions**

250

251 *Arabidopsis* (*A. thaliana* ecotype Columbia [Col-0]) seeds from wild-type
252 and antisense lines were germinated on half-strength Murashige and Skoog
253 (MS) medium plates, pH 5.7 [67], containing 1% (w/v) sucrose in a growth

254 chamber (150 $\mu\text{mol photons m}^{-2} \text{ s}^{-1}$ white light, 22 °C) under short-day
255 conditions (8 h of light/16 h of dark). After ten days under these conditions, the
256 seedlings were transferred to a commercial substrate (Tropstrato HT[®]) in a
257 climate-controlled chamber under the same photoperiod and climate conditions.

258

259 **Generation of *AtSCF1* transgenic lines**

260

261 The transgenic plants were generated with suppressed expression of
262 *AtSCF1* gene by expressing antisense cDNA under the control of the 35S
263 promoter. Primers were designed (forward 5'- ATGGCGACGAGAACGGAATC-
264 3' and reverse 5'- CTATAAAGGAGCATTCCGAAGATATCTCA-3') for the PCR
265 amplification of full-length coding sequence of *At5g01340* gene from a cDNA
266 library derived from Arabidopsis seedlings. The purified PCR fragment was
267 cloned into pDONR207 vector using pDONR207 directional cloning kit (Thermo
268 Fischer Scientific). The resultant ENTRY vector was used in the Gateway LR
269 reaction (Thermo Fischer Scientific) with pH2WG7 destination vector [68]
270 between the cauliflower mosaic virus 35S promoter and the *t-nos* terminator in
271 the sense orientation and cloning of *SCF1* coding sequence in antisense
272 orientation in the expression vector. The resulting construct was introduced into
273 Arabidopsis Col-0 plants by *Agrobacterium tumefaciens* transformation
274 according to the floral dip method [69]. To select transgenic lines, seeds were
275 germinated on MS medium plates containing 1% (w/v) of sucrose and
276 supplemented with *Hygromycin* 50 mg L⁻¹ in a climate-controlled chamber in the
277 same conditions described above.

278 All physiological measurements were carried out with homozygous plants
279 obtained after two self-crosses of the initial T2 hemizygous line and therefore
280 showed 100% resistance to *hygromycin* (T4 generation). The expression of the
281 antisense transcript was also confirmed via PCR using specific primers for the
282 resistance marker *hygromycin* open reading frame (forward primer 5'-
283 CGTGTTGGCTTGTATGGAG-3' and reverse primer 5'-
284 CCCAAGCTGCATCATCGAAA-3'). Real-time PCR experiments were carried
285 out as indicated below.

286

287

288

289 **Expression analysis by real-time PCR**

290

291 Total RNAs from different organs were reverse transcribed using Kit
292 ImProm-II™ Reverse transcription system and oligo dT₍₁₅₎ primers (Promega,
293 Brazil). Real-time PCR were performed using an Applied Biosystem StepOne™
294 Real-Time PCR System and Power SYBR® Green qPCR Master Mix (Applied
295 Biosystem). Antisense lines were screened at the expression level by real-time
296 PCR using primers based on the cDNA sequence of SFC1 and the 3'
297 untranslated region sequence in order to discriminate the endogenous SFC1
298 mRNA from the introduced antisense SFC1 mRNA (forward primer 5'-
299 TGAGATATCTTCGGAATGCTCC-3' and reverse primer 5'-
300 TCTTGATCAAATCAAAATCCTAACA-3'). To correct for differences in the
301 amount of starting first-strand cDNAs, the actin gene (*At3g18780*) was amplified
302 in parallel as a reference gene (forward primer 5'-
303 CTTGCACCAAGCAGCATGAA-3' and reverse primer 5'-
304 CCGATCCAGACACTGTACTTCCTT-3'). The relative quantification of SFC1
305 was performed according to the comparative method ($2^{-\Delta\Delta C_t}$). For the remaining
306 organs and seedlings, the value of $2^{-\Delta\Delta C_t}$ indicates the fold change expression
307 relative to internal calibrator (ΔC_t mature leaf ($\Delta\Delta C_t = 0$ and $2^{-\Delta\Delta C_t} = 1$). For the
308 antisense lines $2^{-\Delta\Delta C_t} = 2^{\Delta C_t \text{ sample} - \Delta C_t \text{ control}}$.

309

310 **Germination, root growth and root respiration measurements**

311

312 The germination experiments were conducted in two different conditions:
313 half-strength medium supplemented with 1% sucrose (w/v) and sucrose-free. A
314 total of 560 seeds/genotype were surface sterilized and plated in plastic Petri
315 dishes (90 x 15mm) and stratified at 4 °C in the dark for 2 days, and then
316 incubated at 22 °C in the photoperiod 16 h of light/ 8 h of dark. The germinated
317 seed count was made daily. Radicle emergence was used as a morphological
318 marker for germination. The results were evaluated as a percentage of daily
319 germinated seeds. Root growth measurement was performed as described by
320 [49] with minor modifications. Seeds were germinated on plates vertically
321 square (120x120mm) containing MS medium supplemented with 1% sucrose,

10

322 60 seeds in total per genotype. After germination plates were transferred to a
323 growth chamber at 150 $\mu\text{mol photons m}^{-2} \text{s}^{-1}$, maximum temperature of 22 °C
324 and a minimum of 18°C, 60% relative humidity and photoperiod of 8 h of light
325 /16 h of dark. Root respiration was measured following the protocol [70].

326

327 **Measurements of photosynthetic parameters**

328

329 Gas exchange parameters were determined on fully expanded leaves
330 from five weeks old plants simultaneously with chlorophyll *a* (Chl *a*)
331 fluorescence measurements using an open-flow infrared gas exchange
332 analyzer system (LI-6400XT; LI-COR Inc., Lincoln, NE) equipped with an
333 integrated fluorescence chamber (LI-6400-40; LI-COR Inc.). Instantaneous gas
334 exchange parameters were measured after 1 h illumination during the light
335 period under 1000 $\mu\text{mol photons m}^{-2} \text{s}^{-1}$. The reference CO_2 concentration was
336 set at 400 $\mu\text{mol CO}_2 \text{ mol}^{-1} \text{ air}$. The stomatal conductance (g_s , $\text{mol H}_2\text{O m}^{-2} \text{s}^{-1}$),
337 CO_2 assimilation rate (A , $\mu\text{mol CO}_2 \text{ m}^{-2} \text{s}^{-1}$) and dark respiration (R_d , $\mu\text{mol CO}_2$
338 $\text{m}^{-2} \text{s}^{-1}$) were calculated as previously described [71]. Dark respiration was
339 measured using the same gas exchange system as described above after 1 h in
340 the dark period.

341

342 **Metabolite measurements of seeds, seedlings and leaves**

343

344 Aliquots of 50–60 mg frozen leaf material and 5-10 mg of seeds or
345 seedlings were extracted with a mixture of chloroform-methanol-water for
346 analysis of sugars, organic acids and amino acids by gas chromatography-
347 mass spectrometry (GC-MS) [72]. Peak integration was conducted with Mass
348 Hunter Software from Agilent. For relative quantification, metabolite peak areas
349 were normalized to the amount of extracted plant material and the peak area of
350 the internal standard ribitol added to the extraction solution. Fatty acids in
351 seedlings were analyzed by GC-MS, following conversion to methyl esters as
352 described in [73]. The fatty acid 17:0 was used as an internal standard to
353 enable quantification.

354

355

356

357

358 Statistical analysis

359

360 The experiments were conducted in a completely randomized design.
361 The *t* test was performed using algorithms embedded into Microsoft Excel®. The
362 term significant is used in the text only when the difference between the data
363 sets in analysis was confirmed to be significant ($P < 0.05$).

364

365

366 RESULTS

367

368 Bacterial expression of AtSFC1

369

370 Reconstitution of recombinant proteins in liposomes is a method
371 frequently used to identify transport properties of carrier proteins [10]. For this
372 reason, the DNA sequence of *AtSFC1* was expressed in *E. coli* C0214 (DE3)
373 cells (Supplemental Figure S1, lane 4). The gene product accumulated as
374 inclusion bodies in the *E. coli* cells and was purified by centrifugation and
375 washing (Supplemental Figure S1, lane 5). The apparent molecular mass of the
376 purified protein was about 35 kDa, in good agreement with the calculated value
377 (34.1 kDa). The identity of the recombinant protein was confirmed by MALDI-
378 TOF mass spectrometry. The yield of the purified protein was about 15 mg per
379 liter of culture. By contrast, the recombinant protein was not detected in bacteria
380 harvested immediately before induction of expression (Supplemental Figure S1,
381 lane 2) nor in cells harvested after induction but lacking the coding sequence in
382 the expression vector (Supplemental Figure 1, lane 3).

383

384 Biochemical functional characterization of AtSFC1

385

386 Recombinant purified *AtSFC1* was reconstituted into liposomes, and its
387 transport activities for a variety of potential substrates were tested in homo-
388 exchange experiments (i. e. with the same substrate inside and outside). Using
389 external and internal substrate concentrations of 1 and 10 mM, respectively, this

12

390 protein catalyzed an active [^{14}C]succinate/succinate homo-exchange and,
391 surprisingly, an even more efficient [^{14}C]citrate/citrate exchange (Figure 1). By
392 contrast, despite the long incubation period (i. e. 60 min) very low homo-
393 exchange activity was measured for [^{14}C]malate, [^{14}C]malonate and [^{14}C] α -
394 oxoglutarate, and negligible activity for [^{14}C]pyruvate, [^{33}P]phosphate,
395 [^{35}S]sulfate, [^{14}C]aspartate, [^{14}C]glutamate, [^3H]ornithine, [^3H]lysine, [^{14}C] γ -
396 aminobutyrate, [^{14}C]threonine, [^{14}C]valine, [^3H]S-adenosylmethionine, [^{14}C]ADP
397 and [^3H]ATP (Figure 1). Notably, no [^{14}C]citrate/citrate and
398 [^{14}C]succinate/succinate exchange activities were detected when *AtSFC1* was
399 inactivated by boiling before reconstitution into liposomes or when liposomes
400 were reconstituted with sarkosyl-solubilized protein from bacterial cells either
401 lacking the expression vector or harvested immediately before induction of
402 expression. Likewise, no such activities were observed using pure liposomes, i.
403 e. liposomes without incorporated *AtSFC1* (not shown).

404 To investigate the substrate specificity of *AtSFC1* in detail, the initial rate
405 of 0.13 mM [^{14}C]citrate uptake into proteoliposomes, that had been preloaded
406 with a variety of potential substrates, was measured (Figure 2). The highest
407 activities of [^{14}C]citrate uptake into proteoliposomes were with internal citrate,
408 isocitrate, *cis*- and *trans*-aconitate. [^{14}C]citrate also exchanged substantially with
409 internal succinate and fumarate and, to a much lower extent, with oxaloacetate,
410 malate, maleate and α -oxoglutarate. By contrast, the *AtSFC1*-mediated
411 [^{14}C]citrate uptake in the presence of internal pyruvate, glutamate, aspartate,
412 ornithine, ADP, phospho*eno*pyruvate, phosphate and NaCl (Figure 2) and
413 carnitine, α -ketoisovalerate, 2-oxoadipate, glutamine, methionine, cysteine,
414 alanine, valine, leucine, SAM, glutathione, ATP, GDP, GTP, UDP, UTP, CDP,
415 CTP, NAD^+ , FAD, thiamine pyrophosphate and coenzyme A (not shown) was
416 negligible or not significantly higher than that found in the presence of NaCl and
417 no substrate. Therefore, the substrate specificity of *AtSFC1* is confined to some
418 tricarboxylic and dicarboxylic acids.

419 The effects of mitochondrial carrier inhibitors on the [^{14}C]citrate/citrate
420 exchange reaction catalyzed by reconstituted *AtSFC1* were also examined
421 (Supplemental Figure S2). This transport activity was inhibited strongly by
422 pyridoxal-5'-phosphate, bathophenanthroline and tannic acid. Unlike most
423 mitochondrial carriers, *AtSFC1* activity was inhibited only partially by the SH-

424 blocking reagents mersalyl, p-hydroxymercurybenzoate and mercury chloride.
425 Bromocresol purple and 1,2,3-benzenetricarboxylate [inhibitors of the glutamate
426 and citrate carriers, respectively [15,16]] also decreased the activity of A/SFC1
427 partially, and butylmalonate and phenylsuccinate [inhibitors of the dicarboxylate
428 carrier [17]] decreased it still less. Notably, A/SFC1 activity was also affected
429 by another tricarboxylate analogue, 1,3,5-benzenetricarboxylate, that does not
430 inhibit the citrate carrier [16]. Furthermore, carboxyatractyloside and bongkreikic
431 acid [inhibitors of the ADP/ATP carrier [18]] and N-ethylmaleimide, an inhibitor
432 of the phosphate carrier [19], had very little effect on A/SFC1 activity.

433

434 **Kinetic characteristics of recombinant A/SFC1**

435

436 The time-courses of 1 mM [¹⁴C]citrate uptake by A/SFC1-reconstituted
437 liposomes containing no substrate (uniport) or substrates (exchange) are
438 compared (Figure 3A). All curves fitted first-order kinetics, isotopic equilibrium
439 being approached exponentially. The rate constants (k) for the exchange
440 reactions were about 0.15 (citrate/citrate), 0.16 (citrate/fumarate), 0.06
441 (citrate/succinate), 0.04 (citrate/oxaloacetate) min⁻¹ and for the uniport 0.02 min⁻¹.
442 The initial rates (the products of k and intraliposomal quantities of citrate
443 taken up at equilibrium) [20] were about 0.21, 0.14, 0.04, 0.01 and 0.002 mmol /
444 min per g protein for the citrate/citrate, citrate/fumarate, citrate/succinate,
445 citrate/oxaloacetate exchanges and for the uniport, respectively. These results
446 indicate that A/SFC1 catalyzes fast exchange reactions and a very slow
447 unidirectional transport (uniport).

448 The kinetic constants of the reconstituted A/SFC1 were determined by
449 measuring the initial transport rate of the citrate/citrate exchange at various
450 external [¹⁴C]citrate concentrations in the presence of a constant internal
451 concentration of 10 mM citrate. The transport affinity (K_m) and the specific
452 activity (V_{max}) values for the citrate/citrate exchange at 25°C were 0.13 ± 0.01
453 mM and 0.24 ± 0.03 mmol / min per g of protein, respectively, in 19
454 experiments. *Cis*-aconitate, fumarate, succinate and oxaloacetate inhibited
455 [¹⁴C]citrate/citrate exchange competitively by increasing the apparent K_m
456 without changing the V_{max} of citrate uptake (results not shown). The inhibition
457 constants (K_i) of these compounds for A/SFC1 were the following: 0.15 ± 0.02

14

458 mM (cis-aconitate), 0.23 ± 0.03 mM (fumarate), 0.36 ± 0.03 mM (succinate) and
459 1.4 ± 0.2 mM (oxaloacetate), respectively, in at least three experiments for each
460 inhibitor.

461

462 **Efflux of citrate from AtSFC1-reconstituted liposomes**

463

464 The uniport mode of transport by AtSFC1 was further investigated by
465 measuring the efflux of [^{14}C]citrate from preloaded active proteoliposomes as it
466 provides a more convenient assay for unidirectional transport [20]. As shown in
467 Figure 3B, a slow and small efflux of [^{14}C]citrate from AtSFC1-reconstituted
468 liposomes was observed with the addition of buffer A alone, i.e. in the absence
469 of external substrate. By contrast, a substantial and much faster efflux of citrate
470 occurred upon addition of unlabeled citrate, fumarate or succinate. Notably, the
471 efflux of the radioactive compound was faster with external citrate than with
472 external fumarate and even more so with external succinate. Furthermore, both
473 effluxes, i.e. with and without external substrate, were prevented completely if
474 the inhibitors pyridoxal 5'-phosphate and bathophenanthroline were present
475 from the beginning of the proteoliposome incubation (time zero).

476

477 **Phylogenetic analysis**

478

479 The closest relatives of AtSFC1 are: the plant SFC (having 77-82%
480 identical amino acids), fungal SFC (with 31-34% sequence identity),
481 oxodicarboxylate carriers ODC (with 26-32% identity), citrate transport proteins
482 CTP (with 21-30% identity), dicarboxylate carriers DIC and OAC (with 19-24%
483 identity) and uncoupling proteins UCP and PUMP (with 21-25% identity). The
484 targeted phylogenetic analysis of AtSFC1 and their closest relatives from
485 species representative of various organisms (Supplemental Figure S3)
486 coherently identified three well separated branches consisting of relatives of
487 plant and fungal SFC/CTP/ODC, DIC/OAC and UCP proteins. On the first main
488 branch, plant and fungal SFC form two well separated clusters. Therefore,
489 SFCs from plants differ from the fungal SFCs phylogenetically, although they
490 share a common ancestral sequence. Furthermore, SFC orthologs based on
491 phylogenetic relationships are found only in fungi and plant lineages suggesting

15

492 a loss in metazoa. Finally, to our knowledge, apart from *S. cerevisiae* SFC1 and
493 *AtSFC1* none of the SFC orthologs reported (Supplemental Figure S3) have
494 been characterized biochemically yet.

495

496 **Subcellular localization of *AtSFC1***

497

498 To provide experimental evidence on the subcellular localization of
499 *AtSFC1*, we generated *Agrobacterium*-mediated transient expression of
500 *AtSFC1*-GFP in tobacco epidermal cells. The mitochondrial identity was
501 demonstrated by co-localization with the mitochondrial marker IVD-eqFP611,
502 consisting of the red fluorescent protein eqFP611 fused at the C-terminus of the
503 mitochondrial isovaleryl-CoA-dehydrogenase (IVD). The *AtSFC1*-GFP-
504 expressing cells showed that *AtSFC1* mostly located in the mitochondrial
505 membranes (Supplemental Figure S4A). This interpretation is based on the
506 observation that the green fluorescing organelle is quite similar with the red
507 autofluorescence of the mitochondria (Supplemental Figure S4B) and is further
508 confirmed by the merged image (Supplemental Figure S4D). Additional
509 evidence for mitochondrial localization of *AtSFC1* has been found by proteomic
510 analysis in mitochondria isolated from leaves of the *Arabidopsis thaliana* [21].

511

512 **Expression patterns of *AtSFC1***

513

514 The expression levels of *AtSFC1* were evaluated in different organs
515 during various different developmental stages. To this end, we first performed
516 an *in silico* survey of the expression of the *AtSFC1* carrier-encoding gene
517 (*At5g01340*) by collecting information derived from publicly available data sets
518 (Supplemental Figure S5). *AtSFC1* mRNA is expressed strongly in early stages
519 of silique, seed and embryo development; it also exhibited considerable
520 expression in dried and imbibed seed, sepals and mature pollen and to a lesser
521 extent in mature roots, cotyledons, stems and leaves. Interestingly, when we
522 looked specifically at seed germination, it was clear that *AtSFC1* is highly
523 expressed at early stages and strongly expressed during radicle emergence
524 and root apex tissues (Supplemental Figure S5B). These results are in line with

525 the *AtSFC1* gene expression levels in different organs determined by real-time
526 reverse transcription (qRT)-PCR (Figure 4A).

527

528

529 **Generation and molecular characterization of 35S-*AtSFC1* antisense lines**

530

531 To understand the functional role of *AtSFC1* in plant metabolism, we first
532 looked for Arabidopsis T-DNA insertion lines in general seed stocks.
533 Surprisingly, at the time we performed this physiological characterization, we
534 were not able to isolate homozygous knockout and/or knockdown mutant lines
535 with consistently reduced expression of *AtSFC1*, suggesting that silenced
536 *AtSFC1* expression might be lethal in Arabidopsis. Thus, we decided to
537 generate Arabidopsis *AtSFC1* antisense transgenic lines under control of the
538 35S-Cauliflower Mosaic Virus Promotor (CaMV) (Figure 4B). Firstly, the
539 transgenic plants were selected on agar plates containing the selective agent
540 (*Hygromycin*). Afterwards, leaf samples were harvested from the resistant lines,
541 DNA were isolated and checked by PCR analysis using specific primers for the
542 selective agent. Subsequently, RNA from the lines containing the resistant gene
543 were extracted for expression analysis by qRT-PCR. The results demonstrated
544 that in comparison with wild-type plants, seven lines exhibited reduced
545 expression of the *AtSFC1* gene (Figure 4C). Out of these lines, we isolated
546 three (*sfc1-8*, *sfc1-10* and *sfc1-12*) with reduced expression of *AtSFC1* as
547 compared with wild-type plants (40, 55 and 75% of WT expression levels,
548 respectively) for further physiological and metabolic analyses.

549

550 **Physiological characterization of seed germination and roots of the** 551 ***AtSFC1* antisense lines**

552

553 Based on expression analysis (Supplemental Figure S5 and Figure 4A)
554 and on the biochemical characterization studies of SFC1 (Figure 1 - 3), we
555 examined the role of *AtSFC1* during seed germination and root growth (Figure
556 5). The seeds from three transgenic lines and wild-type were germinated in half-
557 strength Murashige and Skoog (MS) medium in the presence (Figure 5A) or
558 absence (Figure 5B) of sucrose. In the presence of sucrose, the strongest line

17

559 *sfc1-12* exhibited a lower germination rate as compared with wild-type and the
560 other lines (Figure 5A). Surprisingly, in sucrose-free medium, all three lines
561 displayed lower germination rate in the first 24h following stratification. In later
562 time points, only the line *sfc1-8* exhibited a significant reduction in germination
563 efficiency as compared to wild-type (Figure 5B). In addition, the germination and
564 seedling growth in the 35S-*SFC1* lines were slower than in the wild-type, as
565 indicated by the decrease in germination speed index (GSI) in the absence of
566 sucrose (significantly for all lines) and emergence speed index (ESI) values in
567 the presence of sucrose (significantly for lines *sfc1-12* and 10; Supplemental
568 table 1).

569 Since *AtSFC1* is expressed specifically in root tissues (Supplemental
570 Figure S5B and Figure 4A), we further investigated the impact of the *AtSFC1*
571 transporter for roots growth. Therefore, we analyzed the primary root growth in
572 seedlings of the antisense lines during the 10 days following the start of
573 germination, using radicle emergence as the starting time point (Figure 5C). For
574 this, we germinated seeds on vertical agar plates in the presence of sucrose in
575 the medium and recorded the root length on a daily basis. Well-correlated with
576 the expression pattern, the root length of all homozygous transgenic lines was
577 shorter than that of wild-type plants (Figure 5C). Nevertheless, 6 days after
578 imbibition, the root length of the line *sfc1-8* was quite similar to that of the wild-
579 type.

580 Impaired root growth can be associated with low respiration rates. Thus,
581 in order to investigate if the reduced root growth in the *AtSFC1* antisense lines
582 was related with reduced oxygen consumption, we grew the plants on soil. The
583 results revealed that the rate of respiration in roots of all antisense lines was
584 significantly lower than that observed in the wild-type (Figure 5D).

585

586 **Analysis of storage oil mobilization in *AtSFC1* antisense lines**

587

588 Given that the total lipid content was reduced in dried seeds (significantly
589 for lines *sfc1-10* and *sfc1-12*; Supplemental Figure S6) and germination and
590 seedling development was reduced in the antisense lines (Figure 5), we
591 decided to evaluate the fatty acid profile of seedlings at two, four and six days
592 after stratification (Figure 6, Supplemental Figure S7). To analyze the

18

593 breakdown of lipids the fatty acid contents of wild-type and *AtSFC1* transgenic
594 seedlings grown in the absence of sucrose under long-day condition were
595 examined (Figure 6A, Supplemental Figure S7). Since eicosenoic acid (C20:1)
596 is almost exclusively found in TAG in Arabidopsis seeds [22] and has been
597 widely used as a marker for triacylglycerol breakdown [23–25], we analyzed the
598 relative amounts of this storage oil-marker fatty acid. The C20:1 content in
599 seedlings of wild-type and *AtSFC1* lines continuously decreased during the first
600 six days after germination. In comparison to wild-type, the levels of C20:1 was
601 slightly increased in the SFC1 lines in two-day-old seedlings (Figure 6A). With
602 the exception of C16:1 and C16:3, which are components of thylakoid
603 membranes, the contents of other seed fatty acids were also reduced during the
604 germination and seedling development. In addition, these two fatty acids were
605 slightly increased in two-day-old seedlings (significantly for line *sfc1-10*).
606 Interestingly the levels of C18:0 and C18:1 were reduced in four-day-old
607 seedlings in comparison to wild-type (significantly for line *sfc1-12*, *sfc1-12* and
608 *sfc1-10*, respectively). Furthermore, a minor reduction in the levels of long chain
609 fatty acids C22:1 and C24:1 was observed (significantly for the line *sfc1-8*).
610 Taken together, these results suggest that the reduction in the expression of
611 *AtSFC1* does not strongly impair the oil mobilization following germination and
612 seedling development.

613

614 **Metabolite profile of seedlings from *AtSFC1* antisense lines**

615

616 Considering the reduced germination rates and the changes in
617 accumulation of certain fatty acids in seedlings exhibited by the *AtSFC1*
618 transgenic lines, we next evaluated the impact of reduced *AtSFC1* expression
619 on other groups of primary metabolites during seedling establishment (Figure
620 6B-D; Supplemental Figure S8). This analysis revealed a small number of
621 changes in metabolite levels in two-day-old seedlings. The transgenic lines
622 exhibited decreased levels of fumarate (significantly for the lines *sfc1-10* and
623 *sfc1-8*) and raffinose (line *sfc1-10*); and minor increase in the levels of glycolate
624 (line *sfc1-8*), malonate (line *sfc1-12*), mannitol and mannose (lines *sfc1-12* and
625 *sfc1-10*), and putrescine (line *sfc1-12*). A large number of changes in metabolite
626 levels through seedling development and accumulation of several metabolites in

19

627 seedlings from the transgenic lines were particularly observed in four-day-old
628 seedlings. Regarding organic acids, we observed remarkable alterations for
629 shikimate (significantly for all three lines) and malate (significantly for the two
630 strongest lines, *sfc1-10* and *sfc1-12*). Minor alterations were additionally
631 observed for maleate, malonate and glycerate at the same time point and in six-
632 day-old plants. In case of nitrogen and amino acids metabolism, this analysis
633 also revealed accumulation of cysteine, tyrosine and β -alanine in at least two
634 transgenic lines in comparison with wild-type, in four-day-old seedlings. At the
635 same time point, minor increase was also verified for glutamate and serine
636 (significantly for the strongest line *sfc1-12*) and reduction for tryptophan and
637 phenylalanine (significantly for the line *sfc1-10* and *sfc1-8*). Furthermore,
638 massive increase in the levels of putrescine (significantly in all lines), β -alanine
639 and gamma-aminobutyric acid (GABA; line *sfc1-12* and *sfc1-10*) were observed
640 at this developmental stage.

641

642 **Reduction in *AtSFC1* expression results in unaltered photosynthetic** 643 **parameters and plant growth**

644

645 We additionally grew all transgenic plants side-by-side with wild-type on
646 soil and evaluated the photosynthetic activity in leaves of five-weeks-old plants.
647 These analyses indicated that photosynthesis-related parameters as well as
648 dark respiration are not altered by the reduction of *AtSFC1* expression
649 (Supplemental Figure S9). In agreement with these findings, evaluation of
650 growth related parameters were unaltered in all transgenic lines.

651 We next analyzed the major primary pathways of plant photosynthetic
652 metabolism (Supplemental Figure S10). These studies indicated a decrease in
653 the levels of isoleucine, lysine and phenylalanine in all transgenic lines and
654 increase in the levels of glutamate and aspartate (significantly for *sfc1-8* and
655 *sfc1-12* lines). Other inconsistent changes with *AtSFC1* expression were
656 observed in other amino acids. The levels of TCA cycle intermediates were
657 largely unaffected with exception of trends of increase in the levels of citrate
658 and succinate (significantly for the line *sfc1-8*). Interestingly, the levels of
659 shikimate were increase in the transgenic lines (significantly for line *sfc1-8* and

660 *sfc1-10*). Furthermore, the levels of sucrose, maltose, isomaltose and raffinose
661 were increased in two lines.

662

663

664

665 **DISCUSSION**

666 ***AtSFC1* transports citrate, isocitrate and aconitate, and, to a lesser extent, 667 fumarate and succinate** 668

669 In this study we provide evidence that recombinant, purified *AtSFC1*
670 upon reconstitution into liposomes exhibited higher substrate specificity for
671 citrate, aconitate and isocitrate than for fumarate and succinate (Figure 1 and
672 2). Thus, *AtSFC1* differs from the well-characterized succinate/fumarate carrier
673 from *S. cerevisiae* (*ScSfc1p*) [1] with regard to its substrate affinity and
674 mechanism of transport. The yeast carrier transports citrate, aconitate and
675 isocitrate only to a very low extent and catalyzes an obligatory counter-
676 exchange transport. In contrast, *AtSFC1* preferentially transports tricarboxylates
677 via a fast antiport or a slow uniport mode. *AtSFC1* also differs from all the other
678 members of the mitochondrial carrier family [9,26,27]. For example, *AtSFC1* is
679 different from the yeast and mammalian citrate carriers CTPs because (i) it
680 transports fumarate and both *cis*- and *trans*-aconitate (ii) it is inhibited by 1,3,5-
681 benzenetricarboxylate, and (iii) it does not transport L-malate significantly
682 [16,28–30]. Interestingly, the expression of *AtSFC1* was able to restore the
683 capability of yeast *sfc1* mutant to grow on ethanol, which suggested that
684 *AtSFC1* was able to import succinate into mitochondria in exchange for
685 fumarate [2]. This finding can be explained by the results presented in this
686 study, where succinate and fumarate are also transported by *AtSFC1*, but at
687 considerably lower rates than citrate and isocitrate as substrates.

688

689 **A functional role for *AtSFC1* during seed germination and seedling 690 development** 691

692 Given the transport characteristics and the cytosolic concentration of
693 TCA cycle intermediates the primary role of *AtSFC1* in heterotrophic tissues is

21

694 most likely to catalyze the exchange between cytosolic citrate and
695 intramitochondrial isocitrate and, to a lesser extent, succinate/fumarate
696 exchange (Figure 7A). An SFC1-mediated citrate/fumarate exchange might
697 occur across the inner mitochondrial membrane when citrate is present at high
698 concentration in the cytosol. Since plant glyoxysomes lack aconitase activity
699 [31,32], the conversion of citrate into isocitrate must occur within the cytosol,
700 requiring transport of isocitrate into the peroxisome to be converted into
701 succinate by isocitrate lyase, as part of glyoxylate cycle during storage oil
702 mobilization in seeds. Based on aconitase activities, it has been proposed that
703 cytosolic citrate metabolism might be equal to, if not greater than, that observed
704 in mitochondria [31,32]. In this metabolic context, cytosolic citrate or isocitrate
705 might be either imported into mitochondria or metabolized by the glyoxylate
706 cycle [33,34] suggesting an important role for *AtSFC1* during seed germination
707 and seedling development. As previously hypothesized [2] *AtSFC1* might also
708 play an important role as a mitochondrial organic acid transporter during lipid
709 mobilization in seeds and seedling establishment. In agreement, we observed
710 that *AtSFC1* is mainly expressed at early stages of seedling and radicle
711 development (Supplemental Figure S5). Furthermore, we demonstrated that
712 reduced expression of *AtSFC1* affects the speed of seed germination as well as
713 of seedling establishment (Figure 5). Surprisingly, the levels of C20:1, a marker
714 for triacylglycerol breakdown in *Arabidopsis* seeds, was not consistently altered
715 with the reduction in the expression of *AtSFC1* in the transgenic lines (Figure
716 6A), suggesting that *AtSFC1* is not the main transporter involved in the import of
717 glyoxylate cycle products into the mitochondria. However, the fact that reducing
718 the expression of this transporter resulted in accumulation of several amino
719 acids, and other metabolic intermediates such as GABA, shikimate and malate,
720 might indicate that *SFC1* is involved in metabolite adjustments following
721 seedling development.

722

723 **A functional role for *AtSFC1* in radicle growth**

724

725 In this study the characterization of the *AtSFC1* transgenic lines revealed
726 a reduced root growth in seedlings (Figure 5C), which is in agreement with the
727 expression of *AtSFC1* in radicle tissues (Supplemental Figure S5B). These

22

728 results suggest that lower expression of *AtSFC1* restricts the rate of root
729 respiration and reduces energy production in the roots impairing the growth of
730 this organ as confirmed by root respiration analysis (Figure 5D). The combined
731 results thus suggest that an efficient import of cytosolic citrate from glyoxylate
732 cycle or from sucrose via *AtSFC1* carrier in radicles and mature roots is
733 important for respiration rate, energy conversion and root growth (Figure 7B).
734 We thus hypothesize that the primary function of this transporter in the radicle is
735 to catalyze the exchange between cytosolic citrate and mitochondrial matrix
736 isocitrate or dicarboxylate, like fumarate or succinate. In addition, considering
737 that the partitioning of citrate between the glyoxylate cycle and respiratory
738 pathway may be determined by the relative demands for sugar or energy by
739 seedling [33], it seems reasonable to assume that transport of citrate and
740 isocitrate in the opposite direction might occur via *AtSFC1* (Figure 7), catalyzing
741 the exchange between cytosolic isocitrate and intramitochondrial citrate. The
742 latter is known to be stored in the vacuole during the night and broken down
743 during the day primarily as a source of carbon for nitrogen assimilation [35].

744 In summary, given the transport characteristics added to the effects in
745 metabolism, we hypothesize that the primary function of the *AtSFC1* is to
746 catalyze the exchange between cytosolic citrate and intramitochondrial
747 isocitrate at early stages of seed germination and the opposite transport
748 direction in radicle tissues. Furthermore, our results suggest that the partitioning
749 of citrate between the glyoxylate cycle, beta-oxidation of fatty acids and
750 respiratory pathway is determined by the relative demands for energy and
751 nitrogen assimilation.

752

753 **The role of *AtSFC1* in illuminated leaves**

754

755 Surprisingly, no phenotype indicative of altered source-to-sink carbon
756 transport phenotype was observed in down-regulated *AtSFC1* transgenic lines,
757 despite the fact that such phenotypes would be anticipated since fumarate is
758 demonstrated to be a major carbon transport form in Arabidopsis [36,37]. In
759 addition, considering the importance of succinate and fumarate metabolism and
760 transport in illuminated tissues regulating stomatal aperture and CO₂
761 assimilation [38,39], the lack of a stomatal conductance or photosynthesis in

23

762 plants impaired in SFC1 transporter was surprising. The absence of clear
763 physiological phenotypes in *AtSFC1* deficient plants can be explained by the
764 fact that the expression of *AtSFC1* is minor in mature leaves (Figure 4 and
765 Supplementary Figure S5). Moreover, the biochemical characteristics of
766 *AtSFC1* described here are in agreement with the observed phenotypes in
767 leaves, suggesting that fumarate and succinate are not the main organic acids
768 transported by this carrier.

769 Studies with isolated mitochondria demonstrated that this organelle is
770 able to convert pyruvate and oxaloacetate into citrate, which is then released at
771 a high rate [40]. Similarly, it has been demonstrated that in the light citrate is the
772 major organic acid exported from the mitochondria [41]. Thus, the export of
773 citrate from mitochondria by *AtSFC1* can provide the carbon skeletons needed
774 for nitrogen assimilation in illuminated leaves (Figure 7B). In this model citrate in
775 the cytosol is converted into 2-oxoglutarate by the cytosolic isoforms of
776 aconitase and isocitrate dehydrogenase. Finally, 2-oxoglutarate (as previously
777 proposed [40,42]) is used to produce glutamate. Indeed, despite the lower
778 expression of *AtSFC1* in mature leaves, down-regulation of the *AtSFC1* carrier
779 in illuminated leaves promoted the increase in the levels of total amino acids
780 and protein contents in the transgenic lines (Supplemental Figure S11).
781 Furthermore, several amino acids were reduced including isoleucine, lysine and
782 phenylalanine whilst aspartate and glutamate were increased in two of the
783 *AtSFC1* transgenic lines (Supplementary Figure S10). Interestingly, the
784 changes in N metabolism were accompanied by minor alterations in citrate and
785 succinate levels (Supplemental Figure S10) and a large increase in starch
786 (Supplementary Figure S11A). Together, these results demonstrate that
787 transport of citrate via *AtSFC1* activity has an important function in leaf N
788 metabolism, but that reducing the expression of this carrier by up to 60 % has
789 little consequence on photosynthesis, respiration, plant growth or development.

790

791

792 **Acknowledgements**

793

794 Financial support was provided by Conselho Nacional de
795 Desenvolvimento Científico e Tecnológico (CNPq) (Grant 204133/2017-3 to
796 ANN), Fundação de Amparo à Pesquisa do Estado de Minas Gerais
797 (FAPEMIG) [Grant RED-00053-16] and Max Planck Society to ANN, TO and
798 WLA. This work was also supported by the Ministero dell'Università e della
799 Ricerca (MIUR) [the Italian Human ProteomeNet GrantRBRN07BMCT_009 to F.
800 P.]. ARF acknowledges the support of the Deutsche Forschungsgemeinschaft in
801 the framework of the trans-regional collaborative research centre TRR175.
802 Research fellowships granted by CNPq to ANN and WLA, Coordenação de
803 Aperfeiçoamento de Pessoal de Nível Superior (CAPES) to DSB are also
804 gratefully acknowledged. The CEPLAS Plant Metabolism and Metabolomics
805 Laboratory is funded by the Deutsche Forschungsgemeinschaft (DFG, German
806 Research Foundation) under Germany's Excellence Strategy – EXC-2048/1 –
807 Project ID: 390686111. APMW appreciates funding from CRC 1208. We
808 acknowledge the excellent technical assistance of Elisabeth Klemp, Katrin
809 Weber, and Maria Graf for GC-MS measurements as well as Jessica Albers for
810 manual data curation.

811

812 **Conflict of Interest**

813 The authors declare that they have no conflicts of interest with the contents of
814 this article.

815

816

817

818 **Author contribution**

819

820 A.N.-N., F.P. and A.R.F. designed the research; D.S.B., C.P.N, J.L.-C., and E.F.
821 characterized the transgenic lines under supervision of W.L.A and A.N.-N.; N.L.
822 supervised L.C. in the *AtSFC1* protein localization analysis; D.B., L.C., N.L. and
823 A.N.-N. performed the lipid and metabolite analyses; G.A., M.G.B., V.P.
824 performed the biochemical characterization of *AtSFC1* protein under
825 supervision of F.P.; M.V.P. performed the cloning and plant transformation
826 under supervision T.O.; D.S.B., A.N.-N., A.R.F and F.P. analyzed the data;
827 D.S.B., A.R.F., F.P. and A.N.-N. wrote the article with input from all the others.
828 V.P., L.P., N.L. and A.P.M.W. complemented the writing.

829

830

831

832 **Figure Legends**

833

834

835 **Figure 1. Homo-exchange activities of various substrates in**
836 **proteoliposomes reconstituted with *AtSFC1*.** Transport was initiated by
837 adding radioactive substrate (final concentration, 1 mM) to proteoliposomes
838 preloaded internally with the same substrate (concentration, 10 mM). The
839 reaction was terminated after 60 minutes. The data are means \pm SE of at least
840 three independent experiments in duplicate. Differences between the
841 [14 C]citrate/citrate and [14 C]succinate/succinate homo-exchanges and between
842 these and all the other homo-exchanges were significant (Student's *t*-test, $P <$
843 0.05). Abbreviations: GABA, γ -aminobutyrate; SAM, S-adenosylmethionine.

844

845

846 **Figure 2. Substrate specificity of *AtSFC1*.** Liposomes reconstituted with
847 *AtSFC1* were preloaded internally with various substrates (concentration, 10
848 mM). Transport was started by adding 0.13 mM [14 C]citrate and terminated after
849 1 min. The values are means \pm SE of at least three independent experiments in
850 duplicate for each internal substrate investigated. Differences between the
851 activities of [14 C]citrate uptake with internal citrate, isocitrate and *cis*-aconitate
852 and the activities with internal succinate and fumarate were significant

26

853 (Student's *t*-test, $P < 0.05$). Differences between the activities of [^{14}C]citrate
854 uptake with internal fumarate and succinate and the activity with internal NaCl
855 and no substrate were significant (Student's *t*-test, $P < 0.05$). Differences
856 between the activities of [^{14}C]citrate uptake with internal malate, maleate,
857 oxoglutarate and oxaloacetate and the activity with internal NaCl and no
858 substrate were not significant (Student's *t*-test, $P > 0.05$). Abbreviation: PEP,
859 phosphoenolpyruvate.

860

861

862 **Figure 3. Kinetics of [^{14}C]citrate transport in proteoliposomes**
863 **reconstituted with AtSFC1.** (A) Time courses of [^{14}C]citrate uptake by
864 AtSFC1-reconstituted liposomes containing no substrate or various substrates.
865 Proteoliposomes were preloaded internally with 10 mM citrate (●), fumarate
866 (■), succinate (□), oxaloacetate (△) or NaCl and no substrate (O). Transport
867 was initiated by adding 1 mM [^{14}C]citrate and terminated at the indicated times.
868 Similar results were obtained in at least four independent experiments in
869 duplicate. (B) Efflux of [^{14}C]citrate from liposomes reconstituted with AtSFC1
870 and preloaded internally with 2 mM citrate. The internal substrate pool was
871 labeled with [^{14}C]citrate by carrier-mediated exchange equilibration. Then the
872 proteoliposomes were passed through Sephadex G-75. The efflux of [^{14}C]citrate
873 was started by adding buffer A alone (▼) or in buffer A 5 mM citrate (●),
874 fumarate (□), succinate (▲), 5 mM citrate plus 30 mM pyridoxal 5'-phosphate
875 and 20 mM bathophenanthroline (○) or 30 mM pyridoxal 5'-phosphate and 20
876 mM bathophenanthroline (■). Similar results were obtained in three
877 independent experiments in duplicate.

878

879

880 **Figure 4. Characterization and expression of SFC1 in Arabidopsis.** (A)
881 Expression analysis in wild-type plants in different stages of development. The
882 relative quantification was performed according to the comparative method ($2^{-\Delta\Delta\text{Ct}}$).
883 *Actin2* was employed as a reference gene. (B) Schematic representation
884 of the antisense construct. A fragment of 930 bp of the gene AtSFC1 was
885 inserted in the antisense orientation under the control of the 35S promoter. The

27

886 cassette also contained a hygromycin resistance marker gene (Hyg^R) and *nos*
887 terminator. (C) Real-time PCR analysis for *AtSFC1* in leaves of wild-type and
888 antisense lines. Values are means \pm SE of three independent biological
889 replicates; an asterisk indicates values that were determined by the Student's *t*-
890 test to be significantly different ($P < 0.05$) from the wild-type.

891

892

893 **Figure 5. Phenotypic characterization of *AtSFC1* mitochondrial carrier.**

894 Seed germination rate of wild-type (Wt) and 35S *SFC1* antisense lines grown
895 on agar plates containing half-strength Murashige and Skoog (MS) medium plus
896 1% (w/v) (A) sucrose or (B) sucrose-free. Radicle emergence was used as a
897 morphological marker for germination. Values are means \pm standard error (SE)
898 of four independent biological replicates. (C) Root length of the Wt and 35S
899 *SFC1* antisense lines at 11 days after germination. Ten seeds per genotype
900 were germinated on vertical plates for 2 days in the dark and then transferred to
901 8 h of light/16 h of dark regime. Values are means \pm SE of ten measurements
902 from six biological replicates. (D) Root oxygen consumption in darkness. The
903 measurements were performed in 4-week-old plants. Values are means \pm SE of
904 four individual determinations per line. The asterisk indicates values that were
905 determined by the Student's *t*-test to be significantly different ($P < 0.05$) from the
906 Wt. Abbreviation: FW, fresh weight.

907

908

909 **Figure 6. Relative amount of fatty acids and metabolites in seedlings.**

910 Seedlings of 35S *SFC1* antisense lines and wild-type (Wt) grown on agar plates
911 containing half-strength Murashige and Skoog (MS) medium without sucrose.
912 (A) Fatty acids; (B) organic acids; (C) nitrogen and amino acids metabolism;
913 and (D) sugars that presented a substantial changes. Values are mean \pm SE of
914 three biological replicates. Asterisks indicate values that were determined by the
915 Student's *t*-test to be significantly different ($P < 0.05$) from the Wt. Additional
916 determinations of metabolites and fatty acids are provided in supplemental
917 Figure S7 and S8.

918

919

920 **Figure 7. Proposed roles of the mitochondrial SFC1 carrier in *Arabidopsis***
921 ***thaliana*.** (A) Hypothesized model for seeds and seedlings. The citrate
922 produced in the glyoxylate cycle, after the onset of germination, is exported to
923 cytosol. The transport of citrate out of the glyoxysome is necessary because
924 aconitase (enzyme that converts citrate to isocitrate) is cytosolic. The cytosolic
925 citrate can be imported into mitochondria by the *At*SFC1 carrier in exchange by
926 intramitochondrial isocitrate or to a lower extent fumarate or succinate. The
927 isocitrate in the cytosol can be imported by glyoxysome or provide carbon
928 skeletons for nitrogen assimilation. The cytosolic fumarate can be converted
929 ultimately to OAA and fuels the synthesis of soluble carbohydrates via
930 gluconeogenesis. Succinate can also be imported into the mitochondria through
931 the SFC1 transporter, or other mitochondrial transporters, such as DTC or DIC
932 carrier, and enters the TCA cycle, where it is converted to fumarate. Therefore,
933 it is likely that *At*SFC1 transports other substrates besides citrate and isocitrate.
934 (B) Hypothesized model for radicles and roots. The primary function of this
935 transporter in radicles and roots is to catalyze the exchange between
936 mitochondrial citrate and cytosolic isocitrate. Once into mitochondria, isocitrate
937 can contribute to NADH production acting as a source of reducing equivalents
938 for the electron transport chain. Thus, the reactions of citrate and isocitrate
939 conversions may provide carbon skeletons for amino acid synthesis and
940 reducing equivalents for biosynthetic pathways and energy production,
941 performing important roles in the TCA cycle and energy metabolism. A
942 transporter of organic acids, such as OAA and succinate, from peroxisome
943 metabolism is also shown: PMP22 across the peroxisomal membrane.
944 Abbreviations: ATP, adenosine triphosphate; DTC, dicarboxylate/tricarboxylate
945 carrier; ETC, electron transport chain; e^- , electron; FADH, reduced flavin
946 adenine dinucleotide; GABA, γ -aminobutyric acid; NADH, reduced nicotinamide
947 adenine dinucleotide; OAA, oxaloacetate; PEP, phosphoenolpyruvate; PMP22,
948 peroxisomal membrane protein of 22 kDa; SFC1, citrate/isocitrate carrier 1;
949 SSA, succinic semialdehyde; TCA, tricarboxylic acid cycle; 2-OG, 2-
950 oxoglutarate. Transporter marks (?) denote unknown carriers. The preferential
951 metabolite transport by *At*SFC1 carrier is represented by continuous arrows;
952 dashed arrows means other possibilities.
953

954

955 **Supplementary Files**

956

957 **Supplemental Table 1.** Germination speed index (GSI) and emergence speed
 958 index (ESI) of plants with reduced expression of SFC1 under 12h light/12 h dark
 959 condition. Values are presented as mean \pm SE of determinations on six individual
 960 plates with 50 seeds each per line. Boldface types indicate values that were
 961 determined by Student's *t* test to be significantly different ($P < 0.05$) from the
 962 respective wild type.

963

	GSI		ESI	
	+ Sacarose	- Sacarose	+ Sacarose	- Sacarose
Wt	26.4 \pm 0.23	32.0 \pm 0.36	0.74 \pm 0.01	0.88 \pm 0.01
<i>sfc1-12</i>	24.9 \pm 0.36	29.9 \pm 0.66	0.69 \pm 0.01	0.84 \pm 0.01
<i>sfc1-10</i>	26.2 \pm 0.91	28.6 \pm 0.84	0.83 \pm 0.01	0.85 \pm 0.01
<i>sfc1-8</i>	25.5 \pm 1.04	25.2 \pm 0.59	0.76 \pm 0.01	0.89 \pm 0.01

964

965

966

967 **Supplemental Figure S1. Expression of AtSFC1 in *E. coli* and its**968 **purification.** Proteins were separated by SDS-PAGE and stained with

969 Coomassie Blue dye. The molecular masses of the markers (bovine serum

970 albumin, carbonic anhydrase and cytochrome *c* are shown on the left. Lanes 1–971 4, *E. coli* C014 (DE3) cells containing the expression vector with (lanes 2 and 4)

972 and without (lanes 1 and 3) the coding sequence of AtSFC1. Samples at 37°C

973 were taken immediately before (lanes 1 and 2) and 4 h after induction (lanes 3

974 and 4). The same number of bacteria was analyzed in each sample. Lane 5,

975 purified AtSFC1 (about 10 μ g) derived from the bacteria shown in lane 4.

976

977

978 **Supplemental Figure S2. Effect of inhibitors on the citrate/citrate**979 **exchange by AtSFC1.** Liposomes were reconstituted with AtSFC1 and

980 preloaded internally with 10 mM citrate. Transport was initiated by adding 0.13

981 mM [¹⁴C]citrate and terminated after 1 min. Thiol reagents were added 2

982 minutes before the labeled substrate; the other inhibitors were added together

983 with the labeled substrate. The final concentrations of the inhibitors were 10 μ M

984 (CAT, carboxyatractyloside; BKA, bongkreic acid), 30 mM (PLP, pyridoxal 5'-

985 phosphate), 25 mM (BAT, bathophenanthroline), 0.2 mM (pHMB, *p*-

30

986 hydroxymercuribenzoate; MER, mersalyl), 1 mM (NEM, *N*-ethylmaleimide); 2
987 mM (BM, butylmalonate; Phesuc, phenylsuccinate; 1,2,3-BTA, 1,2,3-
988 benzenetricarboxylate; 1,3,5-BTA, 1,3,5-benzenetricarboxylate), 0.1% (TAN,
989 tannic acid), 0.2 mM (BrCP, bromocresol purple) and 0.1 mM HgCl₂. Similar
990 results were obtained in at least three independent experiments in duplicate.

991

992

993 **Supplemental Figure S3. Phylogenetic tree of AtSFC1 and its closest**
994 **relatives from some plants, fungi and metazoa.** The tree was constructed
995 using 39 sequences comprising the known mitochondrial di- and tri-carboxylic
996 acid carriers from *Arabidopsis thaliana*, *S. cerevisiae* and *H. sapiens*, and the
997 sequences more similar to AtSFC1 from other dicot- (*Glycine max* and *Vitis*
998 *vinifera*) and monocot- plants (*Zea mays* and *Oryza sativa*), other fungi
999 (*Ustilago maydis*, *Trichoderma reesei*, *Neurospora crassa*, *Candida albicans*),
1000 and an insect (*Drosophila melanogaster*); the best hit in a blast search for
1001 vertebrates, the sequence from the fish *Ictalurus punctatus*, was also included in
1002 the tree. The names of the mitochondrial carriers and/or their accession
1003 numbers are found on the terminal nodes. The phylogenetic tree was
1004 constructed as reported in the Methods.

1005

1006

1007 **Supplemental Figure S4.** Subcellular localization of transient expressed
1008 AtSFC1-GFP fusion protein in *N. benthamiana* protoplasts. (A) Fluorescent
1009 signals of AtSFC1-GFP (green); (B) mitochondrial marker IVD-eqFP611 (red);
1010 (C) chlorophyll *a*/chloroplasts (blue); and (D) merge showing the overlap of the
1011 fluorescent signals (yellow) detected by confocal laser-scanning microscopy.

1012

1013

1014 **Supplemental Figure S5.** *In silico* analysis of the expression of AtSFC1 gene. (A)
1015 eFP Browser display of transcript accumulation patterns across a variety of
1016 Arabidopsis organs. Arabidopsis eFP browser presents the transcript
1017 accumulation pattern of At5g01340 in a variety of tissues and organs along the
1018 development (Winter et al., 2007). In all cases, red indicates higher levels of
1019 transcript accumulation and yellow indicates a lower level of transcript

31

1020 accumulation. (B) RNA-seq expression profile of *AtSFC1*. RNA-seq data was
1021 obtained from the (Klepikova et al., 2016) and displayed at Arabidopsis eFP
1022 Browser (Winter et al., 2007). In all cases, red indicates higher levels of
1023 transcript accumulation and yellow indicates a lower level of transcript
1024 accumulation.

1025

1026

1027 **Supplemental Figure S6.** (A) Total lipids; (B) starch; and (C) protein content in
1028 Arabidopsis seeds from wild-type and 35S *SFC1* antisense lines. Values are
1029 mean \pm SE of five independent biological replicates. The data were normalized
1030 by dry weight. Asterisks indicate values that were determined by the Student's *t*-
1031 test to be significantly different ($P < 0.05$) from the wild-type.

1032

1033

1034 **Supplemental Figure S7.** Relative amount of fatty acids in seedlings of 35S
1035 *SFC1* antisense lines and wild-type (Wt) grown on agar plates containing half-
1036 strength Murashige and Skoog (MS) medium without sucrose. Values are
1037 mean \pm SE from three independent biological replicates. Asterisks indicate
1038 values that were determined by the Student's *t*-test to be significantly different
1039 ($P < 0.05$) from the Wt.

1040

1041

1042 **Supplemental Figure S8.** Relative amount of metabolites in seedlings of 35S
1043 *SFC1* antisense lines and wild-type (Wt) grown on agar plates containing half-
1044 strength Murashige and Skoog (MS) medium without sucrose. Values are mean
1045 \pm SE from at three independent biological replicates. Asterisks indicate values
1046 that were determined by the Student's *t*-test to be significantly different ($P <$
1047 0.05) from the Wt.

1048

1049 **Supplemental Figure S9.** Effect of decreased *AtSFC1* expression on
1050 photosynthesis of five-weeks-old plants. (A) CO₂ assimilation rate (A); (B)
1051 stomatal conductance (g_s); (C) dark respiration; (D) transpiration rate (E).
1052 Values are the mean \pm SE of six individual plants per line.

32

1053

1054

1055 **Supplemental Figure S10.** Effect of decreased *AtSFC1* expression on relative
1056 metabolite levels of expanded leaves from five-weeks-old plants. Data are
1057 normalized with respect to the mean response calculated for the wild-type (Wt).
1058 The colors indicate values that represent the mean \pm SE of measurements
1059 made on six individual plants per line. Asterisk indicates differences that were
1060 determined by the Student's *t*-test to be significantly different ($P < 0.05$) from the
1061 Wt.

1062

1063

1064 **Supplemental Figure S11.** Changes in the metabolites content in leaves of
1065 35S *SFC1* antisense lines. (A) Starch; (B) protein; (C) amino acids. Samples
1066 were taken from mature source leaves. Values are means \pm SE of six individual
1067 determinations per line. An asterisk indicates values that were determined by
1068 the Student's *t*-test to be significantly different ($P < 0.05$) from the wild-type. FW:
1069 fresh weight.

1070

1071

1072 **REFERENCES**

1073

- 1074 1 Palmieri, L., Lasorsa, F. M., De Palma, A., Palmieri, F., Runswick, M. J.
1075 and Walker, J. E. (1997) Identification of the yeast ACR1 gene product as
1076 a succinate-fumarate transporter essential for growth on ethanol or
1077 acetate. *FEBS Lett., Federation of European Biochemical Societies* **417**,
1078 114–118.
- 1079 2 Catoni, E., Schwab, R., Hilpert, M., Desimone, M., Schwacke, R., Flügge,
1080 U. I., Schumacher, K. and Frommer, W. B. (2003) Identification of an
1081 *Arabidopsis* mitochondrial succinate-fumarate translocator. *FEBS Lett.*
1082 **534**, 87–92.
- 1083 3 Picault, N., Hodges, M., Palmieri, L. and Palmieri, F. (2004) The growing
1084 family of mitochondrial carriers in *Arabidopsis*. *Trends Plant Sci.* **9**, 138–
1085 146.

33

- 1086 4 Palmieri, F., Pierri, C. L., De Grassi, A., Nunes-Nesi, A. and Fernie, A. R.
1087 (2011) Evolution, structure and function of mitochondrial carriers: A
1088 review with new insights. *Plant J.* **66**, 161–181.
- 1089 5 Palmieri, F. (1994) Mitochondrial carrier proteins. *FEBS Lett.*
- 1090 6 Palmieri, F. (2013) The mitochondrial transporter family SLC25:
1091 Identification, properties and physiopathology. *Mol. Aspects Med.* **34**,
1092 465-484.
- 1093 7 Krämer, R. and Palmieri, F. (1992) Chapter 16 Metabolite carriers in
1094 mitochondria. *New Compr. Biochem.* **23**, 359–384.
- 1095 8 Millar, A. H. and Heazlewood, J. L. (2003) Genomic and proteomic
1096 analysis of mitochondrial carrier proteins in Arabidopsis. *Plant Physiol.*
1097 **131**, 443–53.
- 1098 9 Monné, M. and Palmieri, F. (2014) Antiporters of the mitochondrial carrier
1099 family. In *Current Topics in Membranes* **73**, 289–320.
- 1100 10 Palmieri, F. and Monné, M. (2016) Discoveries, metabolic roles and
1101 diseases of mitochondrial carriers: A review. *Biochim. Biophys. Acta -*
1102 *Mol. Cell Res.* **1863**, 2362–2378.
- 1103 11 Eastmond, P. J. and Graham, I. A. (2001) Re-examining the role of the
1104 glyoxylate cycle in oilseeds. *Trends Plant Sci.* **6**, 72–77.
- 1105 12 Graham, I. A. (2008) Seed Storage Oil Mobilization. *Annu. Rev. Plant*
1106 *Biol.* **59**, 115–142.
- 1107 13 Pracharoenwattana, I., Zhou, W., Keech, O., Francisco, P. B.,
1108 Udomchalothorn, T., Tschoep, H., Stitt, M., Gibon, Y. and Smith, S. M.
1109 (2010) Arabidopsis has a cytosolic fumarase required for the massive
1110 allocation of photosynthate into fumaric acid and for rapid plant growth on
1111 high nitrogen. *Plant J.* **62**, 785–795.
- 1112 14 Dyson, B. C., Miller, M. A. E., Feil, R., Rattray, N., Bowsher, C. G.,
1113 Goodacre, R., Lunn, J. E. and Johnson, G. N. (2016) FUM2, a Cytosolic
1114 Fumarase, Is Essential for Acclimation to Low Temperature in
1115 Arabidopsis thaliana. *Plant Physiol.* **172**, 118–127.
- 1116 15 Fiermonte, G., Palmieri, L., Todisco, S., Agrimi, G., Palmieri, F. and
1117 Walker, J. E. (2002) Identification of the mitochondrial glutamate
1118 transporter. Bacterial expression, reconstitution, functional
1119 characterization, and tissue distribution of two human isoforms. *J. Biol.*

- 1120 Chem. **277**, 19289–19294.
- 1121 16 Palmieri, F., Stipani, I., Quagliariello, E. and Klingenberg, M. (1972)
1122 Kinetic Study of the Tricarboxylate Carrier in Rat Liver Mitochondria. Eur.
1123 J. Biochem. **26**, 587–594.
- 1124 17 Palmieri, F., Prezioso, G., Quagliariello, E. and Klingenberg, M. (1971)
1125 Kinetic Study of the Dicarboxylate Carrier in Rat Liver Mitochondria. Eur.
1126 J. Biochem. **22**, 66–74.
- 1127 18 Klingenberg, M. (2008) The ADP and ATP transport in mitochondria and
1128 its carrier. Biochim. Biophys. Acta - Biomembr. **1778**, 1978–2021.
- 1129 19 McGivan, J. D. and Klingenberg, M. (1971) Correlation Between H⁺ and
1130 Anion Movement in Mitochondria and the Key Role of the Phosphate
1131 Carrier. Eur. J. Biochem. **20**, 392–399.
- 1132 20 Palmieri, F., Indiveri, C., Bisaccia, F. and Iacobazzi, V. (1995)
1133 Mitochondrial metabolite carrier proteins: Purification, reconstitution, and
1134 transport studies. Methods Enzymol., Academic Press **260**, 349–369.
- 1135 21 Senkler, J., Senkler, M., Eubel, H., Hildebrandt, T., Lengwenus, C.,
1136 Schertl, P., Schwarzländer, M., Wagner, S., Wittig, I. and Braun, H. P.
1137 (2017) The mitochondrial complexome of *Arabidopsis thaliana*. Plant J.
1138 **89**, 1079–1092.
- 1139 22 Lemieux, B., Miquel, M., Somerville, C. and Browse, J. (1990) Mutants of
1140 *Arabidopsis* with alterations in seed lipid fatty acid composition. Theor.
1141 Appl. Genet. **80**, 234–240.
- 1142 23 Penfield, S. (2004) Reserve mobilization in the *Arabidopsis* endosperm
1143 fuels hypocotyl elongation in the dark, is independent of abscisic acid,
1144 and requires phosphoenolpyruvate carboxykinase1. Plant Cell **16**, 2705–
1145 2718.
- 1146 24 Pracharoenwattana, I., Cornah, J. E. and Smith, S. M. (2007) *Arabidopsis*
1147 peroxisomal malate dehydrogenase functions in β -oxidation but not in the
1148 glyoxylate cycle. Plant J. **50**, 381–390.
- 1149 25 Bernhardt, K., Wilkinson, S., Weber, A. P. M. and Linka, N. (2012) A
1150 peroxisomal carrier delivers NAD⁺ and contributes to optimal fatty acid
1151 degradation during storage oil mobilization. Plant J. **69**, 1–13.
- 1152 26 Monné, M., Voza, A., Lasorsa, F. M., Porcelli, V. and Palmieri, F. (2019)
1153 Mitochondrial Carriers for Aspartate, Glutamate and Other Amino Acids: A

- 1154 Review. *Int. J. Mol. Sci.* **20**, 4456; doi:10.3390/ijms20184456.
- 1155 27 Yoneshiro, T., Wang, Q., Tajima, K., Matsushita, M., Maki, H., Igarashi,
1156 K., Dai, Z., White, P. J., McGarrah, R. W., Ilkayeva, O. R., et al. (2019)
1157 BCAA catabolism in brown fat controls energy homeostasis through
1158 SLC25A44. *Nature* **572**, 614–619.
- 1159 28 Evans, C. T., scragg, A. H. and Ratledge, C. (1983) A Comparative Study
1160 of Citrate Efflux from Mitochondria of Oleaginous and Non-oleaginous
1161 Yeasts. *Eur. J. Biochem.* **130**, 195–204.
- 1162 29 Kaplan, R. S., Mayor, J. A., Johnston, N. and Oliveira, D. L. (1990)
1163 Purification and characterization of the reconstitutively active
1164 tricarboxylate transporter from rat liver mitochondria. *J. Biol. Chem.* **265**,
1165 13379–13385.
- 1166 30 Bisaccia, F., De Palma, A. and Palmieri, F. (1989) Identification and
1167 purification of the tricarboxylate carrier from rat liver mitochondria. *BBA -*
1168 *Bioenerg.* **977**, 171–176.
- 1169 31 Courtois-Verniquet, F. and Douce, R. (1993) Lack of aconitase in
1170 glyoxysomes and peroxisomes. *Biochem. J.* **294**, 103–7.
- 1171 32 De Bellis, L., Tsugeki, R., Alpi, A. and Nishimura, M. (1993) Purification
1172 and characterization of aconitase isoforms from etiolated pumpkin
1173 cotyledons. *Physiol. Plant.* **88**, 485–492.
- 1174 33 Pracharoenwattana, I., Cornah, J. E. and Smith, S. M. (2005) Arabidopsis
1175 peroxisomal citrate synthase is required for fatty acid respiration and seed
1176 germination. *Plant Cell* **17**, 2037–48.
- 1177 34 Theodoulou, F. L. and Eastmond, P. J. (2012) Seed storage oil
1178 catabolism: a story of give and take. *Curr. Opin. Plant Biol.* **15**, 322–328.
- 1179 35 Cheung, C. Y. M., Poolman, M. G., Fell, D. A., Ratcliffe, R. G. and
1180 Sweetlove, L. J. (2014) A Diel Flux Balance Model Captures Interactions
1181 between Light and Dark Metabolism during Day-Night Cycles in C3 and
1182 Crassulacean Acid Metabolism Leaves. *Plant Physiol.* **165**, 917–929.
- 1183 36 Chia, D. W., Yoder, T. J., Reiter, W. D. and Gibson, S. I. (2000) Fumaric
1184 acid: An overlooked form of fixed carbon in Arabidopsis and other plant
1185 species. *Planta* **211**, 743–751.
- 1186 37 Araújo, W. L., Nunes-Nesi, A. and Fernie, A. R. (2011, June) Fumarate:
1187 Multiple functions of a simple metabolite. *Phytochemistry* **72**, 838-43.

- 1188 38 Araújo, W. L., Nunes-Nesi, A., Osorio, S., Usadel, B., Fuentes, D., Nagy,
1189 R., Balbo, I., Lehmann, M., Studart-Witkowski, C., Tohge, T., et al. (2011)
1190 Antisense Inhibition of the Iron-Sulphur Subunit of Succinate
1191 Dehydrogenase Enhances Photosynthesis and Growth in Tomato via an
1192 Organic Acid-Mediated Effect on Stomatal Aperture. *Plant Cell* **23**, 600–
1193 627.
- 1194 39 Fuentes, D., Meneses, M., Nunes-Nesi, A., Araujo, W. L., Tapia, R.,
1195 Gomez, I., Holuigue, L., Gutierrez, R. A., Fernie, A. R. and Jordana, X.
1196 (2011) A Deficiency in the Flavoprotein of Arabidopsis Mitochondrial
1197 Complex II Results in Elevated Photosynthesis and Better Growth in
1198 Nitrogen-Limiting Conditions. *Plant Physiol.* **157**, 1114–1127.
- 1199 40 Hanning, I. and Heldt, H. W. (1993) On the Function of Mitochondrial
1200 Metabolism during Photosynthesis in Spinach (*Spinacia oleracea* L.)
1201 Leaves (Partitioning between Respiration and Export of Redox
1202 Equivalents and Precursors for Nitrate Assimilation Products). *Plant*
1203 *Physiol.* **103**, 1147–1154.
- 1204 41 Hanning, I., Baumgarten, K., Schott, K. and Heldt, H. W. (1999)
1205 Oxaloacetate Transport into Plant Mitochondria. *Plant Physiol.* **119**,
1206 1025–1031.
- 1207 42 Chen, R. and Gadgil, P. (1990) Do the mitochondria provide the 2-
1208 oxoglutarate needed for glutamate synthesis in higher plant chloroplasts?
1209 *Plant Physiol. Biochem.* **28**, 141–145.
- 1210 43 Fiermonte, G., Walker, J. E. and Palmieri, F. (1993) Abundant bacterial
1211 expression and reconstitution of an intrinsic membrane-transport protein
1212 from bovine mitochondria. *Biochem. J.* **294**, 293–299.
- 1213 44 Hoyos, M. E., Palmieri, L., Wertin, T., Arrigoni, R., Polacco, J. C. and
1214 Palmieri, F. (2003) Identification of a mitochondrial transporter for basic
1215 amino acids in *Arabidopsis thaliana* by functional reconstitution into
1216 liposomes and complementation in yeast. *Plant J.* **33**, 1027–35.
- 1217 45 Marobbio, C. M. T., Giannuzzi, G., Paradies, E., Pierri, C. L. and Palmieri,
1218 F. (2008) α -Isopropylmalate, a leucine biosynthesis intermediate in yeast,
1219 is transported by the mitochondrial oxalacetate carrier. *J. Biol. Chem.*
1220 **283**, 28445–28453.
- 1221 46 Cavero, S., Vozza, A., Del Arco, A., Palmieri, L., Villa, A., Blanco, E.,

- 1222 Runswick, M. J., Walker, J. E., Cerdán, S., Palmieri, F., et al. (2003)
1223 Identification and metabolic role of the mitochondrial aspartate-glutamate
1224 transporter in *Saccharomyces cerevisiae*. *Mol. Microbiol.* **50**, 1257–1269.
- 1225 47 Agrimi, G., Russo, A., Pierri, C. L. and Palmieri, F. (2012) The
1226 peroxisomal NAD⁺ carrier of *Arabidopsis thaliana* transports coenzyme A
1227 and its derivatives. *J. Bioenerg. Biomembr.* **44**, 333–340.
- 1228 48 Agrimi, G., Russo, A., Scarcia, P. and Palmieri, F. (2012) The human
1229 gene SLC25A17 encodes a peroxisomal transporter of coenzyme A, FAD
1230 and NAD⁺. *Biochem. J.* **443**, 241–247.
- 1231 49 Palmieri, L., Santoro, A., Carrari, F., Blanco, E., Nunes-Nesi, A., Arrigoni,
1232 R., Genchi, F., Fernie, A. R. and Palmieri, F. (2008) Identification and
1233 Characterization of ADNT1, a Novel Mitochondrial Adenine Nucleotide
1234 Transporter from *Arabidopsis*. *Plant Physiol.* **148**, 1797–1808.
- 1235 50 Indiveri, C., Iacobazzi, V., Giangregorio, N. and Palmieri, F. (1998)
1236 Bacterial Overexpression, Purification, and Reconstitution of the
1237 Carnitine/Acylcarnitine Carrier from Rat Liver Mitochondria. *Biochem.*
1238 *Biophys. Res. Commun.* **249**, 589–594.
- 1239 51 Monné, M., Miniero, D. V., Obata, T., Daddabbo, L., Palmieri, L., Vozza,
1240 A., Nicolardi, M. C., Fernie, A. R. and Palmieri, F. (2015) Functional
1241 characterization and organ distribution of three mitochondrial ATP-Mg/Pi
1242 carriers in *Arabidopsis thaliana*. *Biochim. Biophys. Acta* **1847**, 1220–
1243 1230.
- 1244 52 Porcelli, V., Fiermonte, G., Longo, A. and Palmieri, F. (2014) The human
1245 gene SLC25A29, of solute carrier family 25, encodes a mitochondrial
1246 transporter of basic amino acids. *J. Biol. Chem.* **289**, 13374–13384.
- 1247 53 Palmieri, L., Arrigoni, R., Blanco, E., Carrari, F., Zanol, M. I., Studart-
1248 Guimaraes, C., Fernie, A. R. and Palmieri, F. (2006) Molecular
1249 Identification of an *Arabidopsis* S-Adenosylmethionine Transporter.
1250 Analysis of Organ Distribution, Bacterial Expression, Reconstitution into
1251 Liposomes, and Functional Characterization. *Plant Physiol.* **142**, 855–
1252 865.
- 1253 54 Monné, M., Daddabbo, L., Gagneul, D., Obata, T., Hielscher, B., Palmieri,
1254 L., Miniero, D. V., Fernie, A. R., Weber, A. P. M. and Palmieri, F. (2018)
1255 Uncoupling proteins 1 and 2 (UCP1 and UCP2) from *Arabidopsis thaliana*

- 1256 are mitochondrial transporters of aspartate, glutamate, and
1257 dicarboxylates. *J. Biol. Chem.* **293**, 4213–4227.
- 1258 55 Bisaccia, F. and Palmieri, F. (1984) Specific elution from hydroxylapatite
1259 of the mitochondrial phosphate carrier by cardiolipin. *Biochim. Biophys.*
1260 *Acta* . **766**, 386–394.
- 1261 56 Kadenbach, B., Mende, P., Kolbe, H. V. J., Stipani, I. and Palmieri, F.
1262 (1982) The mitochondrial phosphate carrier has an essential requirement
1263 for cardiolipin. *FEBS Lett.* **139**, 109–112.
- 1264 57 Indiveri, C., Tonazzi, A. and Palmieri, F. (1991) Characterization of the
1265 unidirectional transport of carnitine catalyzed by the reconstituted
1266 carnitine carrier from rat liver mitochondria. *BBA - Biomembr.* **1069**, 110–
1267 116.
- 1268 58 Palmieri, L., Vozza, A., Hönlinger, A., Dietmeier, K., Palmisano, A., Zara,
1269 V. and Palmieri, F. (1999) The mitochondrial dicarboxylate carrier is
1270 essential for the growth of *Saccharomyces cerevisiae* on ethanol or
1271 acetate as the sole carbon source. *Mol. Microbiol.* **31**, 569–577.
- 1272 59 Castegna, A., Scarcia, P., Agrimi, G., Palmieri, L., Rottensteiner, H.,
1273 Spera, I., Germinario, L. and Palmieri, F. (2010) Identification and
1274 functional characterization of a novel mitochondrial carrier for citrate and
1275 oxoglutarate in *Saccharomyces cerevisiae*. *J. Biol. Chem.* **285**, 17359–
1276 17370.
- 1277 60 Di Noia, M. A., Todisco, S., Cirigliano, A., Rinaldi, T., Agrimi, G.,
1278 Iacobazzi, V. and Palmieri, F. (2014) The Human SLC25A33 and
1279 SLC25A36 Genes of Solute Carrier Family 25 Encode Two Mitochondrial
1280 Pyrimidine Nucleotide Transporters. *J. Biol. Chem.* **289**, 33137–33148.
- 1281 61 Indiveri, C., Tonazzi, A., Prezioso, G. and Palmieri, F. (1991) Kinetic
1282 characterization of the reconstituted carnitine carrier from rat liver
1283 mitochondria. *Biochim. Biophys. Acta* **1065**, 231–8.
- 1284 62 Palmieri, L., Lasorsa, F. M., Iacobazzi, V., Runswick, M. J., Palmieri, F.
1285 and Walker, J. E. (1999) Identification of the mitochondrial carnitine
1286 carrier in *Saccharomyces cerevisiae*. *FEBS Lett.* **462**, 472–6.
- 1287 63 Marobbio, C. M. T., Di Noia, M. A. and Palmieri, F. (2006) Identification of
1288 a mitochondrial transporter for pyrimidine nucleotides in *Saccharomyces*
1289 *cerevisiae*: bacterial expression, reconstitution and functional

- 1290 characterization. *Biochem. J.* **393**, 441–446.
- 1291 64 Nakagawa, T., Suzuki, T., Murata, S., Nakamura, S., Hino, T., Maeo, K.,
1292 Tabata, R., Kawai, T., Tanaka, K., Niwa, Y., et al. (2007) Improved
1293 Gateway Binary Vectors: High-Performance Vectors for Creation of
1294 Fusion Constructs in Transgenic Analysis of Plants. *Biosci. Biotechnol.*
1295 *Biochem.* **71**, 2095–2100.
- 1296 65 Forner, J. and Binder, S. (2007) The red fluorescent protein eqFP611:
1297 Application in subcellular localization studies in higher plants. *BMC Plant*
1298 *Biol.* **7**.
- 1299 66 Schindelin, J., Arganda-Carreras, I., Frise, E., Kaynig, V., Longair, M.,
1300 Pietzsch, T., Preibisch, S., Rueden, C., Saalfeld, S., Schmid, B., et al.
1301 (2012) Fiji: An open-source platform for biological-image analysis. *Nat.*
1302 *Methods* **9**, 676-82.
- 1303 67 Murashige, T. and Skoog, F. (1962) A Revised Medium for Rapid Growth
1304 and Bio Assays with Tobacco Tissue Cultures. *Physiol. Plant.* **15**, 473–
1305 497.
- 1306 68 Karimi, M., Inzé, D. and Depicker, A. (2002, May) GATEWAY™ vectors
1307 for *Agrobacterium*-mediated plant transformation. *Trends Plant Sci.* **7**,
1308 193-5.
- 1309 69 Clough, S. J. and Bent, A. F. (1998) Floral dip: a simplified method for
1310 *Agrobacterium*-mediated transformation of *Arabidopsis thaliana*. *Plant J.*
1311 **16**, 735–43.
- 1312 70 Yoshida, K., Terashima, I. and Noguchi, K. (2007) Up-Regulation of
1313 Mitochondrial Alternative Oxidase Concomitant with Chloroplast Over-
1314 Reduction by Excess Light. *Plant Cell Physiol.* **48**, 606–614.
- 1315 71 Lima, A. L. S., DaMatta, F. M., Pinheiro, H. A., Totola, M. R. and Loureiro,
1316 M. E. (2002) Photochemical responses and oxidative stress in two clones
1317 of *Coffea canephora* under water deficit conditions. *Environ. Exp. Bot.* **47**,
1318 239–247.
- 1319 72 Lisec, J., Schauer, N., Kopka, J., Willmitzer, L. and Fernie, A. R. (2006)
1320 Gas chromatography mass spectrometry-based metabolite profiling in
1321 plants. *Nat. Protoc.* **1**, 387–396.
- 1322 73 Lytovchenko, A., Beleggia, R., Schauer, N., Isaacson, T., Leuendorf, J.
1323 E., Hellmann, H., Rose, J. K. and Fernie, A. R. (2009) Application of GC-

1324 MS for the detection of lipophilic compounds in diverse plant tissues.
 1325 Plant Methods 5, 4.
 1326

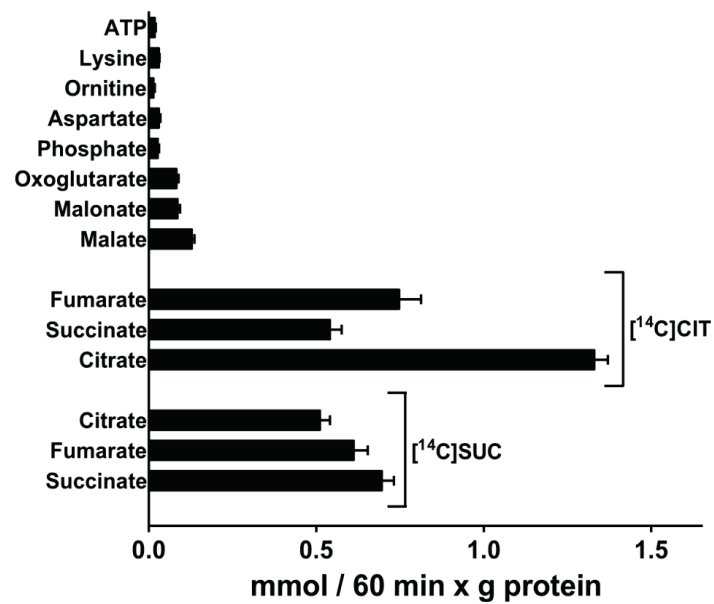


Figure 1. Homo-exchange activities of various substrates in proteoliposomes reconstituted with AtSFC1. Transport was initiated by adding radioactive substrate (final concentration, 1 mM) to proteoliposomes preloaded internally with the same substrate (concentration, 10 mM). The reaction was terminated after 60 minutes. The data are means \pm SE of at least three independent experiments in duplicate. Differences between the [¹⁴C] citrate/citrate and [¹⁴C] succinate/ succinate homoexchanges and between these and all the other homo-exchanges were significant (Student's *t*-test, *P* < 0.05). Abbreviations: GABA, γ -aminobutyrate; SAM, S-adenosylmethionine.

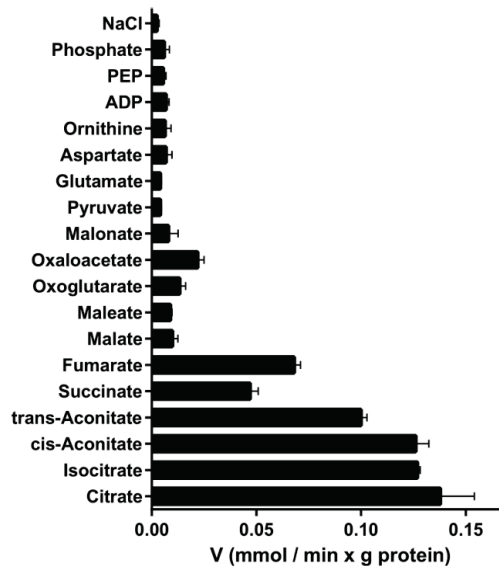


Figure 2. Substrate specificity of AtSFC1. Liposomes reconstituted with AtSFC1 were preloaded internally with various substrates (concentration, 10 mM). Transport was started by adding 0.13 mM [14 C] citrate and terminated after 1 min. The values are means \pm SE of at least three independent experiments in duplicate for each internal substrate investigated. Differences between the activities of [14 C] citrate uptake with internal citrate, isocitrate and *cis*-aconitate and the activities with internal succinate and fumarate were significant (Student's *t*-test, $P < 0.05$). Differences between the activities of [14 C] citrate uptake with internal fumarate and succinate and the activity with internal NaCl and no substrate were significant (Student's *t*-test, $P < 0.05$). Differences between the activities of [14 C] citrate uptake with internal malate, maleate, oxoglutarate and oxaloacetate and the activity with internal NaCl and no substrate were not significant (Student's *t*-test, $P > 0.05$). Abbreviation: PEP, phosphoenolpyruvate.

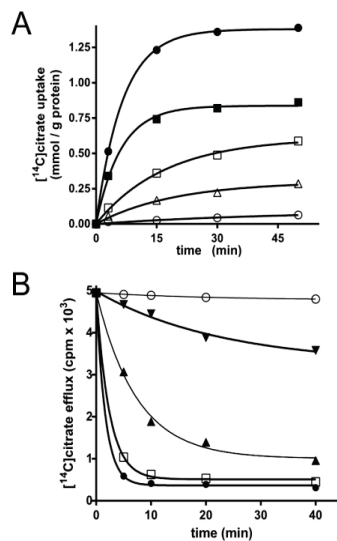


Figure 3. Kinetics of [14 C] citrate transport in proteoliposomes reconstituted with AtSFC1. (A) Time courses of [14 C] citrate uptake by AtSFC1-reconstituted liposomes containing no substrate or various substrates. Proteoliposomes were preloaded internally with 10 mM citrate (●), fumarate (■), succinate (□), oxaloacetate (△) or NaCl and no substrate (○). Transport was initiated by adding 1 mM [14 C] citrate and terminated at the indicated times. Similar results were obtained in at least four independent experiments in duplicate. (B) Efflux of [14 C] citrate from liposomes reconstituted with AtSFC1 and preloaded internally with 2 mM citrate. The internal substrate pool was labeled with [14 C] citrate by carrier-mediated exchange equilibration. Then the proteoliposomes were passed through Sephadex G-75. The efflux of [14 C] citrate was started by adding buffer A alone (▼) or in buffer A 5 mM citrate (●), fumarate (□), succinate (△), 5 mM citrate plus 30 mM pyridoxal 5-phosphate and 20 mM bathophenanthroline (○) or 30 mM pyridoxal 5-phosphate and 20 mM bathophenanthroline (■). Similar results were obtained in three independent experiments in duplicate.

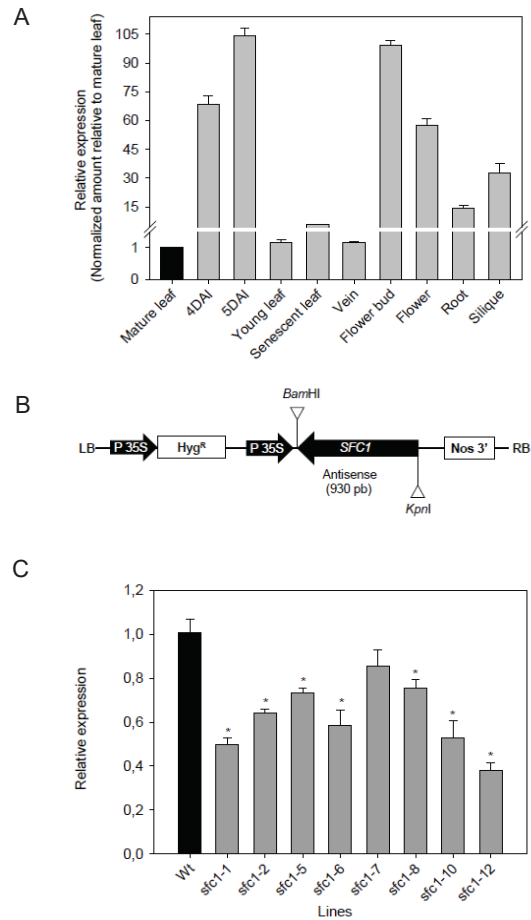


Figure 4. Characterization and expression of SFC1 in Arabidopsis. (A) Expression analysis in wild-type plants in different stages of development. The relative quantification was performed according to the comparative method ($2^{-\Delta\Delta Ct}$). *Actin2* was employed as a reference gene. (B) Schematic representation of the antisense construct. A fragment of 930 bp of the gene *AtSFC1* was inserted in the antisense orientation under the control of the 35S promoter. The cassette also contained a hygromycin resistance marker gene (Hyg^R) and *nos* terminator. (C) Real-time PCR analysis for *AtSFC1* in leaves of wild-type and antisense lines. Values are means \pm SE of three independent biological replicates; an asterisk indicates values that were determined by the Student's *t*-test to be significantly different ($P < 0.05$) from the wild-type.

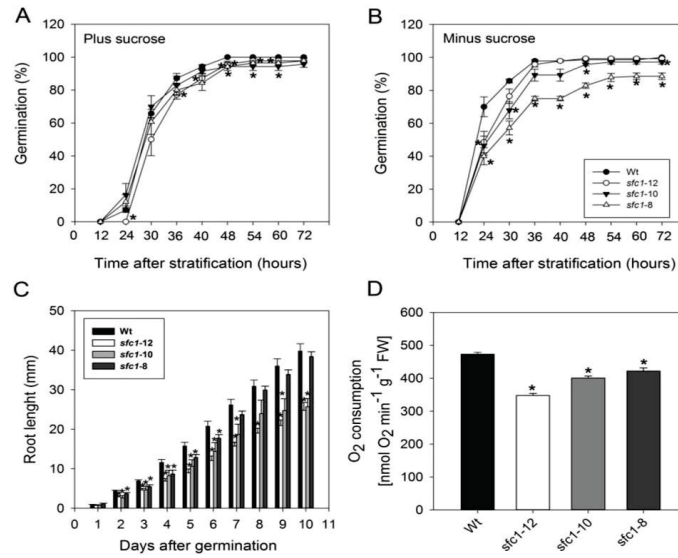


Figure 5. Phenotypic characterization of *AtSFC1* mitochondrial carrier. Seed germination rate of wild-type (Wt) and 35S *SFC1* antisense lines grown on agar plates containing half-strength Murashige and Skoog (MS) medium plus 1% (w/v) (A) sucrose or (B) sucrose-free. Radicle emergence was used as a morphological marker for germination. Values are means \pm standard error (SE) of four independent biological replicates. (C) Root length of the Wt and 35S *SFC1* antisense lines at 11 days after germination. Ten seeds per genotype were germinated on vertical plates for 2 days in the dark and then transferred to 8 h of light/16 h of dark regime. Values are means \pm SE of ten measurements from six biological replicates. (D) Root oxygen consumption in darkness. The measurements were performed in 4-week-old plants. Values are means \pm SE of four individual determinations per line. The asterisk indicates values that were determined by the Student's *t*-test to be significantly different ($P < 0.05$) from the Wt. Abbreviation: FW, fresh weight.

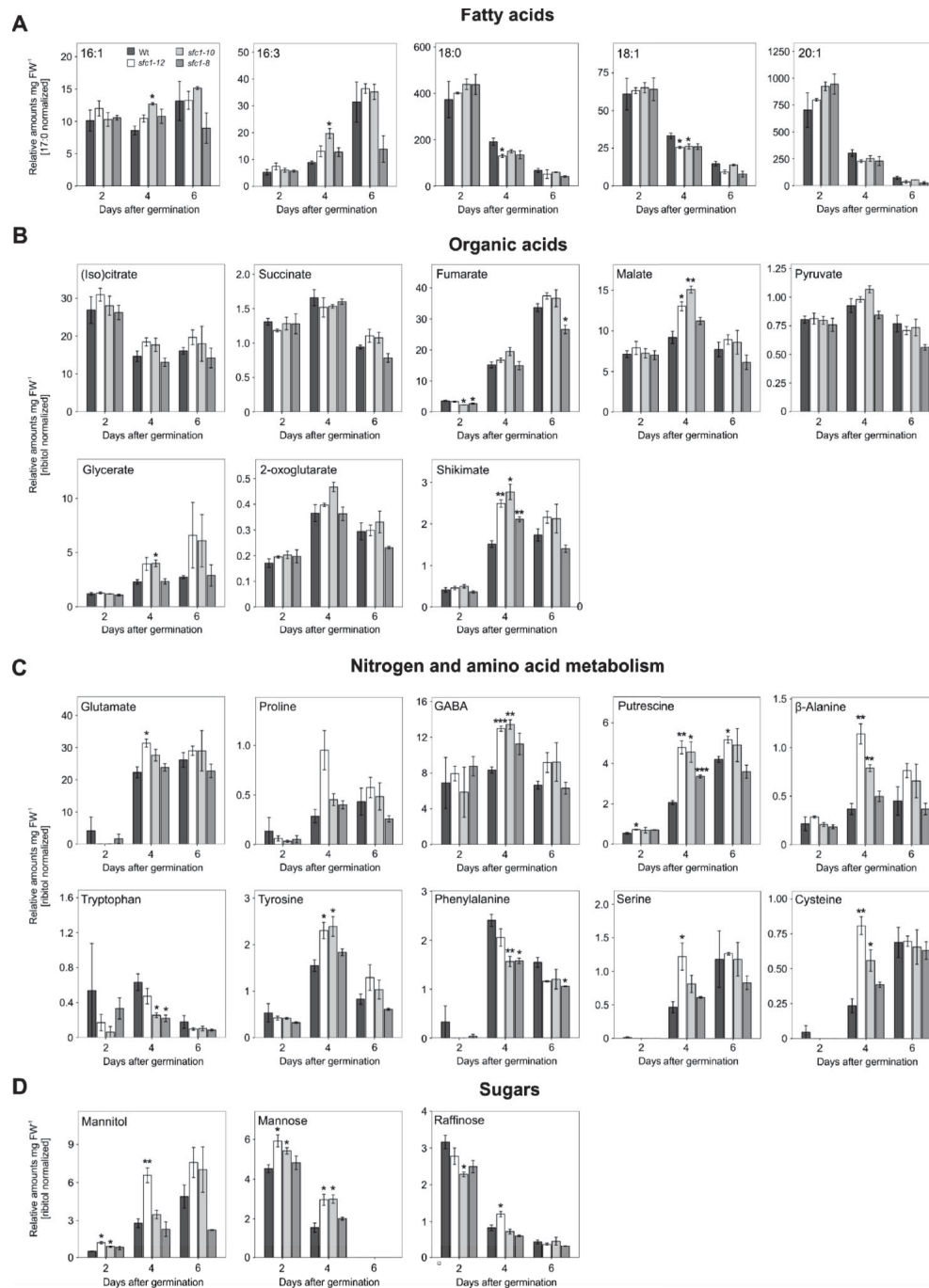


Figure 6. Relative amount of fatty acids and metabolites in seedlings. Seedlings of 35S *SFC1* antisense lines and wild-type (Wt) grown on agar plates containing half-strength Murashige and Skoog (MS) medium without sucrose. (A) Fatty acids; (B) organic acids; (C) nitrogen and amino acids metabolism; and (D) sugars that presented a substantial changes. Values are mean \pm SE of three biological replicates. Asterisks indicate values that were determined by the Student's *t*-test to be significantly different ($P < 0.05$) from the Wt. Additional determinations of metabolites and fatty acids are provided in supplemental Figure S7 and S8.

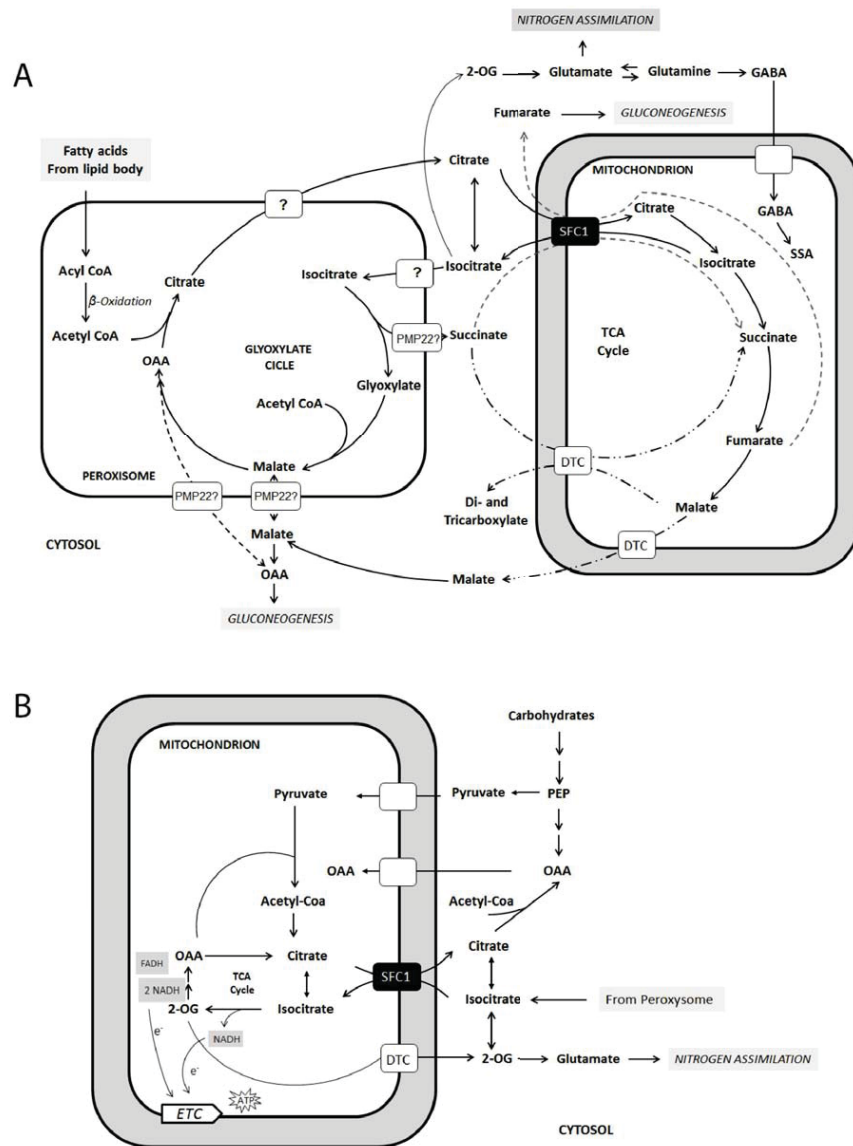
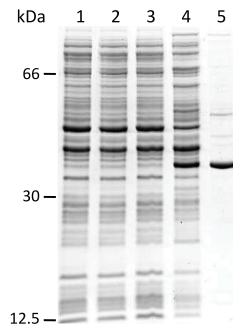
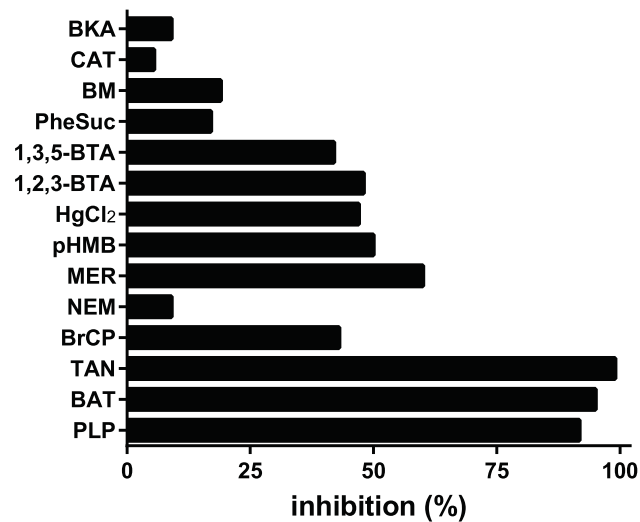


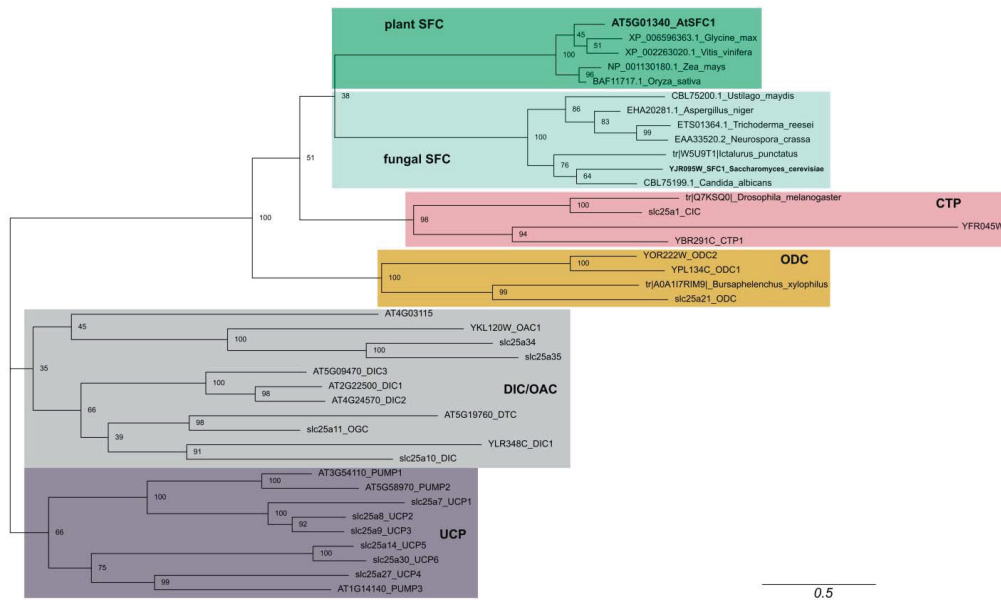
Figure 7. Proposed roles of the mitochondrial SFC1 carrier in *Arabidopsis thaliana*. (A) Hypothesized model for seeds and seedlings. The citrate produced in the glyoxylate cycle, after the onset of germination, is cytosolic. The transport of citrate out of the glyoxysome is necessary because acitase (enzyme that converts citrate to isocitrate) is cytosolic. The cytosolic citrate can be imported into mitochondria by the AtSFC1 carrier in exchange by intramitochondrial isocitrate or to a lower extent fumarate or succinate. The isocitrate in the cytosol can be imported by glyoxysome or provide carbon skeletons for nitrogen assimilation. The cytosolic fumarate can be converted ultimately to OAA and fuels the synthesis of soluble carbohydrates via gluconeogenesis. Succinate can also be imported into the mitochondria through the SFC1 transporter, or other mitochondrial transporters, such as DTC or DIC carrier, and enters the TCA cycle, where it is converted to fumarate. Therefore, it is likely that AtSFC1 transports other substrates besides citrate and isocitrate. (B) Hypothesized model for radicles and roots. The primary function of this transporter in radicles and roots is to catalyze the exchange between mitochondrial citrate and cytosolic isocitrate. Once into mitochondria, isocitrate can contribute to NADH production acting as a source of reducing equivalents for the electron transport chain. Thus, the reactions of citrate and isocitrate conversions may provide carbon skeletons for amino acid synthesis and reducing equivalents for biosynthetic pathways and energy production, performing important roles in the TCA cycle and energy metabolism. A transporter of organic acids, such as OAA and succinate, from peroxisome metabolism is also shown: PMP22 across the peroxisomal membrane. Abbreviations: ATP, adenosine triphosphate; DTC, dicarboxylate/tricarboxylate carrier; ETC, electron transport chain; e⁻, electron; FADH₂, reduced flavin adenine dinucleotide; GABA, γ-aminobutyric acid; NADH, reduced nicotinamide adenine dinucleotide; OAA, oxaloacetate; PEP, phosphoenolpyruvate; PMP22, peroxisomal membrane protein of 22 kDa; SFC1, citrate/isocitrate carrier 1; SSA, succinic semialdehyde; TCA, tricarboxylic acid cycle; 2-OG, 2-oxoglutarate. Transporter marks (?) denote unknown carriers. The preferential metabolite transport by AtSFC1 carrier is represented by continuous arrows; dashed arrows means other possibilities.



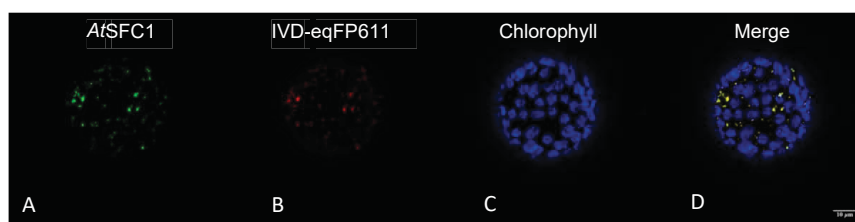
Supplemental Figure S1. Expression of AtSFC1 in *E. coli* and its purification. Proteins were separated by SDS-PAGE and stained with Coomassie Blue dye. The molecular masses of the markers (bovine serum albumin, carbonic anhydrase and cytochrome *c*) are shown on the left. Lanes 1–4, *E. coli* C014 (DE3) cells containing the expression vector with (lanes 2 and 4) and without (lanes 1 and 3) the coding sequence of AtSFC1. Samples at 37°C were taken immediately before (lanes 1 and 2) and 4 h after induction (lanes 3 and 4). The same number of bacteria was analyzed in each sample. Lane 5, purified AtSFC1 (about 10 µg) derived from the bacteria shown in lane 4.



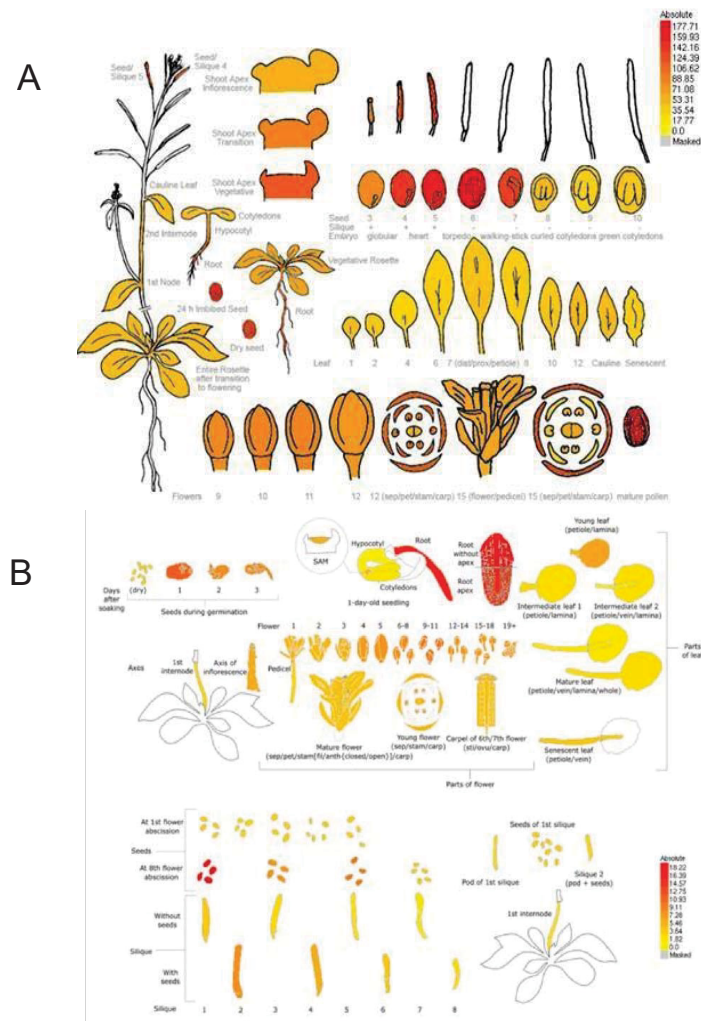
Supplemental Figure S2. Effect of inhibitors on the citrate/citrate exchange by AtSFC1. Liposomes were reconstituted with AtSFC1 and preloaded internally with 10 mM citrate. Transport was initiated by adding 0.13 mM [¹⁴C] citrate and terminated after 1 min. Thiol reagents were added 2 minutes before the labeled substrate; the other inhibitors were added together with the labeled substrate. The final concentrations of the inhibitors were 10 µM (CAT, carboxyatractyloside; BKA, bongkreic acid), 30 mM (PLP, pyridoxal 5-phosphate), 25 mM (BAT, bathophenanthroline), 0.2 mM (pHMB, p-hydroxymercuribenzoate; MER, mersalyl), 1 mM (NEM, N-ethylmaleimide); 2 mM (BM, butylmalonate; PheSuc, phenylsuccinate; 1,2,3-BTA, 1,2,3-benzenetricarboxylate; 1,3,5-BTA, 1,3,5-benzenetricarboxylate), 0.1% (TAN, tannic acid), 0.2 mM (BrCP, bromocresol purple) and 0.1 mM HgCl₂. Similar results were obtained in at least three independent experiments in duplicate.



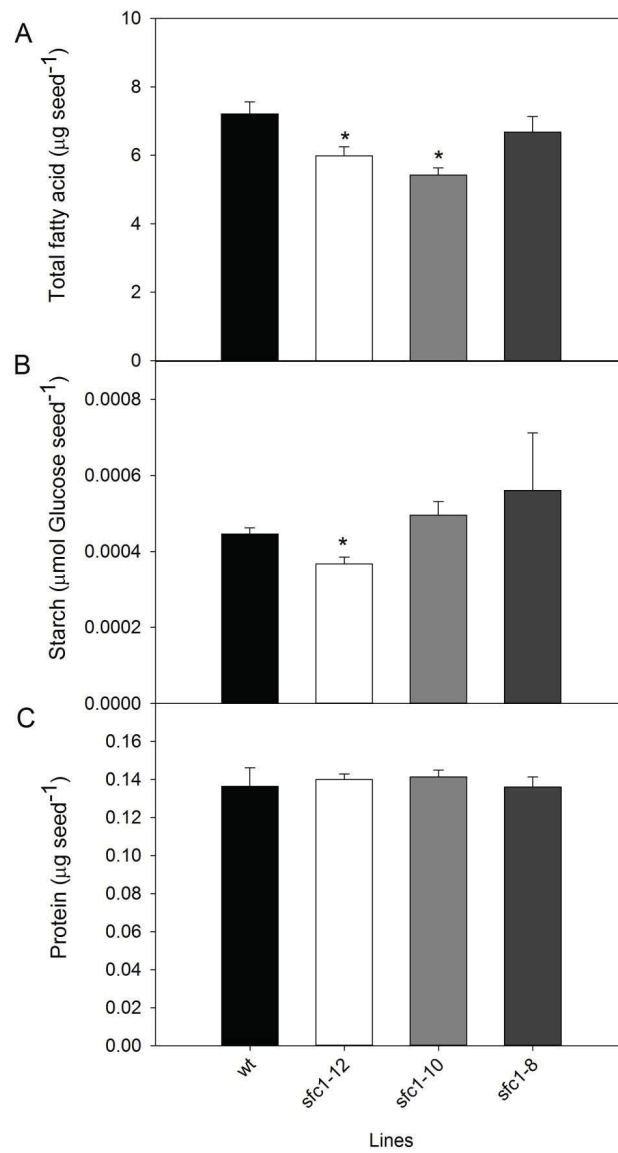
Supplemental Figure S3. Phylogenetic tree of *AtSFC1* and its closest relatives from some plants, fungi and metazoa. The tree was constructed using 39 sequences comprising the known mitochondrial di- and tri-carboxylic acid carriers from *Arabidopsis thaliana*, *S. cerevisiae* and *H. sapiens*, and the sequences more similar to *AtSFC1* from other dicot- (*Glycine max* and *Vitis vinifera*) and monocot- plants (*Zea mays* and *Oryza sativa*), other fungi (*Ustilago maydis*, *Trichoderma reesei*, *Neurospora crassa*, *Candida albicans*), and an insect (*Drosophila melanogaster*); the best hit in a blast search for vertebrates, the sequence from the fish *Ictalurus punctatus*, was also included in the tree. The names of the mitochondrial carriers and/or their accession numbers are found on the terminal nodes. The phylogenetic tree was constructed as reported in the Methods.



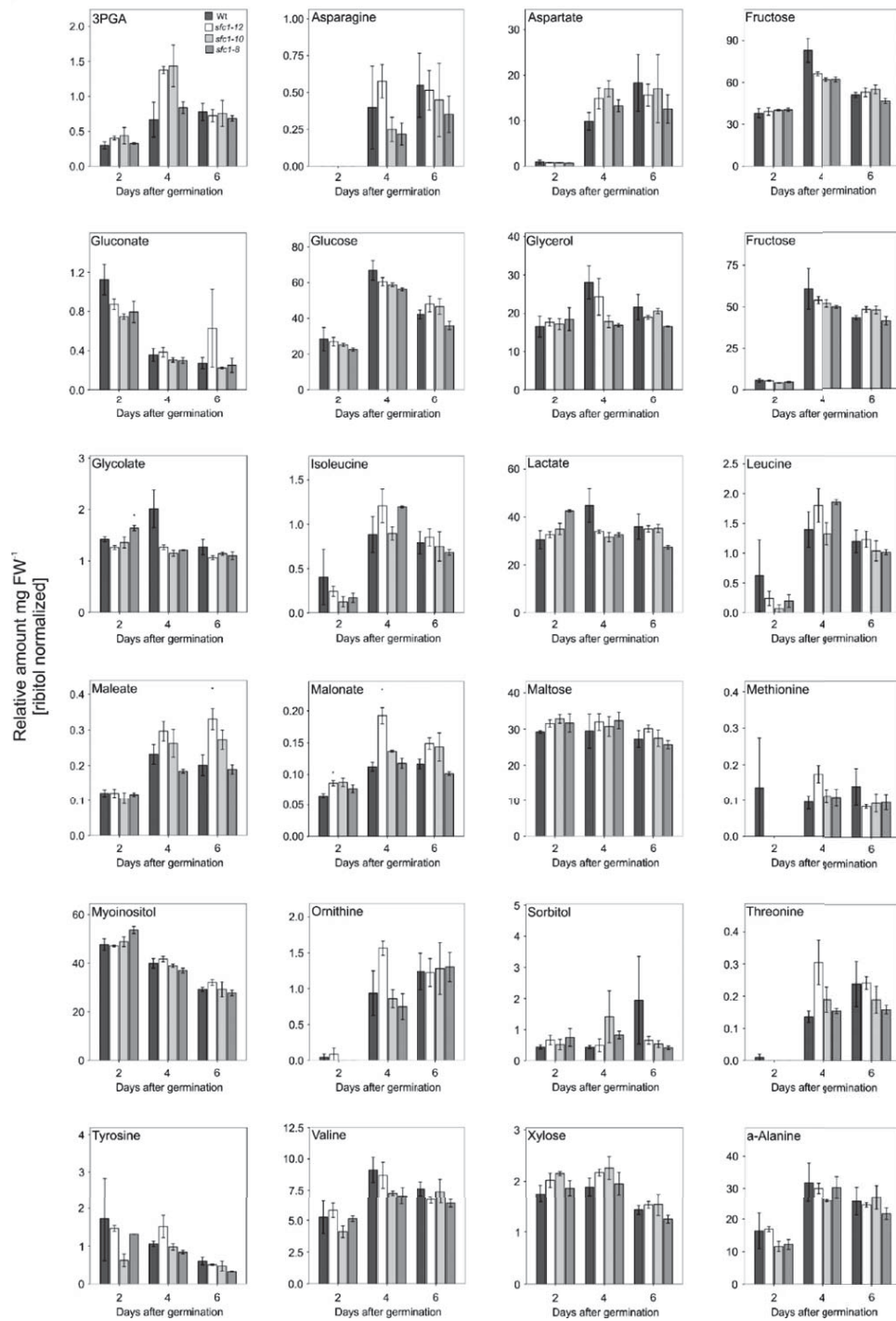
Supplemental Figure S4. Subcellular localization of transiently expressed *AtSFC1*-GFP fusion protein in *N. benthamiana* protoplasts. (A) Fluorescent signals of *AtSFC1*-GFP (green); (B) mitochondrial marker IVD-eqFP611 (red); (C) chlorophyll *a*/chloroplasts (blue); and (D) merge showing the overlap of the fluorescent signals (yellow) detected by confocal laser-scanning microscopy.



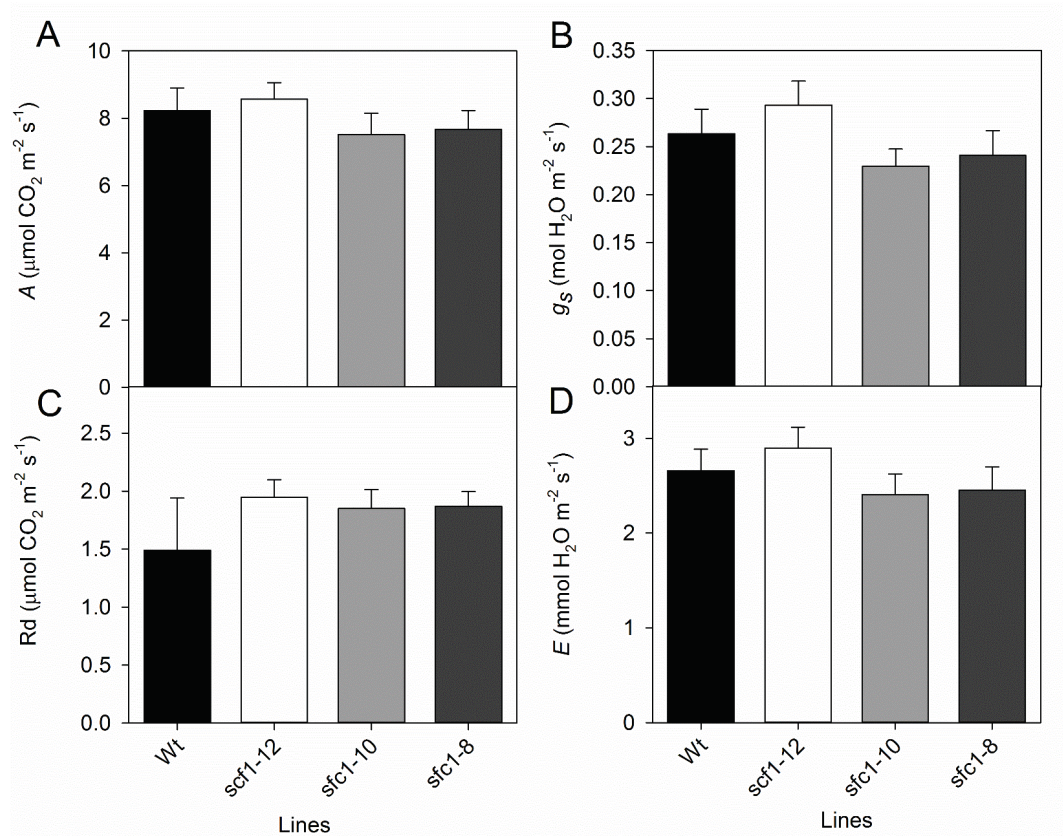
Supplemental Figure S5. *In silico* analysis of the expression of *AtSFC1* gene. (A) eFP Browser display of transcript accumulation patterns across a variety of Arabidopsis organs. Arabidopsis eFP browser presents the transcript accumulation pattern of *At5g01340* in a variety of tissues and organs along the development (Winter et al., 2007). In all cases, red indicates higher levels of transcript accumulation and yellow indicates a lower level of transcript accumulation. (B) RNA-seq expression profile of *AtSFC1*. RNAseq data was obtained from the (Klepikova et al., 2016) and displayed at Arabidopsis eFP Browser (Winter et al., 2007). In all cases, red indicates higher levels of transcript accumulation and yellow indicates a lower level of transcript accumulation.



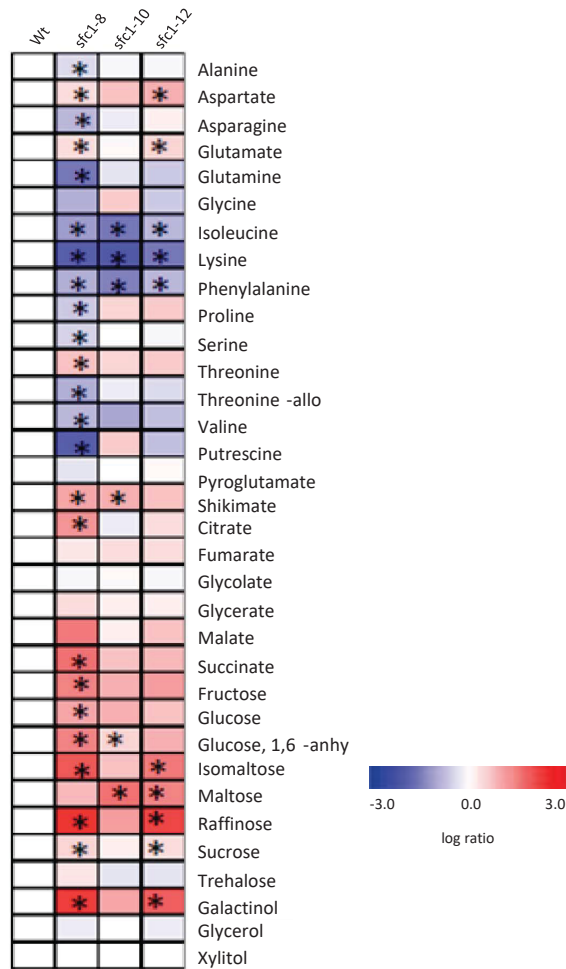
Supplemental Figure S6. (A) Total lipids; (B) starch; and (C) protein content in Arabidopsis seeds from wild-type and 35S *SFC1* antisense lines. Values are mean \pm SE of five independent biological replicates. The data were normalized by dry weight. Asterisks indicate values that were determined by the Student's *t*-test to be significantly different ($P < 0.05$) from the wild-type.



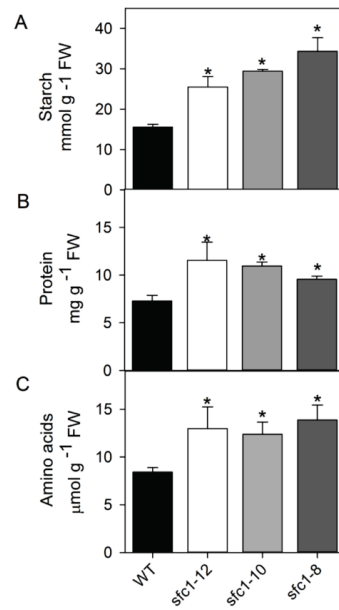
Supplemental Figure S8. Relative amount of metabolites in seedlings of 35S *SFC1* antisense lines and wild-type (Wt) grown on agar plates containing half-strength Murashige and Skoog (MS) medium without sucrose. Values are mean \pm SE from at three biological replicates. Asterisks indicate values that were determined by the Student's *t*-test to be significantly different ($P < 0.05$) from the Wt.



Supplemental Figure S9. Effect of decreased *AtSFC1* expression on photosynthesis of 5 weeks old plants. A, CO₂ assimilation rate (A); B, stomatal conductance (g_s); C, dark respiration; D, transpiration rate (E). Values are the mean \pm SE of measurements made on six individual plants per line.



Supplemental Figure S10. Effect of decreased *AtSFC1* expression on relative metabolite levels of expanded leaves from five-weeks-old plants. Data are normalized with respect to the mean response calculated for the wild-type (Wt). The colors indicate values that represent the mean \pm SE of measurements made on six individual plants per line. Asterisk indicates differences that were determined by the Student's *t*-test to be significantly different ($P < 0.05$) from the Wt.



Supplemental Figure S11. Changes in the metabolites content in leaves of 35S *SFC1* antisense lines. (A) Starch; (B) protein; (C) amino acids. Samples were taken from mature source leaves. Values are means \pm SE of six individual determinations per line. An asterisk indicates values that were determined by the Student's *t*-test to be significantly different ($P < 0.05$) from the wild-type. FW: fresh weight.

Author contribution

Lennart Charton participated in the fatty acid analysis shown in Figure 6a and performed the transient expression of *SFC1* in tobacco leaves followed by subcellular localization shown in Figure S4.

VI. Acknowledgement

Mein Dank geht zu allererst an meine Familie, vor allem an meine Eltern, die mich immer unterstützt und dazu ermutigt haben meinen eigenen Weg zu gehen. Das gleiche gilt für meine Freunde, die sich über Jahre hinweg die Hoch- und Tiefpunkte nicht nur meines wissenschaftlichen Werdegangs anhören mussten.

Ein besonderer Dank geht an Nicole Linka, die mich als studentische Hilfskraft unter ihre Fittiche genommen und mich über Bachelor, Master und Promotion begleitet hat. Ich werde noch lange an unsere (Konferenz-) Reisen denken und die viele Zeit, die wir auch außerhalb des Labors miteinander verbracht haben. Du warst die beste Doktormutter, die ich hätte haben können!

Andreas Weber danke ich vielmals für die jahrelange Unterstützung und die Möglichkeit meine wissenschaftliche „Karriere“ bei ihm anfangen zu dürfen.

Georg Groth möchte ich für die Betreuung als Zweitgutachter und Mentor und die damit verbundene Unterstützung während all meiner Abschlussarbeiten danken.

Petra Fackendahl danke ich für die Koordination des iGRAD-Plant Programms.

Anja Nöcker gebührt ein besonderes Dankeschön, für die Unterstützung mit diversen administrativen Problemen und für all das, was wir gar nicht direkt mitbekommen.

Ana, Franzi und Marc danke ich für die unzähligen Stunden innerhalb und außerhalb des Instituts, die wir gemeinsam auf so vielfältige Weise verbracht haben. Sei es mit einer Tasse Kaffee oder einem anderen Getränk.

Auch möchte ich mich bei den diversen basketballspielenden Kollegen für das Neuentdecken einer Sportart bedanken. Es gibt mehr als 21 Arten, wie ich davon profitiert habe.

Dominik und Marc möchte ich vor allem für das sehr sportliche letzte Jahr danken und hoffe, dass sie sich auch ohne mich weiter motivieren können.

Eichhörnchen an Flughörnchen: Apache bleibt gleich.

An Björn, auch wenn er mich früher verlassen hat: Vielen Dank für die gemeinsame Zeit. Ich sage es auch gerne nochmal: „Uns bleibt immer Paris.“

Ein persönliches Dankeschön an Sam für die vielen lustige Pausen und all die Unterstützung seit dem ersten Tag.

Auch an den Rest des Weberlabs, das MS-Lab und alle ehemaligen Studenten und Kollegen: ein herzliches Dankeschön für die schöne Zeit! Ich bin nicht ohne Grund immer wiedergekommen. Ihr seid ein tolles Institut mit einem großartigen Zusammenhalt, in dem ich mich immer wohl gefühlt habe.

Zu guter Letzt danke ich Kira für all die Jahre, die sie mich unterstützt und an mich geglaubt hat. Einen großen Teil von dem was ich heute bin verdanke ich dir.